

# NEW MACROCYCLES AND THEIR SUPRAMOLECULAR PERSPECTIVES

EDITED BY: Carmine Gaeta and De-Xian Wang  
PUBLISHED IN: Frontiers in Chemistry





# frontiers

## Frontiers eBook Copyright Statement

The copyright in the text of individual articles in this eBook is the property of their respective authors or their respective institutions or funders. The copyright in graphics and images within each article may be subject to copyright of other parties. In both cases this is subject to a license granted to Frontiers.

The compilation of articles constituting this eBook is the property of Frontiers.

Each article within this eBook, and the eBook itself, are published under the most recent version of the Creative Commons CC-BY licence.

The version current at the date of publication of this eBook is CC-BY 4.0. If the CC-BY licence is updated, the licence granted by Frontiers is automatically updated to the new version.

When exercising any right under the CC-BY licence, Frontiers must be attributed as the original publisher of the article or eBook, as applicable.

Authors have the responsibility of ensuring that any graphics or other materials which are the property of others may be included in the CC-BY licence, but this should be checked before relying on the CC-BY licence to reproduce those materials. Any copyright notices relating to those materials must be complied with.

Copyright and source acknowledgement notices may not be removed and must be displayed in any copy, derivative work or partial copy which includes the elements in question.

All copyright, and all rights therein, are protected by national and international copyright laws. The above represents a summary only. For further information please read Frontiers' Conditions for Website Use and Copyright Statement, and the applicable CC-BY licence.

ISSN 1664-8714

ISBN 978-2-88963-630-3

DOI 10.3389/978-2-88963-630-3

## About Frontiers

Frontiers is more than just an open-access publisher of scholarly articles: it is a pioneering approach to the world of academia, radically improving the way scholarly research is managed. The grand vision of Frontiers is a world where all people have an equal opportunity to seek, share and generate knowledge. Frontiers provides immediate and permanent online open access to all its publications, but this alone is not enough to realize our grand goals.

## Frontiers Journal Series

The Frontiers Journal Series is a multi-tier and interdisciplinary set of open-access, online journals, promising a paradigm shift from the current review, selection and dissemination processes in academic publishing. All Frontiers journals are driven by researchers for researchers; therefore, they constitute a service to the scholarly community. At the same time, the Frontiers Journal Series operates on a revolutionary invention, the tiered publishing system, initially addressing specific communities of scholars, and gradually climbing up to broader public understanding, thus serving the interests of the lay society, too.

## Dedication to Quality

Each Frontiers article is a landmark of the highest quality, thanks to genuinely collaborative interactions between authors and review editors, who include some of the world's best academicians. Research must be certified by peers before entering a stream of knowledge that may eventually reach the public – and shape society; therefore, Frontiers only applies the most rigorous and unbiased reviews. Frontiers revolutionizes research publishing by freely delivering the most outstanding research, evaluated with no bias from both the academic and social point of view. By applying the most advanced information technologies, Frontiers is catapulting scholarly publishing into a new generation.

## What are Frontiers Research Topics?

Frontiers Research Topics are very popular trademarks of the Frontiers Journals Series: they are collections of at least ten articles, all centered on a particular subject. With their unique mix of varied contributions from Original Research to Review Articles, Frontiers Research Topics unify the most influential researchers, the latest key findings and historical advances in a hot research area! Find out more on how to host your own Frontiers Research Topic or contribute to one as an author by contacting the Frontiers Editorial Office: [researchtopics@frontiersin.org](mailto:researchtopics@frontiersin.org)

# NEW MACROCYCLES AND THEIR SUPRAMOLECULAR PERSPECTIVES

Topic Editors:

**Carminé Gaeta**, University of Salerno, Italy

**De-Xian Wang**, Institute of Chemistry (CAS), China

**Citation:** Gaeta, C., Wang, D.-X., eds. (2020). New Macrocycles and Their Supramolecular Perspectives. Lausanne: Frontiers Media SA.  
doi: 10.3389/978-2-88963-630-3

# Table of Contents

- 05 Editorial: New Macrocycles and Their Supramolecular Perspectives**  
Carmine Gaeta and De-Xian Wang
- 08 Pillar[5]arene Based [1]rotaxane Systems With Redox-Responsive Host-Guest Property: Design, Synthesis and the Key Role of Chain Length**  
Runmiao Zhang, Chenwei Wang, Renhua Long, Tingting Chen, Chaoguo Yan and Yong Yao
- 15 Modification of Oligo- and Polylactides With Macrocyclic Fragments: Synthesis and Properties**  
Olga A. Mostovaya, Vladimir V. Gorbachuk, Pavel L. Padnya, Alena A. Vavilova, Gennady A. Evtugyn and Ivan I. Stoikov
- 22 Construction of Chiral Nanoassemblies Based on Host-Guest Complexes and Their Responsive CD and CPL Properties: Chirality Transfer From 2,6-helic[6]arenes to a Stilbazolium Derivative**  
Yan Guo, Ying Han and Chuan-Feng Chen
- 31 Hydroxy-Substituted Azacalix[4]Pyridines: Synthesis, Structure, and Construction of Functional Architectures**  
En-Xuan Zhang, De-Xian Wang and Mei-Xiang Wang
- 42 Artificial Gramicidins**  
Zhanhu Sun and Mihail Barboiu
- 48 Applications of Cucurbiturils in Medicinal Chemistry and Chemical Biology**  
Debapratim Das, Khaleel I. Assaf and Werner M. Nau
- 71 Molecular Lysine Tweezers Counteract Aberrant Protein Aggregation**  
Inesa Hadrovic, Philipp Rebmann, Frank-Gerrit Klärner, Gal Bitan and Thomas Schrader
- 80 The Supramolecular Chemistry of Cycloparaphenylenes and Their Analogs**  
Dapeng Lu, Qiang Huang, Shengda Wang, Jinyi Wang, Pingsen Huang and Pingwu Du
- 89 Design of a Thiosemicarbazide-Functionalized Calix[4]arene Ligand and Related Transition Metal Complexes: Synthesis, Characterization, and Biological Studies**  
Ehsan Bahojb Noruzi, Mahsa Kheirkhahi, Behrouz Shaabani, Silvano Geremia, Neal Hickey, Fioretta Asaro, Patrizia Nitti and Hossein Samadi Kafil
- 104 The Hexameric Resorcinarene Capsule as a Brønsted Acid Catalyst for the Synthesis of Bis(heteroaryl)methanes in a Nanoconfined Space**  
Stefania Gambaro, Pellegrino La Manna, Margherita De Rosa, Annunziata Soriente, Carmen Talotta, Carmine Gaeta and Placido Neri
- 113 Ditopic Receptors Based on Dihomooxacalix[4]arenes Bearing Phenylurea Moieties With Electron-Withdrawing Groups for Anions and Organic Ion Pairs**  
Alexandre S. Miranda, Defne Serbetci, Paula M. Marcos, José R. Ascenso, Mário N. Berberan-Santos, Neal Hickey and Silvano Geremia



- 125**  ***$\beta$ -D-Galactose-Functionalized Pillar[5]arene With Interesting Planar-Chirality for Constructing Chiral Nanoparticles***  
Guangping Sun, Liangtao Pu, Srikala Pangannaya, Tangxin Xiao, Xiao-Yu Hu, Juli Jiang and Leyong Wang
- 134** ***Enantiomeric Recognition of  $\alpha$ -Aminoacids by a Uranyl Salen-Bis-Porphyrin Complex***  
Chiara M. A. Gangemi, Ugne Rimkaite, Federica Cipria, Giuseppe Trusso Sfrazzetto and Andrea Pappalardo
- 142** ***Synthesis and Host–Guest Properties of Acyclic Pillar[n]naphthalenes***  
Yuanyin Jia, Ming Dong, Bin Wang and Chunju Li



# Editorial: New Macrocycles and Their Supramolecular Perspectives

Carmine Gaeta<sup>1\*</sup> and De-Xian Wang<sup>2,3\*</sup>

<sup>1</sup> Laboratory of Supramolecular Chemistry, Department of Chemistry and Biology "A. Zambelli", University of Salerno, Fisciano, Italy, <sup>2</sup> Beijing National Laboratory for Molecular Sciences, CAS Key Laboratory of Molecular Recognition and Function, Institute of Chemistry, Chinese Academy of Sciences, Beijing, China, <sup>3</sup> School of Chemical Sciences, University of Chinese Academy of Sciences, Beijing, China

**Keywords:** biomimetic systems, biomedical applications, supramolecular catalysis, cucurbiturils, cycloparaphenylenes, carbon-nanohoops, pillararene, chiral recognition

## Editorial on the Research Topic

### New Macrocycles and Their Supramolecular Perspectives

After more than half a century from the discovery of crown-ethers by Pedersen, macrocyclic hosts continue to be protagonists in supramolecular chemistry. Their peculiar structures make them ideal candidates to perform supramolecular functions such as catalysis, molecular and biomolecular recognition, sensing, self-assembly, and threading to give interpenetrated architectures. In addition, thanks to their synthetic versatility, the macrocycles are useful platforms for the design of more elaborated structures for the self-assembly of supramolecular polymers and for applications in biomimetic chemistry. These aspects have stimulated the creativeness of the scientists that in this way started imagining novel macrocyclic structures with the aim to perform ever more advanced supramolecular functions and properties. Thus, in the last years, in addition to the most innovative aspects regarding the "old" macrocycles, much attention has also been focused on the synthesis of new macrocycles. These studies have led to the discovery of novel classes of hosts such as pillararenes, cycloparaphenylene, biphenarenes, oxatubarene, large resorcinarenes, and a wide class of heteracalixarenes, coronarenes, which have found applications in several areas of supramolecular chemistry.

Starting by these considerations, we organized this article collection in which a considerable attention was devoted to the study of *new macrocycles*, and their applications in the field of molecular recognition and biological application, biomimetic chemistry, including supramolecular catalysis in nanoconfined spaces.

Regarding the biological applications, the review by Hadrovic et al. shows the potentialities of water-soluble molecular tweezers (MTs) which are able to complex the cationic side chains of lysine and arginine inside their cavities. The complexation is driven by secondary interactions between the cationic parts and the electron rich aromatic cavity of MTs. Interestingly, the inclusion of the cationic side chains of biologically-relevant amino acids inside the cavity of MTs prevents the pathologic protein aggregations. The toxic aggregates of protein species are dissolved and redirected to form amorphous, benign assemblies. Thus, MTs can be considered as promising candidates for disease-modifying therapy in early stages of neurodegenerative diseases.

In the last decades many efforts have been directed toward the design of macrocyclic derivatives with applications in the biomedical field. Das et al. show that the cucurbit[n]urils (CBs) are ideal candidates for applications in the area of medicinal-chemistry and chemical-biology thanks to their low toxicity and host-guest properties. In particular, CBs are able to encapsulate drugs for their formulation and delivery and finally show interesting properties in the controlled drug-release.

## OPEN ACCESS

### Edited by:

Tony D. James,  
University of Bath, United Kingdom

### Reviewed by:

Chusen Huang,  
Shanghai Normal University, China

### \*Correspondence:

Carmine Gaeta  
cgaeta@unisa.it  
De-Xian Wang  
dwxwang@iccas.ac.cn

### Specialty section:

This article was submitted to  
Supramolecular Chemistry,  
a section of the journal  
Frontiers in Chemistry

**Received:** 14 December 2019

**Accepted:** 12 February 2020

**Published:** 26 February 2020

### Citation:

Gaeta C and Wang D-X (2020)  
Editorial: New Macrocycles and Their  
Supramolecular Perspectives.  
Front. Chem. 8:128.  
doi: 10.3389/fchem.2020.00128

The host-guest complexes of CBs have found interesting applications for sensing, diagnostic, theranostic, and other relevant medicinal or bioanalytical applications.

The exploration of ever-new biomedical applications led to metal-calix[4]arene complexes able to inhibit the growth of bacteria, fungi, and cancerous tumor cells. As described by Noruzi et al., the biological activity is ascribable to the inorganic ions rather than calixarene ligand.

In the field of biomedical applications of macrocyclic compounds, an interesting review has been reported by Mostovaya et al. The authors show some examples in which the PLA has been modified with various macrocyclic fragments to obtain derivatives with promising properties for drug-delivery systems, photosensitizers in photodynamic therapy, protein binding and biosensing.

Anions play important roles in a wide range of natural and biological processes. Thus, the development of synthetic molecules designed to mimic the efficiency of the natural anion-receptors is an intensively active area of research in supramolecular chemistry. In their work, Miranda et al. report the synthesis of two bidentate dihomooxalix[4]arene receptors bearing phenylurea moieties substituted with electron-withdrawing groups at the lower rim via a butyl spacer. The binding affinity of these receptors toward several relevant anions was investigated and some of them were also studied as ditopic receptors for organic ion pairs, namely monoamine neurotransmitters and trace amine hydrochlorides.

Supramolecular chemistry is always inspired by biological systems and therefore biomimicry plays a crucial role in the design of novel macrocyclic hosts. Among the natural supramolecular systems, Gramicidin A (gA) is a natural peptide channel with a well-established, simple structure, and function: cations and water are transported together along the channel. In their review, Sun and Barboiu report examples of synthetic compounds able to mimic the functions of the natural gA. These systems are channel-type superstructures formed by self-assembly and provide remarkable combinations of functions similar to gA channel: water permeability, proton conductance via Grotts mechanism, cation vs. anion selectivity, single-channel activity.

In the context of the biomimetic systems, the self-assembled hexameric resorcinarene capsule shows peculiar features that make it an efficient biomimetic catalyst for organic reaction. Like a natural enzyme, the resorcinarene capsule shows an internal cavity able to host complementary guests, and able to accelerate the reactions by (i) nano-confinement effect; (ii) stabilization of intermediates and/or transition states. Gambaro et al., in their research article show that the hexameric resorcinarene capsule is able to catalyze the formation of bis(heteroaryl)methanes by reaction between pyrroles or indoles and carbonyl compounds ( $\alpha$ -ketoesters or aldehydes) in excellent yield and selectivity. The authors suggested that the capsule can play a double catalytic role as a H-bond catalyst, for the initial activation of the carbonyl substrate, and as a Brønsted acid catalyst, for the dehydration of the intermediate alcohol.

In natural systems, the receptor-substrate association takes account of the chirality of the individual components and

consequently the preference of a receptor for the given substrate and vice versa, depends on the spatial relationships between the individual interacting species. Taking inspiration from this, many scientists focused their attention on the study of host-guest interactions between chiral species. Guo et al. synthesized a couple of water-soluble chiral 2,6-helic[6]arene macrocycles and showed that they form stable 1:1 complexes with fluorescent cationic pyridinium guests in water. Compared with the free guest, the host-guest complex exhibited enhanced fluorescence. The host-guest complexes between 2,6-helic[6]arene and the cationic pyridinium guest were self-assembled in water to obtain supramolecular aggregates which showed rectangular or hexagonal nanostructures by SEM images. Interestingly, it was found that the assemblies showed clear mirror-image CD and CPL spectra in aqueous solution, which revealed a consecutive chirality transfer from the chiral macrocycle to the achiral guest.

Regarding the chiral recognition, in their paper, Gangemi et al., show that a chiral fluorescent-uranyl salen host acts as a receptor for the enantiomeric recognition of  $\alpha$ -aminoacids derivatives, with high association constants and an excellent enantiomeric discrimination between the two enantiomers of phenylalanine.

The design and the synthesis of chiral macrocyclic hosts has attracted much attention, and therefore the planar chirality shown by pillar[n]arenes was considered very useful for chiral molecular recognition, chirality switches, and catalysis. The planar chirality of pillar[n]arenes is mainly caused by the inherent substitution pattern of the aromatic units. Usually, the synthesized pillar[5]arenes are racemic mixtures and racemization takes place by rotation of its aromatic units. In their work, Sun et al. show that the introduction of  $\beta$ -galactose units on both the rims of the pillar[5]arene prevents the racemization according to dynamic  $^1\text{H}$  NMR studies. After separation, the two stable diastereoisomers (*Sp-D*)-GP5 and (*Rp-D*)-GP5 were able to capture a guest molecule (DNS-CPT) to form a host-guest supramolecular amphiphile. This can further self-assemble into chiral nanoparticles with the *Sp* and *Rp* planar chirality of (*Sp-D*)-GP5 and (*Rp-D*)-GP5 still being retained, suggesting GP5 could be as reliable chiral sources to transfer the *Sp* and *Rp* planar chirality.

The research for new macrocyclic structures often brings to the discovery of new recognition motifs. Thus, in the last years the cycloparaphenylene (CPP) macrocycles and  $\pi$ -extended carbon-nanohoops have attracted much attention due to their intriguing abilities to establish  $\pi\cdots\pi$  and cation $\cdots\pi$  interactions with complementary guests. In their review, Lu et al. highlight the supramolecular properties of CPPs and  $\pi$ -extended carbon-nanohoops mainly focusing on the size-selective encapsulation of fullerenes, endohedral metallofullerenes, small molecules, and CPP-based mechanomolecules.

Regarding the synthesis of mechanomolecules, Zhang R. et al. reported the synthesis of pillar[5]arene-based [1]rotaxanes. Thus, a series of amide-linked pillar[5]arene-based [1]rotaxanes with ferrocene unit as the stopper were obtained. Interestingly, the synthesized monofunctionalized pillar[5]arenes show a self-inclusion property, which gives rise to a pseudo-rotaxane, being the length of the imine chain the key role in this process. A

rotaxane is formed through amidation of a ferrocene dicarboxylic acid which acts as a plug. In addition, due to the ferrocene units, the pillar[5]arene-based [1]rotaxanes exhibit electrochemically reversible property.

The fascinating structure of pillararenes and their amazing supramolecular properties are stimulating the imagination of many scientists. In their work, Jia et al. report acyclic pillar[n]naphthalene ( $n = 2-4$ , dimer, trimer, and tetramer) oligomers, which are made up of 2,3-diethoxynaphthalene units linked by methylene bridges. The crystal structure of the tetramer shows an interesting pseudo-cycle-shaped structure in the solid state. The oligomers show interesting recognition properties toward cationic guests.

Among the new macrocycles, the heterocalixaromatics or heteroatom-bridged calix(het)arenes have gained a role of primary importance thanks to their unique conformational features and versatile recognition properties. In their work, Zhang E-X. et al. synthesized a number of hydroxyl-substituted azacalix[4]pyridines using Pd-catalyzed macrocyclic “2+2” and “3+1” coupling methods and a protection-deprotection

strategy of hydroxyl group. The conformational properties of these hydroxyl-substituted azacalix[4]pyridines have been studied both in solution and in the solid state by X-ray analysis. Taking the hydroxyl substituted azacalix[4]pyridines as molecular platforms, multi macrocycle-containing architectures and functional building blocks were then constructed.

## AUTHOR CONTRIBUTIONS

CG drafted the work. D-XW revised it critically.

**Conflict of Interest:** The authors declare that the research was conducted in the absence of any commercial or financial relationships that could be construed as a potential conflict of interest.

Copyright © 2020 Gaeta and Wang. This is an open-access article distributed under the terms of the Creative Commons Attribution License (CC BY). The use, distribution or reproduction in other forums is permitted, provided the original author(s) and the copyright owner(s) are credited and that the original publication in this journal is cited, in accordance with accepted academic practice. No use, distribution or reproduction is permitted which does not comply with these terms.



# Pillar[5]arene Based [1]rotaxane Systems With Redox-Responsive Host-Guest Property: Design, Synthesis and the Key Role of Chain Length

Runmiao Zhang<sup>1,2</sup>, Chenwei Wang<sup>1</sup>, Renhua Long<sup>1</sup>, Tingting Chen<sup>1\*</sup>, Chaoguo Yan<sup>2\*</sup> and Yong Yao<sup>1\*</sup>

<sup>1</sup> College of Chemistry, Nantong University, Nantong, China, <sup>2</sup> College of Chemistry, Yangzhou University, Yangzhou, China

## OPEN ACCESS

### Edited by:

De-Xian Wang,  
Institute of Chemistry (CAS), China

### Reviewed by:

Xiao-Yu Hu,  
Nanjing University of Aeronautics and  
Astronautics, China  
Tangxin Xiao,  
Changzhou University, China  
Haibo Yang,  
East China Normal University, China

### \*Correspondence:

Tingting Chen  
ttchen1980@126.com  
Chaoguo Yan  
cgyan@yzu.edu.cn  
Yong Yao  
yaoyong1986@ntu.edu.cn

### Specialty section:

This article was submitted to  
Supramolecular Chemistry,  
a section of the journal  
Frontiers in Chemistry

Received: 05 May 2019

Accepted: 02 July 2019

Published: 23 July 2019

### Citation:

Zhang R, Wang C, Long R, Chen T,  
Yan C and Yao Y (2019) Pillar[5]arene  
Based [1]rotaxane Systems With  
Redox-Responsive Host-Guest  
Property: Design, Synthesis and the  
Key Role of Chain Length.  
Front. Chem. 7:508.  
doi: 10.3389/fchem.2019.00508

Pillar[n]arenes are a new type of macrocyclic compounds, which were first reported in 2008 by Ogoshi. They not only have cylindrical, symmetrical, and rigid structures, but also have many advantages, including easy functionalization and rich host-guest properties. On the other hand, mechanically interlocked molecules (MIMs) exist extensively in nature which have been artificially synthesized and widely applied in the fields of nanotechnology and biology. Although pillar[5]arene-based MIMs have been investigated much over recent years, pillar[5]arene-based [1]rotaxanes are very limited. In this report, we synthesized a series of amide-linked pillar[5]arene-based [1]rotaxanes with ferrocene unit as the stopper. Under the catalysis of HOBT/EDCL, the mono-amido-functionalized pillar[5]arenes were amidated with ferrocene carboxylic acid to constructed ferrocene-based [1]rotaxanes, respectively. The structure of the [1]rotaxanes were characterized by <sup>1</sup>H NMR, <sup>13</sup>C NMR, 2D NMR, mass spectroscopy, and single-crystal X-ray structural determination. In the experiment, the monofunctionalized pillar[5]arene was synthesized with a self-inclusion property, which allows for forming a pseudo-rotaxane. The key role is the length of the imine chain in this process. The formation of a rotaxane was realized through amidation of ferrocene dicarboxylic acid, which acted as a plug. In addition, due to the ferrocene units, the pillar[5]arene-based [1]rotaxanes perform electrochemically reversible property. Based on this nature, we hope these pillar[5]arene-based [1]rotaxanes can be applied in battery devices in the future.

**Keywords:** pillar[n]arenes, rotaxanes, electrochemically reversible, single-crystal X-ray, ferrocene

## INTRODUCTION

Mechanically interlocked molecules (MIMs) are a type of “star” molecule due to their beautiful and interesting architectures and wide applications in the area of biology and nanoscience (Bissell et al., 1994; Brouwer et al., 2001; Zhu and Chen, 2005; Crowley et al., 2009; Yonath, 2010; Zhang et al., 2011; Li et al., 2014; Wang et al., 2015, 2018). Among various MIMs, rotaxanes, which have dumbbell-like structures with a wheel sliding along an axle, have attracted great interest due to their wide application in preparation of artificial molecular machines (Green et al., 2007; Lewandowski et al., 2013; Zhang et al., 2013). [1]rotaxanes, whose wheels and axles are connected in one molecule



by covalent bonds, have a stable threaded form in both solution and solid state (Hiratani et al., 2004; Franchi et al., 2008; Li et al., 2012). However, the efficient synthesis of [1]rotaxanes is very difficult due to their subtle structure. To the best of our knowledge, there are very limited studies about the synthesis and properties of macrocycle based [1]rotaxanes. For example, Prof. Yang et al. prepared a functionalized [1]rotaxane and applied it to catalysis Knoevenagel reaction in  $\text{CHCl}_3$  (Du et al., 2017). Prof. Qu et al. fabricated a novel [1]rotaxane-based molecular motion modified with ferrocene groups (Li et al., 2012).

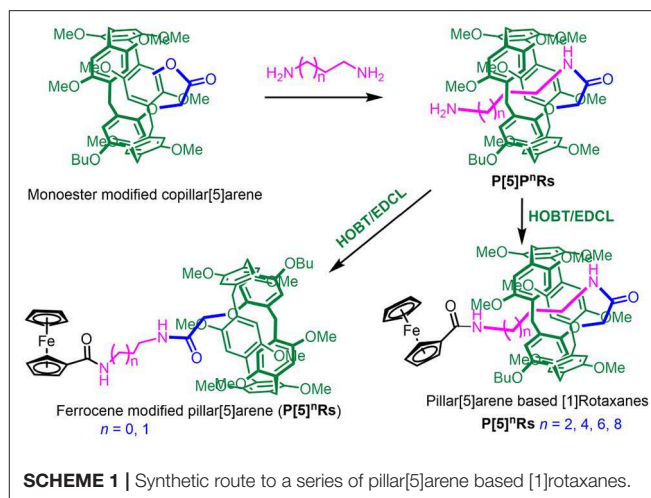
Pillar[ $n$ ]arenes (Ogoshi et al., 2008; Cragg and Sharma, 2012; Xue et al., 2012; Si et al., 2015; Wang et al., 2015, 2016; Sun et al., 2018; Xiao and Wang, 2018; Xiao et al., 2019a,b), which are the newest host compounds in supramolecular chemistry after crown ethers (Liu et al., 2017; Yoo et al., 2019), cyclodextrins (Fu et al., 2019), calix[ $n$ ]arenes (Dalgarno et al., 2007), and cucurbiturils (Murray et al., 2017), have attracted extensive investigations due to their pillar-like topology, rigid structures, electron-rich cavities, and rich host-guest properties (Song and Yang, 2015; Li et al., 2019; Wang et al., 2019). Up to now, pillar[ $n$ ]arene-based pseudo[1]rotaxanes with ammonium units, urea groups, pyridinium salt or biotin units as the axles have been investigated a lot (Strutt et al., 2012; Ni et al., 2014; Wu et al., 2015), but the further formation of [1]rotaxanes is difficult due to the lack of reactivity with stoppers. With the constant efforts by scientists, several examples of pillar[ $n$ ]arene-based [1]rotaxanes have been fabricated successfully. For example, Prof. Xue et al. combined C-H- $\pi$  and ion-pair interactions to construct a pillar[5]arene-based [1]rotaxane in a yield of 73% (Xia and Xue, 2014). Prof. Yan et al. prepared a series of pillar[5]arene-based [1]rotaxanes from mono-amide-modified pillar[5]arenes with different lengths of the axles (Han et al., 2016).

Herein, we designed and synthesized a series of pillar[5]arene-based [1]rotaxanes with  $N$ -aminoalkyl amides as the axles and ferrocenecarboxylic acid as the stoppers through a method called “threading-followed-by-stoppering” (Cao et al., 2000). Self-included pillar[5]arene-based pseudo[1]-rotaxanes **P[5]<sup>n</sup>PRs** were prepared from monoester modified copillar[5]arene according previous research. Then pillar[5]arene based [1]rotaxanes **P[5]<sup>n</sup>Rs** were directly obtained by **P[5]<sup>n</sup>PRs** reacted with ferrocenecarboxylic acid as the stopper under the catalysis of HOBT/EDCL. Importantly, we found that the length of  $N$ -aminoalkyl chains play a key role in the formation of [1]rotaxanes—only when the number of carbon on the  $N$ -aminoalkyl chains larger than three can it form [1]rotaxanes. Moreover, these [1]rotaxanes showed electrochemically reversible properties due to the ferrocene unit on them.

## MATERIALS AND METHODS

### Synthesis of Pillar[5]arenes-Based [1]rotaxanes and Mono-ferrocene Modified Pillar[5]arene

Based on previous work (Han et al., 2016), **P[5]<sup>n</sup>PRs** were obtained directly from mono-ester modified pillar[5]arene



(**Scheme 1**). Then, **P[5]<sup>n</sup>Rs** and mono-ferrocene modified pillar[5]arene were successfully synthesized by **P[5]<sup>n</sup>PRs** reacted with ferrocene-carboxylic acid as the stopper under the catalysis of HOBT/EDCL. We take when  $n = 4$  as a model reaction, **P[5]<sup>4</sup>PR** (0.203 g, 0.2 mmol), ferrocenecarboxylic acid (0.052 g, 0.2 mmol), HOBT (0.038 g, 0.25 mmol), and EDCL (0.055 g, 0.25 mmol) were stirred in 10 mL dry  $\text{CHCl}_3$  over night at room temperature. The reaction solvent was evaporated and the residue was purified by flash column chromatography on silica gel ( $\text{CH}_2\text{Cl}_2/\text{CH}_3\text{OH}$ , v/v 15:1) to give **P[5]<sup>4</sup>R** as a yellow solid (0.195 g). Other **P[5]<sup>n</sup>PRs** and mono-ferrocene modified pillar[5]arene were prepared with the similar method (**Scheme 1**).

### P[5]<sup>2</sup>R

Yellow solid, 78.6%, m.p. 106.9–108.5°C;  $^1\text{H}$  NMR (400 MHz,  $\text{CDCl}_3$ )  $\delta$ : 7.05–6.89 (m, 7 H, ArH), 6.84 (d,  $J = 2.5$  Hz, 1 H, ArH), 6.80 (s, 1 H, ArH), 6.60 (s, 1 H, ArH), 5.04–4.81 (m, 4 H,  $\text{CH}_2$ ), 4.50 (s, 2 H, ArH), 4.39 (s, 2 H, ArH), 4.24 (d,  $J = 2.5$  Hz, 5 H, ArH), 4.05–3.95 (m, 2 H,  $\text{CH}_2$ ), 3.95–3.60 (m, 32 H, 24  $\text{CH}_3$ , 8  $\text{CH}_2$ ), 3.54 (s, 4 H,  $\text{CH}_2$ ), 1.80 (d,  $J = 8.1$  Hz, 2 H,  $\text{CH}_2$ ), 1.55 (d,  $J = 7.6$  Hz, 2 H,  $\text{CH}_2$ ), 1.02 (d,  $J = 7.5$  Hz, 3 H,  $\text{CH}_2$ ), -1.90 (d,  $J = 50.7$  Hz, 2 H,  $\text{CH}_2$ ), -2.19 (d,  $J = 42.0$  Hz, 2 H,  $\text{CH}_2$ );  $^{13}\text{C}$  NMR (101 MHz,  $\text{CDCl}_3$ ) (**Figure S9**)  $\delta$  = 169.0, 168.9, 168.9, 166.7, 151.4, 150.6, 150.6, 150.5, 150.3, 150.3, 150.2, 150.2, 150.2, 150.1, 150.1, 149.7, 148.9, 129.8, 128.8, 128.8, 128.5, 128.4, 128.0, 127.7, 126.6, 126.4, 119.0, 115.5, 113.8, 113.7, 113.5, 113.4, 113.0, 112.9, 112.5, 112.5, 112.4, 112.4, 77.3, 71.8, 71.8, 69.9, 69.9, 69.9, 69.6, 68.5, 67.8, 66.0, 57.0, 56.4, 56.0, 55.8, 55.6, 55.5, 55.3, 55.2, 39.5, 37.5, 31.9, 31.7, 29.8, 29.7, 28.6, 28.5, 27.2, 23.2, 22.3, 22.3, 19.5, 14.1; MS (m/z): HRMS (ESI) Calcd. for  $\text{C}_{64}\text{H}_{75}\text{FeN}_2\text{O}_{12}^+$  ( $[\text{M} + \text{H}]^+$ ): 1119.4671, found: 1119.4669 (**Figure S10**).

### P[5]<sup>4</sup>R

Yellow solid, 42.9%, m.p. 107.4–109.2°C;  $^1\text{H}$  NMR (400 MHz,  $\text{CDCl}_3$ )  $\delta$  7.02–6.76 (m, 10 H, ArH), 5.67 (s, 1 H, NH), 5.26 (s, 1 H, NH), 4.75 (s, 2 H,  $\text{CH}_2$ ), 4.59 (s, 2 H, ArH), 4.40 (s, 2 H, ArH), 4.24 (d,  $J = 2.4$  Hz, 5 H, ArH), 4.05–3.54 (m, 36 H,

24 OCH<sub>3</sub>, 12 CH<sub>2</sub>), 2.72–2.47 (m, 4 H, CH<sub>2</sub>), 1.76 (dd,  $J = 15.2, 8.0$  Hz, 2 H, CH<sub>2</sub>), 1.52 (q,  $J = 7.6$  Hz, 2 H, CH<sub>2</sub>), 0.96 (t,  $J = 7.6$  Hz, 3 H, CH<sub>3</sub>), –0.18 (s, 2 H, CH<sub>2</sub>), –0.90 (s, 1 H, CH<sub>2</sub>), –1.09 (s, 1 H, CH<sub>2</sub>), –1.61 (d,  $J = 23.6$  Hz, 2 H, CH<sub>2</sub>), –2.21 (s, 2 H, CH<sub>2</sub>); <sup>13</sup>C NMR (101 MHz, CDCl<sub>3</sub>) (Figure S13)  $\delta = 169.25, 167.51, 150.91, 150.73, 150.56, 150.45, 150.40, 150.36, 150.32, 150.21, 150.12, 147.21, 129.75, 129.29, 128.75, 128.48, 128.45, 128.19, 127.87, 127.82, 127.05, 115.82, 115.08, 114.71, 114.43, 114.00, 112.80, 112.78, 112.73, 112.23, 70.21, 68.88, 68.09, 67.81, 65.85, 56.83, 56.44, 56.29, 56.26, 56.08, 55.48, 55.43, 55.31, 55.10, 39.73, 37.87, 31.95, 30.15, 29.36, 28.89, 28.60, 28.44, 26.37, 24.41, 23.25, 19.57, 14.06$ ; HRMS (ESI) Calcd. for C<sub>66</sub>H<sub>79</sub>FeN<sub>2</sub>O<sub>12</sub><sup>+</sup> ([M + H]<sup>+</sup>): 1147.4981, found: 1147.4982 (Figure S14).

### P[5]<sup>6</sup>R

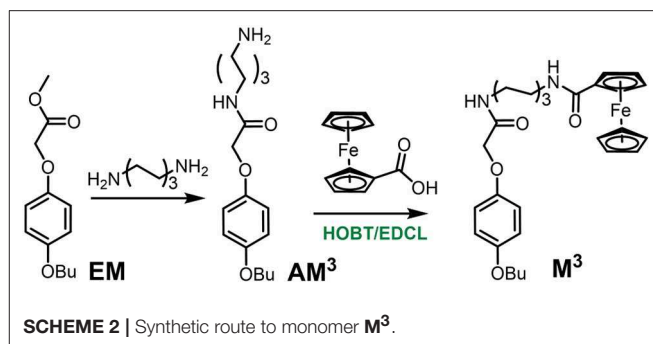
Yellow solid, 38.9%, m.p. 109.9–112.1°C; <sup>1</sup>H NMR (400 MHz, CDCl<sub>3</sub>)  $\delta$ : 6.98–6.70 (m, 10 H, ArH), 5.85 (s, 1 H, NH), 5.18 (s, 1 H, NH), 4.72 (s, 2 H, CH<sub>2</sub>), 4.58 (s, 2 H, ArH), 4.39 (s, 2 H, ArH), 4.24 (s, 5 H, ArH), 4.00–3.59 (m, 36 H, 24 OCH<sub>3</sub>, 12 CH<sub>2</sub>), 3.42 (s, 2 H, CH<sub>2</sub>), 3.29 (s, 2 H, CH<sub>2</sub>), 1.86–1.79 (m, 2 H, CH<sub>2</sub>), 1.60 (q,  $J = 7.6$  Hz, 2 H, CH<sub>2</sub>), 1.35 (s, 2 H, CH<sub>2</sub>), 1.03 (t,  $J = 6.3$  Hz, 3 H, CH<sub>3</sub>), 0.72 (s, 2 H, CH<sub>2</sub>), –0.17 (s, 2 H, CH<sub>2</sub>), –1.11 (s, 1 H, CH<sub>2</sub>), –1.25 (s, 1 H, CH<sub>2</sub>), –1.50 (s, 2 H, CH<sub>2</sub>), –2.32 (s, 2 H, CH<sub>2</sub>); <sup>13</sup>C NMR (101 MHz, CDCl<sub>3</sub>) (Figure S17)  $\delta = 169.86, 150.81, 150.52, 150.48, 150.30, 150.20, 149.99, 129.41, 129.05, 128.35, 128.24, 128.09, 127.85, 127.34, 115.04, 114.18, 114.13, 113.70, 112.76, 112.33, 77.34, 70.43, 69.72, 68.19, 68.11, 55.99, 55.69, 55.46, 55.39, 55.29, 55.12, 40.01, 37.99, 32.02, 30.71, 30.11, 29.27, 29.01, 28.89, 28.62, 28.41, 28.27, 27.72, 19.65, 14.14$ ; MS (m/z): HRMS (ESI) Calcd. for C<sub>68</sub>H<sub>83</sub>FeN<sub>2</sub>O<sub>12</sub><sup>+</sup> ([M + H]<sup>+</sup>): 1175.5294, found: 1175.5295 (Figure S18).

### P[5]<sup>8</sup>R

Yellow solid, 25.9%, m.p. 114.6–116.8°C; <sup>1</sup>H NMR (400 MHz, CDCl<sub>3</sub>)  $\delta$ : 6.95–6.80 (m, 9 H, ArH), 6.71 (s, 1 H, ArH), 5.23 (s, 1 H, NH), 5.02 (s, 1 H, NH), 4.68 (t,  $J = 1.9$  Hz, 2 H, CH<sub>2</sub>), 4.56 (s, 2 H, ArH), 4.37 (t,  $J = 2.0$  Hz, 2 H, ArH), 4.22 (s, 5 H, ArH), 3.92–3.63 (m, 36 H, 24 OCH<sub>3</sub>, 12 CH<sub>2</sub>), 3.42 (q,  $J = 7.0$  Hz, 2 H, CH<sub>2</sub>), 2.41 (s, 2 H, CH<sub>2</sub>), 1.88–1.79 (m, 2 H, CH<sub>2</sub>), 1.62 (td,  $J = 7.4, 2.6$  Hz, 4 H, CH<sub>2</sub>), 1.37 (p,  $J = 7.7$  Hz, 2 H, CH<sub>2</sub>), 1.20 (t,  $J = 7.9$  Hz, 2 H, CH<sub>2</sub>), 1.04 (t,  $J = 7.4$  Hz, 3 H, CH<sub>3</sub>), 0.80 (s, 2 H, CH<sub>2</sub>), –0.05 (s, 2 H, CH<sub>2</sub>), –1.34 (s, 4 H, CH<sub>2</sub>), –2.38 (s, 2 H, CH<sub>2</sub>); <sup>13</sup>C NMR (101 MHz, CDCl<sub>3</sub>) (Figure S21)  $\delta = 170.09, 167.19, 150.80, 150.37, 150.24, 150.12, 150.06, 149.95, 146.97, 129.40, 129.01, 128.32, 128.20, 128.11, 127.94, 127.84, 127.83, 127.08, 114.73, 113.92, 113.58, 113.25, 112.73, 112.42, 76.31, 70.43, 69.72, 68.00, 67.82, 55.48, 55.45, 55.36, 55.32, 55.13, 39.72, 38.02, 32.05, 30.96, 30.66, 30.60, 30.21, 29.64, 29.26, 28.83, 28.76, 28.64, 28.22, 27.94, 19.65, 14.17$ ; IR (KBr)  $\nu$ : 3410, 2932, 2854, 1681, 1499, 1465, 1399, 1295, 1213, 1104, 1047, 929, 879, 855, 774, 704, 647 cm<sup>–1</sup>; MS (m/z): HRMS (ESI) Calcd. for C<sub>70</sub>H<sub>87</sub>FeN<sub>2</sub>O<sub>12</sub><sup>+</sup> ([M + H]<sup>+</sup>): 1203.5602, found: 1203.5508 (Figure S22).

### Mono-ferrocene Modified Pillar[5]arene P[5]<sup>0</sup>R

Yellow solid, 78.6%, m.p. 104.4–106.2°C; <sup>1</sup>H NMR (400 MHz, CDCl<sub>3</sub>) (Figure S1)  $\delta$ : 6.78–6.82 (m, 4 H, ArH), 6.76 (d,  $J =$



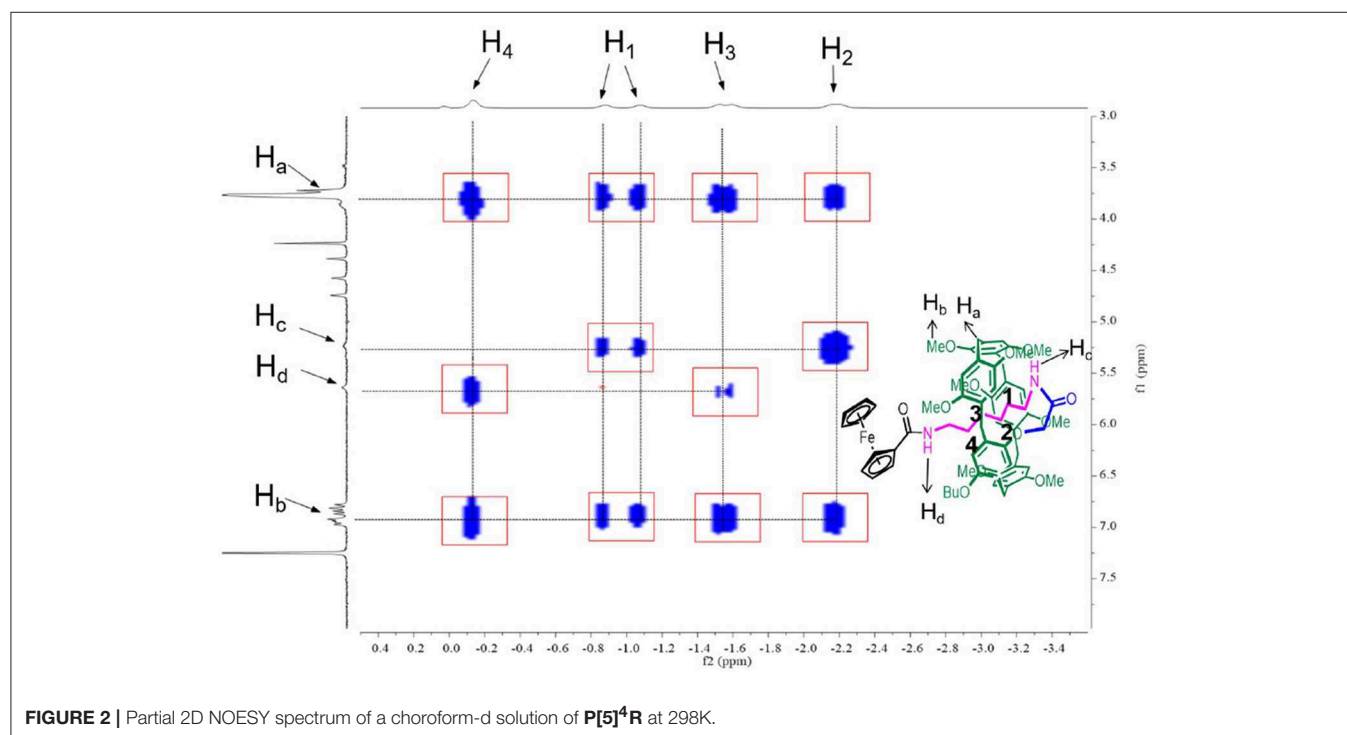
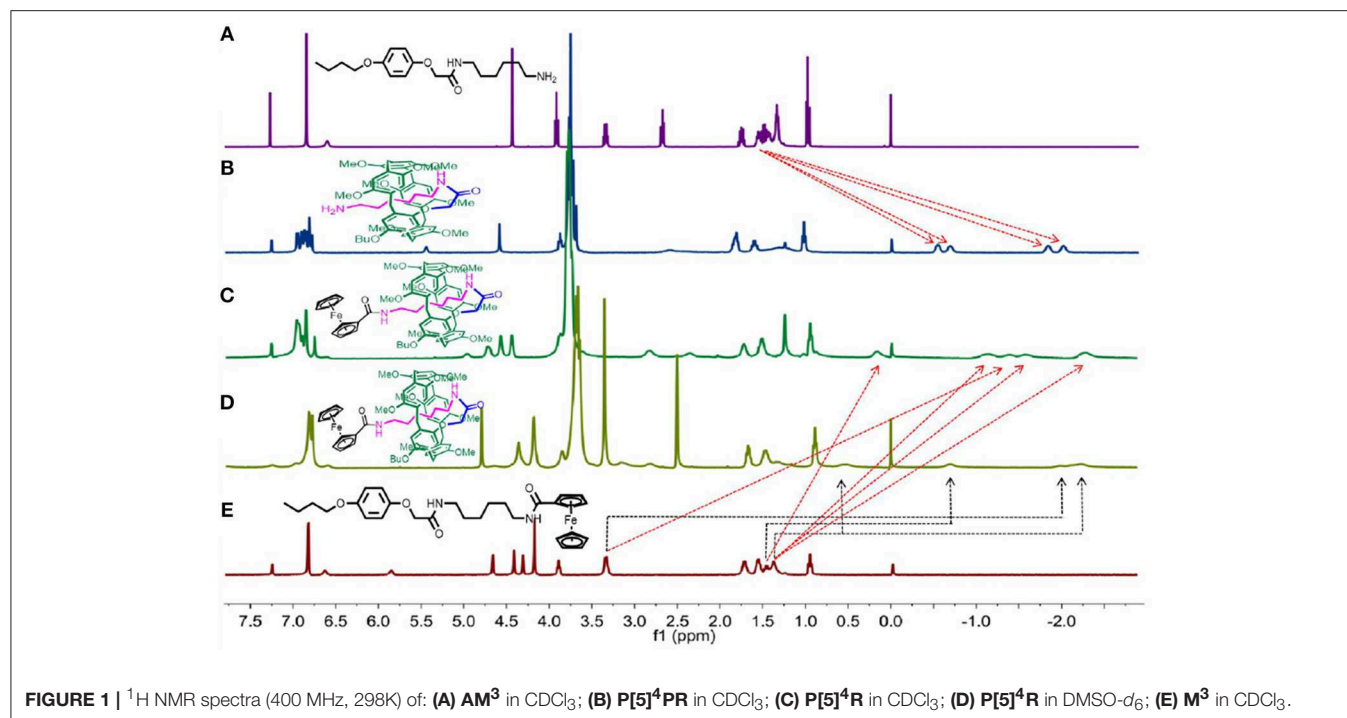
2.7 Hz, 2 H, ArH), 6.70 (s, 1 H, ArH), 6.65 (s, 1 H, ArH), 4.68 (t,  $J = 1.9$  Hz, 2 H, ArH), 4.37 (s, 2 H, CH<sub>2</sub>), 4.32 (t,  $J = 1.9$  Hz, 2 H, ArH), 4.19 (s, 5 H, ArH), 3.88 (t,  $J = 6.4$  Hz, 2 H, CH<sub>2</sub>), 3.85–3.62 (m, 28 H, 24 OCH<sub>3</sub>, 4 CH<sub>2</sub>), 3.60 (s, 3 H, CH<sub>2</sub>), 3.56 (s, 3 H, CH<sub>2</sub>), 3.24 (s, 2 H, CH<sub>2</sub>), 3.11 (s, 2 H, CH<sub>2</sub>), 1.72–1.82 (m, 2 H, CH<sub>2</sub>), 1.53 (h,  $J = 7.4$  Hz, 2 H, CH<sub>2</sub>), 0.97 (t,  $J = 7.4$  Hz, 3 H, CH<sub>3</sub>); <sup>13</sup>C NMR (101 MHz, CDCl<sub>3</sub>) (Figure S2)  $\delta = 170.70, 151.19, 150.87, 150.82, 150.77, 150.76, 150.69, 150.66, 148.15, 129.28, 129.23, 128.62, 128.46, 128.36, 128.08, 127.84, 127.72, 115.41, 115.34, 114.37, 114.31, 114.06, 114.03, 113.97, 113.90, 113.79, 76.13, 70.33, 69.70, 68.37, 68.24, 67.67, 56.68, 56.17, 56.06, 55.91, 55.87, 55.80, 55.77, 41.21, 38.87, 31.80, 30.21, 29.70, 29.64, 28.76, 19.50, 13.96$ ; MS (m/z): HRMS (ESI) Calcd. for C<sub>62</sub>H<sub>71</sub>FeN<sub>2</sub>O<sub>12</sub><sup>+</sup> ([M + H]<sup>+</sup>): 1091.4357, found: 1091.4356 (Figure S3).

### P[5]<sup>1</sup>R

Yellow solid, 71.9 %, m.p. 105.6–107.3°C; <sup>1</sup>H NMR (400 MHz, CDCl<sub>3</sub>) (Figure S5)  $\delta$ : 6.75–6.98 (m, 10 H, ArH), 6.60 (s, 2 H, NH), 4.77 (t,  $J = 2.0$  Hz, 2 H, ArH), 4.39 (s, 2 H, CH<sub>2</sub>), 4.34 (t,  $J = 1.9$  Hz, 2 H, ArH), 4.20 (s, 5 H, ArH), 3.46–3.97 (m, 36 H, 24 OCH<sub>3</sub>, 12 CH<sub>2</sub>), 1.81 (p,  $J = 6.9$  Hz, 2 H, CH<sub>2</sub>), 1.68 (s, 2 H, CH<sub>2</sub>), 1.56 (q,  $J = 7.5$  Hz, CH<sub>2</sub>), 1.01 (t,  $J = 7.4$  Hz, 3 H, CH<sub>3</sub>); <sup>13</sup>C NMR (101 MHz, CDCl<sub>3</sub>) (Figure S6)  $\delta = 150.7, 150.6, 150.4, 148.6, 128.8, 128.3, 128.1, 128.1, 114.6, 114.6, 114.5, 114.4, 113.7, 113.4, 113.3, 113.2, 70.0, 70.0, 69.6, 68.2, 66.9, 56.2, 56.2, 56.2, 55.9, 55.9, 55.7, 55.5, 39.4, 35.7, 34.8, 31.9, 29.7, 29.4, 19.5, 14.1$ ; MS (m/z): HRMS (ESI) Calcd. for C<sub>63</sub>H<sub>73</sub>FeN<sub>2</sub>O<sub>12</sub><sup>+</sup> ([M + H]<sup>+</sup>): 1105.4512, found: 1105.4513 (Figure S7).

## Synthesis of Monomer M<sup>3</sup>

**AM<sup>3</sup>** was obtained from a previous report. Then the monomer **M<sup>3</sup>** was synthesized from **AM<sup>3</sup>** (Figure S23) and ferrocene-carboxylic acid with BOBT and EDCL as the catalyst (Scheme 2). **AM<sup>3</sup>** (0.08 g, 0.25 mmol), ferrocene-carboxylic acid (0.057 g, 0.25 mmol), HOBT (0.054 g, 0.40 mmol), and EDCL (0.076 g, 0.40 mmol) were stirred in 15 mL dry CHCl<sub>3</sub> over night at room temperature. The reaction solvent was evaporated and the residue was purified by flash column chromatography on silica gel (CH<sub>2</sub>Cl<sub>2</sub>/CH<sub>3</sub>OH,  $v/v$  25:1) to give **M<sup>3</sup>** as a yellow solid (0.031 g). <sup>1</sup>H NMR (400 MHz, CDCl<sub>3</sub>) (Figure S24)  $\delta$ : 6.84 (s, 4 H, ArH), 6.65 (s, 1 H, NH), 5.87 (s, 1 H,



NH), 4.68 (s, 2H,  $\text{CH}_2$ ), 4.44 (s, 2H, ArH), 4.33 (s, 2H, ArH), 4.19 (s, 5H, ArH), 3.91 (t,  $J = 5.8$  Hz, 2H,  $\text{CH}_2$ ), 3.36 (d,  $J = 6.2$  Hz, 4H,  $\text{CH}_2$ ), 1.80–1.68 (m, 4H,  $\text{CH}_2$ ), 1.58 (d,  $J = 5.9$  Hz, 4H,  $\text{CH}_2$ ), 1.48 (dd,  $J = 14.6$ , 7.1 Hz, 2H,  $\text{CH}_2$ ), 1.39 (s, 2H,  $\text{CH}_2$ ), 0.97 (t,  $J = 6.9$  Hz, 3H,  $\text{CH}_3$ ).

## MATERIALS

All reactions were performed in atmosphere unless noted. All reagents were commercially available and used as supplied without further purification. NMR spectra were collected on either a Bruker AVIII-400 MHz spectrometer or a Bruker AV-600



MHz spectrometer with internal standard tetramethylsilane (TMS) and signals as internal references, and the chemical shifts ( $\delta$ ) were expressed in ppm. High-resolution Mass (ESI) spectra were obtained with a Bruker Micro-TOF spectrometer. X-ray data were collected on a Bruker Smart APEX-2 CCD diffractometer.

## RESULTS AND DISCUSSION

### $^1\text{H}$ NMR Investigation

The  $^1\text{H}$  NMR spectra of  $\text{AM}^3$  and  $\text{P}[5]^4\text{PR}$  were taken into consideration first. As shown in **Figure 1B**, the chemical shift of four groups of peaks shift below 0 ppm field, indicating that the alkyl chain penetrated into the cavity of pillar[5]arene to form either pseudo[1] rotaxane or [c2]daisy chain (Du et al., 2017). Then  $\text{P}[5]^4\text{R}$  was prepared from  $\text{P}[5]^4\text{PR}$  reacted with ferrocenecarboxylic acid as the stopper.  $^1\text{H}$  NMR spectra of monomer  $\text{M}^3$  and [1] rotaxane  $\text{P}[5]^4\text{R}$  in  $\text{CDCl}_3$  at 293 K are shown in **Figure 1** (spectra c and e). Compared with  $\text{M}^3$ , we found that the signals of protons on the alkyl chain attaching onto the pillar[5]arene platform shifted upfield obviously due to the shielding effect (**Figure 1C**). Then we used a polar solvent,  $\text{DMSO}-d_6$ , for  $^1\text{H}$  NMR investigations to confirm the formation of [1] rotaxane. In  $\text{DMSO}-d_6$ , we also found that the signals of protons on the alkyl chains upfield were below 0 ppm due to the shielding effect (**Figure 1D**), which indicated the formation of a mechanically interlocked structure (Dong et al., 2014). The  $^1\text{H}$  NMR of  $\text{P}[5]^2\text{R}$ ,  $\text{P}[5]^4\text{R}$ ,  $\text{P}[5]^6\text{R}$ ,  $\text{P}[5]^8\text{R}$  all showed several groups of protons on the alkyl chains upfield obviously (**Figures S8, S12, S16, S20**), and the formation of [1] rotaxanes was also confirmed. However, the  $^1\text{H}$  NMR of  $\text{P}[5]^0\text{R}$  and  $\text{P}[5]^1\text{R}$  showed no signal below 0 ppm, indicating the side-chain stayed outside of the cavity of the pillar[5]arene platform (**Figures S1, S5**). The reason for this phenomenon is due to the relatively short length of the axle (only two or three  $\text{CH}_2$  groups) of  $\text{P}[5]^0\text{R}$ , and  $\text{P}[5]^1\text{R}$ , which was not able to allow the large ferrocene group to connect it from the cavity. Thus, the amino-group of the side-chain of  $\text{P}[5]^0\text{PR}$  (or  $\text{P}[5]^1\text{PR}$ ) stayed outside of the cavity and was then reacted with ferrocene-carboxylic acid to obtain free form  $\text{P}[5]^0\text{R}$  (or  $\text{P}[5]^1\text{R}$ ). Furthermore, the temperature-dependent  $^1\text{H}$  NMR of  $\text{P}[5]^4\text{R}$  showed that the peaks became broad as the temperature increased, indicating the chain in the cavity (**Figures S15, S19, S26**).

### 2D NOESY Studies

The formation of [1]rotaxane was then confirmed by 2D Nuclear Overhauser Effect Spectroscopy (NOESY). Here we also take  $\text{P}[5]^4\text{R}$  as the model compound. As shown in **Figure 2**, the hydrogens of the alkyl chain on  $\text{P}[5]^4\text{R}$  were close to the pillar[5]arene platform because  $\text{H}_{1-4}$  showed strong correlation with  $\text{H}_a$  and  $\text{H}_b$ , indicating that the alkyl chain was in close proximity to the cavity. The  $-\text{NH}-$  group  $\text{H}_c$  is close to  $\text{H}_{1-2}$  while  $\text{H}_d$  is close to  $\text{H}_{3-4}$ . Furthermore,  $\text{ArH}-3$  from the ferrocene group showed space correction to the hydrogen- $-\text{OCH}_3$  and  $-\text{OCH}_2-$  on the pillar[5]arene platform (**Data Sheets 1–4**).

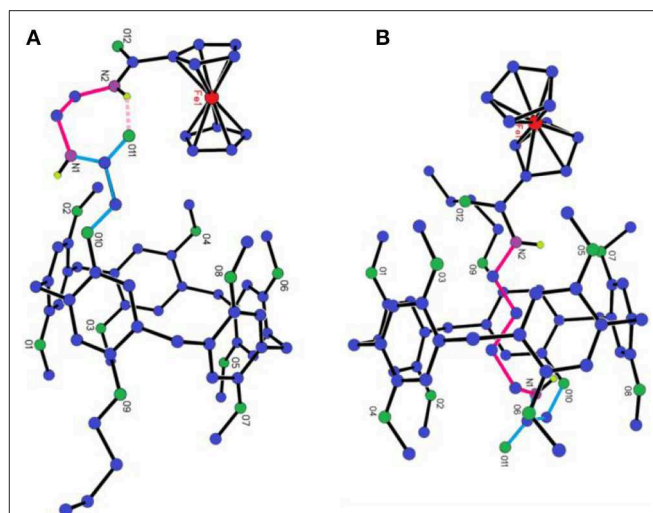


**FIGURE 3** | X-ray single-crystal structure of: (A)  $\text{P}[5]^0\text{R}$ ; (B)  $\text{P}[5]^2\text{R}$ . Color code: C, blue; O, green; Fe, red; N, purple.

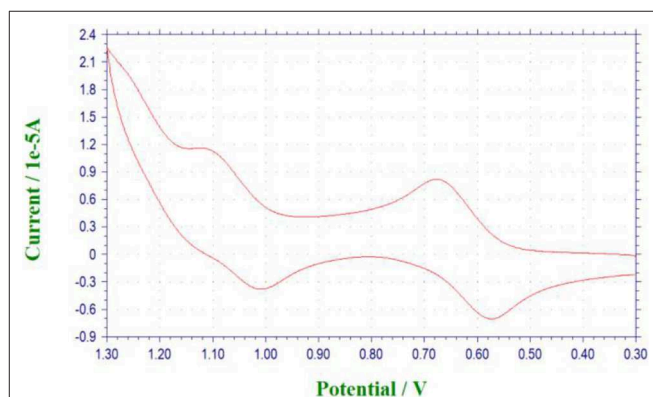


**FIGURE 4** | Cyclic voltammogram (scan rate =  $100 \text{ mV s}^{-1}$ ) of the  $\text{P}[5]^4\text{R}$  ( $5.00 \times 10^{-4} \text{ M}$ ) in  $\text{CH}_2\text{Cl}_2$ .

### Single Crystal Structures

The direct evidence for the formation of [1] rotaxanes only when the length of axle longer than three  $\text{CH}_2$  groups is from single crystal investigation. As shown in **Figure 3A** and **Figure S4**, the whole side chain of  $\text{P}[5]^0\text{R}$  stayed outside of the cavity of pillar[5]arene. It should be pointed that we observed hydrogen bonding between the hydrogen atom of the amine group and the oxygen atom of carbonyl group (**Figure 3A**, pink dash line). However, for  $\text{P}[5]^2\text{R}$ , we can clearly see that the alkyl chain penetrated into the cavity of pillar[5]arene to form a [1] rotaxane (**Figure 3B** and **Figure S11**). The  $\text{C}-\text{H} \cdots \pi$  interactions and  $\text{C}-\text{H} \cdots \text{O}$  interactions were the driving forces for the formation of [1] rotaxane.

### Cyclic Voltammetry Investigation

With the [1]rotaxanes in hand, we then investigated their reversible redox property by electrochemistry methods. Take  $\text{P}[5]^4\text{R}$  as an example, in cyclic voltammetry (CV) experiment (**Figure 4**), the cyclic voltammogram was quasi-reversible with

nearly equal  $i_{pa}$  and  $i_{pc}$ , in which the potential difference  $\Delta E_p$  was around 0.090 V. Compared with ferrocene,  $P[5]^4R$  has a larger half wave potential ( $E_{1/2} = 612$  mV). Further study showed that the free state  $P[5]^0R$  has the similar redox property with  $P[5]^4R$  due to the same ferrocene unit (Figure S25).

## CONCLUSIONS

In this paper, we synthesized a series of amide-linked pillar[5]arene-based [1]rotaxanes with ferrocene unit as the stopper. Under the catalysis of HOBT/EDCL, the mono-amido-functionalized pillar[5]arenes were amidated with ferrocene carboxylic acid, to constructed ferrocene-based [1]rotaxanes, respectively. The structure of the [1]rotaxanes were characterized by  $^1H$  NMR,  $^{13}C$  NMR, 2D NMR, mass spectroscopy and single-crystal X-ray structural determination. In the formation of [1]rotaxane, the key role is the length of the alkyl chain in this process, and only when the number of C on the alkyl chain is larger than three can the formation of [1]rotaxane occur. In addition, due to the ferrocene units, the pillar[5]arene-based [1]rotaxanes display electrochemically reversible properties. Based on this nature, we hope these pillar[5]arene-based [1]rotaxanes can be applied in battery devices in future.

## REFERENCES

- Bissell, S. A., Córdova, E., Kaifer, A. E., and Stoddart, J. F. (1994). A chemically and electrochemically switchable molecular shuttle. *Nature* 369, 133–136. doi: 10.1038/369133a0
- Brouwer, A. M., Frochot, C., Gatti, F. G., Leigh, D. A., Mottier, L., Paolucci, F., et al. (2001). Reversible translation motion in a hydrogen-bonded molecular shuttle. *Science* 291, 2124–2128. doi: 10.1126/science.1057886
- Cao, J., Fyfe, M. C., Stoddart, J. F., Cousins, G. R., and Glink, P. T. (2000). Molecular shuttles by the protecting group approach. *J. Org. Chem.* 65, 1937–1946. doi: 10.1021/jo991397w
- Cragg, P. J., and Sharma, K. (2012). Pillar[5]arene: fascinating cyclophanes with a bright future. *Chem. Soc. Rev.* 41, 597–607. doi: 10.1039/C1CS15164A
- Crowley, J. D., Goldup, S. M., Lee, A.-L., Leigh, D. A., and McBurney, R. T. (2009). Active metal template synthesis of rotaxanes, catenanes and molecular shuttles. *Chem. Soc. Rev.* 38, 1530–1541. doi: 10.1039/b804243h
- Dalgarno, S. J., Thallapally, P. K., Barbour, L. J., and Atwood, J. L. (2007). Engineering void space in organic van der Waals crystals: calixarenes lead the way. *Chem. Soc. Rev.* 36, 236–245. doi: 10.1039/b606047c
- Dong, S., Yuan, J., and Huang, F. (2014). A pillar[5]arene/imidazolium [2]rotaxane: solvent- and thermo-driven molecular motions and supramolecular gel formation. *Chem. Sci.* 5, 247–252. doi: 10.1039/C3SC52481G
- Du, X.-S., Wang, C.-Y., Jia, Q., Deng, R., Tian, H.-S., Zhang, H.-Y., et al. (2017). Pillar[5]arene-based [1]rotaxane: high-yield synthesis, characterization and application in Knoevenagel reaction. *Chem. Comm.* 53, 5326–5329. doi: 10.1039/C7CC02364B
- Franchi, P., Fanì, M., Mezzina, E., and Lucarini, M. (2008). Increasing the persistency of stable free-radicals: synthesis and characterization of a nitroxide based [1]rotaxane. *Org. Lett.* 10, 1901–1904. doi: 10.1021/ol800405b
- Fu, G.-G., Chen, Y., Yu, Q., and Liu, Y. (2019). A tumor-targeting Ru/polysaccharide/protein supramolecular assembly with high photodynamic therapy ability. *Chem. Comm.* 55, 3148–3151. doi: 10.1039/C8CC09964B
- Green, J. E., Choi, J. W., Boukai, A., Bunimovich, Y., Johnston-Halperin, E., Delonno, E., et al. (2007). A 160-kilobit molecular electronic memory patterned at  $10^{11}$  bits per square centimetre. *Nature* 445, 414–417. doi: 10.1038/nature05462
- Han, Y., Huo, G.-F., Sun, J., Xie, J., Yan, C.-G., Zhao, Y., et al. (2016). Formation of a series of stable pillar[5]arene-based pseudo[1]rotaxanes and their [1]rotaxanes in the crystal state. *Sci. Rep.* 6:28748. doi: 10.1038/srep28748
- Hirata, K., Kaneyama, M., Nagawa, Y., Koyama, E., and Kanesato, M. (2004). Synthesis of [1]rotaxane via covalent bond formation and its unidirectional fluorescent response by energy transfer in the presence of lithium ion. *J. Am. Chem. Soc.* 126, 13568–13569. doi: 10.1021/ja046929r
- Lewandowski, B., De Bo, G. D., Ward, J. W., Papmeyer, M., Kuschel, S., Aldegunde, M. J., et al. (2013). Sequence-specific peptide synthesis by an artificial small-molecule machine. *Science* 339, 189–193. doi: 10.1126/science.1229753
- Li, B., Wang, B., Huang, X., Dai, L., Cui, L., Li, J., et al. (2019). Terphenyl[n]arenes and quaterphenyl[n]arenes ( $n = 3-6$ ): one-pot synthesis, self-assembly into supramolecular gel, and iodine capture. *Angew. Chem.* 58, 3885–3889. doi: 10.1002/anie.201813972
- Li, H., Zhang, H., Zhang, Q., Zhang, Q.-W., and Qu, D.-H. (2012). A switchable ferrocene-based [1]rotaxane with an electrochemical signal output. *Org. Lett.* 14, 5900–5903. doi: 10.1021/ol302826g
- Li, Z.-Y., Zhang, Y., Zhang, C.-W., Chen, L.-J., Wang, C., Tan, H., et al. (2014). Cross-linked supramolecular polymer gels constructed from discrete multi-pillar[5]arene metallacycles and their multiple stimuli-responsive behavior. *J. Am. Chem. Soc.* 136, 8577–8589. doi: 10.1021/ja413047r
- Liu, Z., Nalluri, S. K. M., and Stoddart, J. F. (2017). Surveying macrocyclic chemistry: from flexible crown ethers to rigid cyclophanes. *Chem. Soc. Rev.* 46, 2459–2478. doi: 10.1039/C7CS00185A
- Murray, J., Kim, K., Ogoshi, T., Yao, W., and Gibb, B. C. (2017). The aqueous supramolecular chemistry of cucurbit[n]urils, pillar[n]arenes and deep-cavity cavitands. *Chem. Soc. Rev.* 46, 2479–2496. doi: 10.1039/C7CS00095B

## DATA AVAILABILITY

The raw data supporting the conclusions of this manuscript will be made available by the authors, without undue reservation, to any qualified researcher.

## AUTHOR CONTRIBUTIONS

RZ prepared all the pillar[5]arene-based [1]rotaxanes. CW and RL prepared the monomer  $M^3$ . TC and CY analyzed the data. YY analyzed the data and wrote the paper.

## ACKNOWLEDGMENTS

This work was supported by the National Natural Science Foundation of China (21801139), Natural Science Foundation of Jiangsu Province (BK20180942), the Natural Science Foundation of Nantong University for High-Level Talent (03083004), and the Large Instruments Open Foundation of Nantong University (KFJN1814).

## SUPPLEMENTARY MATERIAL

The Supplementary Material for this article can be found online at: <https://www.frontiersin.org/articles/10.3389/fchem.2019.00508/full#supplementary-material>

- Ni, M., Hu, X.-Y., Jiang, J., and Wang, L. (2014). The self-complexation of mono-urea-functionalized pillar[5]arenes with abnormal urea behaviors. *Chem. Comm.* 50, 1317–1319. doi: 10.1039/C3CC47823H
- Ogoshi, T., Kanai, S., Fujinami, S., Yamagishi, T.-A., and Nakamoto, Y. (2008). Para-Bridged symmetrical pillar[5]arenes: their lewis acid catalyzed synthesis and host-guest property. *J. Am. Chem. Soc.* 130, 5022–5023. doi: 10.1021/ja711260m
- Si, W., Xin, P., Li, Z.-T., and Hou, J.-L. (2015). Tubular ubumolecular transmembrane channels: construction strategy and transport activities. *Acc. Chem. Res.* 48, 1612–1619. doi: 10.1021/acs.accounts.5b00143
- Song, N., and Yang, Y.-W. (2015). Molecular and supramolecular switches on *Mesoporous silica* nanoparticles. *Chem. Soc. Rev.* 44, 3474–3504. doi: 10.1039/C5CS00243E
- Strutt, N. L., Zhang, H., Giesener, M. A., Lei, J., and Stoddart, J. F. (2012). A self-complexing and self-assembling pillar[5]arene. *Chem. Comm.* 48, 1647–1649. doi: 10.1039/C2CC16030G
- Sun, S., Geng, M., Huang, L., Chen, Y., Cen, M., Lu, D., et al. (2018). A new amphiphilic pillar[5]arene: synthesis and controllable self-assembly in water and application in white-light-emitting systems. *Chem. Commun.* 54, 13006–13009. doi: 10.1039/C8CC07658H
- Wang, P., Liang, B., and Xia, D. (2019). A linear AIE supramolecular polymer based on a salicylaldehyde azine-containing pillararene and its reversible cross-linking by Cu<sup>II</sup> and cyanide. *Inorg. Chem.* 58, 2252–2256. doi: 10.1021/acs.inorgchem.8b02896
- Wang, W., Chen, L.-J., Wang, X.-Q., Sun, B., Li, X., Zhang, Y., et al. (2015). Organometallic rotaxane dendrimers with fourth-generation mechanically interlocked branches. *Proc. Natl. Acad. Sci. USA* 112, 5597–5601. doi: 10.1073/pnas.1500489112
- Wang, X. Q., Wang, W., Li, W. J., Chen, L. J., Yao, R., Yin, G. Q. et al. (2018). Dual stimuli-responsive rotaxane-branched dendrimers with reversible dimension modulation. *Nat. Commun.* 9:3190. doi: 10.1038/s41467-018-05670-y
- Wang, Y., Ping, G., and Li, C. (2016). efficient complexation between pillar[5]arenes and neutral guests: from host-guest chemistry to functional materials. *Chem. Commun.* 52, 9858–9872. doi: 10.1039/C6CC03999E
- Wu, X., Ni, M., Xia, W., Hu, X.-Y., and Wang, L. (2015). A novel dynamic pseudo[1]rotaxane based on a mono-biotin-functionalized pillar[5]arene. *Org. Chem. Front.* 2, 1013–1017. doi: 10.1039/C5QO00159E
- Xia, B., and Xue, M. (2014). Design and efficient synthesis of a pillar[5]arene-based [1]rotaxane. *Chem. Comm.* 50, 1021–1023. doi: 10.1039/C3CC48014C
- Xiao, T., and Wang, L. (2018). Recent advances of functional gels controlled by pillar[n]arene-based host–guest interactions. *Tetrahedron Lett.* 59, 1172–1182. doi: 10.1016/j.tetlet.2018.02.028
- Xiao, T., Zhong, W., Xu, L., Sun, X.-Q., Hu, X.-Y., and Wang, L. (2019a). Supramolecular vesicles based on pillar[n]arenes: design, construction, and applications. *Org. Biomol. Chem.* 17, 1336–1350. doi: 10.1039/C8OB03095B
- Xiao, T., Zhou, L., Xu, L., Zhong, W., Zhao, W., Sun, X.-Q., et al. (2019b). Dynamic materials fabricated from water soluble pillar[n]arenes bearing triethylene oxide groups. *Chin. Chem. Lett.* 30, 271–276. doi: 10.1016/j.cclet.2018.05.039
- Xue, M., Yang, Y., Chi, X., Zhang, Z., and Huang, F. (2012). Pillararenes, a new class of macrocycles for supramolecular chemistry. *Acc. Chem. Res.* 45, 1294–1308. doi: 10.1021/ar2003418
- Yonath, A. (2010). Hibernating bears, antibiotics, and the evolving ribosome. *Angew. Chem.* 49, 4340–4354. doi: 10.1002/anie.201001297
- Yoo, C., Dodge, H. M., and Miller, A. J. M. (2019). Cation-controlled catalysis with crown ether-containing transition metal complexes. *Chem. Comm.* 55, 5047–5059. doi: 10.1039/C9CC00803A
- Zhang, H., Zhou, B., Li, H., Qu, D.-H., and Tian, H. (2013). A ferrocene-functionalized [2]rotaxane with fluorophores as stoppers. *J. Org. Chem.* 78, 2091–2098. doi: 10.1021/jo302107a
- Zhang, Z.-J., Zhang, H.-Y., Wang, H., and Liu, Y. (2011). A twin-axial hetero[7]rotaxane. *Angew. Chem.* 50, 10834–10839. doi: 10.1002/anie.201105375
- Zhu, X.-Z., and Chen, C.-F. (2005). A highly efficient approach to [4]pseudocatenanes by threefold metathesis reactions of a triptycene-based tris[2]pseudorotaxane. *J. Am. Chem. Soc.* 127, 13158–13159. doi: 10.1021/ja0546020

**Conflict of Interest Statement:** The authors declare that the research was conducted in the absence of any commercial or financial relationships that could be construed as a potential conflict of interest.

Copyright © 2019 Zhang, Wang, Long, Chen, Yan and Yao. This is an open-access article distributed under the terms of the Creative Commons Attribution License (CC BY). The use, distribution or reproduction in other forums is permitted, provided the original author(s) and the copyright owner(s) are credited and that the original publication in this journal is cited, in accordance with accepted academic practice. No use, distribution or reproduction is permitted which does not comply with these terms.



# Modification of Oligo- and Polylactides With Macrocyclic Fragments: Synthesis and Properties

Olga A. Mostovaya<sup>1</sup>, Vladimir V. Gorbachuk<sup>1</sup>, Pavel L. Padnya<sup>1</sup>, Alena A. Vavilova<sup>1</sup>, Gennady A. Evtugyn<sup>2</sup> and Ivan I. Stoikov<sup>1\*</sup>

<sup>1</sup> Department of Organic Chemistry, A. M. Butlerov' Chemistry Institute, Kazan Federal University, Kazan, Russia,

<sup>2</sup> Department of Analytical Chemistry, A. M. Butlerov' Chemistry Institute, Kazan Federal University, Kazan, Russia

## OPEN ACCESS

### Edited by:

Carmine Gaeta,  
University of Salerno, Italy

### Reviewed by:

Andrea Pappalardo,  
University of Catania, Italy  
Tsukuru Minamiki,  
National Institute of Advanced  
Industrial Science and Technology,  
Japan

### \*Correspondence:

Ivan I. Stoikov  
ivan.stoikov@mail.ru

### Specialty section:

This article was submitted to  
Supramolecular Chemistry,  
a section of the journal  
Frontiers in Chemistry

Received: 17 June 2019

Accepted: 22 July 2019

Published: 02 August 2019

### Citation:

Mostovaya OA, Gorbachuk VV,  
Padnya PL, Vavilova AA, Evtugyn GA  
and Stoikov II (2019) Modification of  
Oligo- and Polylactides With  
Macrocyclic Fragments: Synthesis  
and Properties. *Front. Chem.* 7:554.  
doi: 10.3389/fchem.2019.00554

Products of lactic acid polycondensation (poly- and oligolactic acids) are widely used as packaging materials, drug delivery agents, implants etc. Variety of their applications is caused by a number of practically important properties, e.g., biocompatibility and biodegradability, non-toxicity, and mechanical durability. Modification of these polymers with different additives allows improving their properties and extending future applications. In this manner, stability toward degradation, recognition of some substrates, extended thermal stability etc. can be improved. Macrocyclic compounds are promising candidates as modifiers. They are able to provide polymer materials with additional binding sites, impart certain orientation to spatial arrangement of polymer chains, change hydrophilic-lipophilic balance, and redox properties. The latter one can be used for assembling various electrochemical sensors and biosensors that combine steric discrimination of the analytes caused by oligolactides and highly sensitive response to their quantities caused by redox labels introduced. Different composite materials based on oligolactides as matrices for such redox labels were described in the assemblies of biosensors for drugs, pesticides, and antioxidants detection. In this mini-review, methods for the synthesis of the lactic acid oligomers and those modified with the macrocyclic fragments (porphyrin, cyclodextrin, and cyclophane) have been described. The effects of modifiers on complexation, thermal, and aggregation properties of materials are described. Analytical performance of oligolactide based sensors and biosensors has been considered with particular emphasis to the mechanism of signal generation.

**Keywords:** oligolactide, polylactide, synthesis, calixarene, cyclodextrin, tetrapyrrole, porphyrin, macrocycle

## INTRODUCTION

Recently, polylactic acids (PLA) and their modification products have found increasing attention as functional materials due to non-toxicity, biodegradability, biocompatibility, and mechanical durability (Garlotta, 2001). Hydrophilicity, chemical, and thermal stability of such materials was varied by introduction of appropriate modifiers (Marcincinova-Benabdillah et al., 2001; Kumar et al., 2017). As a result, PLA was utilized in drug delivery systems [1986, Decapeptyl® (Jain et al., 2016)] and as a component of drug formulations. A particular PLA advantage is that drug can release from such a matrix for several months (Andreopoulos et al., 2000). Inflammatory reactions mentioned as a negative effect of PLA application related to the removal of the polymer



degradation products can be suppressed by addition magnesium hydroxide or calcium carbonate able to neutralize lactic acid (LA) (Kum et al., 2013; Murariu and Dubois, 2016).

The PLA is usually synthesized in three ways, LA condensation/coupling, azeotropic dehydrative condensation, and by ring opening polymerization (ROP) of lactide (Garlotta, 2001; Pretula et al., 2016; Ren et al., 2016). Polymer modification is achieved by introduction of additives containing carboxyl or hydroxyl groups and acid anhydrides into the reaction media. Recently, macrocyclic fragments have been actively studied for this purpose. They offer fixed spatial separation of the binding groups to get variety of ligands toward different molecules to be recognized (Poulsen et al., 2015; Imran et al., 2018) (**Figure 1**).

## HYBRIDS WITH CYCLODEXTRINS

Cyclodextrins applied in the pharmacy, food and cosmetic industries, biotechnology are produced by enzymatic degradation of starch (van de Manakker et al., 2009; Crini, 2014) (**Figure 1A**). They contain spatially stable hydrophobic cavity that captures small molecules.

In 2008, one-handed lactide derivative of  $\beta$ -cyclodextrin (CD) was obtained by ROP of 3,6-dimethyl-1,4-dioxane-2,5-dione (lactide) in the absence of any catalyst (Shen et al., 2008; **Figure 2A**). Its functionalization was carried out via primary hydroxyl group farthest from the macrocycle (**Figure 1A**,  $R^1$ ). Introduction of oligomeric lactic acid (OLA) into the CD platform increased solubility of the product in the water. The resulting hybrid formed an inclusion complex with amoxicillin, a common antibiotic.

In the same year, copolymers with 14 polylactic “arms” were obtained from tosylated CD via secondary hydroxyl groups by ROP with lactide (**Figure 1A**,  $R^2$ ; Adeli et al., 2008). Further ROP with 2-ethyl-2-oxazoline resulted in formation of block copolymers consisting of the CD core, PLA and seven polyoxazoline fragments. They formed micelles in chloroform and encapsulated the Congo red dye. The rate of the dye release increased with the length of both types of fragments (Adeli et al., 2008).

The CD substituted by a single amino group was functionalized with the PLA in the presence of  $N,N'$ -dicyclohexylcarbodiimide (DCC) as an activating agent (**1**, **Figure 2B**; Gao et al., 2005). The TG/DSC showed that grafting the PLA onto the CD reduced the glass transition temperature ( $T_g$ ). Introduction of a hydrophilic CD fragment led to significant increase in the biodegradation rate of the copolymer compared with unmodified PLA due to increased water diffusion into the copolymer. Resulting copolymers formed in aqueous solution negatively charged monodisperse particles of submicron size. The higher the content of CD in the copolymer the smaller their size and the lower their charge were (Gao et al., 2005). Micelles described could encapsulate BSA. Again, the higher the content of the CD fragment the more pronounced this ability was.

Block-copolymers **2** containing poly(ethylene glycol) fragments together with PLA were synthesized in a similar manner (**Figure 2**; Qiu et al., 2010). They could bind

doxorubicin, an anticancer drug. A series of poly(ethylene glycol) copolymers with PLA was obtained by ROP of lactide with monomethoxypoly(ethylene glycol) as an initiator in the presence of stannous 2-ethylhexanoate (Kricheldorf and Serra, 1985). Terminal hydroxyl group of the polylactic unit was replaced by a carboxyl group by interaction with succinic anhydride in dioxane. Then, CD derivative containing seven ethylenediamine fragments was functionalized at primary amino groups by resulting acid in the presence of DCC and 4-(dimethylamino)pyridine (DMAP). Hybrids obtained could form micelles. Increase in the content of hydrophobic polylactide fragments decreased their critical micelle concentration and size. Most complete doxorubicin release was observed at pH 5.0. Cytotoxicity of the systems was observed only after the doxorubicin implementation. It significantly depended on the length of the polylactic chain. Longer chain showed higher cytotoxicity measured with the MCF-7/ADR cells.

21 polylactide fragments (**Figure 1A**,  $R^1$ ,  $R^2$ ) were introduced in the CD platform by ROP of D,L-lactide in the presence of tin octoate as catalyst (Yao et al., 2016). The substitution was observed at both primary and secondary hydroxyl groups of CD. The resulting 21-arm star copolymer was further modified with 2-(dimethylamino)ethylmethacrylate and 2-ethyl-2-oxazoline to corresponding block-copolymer. 2-(Dimethylamino)ethyl methacrylate block containing tertiary amino group was chosen to *in situ* reduction of the  $Au^{3+}$  ions to zero-valent gold via coordination—reduction mechanism without additional reductants. Monodisperse and structurally stable spherical unimolecular micelles containing CD and PLA as an inner core, poly(2-(dimethylamino)ethyl methacrylate) block as the middle layer and poly[oligo(2-ethyl-2-oxazoline)methacrylate] block as the outer shell have been obtained by dialysis. The size of the micelles depended on the degree of polymerization of the monomers in the blocks and ranged from 20.9 to 28.5 nm (Yao et al., 2016; Zhang et al., 2016). The resulting products showed low cytotoxicity indicating advantages of the products as a nanoplatform for anticancer drug delivery and as contrast agents in computed tomography. They could also accumulate doxorubicin (Lin et al., 2017) separated between middle layer and micellar core (PLA block). The release of doxorubicin was pH dependent (max at pH 5.0) due to protonation of nitrogen atoms and accelerated PLA degradation in acidic media (Qiu et al., 2010). Doxorubicin loaded micelles were tested for antitumor efficiency against HepG2 cells (Yao et al., 2016; Lin et al., 2017).

The block-copolymer was also able to load imiquimod (synthetic immune response modifier) and plasmid DNA (Lin et al., 2016). Imiquimod was released most rapidly in acidic conditions in agreement with the above mentioned mechanism (Qiu et al., 2010; Lin et al., 2017). Cationic poly(2-(dimethylamino)ethyl methacrylate) block played a key role in formation of the complex with plasmid DNA.

In 2016, the synthesis of dendrimer like star polymer by click chemistry was reported (Tungala et al., 2016; **Figure 1A**,  $R^1$ , **Figure 2A**). The CD primary hydroxyl groups were replaced by azide groups. Then three types of polymers (poly(methyl methacrylate), poly( $N$ -isopropylacrylamide), PLA) were synthesized. The core was

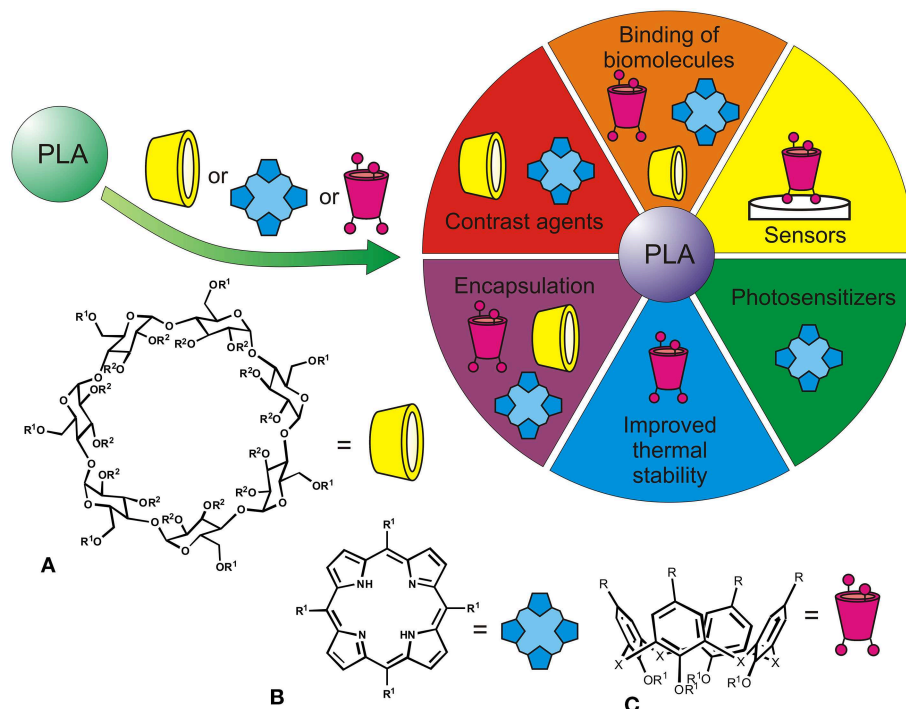


**FIGURE 1** | Applications of PLA functionalized with macrocyclic structures [ $\beta$ -cyclodextrins (A), tetrapyrroles (B), calixarenes (C),  $R^1$ ,  $R^2$  indicate possible modification by PLA fragments].

functionalized with polymethylmethacrylate and then re-azidated. The polylactide fragment was obtained by ROP of D,L-lactide at room temperature in the presence of 1,8-diazabicyclo[5.4.0]undec-7-ene (DBU) as a catalyst. Further, this fragment was modified by poly(*N*-isopropylacrylamide) to amphiphilic block-copolymer containing terminal alkyne group involved in the click reaction with an azide-polymethylmethacrylate block.

Pseudo-block copolymer based on the CD terminated poly(*N*-acryloylmorpholine) and adamantane-terminated linear poly(D,L-lactide) was obtained 2 years later (Ramesh et al., 2018) by ROP in the presence of DBU as a catalyst. The reaction was based on host-guest interactions, in which the inclusion complex of adamantane and CD moiety was formed. The obtained copolymer formed micelles with the size of 103 nm that were able to incorporate doxorubicin into the core. Doxorubicin release from the micelles was faster in acidic medium (Qiu et al., 2010; Lin et al., 2016, 2017).

## HYBRIDS WITH TETRAPYRROLES

Porphyrins represent a unique class of synthetic and natural tetrapyrrole heterocyclic organic molecules (Imran et al., 2018), in which four pyrrole rings are linked together by methine bridges to form a plane macrocyclic structure with conjugated  $\pi$ -electrons (Figure 1B). Aromatic properties combined with the presence of a cavity make for them possible to bind various substrates.

In 2011, a star-shaped four-arm copolymer based on *meso*-tetra-(*p*-hydroxymethylphenyl) porphyrin was obtained by ROP of lactide in the presence of 2-[(2-dimethylamino-ethylimino) methyl] phenol) as a catalyst (Shieh et al., 2011; Hsu et al., 2012; Figures 1B, 2A). The photosensitizing properties caused by porphyrin macrocycle and ability to accumulate doxorubicin resulted in cytotoxic effect of the product toward MCF-7 cells resistant to doxorubicin.

A year later, poly(lactide-co-glycolide) with chlorine containing polymer **3** was synthesized using Steglich esterification (Lee et al., 2012; Figure 2). Further combination with a poly(lactide-co-glycolide) block-copolymer- polyethylene glycol gave water soluble product with low immune response and photo-sensitizing properties. Nanoparticles of about 160 nm were obtained which encapsulated magnetite required for high contrast magnetic resonance tumor imaging *in vivo*.

In 2016, poly(lactide-co-glycolide) fragment was covalently linked to porphyrin blocks by click reaction (Boix-Garriga et al., 2016; Figure 2A). The resulting copolymers **4** and **5** (Figure 2B) formed in aqueous solutions negatively charged nanoparticles of 114–148 nm in size, in which porphyrin fragments were located at the outer layer. They showed high photosensitizing ability to generate singlet oxygen, especially in the case of a hydrophilic porphyrin derivative **5**.

Four-armed copolymer was obtained from tetra(hydroxyethyl) terminated porphyrin and L-lactide by ROP in the presence of DMAP (Figure 1B; Dai et al., 2011, 2014a,b,c, 2015). Terminal hydroxyl groups of the copolymer were then

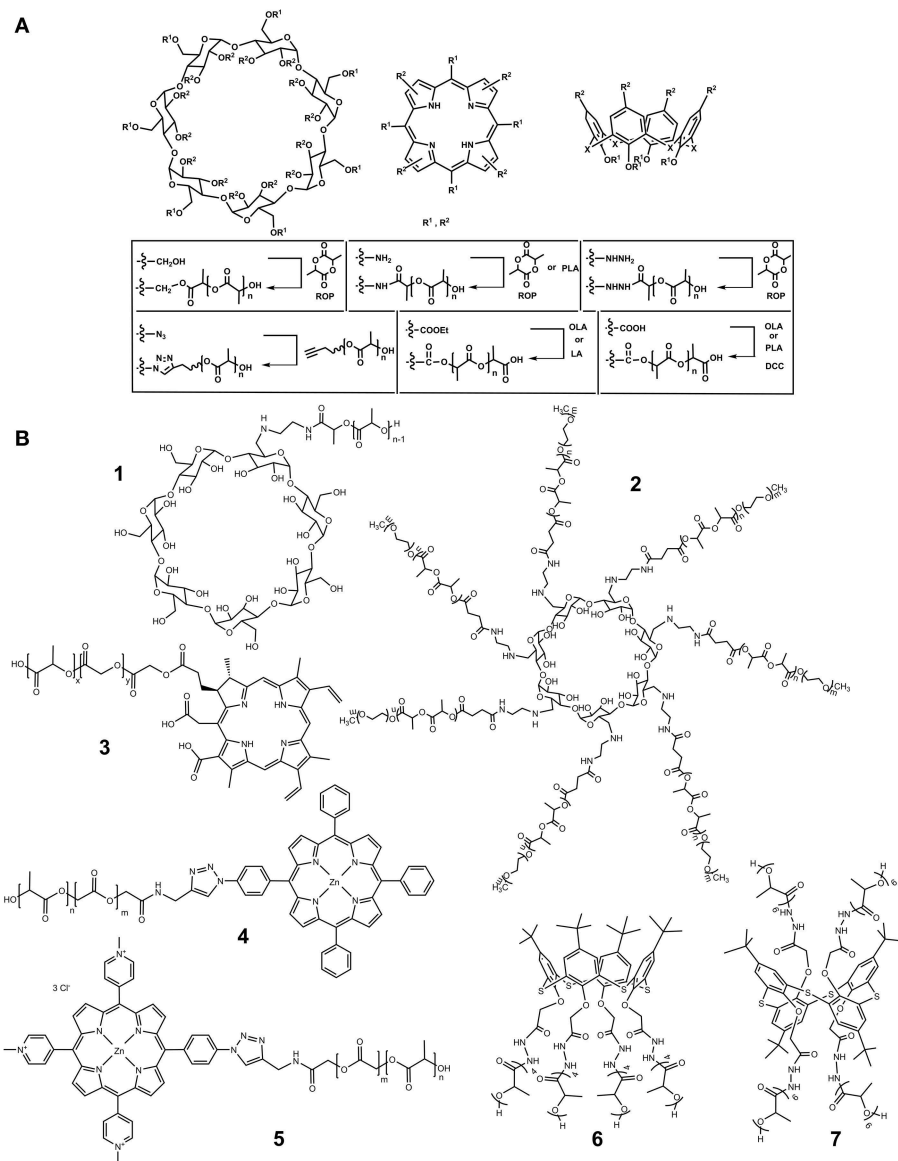


**FIGURE 2 | (A)** Synthetic approaches to PLA modification by macrocycles. **(B)** Macrocycles functionalized by PLA fragments.

modified with benzylsulfanylthiocarbonylsulfanylpropionic acid (Dai et al., 2015). The poly(*N*-isopropylacrylamide) block was polymerized with corresponding monomer in the presence of azobisisobutyronitrile as an initiator. Resulting hybrid formed micelles in aqueous media able to change their shape (through cylinders to vesicles) at temperature near that of a body (37.2°C). It was also proved to be effective in generation of the singlet oxygen and inhibited BEL-7402 cancer cells. Similar hybrid with poly(ethylene glycol) block instead of poly(*N*-isopropylacrylamide) (Dai et al., 2014a) formed micelles in aqueous media that encapsulated doxorubicin released in acidic media (Qiu et al., 2010; Lin et al., 2016, 2017). The ability to generate singlet oxygen was retained.

Glycopolymers based on porphyrin containing four-arm copolymer were in 1-methyl-2-pyrrolidinone solution at 70°C

obtained (Dai et al., 2014b,c). The copolymers generate singlet oxygen and fluorescence with a high quantum yield. Low dark cytotoxicity of the block-copolymers toward the COS-7 cells was shown (Dai et al., 2014b).

Based on tetrakis(4-aminophenyl) porphyrin, a four-arm star-shaped block copolymer including PLA fragment was obtained (Wang et al., 2015). First, D- $\alpha$ -tocopheryl polyethylene glycol 1,000 succinate was modified by D,L-lactide using the ROP in the presence of tin octoate. Further modification of block-copolymer with porphyrin was carried out in the presence of DCC and DMAP. For this purpose, terminal hydroxyl group of the polylactide block was first converted into carboxyl group with *N*-hydroxysuccinimide. Negatively charged nanoparticles up to 130 nm in size were obtained by nanoprecipitation from the copolymer to encapsulate cytostatic

drug Docetaxel (Dai et al., 2014a) released back in acidic media (pH 5.0).

Nanocomposite based on carbon nanotubes and a four-arm PLA copolymer with zinc *p*-tetraaminophenylporphyrin was obtained by sonication due to non-covalent interactions caused by strong  $\pi$ - $\pi$  interactions between carbon nanotubes and the porphyrin block of the copolymer (Li et al., 2016). Polymer with fully retained structure part was positioned outside the nanotubes.

## HYBRIDS WITH CALIXARENES

Calixarenes are fully synthetic macrocycles of cup-shaped form produced by cyclic oligomerization of phenol with formaldehyde (Figure 1C; Gutsche, 1998). The presence of a hydrophobic cavity and the possibility of combining with hydrophilic substituents open up wide possibilities for their use as catalytic systems and receptors for recognition of numerous substrates (Gutsche, 1998; Ludwig and Dzung, 2002). Derivatives of classical calixarene and resorcinarene were first examples of hybrids with cyclophanes (Dria et al., 2012) obtained by ROP of lactide using stannous (II) octoate (Figure 1C). Using macrocycles with unsubstituted phenolic groups as “knot” elements, functionalization with lactide fragments proceeded slowly and not fully. Separation of the reaction centers from the macrocyclic platform showed possibility of the synthesis of target copolyesters with good yields and formation of completely substituted products (with 4 or 8 “arms”). The authors noted the effect of the macrocyclic center on thermal properties of the copolyesters. With smaller number of arms, both average molecular weight of the “arm” fragment and crystallinity degree of the sample decreased.

Thiacalixarene platform is favorably different from classical calixarene by the possibility of easy synthesis of different spatial isomers with intended position of the binding groups against cyclophane platform (Morohashi et al., 2006). Rather rigid fixation of the binding sites in the space allows high binding selectivity for different types of guests. All of this in combination with the non-toxicity of the macrocycle (Perret and Coleman, 2011) offers wide opportunities for its application. In 2018, amino derivative of *p*-*tert*-butylthiacalix[4]arene was firstly modified by L-lactide (Mostovaya et al., 2018) with preservation of the lactide fragment configuration. The resulting compound could bind dopamine. Fragments of the substituent but not the macrocycle itself played key role in the recognition. Endohedral complex was formed with dopamine coordinated outside the macrocycle cavity.

Modification of hydrazide derivatives of *p*-*tert*-butylthiacalix[4]arene in different conformations by LA led to formation of various products depending on the spatial loading of the reaction centers. In the case of their proximity (*cone* conformation), product **6** (Figure 2B) with four LA residues in oligolactide (OLA) fragments was obtained. More freely spaced substituents (*1,3-alternate*) were acylated with six residues (**7**, Figure 2B; Gorbachuk et al., 2018). The OLA obtained were able to self-association in methylene chloride.

The associate size essentially depended on the spatial structure of thiacalix[4]arene stereoisomers. In *cone* conformation, all the OLA fragments were on one side of the macrocyclic rim. For the *1,3-alternate*, the OLA fragments interfere with the efficient packing of cyclophane, which results in much larger size of self-associates. The addition of silver nitrate to the copolymers resulted in disaggregation of self-associates.

Modification of the thiacalixarene platform by L-lactide could be carried out rather easily. However, a number of difficulties appeared in functionalization of the macrocycle directly with L-LA even for the most spatially unloaded *1,3-alternate* (Vavilova et al., 2019). “Knot” element of the tetracarboxyl macrocycle catalyzes the LA condensation with the formation of its pentamer. The replacement of carboxyl groups by ethoxycarbonyl did not lead to the positive result either. However, in the presence of  $\text{MgSO}_4/p$ -toluenesulfonic acid mixture, the tetraester was modified by trilactide fragments over all ethoxycarbonyl groups (Figure 2A).

Introduction of a macrocyclic fragment significantly increased the decomposition temperature against that of unmodified pentalactide. Besides, resulting product was able to self-associate in polar solvents (Vavilova et al., 2019).

*p*-*tert*-Butylthiacalix[4]arene in *cone*, *partial cone*, and *1,3-alternate* conformations containing five lactide units in substituents was obtained by co-polycondensation in the melt (180°C) with pentameric LA (Gorbachuk et al., 2017; Gorbachuk et al., 2017). Although a mixture of appropriate products was obtained, it was thermally more stable than unmodified penta-LA (Vavilova et al., 2019). In  $\text{CH}_2\text{Cl}_2$ , the mixture formed submicron particles by self-association. Their size significantly depended on the conformation of the “knot.” The largest associates were observed for *1,3-alternate* and the smallest ones for *cone*. Inverse relationship was found in water solution (Gorbachuk et al., 2017). Probably, decrease in the associate size with a higher solvent polarity could be explained by different packaging of the self-associates formed. They swell in dichloromethane by forming loose package, but do not swell in water. This significantly reduced particle size due to the denser packing of the copolyester molecules in micelles.

Largest oligolactide fragments were obtained by copolycondensation with penta-LA and tetra(penta-LA) derivatives of *p*-*tert*-butylthiacalix[4]arene (Gorbachuk et al., 2017) at 180°C in the presence of tin octoate (Mostovaya et al., 2019) (Figure 2A). In these conditions, lengthening of the chain of lactide residues to eight fragments in average occurred. However, the products obtained showed lower thermal stability (Gorbachuk et al., 2017; Vavilova et al., 2019). Probably, higher number of monomer units increased energy of inter- and intramolecular bonds. This explained higher decomposition temperature of unmodified octa-LA compared to penta-LA. The macrocyclic block acts as additional “loosening” element that weakens the bonds between OLA chains (Mostovaya et al., 2019). The resulting copolyesters form stable negatively charged submicron particles able to bind proteins. The coagulation was observed in the presence of positively charged lysozyme. In the case of BSA and hemoglobin, the associates retain submicron size exceeding 400 nm for



1,3-alternate, and <200 nm for other isomers of the core. OLA modified by *partial cone* macrocycle interacted most efficiently with all the model proteins, while unmodified octalactide did not interact with them at all. Probably, interactions with biopolymers is mostly dependent on hydrophobic force between macrocyclic fragments of copolyesters and protein binding sites.

Self-association of the OLA modified thiacalixarenes has been used for assembling of electrochemical sensors where modifiers provided both accumulation of auxiliary agents and analytes. This resulted in significant improvement of analytical performance of the sensors. The permeability of the surface layer formed by drop-casting of the thiacalixarenes bearing five OLA fragments in each substituent was explored using electrochemical impedance spectroscopy and direct current voltammetry (Gorbachuk et al., 2017). In both cases, negatively charged ferricyanide ion was utilized as redox probe. Its signals, i.e., cathodic current or charge transfer resistance, were sensitive to the charge density of the surface layer caused by carboxylic terminal groups of OLA fragments. The surface concentration and configuration of thiacalixarene core both influenced above parameters. Treatment of the OLA-thiacalixarene hybrids with AgNO<sub>3</sub> followed by cathodic reduction of accumulated Ag<sup>+</sup> ions resulted in formation of nanodendrites exerting electrocatalytic signals toward hydrogen peroxide, thiocholine, hydroquinone, tryptophan (Porifreva et al., 2018). As a result, their working concentrations have been decreased by more than one order of magnitude against bare glassy carbon electrode. OLA-thiacalixarene hybrids were also used as transducers in acetylcholinesterase sensors for determination of

organophosphate pesticides and anti-dementia drugs exerting inhibitory effect on immobilized enzyme (Gorbachuk et al., 2017; Shamagsumova et al., 2019).

## CONCLUSIONS

PLA has been modified by various macrocyclic fragments to obtain derivatives with the properties promising for drug delivery systems, photosensitizers in photodynamic therapy, and protein binding. These properties are determined by both the types of macrocyclic block and the number of lactide fragments in them. Variation in the above parameters as well as introduction of other substituents with functional groups can offer new opportunities for directional design of synthetic receptors and drug delivery systems with specific properties sensitive to the analyte properties and structural factors of macrocyclic core. Some of the advantages described have been already shown on the example of electrochemical sensors and biosensors with extended characteristics of drug, metabolite, antioxidant determination.

## AUTHOR CONTRIBUTIONS

All authors listed have made a substantial, direct and intellectual contribution to the work, and approved it for publication.

## FUNDING

This work was financially supported by the Russian Science Foundation (Grant No. 16-13-00005).

## REFERENCES

- Adeli, M., Zarnegar, Z., and Kabiri, R. (2008). Amphiphilic star copolymers containing cyclodextrin core and their application as nanocarrier. *Eur. Polym. J.* 44, 1921–1930. doi: 10.1016/j.eurpolymj.2008.03.028
- Andreopoulos, A. G., Hatz, E. C., and Doxastakis, M. (2000). Controlled release systems based on poly(lactic acid). An *in vitro* and *in vivo* study. *J. Mater. Sci. Mater. Med.* 11, 393–397. doi: 10.1023/A:1008990109419
- Boix-Garriga, E., Bryden, F., Savoie, H., Sagristá, M. L., Mora, M., Boyle, R. W., et al. (2016). Poly-(D,L-lactide-co-glycolide) nanoparticles with covalently-bound porphyrins for efficient singlet oxygen photosensitization. *J. Porphyrins Phthaloc.* 20, 1306–1318. doi: 10.1142/S108842461650108X
- Crini, G. (2014). Review: a history of cyclodextrins. *Chem. Rev.* 114, 10940–10975. doi: 10.1021/cr500081p
- Dai, X.-H., Jin, H., Cai, M.-H., Wang, H., Zhou, Z.-P., Pan, J.-M., et al. (2015). Fabrication of thermosensitive, star-shaped poly(L-lactide)-blockpoly(N-isopropylacrylamide) copolymers with porphyrin core for photodynamic therapy. *React. Funct. Polym.* 89, 9–17. doi: 10.1016/j.reactfunctpolym.2015.02.002
- Dai, X.-H., Liu, W., Huang, Y.-F., and Dong, C.-M. (2011). Synthesis and characterization of star-shaped porphyrin-cored poly(L-lactide). *Adv. Mater. Res.* 239–242, 1703–1706. doi: 10.4028/www.scientific.net/AMR.239-242.1703
- Dai, X.-H., Wang, Z.-M., Gao, L.-Y., Pan, J.-M., Wang, X.-H., Yan, Y.-S., et al. (2014a). Star-shaped poly(L-lactide)-b-poly(ethylene glycol) with porphyrin core: synthesis, self-assembly, drug-release behavior, and singlet oxygen research. *New J. Chem.* 38, 3569–3578. doi: 10.1039/C3NJ01621H
- Dai, X.-H., Wang, Z.-M., Liu, W., Dong, C.-M., Pan, J.-M., Yuan, S.-S., et al. (2014b). Biomimetic star-shaped porphyrin-cored poly(L-lactide)-b-glycopolymer block copolymers for targeted photodynamic therapy. *Colloid. Polym. Sci.* 292, 2111–2122. doi: 10.1007/s00396-014-3244-6
- Dai, X.-H., Wang, Z.-M., Pan, J.-M., Yuan, S.-S., Yan, Y.-S., Liu, D.-M., et al. (2014c). Star-shaped poly(L-lactide)-b-poly(lactobionamidoethyl methacrylate) with porphyrin core: synthesis, self-assembly, singlet oxygen research and recognition properties. *J. Biomater. Sci. Polym. Ed.* 25, 1755–1770. doi: 10.1080/09205063.2014.946878
- Dria, D., Goudy, B. A., Moga, K. A., and Corbin, P. S. (2012). Synthesis and characterization of multi-armed calixarene- and resorcinarene-core polylactide star polymers. *Polym. Chem.* 3, 2070–2081. doi: 10.1039/c2py20188g
- Gao, H., Wang, Y. N., Fan, Y. G., and Ma, J. B. (2005). Synthesis of a biodegradable tadpole-shaped polymer via the coupling reaction of polylactide onto mono(6-(2-aminoethyl)amino-6-deoxy)-β-cyclodextrin and its properties as the new carrier of protein delivery system. *J. Controlled Release*. 107, 158–173. doi: 10.1016/j.jconrel.2005.06.010
- Garlotta, D. (2001). A literature review of poly(Lactic Acid). *J. Polym. Environ.* 9, 63–84. doi: 10.1023/A:1020200822435
- Gorbachuk, V. V., Mostovaya, O. A., Evtugyn, V. G., Osin, Y. N., Kh. Rizvanov, I., Gerasimov, A. V., et al. (2017). Modification of oligolactic acid with tetracarboxylic *p*-tert-butylthiacalix[4]arene derivatives: effect of macrocyclic fragment configuration on aggregation and thermal properties of copolyesters. *Macromolecules*. 10, 174–181. doi: 10.6060/mhc170513s
- Gorbachuk, V. V., Padnya, P. L., and Stoikov, I. I. (2018). Synthesis of macrocyclic stereoisomers substituted with oligolactide fragments. *Russ. J. Gen. Chem.* 88, 1838–1841. doi: 10.1134/S1070363218090128
- Gorbachuk, V. V., Porifreva, A. V., Stepanova, V. B., Yu Kuzin, I., Evtugyn, V. G., Shamagsumova, R.V., et al. (2017). Co-polymers of oligolactic acid and tetrasubstituted thiacalix[4]arenes as a new material for electrochemical sensor development. *Sens. Actu B Chem.* 246, 136–145. doi: 10.1016/j.snb.2017.02.061
- Gutsche, C. D. (1998). *Calixarenes Revisited, Monographs in Supramolecular Chemistry*. ed Stoddart, J.F. Cambridge: The Royal Society of Chemistry.

- Hsu, C.-Y., Nieh, M.-P., and Lai, P.-S. (2012). Facile self-assembly of porphyrin-embedded polymeric vesicles for theranostic applications. *Chem. Commun.* 48, 9343–9345. doi: 10.1039/c2cc33851c
- Imran, M., Ramzan, M., Qureshi, A. K., Khan, M. A., and Tariq, M. (2018). Emerging applications of porphyrins and metalloporphyrins in biomedicine and diagnostic magnetic resonance imaging. *Biosensors* 8:95. doi: 10.3390/bios8040095
- Jain, A., Kunduru, K. R., Basu, A., Mizrahi, B., Domb, A. J., and Khan, W. (2016). Injectable formulations of poly(lactic acid) and its copolymers in clinical use. *Adv. Drug Del. Rev.* 107, 213–227. doi: 10.1016/j.addr.2016.07.002
- Kricheldorf, H. R., and Serra, A. (1985). Polylactones. 6. Influence of various metal salts on the optical purity of poly(L-lactide). *Polym. Bull.* 14, 497–502. doi: 10.1007/BF00271606
- Kum, C. H., Cho, Y., Joong, Y. K., Choi, J., Park, K., Seo, S. H., et al. (2013). Biodegradable poly(L-lactide) composites by oligolactide-grafted magnesium hydroxide for mechanical reinforcement and reduced inflammation. *J. Mater. Chem. B* 1, 2764–2772. doi: 10.1039/c3tb00490b
- Kumar, S., Singh, S., Senapati, S., Singh, A. P., Ray, B., and Maiti, P. (2017). Controlled drug release through regulated biodegradation of poly(lactic acid) using inorganic salts. *Int. J. Biol. Macromol.* 104, 487–497. doi: 10.1016/j.ijbiomac.2017.06.033
- Lee, D. J., Park, G. Y., Oh, K. T., Oh, N. M., Kwag, D. S., Youn, Y. S., et al. (2012). Multifunctional poly (lactide-co-glycolide) nanoparticles for luminescence/magnetic resonance imaging and photodynamic therapy. *Int. J. Pharm.* 434, 257–263. doi: 10.1016/j.ijpharm.2012.05.068
- Li, J., Song, Z., Gao, L., and Shan, H. (2016). Preparation of carbon nanotubes/poly(lactic acid) nanocomposites using a non-covalent method. *Polym. Bull.* 73, 2121–2128. doi: 10.1007/s00289-015-1597-8
- Lin, W., Yao, N., Li, H., Hanson, S., Han, W., Wang, C., et al. (2016). Co-delivery of imiquimod and plasmid DNA via an amphiphilic pH-responsive star polymer that forms unimolecular micelles in water. *Polymers* 8:397. doi: 10.3390/polym8110397
- Lin, W., Yao, N., Qian, L., Zhang, X., Chen, Q., Wang, J., et al. (2017). pH-responsive unimolecular micelle-gold nanoparticles-drug nanohybrid system for cancer theranostics. *Acta Biomaterialia* 58, 455–465. doi: 10.1016/j.actbio.2017.06.003
- Ludwig, R., and Dzung, N. T. K. (2002). Calixarene-based molecules for cation recognition. *Sensors* 2, 397–416. doi: 10.3390/s21000397
- Marcincinova-Benabdillah, K., Boustta, M., Coudane, J., and Vert, M. (2001). Novel degradable polymers combining D-gluconic acid, a sugar of vegetal origin, with lactic and glycolic acids. *Biomacromolecules* 2, 1279–1284. doi: 10.1021/bm015585j
- Morohashi, N., Narumi, F., Iki, N., Hattori, T., and Miyano, S. (2006). Thiacalixarenes. *Chem. Rev.* 106, 5291–5316. doi: 10.1021/cr050565j
- Mostovaya, O. A., Gorbachuk, V. V., Bazanova, O. B., Gerasimov, A. V., Evtugyn, V. G., Osin, Y. N., et al. (2019). Thiacalixarene “knot” effect on protein binding by oligolactide acid particles. *Mater. Chem. Front.* 3, 292–300. doi: 10.1039/C8QM00435H
- Mostovaya, O. A., Padnya, P. L., Vavilova, A. A., Shurpik, D. N., Khairutdinov, B. I., Mukhametzyanov, et al. (2018). Tetracarboxylic acids on a thiacalixarene scaffold: synthesis and binding of dopamine hydrochloride. *New J. Chem.* 42, 177–183. doi: 10.1039/C7NJ03953K
- Murariu, M., and Dubois, P. (2016). PLA composites: from production to properties. *Adv. Drug Delivery Rev.* 107, 17–46. doi: 10.1016/j.addr.2016.04.003
- Perret, F., and Coleman, A. W. (2011). Biochemistry of anionic calix[n]arenes. *Chem. Commun.* 47, 7303–7319. doi: 10.1039/c1cc11541c
- Porifreva, A. V., Gorbachuk, V. V., Evtugyn, V. G., Stoikov, I. I., and Evtugyn, G. A. (2018). Glassy carbon electrode modified with silver nanodendrites implemented in polylactide-thiacalix[4]arene copolymer for the electrochemical determination of tryptophan. *Electroanalysis* 30, 641–649. doi: 10.1002/elan.201700638
- Poulsen, A., William, A. D., and Dymock, B. W. (2015). “Designed macrocyclic kinase inhibitors” in *RSC Drug Discovery Series, Macrocycles in Drug Discovery*, ed J. Levin (London: Royal Society of Chemistry), 141–205. doi: 10.1039/9781782623113-00141
- Pretula, J., Slomkowski, S., and Penczek, S. (2016). Polylactides—Methods of synthesis and characterization. *Adv. Drug Delivery Rev.* 107, 3–16. doi: 10.1016/j.addr.2016.05.002
- Qiu, L. Y., Wang, R. J., Zheng, C., Jin, Y., and Jin, L. Q. (2010).  $\beta$ -Cyclodextrin-centered star-shaped amphiphilic polymers for doxorubicin delivery. *Nanomedicine* 5, 193–208. doi: 10.2217/nnm.09.108
- Ramesh, K., Anugrah, D. S. B., and Lim, K. T. (2018). Supramolecular poly(N-acryloylmorpholine)-b-poly(D,L-lactide) pseudoblock copolymer via host-guest interaction for drug delivery. *React. Funct. Polym.* 131, 12–21. doi: 10.1016/j.reactfunctpolym.2018.06.011
- Ren, J. M., McKenzie, T. G., Fu, Q., Wong, E. H. H., Xu, J., An, Z., et al. (2016). Star polymers. *Chem. Rev.* 116, 6743–6836. doi: 10.1021/acs.chemrev.6b00008
- Shamagsumova, R. V., Efimova, Olga, Yu., Gorbachuk, V. V., Evtugyn, V. G., Stoikov, I. I., et al. (2019). Electrochemical acetylcholinesterase biosensor based on Polylactide–nanosilver composite for the determination of anti-dementia drugs. *Anal. Lett.* 52, 1558–1578. doi: 10.1080/00032719.2018.1557202
- Shen, J., Hao, A., Du, G., Zhang, H., and Sun, H. (2008). A convenient preparation of 6-oligo(lactic acid)cyclomaltoheptaose as kinetically degradable derivative for controlled release of amoxicillin. *Carbohydr. Res.* 343, 2517–2522. doi: 10.1016/j.carres.2008.06.010
- Shieh, M.-J., Hsu, C.-Y., Huang, L.-Y., Chen, H.-Y., Huang, F.-H., and Lai, P.-S. (2011). Reversal of doxorubicin-resistance by multifunctional nanoparticles in MCF-7/ADR cells. *J. Controlled Release* 152, 418–425. doi: 10.1016/j.jconrel.2011.03.017
- Tungala, K., Adhikary, P., Azmeera, V., Kumar, K., Ramesh, K., and Krishnamoorthi, S. (2016). Dendrimer like star polymer based on  $\beta$ -cyclodextrin with ABC type miktoarms. *RSC Adv.* 6, 41594–41607. doi: 10.1039/C6RA09660C
- van de Manaker, F., Vermonden, T., van Nostrum, C. F., and Hennink, W. E. (2009). Cyclodextrin-based polymeric materials: synthesis, properties, and pharmaceutical/biomedical applications. *Biomacromolecules* 10, 3157–3175. doi: 10.1021/bm901065f
- Vavilova, A. A., Gorbachuk, V. V., Shurpik, D. N., Gerasimov, A. V., Yakimova, L. S., Padnya, P. L., et al. (2019). Synthesis, self-assembly and the effect of the macrocyclic platform on thermal properties of lactic acid oligomer modified by *p*-tert-butylthiacalix[4]arene. *J. Mol. Liq.* 281, 243–251. doi: 10.1016/j.molliq.2019.02.086
- Wang, T., Zhu, D., Liu, G., Tao, W., Cao, W., Zhang, L., et al. (2015). DTX-loaded star-shaped TAPP-PLA-b-TPGS nanoparticles for cancer chemical and photodynamic combination therapy. *RSC Adv.* 5, 50617–50627. doi: 10.1039/C5RA09042C
- Yao, N., Lin, W., Zhang, X., Gu, H., and Zhang, L. (2016). Amphiphilic  $\beta$ -cyclodextrin-based star-like block copolymer unimolecular micelles for facile *in situ* preparation of gold nanoparticles. *J. Polym. Sci. A Polym. Chem.* 54, 186–196. doi: 10.1002/pola.27889
- Zhang, X., Lin, W., Wen, L., Yao, N., Nie, S., and Zhang, L. (2016). Systematic design and application of unimolecular star-like block copolymer micelles: a coarse-grained simulation study. *Phys. Chem. Chem. Phys.* 18, 26519–26529. doi: 10.1039/C6CP05039E

**Conflict of Interest Statement:** The authors declare that the research was conducted in the absence of any commercial or financial relationships that could be construed as a potential conflict of interest.

Copyright © 2019 Mostovaya, Gorbachuk, Padnya, Vavilova, Evtugyn and Stoikov. This is an open-access article distributed under the terms of the Creative Commons Attribution License (CC BY). The use, distribution or reproduction in other forums is permitted, provided the original author(s) and the copyright owner(s) are credited and that the original publication in this journal is cited, in accordance with accepted academic practice. No use, distribution or reproduction is permitted which does not comply with these terms.



# Construction of Chiral Nanoassemblies Based on Host-Guest Complexes and Their Responsive CD and CPL Properties: Chirality Transfer From 2,6-helic[6]arenes to a Stilbazolium Derivative

Yan Guo<sup>1,2</sup>, Ying Han<sup>1\*</sup> and Chuan-Feng Chen<sup>1,2\*</sup>

<sup>1</sup> Beijing National Laboratory for Molecular Sciences, CAS Key Laboratory of Molecular Recognition and Function, Institute of Chemistry, Chinese Academy of Sciences, Beijing, China, <sup>2</sup> University of Chinese Academy of Sciences, Beijing, China

## OPEN ACCESS

### Edited by:

De-Xian Wang,  
Institute of Chemistry (CAS), China

### Reviewed by:

Dong-Sheng Guo,  
Nankai University, China  
Chunju Li,  
Tianjin Normal University, China

### \*Correspondence:

Ying Han  
hanying463@iccas.ac.cn  
Chuan-Feng Chen  
cchen@iccas.ac.cn

### Specialty section:

This article was submitted to  
Supramolecular Chemistry,  
a section of the journal  
Frontiers in Chemistry

Received: 17 June 2019

Accepted: 16 July 2019

Published: 02 August 2019

### Citation:

Guo Y, Han Y and Chen C-F (2019)  
Construction of Chiral  
Nanoassemblies Based on  
Host-Guest Complexes and Their  
Responsive CD and CPL Properties:  
Chirality Transfer From  
2,6-helic[6]arenes to a Stilbazolium  
Derivative. *Front. Chem.* 7:543.  
doi: 10.3389/fchem.2019.00543

A couple of water-soluble chiral 2,6-helic[6]arene derivatives **P-H1** and **M-H1** were synthesized, and they could form 1:1 stable complexes with 4-[(4'-N, N-diphenylamino)-styryl]-N-methylpyridinium iodide (**G**) in water. Compared with **G**, the host-guest complexes exhibited enhanced fluorescence, which might be attributed to the spatial confinement of **G** and restriction of aggregation-caused quenching (ACQ) effects. Based on the host-guest complexation, the first helic[6]arene-based chiral assemblies were then constructed, and they showed rectangular or hexagonal nanostructures by scanning electron microscopy (SEM) images. Interestingly, the assemblies showed clear mirror-image circular dichroism (CD) and circularly polarized luminescence (CPL) spectra in aqueous solution, revealing a consecutive chirality transfer from the chiral macrocyclic cavities of the hosts to **G**. Moreover, the supramolecular chirality of the assemblies could also show responsiveness to the pH values and temperatures of the system.

**Keywords:** helic[6]arene, host-guest complexation, self-assembly, chirality transfer, circularly polarized luminescence

## INTRODUCTION

Circularly polarized luminescent (CPL) materials have aroused extensively interest for their potential applications in the fields of biological probes (Carr et al., 2012), photoelectric devices (Grell et al., 2001; Shimada et al., 2017; Li et al., 2018a), asymmetric synthesis (Kawasaki et al., 2005; Xu et al., 2014), and chiral sensing (Yang et al., 2013). It is well-known that chirality and luminophores are two essential factors to realize CPL, and most organic CPL materials combined the two factors, but the construction of the materials is generally inconvenient (Han et al., 2017; Li et al., 2017; Chen et al., 2018). As an alternative way, supramolecular assembling based on the complexation motif between a chiral host and an achiral organic fluorescent dye will be convenient and efficient for construction of the CPL materials (Liu et al., 2015). Recently, Inouye's group reported two doubly threaded [4]rotaxanes with strong CPL based on  $\gamma$ -cyclodextrins

(Inouye et al., 2014; Hayashi et al., 2018). Liu's group reported a pyrene-cyclodextrin supra-dendron which showed 1D and 2D nanostructures with CPL activities (Zhang Y. et al., 2018). Because of their commercial availability and chiral cavities, cyclodextrins were often utilized as hosts to construct chiral assemblies or nanostructures based on the chirality transfer motifs (Maeda et al., 2011; Yamaguchi et al., 2011; Sun et al., 2013; Yoshihara et al., 2013; Zhang et al., 2014; Zhang W. et al., 2016; Krishnan and Gopidas, 2017; Zhang B. et al., 2018). However, single enantiomer of cyclodextrins would affect their potential applications in chiral functional materials to some extent. Especially, the lack of chiral macrocyclic hosts could limit the development of such a research area in the host-guest complexation induced CLP materials. As a result, the examples on supramolecular assemblies with CPL properties based on host-guest complexation motif are very limited. Moreover, still no such assemblies with responsive CPL activities have been reported so far.

Recently, we reported a new type of chiral macrocyclic arenes, 2,6-helic[6]arenes (Zhang G. W. et al., 2016; Chen and Han, 2018), which could not only show efficient and enantioselective recognition toward chiral organic ammonium salts, but also form host-guest complexes with various organic guests (Shi and Chen, 2017; Shi et al., 2017; Zhang et al., 2017a,b,c; Wang et al., 2018). It was further deduced that chiral macrocyclic arenes could provide an opportunity to develop the CPL materials based on the host-guest complexation. In this paper, we report a couple of water-soluble chiral 2,6-helic[6]arene derivatives **P-H1** and **M-H1**, which could form 1:1 stable complexes with 4-[(4'-N, N-diphenylamino)styryl]-N-methylpyridinium iodide (**G**) in water (Figure 1). Compared with **G**, the host-guest complexes exhibited enhanced fluorescence, which might be attributed to the spatial confinement of **G** and restriction of aggregation-caused quenching (ACQ) effects. Based on the host-guest complexation, the first helic[6]arene-based chiral assemblies with rectangular or hexagonal nanostructures were then constructed. Interestingly, the supramolecular assemblies showed clear mirror-image CD and CPL spectra in aqueous solution, revealing a consecutive chirality transfer from the chiral macrocyclic cavities to **G**. Moreover, the assemblies could also show the pH and temperature responsive CD and CPL properties.

## RESULTS AND DISCUSSION

### Synthesis

As shown in Scheme 1, treatment of **P-H4** and methyl bromoacetate in acetonitrile in the presence of  $K_2CO_3$  provided methoxycarbonyl-substituted 2,6-helic[6]arene **P-H3** in 93% yield, which were then followed by the hydrolysis with sodium hydroxide aqueous solution and acidification with hydrochloric acid to give the 2,6-helic[6]arene derivative **P-H2**. Finally, the water-soluble **P-H1** was obtained in 100% yield by treatment of **P-H2** with equivalent sodium hydroxide. According to the same method as described above, 2,6-helic[6]arene derivative **M-H1** could also be conveniently synthesized starting from **M-H4**. The new

compounds were all characterized by NMR and MS spectra (Figures S1–S4, S12, S13).

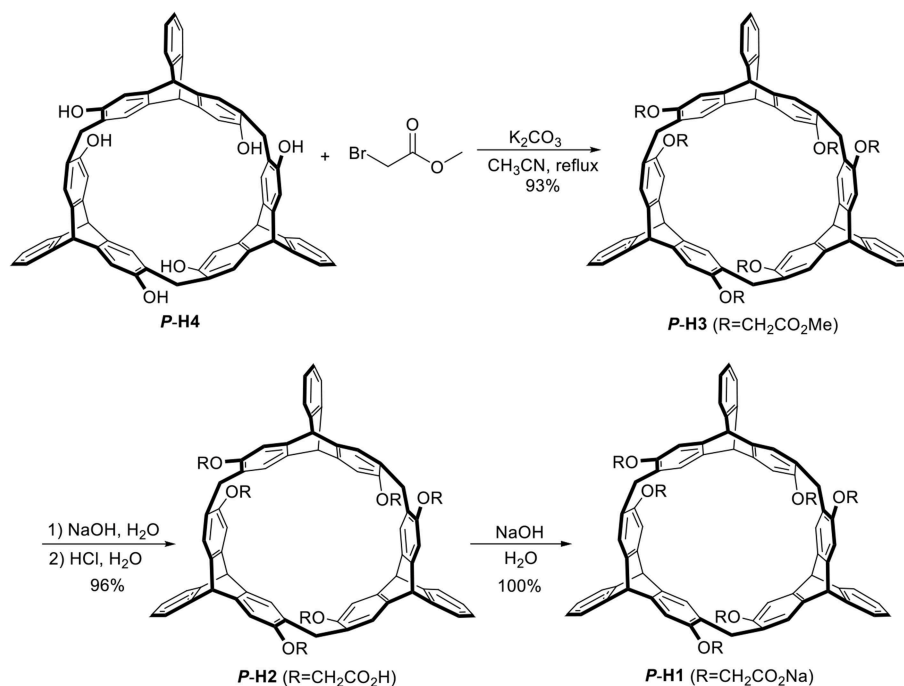
### Host-Guest Complexation

Enantiomers **P-H1** and **M-H1** should show the same host-guest complexation with the guest, so **P-H1** as an example was used to investigate the complexation, which was carried out in solution by  $^1H$  NMR spectroscopy (Figure 2 and Figure S6 for **P-H1-G**, Figures S5, S7 for **M-H1-G**). As shown in Figure 2, when 1.0 equiv of host **P-H1** was added into a solution of **G**, significant chemical shift changes of the protons on **P-H1** and **G** appeared. It was found that protons  $H_1$ ,  $H_2$ ,  $H_3$ , and  $H_4$  of the guest shifted upfield dramatically by 0.47, 1.02, 0.50, and 0.48 ppm, respectively. While the resonance peaks related to protons  $H_7$ ,  $H_8$ ,  $H_{10}$  showed downfield shifts compared with free guest **G** ( $\Delta\delta = 0.11$ , 0.08 and 0.06 ppm, respectively). Moreover, the signals of protons  $H_a$ ,  $H_b$ ,  $H_c$ , and  $H_d$  on **P-H1** also showed upfield shifts due to the host-guest interaction. These observations suggested that host **P-H1** could form 1:1 stable complex with guest **G**, and the complexation between **P-H1** and **G** was a fast exchange process on the NMR spectroscopic timescale. From the 2D ROESY spectrum of a solution of 2.0 mM **P-H1** and 2.0 mM **G** (Figures S10, S11), correlations were observed between protons  $H_2$ ,  $H_3$  of guest **G** and protons  $H_a$  on **P-H1**, which further indicated that in the complex, the methylpyridinium group of **G** was located inside the cavity of **P-H1**, while the benzene ring connected with the double bond of **G** might be located outside the cavity. Furthermore, the electrospray ionization (ESI) mass spectra confirmed the formation of the 1:1 complex between **P-H1** and **G** (Figures S14, S15) as well, in which the signal corresponding to  $[P-H1 \cdot G - 6Na + 3H-I]^{2+}$  was monitored at  $m/z$  801.24776. To quantitatively investigate the complexation between **P-H1** and **G**, isothermal titration calorimetry (ITC) experiments were then carried out in aqueous solution (Figure S16). Consequently, it was found that the association constant ( $K_a$ ) for 1:1 complex **P-H1-G** was determined to be  $(3.84 \pm 0.24) \times 10^5 M^{-1}$ . Similarly, **M-H1** could also form 1:1 stable complex with guest **G** in water, and the  $K_a$  value for the 1:1 complex **M-H1-G** was determined to be  $(3.21 \pm 0.23) \times 10^5 M^{-1}$ .

UV/Vis and fluorescence experiments were also performed to investigate the host-guest complexation. As shown in Figure S17, the absorption and emission spectra of  $2.00 \times 10^{-5} M$  **G** in aqueous solution exhibited an absorption maximum at 450 nm and a weak emission band at about 600 nm, respectively. When equimolar **P-H1** was added into the solution of **G**, distinct bathochromic shifts of absorption maximum occurred from 450 to 475 nm, while a new emission band centered at 618 nm appeared. Probably due to the cavity inclusion and rotation restriction of **G**, the ACQ effects of **G** were avoided and an intensive emission signal was observed in the aqueous solution of **P-H1-G**.

Since **P-H1** contained six carboxyl groups, we further explored the acid/base controlled complexation of **P-H1-G** by  $^1H$  NMR spectroscopy. As shown in Figures S8, S9, upon the





**SCHEME 1** | Synthesis of **P-H1** and **M-H1**.

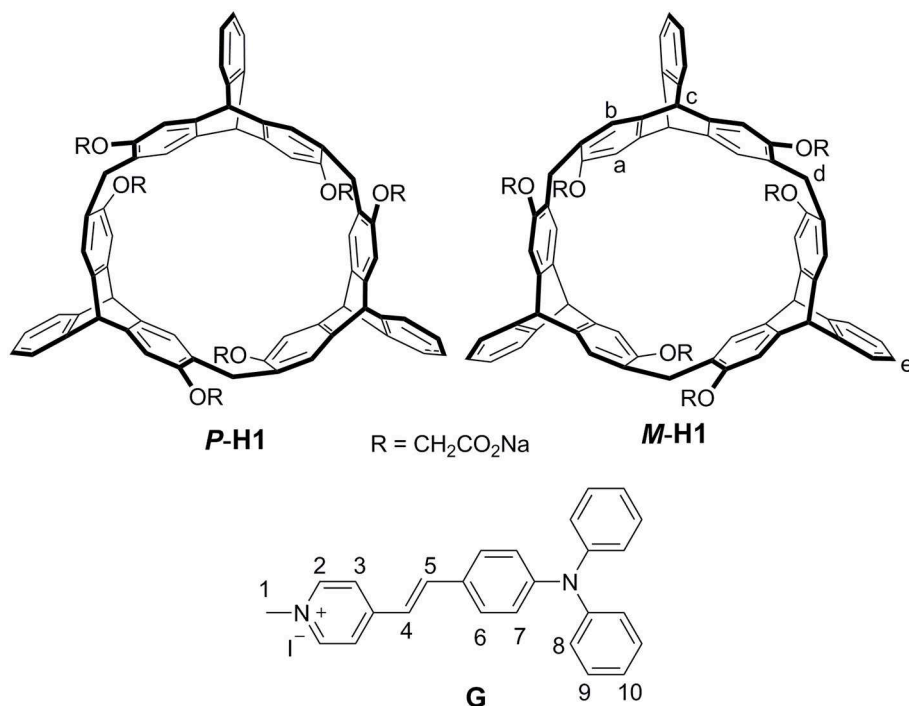


**FIGURE 1** | Structures and proton designations of hosts **P-H1/M-H1** and guest **G**.

addition of an aqueous DCl solution into complex **P-H1**·**G** in  $\text{D}_2\text{O}$ , the carboxylate groups in **P-H1** were acidified into carboxylic acids, and the protonated host was then precipitated

from the solution. Although the guest was also protonated and possessed good water solubility, most of them might be absorbed by the **P-H1** sediment, leading to no signals in the

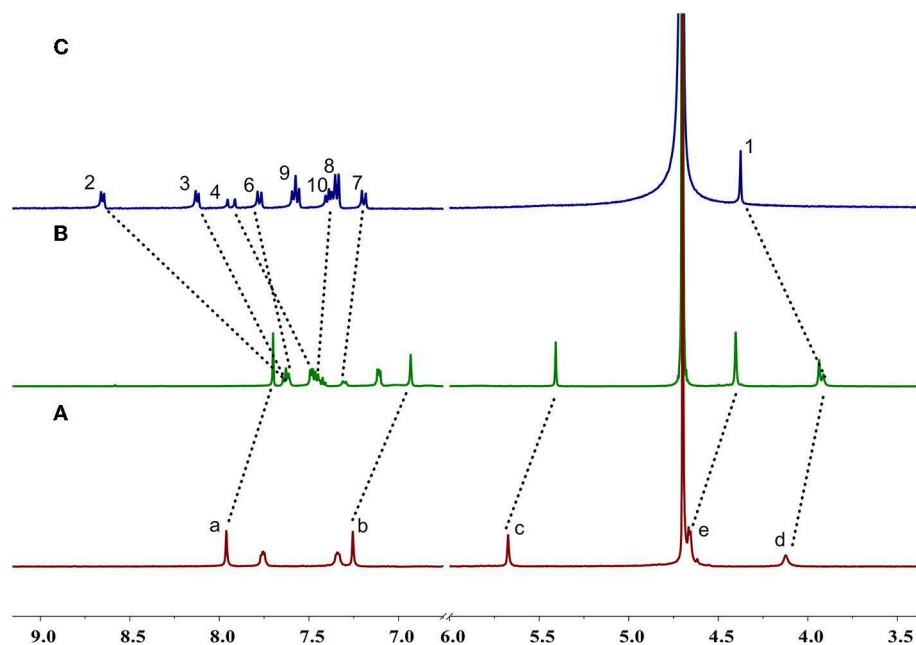


**FIGURE 2** | Partial  $^1\text{H}$  NMR spectra (400 MHz  $\text{D}_2\text{O}$ , 298 K) of (A) free *P*-H1, (B) *P*-H1 with 1.0 equiv. *G*, (C) free *G*. [*P*-H1] = [*G*] = 2.0 mM.

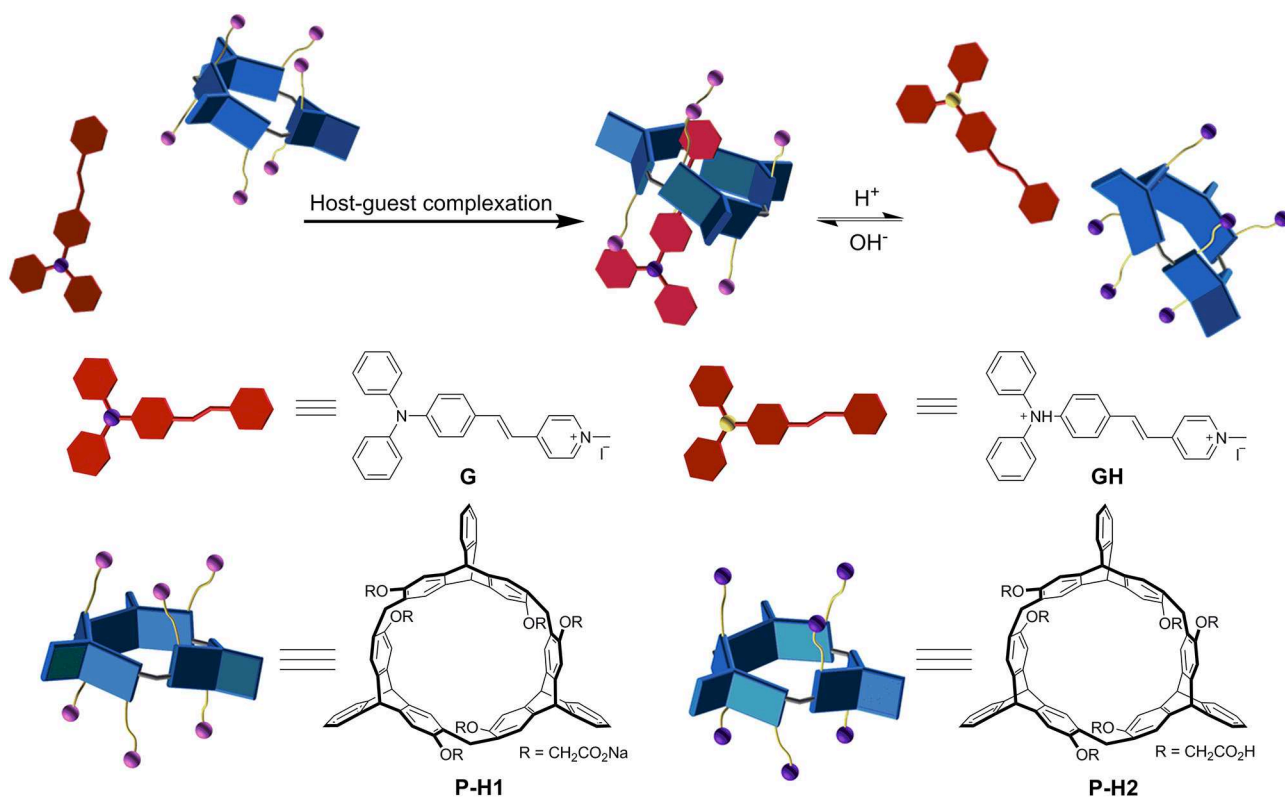
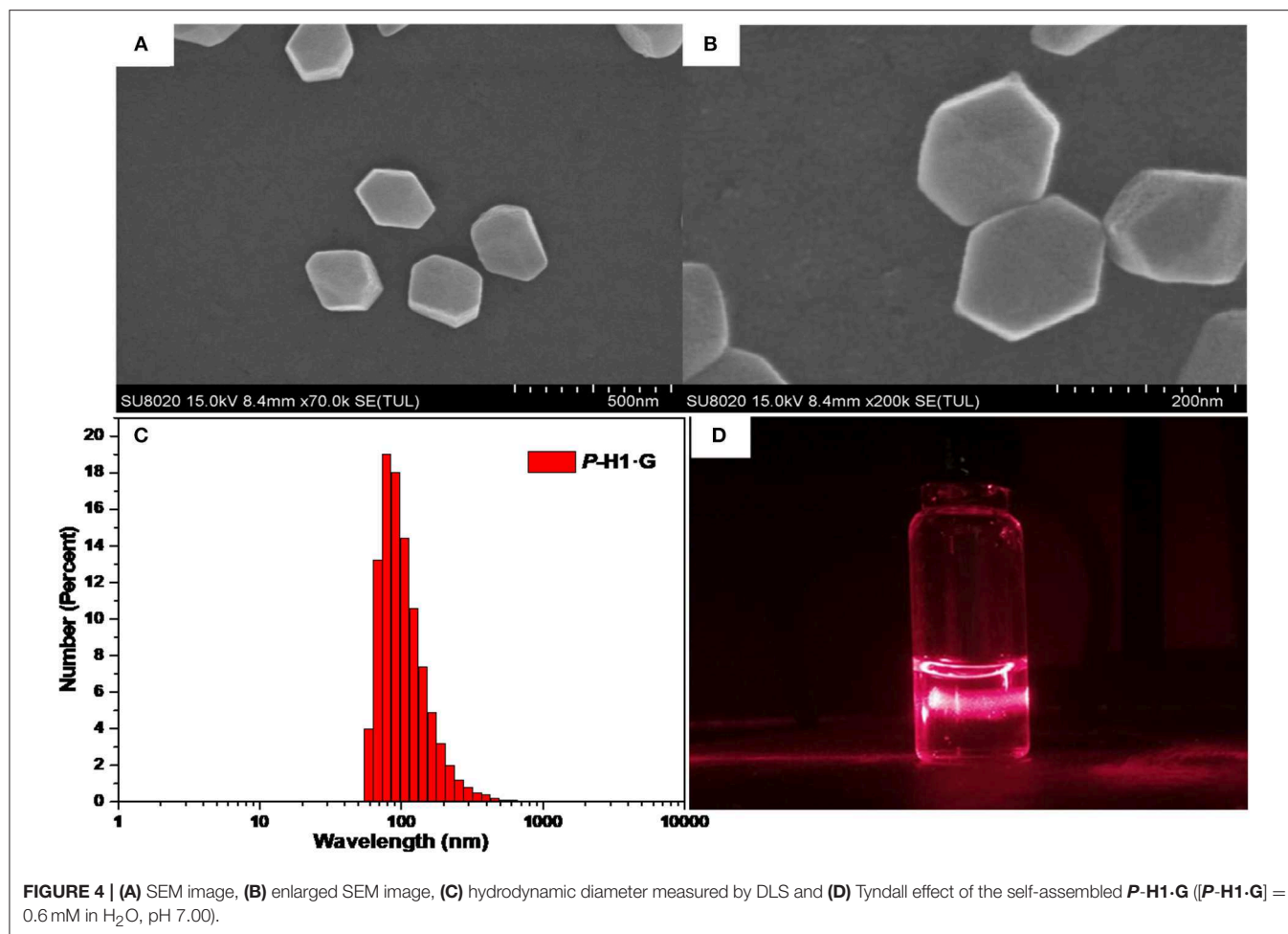


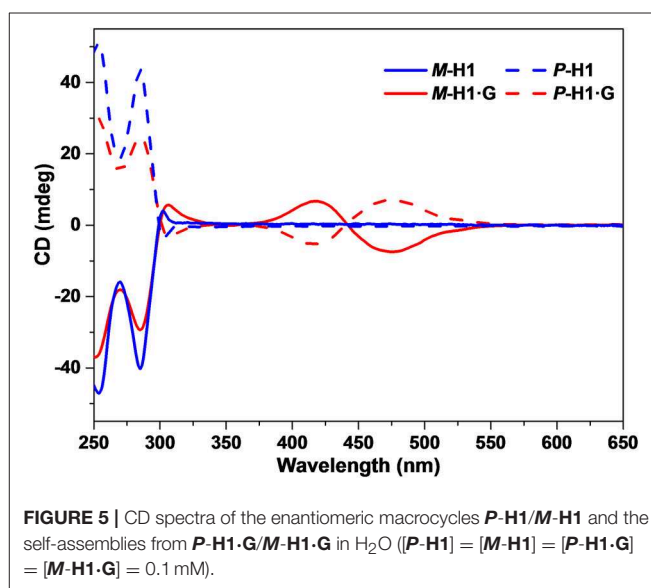
**FIGURE 3** | Cartoon representation of pH responsive complex *P*-H1-*G*.



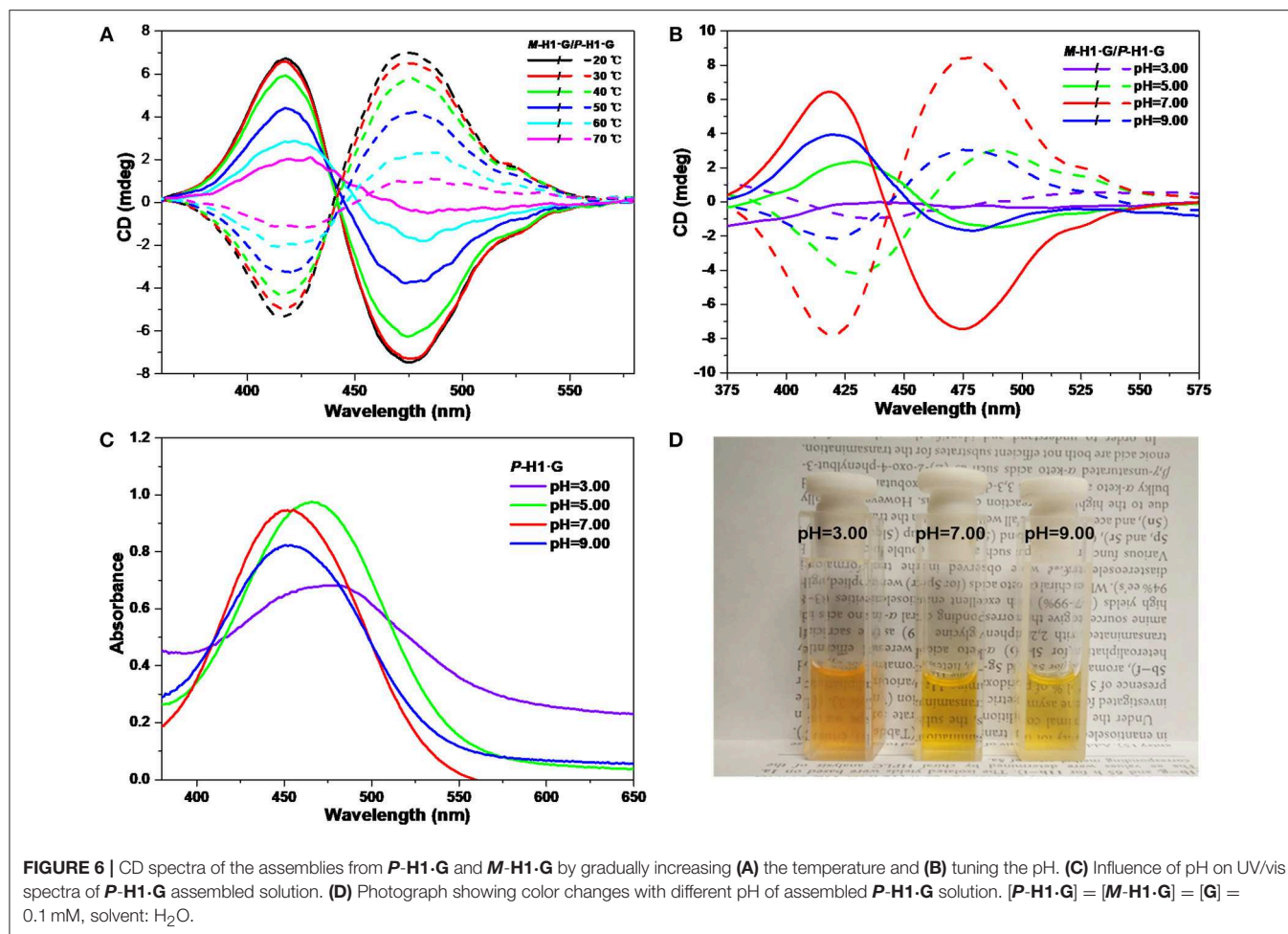
spectrum. Followed by adding an excess of NaOD aqueous solution to the above system, the protonated host dissolved in the solution, and the proton signals of complex  $P-H1 \cdot G$  recovered, which suggested that complex  $P-H1 \cdot G$  formed again. These results indicated that the acid/base stimuli-responsive complexation between  $P-H1$  and  $G$  could be efficiently controlled (Figure 3).

### Morphology of the Aggregates

Based on the formation of complex  $P-H1 \cdot G$ , we further constructed the supramolecular assemblies in water by the reported method (Li et al., 2018b). Consequently, 100 or 600  $\mu\text{L}$  aqueous solution of  $P-H1 \cdot G$  (5 mM) was rapidly injected into 9 mL of water/THF 2:1 (v/v) solution under ultrasonic condition. After the ultrasound was sustained for 5 min, the solution was bubbled by Ar for about 1 h to remove the THF. Then, by continual bubbling, the obtained solution was heated to  $100^\circ\text{C}$  until 5 mL of water remained. Thus, the uniformly distributed self-assemblies in  $\text{H}_2\text{O}$  were obtained with 0.1 and 0.6 mM, respectively. To study the topological influence of  $P-H1$  and  $G$  on the self-assemblies, the similar assembled experiments for free  $P-H1$  and free  $G$  were also carried out, respectively. Scanning electron microscopy (SEM)



and dynamic light scattering (DLS) were used to investigate the assembled structures of  $P-H1 \cdot G$ . SEM images of the assembled  $P-H1 \cdot G$  (0.6 mM) showed hexagon nanostructures



with diameters of about 160 nm (Figures 4A,B). Meanwhile, DLS data showed that the assemblies possessed an average hydrodynamic diameter of 180.4 nm in solution with an obvious Tyndall effect (Figures 4C,D). For the assemblies from the 0.1 mM complex, rectangular nanosheets with the length ranging from 100 to 150 nm were found, which were in agreement with the DLS results (Figures S21–S23). Comparatively, the morphologies of both *P*-H1 and G showed strip-like structures with a length of several micrometers (Figure S18), which were distinctly different from that of complex *P*-H1·G. For the assemblies of *M*-H1·G formed under the same conditions, similar nanostructures to complex *P*-H1·G were obtained (Figures S20, S24). These results suggested that the macrocyclic compounds have a dramatic influence on the spatial alignment of G, and the morphological modulation of the assemblies from the complex could also be realized by simply tuning the concentration of host-guest complex.

Since complex *P*-H1·G could be easily destroyed by acid (Zhang et al., 2017b), we found that when the pH of the assembled solution of *P*-H1·G (0.6 mM) decreased to 3.00, the self-assembly morphology of *P*-H1·G changed from nanohexagon to irregular structures (Figure S19). Moreover, it was also found that when the pH of above system reached

9.00 by adding NaOH solution, irregular aggregates were also generated probably because the existence of excess NaOH could increase the ionic strength of the system and subsequently weaken the host-guest interaction of *P*-H1·G (Figure S19) [17a]. Similarly, the regular nanosheets for the assemblies of 0.1 mM system could also be destroyed upon addition of HCl or NaOH (Figures S21, S22). These results indicated that the self-assembly morphology based on complex *P*-H1·G showed pH responsiveness.

## CD and CPL Properties of the Aggregates

Based on the spatial confinement of G by the chiral cavity of the macrocycles and strong absorption and emission properties of the complexes, we deduced that the assembled nanostructures could show induced CD and CPL properties, attributed to the chiral transfer from the chiral cavity of *P*-H1/*M*-H1 to the dye guest G. As shown in Figure 5, mirror-image CD signals for *P*-H1 and *M*-H1 at 285 nm were observed in agreement with their absorption regions. For the assemblies from complexes *P*-H1·G/*M*-H1·G, a pair of new mirror-image CD signals at 425 and 475 nm appeared, which could be ascribed to the host-guest complexation induced chiral transfer from the enantiomeric macrocycles to G. Moreover, when 0.6 mM solution of assembled



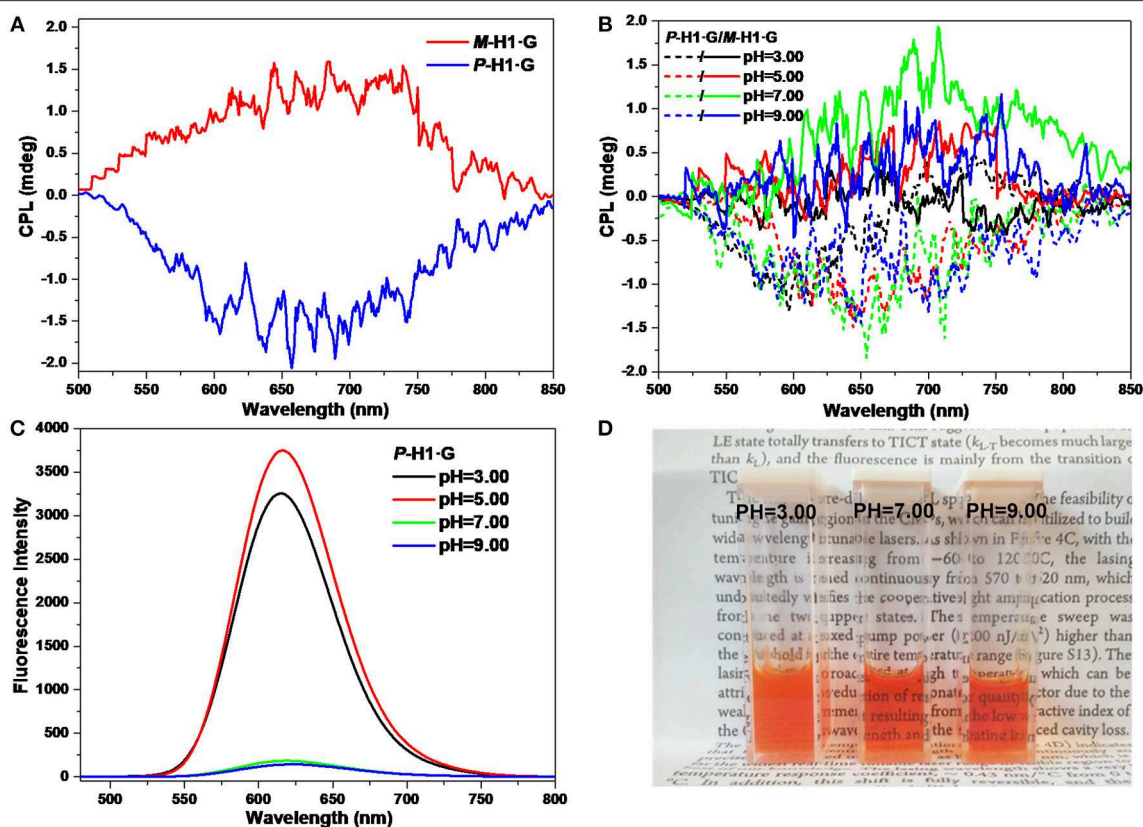


**FIGURE 7 | (A)** CPL spectra of the assemblies from *P*-H1·G and *M*-H1·G in water. **(B)** CPL spectra, **(C)** FL spectra, and **(D)** photograph showing color changes with different pH values of the assemblies from *P*-H1·G and *M*-H1·G in water ([*P*-H1·G] = [*M*-H1·G] = 0.6 mM,  $\lambda_{\text{ex}}$  = 450 nm).

complexes *P*-H1·G/*M*-H1·G was used, the CD signals enhanced distinctly, suggesting that the system with higher concentration could induce stronger chirality.

We further explored the CD changes of the assemblies under alternative temperatures and pH values. It was found that with the increase of temperature from 20 to 70°C, the intensity of the mirror-image CD signals induced by the host-guest complexation decreased gradually (**Figure 6A**). These changes implied that the accelerated rotation and motion of the chiral macrocycle and guest *G* emerged under heating conditions, which resulted in the interruptive chirality transfer. It was also found that when dilute HCl solution was added into the neutral system, the mirror-image CD signals exhibited reduced intensity as well as bathochromic shifts (**Figure 6B**), indicating that the assemblies dissociated gradually while the host and the guest were protonated. Simultaneously, when pH increased to 9.00, only the weakened CD signal intensities were observed due to no structural change of guest *G*. The pH responsive CD signal changes of the assemblies from the complexes were basically in agreement with the change tendency of UV/vis spectra and color changes in **Figures 6C,D**.

The CPL properties of the assemblies from the complexes were further explored. As shown in **Figure 7A**, it is found that with chiral microenvironment of the macrocycles and luminophore of the guest, the *P*-H1·G/*M*-H1·G assembled solution (0.6 mM)

also showed a pair of mirror-image CPL signals ranging from 500 to 850 nm, which might be attributed to the chirality transfer from the macrocycles to guest *G* by the strong host-guest interactions and the well-ordered assembled nanostructures. Correspondingly, the maximum  $g_{\text{lum}}$  values of CPL for *P*-H1·G and *M*-H1·G were determined to be  $-2.67 \times 10^{-4}$  and  $1.48 \times 10^{-4}$  at 655 nm, respectively. Moreover, the pH values dependent on CPL signal changes of the assembled solution could also be found. As shown in **Figure 7B**, the mirror-image CPL signals weakened under either the acidic or basic conditions. These observations might be due to the destruction of the assemblies from complex *P*-H1·G/*M*-H1·G by acid, and the weakened host-guest interactions by base, which were further proved by FL spectra and photograph showing color changes (**Figures 7C,D**). The acid/base controlled CPL properties of the assemblies could provide an opportunity to further design and construct new chiral assembled materials with responsive properties.

## CONCLUSION

In summary, we have synthesized a couple of water-soluble chiral 2,6-helic[6]arene derivatives *P*-H1 and *M*-H1, and found that they could form 1:1 stable complexes with 4'-[(4'-N, N-diphenylamino)styryl]-N-methylpyridinium iodide in water. Compared with the guest, the host-guest complexes exhibited

enhanced fluorescence, which might be attributed to the spatial confinement of the guest and restriction of ACQ effects. Based on the host-guest complexation, the first helic[6]arene-based chiral assemblies were then constructed, and they showed rectangular or hexagonal nanostructures by SEM images. Interestingly, it was found that the assemblies showed clear mirror-image CD and CPL spectra in aqueous solution, which revealed a consecutive chirality transfer from the chiral macrocycles to the achiral guest. Moreover, the assemblies could also show the responsive CD and CPL activities to the pH and temperatures, which would provide an opportunity to further construct new chiral functional materials.

## DATA AVAILABILITY

All datasets generated for this study are included in the manuscript/**Supplementary Files**.

## REFERENCES

- Carr, R., Evans, N. H., and Parker, D. (2012). Lanthanide complexes as chiral probes exploiting circularly polarized luminescence. *Chem. Soc. Rev.* 41, 7673–7686. doi: 10.1039/C2CS35242
- Chen, C.-F., and Han, Y. (2018). Triptycene-derived macrocyclic arenes: from calixarenes to helicarenes. *Acc. Chem. Res.* 51, 2093–2106. doi: 10.1021/acs.accounts.8b00268
- Chen, X.-M., Chen, Y., Liang, L., Liu, Q.-J., and Liu, Y. (2018). Chiral binaphthylbis(4,4'-bipyridin-1-ium)/cucurbit[8]uril supramolecular system and its induced circularly polarized luminescence. *Macromol. Rapid Commun.* 39:1700869. doi: 10.1002/marc.201700869
- Grell, M., Oda, M., Whitehead, K. S., Asimakis, A., Neher, D., and Bradley, D. D. C. (2001). A compact device for the efficient, electrically driven generation of highly circularly polarized light. *Adv. Mater. Weinheim.* 13, 577–580. doi: 10.1002/1521-4095(200104)13:8<577::AID-ADMA577>3.0.CO;2-K
- Han, J., You, J., Li, X., Duan, P., and Liu, M. (2017). Full-color tunable circularly polarized luminescent nanoassemblies of achiral aiegens in confined chiral nanotubes. *Adv. Mater. Weinheim.* 29:1606503. doi: 10.1002/adma.201606503
- Hayashi, K., Miyaoka, Y., Ohishi, Y., Uchida, T., Iwamura, M., Nozaki, K., et al. (2018). Observation of circularly polarized luminescence of the excimer from two perylene cores in the form of [4]rotaxane. *Chem. Eur. J.* 24, 1–5. doi: 10.1002/chem.201803215
- Inouye, M., Hayashi, K., Yonenaga, Y., Itou, T., Fujimoto, K., Uchida, T., et al. (2014). A doubly alkynylpyrene-threaded [4] rotaxane that exhibits strong circularly polarized luminescence from the spatially restricted excimer. *Angew. Chem. Int. Ed.* 53, 14392–14396. doi: 10.1002/anie.201408193
- Kawasaki, T., Sato, M., Ishiguro, S., Saito, T., Morishita, Y., Sato, I., et al. (2005). Enantioselective synthesis of near enantiopure compound by asymmetric autocatalysis triggered by asymmetric photolysis with circularly polarized light. *J. Am. Chem. Soc.* 127, 3274–3275. doi: 10.1021/ja0422108
- Krishnan, S. B., and Gopidas, K. R. (2017). Observation of supramolecular chirality in a hierarchically self-assembled mixed-stack charge-transfer complex. *Chem. Eur. J.* 23, 9600–9606. doi: 10.1002/chem.201701123
- Li, M., Li, S.-H., Zhang, D., Cai, M., Duan, L., Fung, M.-K., et al. (2018a). Stable enantiomers displaying thermally activated delayed fluorescence: efficient OLEDs with circularly polarized electroluminescence. *Angew. Chem. Int. Ed.* 57, 2889–2893. doi: 10.1002/anie.201800198
- Li, M., Lin, W.-B., Fang, L., and Chen, C.-F. (2017). Recent progress on circularly polarized luminescence of chiral organic small molecules. *Acta Chim. Sinica* 75, 1150–1163. doi: 10.6023/A17090440
- Li, M., Zhang, C., Fang, L., Shi, L., Tang, Z., Lu, H.-Y., et al. (2018b). Chiral nanoparticles with full-color and white CPL properties based on optically stable helical aromatic imide enantiomers. *ACS Appl. Mater. Interfaces* 10, 8225–8230. doi: 10.1021/acsami.8b00341
- Liu, M., Zhang, L., and Wang, T. (2015). Supramolecular chirality in self-assembled systems. *Chem. Rev.* 115, 7304–7397. doi: 10.1021/cr500671p
- Maeda, K., Mochizuki, H., Osato, K., and Yashima, E. (2011). Stimuli-responsive helical poly(phenylacetylene)s bearing cyclodextrin pendants that exhibit enantioselective gelation in response to chirality of a chiral amine and hierarchical super-structured helix formation. *Macromolecules* 44, 3217–3226. doi: 10.1021/ma200537p
- Shi, Q., and Chen, C.-F. (2017). Switchable complexation between (O-methyl)<sub>6</sub>-2,6-helic[6]arene and protonated pyridinium salts controlled by acid/base and photoacid. *Org. Lett.* 19, 3175–3178. doi: 10.1021/acs.orglett.7b01296
- Shi, Q., Han, Y., and Chen, C.-F. (2017). Complexation between (O-methyl)<sub>6</sub>-2,6-helic[6]arene and tertiary ammonium salts: acid-base/chloride ion responsive host-guest systems and synthesis of [2]rotaxane. *Chem. Asian J.* 12, 2576–2582. doi: 10.1002/asia.201700857
- Shimada, M., Yamanoi, Y., Ohto, T., Pham, S.-T., Yamada, R., Tada, H., et al. (2017). Multifunctional octamethyltetrasila[2.2]cyclophanes: conformational variations, circularly polarized luminescence, and organic electroluminescence. *J. Am. Chem. Soc.* 139, 11214–11221. doi: 10.1021/jacs.7b05671
- Sun, R., Xue, C., Ma, X., Gao, M., Tian, H., and Li, Q. (2013). Light-driven linear helical supramolecular polymer formed by molecular-recognition-directed self-assembly of bis(p-sulfonatocalix[4]arene) and pseudorotaxane. *J. Am. Chem. Soc.* 135, 5990–5993. doi: 10.1021/ja4016952
- Wang, J.-Q., Li, J., Zhang, G.-W., and Chen, C.-F. (2018). A route to enantiopure (O-methyl)<sub>6</sub>-2,6-helic[6]arenes: synthesis of hexabromo-substituted 2,6-helic[6]arene derivatives and their Suzuki–Miyaura coupling reactions. *J. Org. Chem.* 83, 11532–11540. doi: 10.1021/acs.joc.8b01437
- Xu, Y., Jiang, H., Zhang, Q., Wang, F., and Zou, G. (2014). Helical polydiacetylene prepared in the liquid crystal phase using circular polarized ultraviolet light. *Chem. Commun.* 50, 365–367. doi: 10.1039/C3CC47245K
- Yamaguchi, H., Kobayashi, Y., Kobayashi, R., Takashima, Y., Hashidzume, A., and Harada, A. (2011). A high-rate long-life Li<sub>4</sub>Ti<sub>5</sub>O<sub>12</sub>/Li[Ni<sub>0.45</sub>Co<sub>0.1</sub>Mn<sub>1.45</sub>]O<sub>4</sub> lithium-ion battery. *Nat. Commun.* 2, 511–515. doi: 10.1038/ncomms1527
- Yang, Y., da Costa, R. C., Fuchter, M. J., and Campbell, A. J. (2013). Circularly polarized light detection by a chiral organic semiconductor transistor. *Nat. Photonics* 7, 634–638. doi: 10.1038/NPHOTON.2013.176
- Yoshihara, D., Tsuchiya, Y., Noguchi, T., Yamamoto, T., Dawn, A., and Shinkai, S. (2013). Cyclodextrin-assisted synthesis of a metallosupramolecular terbium(III) polymer and its fluorescence properties and chiral recognition. *Chem. Eur. J.* 19, 15485–15488. doi: 10.1002/chem.201302138
- Zhang, B., Guan, W., Yin, F., Wang, J., Li, B., and Wu, L. (2018). Induced chirality and reversal of phosphomolybdate cluster via modulating its interaction with cyclodextrins. *Dalton Trans.* 47, 1388–1392. doi: 10.1039/C7DT03669H

## AUTHOR CONTRIBUTIONS

This work was done mainly by YG, and the manuscript was written by YG with the guidance of YH and C-FC.

## ACKNOWLEDGMENTS

We thank the National Natural Science Foundation of China (91856117 and 21572233) and the Strategic Priority Research Program of CAS (XDB12010400) for financial support.

## SUPPLEMENTARY MATERIAL

The Supplementary Material for this article can be found online at: <https://www.frontiersin.org/articles/10.3389/fchem.2019.00543/full#supplementary-material>

- Zhang, B., Yue, L.i., Wang, Y., Yang, Y., and Wu, L. (2014). A novel single-side azobenzene-grafted Anderson-type polyoxometalate for recognition-induced chiral migration. *Chem. Commun.* 50, 10823–10826. doi: 10.1039/C4CC04442H
- Zhang, G.-W., Han, Y., Wang, Y.-L., and Chen, C.-F. (2017b). Synthesis of a water-soluble 2,6-helic[6]arene derivative and its strong binding abilities towards quaternary phosphonium salts: an acid/base controlled switchable complexation process. *Chem. Commun.* 53, 10433–10436. doi: 10.1039/C7CC05489K
- Zhang, G.-W., Li, P.-F., Wang, H.-X., Han, Y., and Chen, C.-F. (2017a). Complexation of racemic 2,6-helic[6]arene and its hexamethyl-substituted derivative with quaternary ammonium salts, N-heterocyclic salts, and tetracyanoquinodimethane. *Chem. Eur. J.* 23, 3735–3742. doi: 10.1002/chem.201605394
- Zhang, G.-W., Shi, Q., and Chen, C.-F. (2017c). Formation of charge-transfer complexes based on a tropylium cation and 2, 6-helic[6]arenes: a visible redox stimulus-responsive process. *Chem. Commun.* 53, 2582–2585. doi: 10.1039/C7CC00600D
- Zhang, G. W., Li, P.-F., Meng, Z., Wang, H.-X., Han, Y., and Chen, C.-F. (2016). Triptycene-based chiral macrocyclic hosts for highly enantioselective recognition of chiral guests containing a trimethylamino group. *Angew. Chem. Int. Ed.* 55, 5304–5308. doi: 10.1002/anie.201600911
- Zhang, W., Chen, Y., Yu, J., Zhang, X.-J., and Liu, Y. (2016). Photo/chemo dual-controlled reversible morphological conversion and chiral modulation of supramolecular nanohelices with nanosquares and nanofibers. *Chem. Commun.* 52, 14274–14277. doi: 10.1039/C6CC07089B
- Zhang, Y., Yang, D., Han, J., Zhou, J., Jin, Q., Liu, M., et al. (2018). Circularly polarized luminescence from a pyrene-cyclodextrin supra-dendron. *Langmuir* 34, 5821–5830. doi: 10.1021/acs.langmuir.8b01035

**Conflict of Interest Statement:** The authors declare that the research was conducted in the absence of any commercial or financial relationships that could be construed as a potential conflict of interest.

The handling editor declared a shared affiliation, though no other collaboration, with the authors [YG, YH, C-FC] at time of review.

Copyright © 2019 Guo, Han and Chen. This is an open-access article distributed under the terms of the Creative Commons Attribution License (CC BY). The use, distribution or reproduction in other forums is permitted, provided the original author(s) and the copyright owner(s) are credited and that the original publication in this journal is cited, in accordance with accepted academic practice. No use, distribution or reproduction is permitted which does not comply with these terms.



# Hydroxy-Substituted Azacalix[4]Pyridines: Synthesis, Structure, and Construction of Functional Architectures

En-Xuan Zhang<sup>1</sup>, De-Xian Wang<sup>1,2\*</sup> and Mei-Xiang Wang<sup>3\*</sup>

<sup>1</sup> Beijing National Laboratory for Molecular Sciences, CAS Key Laboratory of Molecular Recognition and Function, Institute of Chemistry, Chinese Academy of Sciences, Beijing, China, <sup>2</sup> School of Chemical Sciences, University of Chinese Academy of Sciences, Beijing, China, <sup>3</sup> The Key Laboratory of Bioorganic Phosphorus Chemistry and Chemical Biology (Ministry of Education), Department of Chemistry, Tsinghua University, Beijing, China

## OPEN ACCESS

### Edited by:

Sébastien Vidal,  
Centre National de la Recherche  
Scientifique (CNRS), France

### Reviewed by:

Dario Pasini,  
University of Pavia, Italy  
Khaleel Assaf,  
Jacobs University Bremen, Germany  
Mark W. Pecuh,  
University of Connecticut,  
United States

### \*Correspondence:

De-Xian Wang  
dxwang@iccas.ac.cn  
Mei-Xiang Wang  
wangmx@mail.tsinghua.edu.cn

### Specialty section:

This article was submitted to  
Supramolecular Chemistry,  
a section of the journal  
Frontiers in Chemistry

Received: 01 June 2019

Accepted: 22 July 2019

Published: 16 August 2019

### Citation:

Zhang E-X, Wang D-X and Wang M-X  
(2019) Hydroxy-Substituted  
Azacalix[4]Pyridines: Synthesis,  
Structure, and Construction of  
Functional Architectures.  
Front. Chem. 7:553.  
doi: 10.3389/fchem.2019.00553

A number of hydroxyl-substituted azacalix[4]pyridines were synthesized using Pd-catalyzed macrocyclic “2+2” and “3+1” coupling methods and the protection-deprotection strategy of hydroxyl group. While the conformation of these hydroxyl-substituted azacalix[4]pyridines is fluxional in solution, in the solid state, they adopted shape-persistent 1,3-alternate conformations. Besides, X-ray analysis revealed that the existence of hydroxy groups on the *para*-position of pyridine facilitated the formation of solvent-bridged intermolecular hydrogen bonding for mono-hydroxyl-substituted while partial tautomerization for four-hydroxyl-substituted macrocycles, respectively. Taking the hydroxyl-substituted azacalix[4]pyridines as molecular platforms, multi-macrocycle-containing architectures and functional building blocks were constructed. The self-assembly behavior of the resulting building blocks was investigated in crystalline state.

**Keywords:** heteracalixaromatics, azacalix[4]pyridine, fragment coupling, functionalization, self-assembly

## INTRODUCTION

Design of ingenious macrocyclic molecules has been one of the driving forces to promote the major advances of supramolecular chemistry, which has been manifested by examples of crownether, cyclodextrin, calixarene, resorcinarene, cucurbituril, calixpyrrole, pillarenes, etc. (Lehn et al., 1996). Indeed, macrocyclic compounds provide unique models in the study of non-covalent interactions, and they have been serving as building blocks in the construction of high-level supramolecular architectures. Typical examples such as by anchoring derivative groups on the macrocycles, versatile building blocks, have been prepared and widely applied to the fabrication of molecular devices and smart materials (Chen and Liu, 2010; Guo and Liu, 2014; Ma and Tian, 2014; Strutt et al., 2014; Caricato et al., 2015; Le Poul et al., 2015; Parisi et al., 2016; Murray et al., 2017; Pazos et al., 2018; Wang, 2018; Ogoshi et al., 2019).

Heteracalixaromatics, or heteroatom-bridged calix(het)arenes, are a new type of macrocyclic host molecules (König and Fonseca, 2000; Lhoták, 2004; Morohashi et al., 2006; Maes and Dehaen, 2008; Wang, 2008, 2012; Thomas et al., 2012; Ma and Chen, 2014; Chen and Han, 2018). In comparison with the classical calix[n]arenes in which the phenol moieties are linked by methylene units, heteracalixaromatics enjoy much richer molecular diversity and complexity as the different combinations of various heteroatoms and heteroaromatic rings afford almost limitless macrocyclic



compounds. Because of the electronic nature of heteroatoms are different from that of carbon and they are able to conjugate differently with their adjacent aromatics, the incorporation of heteroatoms into the bridging positions and aromatic rings endows heteracalixaromatics unique conformational structures and versatile recognition properties. In particular, heteracalixaromatics show unique association property toward ionic species including cations (Gong et al., 2006a; Ma et al., 2009; Zhang et al., 2009; Fang et al., 2012; Wu et al., 2012, 2013), metal clusters (Gao et al., 2011, Gao et al., 2012; Zhang and Zhao, 2018), anions (Wang et al., 2008, 2010; Wang and Wang, 2013; Luo et al., 2018), and neutral molecules (Wang et al., 2004; Gong et al., 2007; Hu and Chen, 2010). Despite the powerful ability as host molecules, surprisingly, the application of heteracalixaromatics as functional building blocks is obviously underexplored. Herein, we report the facile synthesis and structure of a number of hydroxy-substituted azacalix[4]pyridines. These functionalized macrocycles as molecular platform to construct high-level architectures and functional building blocks were also demonstrated.

## RESULTS AND DISCUSSION

### Synthesis

We attempted to synthesize the hydroxyl-substituted macrocycles from deprotection of the 4-methoxyphenyl (PMB) protected macrocycles. The PMB-protected macrocycle could be obtained from a Pd-catalyzed 3 + 1 coupling method. To access the target macrocycles, the mono-PMB-protected macrocycle **3** was initially examined (Scheme 1). **1a**, which was prepared from nucleophilic substitution reaction between 4-(methoxyphenyl)oxy-substituted 2,6-dibromopyridine **1a'** and CH<sub>3</sub>NH<sub>2</sub> (Figure S1), was applied as the monomeric fragment and reacted with a nitrogen-linked linear trimeric aromatic fragment **2a** (Gong et al., 2006b). The effects of catalyst, ligand and solvent, temperature, and concentration of the substrate were carefully examined (Table S1). It was found that Pd<sub>2</sub>(dba)<sub>3</sub> (dba = trans,trans-dibenzylideneacetone) showed higher catalytic efficiency than PdCl<sub>2</sub> and Pd(OAc)<sub>2</sub> (entries 1–3, Table S1). Dppp [1,3-bis(diphenylphosphino)propane] was shown a better ligand than dppe [1,2-bis(diphenylphosphino)ethane], P(c-Hex)<sub>3</sub> (tricyclohexylphosphine), and DPEphos [bis(2-dicyclohexylphosphinophenyl)ether] (entries 3–6, Table S1). Among the tested solvents including THF, 1,4-dioxane, o-xylene, and toluene, toluene turned out to be the best to facilitate the macrocyclization (entries 3 and 7–9, Table S1). Reaction temperature is crucial to the cross-coupling reaction. While lower temperature (70°C and 90°C) had a detrimental effect on the reaction, reaction in refluxing toluene could give the macrocyclic product **3** in chemical yield of 32% (entries 3, 10, and 11, Table S1). When 10% mol Pd<sub>2</sub>(dba)<sub>3</sub>, 20% mol dppp, and monomer **1a** at a concentration of 10 mM were employed in refluxing toluene, the macrocyclization gave the highest chemical yield of 40% (entries 12–20, Table S1).

Encouraged by the synthesis of **3**, the synthesis of other PMB-protected macrocycles was then attempted. We envisioned that the 3 + 1 and 2 + 2 coupling strategy could

be applicable to obtain these macrocycles. Based on such hypothesis, we prepared different 4-(methoxyphenyl)oxy-substituted di-bromopyridine and di-methylaminopyridine fragments, respectively (Figure S1). Pleasantly, both 3 + 1 and 2 + 2 cross-coupling methods worked equally well. Under the optimized conditions for synthesis **3**, the macrocycles **6–9** bearing different numbers ( $n = 2–4$ ) of (4-methoxybenzyl)oxy groups were obtained in acceptable yields (30–34%) (Table 1).

For the synthesis of hydroxyl-substituted azacalix[4]pyridines **10–14**, the Pb/C-catalyzed hydrogenation reactions were performed on the different protected macrocycles. As shown in Scheme 2, all the reactions proceeded with high efficiency to afford the desired products in the yields ranging from 95 to 99%.

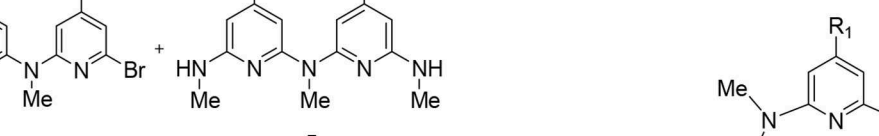
### Structure

The characterization of **10–14** was established on spectroscopic data and elemental analysis. In solution, all the macrocyclic compounds gave one set of <sup>1</sup>H and <sup>13</sup>C NMR signals, indicating that they are very fluxional at room temperature and the various conformational structures most probably interconvert rapidly relative to the NMR time scale (Figures S2, S3). Under decreased temperatures (from 298 to 178 K), the conformational interconversion became slow and coexistence of different conformations was clearly observed at 178 K (Figure S4). To probe the structure in solid state, single crystals were cultivated and analyzed by X-ray diffraction method. Pleasantly, slow evaporation of the solutions of **10** (Supplementary Data Sheet 2) and **14** (Supplementary Data Sheet 3) produced single crystals with high quality; the structural details are demonstrated in Figures 1, 2, and Table S2 respectively. In the case of **10**, the molecule shows a similar 1,3-alternate conformation with other azacalix[4]pyridines (Figures 1A,B). While the existence of hydroxyl group on the *para*-position of one pyridine does not affect the conformation of the macrocyclic backbone; it leads to interesting hydrogen-bonded packing. For example, each hydroxyl group as hydrogen bond donor interacts with the oxygen of DMSO; an infinite DMSO-separated layer structure is then produced (Figure 1C).

Surprisingly, the structure crystallized from **14** might not be this compound itself. Representative parameters such as two of the C–O distances ( $d_{C8-O2} = 1.291 \text{ \AA}$ ) is shorter than the other pair ( $d_{C3-O1} = 1.349 \text{ \AA}$ ). The former distance is typical of C = O double bond, while the latter is C–O single bond as expected (Figure 2). Besides, a dimer structure linked by an O2–O1–O3–O2 hydrogen bonding network could be observed. Here, O2 serves as a hydrogen bond acceptor while the hydroxyl group (O1) or a water molecule (O3) serves as a hydrogen bond donor (Figure 2B). The function of O2 in the hydrogen bonding network is consistent with the nature of carbonyl oxygen. These structural features therefore indicate that the obtained structure is a partially tautomerized compound **14'**, i.e., two of the 4-hydroxyl pyridine of **14** turn to pyridine-4-one moieties. As in solution, **14** gives one set of NMR signals, and the partial tautomerization product is most probably facilitated in solid state (Scheme 3).



**2+2**



**4** + **5** → **6-9**

**3+1**

**2** + **1** → **6-9**

or

$\text{Pd}_2(\text{dba})_3$ , dppp

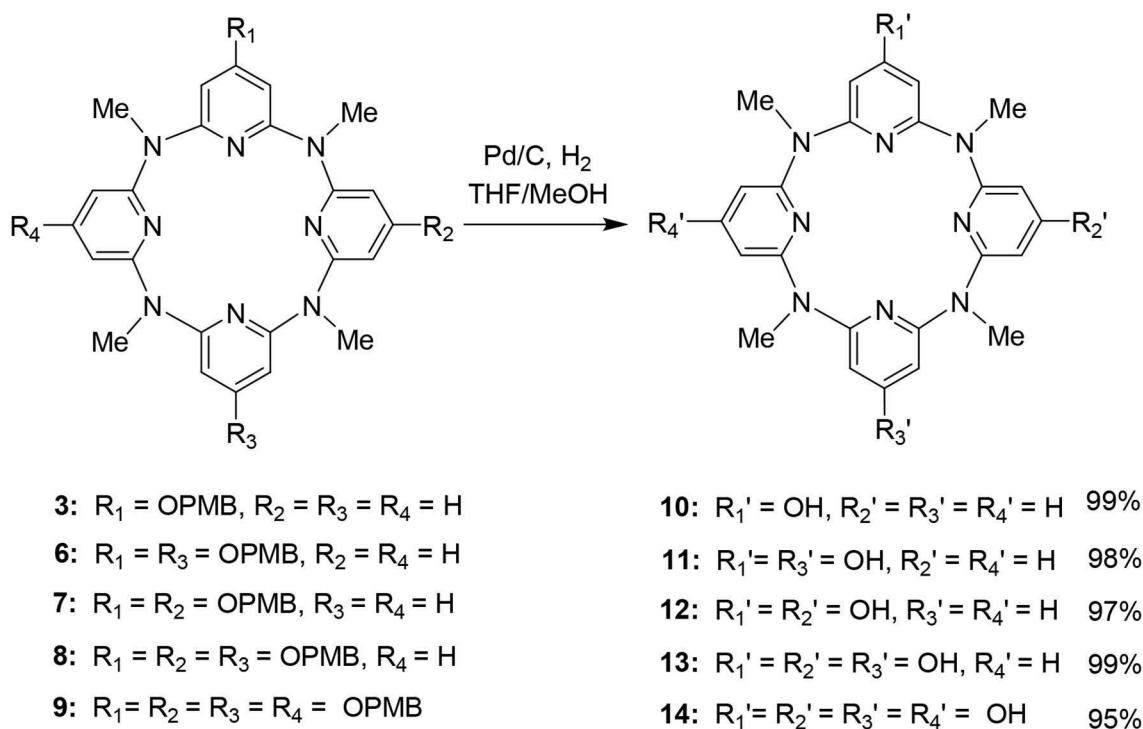
$t\text{-BuONa}$ , toluene

reflux, 5h

<sup>a</sup> Isolated yields.

On the other hand, we applied **14** as the starting materials to react with pyridine-2-acylchloride hydrochloride **19** and pyridine-4-acylchloride hydrochloride **20**, respectively. The reactions in the presence of trimethylammonium in  $\text{CH}_2\text{Cl}_2$

The introduction of the pyridine substituents on azacalix[4]pyridine provides diverse binding sites to facilitate intermolecular self-assembly. To demonstrate the application of the functional building blocks, the self-assembly of **21** and **22** in crystalline state was investigated (**Table S3**). It is worth addressing that the different pyridine substituents caused significant changes in the conformations. In the case of **21**, the azacalix[4]pyridine backbone maintains the typical 1,3-alternate conformation, i.e., two of the pyridines tend to be edge-to-edge flattened while the other two pyridines tend to be face-to-face paralleled (**Figure 3A**). For **22**, the molecule exhibits a non-typical orthorhombic 1,3-alternate conformation (**Figure 4A**). Moreover, due to the different shapes of the building block and different position of nitrogen



**SCHEME 2** | Synthesis of hydroxyl-substituted azacalix[4]pyridines **10–14**.

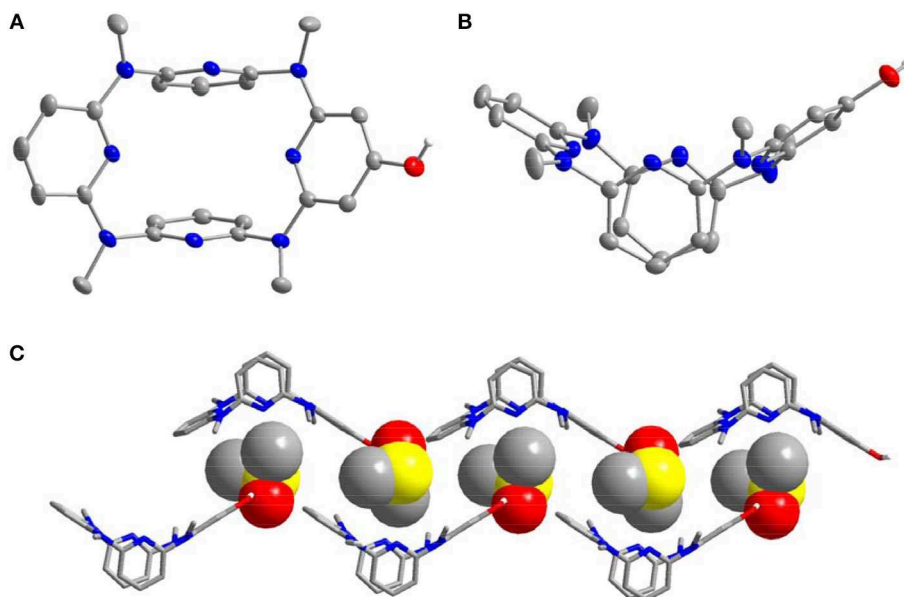


**FIGURE 1** | Crystal structure of **10**, top view (A) and side view (B), DMSO-separated layer structure through hydrogen bonding (C). Probability is 25%, parts of the hydrogens are omitted for clarity.

on the substituent pyridines, the intermolecular hydrogen bonding between pyridine-N and pyridine-H yielded different 2D networks for **21** (Supplementary Data Sheet 4) and **22** (Supplementary Data Sheet 5), respectively. For building

block **21**, hydrogen bonding is formed between the substituent pyridines; the interaction of pyridine-N with pyridine-2-H or pyridine-4-H contributes to the formation of hydrogen bond network (Figure 3B), while for **22**, the substituent pyridine-N

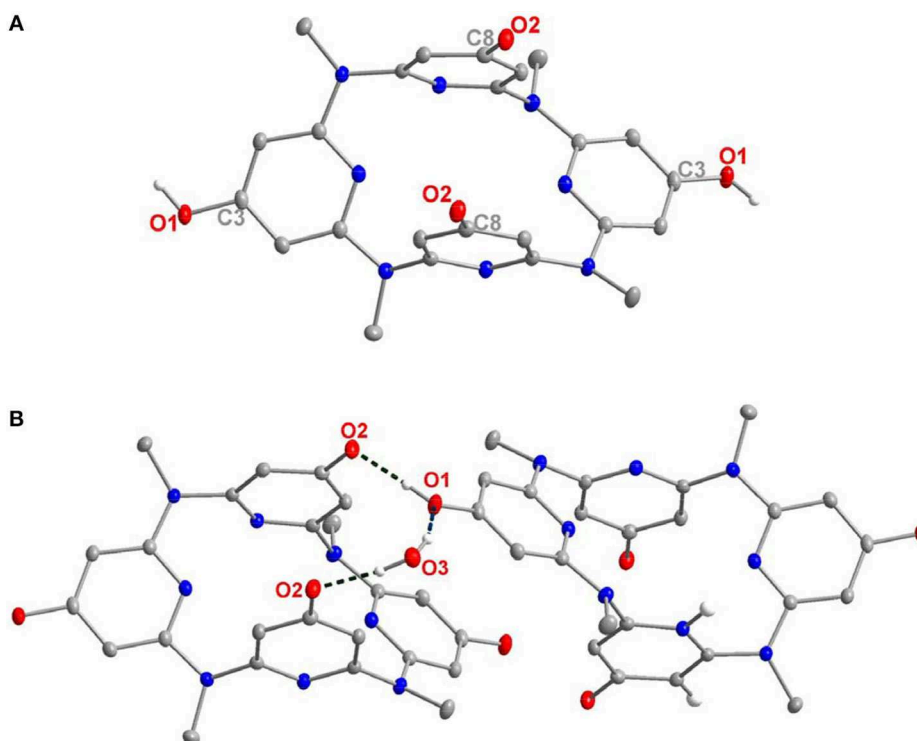
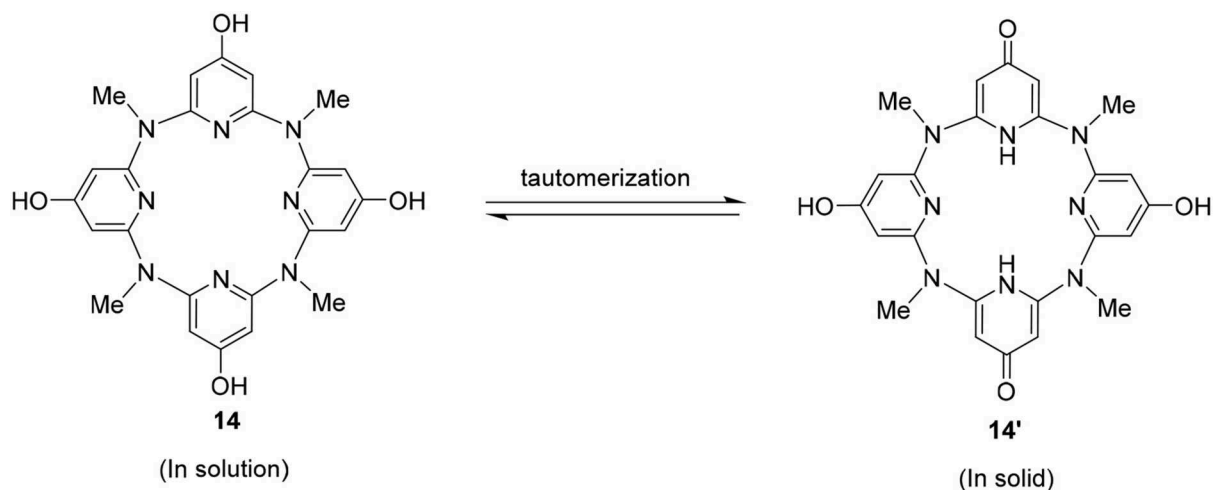


**FIGURE 2 |** Crystal structure of **14'**, top view **(A)** and dimer structure linked by hydrogen bonding network **(B)**. Selected bond length (Å): C8–O2 1.291, C3–O1 1.349. Selected distance (Å): O2–O1 2.574, O2–O3 2.700, O3–O1 2.887.



**SCHEME 3 |** Tautomerization of **14**.

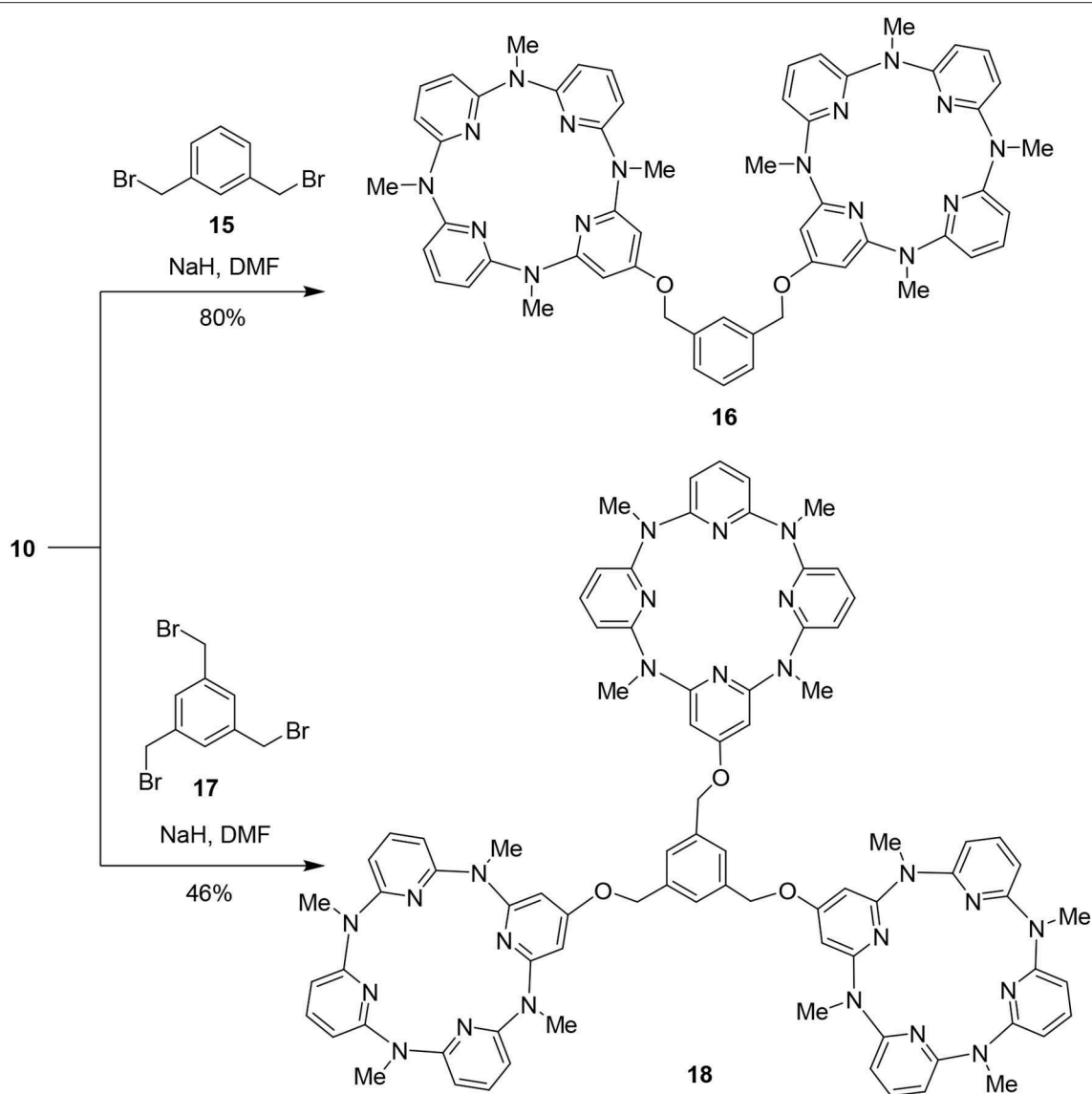
forms hydrogen bond with the aryl hydrogen of pyridine on the backbone, which produces network with rhombic porosity (**Figure 4B**).

## CONCLUSION

In summary, we have synthesized hydroxyl-substituted azacalix[4]pyridines using an efficient protection–deprotection

strategy and Pd-catalyzed macrocyclic “2+2” and “3+1” coupling methods. The unique structure and tautomerization of the macrocycle in solid state were revealed by X-ray analysis. This work demonstrated that the synthesized macrocycles could be useful molecular platforms for highly efficient construction of multi-macrocycle-containing architectures and functional building blocks. The high-level architectures and the functional building blocks could find the potential application in





**SCHEME 4** | Synthesis of di- and tri-cavity architectures **16** and **18**.

fabricating supramolecular or metal-organic porous framework in the future.

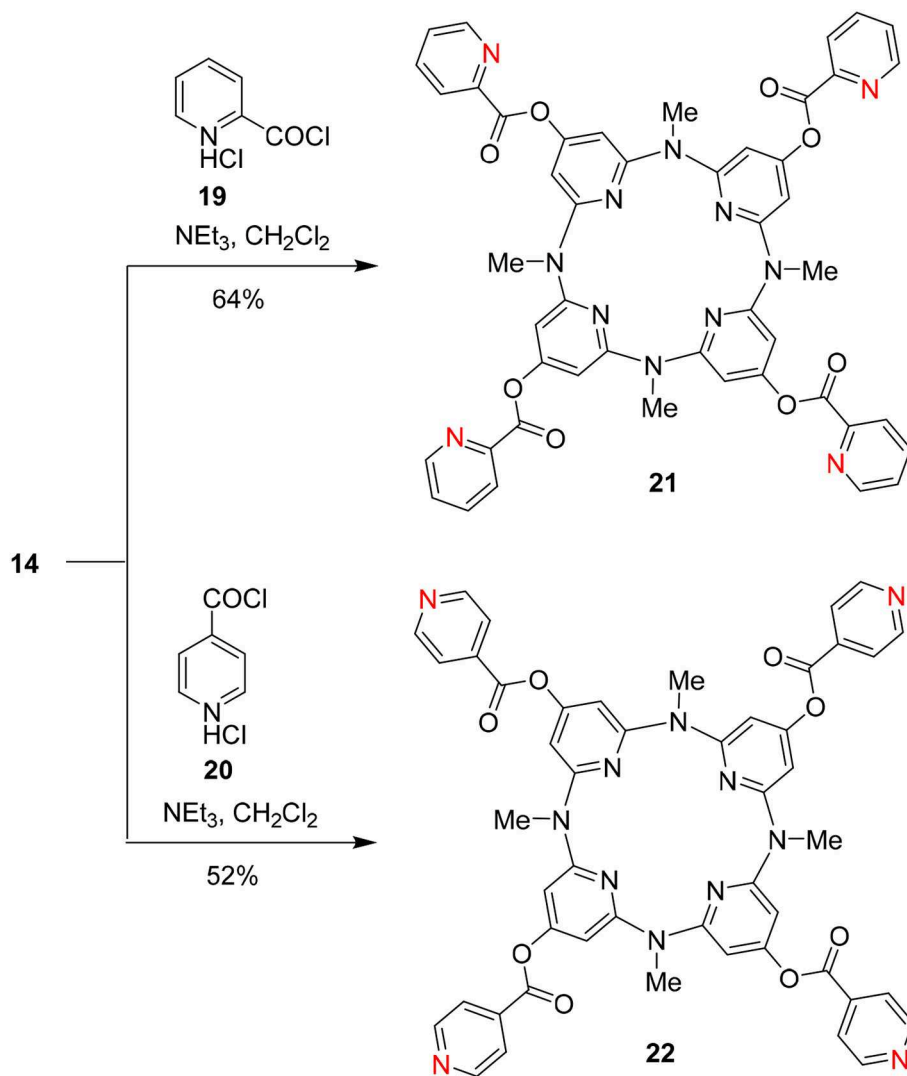
## EXPERIMENTAL

### General Information

Chemical shifts are reported in parts per million vs. tetramethylsilane with either tetramethylsilane or the residual solvent resonance used as an internal standard. Melting points are uncorrected. Elemental analyses, mass spectrometry, and X-ray crystallography were performed at the Analytical Laboratory of the Institute. All solvents were dried according to standard procedures prior to use. All other major chemicals were obtained from commercial sources and used without further purification.

### General Procedure for the Synthesis of (4-methoxybenzyl)Oxy-substituted Macrocycles **3**, **6–9**

Under argon protection, a mixture of di-methylaminopyridine fragment (2 mmol) and di-bromopyridine fragment (2.2 mmol),  $\text{Pd}_2(\text{dba})_3$  (184 mg, 0.2 mmol), dppp (164 mg, 0.2 mmol), and sodium tert-butoxide (576 mg, 3 mmol) in anhydrous toluene (400 ml) was heated at reflux for 5 h. The reaction mixture was cooled down to room temperature and filtered through a Celite pad. The filtrate was concentrated under vacuum to remove toluene and the residue was dissolved in dichloromethane (50 ml) and washed with brine ( $3 \times 15$  ml). The aqueous phase was re-extracted with dichloromethane ( $3 \times 20$  ml), and the combined organic phase was dried over anhydrous  $\text{Na}_2\text{SO}_4$ . After removal of solvent, the residue was



**SCHEME 5** | Construction of functional building blocks **21** and **22**.

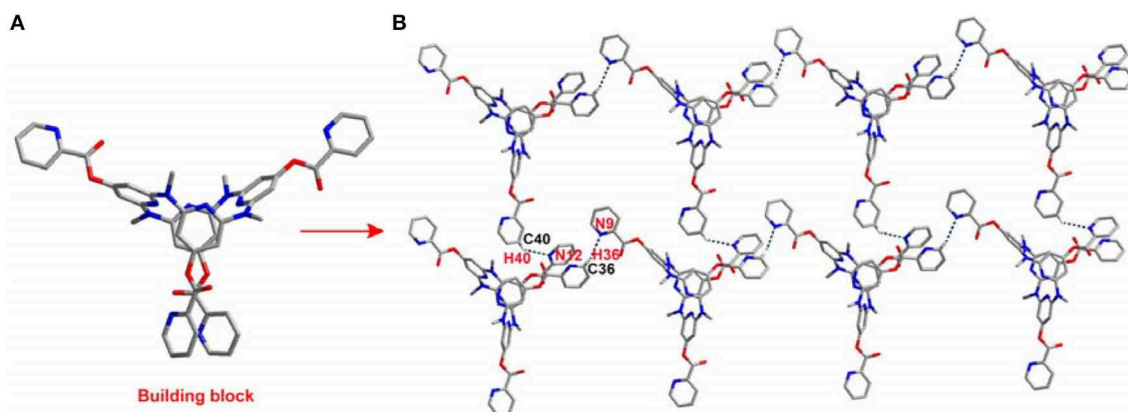


**FIGURE 3** | Self-assembly of **21**, (A) side view of building block and (B) self-assembly structure. Selected hydrogen bonding distance (Å):  $\text{N9} \cdots \text{H36}$  2.721,  $\text{N12} \cdots \text{H40}$  2.626. Selected hydrogen bonding angle (°):  $\text{N9-H36-C36}$  159.6,  $\text{N12-H40-C40}$  139.5.

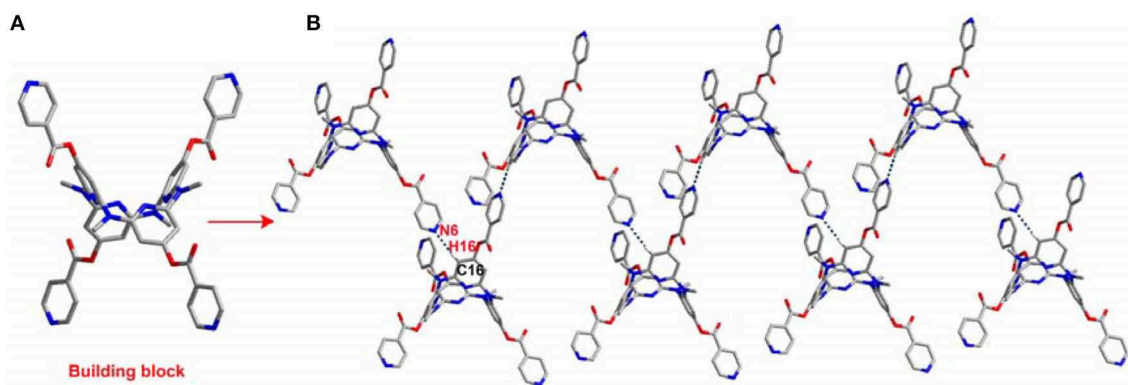


**FIGURE 4 |** Self-assembly of **22**, **(A)** side view of building block and **(B)** self-assembly structure. Selected hydrogen bonding distance (Å): N6...H16 2.555. Selected hydrogen bonding angle (°): N6-H16-C16 172.3.

chromatographed on a silica gel column (100–200) with a mixture of petroleum ether and acetone as the mobile phase to give the products.

#### (4-Methoxybenzyl)Oxy-Substituted Macrocycle 3

A white solid (449 mg, 40% yield); mp 191–193°C;  $^1\text{H}$  NMR (300 MHz,  $\text{CDCl}_3$ )  $\delta$  7.39–7.32 (m, 5H), 6.94 (d,  $J = 8.7$  Hz, 2H), 6.39 (d,  $J = 8.7$  Hz, 2H), 6.34–6.30 (m, 4H), 6.04 (s, 2H), 4.97 (s, 2H), 3.82 (s, 3H), 3.20 (s, 6H), 3.17 (s, 6H);  $^{13}\text{C}$  NMR (75 MHz,  $\text{CDCl}_3$ )  $\delta$  167.2, 160.2, 159.6, 159.2, 159.0, 138.3, 137.8, 129.2, 128.5, 114.1, 109.5, 107.5, 96.9, 69.4, 55.3, 36.6; IR (KBr)  $\nu$  1,578, 1,559, 1,515, and 1,473  $\text{cm}^{-1}$ ; MS (MALDI-TOF)  $m/z$  (%) 599  $[\text{M}+\text{K}]^+$  (28), 583  $[\text{M}+\text{Na}]^+$  (50), 561  $[\text{M}+\text{H}]^+$  (100). Anal. Calcd. for  $\text{C}_{32}\text{H}_{32}\text{N}_8\text{O}_2$ : C, 68.55; H, 5.75; N, 19.99. Found: C, 68.49; H, 5.83; N, 19.91.

#### (4-Methoxybenzyl)Oxy-substituted Macrocycle 6

A white solid (457 mg, 33% yield); mp 273–274°C;  $^1\text{H}$  NMR (300 MHz,  $\text{CDCl}_3$ ) 7.35 (t,  $J = 7.8$  Hz, 2H), 7.30 (d,  $J = 8.6$  Hz, 4H), 6.86 (d,  $J = 8.6$  Hz, 4H), 6.42 (d,  $J = 7.8$  Hz, 4H), 5.96 (s, 4H), 4.96 (s, 4H), 3.81 (s, 6H), 3.18 (s, 12H);  $^{13}\text{C}$  NMR (75 MHz,  $\text{CDCl}_3$ )  $\delta$  167.7, 160.2, 159.5, 159.1, 138.0, 129.2, 128.7, 114.0, 111.9, 92.4, 69.4, 55.2, 36.6; IR (KBr)  $\nu$  1,580, 1,559, and 1,515  $\text{cm}^{-1}$ ; MS (MALDI-TOF)  $m/z$  (%) 719  $[\text{M}+\text{Na}]^+$  (40), 697  $[\text{M}+\text{H}]^+$  (100). Anal. Calcd. for  $\text{C}_{40}\text{H}_{40}\text{N}_8\text{O}_4$ : C, 68.95; H, 5.79; N, 16.08. Found: C, 68.77; H, 5.49; N, 16.28.

#### (4-Methoxybenzyl)Oxy-substituted Macrocycle 7

A white solid (415 mg, 30% yield); mp 98–99°C;  $^1\text{H}$  NMR (300 MHz,  $\text{CDCl}_3$ ) 7.38 (d,  $J = 8.5$  Hz, 4H), 7.35 (t,  $J = 7.8$  Hz, 2H), 6.94 (d,  $J = 8.5$  Hz, 4H), 6.37 (d,  $J = 7.8$  Hz, 2H), 6.36 (d,  $J = 7.8$  Hz, 2H), 6.01 (s, 2H), 6.00 (s, 2H), 4.97 (s, 4H), 3.82 (s, 6H), 3.21 (s, 3H), 3.18 (s, 6H), 3.15 (s, 3H);  $\delta$  167.3, 160.1, 159.6, 159.1, 137.9, 129.3, 128.4, 114.1, 108.6, 95.9, 69.4, 55.4, 36.6; IR (KBr)  $\nu$  1,581, 1,560, 1,514, and 1,468  $\text{cm}^{-1}$ ; MS (MALDI-TOF)  $m/z$  (%) 735  $[\text{M}+\text{K}]^+$  (6), 719  $[\text{M}+\text{Na}]^+$  (14), 697  $[\text{M}+\text{H}]^+$  (100). Anal. Calcd. for  $\text{C}_{40}\text{H}_{40}\text{N}_8\text{O}_4$ : C, 68.95; H, 5.79; N, 16.08. Found: C, 68.75; H, 5.70; N, 16.21.

#### (4-Methoxybenzyl)Oxy-substituted Macrocycle 8

A white solid (566 mg, 34% yield); mp 101–102°C;  $^1\text{H}$  NMR (300 MHz,  $\text{CDCl}_3$ ) 7.37 (d,  $J = 8.6$  Hz, 2H), 7.30 (t,  $J = 7.8$  Hz, 1H), 7.29 (d,  $J = 8.6$  Hz, 4H), 6.94 (d,  $J = 8.6$  Hz, 2H), 6.86 (d,  $J = 8.6$  Hz, 4H), 6.45 (d,  $J = 7.8$  Hz, 2H), 6.10 (s, 2H), 5.93 (s, 2H), 5.92 (s, 2H), 4.96 (s, 6H), 3.82 (s, 3H), 3.80 (s, 6H), 3.18 (s, 6H), 3.14 (s, 6H);  $^{13}\text{C}$  NMR (75 MHz,  $\text{CDCl}_3$ )  $\delta$  167.7, 166.8, 160.2, 160.1, 159.7, 159.4, 159.1, 137.5, 129.3, 129.2, 128.6, 128.4, 114.2, 114.0, 112.6, 100.0, 91.7, 69.4, 55.3(4), 55.2(8), 36.6; IR (KBr)  $\nu$  1,583, 1,559, and 1,514  $\text{cm}^{-1}$ ; MS (MALDI-TOF)  $m/z$  (%) 871  $[\text{M}+\text{K}]^+$  (1), 855  $[\text{M}+\text{Na}]^+$  (26), 833  $[\text{M}+\text{H}]^+$  (100). Anal. Calcd. for  $\text{C}_{48}\text{H}_{48}\text{N}_8\text{O}_6$ : C, 69.21; H, 5.81; N, 13.45. Found: C, 69.19; H, 5.93; N, 13.45.

#### (4-Methoxybenzyl)Oxy-substituted Macrocycle 9

A white solid (620 mg, 32% yield); mp 203–204°C;  $^1\text{H}$  NMR (300 MHz,  $\text{CDCl}_3$ ) 7.26 (d,  $J = 8.6$  Hz, 8H), 6.83 (d,  $J = 8.6$  Hz, 8H), 6.03 (s, 8H), 4.92 (s, 8H), 3.79 (s, 12H), 3.16 (s, 12H);  $^{13}\text{C}$  NMR (75 MHz,  $\text{CDCl}_3$ )  $\delta$  167.4, 160.1, 159.4, 129.3, 128.5, 113.9, 95.7, 69.4, 55.2, 36.8; IR (KBr)  $\nu$  1,583, 1,559, and 1,514  $\text{cm}^{-1}$ ; MS (MALDI-TOF)  $m/z$  (%) 991  $[\text{M}+\text{Na}]^+$  (39), 969  $[\text{M}+\text{H}]^+$  (100). Anal. Calcd. for  $\text{C}_{56}\text{H}_{56}\text{N}_8\text{O}_8$ : C, 69.41; H, 5.82; N, 11.56. Found: C, 69.29; H, 5.89; N, 11.63.

#### General Procedure for the Synthesis of Hydroxyl-Substituted Azacalix[4]pyridines 10–14

Under nitrogen protection, Pd/C (150 mg, 10 wt%) was added rapidly in a 100-ml round bottom flask with a mixture of PMB-protected macrocycles (2 mmol), THF (20 ml), and methanol (20 ml). The flask was switched three times with hydrogen balloon. The reaction was stopped after reacting at room temperature for 24 h. The reaction mixture was worked up in two ways. Method A: After filtration of the catalyst and removal of the solvent, the residue was chromatographed on a silica gel column (100–200) with a mixture of dichloromethane and methanol as the mobile phase to give the product. Method B: Before filtration of catalyst, the concentrated aqueous ammonia solution was added to the reaction mixture to dissolve the precipitated product. After filtration of the catalyst and removal of the solvent,

acetone was added to slurry the residue. The solid was filtered out and washed with a small amount of acetone and dried to give the product.

### Hydroxyl-Substituted Azacalix[4]pyridine 10

Workup by method A, the product was a white solid (872 mg, 99% yield): 260–262°C;  $^1\text{H}$  NMR (300 MHz,  $d_6$ -DMSO) 10.05 (s, 1H), 7.49–7.40 (m, 3H), 6.40–6.34 (m, 6H), 5.82 (s, 2H), 3.10 (s, 6H), 3.03 (s, 6H);  $^{13}\text{C}$  NMR (75 MHz,  $d_6$ -DMSO)  $\delta$  166.2, 159.4, 158.4, 158.3, 158.2, 138.6, 138.3, 108.4, 108.2, 96.5, 36.2; IR (KBr)  $\nu$  3,388, 1,578, and 1,470  $\text{cm}^{-1}$ ; MS (MALDI-TOF)  $m/z$  (%) 479  $[\text{M}+\text{K}]^+$  (5), 463  $[\text{M}+\text{Na}]^+$  (45), 441  $[\text{M}+\text{H}]^+$  (100). Anal. Calcd. for  $\text{C}_{24}\text{H}_{24}\text{N}_8\text{O}$ : C, 65.44; H, 5.49; N, 25.44. Found: C, 65.21; H, 5.54; N, 25.34.

### Hydroxyl-Substituted Azacalix[4]pyridine 11

Workup by method A, the product was obtained as a white solid (904 mg, 99% yield): > 300°C;  $^1\text{H}$  NMR (300 MHz,  $d_6$ -DMSO) 9.93 (s, 2H), 7.39 (t,  $J = 7.7$  Hz, 2H), 6.48 (d,  $J = 7.7$  Hz, 4H), 5.70 (s, 4H), 3.03 (s, 12H);  $^{13}\text{C}$  NMR (75 MHz,  $d_6$ -DMSO)  $\delta$  166.6, 159.4, 158.5, 138.0, 116.2, 88.6, 36.3; IR (KBr)  $\nu$  3,368, 3,260, 1,588, and 1,475  $\text{cm}^{-1}$ ; MS (MALDI-TOF)  $m/z$  (%) 495  $[\text{M}+\text{K}]^+$  (5), 479  $[\text{M}+\text{Na}]^+$  (20), 457  $[\text{M}+\text{H}]^+$  (100). exact mass (HRESI) found 457.2092,  $\text{C}_{24}\text{H}_{25}\text{N}_8\text{O}_2$  requires: 457.2095.

### Hydroxyl-Substituted Azacalix[4]pyridine 12

Workup by method A, the product was obtained as a white solid (886 mg, 97% yield): 239–241°C;  $^1\text{H}$  NMR (300 MHz,  $d_6$ -DMSO) 10.08 (s, 2H), 7.46 (t,  $J = 7.8$  Hz, 2H), 6.41 (d,  $J = 7.8$  Hz, 2H), 6.38 (d,  $J = 7.8$  Hz, 2H), 5.85 (s, 4H), 3.12 (s, 3H), 3.05 (s, 6H), 2.99 (s, 3H);  $^{13}\text{C}$  NMR (75 MHz,  $d_6$ -DMSO)  $\delta$  158.1, 138.3, 108.3, 96.8, 36.3, 36.2; IR (KBr)  $\nu$  3,401, 1,573, and 1,477  $\text{cm}^{-1}$ ; MS (MALDI-TOF)  $m/z$  (%) 479  $[\text{M}+\text{Na}]^+$  (25), 457  $[\text{M}+\text{H}]^+$  (100). Exact mass (HRESI) found 457.2094,  $\text{C}_{24}\text{H}_{25}\text{N}_8\text{O}_2$  requires: 457.2095.

### Hydroxyl-Substituted Azacalix[4]pyridine 13

Workup by method A, the product was obtained as a white solid (936 mg, 99% yield): > 300°C;  $^1\text{H}$  NMR (300 MHz,  $d_6$ -DMSO) 10.08 (s, 1H), 9.90 (s, 2H), 7.41 (t,  $J = 7.8$  Hz, 1H), 6.49 (d,  $J = 7.8$  Hz, 2H), 5.92 (s, 2H), 5.67 (s, 2H), 5.64 (s, 2H), 3.06 (s, 6H), 2.96 (s, 6H);  $^{13}\text{C}$  NMR (75 MHz,  $d_6$ -DMSO)  $\delta$  166.6, 165.4, 159.5, 159.4, 159.3, 158.4, 137.3, 116.2, 104.5, 88.5, 36.3; IR (KBr)  $\nu$  3,259, 1,586, and 1,477  $\text{cm}^{-1}$ ; MS (MALDI-TOF)  $m/z$  (%) 495  $[\text{M}+\text{Na}]^+$  (100), 473  $[\text{M}+\text{H}]^+$  (20). Exact mass (HRESI) found 473.2033,  $\text{C}_{24}\text{H}_{25}\text{N}_8\text{O}_3$  requires: 473.2044.

### Hydroxyl-Substituted Azacalix[4]pyridine 14

Workup by method B, the product was obtained as a white solid (928 mg, 95% yield): > 300°C;  $^1\text{H}$  NMR (300 MHz,  $d_6$ -DMSO) 9.90 (s, 4H), 5.79 (s, 8H), 2.96 (s, 12H);  $^{13}\text{C}$  NMR (75 MHz,  $d_6$ -DMSO)  $\delta$  166.0, 159.4, 95.9, 36.6; IR (KBr)  $\nu$  3,512, 3,398, 1,578, and 1,490  $\text{cm}^{-1}$ ; MS (MALDI-TOF)  $m/z$  (%) 511  $[\text{M}+\text{Na}]^+$  (74), 489  $[\text{M}+\text{H}]^+$  (100). Exact mass (HRESI) found 489.1983,  $\text{C}_{24}\text{H}_{25}\text{N}_8\text{O}_4$  requires: 489.1993.

### Preparation of Di-Cavity Compound 17

To a solution of **10** (92.5 mg, 0.21 mmol) in dry DMF (2 ml) at room temperature was added NaH (7.2 mg, 0.3 mmol) slowly and the mixture was agitated for 1 h. 1,3-Bis(bromomethyl)benzene **15** (26 mg, 0.1 mmol) was added to the mixture slowly and the reaction mixture was agitated for another 4 h, and then water (20 mL) was added and extracted by ethyl acetate ( $3 \times 20$  ml). The organic phase was washed by saturated brine ( $2 \times 20$  ml) and dried over anhydrous  $\text{Na}_2\text{SO}_4$ . After removal of solvent, the residue was chromatographed on a silica gel column (100–200) with a mixture of dichloromethane and ethyl acetate as the mobile phase to give pure **16** (79 mg, 80%) as a white solid: 253–254°C;  $^1\text{H}$  NMR (300 MHz,  $\text{CDCl}_3$ ) 7.56 (s, 1H), 7.46–7.45 (m, 3H), 7.35 (t,  $J = 7.8$  Hz, 6H), 6.38 (d,  $J = 7.8$  Hz, 4H), 6.35 (d,  $J = 7.8$  Hz, 4H), 6.33 (d,  $J = 7.8$  Hz, 4H), 6.04 (s, 4H), 5.10 (s, 4H), 3.20 (s, 12H), 3.17 (s, 12H);  $^{13}\text{C}$  NMR (75 MHz,  $\text{CDCl}_3$ )  $\delta$  167.1, 160.2, 159.1, 159.0, 158.9, 138.4, 137.9, 137.0, 129.1, 127.2, 126.4, 108.8, 108.2, 96.1, 69.3, 36.6; IR (KBr)  $\nu$  1,583  $\text{cm}^{-1}$ ; MS (MALDI-TOF)  $m/z$  (%) 1,005  $[\text{M}+\text{Na}]^+$  (7), 983  $[\text{M}+\text{H}]^+$  (100). Anal. Calcd. for  $\text{C}_{56}\text{H}_{54}\text{N}_{16}\text{O}_2$ : C, 68.41; H, 5.54; N, 22.80. Found: C, 68.44; H, 5.55; N, 22.71.

### Preparation of Tri-Cavity Compound 18

Compound **18** was prepared from **10** and 1,3,5-tribromomesitylene **17** by a similar procedure to the synthesis of **16**. Quantities: **10** (132 mg, 0.3 mmol), NaH (10.8 mg, 0.45 mmol), 1,3,5-tribromomesitylene **17** (35.7 mg, 0.1 mmol), and DMF (2 mL). The product was obtained as a light yellow solid (66 mg, 46%): 208–210°C;  $^1\text{H}$  NMR (300 MHz,  $\text{CDCl}_3$ ) 7.54 (s, 3H), 7.38–7.33 (m, 9H), 6.39–6.35 (m, 18H), 6.04 (s, 6H), 5.14 (s, 6H), 3.20 (s, 18H), 3.18 (s, 18H);  $^{13}\text{C}$  NMR (75 MHz,  $\text{CDCl}_3$ )  $\delta$  167.1, 160.1, 159.1, 159.0, 158.9, 138.4, 138.0, 137.6, 125.9, 108.8(1), 108.7(6), 108.4, 95.6, 69.1, 36.6(4), 36.6(2); IR (KBr)  $\nu$  1,582  $\text{cm}^{-1}$ ; MS (MALDI-TOF)  $m/z$  (%) 1,473  $[\text{M}+\text{K}]^+$  (2), 1,457  $[\text{M}+\text{Na}]^+$  (9), 1,435  $[\text{M}+\text{H}]^+$  (100). Anal. Calcd. for  $\text{C}_{81}\text{H}_{78}\text{N}_{24}\text{O}_3$ : C, 67.77; H, 5.48; N, 23.42. Found: C, 67.60; H, 5.58; N, 23.02.

### Preparation of Functional Building Block 21

To a solution of **14** (98 mg, 0.2 mmol) in dry dichloromethane (20 ml) at room temperature was added pyridine-2-acylchloride hydrochloride **19** (156 mg, 0.88 mmol) and triethylamine (0.55 ml). After reacting for 24 h, the reaction mixture was washed by saturated  $\text{Na}_2\text{CO}_3$  solution (10 ml) and saturated brine ( $3 \times 20$  ml) and then dried over anhydrous  $\text{Na}_2\text{SO}_4$ . After removal of solvent, the residue was crystallized by dichloromethane and ethyl acetate to give pure **21** as a light yellow solid (117 mg, 64%): > 300°C;  $^1\text{H}$  NMR (300 MHz,  $\text{CDCl}_3$ ) 8.68 (d,  $J = 4.6$  Hz, 4H), 8.13 (d,  $J = 7.8$  Hz, 4H), 7.76–7.70 (m, 4H), 7.44–7.39 (m, 4H), 6.50 (s, 8H), 3.25 (s, 12H);  $^{13}\text{C}$  NMR (75 MHz,  $\text{CDCl}_3$ )  $\delta$  162.5, 160.1, 159.8, 150.0, 147.2, 137.0, 127.2, 125.8, 102.2, 36.8; IR (KBr)  $\nu$  1,763, 1,744, and 1,581  $\text{cm}^{-1}$ ; MS (ESI)  $m/z$  (%) 931  $[\text{M}+\text{Na}]^+$  (100), 909  $[\text{M}+\text{H}]^+$  (86). Exact mass (HRESI) found 909.2828,  $\text{C}_{48}\text{H}_{37}\text{N}_{12}\text{O}_8$  requires: 909.2852.



## Preparation of Functional Building Block 22

Compound **22** was prepared from **14** and pyridine-4-acylchloride hydrochloride **20** by a similar procedure to the synthesis of **21**. Quantities: **14** (195 mg, 0.4 mmol), **20** (331 mg, 1.76 mmol), dichloromethane (20 ml), and triethylamine (1.11 ml). The product was obtained as a light yellow solid (190 mg, 52%): 289–291°C;  $^1\text{H}$  NMR (300 MHz,  $\text{CDCl}_3$ ) 8.74 (d,  $J = 6.0$  Hz, 8H), 7.84 (d,  $J = 6.0$  Hz, 8H), 6.46 (s, 8H), 3.26 (s, 12H);  $^{13}\text{C}$  NMR (75 MHz,  $\text{CDCl}_3$ )  $\delta$  162.5, 159.8, 159.7, 150.7, 136.4, 123.0, 101.9, 36.8; IR (KBr)  $\nu$  1,748, 1,607, and 1,571  $\text{cm}^{-1}$ ; MS (ESI)  $m/z$  (%) 931  $[\text{M}+\text{Na}]^+$  (100), 909  $[\text{M}+\text{H}]^+$  (40). Exact mass (HRESI) found 909.2848,  $\text{C}_{48}\text{H}_{37}\text{N}_{12}\text{O}_8$  requires: 909.2852.

## DATA AVAILABILITY

The raw data supporting the conclusions of this manuscript will be made available by the authors, without undue reservation, to any qualified researcher.

## REFERENCES

- Caricato, M., Delforge, A., Bonifazi, D., Dondi, D., Mazzanti, A., and Pasini, D. (2015). Chiral nanostructuring multivalent macrocycles in solution and on surfaces. *Org. Biomol. Chem.* 13, 3593–3601. doi: 10.1039/c4ob02643h
- Chen, C.-F., and Han, Y. (2018). Triptycene-derived macrocyclic arenes: from calixarenes to helicenes. *Acc. Chem. Res.* 51, 2093–2106. doi: 10.1021/acs.accounts.8b00268
- Chen, Y., and Liu, Y. (2010). Cyclodextrin-based bioactive supramolecular assemblies. *Chem. Soc. Rev.* 39, 495–505. doi: 10.1039/b816354p
- Fang, Y.-X., Zhao, L., Wang, D.-X., and Wang, M.-X. (2012). Synthesis, structure and metal binding property of internally 1,3-arylene-bridged azacalix[6]aromatics. *J. Org. Chem.* 77, 10073–10082. doi: 10.1021/jo301528f
- Gao, C.-Y., Zhao, L., and Wang, M.-X. (2011). Designed synthesis of metal cluster-centered pseudo-rotaxane supramolecular architectures. *J. Am. Chem. Soc.* 133, 8448–8451. doi: 10.1021/ja202294v
- Gao, C.-Y., Zhao, L., and Wang, M.-X. (2012). Stabilization of a reactive polynuclear silver carbide cluster through the encapsulation within a supramolecular cage. *J. Am. Chem. Soc.* 134, 824–827. doi: 10.1021/ja209729h
- Gong, H.-Y., Wang, D.-X., Xiang, J.-F., Zheng, Q.-Y., and Wang, M.-X. (2007). Highly selective recognition of diols by a self-regulating fine-tunable methylazacalix[4]pyridine cavity: guest-dependent formation of molecular-sandwich and molecular-capsule complexes in solution and the solid state. *Chem. Eur. J.* 13, 7791–7802. doi: 10.1002/chem.200700498
- Gong, H.-Y., Zhang, X.-H., Wang, D.-X., Ma, H.-W., Zheng, Q.-Y., and Wang, M.-X. (2006a). Methylazacalixpyridines: remarkable bridging nitrogen-tuned conformations and cavities with unique recognition properties. *Chem. Eur. J.* 12, 9262–9275. doi: 10.1002/chem.200600377
- Gong, H.-Y., Zheng, Q.-Y., Zhang, X.-H., Wang, D.-X., and Wang, M.-X. (2006b). Methylazacalix[4]pyridine: en route to  $\text{Zn}^{2+}$ -specific fluorescence sensors. *Org. Lett.* 8, 4895–4898. doi: 10.1021/ol061928k
- Guo, D.-S., and Liu, Y. (2014). Supramolecular chemistry of *p*-sulfonatocalix[n]arenes and its biological applications. *Acc. Chem. Res.* 47, 1925–1934. doi: 10.1021/ar500309g
- Hu, S.-Z., and Chen, C.-F. (2010). Triptycene-derived oxacalixarene with expanded cavity: synthesis, structure and its complexation with fullerenes  $\text{C}_{60}$  and  $\text{C}_{70}$ . *Chem. Commun.* 46, 4199–4201. doi: 10.1039/c002944k
- König, B., and Fonseca, M. H. (2000). Heteroatom-bridged calixarenes. *Eur. J. Inorg. Chem.* 2000, 2303–2310. doi: 10.1002/1099-0682(200011)2000%3A11<2303%3A%3AAID-EJIC2303>3.0.CO%3B2-Y
- Le Poul, N., Le Mest, Y., Jabin, I., and Reinaud, O. (2015). Supramolecular modeling of mono-copper enzyme active sites with calix[6]arene-based funnel complexes. *Acc. Chem. Res.* 48, 2097–2106. doi: 10.1021/acs.accounts.5b00152
- Lehn, J.-M., Atwood, J. L., Davies, J. D., Macnicol, D. D., and Vögtle, F. (1996). *Comprehensive Supramolecular Chemistry*. Oxford: Pergamon.
- Lhoták, P. (2004). Chemistry of thiacalixarenes. *Eur. J. Org. Chem.* 2004, 1675–1692. doi: 10.1002/ejoc.200300492
- Luo, J., Ao, Y.-F., Wang, Q.-Q., and Wang, D.-X. (2018). Diversity-oriented construction and interconversion of multicavity supermacrocycles for cooperative anion- $\pi$  binding. *Angew. Chem. Int. Ed.* 57, 15827–15831. doi: 10.1002/anie.201810836
- Ma, M.-L., Li, X.-Y., and Wen, K. (2009). Coordination-driven self-Assembly of a discrete molecular cage and an infinite chain of coordination cages based on ortho-linked oxacalix[2]benzene[2]pyrazine and oxacalix[2]arene[2]pyrazine. *J. Am. Chem. Soc.* 131, 8338–8339. doi: 10.1021/ja900291w
- Ma, X., and Tian, H. (2014). Stimuli-responsive supramolecular polymers in aqueous solution. *Acc. Chem. Res.* 47, 1971–1981. doi: 10.1021/ar500033n
- Ma, Y.-X., and Chen, C.-F. (2014). Triptycene-derived calixarenes. *Incl. Phenom. Macrocycl. Chem.* 79, 261–281. doi: 10.1007/s10847-013-0372-4
- Maes, W., and Dehaen, W. (2008). Oxacalix[n](het)arenes. *Chem. Soc. Rev.* 37, 2393–2402. doi: 10.1039/b718356a
- Morohashi, N., Narumi, F., Iki, N., Hattori, T., and Miyano, S. (2006). Thiacalixarenes. *Chem. Rev.* 106, 5291–5316. doi: 10.1021/cr050565j
- Murray, J., Kim, K., Ogoshi, T., Yao, W., and Gibb, B. C. (2017). The aqueous supramolecular chemistry of cucurbit[n]urils, pillar[n]arenes and deep-cavity cavitands. *Chem. Soc. Rev.* 46, 2479–2496. doi: 10.1039/c7cs00095b
- Ogoshi, T., Kakuta, T., and Yamagishi, T.-A. (2019). Applications of pillar[n]arene-based supramolecular assemblies. *Angew. Chem. Int. Ed.* 58, 2197–2206. doi: 10.1002/anie.201805884
- Parisi, M. F., Gattuso, G., Notti, A., Pisagatti, H., and Pappalardo, S. (2016). *Calix[5]arene: From Capsules to Polymers in Calixarenes and Beyond*. eds P. Neri, J. L. Sessler, M.-X. Wang. Oxford: Springer.
- Pazos, E., Novo, P., Peinador, C., Kaifer, A. E., and García, M. D. (2018). Cucurbit[8]uril (CB[8])-based supramolecular switches. *Angew. Chem. Int. Ed.* 57, 2–16. doi: 10.1002/ange.201806575
- Strutt, N. L., Zhang, H., Schneebeli, S. T., and Stoddart, J. F. (2014). Functionalizing pillar[n]arenes. *Acc. Chem. Res.* 47, 2630–2642. doi: 10.1021/ar500177d
- Thomas, J., Van Rossom, W., Van Hecke, K., Van Meervelt, L., Smet, M., Maes, W., et al. (2012). Selenacalix[3]triazines: synthesis and host–guest chemistry. *Chem. Commun.* 48, 43–45. doi: 10.1039/c1cc15473g
- Wang, D.-X., and Wang, M.-X. (2013). Anion- $\pi$  interactions: generality, binding strength, and structure. *J. Am. Chem. Soc.* 135, 892–897. doi: 10.1021/ja310834w
- Wang, D.-X., Wang, Q.-Q., Han, Y., Wang, Y., Huang, Z.-T., and Wang, M.-X. (2010). Versatile anion- $\pi$  interactions between halides and a conformationally rigid bis(tetraoxacalix[2]arene[2]triazine) cage and their

## AUTHOR CONTRIBUTIONS

E-XZ performed the experiments and participated in manuscript preparation. D-XW and M-XW prepared the manuscript.

## FUNDING

We are grateful for the financial support by the National Natural Science Foundation of China (21772203, 21732004, and 21521002) and the Chinese Academy of Sciences (QYZDJ-SSW-SLH023).

## SUPPLEMENTARY MATERIAL

The Supplementary Material for this article can be found online at: <https://www.frontiersin.org/articles/10.3389/fchem.2019.00553/full#supplementary-material>



- directing effect on molecular assembly. *Chem. Eur. J.* 16, 13053–13057. doi: 10.1002/chem.201002307
- Wang, D.-X., Zheng, Q.-Y., Wang, Q.-Q., and Wang, M.-X. (2008). Halide recognition by tetraoxacalix[2]arene[2]triazine receptors: concurrent noncovalent halide- $\pi$  and lone pair- $\pi$  interactions in host-halide-water ternary complexes. *Angew. Chem. Int. Ed.* 47, 7485–7488. doi: 10.1002/anie.200801705
- Wang, M.-X. (2008). Heterocalixaromatics, new generation macrocyclic host molecules in supramolecular chemistry. *Chem. Commun.* 2008, 4541–4551. doi: 10.1039/b809287g
- Wang, M.-X. (2012). Nitrogen and oxygen bridged calixaromatics: synthesis, structure, functionalization, and molecular recognition. *Acc. Chem. Res.* 45, 182–195. doi: 10.1021/ar200108c
- Wang, M.-X. (2018). Coronarenes: recent advances and perspectives on macrocyclic and supramolecular chemistry. *Sci. China Chem.* 61, 993–1003. doi: 10.1007/s11426-018-9328-8
- Wang, M.-X., Zhang, X.-H., and Zheng, Q.-Y. (2004). Synthesis, structure, and [60]fullerene complexation properties of azacalix[m]arene[n]pyridines. *Angew. Chem. Int. Ed.* 43, 838–842. doi: 10.1002/anie.200351975
- Wu, J.-C., Zhao, L., Wang, D.-X., and Wang, M.-X. (2012). Structural diversity in coordination self-assembled networks of a multimodal ligand azacalix[4]pyrazine. *Inorg. Chem.* 51, 3860–3867. doi: 10.1021/ic3000679
- Wu, J.-C., Zhao, L., Wang, D.-X., and Wang, M.-X. (2013). Synthesis, structure and coordination self-assembly of azacalix[4-*n*]pyridine[*n*]pyrazines (*n*-1-3). *Chin. J. Chem.* 31, 589–597. doi: 10.1002/cjoc.201300078
- Zhang, E.-X., Wang, D.-X., Huang, Z.-T., and Wang, M.-X. (2009). Synthesis of (NH)<sub>m</sub>(NMe)<sub>4-m</sub>-bridged calix[4]pyridines and the effect of NH bridge on structure and properties. *J. Org. Chem.* 74, 8595–8603. doi: 10.1021/jo901609u
- Zhang, S., and Zhao, L. (2018). Macrocyclic-encircled polynuclear metal clusters: controllable synthesis, reactivity studies, and applications. *Acc. Chem. Res.* 51, 2535–2545. doi: 10.1021/acs.accounts.8b00283

**Conflict of Interest Statement:** The authors declare that the research was conducted in the absence of any commercial or financial relationships that could be construed as a potential conflict of interest.

Copyright © 2019 Zhang, Wang and Wang. This is an open-access article distributed under the terms of the Creative Commons Attribution License (CC BY). The use, distribution or reproduction in other forums is permitted, provided the original author(s) and the copyright owner(s) are credited and that the original publication in this journal is cited, in accordance with accepted academic practice. No use, distribution or reproduction is permitted which does not comply with these terms.



# Artificial Gramicidins

Zhanhu Sun and Mihail Barboiu\*

*Institut Européen des Membranes, Adaptive Supramolecular Nanosystems Group, University of Montpellier, ENSCM-CNRS, Montpellier, France*

Gramicidin A, gA is a natural protein channel with a well-established, simple structure, and function: cations and water are transported together along the channel. Importantly, the dipolar orientation of water molecules within the pore can influence the ionic translocation. The need for simple artificial systems biomimicking the gA functions has been desired and they were until last decade unknown. Several interesting papers highlighted in this minireview have been published and supramolecular systems described here can be considered as primitive gA mimics. The dynamics of ions/water and protons confined within gA channels is difficult to structurally analyze and simpler artificial systems designed at the atomic level would have a crucial relevance for understanding such translocation scenarios at the molecular level. The directional ordering of confined water-wires or ions, as observed inside primitive gA channels is reminiscent with specific interactions between water and the natural gA. This dipolar orientation may induce specific dielectric properties which most probably influence the biological recognition at bio-interfaces or translocation of charge species along artificial channel pathways.

## OPEN ACCESS

### Edited by:

Carminé Gaeta,  
University of Salerno, Italy

### Reviewed by:

Narayanan Selvapalam,  
Kalasalingam University, India  
Ana Maria Carmona-Ribeiro,  
University of São Paulo, Brazil

### \*Correspondence:

Mihail Barboiu  
mihail-dumitru.barboiu@umontpellier.fr

### Specialty section:

This article was submitted to  
Supramolecular Chemistry,  
a section of the journal  
Frontiers in Chemistry

**Received:** 13 July 2019

**Accepted:** 20 August 2019

**Published:** 04 September 2019

### Citation:

Sun Z and Barboiu M (2019) Artificial  
Gramicidins. *Front. Chem.* 7:611.  
doi: 10.3389/fchem.2019.00611

**Keywords:** gramicidin A, biomimetic, ion channels, hydrophobic, hydrophilic

## INTRODUCTION

Gramicidin A, gA discovered during the late 30 s (Dubos, 1939), is one of the most studied natural channels (Burkhart et al., 1998; Roux, 2002; Allen et al., 2007) and important insights were obtained with synthetically modified gAs to improve their membrane transport activity (Pfeifer et al., 2006).

Concerning translocation mechanisms along gA pore, its polarized structure helps to compensate the high energy barrier to water and ion dehydration, which are transported sharing the unique pore pathway, through the bilayer membrane (Burkhart et al., 1998; Roux, 2002). Importantly, the dipolar orientation of water molecules within the pore can influence the ionic translocation and this process is also a determinant for their selective pumping in other protein-channels (Allen et al., 2007). Water, can influence, by its dynamic structure and orientation, ion and proton translocation and ion-valence selectivity of the gA channel.

The field of artificial ion channels have been extensively reviewed (Gokel and Mukhopadhyay, 2001; Sakai et al., 2005; Sakai and Matile, 2013). Understanding the dynamics of water molecules at the molecular level, hydrated ions, and protons within structurally simpler artificial channels would have a crucial relevance in order to understand many biological translocation processes involving dynamic transport through complicated protein channels (Barboiu, 2012; Barboiu and Gilles, 2013). The ability to know how ions or water-clusters are confined in structurally well-defined architectures might shed-light on the water structural behaviors within pores as observed with biological water (Kocsis et al., 2018),

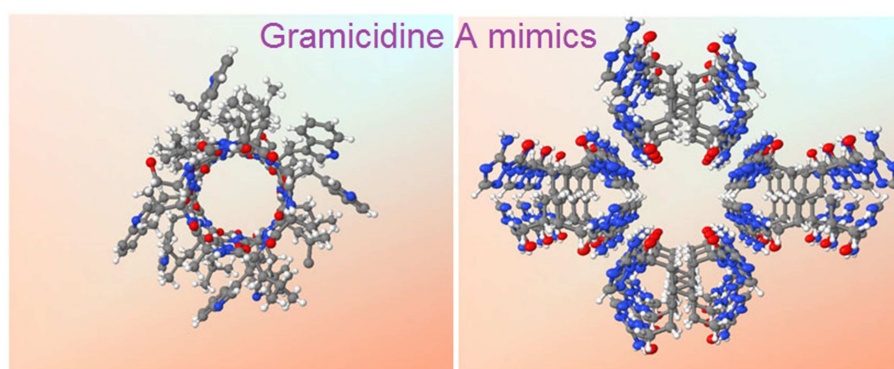
with properties at the boundaries between solid and liquid phases. Despite multiple studies of entrapping water or water/ion clusters within complex supramolecular structures, few synthetic channels have been tested to selectively transport water (Le Duc et al., 2011) and ions (Barboiu et al., 2014) efficiently through bilayer membranes.

Among the successful investigations for the construction of active artificial channels, one way is to use unimolecular channels (Hu et al., 2012). Another way is the bottom-up supramolecular strategy, in which biomimetic or bio-inspired artificial channel architectures are constructed *via* the self-assembly of synthetic molecular components through non-covalent self-assembly (Sakai et al., 2005; Cazacu et al., 2006; Ma et al., 2008).

Within this context, the need for simplest artificial systems biomimicking the complex natural gA functions has been desired and they were unknown until last 5 years. This Minireview will focus on recent accomplishments on artificial biomimetic ion channels, which can be envisioned as primitive gA mimics, presenting ion/proton, and water-channel conductance states in lipid bilayer membranes.

## ARTIFICIAL gA CHANNELS

Although gA is one of the most-simple and well-studied natural channels, important works in improving natural transport activity has been described in several findings, showing that gA



**Graphical Abstract** | X-ray crystal structures of gA (**left**) and the hydrophilic T-channel of triazole 3 (**right**) at the same dimensional scale.

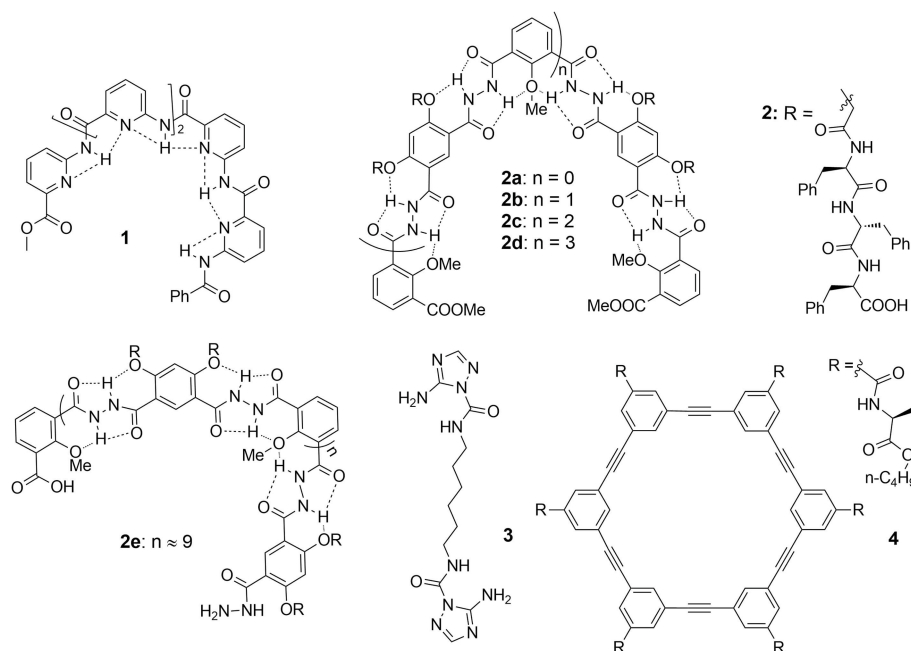


**FIGURE 1** | Artificial Gramicidin A ion channel forming compounds: aromatic foldameric polyamide **1**, aromatic foldameric hydrazides **2a–2e**, bola-amphiphile triazole **3** and arylene-ethynylene macrocycle **4**.

can be bio-mimicked using artificial compounds with similar functions like the natural gA, in order to obtain artificial gAs by using simple compounds approaches. These systems are channel-type superstructures formed by self-assembly and provide remarkable combinations of functions similar to gA channel: water permeability, proton conductance via Grotthus mechanism, cation vs. anion selectivity, single-channel activity. Within this context, the novel artificial systems may provide interesting information about the translocation mechanisms of water molecules or ions through channels within lipid bilayers. Meanwhile, their functions are close or comparable, even superior to the natural ion channel proteins.

Among the numerous investigations on ion channels, the bottom-up supramolecular biomimetic strategy uses simple synthetic molecules that self-assemble through non-covalent interactions: H- bonding, charge compensation or hydrophobic effects. Due to their easy manipulation, convenient modification and versatility, supramolecular biomimetic strategies are envisioned as an excellent method to further understand the functions, structures and mechanisms of ion channels, even to create substitutes for natural channels. Supramolecular chemists have concentrated their research on the study on artificial biomimetic structures of gA.

Zeng et al. prepared foldameric channels for synergetic transport of protons and of water (Zhao et al., 2014). They discovered that pentamer **1** (Figure 1) made from 6-aminopyridine-2-carboxylic components, which clearly shows the formation of a chiral helical structure, providing like in

natural gA, a perfect pore dimensionally adapted ( $\sim 2.8$  Å) for water recognition. This structure is regarded as a model for the building of ion channels using a bottom-up self-assembling method. Interestingly, oriented water wires are oriented in one direction following the supramolecular chiral orientation of the helical molecules (Figure 2a). After unsuccessful tests on water transport under salt-induced osmotic conditions, the helical channels can effectively transport water only when a proton gradient is applied. Using the dynamic light scattering, the size of LUVs containing the pentamer **1** rapidly increased 40% within the first 15 min, in comparison to the inactivity of gA under the same conditions. The authors define this behavior as “proton gradient-induced water transport.” More interestingly, the pentamer **1** facilitates transmembrane proton transport, which is efficient and very similar to that of gA.

Li et al. have constructed hydrogen bonding-mediated hydrazide foldamers and have focused on building artificial biomimetic structures and responsive materials based on hydrogen bonding-mediated hydrazides and amides (Zhang et al., 2014). They have conceived and carried out a series of unimolecular channels (2a–e, Figure 1), whose selectivities and permeabilities even outmatch the natural gA. The structural stabilization in the lipid bilayers results from the multiple intramolecular hydrogen bonding, which direct half of the carbonyl groups toward the internal cavity, similar to gA and from the phenylalanine tripeptides acting as the lipophilic anchors. Patch clamp experiments show that the selectivities toward alkali ions correspond to the energetic penalty for ions

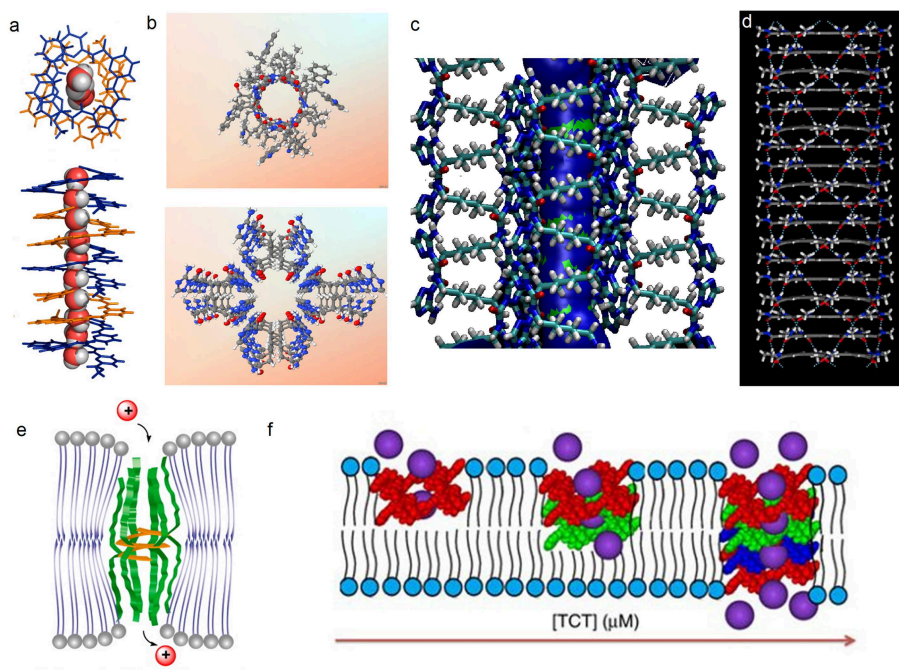


**FIGURE 2 |** (a) Single crystal structure of **1** and the accompanying water wires; (b) X-ray crystal structures of gA (top) and the hydrophilic T-channel of triazole **3** (bottom) at the same dimensional scale, (c) Probability plots describing the average distribution of water molecules confined within the T-channels (d) simulated hydrophobic tubular pores from macrocycle **4**. Schematic representation on reconstitution of (e) **2b** and **2c** and (f) **3** in bilayer membrane models.

**TABLE 1** | A summary of various artificial gA channels.

Compound	Nature of the channel	Net permeability/selectivity/single channel permeability or ion flux	References
<b>1</b>	Hydrophilic helical channel (2.8 Å) via $\pi$ - $\pi$ stacking of aromatic units	No permeability reported/high selectivity for water, reject all ions except protons	Zhao et al., 2014
<b>2a–2e</b>	Hydrophilic helical channel (1.0 nm) via intramolecular hydrogen bonding in aromatic hydrazide foldamers	No permeability reported/higher $\text{NH}_4^+/\text{K}^+$ selectivity than that of gA	Xin et al., 2014
<b>3</b>	Self-assembled helical pores (~2.5–4 Å); double helical water channels with double helix net-dipolar orientation	No permeability reported for water/enhanced conduction states for alkali cations and for protons	Barboiu et al., 2015
<b>4</b>	Hydrophobic tubular channel (6.4 Å) via tubular $\pi$ - $\pi$ stacking of macrocyclic arylene-ethynylenes and H-bonding of marginal dipeptides	$51 \mu\text{m s}^{-1}$ /no selectivity for water, high conduction for $\text{K}^+$ , and protons/ $4.9 \times 10^7$ water molecules per s per channel	Zhou et al., 2012
<b>5</b>	Inherent hydrophobic cavity (~2.4–5.5 Å)	No permeability reported for water/enhanced conduction states for alkali cations and for protons/ $\sim 3 \times 10^7$ $\text{Cs}^+$ ions per s per channel	Jeon et al., 2004

dehydration. The helical **2d** and **2e** show higher  $\text{NH}_4^+/\text{K}^+$  selectivity than gA, under the identical performed conditions. The authors attribute this feature to the addition hydrogen bonding between ammonium cations and the hydrazide carbonyl moieties, which is supported by the increasing transporting ability toward ammonium with the elongation of the channel-forming compounds. In addition, stopped-flow experiments point out that these hydrazides display positive transporting activities toward  $\text{Ti}^+$  ions and function as a unimolecular channel process. Interestingly, the short helical **2b** transports  $\text{Ti}^+$  almost as effectively as gramicidin A does (Xin et al., 2014). According to stopped-flow experiments for the transport of  $\text{Ti}^+$ , compounds **2b** and **2c** most probably formed a unimolecular channel in lipid bilayers (Figure 2e).

Barboiu et al. have described one of the most appropriate primitive artificial gA channels, showing amazing similarities in both structure and function aspects (Barboiu et al., 2014). The synthesis of a bola-amphiphile compound **3** (Figure 1) is the result of serendipity. It results in the formation of T-channels with a water filled interior free channel of 5 Å in van der Waals diameter, which is dimensionally similar to the gA channel (Figures 2b,c). The chiral T-channel is regarded as hydrophilic, because the carbonyl groups directing the channel inward toward the transport void, are in close contact with water like the carbonyl strings in gA. The total dipolar orientation of water molecules within the chiral pore determine the translocation of both protons and ions, that diffuse along such hydrophilic directional pathways. From a functional aspect, compound **3** is able to form transmembrane channels to facilitate water permeability and selective ion/proton transporting as well as single channel ion transporting. Based on molecular simulations and the transport data, compound **3** was likely to form T-channels in lipid bilayers (Figure 2e). Dynamic light scattering measurements prove that **3** effectively transports water. Compound **3** shows fifty times higher water permeability than the control. In addition, compound **3** constructs channels to transport protons via the inside water wires through the Grothuss

mechanism. Furthermore, both cations and anions are effectively transmembrane moved, thus good cation/anion selectivity is accomplished. Theoretical simulations and experimental assays reveal that the conduction through the T-channel, like in gA, presents proton/water conduction, cation/anion selectivity, and large open channel-conductance states. The strong interactions between water molecules and the groups at the inner surface of the T-channel groups determine a net-dipole orientation of confined water molecules. Moreover, even when different ions are present within the channel, confined water remains significantly localized and still presents directional orientation and ordering within the T-channel (Barboiu et al., 2015). The T-channels—associating supramolecular chirality and dipolar water orientation—represent an interesting artificial mimic of gA.

Hydrophobic effects play an important role in biology, such as they are a significant driving force controlling the protein folding or facilitating the transmembrane ion and water transport. Within this context, Gong et al. have constructed a series of tubular hydrophobic adjustable nanopores (Figure 2D) generated *via* multiple hydrogen bonding and stacking (Zhou et al., 2012). Meanwhile, the internal pores are adjustable through the choice of appropriate monomers. Computational studies, X-ray diffraction, and microscopy results are in agreement with the construction of well-defined shaped-persistent nanotubes able to define stable nanopores.

The cyclic arylene-ethynylene macrocycle **4** (Figure 1) demonstrates excellent selective ion transport and high-water permeability. Its conductance reaches  $\sim 5.8$  pS for  $\text{K}^+$  cations, while no transport is observed for  $\text{Li}^+$  or  $\text{Na}^+$  cations. The authors attribute this selectivity to the dehydration energy of cations based on MD simulations. Compound **4** also shows significant water permeability ( $2.6 \pm 0.4 \times 10^{-14} \text{ cm}^3 \text{ s}^{-1}$ ,  $\sim 22\%$  that of Aquaporin-AQP1) and single ion channel transport behaviors.

In addition, Kim and co-workers developed macrocyclic cucurbit[n]uril (CB[n]) derivatives as artificial ion channels (Jeon et al., 2004). By introduction of 3-octylsulfanylpropyl-O



moieties into CB[n] ( $n = 6, 5$ ), novel CB[n] derivatives effectively mediate the transmembrane proton/ion transport by a membrane mechanism. The results showed that the inherent cavity of the CB[n] play an important role in the transport of ions. With different hydrophobic cavities (CB[6], diameter  $\sim 5.5$  Å; CB[5], diameter  $\sim 4.4$  Å), the two CB[n]s show different ion selectivities. Based on the transport data and selectivity, the authors imply that CB[n] derivatives transport ions through their inherent cavities. Yet, the authors do not study the reconstitution of CB[6] derivatives in lipid bilayers and how they form ion channels. Notably, CB[6] derivative shows high ion flux of  $\sim 3 \times 10^7$  ion/s, comparable to that of gA.

## DISCUSSIONS

The aforementioned five artificial gA mimics demonstrate some similarities but also some differences. With respect to similarities, all of them were generated *via* self-assembly of molecular components through non-covalent interactions. All of the channels forming compounds are amphiphilic so that they present good partition into the lipid bilayers and facilitate the water/ion transporting. The absence of ion-exclusion sites causes them to form the non-exclusive channels but show many similarities with the natural gA. With respect to the differences, the first three channels 1–3 provide the hydrophilic pores for ion/water transport. The last two systems, 4 and CB[n] derivatives, offer a hydrophobic pore, able to provide a high flow velocity for ions and/or water owing to less friction like carbon nanotubes. The pores formed by 1 and 3 are chiral and contain oriented water wires in their confined space (Table 1).

The behaviors of channels presented here may lead to more general conclusions. Structured water and derived physical theories have been the sources of continuous controversies. However, it should be stressed that moving from conventional bulk water to confined water is not simply a change of the scale, as the dynamics of confined water is quite fundamentally complex and different from that observed in bulk liquid water. Compartmentalization and chiral surfaces are basic features of biomolecules. The directional ordering of confined water-wires, as observed inside all presented gA mimics, is reminiscent with specific interactions between water and the biosurfaces, of which most are chiral. This dipolar orientation may induce important

dielectric behaviors, which may certainly influence the biological recognition at biointerfaces or inside biocavities. The dipolar orientation of waters within ion-water single file through gA channel is an important driving force for the permeation of ions. The single-file columns of water are like a lubricant between the inner surface of the pore and the diffusing ions. On the other hand, such association of simple asymmetric properties: the *chirality of the pore structures* and one directional *orientation of the dipolar water-wires*, enables the idea for a novel strategy of much interest for artificial ion-pumping processes.

## OUTLOOK

Nature has developed various ion/water channels over a million years or more. As an example of natural channels, gA has showed interesting and important functions, especially on water/ion transport. However, biomimetic on artificial ion/water channels has emerged in <4 decades, dating back to the seminal paper published in Tetrahedron Letters in 1982 by Tabushi et al. (1982) when  $\text{Co}^{2+}$  ions have been efficiently transported by a functionalized cyclodextrin carrier, with the rate  $4.5 \times 10^{-4} \text{ sec}^{-1}$ , through a bilayer membrane. Since this period, some artificial ion channels have surpassed gA in both cation/anion selectivity and proton/water transport efficiency, as well as active open channel-activity in bilayer membranes. It shows the bright future of research on artificial gA. It is still challenging for researchers to design the structures of artificial gA with expected selectivity and efficiency. The development of this field not only relies on further understanding on biology but also on organic synthetic strategies. With its progress, the applications of artificial gA will blossom.

## AUTHOR CONTRIBUTIONS

ZS collected the references and wrote the draft. MB finalized the manuscript.

## FUNDING

Financial support from the framework of WATERCHANNELS, ANR-18-CE06-0004-02, and ANR LABEX Chemisyst ANR-10-LABX-05-01 awarded by Pole Balard Montpellier.

## REFERENCES

- Allen, O., Andersen, S., and Roux, B. (2007). Energetics of ion conduction through the gramicidin channel. *Proc. Natl. Acad. Sci. U.S.A.* 101, 117–122. doi: 10.1073/pnas.2635314100
- Barboiu, M. (2012). Artificial water channels. *Angew. Chem. Int. Ed.* 51, 11674–11676. doi: 10.1002/anie.201205819
- Barboiu, M., Cazade, P. A., Le Duc, Y., Legrand, Y. M., van der Lee, A., and Coasne, B. (2015). Polarized water wires under confinement in chiral channels. *J. Phys. Chem. B* 119, 8707–8717. doi: 10.1021/acs.jpcc.5b03322
- Barboiu, M., and Gilles, A. (2013). From natural to bioassisted and biomimetic artificial water channel systems *Acc. Chem. Res.* 46, 2814–2823. doi: 10.1021/ar400025e
- Barboiu, M., Le Duc, Y., Gilles, A., Cazade, P.-A., Michau, M., Legrand, Y.-M., et al. (2014). An artificial primitive mimic of Gramicidin-A channel. *Nature Comm.* 5:4142. doi: 10.1038/ncomms5142
- Burkhart, B. M., Li, N., Langs, D. A., Pangborn, W. A., and Duax, W. L. (1998). The conducting form of gramicidin A is a right-handed double-stranded double helix. *Proc. Natl. Acad. Sci. U.S.A.* 95:12950. doi: 10.1073/pnas.95.22.12950
- Cazacu, A., Tong, C., van der Lee, A., Fyles, T. M., and Barboiu, M. (2006). Columnar self-assembled ureidocrown-ethers – an example of ion-channel organization in lipid bilayers. *J. Am. Chem. Soc.* 128, 9541–9548. doi: 10.1021/ja061861w
- Dubos, R. J. (1939). Studies on a bactericidal agent extracted from a soil bacillus: I preparation of the agent. Its activity *in vitro*. *J. Exp. Med.* 70, 1–10. doi: 10.1084/jem.70.1.1

- Gokel, G. W., and Mukhopadhyay, A. (2001). Synthetic models of cation-conducting channels. *Chem. Soc. Rev.* 30, 274–286. doi: 10.1039/b008667n
- Hu, X. B., Chen, Z., Tang, G., Hou, J. L., and Li, Z. T. (2012). Single-molecular artificial transmembrane water channels. *J. Am. Chem. Soc.* 134, 8387–8387. doi: 10.1021/ja302292c
- Jeon, Y. J., Kim, H., Sangyong, J., Selvapalam, N., Oh, D. H., Seo, I., et al. (2004). Artificial ion channel formed by cucurbit[n]uril derivatives with a carbonyl group fringed portal reminiscent of the selectivity filter of K<sup>+</sup> channels. *J. Am. Chem. Soc.* 126, 15944–15945. doi: 10.1021/ja044748j
- Kocsis, I., Sorci, M., Vanselous, H., Murail, S., Sanders, S. E., Licsandru, E., et al. (2018). Oriented chiral water wires in artificial transmembrane channels. *Sci. Adv.* 4:eao5603. doi: 10.1126/sciadv.aao5603
- Le Duc, Y., Michau, M., Gilles, A., Gence, V., Legrand, Y.-M., van der Lee, A., et al. (2011). Imidazole I-quartet water and proton dipolar channels. *Angew. Chem. Int. Ed.* 50, 11366–11372. doi: 10.1002/anie.201103312
- Ma, L., Melegari, M., Colombini, M., and Davis, J. T. (2008). Large and stable transmembrane pores from guanosine-bile acid conjugates. *J. Am. Chem. Soc.* 130, 2938–2939. doi: 10.1021/ja7110702
- Pfeifer, J. R., Reiss, P., and Koert, U. (2006). Crown-ether gramicidin hybrid ion channels: dehydration-assisted ion selectivity. *Angew. Chem. Int. Ed.* 45, 501–504. doi: 10.1002/anie.200502570
- Roux, B. (2002). Computational studies of the gramicidin channel. *Acc. Chem. Res.* 35, 366–375. doi: 10.1021/ar010028v
- Sakai, N., Mareda, J., and Matile, S. (2005). Rigid-rod molecules in biomembrane models: from hydrogen-bonded chains to synthetic multifunctional pores. *Acc. Chem. Res.* 38, 79–87. doi: 10.1021/ar0400802
- Sakai, N., and Matile, S. (2013). Synthetic ion channels. *Langmuir* 29, 9031–9040. doi: 10.1021/la400716c
- Tabushi, I., Kuroda, Y., and Yokota, K. (1982). A,B,D,F-tetrasubstituted  $\beta$ -Cyclodextrin as artificial channel compound. *Tetrahedron Lett.* 23, 4601–4604. doi: 10.1016/S0040-4039(00)85664-6
- Xin, P., Zhu, P., Su, P., Hou, J. L., and Li, Z. T. (2014). Hydrogen-bonded helical hydrazide oligomers and polymer that mimic the ion transport of gramicidin A. *J. Am. Chem. Soc.* 136, 13078–13081. doi: 10.1021/ja503376s
- Zhang, D. W., Zhao, X., and Li, Z. T. (2014). Aromatic amide and hydrazide foldamer-based responsive host–guest systems. *Acc. Chem. Res.* 47, 1961–1970. doi: 10.1021/ar5000242
- Zhao, H., Sheng, S., Hong, Y., and Zeng, H. (2014). Proton gradient-induced water transport mediated by water wires inside narrow aquapores of aquafoldamer molecules. *J. Am. Chem. Soc.* 136:14270. doi: 10.1021/ja5077537
- Zhou, X., Liu, G., Yamato, K., Shen, Y., Cheng, R., Wei, X., et al. (2012). Self-assembling subnanometer pores with unusual mass-transport properties. *Nat. Commun.* 3:949. doi: 10.1038/ncomms1949

**Conflict of Interest Statement:** The authors declare that the research was conducted in the absence of any commercial or financial relationships that could be construed as a potential conflict of interest.

Copyright © 2019 Sun and Barboiu. This is an open-access article distributed under the terms of the Creative Commons Attribution License (CC BY). The use, distribution or reproduction in other forums is permitted, provided the original author(s) and the copyright owner(s) are credited and that the original publication in this journal is cited, in accordance with accepted academic practice. No use, distribution or reproduction is permitted which does not comply with these terms.



# Applications of Cucurbiturils in Medicinal Chemistry and Chemical Biology

Debapratim Das<sup>1\*</sup>, Khaleel I. Assaf<sup>2,3\*</sup> and Werner M. Nau<sup>2\*</sup>

<sup>1</sup> Department of Chemistry, Indian Institute of Technology Guwahati, Guwahati, India, <sup>2</sup> Department of Life Sciences and Chemistry, Jacobs University Bremen, Bremen, Germany, <sup>3</sup> Department of Chemistry, Faculty of Science, Al-Balqa Applied University, Al-Salt, Jordan

The supramolecular chemistry of cucurbit[n]urils (CBn) has been rapidly developing to encompass diverse medicinal applications, including drug formulation and delivery, controlled drug release, and sensing for bioanalytical purposes. This is made possible by their unique recognition properties and very low cytotoxicity. In this review, we summarize the host-guest complexation of biologically important molecules with CBn, and highlight their implementation in medicinal chemistry and chemical biology.

**Keywords:** molecular containers, host-guest complexes, drug delivery, supramolecular chemistry, drug release, molecular recognition, chemosensing

## OPEN ACCESS

### Edited by:

De-Xian Wang,  
Institute of Chemistry (CAS), China

### Reviewed by:

Ruibing Wang,  
University of Macau, China  
Yu Liu,  
Nankai University, China

### \*Correspondence:

Debapratim Das  
ddas@iitg.ac.in  
Khaleel I. Assaf  
k.assaf@jacobs-university.de;  
khaleel.assaf@bau.edu.jo  
Werner M. Nau  
w.nau@jacobs-university.de

### Specialty section:

This article was submitted to  
Supramolecular Chemistry,  
a section of the journal  
Frontiers in Chemistry

**Received:** 21 June 2019

**Accepted:** 28 August 2019

**Published:** 13 September 2019

### Citation:

Das D, Assaf KI and Nau WM (2019)  
Applications of Cucurbiturils in  
Medicinal Chemistry and Chemical  
Biology. *Front. Chem.* 7:619.  
doi: 10.3389/fchem.2019.00619

## INTRODUCTION

One of the major challenges in modern-day pharmacology and medicine is the stable formulation and targeted delivery of therapeutics (Ghosh and Nau, 2012; Sreenivasolu, 2012; Sanku et al., 2019). A major effort in pharmaceutical research is being invested with the aim to achieve the highest impact of a particular therapeutic agent or drug on living systems by creating appropriate delivery vehicles that affect, on one hand, delivery at the desired target and that protect, on the other hand, drug molecules from degradation. In part, the focus of pharmaceutical research has recently moved more toward the development of new nanoscale biocompatible delivery vehicles and away from the *de-novo* design of new drugs.

Macrocyclic receptors, such as cyclodextrins (CDs), calixarenes (CXs), and cucurbiturils (CBs), have received enormous attention owing to their ability to encapsulate therapeutic agents non-covalently and to release them by appropriate stimuli (Saleh et al., 2013; Liu, 2017). Macrocyclic hosts show considerable advantages over other forms of nano-sized drug carriers (Schneider and Yatsimirsky, 2008). The thermal and chemical stability, formation of different nano-structured assemblies, availability of various sizes, and most importantly, the biocompatibility of these macrocyclic hosts are some of the essential features which differentiate them from alternative drug-delivery vehicles such as dendrimers, liposomes, hydrogels, micelles, carbon nanotubes, or polymers.

Amidst macrocyclic hosts, CDs (Li and Loh, 2008) are the most common choice due to their ready availability, low cost, and high water solubility. However, there are several limitations arising from their poor selectivity and low affinity ( $K_a < 10^4 \text{ M}^{-1}$ ) (Rekharsky and Inoue, 1998). Moreover, their use in clinical formulations is generally limited to oral and topical drug delivery because they can be nephrotoxic if administered in non-metabolized form (Shchepotina et al., 2011). The low binding constants, especially toward drug molecules, lead to the requirement of excess concentrations of CDs in order to form host-guest complexes quantitatively.

Several other macrocyclic hosts are under the scanner for development of effective host-guest complexes with drugs in order to stabilize and effectively deliver them. In recent years, CBs (**Figure 1**) have come out as attractive macrocyclic hosts for applications in medicinal chemistry and chemical biology (Ma and Zhao, 2015; Masson, 2017; Yin and Wang, 2018; Yin et al., 2019). The binding constants ( $K_a$ ) of their host-guest complexes are several orders of magnitude higher than those of CDs in aqueous medium (Cao et al., 2014; Assaf and Nau, 2015; Barrow et al., 2015; Shetty et al., 2015). Most importantly, CBs hold promise as being non-toxic and highly biocompatible (Montes-Navajas et al., 2009; Hettiarachchi et al., 2010; Uzunova et al., 2010; Zhang et al., 2018b).

CB $n$  ( $n = 5$ – $10$ , 9 yet to be isolated, **Figure 1** and **Table 1**) are readily synthesized from the condensation of glycoluril and formaldehyde in strongly acidic media. Interestingly, though the synthesis was reported back in 1905 by Behrend et al. (1905) the determination of the chemical structure of CB6 took 70 years when Mock and coworkers refined it for the first time crystallographically (Freeman et al., 1981). CB9 is yet to be isolated, but other homologs of CBs (5–10) have in the meantime been purified. Structural analysis of these analogs showed that CBs are macrocycles containing 5 to 10 glycoluril units connected by two methylene bridges on each side of the glycoluril segments. The cyclic structure, thus, creates two identical partially negatively charged hydrophilic carbonyl portals on each sides and a hydrophobic cavity with low polarity and polarizability (**Figure 1**) (Márquez and Nau, 2001a; Assaf and Nau, 2014).

The first two decades on research with CBs were mostly focused on synthesis, structural evaluation, and their guest binding properties. However, with the newer, more economic synthetic and purification strategies, along with considerable knowledge about their properties, the focus has shifted toward applications of this interesting family of water-soluble macrocycles. One of the prominent dimensions of recent publications on CBs is their use in the areas of medicinal chemistry and chemical biology. Though *in vivo* applications of CBs for medicinal and diagnostic purposes are emerging relatively slowly, the increasing number of reports on CB-based drug delivery systems has become overwhelming in the last decade. In this review, we aim to provide an overview of the recent achievements in the area of drug delivery and diagnostics involving host-guest chemistry of CBs. The review focuses on the applications of the parent macrocyclic homologs in medicinal chemistry and chemical biology; applications of acyclic and other variants or derivatives are reviewed elsewhere (Ganapati and Isaacs, 2018).

CBs are well-known to bind a wide range of guest molecules, including small organic molecules, amino acids, peptides, and proteins (Macartney, 2011; Shchepotina et al., 2011; Barrow et al., 2015; Sanku et al., 2019). The association of guest molecules to CBs is generally driven by ion-dipole interactions, as well as the classical and non-classical hydrophobic effect (Nau et al., 2011; Assaf and Nau, 2015). The CB cavity provides a hydrophobic void for the binding of neutral hydrophobic molecules, while the two identical carbonyl rims represent docking sites for

positively charged groups, in most cases ammonium groups or other cations. The complexation of hydrophobic residues inside the cavity is associated with the release of high-energy water molecules from the CB cavity, which contributes to the high association constants (Biedermann et al., 2012b, 2014). The size and shape of the guest molecules also modulate the binding process (Nau et al., 2011; Lee et al., 2013; Assaf and Nau, 2015; Assaf et al., 2017). An ideal binding is generally obtained when the guest volume is around 55% of that of the inner cavity of CBs (Mecozzi and Rebek, 1998; Nau et al., 2011). Among the CB homologs, CB7 can bind guest molecules with extremely high binding affinities, which exceed that of the biotin-avidin pair, the strongest non-covalent interaction between two partners found in nature (Moghaddam et al., 2011; Cao et al., 2014). The highest binding affinity measured with CBs is  $7.2 \times 10^{17} \text{ M}^{-1}$ , observed between CB7 and a diamantane diammonium guest molecule (Cao et al., 2014).

The encapsulation of molecules inside the CB cavity leads usually to (real or apparent) changes in their physical and chemical properties due to an altered microenvironment as well as confinement and isolation from the surrounding medium (Koner and Nau, 2007; Dsouza et al., 2011; Koner et al., 2011). For example, the solubility of poorly soluble drug molecules can be significantly enhanced upon complexation with CBs (Zhao et al., 2008; Koner et al., 2011; Ma et al., 2012a; Lazar et al., 2016). The use of even-numbered CB $n$  homologs ( $n = 6$  and  $8$ ) as drug solubilizing agents is limited due to their low intrinsic solubilities ( $\mu\text{M}$ , see **Table 1**) in water, which can be enhanced to a certain degree in the presence of cations or positively charged guest molecules (Lagona et al., 2005; Masson et al., 2012). Guest molecules can also take advantage of isolation or protection from the bulk solvent upon complexation with CBs. Mohanty et al. reported that CB7 can induce deaggregation and photostabilization of fluorescent dyes, such as Rhodamine 6G, which is commonly used in cell-biological applications such as fluorescence microscopy and fluorescence correlation spectroscopy (Mohanty and Nau, 2005; Nau and Mohanty, 2005). CBs are also known to affect the  $pK_a$  values of the guest molecules and, thereby, alter their chemical reactivities (Koner et al., 2011; Barooah et al., 2012; Ghosh and Nau, 2012; Lazar et al., 2017). The preferential binding of the protonated form of the guest molecule over its neutral form increases the  $pK_a$  values of the conjugate acids of basic guests, leading to complexation-induced  $pK_a$  shifts. The high affinity of the protonated guest is mainly attributed to additional ion-dipole interactions between the cationic sites of the guest molecules with the carbonyl portals of CBs (Márquez et al., 2004b). Also important, the high thermal stability of CBs allows their implementation to improve the thermal stability of many drugs in the solid state (Bardelang et al., 2011; Saleh et al., 2012).

## ENCAPSULATION OF DRUGS

CB complexation has been established for different classes of drug molecules, pharmaceutical agents, and other bioactive molecules (Hettiarachchi et al., 2010; Huang et al., 2011;

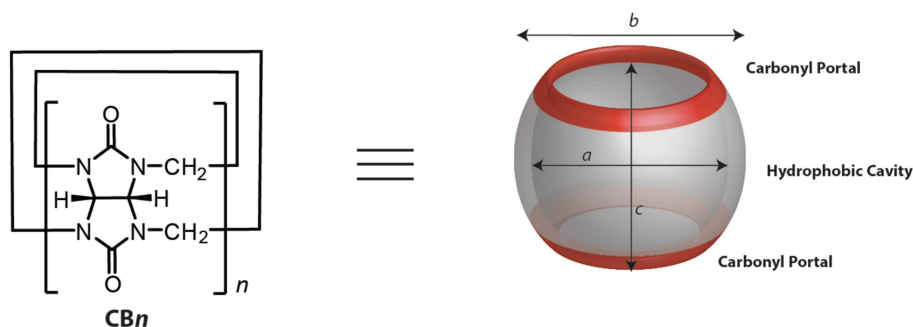


**FIGURE 1** | Chemical and model representations of CBn.

**TABLE 1** | Structural parameters<sup>a</sup> of CBn (see **Figure 1**) and selected physicochemical properties.

<i>n</i>	CBn	Molecular weight	Inner diameter <i>a</i> [Å]	Outer diameter <i>b</i> [Å]	Height <i>c</i> [Å]	Inner cavity volume [Å <sup>3</sup> ]	Aqueous solubility <i>S</i> <sub>H2O</sub> [mM]
5	CB5	830	4.4	13.1	9.1	68	20–30 <sup>b</sup>
6	CB6	996	5.8	14.4	9.1	142	0.03 <sup>c</sup>
7	CB7	1163	7.3	16.0	9.1	242	5 <sup>d</sup>
8	CB8	1329	8.8	17.5	9.1	367	<0.01 <sup>b</sup>
10	CB10	1661	11.7	20.0	9.1	691	<0.05 <sup>e</sup>

<sup>a</sup>From Assaf and Nau (2015).

<sup>b</sup>From Lagona et al. (2005).

<sup>c</sup>From Márquez et al. (2004b).

<sup>d</sup>From Márquez et al. (2004a).

<sup>e</sup>From Liu et al. (2005b).

Walker et al., 2011; Day and Collins, 2012; Yin et al., 2019). Drug molecules that have been studied for their inclusion complexation with CBs to date include anti-neoplastic, anti-pathogenic, antagonist agents, vitamins and hormones, enzyme inhibitors, neurotransmitters, neuromuscular blockers, anti-tuberculosis agents, local anesthetics, and others. In this section, we provide an overview of the different types of biologically relevant guest molecules in regard to their encapsulation inside CBs.

The supramolecular complexation of benzimidazole-based drugs (**Figure 2**) has been systematically studied by Nau and coworkers (Saleh et al., 2008; Koner et al., 2011). CB7, in particular, is capable of encapsulating the benzimidazole derivatives albendazole, carbendazim, thiabendazole, and fuberidazole (Saleh et al., 2008; Koner et al., 2011; Tang et al., 2018). These molecules possess very low water solubility in their neutral forms. The *pK<sub>a</sub>* values of this class of molecules are in the range of 3.5–4.8, and, therefore, they are neutral at physiological pH, which hinders their usability. The binding affinities of benzimidazole derivatives to CB7 in their neutral forms are in the millimolar range; these increase significantly for the protonated forms, reaching micromolar values (Koner et al., 2011). The preferential binding of the protonated forms increases the *pK<sub>a</sub>* values of the conjugate acids of these drug molecules by 2–5 units and, thereby, improves their solubilities by stabilizing the protonated forms at pH 7.2. For example, CB7 increased the aqueous solubility of albendazole by 2,000-fold

(Zhao et al., 2008). Other CBn homologs and acyclic derivatives can also enhance the solubility of albendazole (Ma et al., 2012a; Vinciguerra et al., 2012). Beyond the enhanced solubility, CB7 was found to improve the photostability of several benzimidazole drugs (Koner et al., 2011). For example, fuberidazole, and thiabendazole photobleached less effectively in the presence of CB7, with photostabilization factors amounting to 7 and 3, respectively. In addition, CB7 prevents the interconversion of crystal polymorphs of albendazole and retained the amorphous structure in the resulting complex (Saleh et al., 2012).

Sanguinarine (**Figure 2**), which has anti-oxidant, anti-tumor, anti-bacterial, and anti-inflammatory properties, forms a stable complex with CB7 (Miskolczy et al., 2011). The binding inside CB7 stabilizes the active form of sanguinarine by a complexation-induced *pK<sub>a</sub>* shift of the alkanolamine from 7.2 to 10.8, allowing its usability in the active form at higher pH values. Further, the complexed sanguinarine was stabilized toward photoirradiation relative to the free drug. CB7 forms a stable host-guest complex with berberine (**Figure 2**), an antimicrobial agent. The binding was monitored by the fluorescence change of berberine upon complexation, in which the fluorescence of berberine was enhanced by a factor of 500 upon complexation with CB7 (Miskolczy and Biczók, 2014a). With CB8, two berberine units are encapsulated (Miskolczy and Biczók, 2014b). The antimicrobial alkaloid coptisine forms also complexes with CBs, as reflected again in fluorescence changes. The fluorescence intensity of coptisine was greatly enhanced in the presence



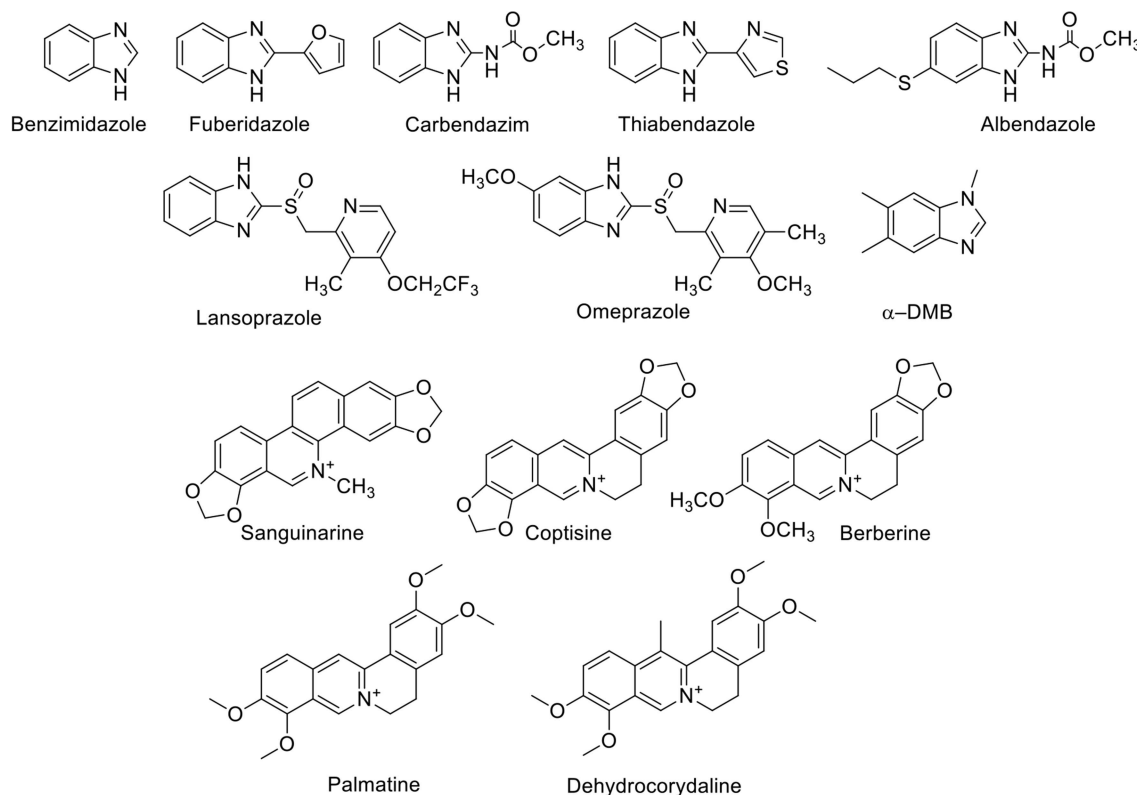


**FIGURE 2** | Chemical structures of benzimidazole derivatives and alkaloids which form host-guest complexes with CBn.

of CB7, affording a highly sensitive and selective method for the determination of coptisine in aqueous solution (Li et al., 2010). CB7 binds to isoquinoline alkaloids, namely palmatine and dehydrocorydaline (**Figure 2**) with binding affinities of  $2.4 \times 10^6$  and  $3.2 \times 10^4 \text{ M}^{-1}$ , respectively (Li et al., 2009). The dramatic fluorescence enhancement upon complexation with CB7 can be observed by naked eye.

Dye displacement was employed to study the complexation of nicotine (**Figure 3**) by CB7 in aqueous solution (Zhou et al., 2009a). Methylene blue was used as a dye that forms an inclusion complex with CB7 and shows a significant fluorescence response upon complexation. The addition of nicotine, as a competitor guest and analyte, displaced the dye, leading to the restoration of the original dye fluorescence. This allows for the detection of nicotine in concentrations as low as  $0.05 \mu\text{g mL}^{-1}$  (Zhou et al., 2009a). Tropicamide (**Figure 3**), an antimuscarinic drug routinely applied in eye drops to cause a mydriatic response (pupil dilation) in preparation for ophthalmological examinations and surgery, forms inclusion complexes with CB7 and CB8 in aqueous solution (Saleh et al., 2011). The protonated tropicamide showed high binding affinity with both hosts ( $K_a = 1.3 \times 10^3$  and  $4 \times 10^4 \text{ M}^{-1}$  with CB7 and CB8, respectively) (Saleh et al., 2011). Saleh et al. also reported the formation of a host-guest complex between CB7 and the antihistamine drug tripeleennamine (Saleh et al., 2016). The binding was studied by means of optical

and NMR titrations (Saleh et al., 2016). Macartney and coworkers studied the complexation of local anesthetics with CB7 (Wyman and Macartney, 2010). They found that CB7 can bind procaine ( $K_a = 3.5 \times 10^4 \text{ M}^{-1}$ ), tetracaine ( $K_a = 1.5 \times 10^4 \text{ M}^{-1}$ ), procainamide ( $K_a = 7.8 \times 10^4 \text{ M}^{-1}$ ), dibucaine ( $K_a = 1.8 \times 10^5 \text{ M}^{-1}$ ), and prilocaine ( $K_a = 2.6 \times 10^4 \text{ M}^{-1}$ ) in acidic aqueous solution. These binding affinities are much higher than those measured for CDs (Wyman and Macartney, 2010). Recently, benzocaine, and its metabolite, *p*-aminobenzoic acid, have been reported to form host-guest complexes with CB7 in water (Li et al., 2016a). The binding affinities are  $2.2 \times 10^4 \text{ M}^{-1}$  and  $1.5 \times 10^4 \text{ M}^{-1}$  for the protonated guests, respectively (Li et al., 2016a). The supramolecular interactions of a bactericidal agent against tuberculosis, namely isonicotinic acid hydrazide, commonly known as isoniazid, have been studied with CB6 and CB7 (Cong et al., 2011). The complexation with the macrocyclic hosts hindered the acylation reaction of isonicotinic acid hydrazide (Cong et al., 2011). Complexation of carboxin, a fungicide, with CB8 was found to promote the inhibition activity of carboxin on mycelial growth of *Rhizoctonia solani* (Liu et al., 2011). Relative improvement was evaluated in terms of area covered by the mycelia of *R. solani* and their growth inhibition rate (Liu et al., 2011).

The binding of drug molecules to biomacromolecules can be mediated by the complexation to macrocyclic hosts. For

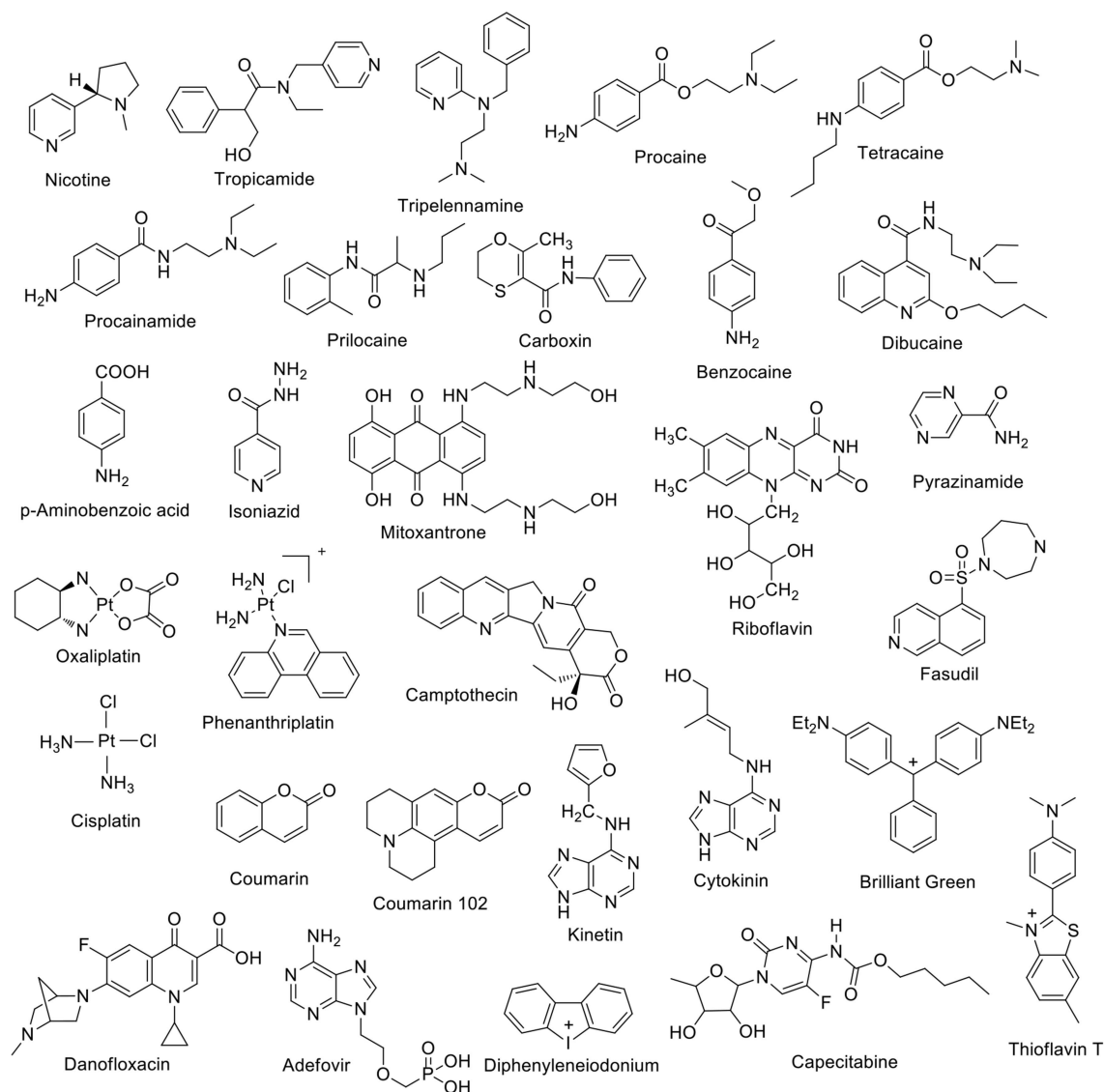


**FIGURE 3** | Chemical structures of a first set of selected drug molecules which form host-guest complexes with CBn.

example, the binding affinity of Brilliant Green (BG) to bovine serum albumin (BSA) was enhanced in the presence of CB7 (Bhasikuttan et al., 2007). The CB7 cavity can encapsulate part of the BG molecule, while the unencapsulated part remained accessible to associate to BSA. Mitoxantrone, an anthracenedione antineoplastic agent used to treat certain types of cancer, forms a 2:1 host:guest complex with CB8 (Konda et al., 2017). The complexation increased the mitoxantrone uptake in mouse breast cancer cells and decreased its toxicity (Konda et al., 2017). The complexation of capecitabine with CB7 was investigated by Wang et al. (2018). ITC experiments revealed a 1:1 binding stoichiometry with  $K_a = 2.8 \times 10^5 \text{ M}^{-1}$ . The encapsulation of platinum anticancer drug was reported by Kim and coworkers (Jeon et al., 2005). Oxaliplatin was found to form a 1:1 inclusion complex with CB7 in aqueous solution with a  $K_a$  value of  $2.3 \times 10^6 \text{ M}^{-1}$ . The complexation inside

the cavity of CB7 resulted in an enhanced stability (Jeon et al., 2005). The CB7•oxaliplatin complex exhibited cooperatively enhanced antitumor activity compared to oxaliplatin itself (Chen et al., 2017). Phenanthriplatin, an anticancer drug, forms supramolecular complexes with CBs as well (Kahwajy et al., 2017). CB7 accommodates one phenanthriplatin molecule, while the larger cavity of CB8 can simultaneously bind two molecules. The release of phenanthriplatin can be achieved by the addition of cations. NMR studies suggest that cisplatin forms an inclusion complex with CB7, while  $\text{cis-[PtCl(NH}_3)_2(\text{H}_2\text{O})]^+$  only binds at the portals (Wheate et al., 2006). The formation of a 1:1 riboflavin•CB7 complex in aqueous solution ( $K_a = 1.25 \times 10^4 \text{ M}^{-1}$ ) has also been reported (Zhou et al., 2009b). Coumarin, an anti-coagulant, was found to form stable inclusion complexes with CB7 and CB8 in aqueous solution (Wang et al., 2009). The binding constant with CB7 was measured as  $2.6 \times 10^5 \text{ M}^{-1}$ .

Crystal structures revealed the encapsulation of two coumarin units inside CB8 (Wang et al., 2009). Fasudil (FSD), a *roh* kinase inhibitor, forms a stable supramolecular host-guest inclusion complex with CB7 with a binding constant of  $K_a = 4.28 \times 10^6 \text{ M}^{-1}$  under acidic conditions (pH = 2.0) (Yin et al., 2017). The effect of camptothecin complexation with CBn ( $n = 7$  and  $8$ ) on its solubility and reactivity as an anticancer drug was reported by Dong et al. (2008). The solubility of camptothecin was enhanced up to 70 and 8 times at pH 2 due to the formation of host-guest complexes with CB7 and CB8, respectively. Further, the formed host-guest complexes retained the characteristic camptothecin activity (Dong et al., 2008). Kinetin (**Figure 3**), a plant hormone that promotes cell division, forms inclusion complexes with CB7 and substituted CB6 derivatives in aqueous solution as well as in the solid state (Huang et al., 2008b). A magnetic perhydroxy-CB8 material was prepared that showed good adsorption capacity for cytokinins (Zhang et al., 2016). CB7 was reported to form stable complexes with the H2-receptor antagonist ranitidine, the administration of which is one of the most popular treatments of stomach ulcer symptoms (Wang and Macartney, 2008). The stability of the ranitidine complexes varies for the diprotonated ( $K_{a1} = 1.8 \times 10^8 \text{ M}^{-1}$ ), monoprotonated ( $K_{a2} = 1.0 \times 10^7 \text{ M}^{-1}$ ), and neutral form ( $K_{a3} = 1.2 \times 10^3 \text{ M}^{-1}$ ). The CB7 complex was also found to improve the thermal stability of the drug (Wang and Macartney, 2008).

The complexation of diphenyleneiodonium (**Figure 3**), a bioactive halonium ion, with CB7 and CB8 has been recently reported (Yin et al., 2018). Host-guest binding experiments revealed a 1:1 complexation stoichiometry with CB7 ( $K_a = 3 \times 10^4 \text{ M}^{-1}$ ) and a 1:2 one with CB8 ( $K_a = 2 \times 10^{12} \text{ M}^{-1}$ ). Interestingly, the complexation was shown to modulate the inhibitory activity of diphenyleneiodonium against reactive oxygen species generation and to alleviate its cardiotoxicity.

Recently, the complexation of a third-generation fluoroquinone, danofloxacin (**Figure 3**), by CB7 has been investigated (El-Sheshtawy et al., 2018). The complex was found to be stable at different pH values ( $K_a = 10^3$ – $10^5 \text{ M}^{-1}$ ). The antibacterial activity of danofloxacin, and two additional second-generation fluoroquinones, i.e., norfloxacin and ofloxacin, was enhanced in the presence of CB7. Feng et al. studied the interaction between CB7 and the hepatitis B drug Adefovir (**Figure 3**) (Feng et al., 2019). Adefovir forms a 1:1 complex with CB7 with  $K_a = 4.25 \times 10^3 \text{ M}^{-1}$ . The thermal stability of Adefovir was enhanced upon complexation.

The CB6 derivative (allyloxy)<sub>12</sub>CB6 forms a stable supramolecular host-guest complex with acetylcholine ( $K_a = 5 \times 10^3 \text{ M}^{-1}$ , **Figure 4**) and a much weaker complex with choline (Kim et al., 2012; Ghale and Nau, 2014). An indicator displacement strategy was developed for the detection of ethambutol (**Figure 4**) in water as well as in biological fluids (Wu et al., 2011). The complexation of ethambutol to CB7 was observed upon the release of the precomplexed fluorescent dye (Wu et al., 2011). Adamantane derivatives have found practical application as drugs. The hydrophobic nature of the adamantane residue is well-known in the CB field as a gold-standard with high-binding affinity (Liu et al., 2005a; Assaf and Nau, 2015). For example, amantadine and memantine form exceptionally

stable complexes with CBn ( $n = 7$  and  $8$ ) (Vázquez et al., 2014; Assaf and Nau, 2015). Pyridoxine, also known as vitamin B6 or pyridoxol, could be encapsulated inside the CB7 cavity in aqueous solution ( $K_a = 4.0 \times 10^3 \text{ M}^{-1}$ ) (Li et al., 2016d). The 1:1 complexation pattern was characterized by <sup>1</sup>H NMR and UV-Visible spectroscopy (Li et al., 2016d). The interaction between the CB7 macrocycle and pilocarpine was investigated in aqueous solution by using <sup>1</sup>H NMR and circular dichroism spectroscopic techniques (Saleh et al., 2014). The protection of the lactone group showed a significant enhancement upon the chemical stability of pilocarpine against hydrolysis in basic aqueous solution (Saleh et al., 2014). Thiamine, thiamine monophosphate, and thiamine pyrophosphate form 1:1 host-guest complexes with CB7 as well (Li et al., 2016b). The host-guest stability constants were determined by UV-Visible titrations. The presence of an anionic phosphate/diphosphate group on the molecular structures lowered the binding affinity (Li et al., 2016b).

Collins and Day investigated the interactions of the antibiotic drugs *trans*-[(PtCl(NH<sub>3</sub>)<sub>2</sub>)<sub>2</sub>(μ-NH<sub>2</sub>(CH<sub>2</sub>)<sub>8</sub>NH<sub>2</sub>)]<sup>2+</sup> and [(Ru(phen)<sub>2</sub>)<sub>2</sub>(m-bb<sub>5</sub>)]<sup>4+</sup> {phen = 1,10-phenanthroline; bb<sub>5</sub> = 1,5-bis[4(4'-methyl-2,2'-bipyridyl)]-pentane} (Rubb5, **Figure 4**) with CB macrocycles. <sup>1</sup>H NMR experiments indicated that the platinum group at both ends of the *trans*-[(PtCl(NH<sub>3</sub>)<sub>2</sub>)<sub>2</sub>(μ-NH<sub>2</sub>(CH<sub>2</sub>)<sub>8</sub>NH<sub>2</sub>)]<sup>2+</sup> were too large to allow the threading through the portal of CB6. On other hand, CB7 and CB8 were able to bind the platinum complex, in which all methylene groups are located inside the cavity, while the platinum centers docked at the CB portals (Pisani et al., 2010). The complexation with CBs prevented the degradation by biological nucleophiles. The large cavity of CB10 could also serve as a delivery vehicle for these potential drugs (Pisani et al., 2010; Deng et al., 2018).

CBn ( $n = 7$  and  $8$ ) act as artificial organic receptors for steroids (**Figure 5**), including the hormones testosterone and estradiol, the inflammation inhibitor cortisol, as well as the muscle relaxants pancuronium and vecuronium, with extraordinarily high binding affinities (Lazar et al., 2016). For example, CB8 binds preferentially estranes, androstanes, and pregnanes, while CB7 binds nandrolone selectively. The high affinities are also retained in buffered water as well as in biological media such as gastric acid and blood serum. Three steroidal neuromuscular blocking agents, rocuronium, vecuronium, and pancuronium have been investigated as candidate guest molecules for CB7. In aqueous solution, CB7 binds the steroidal neuromuscular blockers with high affinity, following the order: vecuronium > pancuronium > rocuronium (Gamal-Eldin and Macartney, 2014).

CBs can selectively accommodate and interact with amino acids and small peptides in water (Bush et al., 2005; Urbach and Ramalingam, 2011; Gamal-Eldin and Macartney, 2013; Biedermann and Nau, 2014; Lee et al., 2015; Smith et al., 2015; Kovalenko et al., 2016; Bai et al., 2017). The binding of amino acids and their corresponding decarboxylated adducts to CB7 was explored by Bailey et al. The study revealed a higher affinity for the decarboxylated molecules (Bailey et al., 2008). Urbach and coworkers showed that the binary CB8•methyl viologen complex can selectively bind peptides with N-terminal

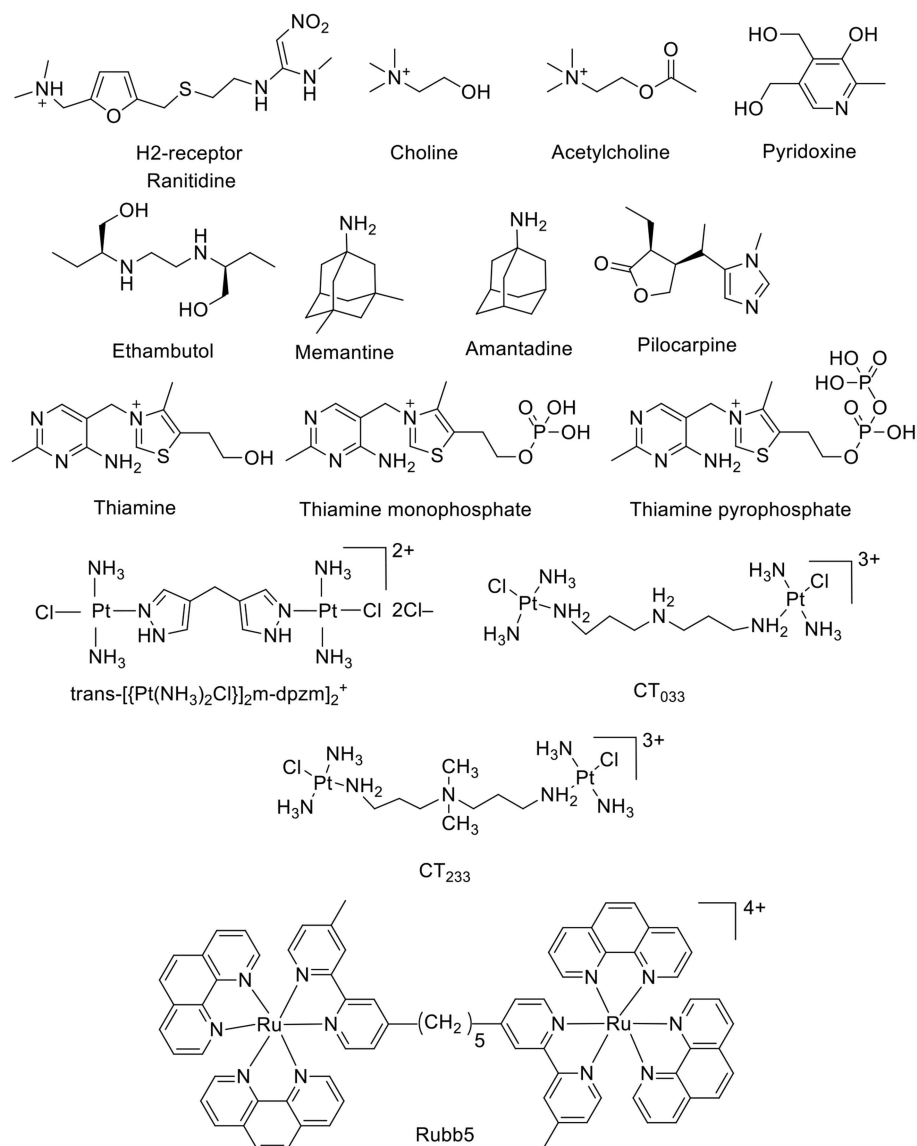


**FIGURE 4** | Chemical structures of a second set of selected drug-based molecules which form host-guest complexes with CBn.

tryptophan compared to C-terminal or internal tryptophan residues through the formation of a ternary complex (Bush et al., 2005). Recently, selective peptide recognition has also been documented for methionine-terminated peptides with CB8 as a receptor without any auxiliary guest (Hirani et al., 2018). The binding of human insulin by CB7 *in vitro* was also reported (Chinai et al., 2011). Its recognition relies on the binding of N-terminal phenylalanine to CB7 ( $K_a = 1.5 \times 10^6 \text{ M}^{-1}$ ) (Chinai et al., 2011).

## MECHANISMS OF DRUG RELEASE FROM CUCURBITURIL-BASED SYSTEMS

A schematic presentation of various ways to release encapsulated drugs from CB•drug complexes is shown in **Figure 6**.

## Dilution Effect

Dissociation of CB•drug complexes to release the drug molecules in general follows a fast kinetics and the association and dissociation rate constants fall in the order of seconds or faster which ensures a fast dynamic equilibrium for rapid drug release. However, very slow release with dissociation rate constants in the range of hours has also been reported, potentially suitable for sustained release. Albendazole (**Figure 2**), an antiparasitic agent, was found to be released within seconds from CB7, while the release of dinuclear ruthenium complexes (**Figure 4**) from the cavity of CB10 takes several hours (Zhao et al., 2008; Pisani et al., 2010). One important factor controlling the dissociation is the dilution, which inevitably occurs when a CB•drug complex enters the body fluid. Complexes with macrocycles are held together by weak non-covalent forces, which can be disrupted

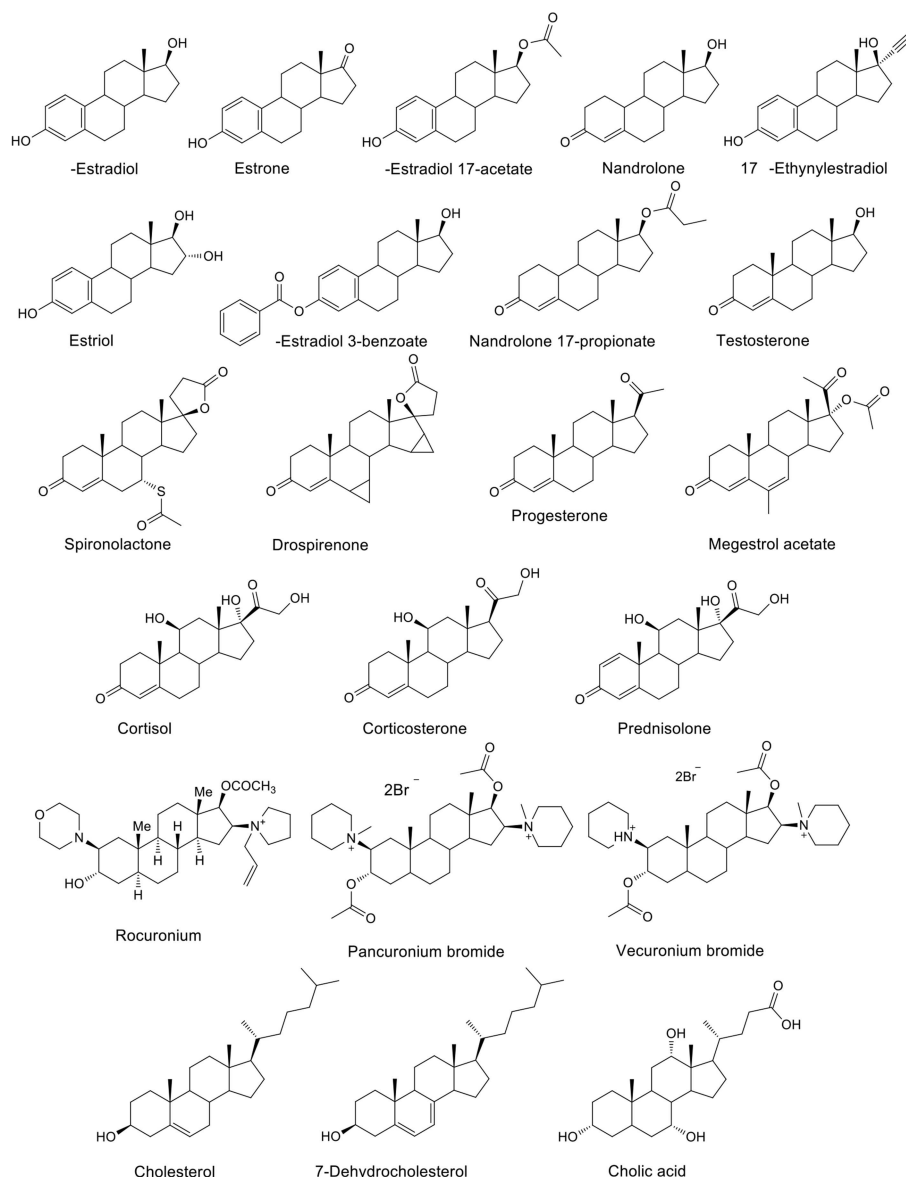


**FIGURE 5** | Chemical structures of steroids which form host-guest complexes with CB7 and CB8.

after administration, such that the CB•drug complexes encounter a lowering in concentration. Invariably, dilution decreases the degree of complexation. Thus, the release of the administered drug will spontaneously occur simply because of the associated dilution effect. It is worth mentioning that an accelerated release of drugs is not always desirable; for certain treatments, a sustained and slow release may be preferred to achieve the highest therapeutic effect. In the case of *cis*-platin (**Figure 3**), as reported by Wheate and coworkers, the encapsulated drug inside CB7 showed a much slower release rate *in vivo* than in the *in vitro* experiments (Plumb et al., 2012). A direct consequence is the retention of complexed *cis*-platin in circulation for a longer

time than of the free drug which leads to better efficacy of the drug. In this regard, one also needs to consider that the absolute binding affinities of the guest molecules with CBs are not always a useful measure of the kinetics of drug release; the tight carbonyl portals of CBs may present a steric/mechanical barrier toward ingress and egress of larger guests, a phenomenon known as constrictive binding (Márquez and Nau, 2001b; Márquez et al., 2004b; Pisani et al., 2010). Though the dynamic complexation-decomplexation of the drug molecules from the CB cavity is found effective in certain cases, it is equally important to incorporate stimuli responsiveness to the complexes which may lead to the release of drugs at a specific location, time, or rate.



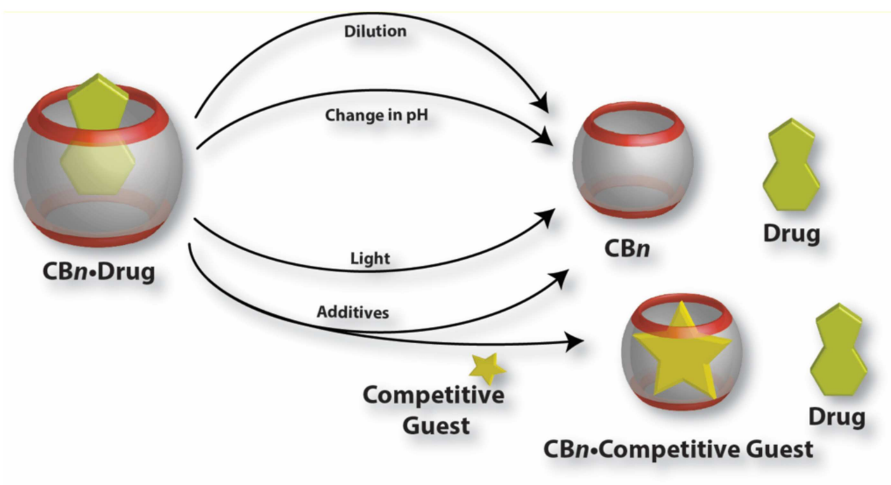


**FIGURE 6** | Graphical presentation of various mechanisms for the release of drug molecules from CB•drug complexes.

## Effect of Additives

Another viable way of releasing encapsulated drugs is the use of inorganic cations. Inorganic cations competitively displace cationic guests (Shaikh et al., 2008) from the CB cavity by binding at the portals. As a consequence, the effective binding constants of the guests always get reduced in the presence of salts (Márquez et al., 2004b; Bhasikuttan et al., 2011). Importantly, biological fluids naturally contain large amounts of salts which can trigger the release of drugs from CB complexes. As a proof of concept, it was shown that salts can shift the equilibrium from CB7-bound methyl red to the dye bound in the hydrophobic pocket of BSA (Shaikh et al., 2008). Shaikh et al. have shown that the 1:1 and 1:2 complexes of Thioflavin T (ThT, **Figure 3**) and CB7 respond differently to the presence of salts. In case of the 1:1 complex, the consequence of addition of salts is the release of the dye while in case of the 1:2 complex, metal ions result in the formation of a capsule-like structure (Choudhury et al., 2009, 2010). The addition of a competitive guest in the form of 1-adamantylamine (ADA), an antiviral and antiparkinsonian drug itself, leads to the destruction of the capsular complex. A competitive guest can also be effective in releasing the drug molecules from the CB cavity. Kim et al. demonstrated that CB7-stabilized amine-functionalized gold nanoparticles (AuNP-NH<sub>2</sub>) can be ruptured by ADA to release AuNP-NH<sub>2</sub> (**Figure 7**) and, thereby, enhance their cytotoxicity toward MCF-7 cells (Kim et al., 2010a).

The release of entrapped drugs from self-assembled systems can also be achieved by addition of macrocycles other than the ones used to form the self-assembly (Wu et al., 2016). The affinity of two macrocycles for different regions of the drug can be used to disassemble the system. As demonstrated by Wu et al., noncovalent association of alkyl-chain modified polyamines with CB6 decreased the critical aggregation concentration significantly and led to the formation of self-aggregated nanoparticles (Wu et al., 2016). CDs, which have a higher binding affinity to the hydrophobic chain, disrupt these doxorubicin-(DOX)-loaded nanoparticles to release

the drug molecules. The DOX-loaded nanoassembly exhibited better anticancer activity toward MCF-7 cancer cells, but was safe to normal cells. Singharoy et al. showed that the release of a naphthalimide derivative, [2-(2-aminoethyl)-1H-benzo[deisoquinoline-1,3(2H)-dione], from the cavity of CB7 can be modulated by the addition of surfactants (Singharoy et al., 2017). In the presence of non-ionic surfactants, e.g., Ig-720, the drug can be effectively released from CB7, while ionic surfactants were less effective (Singharoy et al., 2017).

## Changes in pH

The inclusion of protonated guests by macrocyclic hosts often results in a shift in the  $pK_a$  values of the guests (Márquez and Nau, 2001b; Saleh et al., 2008). The observed direction of the shift depends on the host and its inclination for binding with the protonated guest compared to its conjugate base. In case of CBs, in general, the  $pK_a$  values of basic guests increase as they are encapsulated inside the CB cavity. The switch in the  $pK_a$  value can be of great importance for the release of the guest molecule. A subtle change in pH of the system can lead to the decomplexation of the CB•drug complexes. A pH jump of the medium from below the  $pK_a'$  (the  $pK_a$  value of the complex) to above effectively reduces the binding constant of the drug and affects its fast release through changes of the chemical equilibrium toward the uncomplexed guest (and host).

A pH-responsive drug release was demonstrated by Zink and Stoddart in the form of surface-immobilized pseudorotaxane-based nanovalves (**Figure 8**) (Angelos et al., 2008, 2009). Mesoporous silica nanoparticles functionalized with alkyne groups were loaded with Rhodamine B and, subsequently, the surface was functionalized by means of an interfacial CB6-catalyzed 1,3-dipolar cycloaddition of the alkyne groups and 2-azidoethylamine. This resulted in the formation of CB6/disubstituted 1,2,3-triazole[2]pseudorotaxanes which acted as nanovalves. An increase in pH of the system leads to the opening of nanovalves as the inclusion complex breaks and

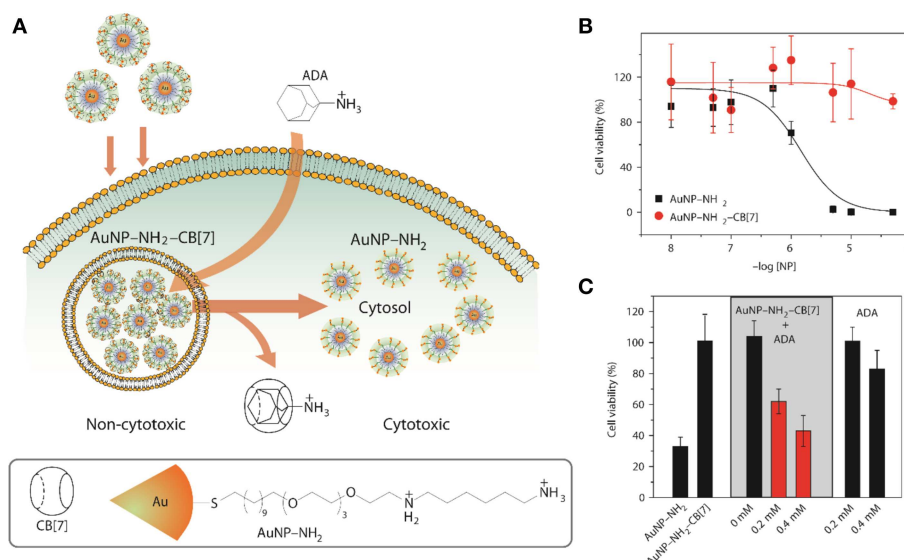


**FIGURE 7 | (A)** Schematic illustration for the use of intracellular supramolecular host-guest complexation to trigger nanoparticle cytotoxicity; **(B,C)** Cytotoxicity of AuNP-NH<sub>2</sub> and AuNP-NH<sub>2</sub>-CB7 and modulation of cytotoxicity of the gold nanoparticles (Kim et al., 2010a) (Reproduced with permission, Copyright 2010, Nature publishing group).

consequently, the loaded dye gets released. The pH-dependent binding of CB6 with the bisammonium stalks presents the operational principle of these nanovalves.

## Light-Triggered Release of Drugs From Cucurbituril•Drug Complexes

A photo-triggered change in pH and associated release of the guest from the complexed form is also possible, as demonstrated by Carvalho et al. (2011). In this model, the authors used Hoechst 33258 as a guest for CB7 and malachite green leuco hydroxide (MGOH) as a photo-base. The binding constant of protonated Hoechst 33258 with CB7 is 100 times higher than that of the neutral form of the dye. Upon irradiation with UV light, MGOH generates OH<sup>-</sup> and increases the pH of the solution from 7 to 9. This stimulus affects the release of Hoechst 33258 from the host cavity (**Figure 9**). A negative control in buffer resulted in no release of the drug. Photo-induced release of drugs can also be materialized by using appropriate photo-responsive molecules. Basilio and Pischel described the photo-controlled release of a widely used Alzheimer's drug, 3,5-dimethyl-1-aminoadamantane, also known as memantine, based on the photo-induced transformation of chalcone to flavylum (Basilio and Pischel, 2016). Charged flavylum can be generated by irradiating non-charged chalcone (three orders of magnitude lower affinity to CB7 than flavylum), which can effectively release the drug from its CB7•drug complex. Recently, Romero et al. reported a light-induced release of a tripeptide from the cavity of CB8 by employing the chalcone/flavylum photo-switch in conjunction with light and acid as input signals (Romero et al., 2018). The flavylum cation, which resulted from a pH-dependent and light-induced transformation of chalcone upon irradiation at

365 nm, acts as a competitive binder for CB8 and, thus, triggers the release of the tripeptide from the cavity (Romero et al., 2018).

The concept of nanovalves on mesoporous silica nanoparticles (**Figure 8**) was further extended to the controlled release of entrapped guests by light through a photothermal mechanism involving the plasmonic properties of a gold nanoparticle core (Croissant and Zink, 2012). For the preloaded guests (inside the pores) of a mesoporous silica matrix containing embedded gold nanoparticles, the release of the guest molecule could be triggered by laser irradiation. Laser irradiation with low intensity at the wavelength corresponding to the plasmon resonance of the gold nanoparticles causes a local internal heating through dissipation of the photonic energy, which raises the local temperature above 60°C to significantly decrease the ring-stalk binding and, thus, release the guest molecules. This light-sensitive nanostructure can increase the local temperature without significantly changing the bulk temperature, which could potentially be used for (spatially) controlled dual therapy involving the delivery of drug molecules to cells and necrosis through hyperthermia.

## Release From Micro-Heterogeneous Systems

Apart from inclusion complexation-based drug release, CBs were successfully implemented in constructing micro-heterogeneous systems which can entrap and release drug molecules. Construction of supramolecular peptide-amphiphiles using ternary complexation presents one example (Jiao et al., 2012; Mondal et al., 2015). Supramolecular peptide amphiphiles (SPAs) and their vesicle formation were reported where the SPAs were prepared with a viologen amphiphile and peptides containing an appropriate second guest. In

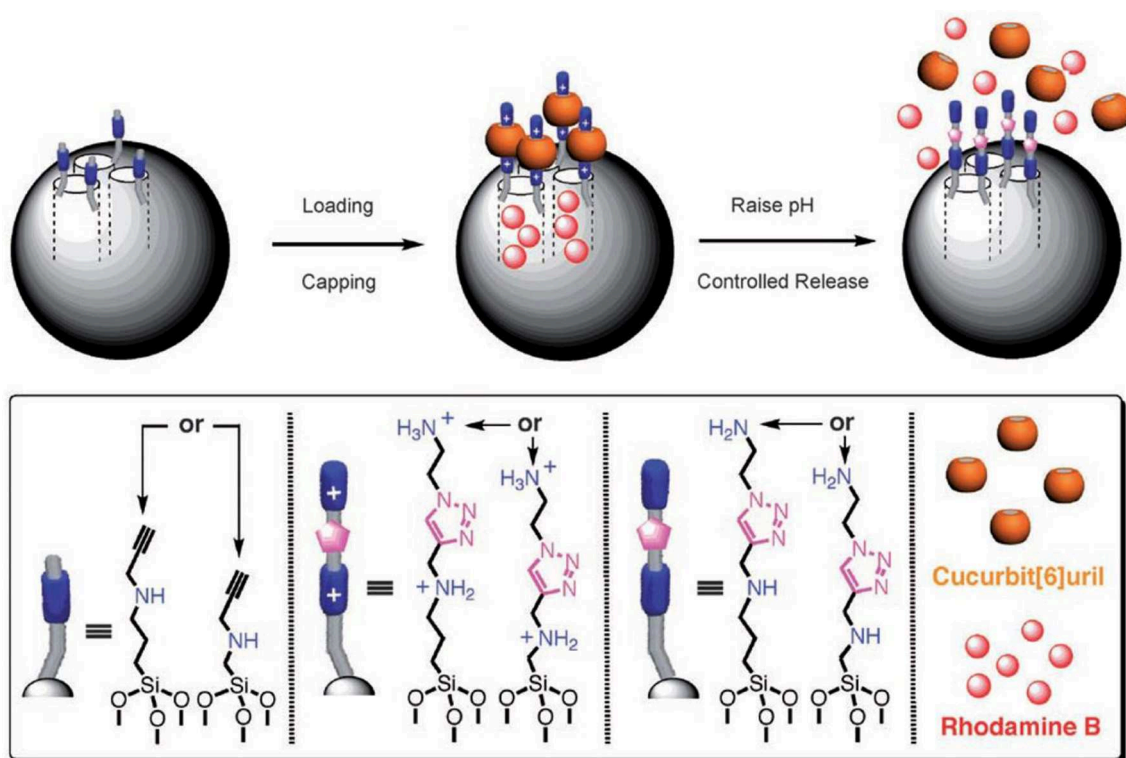


**FIGURE 8** | Graphical representations of operational supramolecular nanovalves (Angelos et al., 2008) (Reproduced with permission, Copyright 2008, Wiley-VCH Verlag GmbH and Co. KGaA, Weinheim).

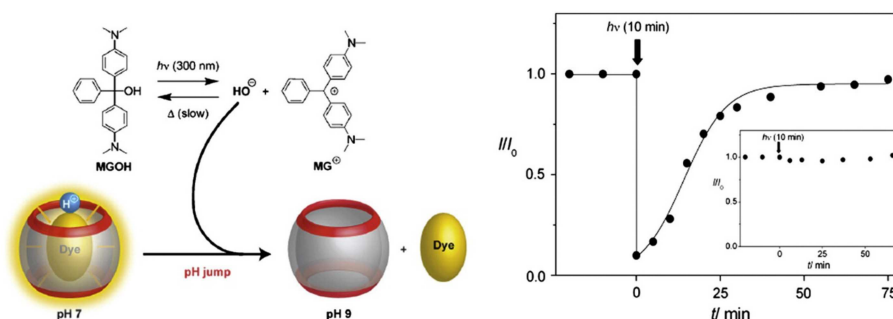
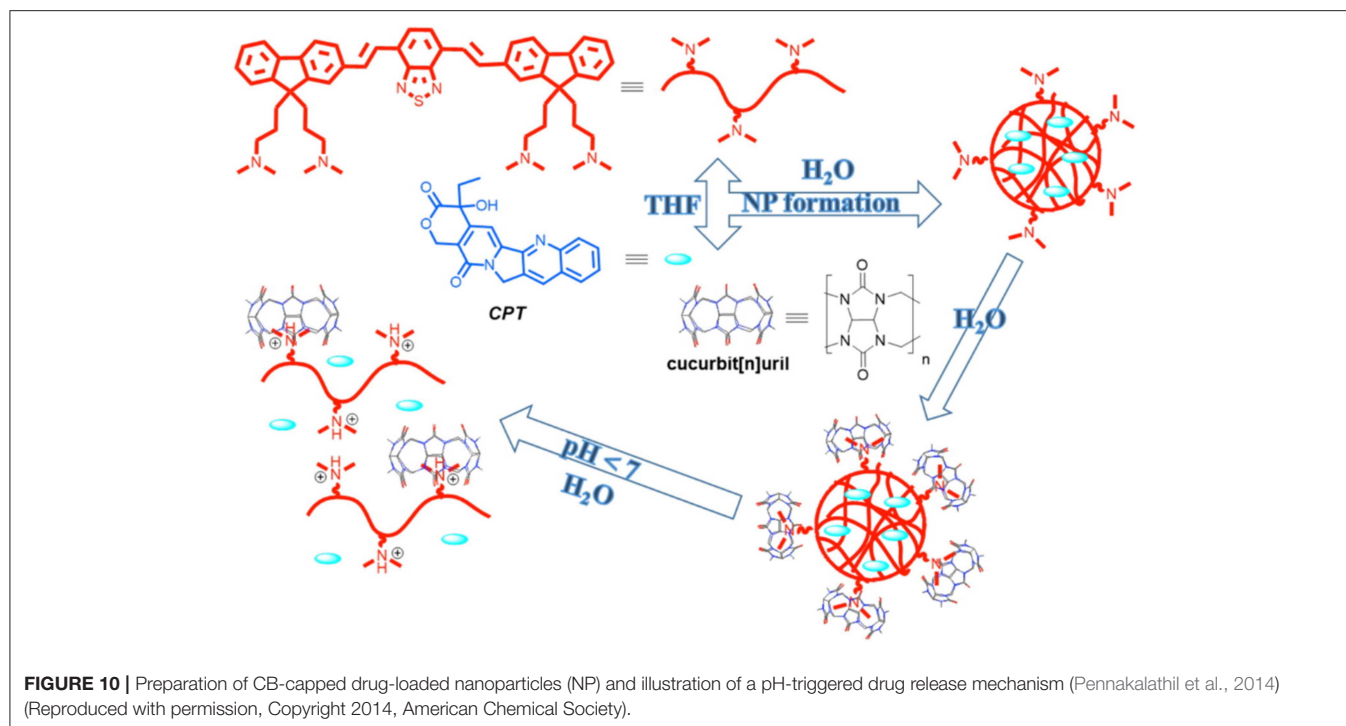


**FIGURE 9** | Graphical representation of a photo-triggered pH jump-induced release of an encapsulated dye (MGOH, malachite green leuco hydroxide) from the cavity of CB7 (Carvalho et al., 2011) (Reproduced with permission, Copyright 2011, The Royal Society of Chemistry).

their pioneering work, Scherman and coworkers have shown that the vesicles formed by the SPAs were taken up by HeLa cells and responded to multiple external triggers, which could modulate the toxicity of the supramolecular system (Jiao et al., 2012).

Hydrogels are another class of materials, which are being considered as potential targeted drug delivery vehicles. CB6-containing alginate hydrogel beads were found to load an anti-cancer drug, 5-fluorocil (FU), with a loading capacity of 3.87–6.13 wt%. These drugs can then be slowly released. The optimal (slowest) release, with a half-life of 2.7 h, was found for a loading of 5.94% (Huang et al., 2008a).

Nano-assemblies of CBs with proteins were also used as an effective way for the construction of stimuli-responsive materials for controlled release of drugs. A hybrid of bovine serum albumin (BSA) and CB7 formed a non-toxic nano-assembly which can load an anti-cancer drug, DOX and effectively release it in the presence of ADA or a change in pH. Importantly, the dis-assembly of the composite led to restoration of the BSA structure and its recognition property. The DOX-loaded assembly was observed to mask the cytotoxicity of DOX and the toxicity can be restored at the target on demand, triggering its therapeutic activity (Barooah et al., 2017).



Another important type of nanoscale assemblies are supramolecular polymers (Yang et al., 2015). In recent years, a considerable number of such supramolecular polymers have been reported that are based on CBs (Appel et al., 2012; Stoffelen et al., 2015; Ahmed et al., 2016). Loh et al. reported a micelle-like structure formed by supramolecular assembly of poly(*N*-isopropylacrylamide) (as a thermoresponsive block) and poly(dimethylamino-ethylmethacrylate) (as the pH-responsive block) (Loh et al., 2012). These two blocks are held together by ternary complexation of CB8. DOX was encapsulated inside this micelle-like structure and intracellular delivery of the drug was demonstrated using three stimuli, namely, pH, temperature, and a competitive binder. The micellar structure disrupted upon changing the pH from 7 to 4, upon lowering the temperature from 37°C to 15°C, and upon addition of ADA. The release of DOX from the micellar core to the nuclei of HeLa cells was also observed within a desirable time frame.

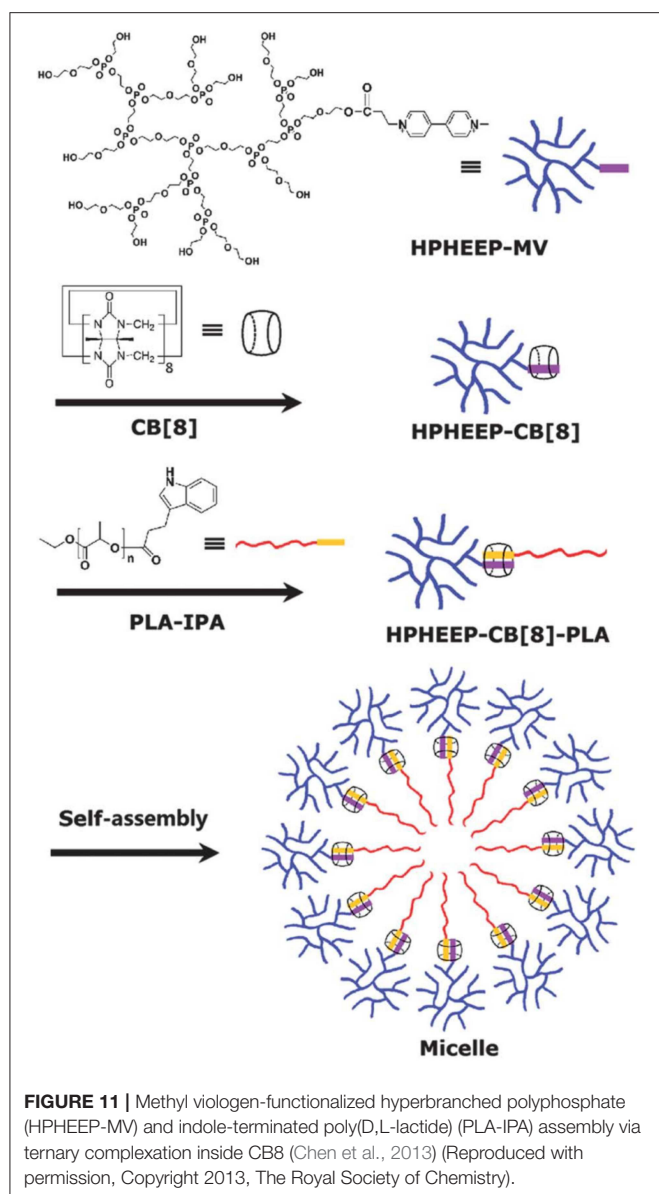
In a recent study, Tuncel and coworkers reported the synthesis of nanoparticles based on a conjugated oligomer (Pennakalathil et al., 2014). The nanoparticles could carry camptothecin, an anticancer drug, with high loading efficiency. The cell viability studies with breast cancer cell lines showed that the  $IC_{50}$  values of the nanoparticles for MCF7 and MDA-MB-231 were 44.7 and 24.8  $\mu$ M, respectively. The cytotoxicity of the nanoparticles was further decreased by capping the amine groups with CB7.  $IC_{50}$  values for camptothecin in the presence of nanoparticles with or without CB7 were significantly reduced in MCF7 and MDAMB-231 cells. CB7-capped drug-loaded nanoparticles regulated the release rate by providing much slower release at pH 7.4 than the nanoparticles in the absence of CB7 (Figure 10).

Alternatively, a redox trigger can be applied to release entrapped drug molecules from polymeric materials. Methyl viologen-(MV)-functionalized hyperbranched polyphosphate (HPHEEP-MV) and indole-terminated poly(D,L-lactide) (PLA-IPA) can be conjugated via ternary complexation inside CB8 (Figure 11) (Chen et al., 2013). The amphiphilic ternary complex could form micelles where HPHEEP remains at the surface while the interior is made of PLA. The micelles could be disrupted by the addition of ADA or  $Na_2S_2O_4$  through competitive binding or formation of radical cations of MV, respectively. The disruption of the micellar structure results in the release of the loaded hydrophobic drug Coumarin 102 (Figure 3). In another example, the team has reported a micellar assembly via ternary complexation of viologen-functionalized poly(ethylene oxide) (PEO) and PLAIPA (Zhao et al., 2014). The micelles were loaded with DOX and the release of the drug could be triggered by reduction with  $Na_2S_2O_4$ . *In vitro* cell viability studies indicated good biocompatibility of the micelles toward two cell lines, that is, human umbilical vein endothelial cells (HUVEC) and human liver cancer HepG2 cells. Enhanced toxicity was observed.

## TARGETED DRUG DELIVERY FROM CUCURBITURIL-BASED SYSTEMS

In the previous section, we have discussed the different mechanisms which can be used to release encapsulated drugs from either inside CBs or CB-based self-assemblies. However, the bigger challenge is to create the “magic bullet” which can specifically target the diseased cell and deliver the therapeutic





site-selectively. Researchers have recently concentrated their efforts on preparing new CB-based systems which can deliver drugs at the targeted site. The present section encompasses a summary for most of the reports on such CB-based targeted drug delivery systems.

Targeting can be achieved via appropriate functionalization of the carrier system with functional groups that are recognized by specific receptors present at the cell surface. Incorporation of these functional groups into the system can either be achieved by covalent or non-covalent attachment of such groups to the self-assembled delivery vehicle. A promising example is the synthesis of a functionalized CB6 derivative that assembles into vesicles (Lee et al., 2005). The surface of the vesicles can be decorated via non-covalent interactions of alkylammonium-tagged guests with free CB6 cavities. When the surface of the vesicles was decorated with a thiourea-linked  $\alpha$ -mannose-spermidine conjugate and

mixed with a solution containing Concanavalin A (ConA), a lectin that shows specificity toward  $\alpha$ -mannose, immediate aggregation was observed. The use of a galactose derivative instead of mannose did not show any aggregation. The resulting system can be potentially applied to diseases where mannose receptors are over-expressed.

Functionalized CB6 was also used to prepare nanoparticles loaded with Nile red (NR, as a model hydrophobic drug) and decorated with spermidine-conjugated folate via host-guest chemistry of CB6 and spermidine (Park et al., 2009). The folate-decorated system showed effective uptake of the dye into HeLa cells whose surface has overexpressed folate receptors. A negative control with nanoparticles lacking folate resulted in no or minimal uptake of the dye. Folate receptor-mediated endocytosis was confirmed as uptake mechanism. After endocytosis, Nile red was released, as monitored by confocal laser scanning microscopy. Building on these findings, the unloading of the antitumor drug, PTX, to HeLa cells was also established. A galactose-functionalized CB6-based carbohydrate wheel was also used to demonstrate galactose-receptor mediated endocytosis into HepG2 hepatocellular carcinoma cells (Kim et al., 2007). In a complementary study, the same CB6-galactose conjugate was utilized to non-covalently encapsulate dextran-spermine conjugates into hepatocyte cells containing asialoglycoprotein (ASGPR) receptors. This model was also used to demonstrate the viability of a non-toxic and biocompatible receptor-mediated gene delivery system (Kim et al., 2010c).

A polymeric nanocapsule consisting of a disulfide-bridged CB6 was reported by Kim et al. Treatment with dithiothreitol (DDT), a reducing agent, breaks the disulfide linkage and ruptures the nanocapsule to release the pre-loaded dye (Kim et al., 2010b). The potential application of this system in targeted drug delivery was illustrated by encapsulating a galactose-spermidine conjugate into the CB cavity and, thereby, bringing the galactose moiety to the surface of the nanocapsules. Carboxyfluorescein was used as an imaging probe. After incubation with HepG2 hepatocellular carcinoma cells, a change in fluorescence inside the cells was observed, indicating the cellular uptake of the entire system. Controlled *in vitro* targeted release of DOX in HeLa cells has also been reported according to the same principle (Park et al., 2010).

In another work, CB6-conjugated hyaluronate (CB6-HA) was synthesized and non-covalently decorated with a peptide-spermidine conjugate (Jung et al., 2011). The peptide-spermidine was used as a model for a drug that binds to and activates the formyl peptide receptor (FPR1). A FITC-spermidine conjugate was used as imaging probe (Figure 12). Controlled drug targeting into B16F1 cells with HA receptors was confirmed *in vitro* by simultaneous bioimaging of FITC-spermidine-conjugated CB6-HA. Activation of the FPR1 receptor results in enhanced intracellular  $\text{Ca}^{2+}$  levels, through which the delivery of the CB6-HA-peptide-spermidine conjugate could be demonstrated in FPR1-expressing human breast adenocarcinoma (FPR1/MCF-7) cells. The bright fluorescence signal of FLUO-3/AM served as indicator for enhanced  $\text{Ca}^{2+}$  concentrations. The stability of the system



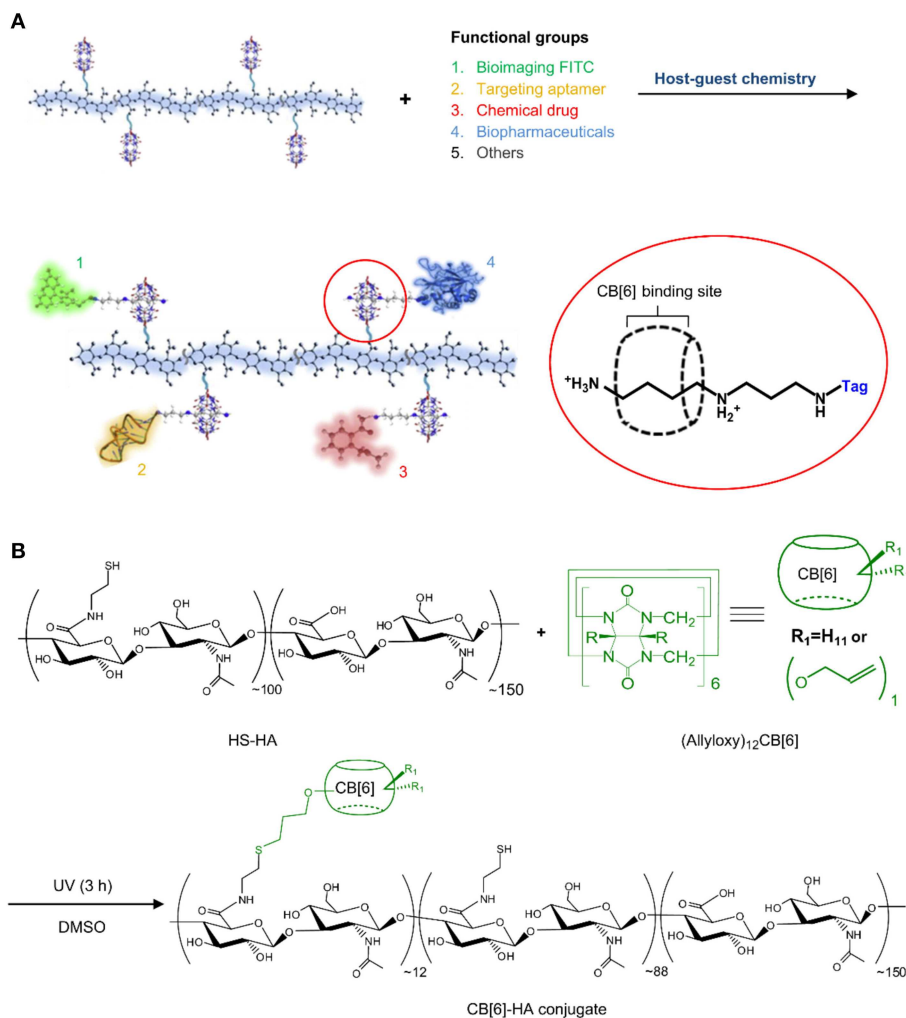


**FIGURE 12 | (A)** Schematic illustration of a multi-functional theranostic system using CB6-HA tethered with various functional “tag”-spermidine conjugates by the host-guest complexation between spermidine and CB6. **(B)** Preparation of a CB6-HA conjugate by UV photoreaction of thiolated hyaluronate (HS-HA) with (allyloxy)<sub>12</sub>CB6. FITC, fluorescein isothiocyanate (Jung et al., 2011) (Reproduced with permission, Copyright 2013, Elsevier).

in biological media was also demonstrated *in vitro* as well as *in vivo*.

Recently, a CB7-PEG copolymer was developed as drug carrier. The accessible cavity of CB7 was able to encapsulate the anticancer drug oxaliplatin. The supramolecular polymeric material displayed low cytotoxicity to normal cells. However, the cytotoxicity of the encapsulated oxaliplatin was recovered in cancer cells. The release of the anticancer drug is attributed to the high concentration of spermine in cancer cells, which acts as a competitive guest and, thereby, trigger the release of the complexed drug in a targeted manner (Chen et al., 2018).

Zhang and coworkers selected MV as model antitumor agent and demonstrated an elegant targeted delivery application, which is also based on overexpressed spermine (Chen et al., 2016). MV is highly toxic in nature and affects both tumor and normal cells without specificity. When encapsulated in CB7, the cytotoxicity of MV to normal cells decreased significantly.

However, for tumor cells, the overexpressed spermine displaces the encapsulated MV from the complex, thereby allowing the recovery of cytotoxicity of MV.

## CUCURBITURIL•DRUG COMPLEXES IN PHARMACEUTICAL FORMULATIONS

As discussed before, the stability of CB•drug complexes depends on the medium and presence of other components in the system. Similarly, the property and, hence, the preferred administration mode also depends on the biological media. The presence of salt and acid in biological media affect the solubility of CBs significantly (Steed and Gale, 2012). For example, the solubility of CB6 in simulated gastric fluid increases up to 4 mM (Walker et al., 2010) compared to 0.03 mM (Márquez et al., 2004a) in water. Moreover, the different solubilities of the members

of the CB family may dictate the most promising way of administration of the CB•drug complexes (Steed and Gale, 2012; Venkataramanan et al., 2012; Saleh et al., 2013).

The production of CB-based host-guest complexes as solid products involves mixing of the hosts and guests in appropriate stoichiometry, isolation of the complexes in solid form using either lyophilization (Zhao et al., 2008), co-solvent processing (Blanch et al., 2002), or ball-mill grinding (Constabel and Geckeler, 2004; Jiang and Li, 2006; Walker et al., 2010). A fundamental issue which needs to be taken care of is to ensure that the components are held together by non-covalent interactions. To shift the dynamic chemical equilibrium toward the bound drug in solution, the concentration of the host needs to be adjusted such that the drugs are mostly present in their complexed forms. As an asset, the guest binding affinity of CBs is exceptionally high which facilitates the preparation of solutions with 99% or even higher content of the complexed drug even at relatively low (excess) CB concentrations.

The simplest, safest, most convenient, and most common drug administration way is the oral route. Thus, formulation and production of CB-drug complexes in the form of tablets is essential (Walker et al., 2011). These cannot be produced from the CB•drug complexes alone but several pharmaceutical adjuvants need to be incorporated in the formulation. Walker et al. reported a tablet formulation in which up to 50% microcrystalline CB6 (w/w) was mixed with other excipients such as lactose (as diluent/bulking agent), Avicel (aids tablet compaction), talc, magnesium stearate (as lubricants and glidants), and Ac-Di-Sol (as disintegrant) (Walker et al., 2010). The compatibility of CB6 with other excipients was confirmed by various techniques (Walker et al., 2010, 2011). The same group has successfully used CB6 in a nasal drug formulation containing hydroxypropyl methylcellulose (HPMC) and sodium carboxymethylcellulose (NaCMC) (Walker et al., 2011).

Use of CB7 in drug formulation was found to have the additional advantage that it prevents interconversion of crystal polymorphs of the drugs and allows them to retain the amorphous structure in the resulting CB7 complex (Jeon et al., 2005; Kennedy et al., 2009; Wheate et al., 2010; Saleh et al., 2012). It is also noteworthy that CB7 does not affect the surface area and pore size distribution which is beneficial for processing and robust formulation (Saleh et al., 2012).

In a very recent report, a “Trojan antibiotic” has been formulated by a host-guest complex of CB7 and a bola-type azobenzene compound with glycosylamine heads at both ends (Wang et al., 2019). Similar to the bacterial wall, this supramolecular assembly displays a surface that is fully decorated with sugar-like components. This Trojan antibiotic was found to be benign to a wide spectrum of bacteria at a weak basic pH of approximately 9.0 under daylight conditions but became a potent bactericide toward both Gram-negative and Gram-positive bacteria at pH 4.0 under 365 nm UV irradiation. The dual use of pH and UV light greatly enhanced the efficacy of the bactericidal effect such that the  $MIC_{50}$  value of the Trojan antibiotic was observed to be at least 10 times smaller than that of conventional drugs. The activity of the Trojan antibiotic automatically stopped upon removal of the UV source and

reversal of pH which prevents the buildup of active antimicrobial materials in the environment. This novel approach may pave the way to a new era in the fight against bacterial resistance.

## CUCURBITURILS IN PHOTODYNAMIC THERAPY

CBs have also been explored in regard to their potential to serve as enhancement agents for photosensitizer drugs utilized in photodynamic therapy (PDT), which has recently been reviewed (Robinson-Duggon et al., 2018). PDT applications have been extended from discrete CB•photosensitizer host-guest complexes to elaborate nanomaterials and supramolecular assemblies. Wang and coworkers prepared, for example, CB6-based nano-capsules through direct alkylation of perhydroxycucurbit[6]uril with a ditopic linker. A photosensitive therapeutic payload, such as chlorin e6, was encapsulated within these nano-capsules for targeted PDT against cancer cells (Sun et al., 2019).

Another nanoscale CB-based PDT agent was constructed through a multi-step assembly by using a dipolar fluorescence compound (with carbazole as the electron-donor motif and pyridinium as the electron acceptor), CB8, and  $\alpha$ -cyclodextrin-modified hyaluronic acid (HA-CD) (Wu et al., 2019). The carbazole fluorophore was a non-NIR emissive dye with an emission wavelength of 568 nm that was used as photosensitizer. Host-guest complexation with CB8 exhibited a marked red shift of the emission maxima of the dye to 662 nm, such that the binary assembly could not only be used as an efficient PDT agent but also as a targeted NIR lysosome imaging probe. When HA-CD was incorporated into the assembly, owing to the strong interactions between  $\alpha$ -CD and the alkyl chain, the mixture resulted in a ternary nano-supramolecular assembly with targeting properties. In the presence of overexpressed acceptors on cancer cell surfaces, the assembly showed light toxicity toward cancer cells (A549) while the light cytotoxicity was found to be remarkably reduced for normal cells (293T). Thus, a complex system with an ability for NIR imaging and enhanced targeted PDT efficiency was successfully constructed using the orthogonal host-guest recognition with different macrocyclic molecules.

## CUCURBITURILS FOR ALLEVIATING AND MODULATING SIDE EFFECTS OF DRUG ADMINISTRATION

CBs can also reduce the toxicity or mask other properties of encapsulated guest molecules. The reversal of the action of neuromuscular blocking agents is a prominent example in this line of successful applications of the action of CBs and their derivatives (Ma et al., 2012b). CB7 was found to reduce the cytotoxicity of polycations such as polyethylenimine or cationic dendrimers through complexation (Lim et al., 2002; Li et al., 2017; Huang et al., 2018c). At the same time, these systems were demonstrated to act as efficient gene carriers. It has also been demonstrated recently that CB7 complexation of paraquat (methyl viologen dichloride hydrate), a widely used herbicide, decreases under various conditions and effectively the toxicity *in*

*vitro* and *in vivo* (Zhang et al., 2019b). In a recent report, CB7 was shown to inhibit seizures induced by small toxic molecules in both, zebrafish and mice models (Huang et al., 2018b), which has also been related to their complexation potential, which results in an effective detoxification. It has also been demonstrated that hexadimethrine bromide (HB), an agent which causes internal blood coagulation, can be efficiently captured by CB7 to control blood coagulation both *in vitro* and *in vivo* (Huang et al., 2018a). In another interesting application, it was found that CB7 is able to conceal the taste of the bitterest substance, denatonium benzoate (Yang et al., 2017).

A pH-induced toxicity switch has also been described by employing CB7 (Cheng et al., 2018). A triple-station guest (viologen-phenylene-imidazole or V-P-I) is used for CB7 complexation. The complex exhibits pH-directed translocation with high fatigue resistance (up to more than 100 cycles). Under basic pH, due to deprotonation of the imidazolium group (I station), CB7 positions itself around the viologen moiety (V station) and, thus, masks the toxicity of the viologen. Decreasing the pH into the acidic region protonates the imidazole group, affects a locomotion of CB7 to the phenylene (P) station, and thereby, the toxicity of the viologen unit becomes prominent. Cytotoxicity testing was performed *in vitro* on RAW 264.7 (murine macrophage) and BEL 7402 (human liver cancer) cell lines. It was observed that, in case of normal non-cancerous RAW 264.7 cells, there is significant masking of the toxicity when the guest is complexed within CB7. However, for cancerous BEL 7402 cells, no such difference could be observed. In RAW 264.7 cells CB7 is presumed to remain on station V since the local pH is  $\sim 7.4$  while in the case of BEL 7402 cells, it shuttles to station P as their pH is significantly lower, around 6.8 (similar to the  $pK_a$  of the guest).

## CUCURBITURIL-BASED SYSTEMS FOR DIAGNOSTICS AND OTHER BIOMEDICAL APPLICATIONS

Host-guest complexes of CBs have also been used for sensing, diagnostic, theranostic, and other relevant medicinal or bioanalytical applications. Monitoring enzymatic reactions by the tandem assay principle has been successfully implemented. The basic principle applied here is to form an inclusion complex of CB with an appropriate fluorescent dye whose affinity with CB lies ideally in between the binding constant of the substrate and the product of the enzymatic reaction of interest. For example, by using the Dapoxyl (a fluorescent dye)/CB7 reporter pair, the decarboxylation processes of different amino acids (Lys, Arg, His, Tyr, and Trp) to their corresponding biogenic amines (cadaverine, agmatine, histamine, tyramine, and tryptamine) can be conveniently monitored (Hennig et al., 2007; Nau et al., 2009). By using this principle along with the intrinsic enantiospecificity of decarboxylases for L-amino acid substrates, multi-parameter sensor arrays (for measuring concentrations of several amino acids in parallel) were designed that selectively signal the presence of a reactive pair of an L-amino acid and its corresponding decarboxylase (Bailey et al., 2008).

Numerous reports by Urbach and others have demonstrated binding of CBs to amino acids, peptides, proteins, biomolecules (e.g., neurotransmitters), and dyes, signifying applicability to extremely accurate biosensing applications at sub-nanomolar concentrations (Bush et al., 2005; Chinai et al., 2011; Smith et al., 2015). Indeed, sensors for various biomolecules using host-guest chemistry have been developed by several research groups (Biedermann et al., 2012a; Minami et al., 2012; Kasera et al., 2014; Sinn and Biedermann, 2018). The sequence-specific recognition property of CB7 can be transferred from sensing to separation applications. The groups of Urbach and Isaacs have, for example, coated mono-functionalized CB7 on a solid sepharose resin in order to separate proteins, namely human growth hormone as well as native insulin, in complex mixtures (Li et al., 2016c).

The binding pairs between CB7 and adamantyl- (AdA) or ferrocenyl-ammonium (FcA) were recently utilized by Kim as a supramolecular latching system for protein imaging, overcoming the limitations of protein-based binding pairs (Kim et al., 2018). Proteins in (or on) the cells were adamantylated/ferrocenylated using various labeling approaches. The strong affinity of AdA or FcA allows these proteins to latch to Cy3-CB7 which results in the successful visualization of the proteins with cells and *Caenorhabditis elegans*. Importantly, no interference from endogenous biomolecules was observed, enabling clear fluorescence images for accurate and precise analysis of protein locations using fluorescence microscopy.

Application of the sequence selectivity of CBs for aromatic peptides has been utilized to determine protease substrate selectivity and inhibition (Ghale et al., 2011). The selectivity of thermolysin to cleave the amide bond at the nitrogen side of Phe residues in peptides leads to the formation of peptide fragments with N-terminal Phe residues. The selectivity of CB7 toward N-terminal Phe residues has been used to create the assay. Scherman et al. have utilized this sequence selectivity of CBs to create a surface immobilized CB8 system which can be used to separate peptides with N-terminal tryptophan (Tian et al., 2011). Larger structures such as cells can also be adsorbed and released using surface-bound CB8 ternary complexes as shown by Sankaran et al. (2017). RGD-based tripeptide ligands were immobilized onto gold substrates fabricating an electrochemically controlled cell-adhesive surface (An et al., 2012). The RGD sequence can selectively adsorb cells on the surface. Electrochemical activation led to the dissociation of the host-guest complex and, thereby, the release of the adsorbed cells. A bio-interface has been developed by Kim and coworkers for isolating plasma membrane proteins by using highly selective binding of CB7 and a ferrocene derivative (AFc, **Figure 13**) (Lee et al., 2011). The system can capture model proteins from protein mixtures and the captured proteins were readily removed from the interface via addition of a second ferrocene derivative (BAFc) with higher binding affinity for CB7 than AFc. In a recent work, iron oxide nanoparticle surfaces were immobilized with CB7 and the modified particles were observed to be stable under a wide range of pH (2–12) (Benyettou et al., 2013). Nile red (NR) was loaded on the surface-bound CB7 and the nanoparticles were used for intracellular delivery of the dye and as MRI contrast agent demonstrating its potential for theranostics.

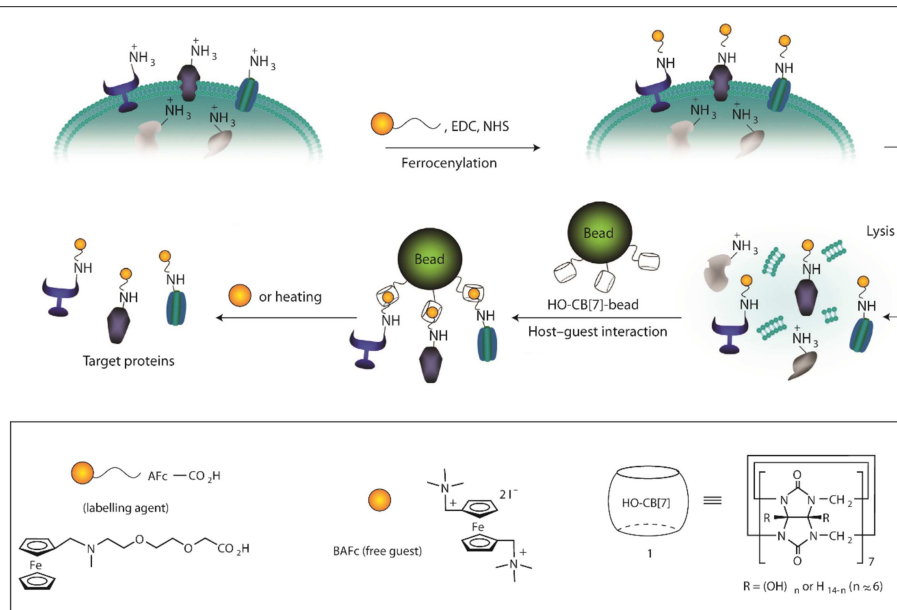


**FIGURE 13** | Schematic illustration for the isolation of plasma membrane proteins using a synthetic binding pair. EDC, 1-ethyl-3-(3-dimethylaminopropyl) carbodiimide; NHS, N-hydroxysuccinimidyl sepharose (Lee et al., 2011) (Reproduced with permission, Copyright 2011, Nature Publishing Group).

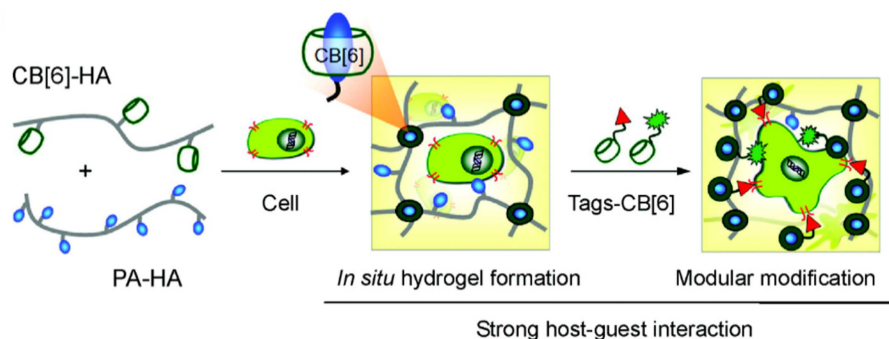


**FIGURE 14** | Schematic illustration for *in situ* formation of supramolecular biocompatible hydrogels (PA-HA, polyamine-hyaluronic acid assembly) and their modular modification using highly selective and strong supramolecular host-guest complexation (Park et al., 2012) (Reproduced with permission, Copyright 2013, American Chemical Society).

Tissue culture is another area where CBs have recently been successfully used. A facile *in situ* supramolecular assembly and modular modification of biocompatible hydrogels were demonstrated by Kim and coworkers (Park et al., 2012). CB6-conjugated hyaluronic acid (CB6-HA), diaminohexaneconjugated HA (DAH-HA), and tags-CB6 were used to create the hydrogel. When these hydrogels were modified with the c(RGDyK) peptide, the entrapped NHDF human fibroblast cells and NIH3T3 mouse fibroblast cells proliferated 5-fold within 14 and 3 days, respectively, compared to the untreated hydrogels (Figure 14). The 3D environment of the hydrogel was modularly modified by the simple treatment with various multifunctional tags-CB6. Furthermore, *in situ* formation of CB6/DAH-HA hydrogels under the skin of nude mice by sequential subcutaneous injections of CB6-HA and

DAH-HA solutions was also confirmed. The fluorescence of modified FITC-CB6 in the hydrogels could be monitored for up to 11 days, showing the feasibility to deliver signals for cellular proliferation and differentiation in the body. To extend the work, the same group prepared 3D tissue-engineered supramolecular hydrogels using CB6-HA, DAH-HA, and drug-conjugated CB6 (drug-CB6) for the controlled chondrogenesis of human mesenchymal stem cells (hMSCs) (Jung et al., 2014). The system can be used as a platform for controlled drug delivery for cartilage regeneration and other various tissue-engineering applications.

In a recent study, Dowari et al. reported a three-way cross-linked peptide-based polymer (Dowari et al., 2018). The cross-linking was achieved *via* disulfide bond formation, enzymatic cross-linking by HRP-mediated dimerization of tyrosine, and



supramolecular linkage using homoternary complexation by CB8. The supramolecular cross-linking was found to play a crucial role in controlling the size of the polymer. The surfaces of the polymer particles were decorated with an RGDS sequence which was utilized for efficient cell adhesion and proliferation of RAW 264.7 cells. The cross-linked polymers could bind cells effectively and the cells proliferated significantly. Jonkheijm and coworkers studied cell adhesion on multivalent knottins displaying RGD ligands with high affinity for integrin receptors (Sankaran et al., 2017). The integrin receptors were assembled on CB8/viologen-modified surfaces. The number of tryptophan units in the knottins varied between 0 and 4 which can form a heteroternary complex with CB8 and surface-tethered viologen. Specific binding occurred, and the affinity increased with the valency of the tryptophan residues on the knottin. Additionally, increased multilayer formation was observed, attributed to homoternary complex formation between tryptophan residues of different knottins and CB8. Control over the surface coverage of the knottins could thus be achieved by valency and concentration. Experiments with mouse myoblast (C2C12) cells on the self-assembled knottin surfaces showed specific integrin recognition by the RGD-displaying knottins. Cells were observed to elongate more on the knottin surfaces with higher valency. Moreover, more pronounced focal adhesion formation was observed on the higher-valency knottin surfaces.

## TOXICITY AND PERMEABILITY OF CUCURBITURIL MACROCYCLES

Any potential biological or medicinal application depends on the cytotoxicity and biocompatibility of the employed formulations. In regard to CB-based compounds and nanomaterials, Kim and coworkers demonstrated the non-toxicity of CB molecules with  $ED_{50}$  levels of more than  $100\ \mu\text{M}$  against human lung and ovarian cancer cells (Jeon et al., 2005). *In vitro* cell viability testing of CB7 by using MTT assay in CHO-K1 cells showed no significant cytotoxicity up to 1 mM and 3 h incubation time; after 48 h incubation time an  $IC_{50}$  value of 0.53 mM was determined (Uzunova et al., 2010). Owing to the low solubility of CB8, a precise determination of its toxicity level is difficult. However,  $20\ \mu\text{M}$  CB8 caused a minor drop in cell viability (86%) within 48 h of incubation. A single oral dose of CB7 and CB8 as a mixture in equal proportions showed no toxicity up to  $600\ \text{mg kg}^{-1}$  (Uzunova et al., 2010). CB5, CB7, and several acyclic CB containers were also tested for their toxicology and bioactivity; they were found to be non-toxic within the desired concentration range (Hettiarachchi et al., 2010).

Another important question which needs to be addressed before using any system for biological application is their cell

permeability. Acridine orange and pyronine Y complexes of CB7 and CB8 were employed to show that the complexes can penetrate the cell membrane of mouse embryo muscle cells (Montes-Navajas et al., 2009). CB7 complexes with dye molecules (fluorophores conjugated with spermidine and adamantylamine) were shown by Isaacs and coworkers to be able to cross the cell membranes of murine macrophage cells; within 20 min, 86% of the cells incorporated the complex. The host-guest complex was observed to be stable within the cells up to 2 h (Hettiarachchi et al., 2010). A CB7-labeled antibody has also been reported to be spontaneously taken up into living cells (Sasmal et al., 2018).

## CONCLUSIONS

We provided an overview of the recent achievements in the area of medicinal-chemical and chemical-biological applications utilizing the host-guest chemistry of CBs. Over the last decade, there has been a paradigm shift in the research with CBs and the focus is now more on the actual applications of these fascinating macrocyclic hosts. A major thrust is in the area of biological and specifically toward biomedical applications. CBs have been widely used to bind bioactive molecules, which helps to overcome the poor solubility of hydrophobic molecules, in particular drug candidates. The unique recognition properties and biocompatibility enables their implementation as excipients (Lim et al., 2002; Kuok et al., 2017). Recent achievements in the preparation of CB derivatives and analogs allow their incorporation into more intricate and applied research lines (Ayhan et al., 2015; Kim et al., 2018; Koc et al., 2018; Park et al., 2018; Sun et al., 2018; Zhang et al., 2018a, 2019a) in an effort to by-pass intrinsic limitations of the parent CBs, such as their stringent selectivity for guest binding and the low intrinsic solubility of CB6 and CB8. We contend that this account will provide a platform for understanding the potential of CBs toward applications in pharmaceutically and medicinally research and assist us in designing and creating new CB-based assemblies.

## AUTHOR CONTRIBUTIONS

All authors contributed to the design and write-up of the review.

## ACKNOWLEDGMENTS

DD thanks the Alexander von Humboldt Foundation for a renewed research stay fellowship and SERB (EMR/2016/000857), India, for financial assistance. WN and KA are grateful to the DFG for grant NA-686/8 within the priority program SPP 1807 Control of London Dispersion Interactions in Molecular Chemistry.

## REFERENCES

- Ahmed, S., Singha, N., Pramanik, B., Mondal, J. H., and Das, D. (2016). Redox controlled reversible transformation of a supramolecular alternating copolymer to a radical cation containing homo-polymer. *Polym. Chem.* 7, 4393–4401. doi: 10.1039/C6PY00809G
- An, Q., Brinkmann, J., Huskens, J., Krabbenborg, S., de Boer, J., and Jonkheijm, P. (2012). A supramolecular system for the electrochemically controlled release of cells. *Angew. Chem. Int. Ed.* 51, 12233–12237. doi: 10.1002/anie.201205651
- Angelos, S., Khashab, N. M., Yang, Y. W., Trabolsi, A., Khatib, H. A., Stoddart, J. F., et al. (2009). pH clock-operated mechanized nanoparticles. *J. Am. Chem. Soc.* 131, 12912–12914. doi: 10.1021/ja9010157



- Angelos, S., Yang, Y. W., Patel, K., Stoddart, J. F., and Zink, J. I. (2008). pH-responsive supramolecular nanovalves based on cucurbit[6]uril pseudorotaxanes. *Angew. Chem. Int. Ed.* 47, 2222–2226. doi: 10.1002/anie.200705211
- Appel, E. A., Loh, X. J., Jones, S. T., Biedermann, F., Dreiss, C. A., and Scherman, O. A. (2012). Ultrahigh-water-content supramolecular hydrogels exhibiting multistimuli responsiveness. *J. Am. Chem. Soc.* 134, 11767–11773. doi: 10.1021/ja3044568
- Assaf, K. I., Florea, M., Antony, J., Henriksen, N. M., Yin, J., Hansen, A., et al. (2017). Hydrophobe challenge: a joint experimental and computational study on the host–guest binding of hydrocarbons to cucurbiturils, allowing explicit evaluation of guest hydration free-energy contributions. *J. Phys. Chem. B* 121, 11144–11162. doi: 10.1021/acs.jpcc.7b09175
- Assaf, K. I., and Nau, W. M. (2014). Cucurbiturils as fluorophilic receptors. *Supramol. Chem.* 26, 657–669. doi: 10.1080/10610278.2014.929130
- Assaf, K. I., and Nau, W. M. (2015). Cucurbiturils: from synthesis to high-affinity binding and catalysis. *Chem. Soc. Rev.* 44, 394–418. doi: 10.1039/C4CS00273C
- Ayhan, M. M., Karoui, H., Hardy, M., Rockenbauer, A., Charles, L., Rosas, R., et al. (2015). Comprehensive synthesis of monohydroxy–cucurbit[n]urils ( $n = 5, 6, 7, 8$ ): high purity and high conversions. *J. Am. Chem. Soc.* 137, 10238–10245. doi: 10.1021/jacs.5b04553
- Bai, Q., Zhang, S., Chen, H., Sun, T., Redshaw, C., Zhang, J.-X., et al. (2017). Alkyl substituted cucurbit[6]uril assisted competitive fluorescence recognition of lysine and methionine in aqueous solution. *ChemistrySelect* 2, 2569–2573. doi: 10.1002/slct.201700053
- Bailey, D. M., Hennig, A., Uzunova, V. D., and Nau, W. M. (2008). Supramolecular tandem enzyme assays for multiparameter sensor arrays and enantiomeric excess determination of amino acids. *Chem. Eur. J.* 14, 6069–6077. doi: 10.1002/chem.200800463
- Bardelang, D., Udachin, K. A., Leek, D. M., Margeson, J. C., Chan, G., Ratcliffe, C. I., et al. (2011). Cucurbit[n]urils ( $n = 5–8$ ): a comprehensive solid state study. *Cryst. Growth Des.* 11, 5598–5614. doi: 10.1021/cg201173j
- Barooah, N., Kunwar, A., Khurana, R., Bhasikuttan, A. C., and Mohanty, J. (2017). Stimuli-responsive cucurbit[7]uril-mediated BSA nanoassembly for uptake and release of doxorubicin. *Chem. Asian J.* 12, 122–129. doi: 10.1002/asia.201601411
- Barooah, N., Mohanty, J., Pal, H., and Bhasikuttan, A. C. (2012). Stimulus-responsive supramolecular  $pK_a$  tuning of cucurbit[7]uril encapsulated coumarin 6 dye. *J. Phys. Chem. B* 116, 3683–3689. doi: 10.1021/jp212459r
- Barrow, S. J., Kasera, S., Rowland, M. J., del Barrio, J., and Scherman, O. A. (2015). Cucurbituril-based molecular recognition. *Chem. Rev.* 115, 12320–12406. doi: 10.1021/acs.chemrev.5b00341
- Basilio, N., and Pischel, U. (2016). Drug delivery by controlling a supramolecular host–guest assembly with a reversible photoswitch. *Chem. Eur. J.* 22, 15208–15211. doi: 10.1002/chem.201603331
- Behrend, R., Meyer, E., and Rusche, F. (1905). Ueber condensationsproducte aus glycurilur und formaldehyd. *Justus Liebigs Ann. Chem.* 339, 1–37. doi: 10.1002/jlac.19053390102
- Benyettou, F., Milosevic, I., Lalatonne, Y., Warmont, F., Assah, R., Olsen, J.-C., et al. (2013). Toward theranostic nanoparticles: CB[7]-functionalized iron oxide for drug delivery and mri. *J. Mater. Chem. B* 1, 5076–5082. doi: 10.1039/c3tb20852d
- Bhasikuttan, A. C., Mohanty, J., Nau, W. M., and Pal, H. (2007). Efficient fluorescence enhancement and cooperative binding of an organic dye in a supra-biomolecular host-protein assembly. *Angew. Chem. Int. Ed.* 46, 4120–4122. doi: 10.1002/anie.200604757
- Bhasikuttan, A. C., Pal, H., and Mohanty, J. (2011). Cucurbit[n]uril based supramolecular assemblies: tunable physico-chemical properties and their prospects. *Chem. Commun.* 47, 9959–9971. doi: 10.1039/c1cc12091c
- Biedermann, F., Elmaleh, E., Ghosh, I., Nau, W. M., and Scherman, O. A. (2012a). Strongly fluorescent, switchable perylene bis(diimide) host-guest complexes with cucurbit[8]uril in water. *Angew. Chem. Int. Ed.* 51, 7739–7743. doi: 10.1002/anie.201202385
- Biedermann, F., and Nau, W. M. (2014). Noncovalent chirality sensing ensembles for the detection and reaction monitoring of amino acids, peptides, proteins, and aromatic drugs. *Angew. Chem. Int. Ed.* 53, 5694–5699. doi: 10.1002/anie.201400718
- Biedermann, F., Nau, W. M., and Schneider, H.-J. (2014). The hydrophobic effect revisited-studies with supramolecular complexes imply high-energy water as a noncovalent driving force. *Angew. Chem. Int. Ed.* 53, 11158–11171. doi: 10.1002/anie.201310958
- Biedermann, F., Uzunova, V. D., Scherman, O. A., Nau, W. M., and De Simone, A. (2012b). Release of high-energy water as an essential driving force for the high-affinity binding of cucurbit[n]urils. *J. Am. Chem. Soc.* 134, 15318–15323. doi: 10.1021/ja303309e
- Blanch, R. J., Sleeman, A. J., White, T. J., Arnold, A. P., and Day, A. I. (2002). Cucurbit[7]uril and *o*-carborane self-assemble to form a molecular ball bearing. *Nano Lett.* 2, 147–149. doi: 10.1021/nl015655s
- Bush, M. E., Bouley, N. D., and Urbach, A. R. (2005). Charge-mediated recognition of N-terminal tryptophan in aqueous solution by a synthetic host. *J. Am. Chem. Soc.* 127, 14511–14517. doi: 10.1021/ja0548440
- Cao, L., Sekutor, M., Zavalij, P. Y., Mlinaric-Majerski, K., Glaser, R., and Isaacs, L. (2014). Cucurbit[7]uril•guest pair with an attomolar dissociation constant. *Angew. Chem. Int. Ed.* 53, 988–993. doi: 10.1002/anie.201309635
- Carvalho, C. P., Uzunova, V. D., Da Silva, J. P., Nau, W. M., and Pischel, U. (2011). A photoinduced pH jump applied to drug release from cucurbit[7]uril. *Chem. Commun.* 47, 8793–8795. doi: 10.1039/c1cc12954f
- Chen, C.-J., Li, D.-D., Wang, H.-B., Zhao, J., and Ji, J. (2013). Fabrication of dual-responsive micelles based on the supramolecular interaction of cucurbit[8]uril. *Polym. Chem.* 4, 242–245. doi: 10.1039/C2PY20549A
- Chen, H., Chen, Y., Wu, H., Xu, J.-F., Sun, Z., and Zhang, X. (2018). Supramolecular polymeric chemotherapy based on cucurbit[7]uril-PEG copolymer. *Biomaterials* 178, 697–705. doi: 10.1016/j.biomaterials.2018.02.051
- Chen, Y., Huang, Z., Xu, J.-F., Sun, Z., and Zhang, X. (2016). Cytotoxicity regulated by host–guest interactions: a supramolecular strategy to realize controlled disguise and exposure. *ACS Appl. Mater. Interfaces* 8, 22780–22784. doi: 10.1021/acsami.6b08295
- Chen, Y., Huang, Z., Zhao, H., Xu, J.-F., Sun, Z., and Zhang, X. (2017). Supramolecular chemotherapy: cooperative enhancement of antitumor activity by combining controlled release of oxaliplatin and consuming of spermine by cucurbit[7]uril. *ACS Appl. Mater. Interfaces* 9, 8602–8608. doi: 10.1021/acsami.7b01157
- Cheng, Q., Yin, H., Rosas, R., Gimes, D., Ouari, O., Wang, R., et al. (2018). A pH-driven ring translocation switch against cancer cells. *Chem. Commun.* 54, 13825–13828. doi: 10.1039/C8CC08681H
- Chinai, J. M., Taylor, A. B., Ryno, L. M., Hargreaves, N. D., Morris, C. A., Hart, P. J., et al. (2011). Molecular recognition of insulin by a synthetic receptor. *J. Am. Chem. Soc.* 133, 8810–8813. doi: 10.1021/ja201581x
- Choudhury, S. D., Mohanty, J., Pal, H., and Bhasikuttan, A. C. (2010). Cooperative metal ion binding to a cucurbit[7]uril-thioflavin T complex: demonstration of a stimulus-responsive fluorescent supramolecular capsule. *J. Am. Chem. Soc.* 132, 1395–1401. doi: 10.1021/ja908795y
- Choudhury, S. D., Mohanty, J., Upadhyaya, H. P., Bhasikuttan, A. C., and Pal, H. (2009). Photophysical studies on the noncovalent interaction of thioflavin T with cucurbit[n]uril macrocycles. *J. Phys. Chem. B* 113, 1891–1898. doi: 10.1021/jp8103062
- Cong, H., Li, C.-R., Xue, S.-F., Tao, Z., Zhu, Q.-J., and Wei, G. (2011). Cucurbituril-resisted acylation of the anti-tuberculosis drug isoniazid via a supramolecular strategy. *Org. Biomol. Chem.* 9, 1041–1046. doi: 10.1039/C0OB00114G
- Constabel, F., and Geckeler, K. E. (2004). Solvent-free self-assembly of  $C_{60}$  and cucurbit[7]uril using high-speed vibration milling. *Tetrahedron Lett.* 45, 2071–2073. doi: 10.1016/j.tetlet.2004.01.071
- Croissant, J., and Zink, J. I. (2012). Nanovalve-controlled cargo release activated by plasmonic heating. *J. Am. Chem. Soc.* 134, 7628–7631. doi: 10.1021/ja301880x
- Day, A. I., and Collins, J. G. (2012). “Cucurbituril receptors and drug delivery,” in *Supramolecular Chemistry: From Molecules to Nanomaterials*, eds P. A. Gale and J. W. Steed (Chichester, UK: John Wiley and Sons Ltd.), 983–1000.
- Deng, Y., Yin, H., Zhao, Z., Wang, R., and Liu, S. (2018). A study of binding interactions between terpyridine derivatives and cucurbit[10]uril. *Supramol. Chem.* 30, 706–712. doi: 10.1080/10610278.2018.1455977
- Dong, N., Xue, S.-F., Zhu, Q.-J., Tao, Z., Zhao, Y., and Yang, L.-X. (2008). Cucurbit[n]urils ( $n=7, 8$ ) binding of camptothecin and the effects on solubility and reactivity of the anticancer drug. *Supramol. Chem.* 20, 663–671. doi: 10.1080/10610270701666018
- Dowari, P., Saha, S., Pramanik, B., Ahmed, S., Singha, N., Ukil, A., et al. (2018). Multiple cross-linking of a small peptide to form a size tunable biopolymer

- with efficient cell adhesion and proliferation property. *Biomacromolecules* 19, 3994–4002. doi: 10.1021/acs.biomac.8b00950
- Dsouza, R. N., Pischel, U., and Nau, W. M. (2011). Fluorescent dyes and their supramolecular host/guest complexes with macrocycles in aqueous solution. *Chem. Rev.* 111, 7941–7980. doi: 10.1021/cr200213s
- El-Sheshtawy, H. S., Chatterjee, S., Assaf, K. I., Shinde, M. N., Nau, W. M., and Mohanty, J. (2018). A supramolecular approach for enhanced antibacterial activity and extended shelf-life of fluoroquinolone drugs with cucurbit[7]uril. *Sci. Rep.* 8:13925. doi: 10.1038/s41598-018-32312-6
- Feng, H., Kan, J., Redshaw, C., Bian, B., Tao, Z., and Xiao, X. (2019). Supramolecular drug inclusion complex constructed from cucurbit[7]uril and the Hepatitis B drug Adefovir. *Supramol. Chem.* 31, 260–267. doi: 10.1080/10610278.2018.1562193
- Freeman, W. A., Mock, W. L., and Shih, N. Y. (1981). Cucurbituril. *J. Am. Chem. Soc.* 103, 7367–7368. doi: 10.1021/ja00414a070
- Gamal-Eldin, M. A., and Macartney, D. H. (2013). Selective molecular recognition of methylated lysines and arginines by cucurbit[6]uril and cucurbit[7]uril in aqueous solution. *Org. Biomol. Chem.* 11, 488–495. doi: 10.1039/C2OB27007B
- Gamal-Eldin, M. A., and Macartney, D. H. (2014). Cucurbit[7]uril host–guest complexations of steroidal neuromuscular blocking agents in aqueous solution. *Can. J. Chem.* 92, 243–249. doi: 10.1139/cjc-2013-0490
- Ganapati, S., and Isaacs, L. (2018). Acyclic cucurbit[n]uril-type receptors: preparation, molecular recognition properties and biological applications. *Isr. J. Chem.* 58, 250–263. doi: 10.1002/ijch.201700098
- Ghale, G., and Nau, W. M. (2014). Dynamically analyte-responsive macrocyclic host–fluorophore systems. *Acc. Chem. Res.* 47, 2150–2159. doi: 10.1021/ar500116d
- Ghale, G., Ramalingam, V., Urbach, A. R., and Nau, W. M. (2011). Determining protease substrate selectivity and inhibition by label-free supramolecular tandem enzyme assays. *J. Am. Chem. Soc.* 133, 7528–7535. doi: 10.1021/ja2013467
- Ghosh, I., and Nau, W. M. (2012). The strategic use of supramolecular pK<sub>a</sub> shifts to enhance the bioavailability of drugs. *Adv. Drug. Deliv. Rev.* 64, 764–783. doi: 10.1016/j.addr.2012.01.015
- Hennig, A., Bakirci, H., and Nau, W. M. (2007). Label-free continuous enzyme assays with macrocycle-fluorescent dye complexes. *Nat. Methods* 4, 629–632. doi: 10.1038/nmeth1064
- Hettiarachchi, G., Nguyen, D., Wu, J., Lucas, D., Ma, D., Isaacs, L., et al. (2010). Toxicology and drug delivery by cucurbit[n]uril type molecular containers. *PLoS ONE* 5:e10514. doi: 10.1371/journal.pone.0010514
- Hirani, Z., Taylor, H. F., Babcock, E. F., Bockus, A. T., Varnado, C. D., Bielawski, C. W., et al. (2018). Molecular recognition of methionine-terminated peptides by cucurbit[8]uril. *J. Am. Chem. Soc.* 140, 12263–12269. doi: 10.1021/jacs.8b07865
- Huang, Q., Cheng, Q., Zhang, X., Yin, H., Wang, L.-H., and Wang, R. (2018a). Alleviation of polycation-induced blood coagulation by the formation of polypseudorotaxanes with macrocyclic cucurbit[7]uril. *ACS Appl. Bio Mater.* 1, 544–548. doi: 10.1021/acsabm.8b00401
- Huang, Q., Kuok, K. I., Zhang, X., Yue, L., Lee, S. M. Y., Zhang, J., et al. (2018b). Inhibition of drug-induced seizure development in both zebrafish and mouse models by a synthetic nanoreceptor. *Nanoscale* 10, 10333–10336. doi: 10.1039/C8NR02041H
- Huang, Q., Li, S., Ding, Y.-F., Yin, H., Wang, L.-H., and Wang, R. (2018c). Macrocyclic-wrapped polyethylenimine for gene delivery with reduced cytotoxicity. *Biomater. Sci.* 6, 1031–1039. doi: 10.1039/C8BM00022K
- Huang, X. L., Tan, Y. B., Zhou, Q. F., and Wang, Y. X. (2008a). Fabrication of cucurbit[6]uril mediated alginate physical hydrogel beads and their application as a drug carriers. *e-Polymers* 95, 1–11. doi: 10.1515/epoly.2008.8.1.1098
- Huang, Y., Tao, Z., Xue, S.-F., and Zhu, Q.-J. (2011). Progress of cucurbit[n]urils in drug delivery system. *Chem. J. Chin.* 32, 2022–2031.
- Huang, Y., Xue, S.-F., Tao, Z., Zhu, Q.-J., Zhang, H., Lin, J.-X., et al. (2008b). Solubility enhancement of kinetin through host–guest interactions with cucurbiturils. *J. Incl. Phenom. Macrocycl. Chem.* 61, 171–177. doi: 10.1007/s10847-008-9410-z
- Jeon, Y. J., Kim, S. Y., Ko, Y. H., Sakamoto, S., Yamaguchi, K., and Kim, K. (2005). Novel molecular drug carrier: encapsulation of oxaliplatin in cucurbit[7]uril and its effects on stability and reactivity of the drug. *Org. Biomol. Chem.* 3, 2122–2125. doi: 10.1039/b504487a
- Jiang, G., and Li, G. (2006). Preparation and biological activity of novel cucurbit[8]uril-fullerene complex. *J. Photochem. Photobiol. B* 85, 223–227. doi: 10.1016/j.jphotobiol.2006.08.001
- Jiao, D., Geng, J., Loh, X. J., Das, D., Lee, T.-C., and Scherman, O. A. (2012). Supramolecular peptide amphiphile vesicles through host–guest complexation. *Angew. Chem. Int. Ed.* 51, 9633–9637. doi: 10.1002/anie.201202947
- Jung, H., Park, J. S., Yeom, J., Selvapalam, N., Park, K. M., Oh, K., et al. (2014). 3D tissue engineered supramolecular hydrogels for controlled chondrogenesis of human mesenchymal stem cells. *Biomacromolecules* 15, 707–714. doi: 10.1021/bm401123m
- Jung, H., Park, K. M., Yang, J. A., Oh, E. J., Lee, D. W., Park, K., et al. (2011). Theranostic systems assembled *in situ* on demand by host–guest chemistry. *Biomaterials* 32, 7687–7694. doi: 10.1016/j.biomaterials.2011.06.060
- Kahwajy, N., Nematollahi, A., Kim, R. R., Church, W. B., and Wheate, N. J. (2017). Comparative macrocycle binding of the anticancer drug phenanthriplatin by cucurbit[n]urils,  $\beta$ -cyclodextrin and para-sulfonatocalix[4]arene: a <sup>1</sup>H NMR and molecular modelling study. *J. Incl. Phenom. Macrocycl. Chem.* 87, 251–258. doi: 10.1007/s10847-017-0694-8
- Kasera, S., Herrmann, L. O., del Barrio, J., Baumberg, J. J., and Scherman, O. A. (2014). Quantitative multiplexing with nano-self-assemblies in sers. *Sci. Rep.* 4:6785. doi: 10.1038/srep06785
- Kennedy, A. R., Florence, A. J., McInnes, F. J., and Wheate, N. J. (2009). A chemical preformulation study of a host–guest complex of cucurbit[7]uril and a multinuclear platinum agent for enhanced anticancer drug delivery. *Dalton Trans.* 7695–7700. doi: 10.1039/b909717c
- Kim, C., Agasti, S. S., Zhu, Z., Isaacs, L., and Rotello, V. M. (2010a). Recognition-mediated activation of therapeutic gold nanoparticles inside living cells. *Nat. Chem.* 2, 962–966. doi: 10.1038/nchem.858
- Kim, E., Kim, D., Jung, H., Lee, J., Paul, S., Selvapalam, N., et al. (2010b). Facile, template-free synthesis of stimuli-responsive polymer nanocapsules for targeted drug delivery. *Angew. Chem. Int. Ed.* 49, 4405–4408. doi: 10.1002/anie.201000818
- Kim, H., Oh, J., Jeon, W. S., Selvapalam, N., Hwang, I., Ko, Y. H., et al. (2012). A new cucurbit[6]uril-based ion-selective electrode for acetylcholine with high selectivity over choline and related quaternary ammonium ions. *Supramol. Chem.* 24, 487–491. doi: 10.1080/10610278.2012.688125
- Kim, J., Ahn, Y., Park, K. M., Kim, Y., Ko, Y. H., Oh, D. H., et al. (2007). Carbohydrate wheels: cucurbituril-based carbohydrate clusters. *Angew. Chem. Int. Ed.* 46, 7393–7395. doi: 10.1002/anie.200702540
- Kim, K. L., Sung, G., Sim, J., Murray, J., Li, M., Lee, A., et al. (2018). Supramolecular latching system based on ultrastable synthetic binding pairs as versatile tools for protein imaging. *Nat. Commun.* 9:1712. doi: 10.1038/s41467-018-04161-4
- Kim, S. K., Park, K. M., Singha, K., Kim, J., Ahn, Y., Kim, K., et al. (2010c). Galactosylated cucurbituril-inclusion polyplex for hepatocyte-targeted gene delivery. *Chem. Commun.* 46, 692–694. doi: 10.1039/B920753H
- Koc, A., Khan, R., and Tuncel, D. (2018). “Clicked” porphyrin-cucurbituril conjugate: a new multifunctional supramolecular assembly based on triglycosylated porphyrin and monopropargyloxycucurbit[7]uril. *Chem. Eur. J.* 24, 15550–15555. doi: 10.1002/chem.201804024
- Konda, S. K., Maliki, R., McGrath, S., Parker, B. S., Robinson, T., Spurling, A., et al. (2017). Encapsulation of mitoxantrone within cucurbit[8]uril decreases toxicity and enhances survival in a mouse model of cancer. *ACS Med. Chem. Lett.* 8, 538–542. doi: 10.1021/acsmedchemlett.7b00090
- Koner, A. L., Ghosh, I., Saleh, N., and Nau, W. M. (2011). Supramolecular encapsulation of benzimidazole-derived drugs by cucurbit[7]uril. *Can. J. Chem.* 89, 139–147. doi: 10.1139/V10-079
- Koner, A. L., and Nau, W. M. (2007). Cucurbituril encapsulation of fluorescent dyes. *Supramol. Chem.* 19, 55–66. doi: 10.1080/10610270600910749
- Kovalenko, E., Vilaseca, M., Díaz-Lobo, M., Masliy, A. N., Vicent, C., and Fedin, V. P. (2016). Supramolecular adducts of cucurbit[7]uril and amino acids in the gas phase. *J. Am. Soc. Mass Spectrom.* 27, 265–276. doi: 10.1007/s13361-015-1274-z
- Kuok, K. I., Li, S., Wyman, I. W., and Wang, R. (2017). Cucurbit[7]uril: an emerging candidate for pharmaceutical excipients. *Ann. N. Y. Acad. Sci.* 1398, 108–119. doi: 10.1111/nyas.13376
- Lagona, J., Mukhopadhyay, P., Chakrabarti, S., and Isaacs, L. (2005). The cucurbit[n]uril family. *Angew. Chem. Int. Ed.* 44, 4844–4870. doi: 10.1002/anie.200460675

- Lazar, A. I., Biedermann, F., Mustafina, K. R., Assaf, K. I., Hennig, A., and Nau, W. M. (2016). Nanomolar binding of steroids to cucurbit[n]urils: selectivity and applications. *J. Am. Chem. Soc.* 138, 13022–13029. doi: 10.1021/jacs.6b07655
- Lazar, A. I., Rohacova, J., and Nau, W. M. (2017). Comparison of complexation-induced  $pK_a$  shifts in the ground and excited states of dyes as well as different macrocyclic hosts and their manifestation in host-retarded excited-dye deprotonation. *J. Phys. Chem. B* 121, 11390–11398. doi: 10.1021/acs.jpcc.7b10651
- Lee, D. W., Park, K. M., Banerjee, M., Ha, S. H., Lee, T., Suh, K., et al. (2011). Supramolecular fishing for plasma membrane proteins using an ultrastable synthetic host-guest binding pair. *Nat. Chem.* 3, 154–159. doi: 10.1038/nchem.928
- Lee, H. K., Park, K. M., Jeon, Y. J., Kim, D., Oh, D. H., Kim, H. S., et al. (2005). Vesicle formed by amphiphilic cucurbit[6]uril: versatile, noncovalent modification of the vesicle surface, and multivalent binding of sugar-decorated vesicles to lectin. *J. Am. Chem. Soc.* 127, 5006–5007. doi: 10.1021/ja042172s
- Lee, J. W., Lee, H. H. L., Ko, Y. H., Kim, K., and Kim, H. I. (2015). Deciphering the specific high-affinity binding of cucurbit[7]uril to amino acids in water. *J. Phys. Chem. B* 119, 4628–4636. doi: 10.1021/acs.jpcc.5b00743
- Lee, T.-C., Kalenius, E., Lazar, A. I., Assaf, K. I., Kuhnert, N., Grün, C. H., et al. (2013). Chemistry inside molecular containers in the gas phase. *Nat. Chem.* 5, 376. doi: 10.1038/nchem.1618
- Li, C., Li, J., and Jia, X. (2009). Selective binding and highly sensitive fluorescent sensor of palmitate and dehydrocorydaline alkaloids by cucurbit[7]uril. *Org. Biomol. Chem.* 7, 2699–2703. doi: 10.1039/b820852b
- Li, C.-F., Du, L.-M., Wu, W.-Y., and Sheng, A.-Z. (2010). Supramolecular interaction of cucurbit[n]urils and coptisine by spectrofluorimetry and its analytical application. *Talanta* 80, 1939–1944. doi: 10.1016/j.talanta.2009.10.049
- Li, J., and Loh, X. J. (2008). Cyclodextrin-based supramolecular architectures: syntheses, structures, and applications for drug and gene delivery. *Adv. Drug Deliv. Rev.* 60, 1000–1017. doi: 10.1016/j.addr.2008.02.011
- Li, S., Jiang, N., Zhao, W., Ding, Y.-F., Zheng, Y., Wang, L.-H., et al. (2017). An eco-friendly *in situ* activatable antibiotic via cucurbit[8]uril-mediated supramolecular crosslinking of branched polyethylenimine. *Chem. Commun.* 53, 5870–5873. doi: 10.1039/C7CC02466E
- Li, S., Yin, H., Martinz, G., Wyman, I. W., Bardelang, D., Macartney, D. H., et al. (2016a). Supramolecular encapsulation of benzocaine and its metabolite para-aminobenzoic acid by cucurbit[7]uril. *New J. Chem.* 40, 3484–3490. doi: 10.1039/C5NJ03259H
- Li, S., Yin, H., Wyman, I. W., Zhang, Q., Macartney, D. H., and Wang, R. (2016b). Encapsulation of vitamin B1 and its phosphate derivatives by cucurbit[7]uril: tunability of the binding site and affinity by the presence of phosphate groups. *J. Org. Chem.* 81, 1300–1303. doi: 10.1021/acs.joc.5b02666
- Li, W., Bockus, A. T., Vinciguerra, B., Isaacs, L., and Urbach, A. R. (2016c). Predictive recognition of native proteins by cucurbit[7]uril in a complex mixture. *Chem. Commun.* 52, 8537–8540. doi: 10.1039/C6CC03193E
- Li, W., Li, S., Wyman, I. W., Macartney, D. H., Zhang, Q., Zheng, Y., et al. (2016d). Supramolecular encapsulation of Vitamin B by macrocyclic nanocontainer cucurbit[7]uril. *J. Nanomater.* 16:375. doi: 10.1155/2015/574013
- Lim, Y. B., Kim, T., Lee, J. W., Kim, S. M., Kim, H. J., Kim, K., et al. (2002). Self-assembled ternary complex of cationic dendrimer, cucurbituril, and DNA: noncovalent strategy in developing a gene delivery carrier. *Bioconjug. Chem.* 13, 1181–1185. doi: 10.1021/bc025581r
- Liu, H., Wu, X., Huang, Y., He, J., Xue, S. F., Tao, Z., et al. (2011). Improvement of antifungal activity of carbocin by inclusion complexation with cucurbit[8]uril. *J. Incl. Phenom. Macro. Chem.* 71, 583–587. doi: 10.1007/s10847-011-9982-x
- Liu, L. (2017). Controlled release from cucurbituril. *J. Incl. Phenom. Macrocycl. Chem.* 87, 1–12. doi: 10.1007/s10847-016-0683-3
- Liu, S. M., Ruspice, C., Mukhopadhyay, P., Chakrabarti, S., Zavalij, P. Y., and Isaacs, L. (2005a). The cucurbit[n]uril family: prime components for self-sorting systems. *J. Am. Chem. Soc.* 127, 15959–15967. doi: 10.1021/ja055013x
- Liu, S. M., Zavalij, P. Y., and Isaacs, L. (2005b). Cucurbit[10]uril. *J. Am. Chem. Soc.* 127, 16798–16799. doi: 10.1021/ja056287n
- Loh, X. J., del Barrio, J., Toh, P. P. C., Lee, T.-C., Jiao, D., Rauwald, U., et al. (2012). Triply triggered doxorubicin release from supramolecular nanocontainers. *Biomacromolecules* 13, 84–91. doi: 10.1021/bm201588m
- Ma, D., Hettiarachchi, G., Duc, N., Zhang, B., Wittenberg, J. B., Zavalij, P. Y., et al. (2012a). Acyclic cucurbit[n]uril molecular containers enhance the solubility and bioactivity of poorly soluble pharmaceuticals. *Nat. Chem.* 4, 503–510. doi: 10.1038/nchem.1326
- Ma, D., Zhang, B., Hoffmann, U., Sundrup, M. G., Eikermann, M., and Isaacs, L. (2012b). Acyclic cucurbit[n]uril-type molecular containers bind neuromuscular blocking agents *in vitro* and reverse neuromuscular block *in vivo*. *Angew. Chem. Int. Ed.* 51, 11358–11362. doi: 10.1002/anie.201206031
- Ma, X., and Zhao, Y. (2015). Biomedical applications of supramolecular systems based on host–guest interactions. *Chem. Rev.* 115, 7794–7839. doi: 10.1021/cr500392w
- Macartney, D. H. (2011). Encapsulation of drug molecules by cucurbiturils: effects on their chemical properties in aqueous solution. *Isr. J. Chem.* 51, 600–615. doi: 10.1002/ijch.201100040
- Márquez, C., Huang, F., and Nau, W. M. (2004a). Cucurbiturils: molecular nanocapsules for time-resolved fluorescence-based assays. *IEEE Trans. Nanobiosci.* 3, 39–45. doi: 10.1109/TNB.2004.824269
- Márquez, C., Hudgins, R. R., and Nau, W. M. (2004b). Mechanism of host-guest complexation by cucurbituril. *J. Am. Chem. Soc.* 126, 5806–5816. doi: 10.1021/ja0319846
- Márquez, C., and Nau, W. M. (2001a). Polarizabilities inside molecular containers. *Angew. Chem. Int. Ed.* 40, 4387–4390. doi: 10.1002/1521-3773(20011203)40:23<4387::AID-ANIE4387>3.0.CO;2-H
- Márquez, C., and Nau, W. M. (2001b). Two mechanisms of slow host-guest complexation between cucurbit[6]uril and cyclohexylmethylamine: pH-responsive supramolecular kinetics. *Angew. Chem. Int. Ed.* 40, 3155–3160. doi: 10.1002/1521-3773(20010903)40:17<3155::AID-ANIE3155>3.0.CO;2-7
- Masson, E. (2017). “Biomedical applications of cucurbiturils and derivatives,” in *Comprehensive Supramolecular Chemistry II*, ed J. L. Atwood (Oxford: Elsevier), 21–45.
- Masson, E., Ling, X., Joseph, R., Kyeremeh-Mensah, L., and Lu, X. (2012). Cucurbituril chemistry: a tale of supramolecular success. *RSC Adv.* 2, 1213–1247. doi: 10.1039/C1RA00768H
- Mecozzi, S., and Rebek, J. Jr. (1998). The 55 % solution: a formula for molecular recognition in the liquid state. *Chem. Eur. J.* 4, 1016–1022.
- Minami, T., Esipenko, N. A., Zhang, B., Kozelkova, M. E., Isaacs, L., Nishiyabu, R., et al. (2012). Supramolecular sensor for cancer-associated nitrosamines. *J. Am. Chem. Soc.* 134, 20021–20024. doi: 10.1021/ja3102192
- Miskolczy, Z., and Biczók, L. (2014a). Kinetics and thermodynamics of berberine inclusion in cucurbit[7]uril. *J. Phys. Chem. B* 118, 2499–2505. doi: 10.1021/jp500603g
- Miskolczy, Z., and Biczók, L. (2014b). Sequential inclusion of two berberine cations in cucurbit[8]uril cavity: kinetic and thermodynamic studies. *Phys. Chem. Chem. Phys.* 16, 20147–20156. doi: 10.1039/C4CP02919D
- Miskolczy, Z., Megyesi, M., Tarkanyi, G., Mizsei, R., and Biczók, L. (2011). Inclusion complex formation of sanguinarine alkaloid with cucurbit[7]uril: inhibition of nucleophilic attack and photooxidation. *Org. Biomol. Chem.* 9, 1061–1070. doi: 10.1039/C0OB00666A
- Moghaddam, S., Yang, C., Rekharsky, M., Ko, Y. H., Kim, K., Inoue, Y., et al. (2011). New ultrahigh affinity host-guest complexes of cucurbit[7]uril with bicyclo[2.2.2]octane and adamantane guests: thermodynamic analysis and evaluation of M2 affinity calculations. *J. Am. Chem. Soc.* 133, 3570–3581. doi: 10.1021/ja109904u
- Mohanty, J., and Nau, W. M. (2005). Ultrastable rhodamine with cucurbituril. *Angew. Chem. Int. Ed.* 44, 3750–3754. doi: 10.1002/anie.200500502
- Mondal, J. H., Ahmed, S., Ghosh, T., and Das, D. (2015). Reversible deformation-formation of a multistimuli responsive vesicle by a supramolecular peptide amphiphile. *Soft Matter* 11, 4912–4920. doi: 10.1039/C5SM00491H
- Montes-Navajas, P., Gonzalez-Bejar, M., Scaiano, J. C., and Garcia, H. (2009). Cucurbituril complexes cross the cell membrane. *Photochem. Photobiol. Sci.* 8, 1743–1747. doi: 10.1039/b9pp00041k
- Nau, W. M., Florea, M., and Assaf, K. I. (2011). Deep inside cucurbiturils: physical properties and volume of their inner cavity determine the hydrophobic driving forces for host-guest complexation. *Isr. J. Chem.* 51, 559–577. doi: 10.1002/ijch.201100044
- Nau, W. M., Ghale, G., Hennig, A., Bakirci, H., and Bailey, D. M. (2009). Substrate-selective supramolecular tandem assays: monitoring enzyme inhibition of arginase and diamine oxidase by fluorescent dye displacement from



- calixarene and cucurbituril macrocycles. *J. Am. Chem. Soc.* 131, 11558–11570. doi: 10.1021/ja904165c
- Nau, W. M., and Mohanty, J. (2005). Taming fluorescent dyes with cucurbituril. *Int. J. Photoenergy* 7, 133–141. doi: 10.1155/S1110662X05000206
- Park, K. M., Baek, K., Ko, Y. H., Shrinidhi, A., Murray, J., Jang, W. H., et al. (2018). Mono-allyloxyated cucurbit[7]uril acts as an unconventional amphiphile to form light-responsive vesicles. *Angew. Chem. Int. Ed.* 57, 3132–3136. doi: 10.1002/anie.201713059
- Park, K. M., Lee, D. W., Sarkar, B., Jung, H., Kim, J., Ko, Y. H., et al. (2010). Reduction-sensitive, robust vesicles with a noncovalently modifiable surface as a multifunctional drug-delivery platform. *Small* 6, 1430–1441. doi: 10.1002/sml.201000293
- Park, K. M., Suh, K., Jung, H., Lee, D. W., Ahn, Y., Kim, J., et al. (2009). Cucurbituril-based nanoparticles: a new efficient vehicle for targeted intracellular delivery of hydrophobic drugs. *Chem. Commun.* 71–73. doi: 10.1039/B815009E
- Park, K. M., Yang, J.-A., Jung, H., Yeom, J., Park, J. S., Park, K.-H., et al. (2012). *In situ* supramolecular assembly and modular modification of hyaluronic acid hydrogels for 3D cellular engineering. *ACS Nano* 6, 2960–2968. doi: 10.1021/nn204123p
- Pennakalathil, J., Jahja, E., Özdemir, E. S., Konu, Ö., and Tuncel, D. (2014). Red emitting, cucurbituril-capped, pH-responsive conjugated oligomer-based nanoparticles for drug delivery and cellular imaging. *Biomacromolecules* 15, 3366–3374. doi: 10.1021/bm500839j
- Pisani, M. J., Zhao, Y., Wallace, L., Woodward, C. E., Keene, F. R., Day, A. I., et al. (2010). Cucurbit[10]uril binding of dinuclear platinum(II) and ruthenium(II) complexes: association/dissociation rates from seconds to hours. *Dalton Trans.* 39, 2078–2086. doi: 10.1039/b921172a
- Plumb, J. A., Venugopal, B., Oun, R., Gomez-Roman, N., Kawazoe, Y., Venkataramanan, N. S., et al. (2012). Cucurbit[7]uril encapsulated cisplatin overcomes cisplatin resistance via a pharmacokinetic effect. *Metallomics* 4, 561–567. doi: 10.1039/c2mt20054f
- Rekharsky, M. V., and Inoue, Y. (1998). Complexation thermodynamics of cyclodextrins. *Chem. Rev.* 98, 1875–1917. doi: 10.1021/cr970015o
- Robinson-Duggon, J., Pérez-Mora, F., Dibona-Villanueva, L., and Fuentealba, D. (2018). Potential applications of cucurbit[n]urils inclusion complexes in photodynamic therapy. *Isr. J. Chem.* 58, 199–214. doi: 10.1002/ijch.201700093
- Romero, M. A., Fernandes, R. J., Moro, A. J., Basilio, N., and Pischel, U. (2018). Light-induced cargo release from a cucurbit[8]uril host by means of a sequential logic operation. *Chem. Commun.* 54, 13335–13338. doi: 10.1039/C8CC07404F
- Saleh, N., Al-Handawi, M. B., Al-Kaabi, L., Ali, L., Ashraf, S. S., Thiemann, T., et al. (2014). Intermolecular interactions between cucurbit[7]uril and pilocarpine. *Int. J. Pharm.* 460, 53–62. doi: 10.1016/j.ijpharm.2013.11.010
- Saleh, N., Al-Handawi, M. B., Bufaroosha, M. S., Assaf, K. I., and Nau, W. M. (2016). Tuning protonation states of tripeleannamine antihistamines by cucurbit[7]uril. *J. Phys. Org. Chem.* 29, 101–106. doi: 10.1002/poc.3504
- Saleh, N., Ghosh, I., and Nau, W. M. (2013). “Cucurbiturils in drug delivery and for biomedical applications,” in *Supramolecular Systems in Biomedical Fields*, ed H.-J. Schneider (Cambridge: Royal Society of Chemistry), 164–212.
- Saleh, N., Khaleel, A., Al-Dmour, H., Al-Hindawi, B., and Yakushenko, E. (2012). Host-guest complexes of cucurbit[7]uril with albendazole in solid state - thermal and structural properties. *J. Therm. Anal. Calorim.* 111, 1–8. doi: 10.1007/s10973-012-2376-5
- Saleh, N., Koner, A. L., and Nau, W. M. (2008). Activation and stabilization of drugs by supramolecular  $pK_a$  shifts: drug-delivery applications tailored for cucurbiturils. *Angew. Chem. Int. Ed.* 47, 5398–5401. doi: 10.1002/anie.200801054
- Saleh, N., Meetani, M. A., Al-Kaabi, L., Ghosh, I., and Nau, W. M. (2011). Effect of cucurbit[n]urils on tropicamide and potential application in ocular drug delivery. *Supramol. Chem.* 23, 650–656. doi: 10.1080/10610278.2011.593631
- Sankaran, S., Cavatorta, E., Huskens, J., and Jonkheijm, P. (2017). Cell adhesion on RGD-displaying knottins with varying numbers of tryptophan amino acids to tune the affinity for assembly on cucurbit[8]uril surfaces. *Langmuir* 33, 8813–8820. doi: 10.1021/acs.langmuir.7b00702
- Sanku, R. K. K., Karakus, O. O., Ilies, M., and Ilies, M. A. (2019). “Inclusion complexes in drug delivery and drug targeting: formation, characterization, and biological applications,” in *Targeted Nanosystems for Therapeutic Applications: New Concepts, Dynamic Properties, Efficiency, and Toxicity*, eds K. Sakurai and M. A. Ilies (Washington, DC: American Chemical Society), 187–221.
- Sasmal, R., Das Saha, N., Pahwa, M., Rao, S., Joshi, D., Inamdar, M. S., et al. (2018). Synthetic host-guest assembly in cells and tissues: fast, stable, and selective bioorthogonal imaging via molecular recognition. *Anal. Chem.* 90, 11305–11314. doi: 10.1021/acs.analchem.8b01851
- Schneider, H.-J., and Yatsimirsky, A. K. (2008). Selectivity in supramolecular host-guest complexes. *Chem. Soc. Rev.* 37, 263–277. doi: 10.1039/B612543N
- Shaikh, M., Mohanty, J., Bhasikuttan, A. C., Uzunova, V. D., Nau, W. M., and Pal, H. (2008). Salt-induced guest relocation from a macrocyclic cavity into a biomolecular pocket: interplay between cucurbit[7]uril and albumin. *Chem. Commun.* 3681–3683. doi: 10.1039/b804381g
- Shchepotina, E., Pashkina, E., Yakushenko, E., and Kozlov, V. (2011). Cucurbiturils as containers for medicinal compounds. *Nanotechnol. Russ.* 6, 773–779. doi: 10.1134/S1995078011060127
- Shetty, D., Khedkar, J. K., Park, K. M., and Kim, K. (2015). Can we beat the biotin-avidin pair? cucurbit[7]uril-based ultrahigh affinity host-guest complexes and their applications. *Chem. Soc. Rev.* 44, 8747–8761. doi: 10.1039/C5CS00631G
- Singharoy, D., Mati, S. S., Ghosh, S., and Bhattacharya, S. C. (2017). CB7 as a drug vehicle and controlled release of drug through non ionic surfactant: spectroscopic technique. *Colloids Surf. B* 160, 84–91. doi: 10.1016/j.colsurfb.2017.09.007
- Sinn, S., and Biedermann, F. (2018). Chemical sensors based on cucurbit[n]uril macrocycles. *Isr. J. Chem.* 58, 357–412. doi: 10.1002/ijch.201700118
- Smith, L. C., Leach, D. G., Blaylock, B. E., Ali, O. A., and Urbach, A. R. (2015). Sequence-specific, nanomolar peptide binding via cucurbit[8]uril-induced folding and inclusion of neighboring side chains. *J. Am. Chem. Soc.* 137, 3663–3669. doi: 10.1021/jacs.5b00718
- Sreenivasulu, B. (2012). “Schiff base and reduced schiff base ligands,” in *Supramolecular Chemistry*, eds P. A. Gale and J. W. Steed (Chichester: John Wiley and Sons Ltd), 827–862.
- Steed, J. W., and Gale, P. A. (2012). *Supramolecular Chemistry: From Molecules to Nanomaterials*. Chichester, UK: John Wiley and Sons.
- Stoffelen, C., Staltari-Ferraro, E., and Huskens, J. (2015). Effects of the molecular weight and the valency of guest-modified poly(ethylene glycol)s on the stability, size and dynamics of supramolecular nanoparticles. *J. Mater. Chem. B* 3, 6945–6952. doi: 10.1039/C5TB01111F
- Sun, C., Zhang, H., Li, S., Zhang, X., Cheng, Q., Ding, Y., et al. (2018). Polymeric nanomedicine with “lego” surface allowing modular functionalization and drug encapsulation. *ACS Appl. Mater. Interfaces* 10, 25090–25098. doi: 10.1021/acsami.8b06598
- Sun, C., Zhang, H., Yue, L., Li, S., Cheng, Q., and Wang, R. (2019). Facile preparation of cucurbit[6]uril-based polymer nanocapsules for targeted photodynamic therapy. *ACS Appl. Mater. Interfaces* 11, 22925–22931. doi: 10.1021/acsami.9b04403
- Tang, Q., Zhang, J., Sun, T., Wang, C.-H., Huang, Y., Zhou, Q., et al. (2018). A turn-on supramolecular fluorescent probe for sensing benzimidazole fungicides and its application in living cell imaging. *Spectrochim. Acta Part A* 191, 372–376. doi: 10.1016/j.saa.2017.10.042
- Tian, F., Cziferszky, M., Jiao, D., Wahlström, K., Geng, J., and Scherman, O. A. (2011). Peptide separation through a CB[8]-mediated supramolecular trap-and-release process. *Langmuir* 27, 1387–1390. doi: 10.1021/la104346k
- Urbach, A. R., and Ramalingam, V. (2011). Molecular recognition of amino acids, peptides, and proteins by cucurbit[n]uril receptors. *Isr. J. Chem.* 51, 664–678. doi: 10.1002/ijch.201100035
- Uzunova, V. D., Cullinane, C., Brix, K., Nau, W. M., and Day, A. I. (2010). Toxicity of cucurbit[7]uril and cucurbit[8]uril: an exploratory *in vitro* and *in vivo* study. *Org. Biomol. Chem.* 8, 2037–2042. doi: 10.1039/b925555a
- Vázquez, J., Remón, P., Dsouza, R. N., Lazar, A. I., Arteaga, J. F., Nau, W. M., et al. (2014). A simple assay for quality binders to cucurbiturils. *Chem. Eur. J.* 20, 9897–9901. doi: 10.1002/chem.201403405
- Venkataramanan, N. S., Ambigapathy, S., Mizuseki, H., and Kawazoe, Y. (2012). Theoretical prediction of the complexation behaviors of antitumor platinum drugs with cucurbiturils. *J. Phys. Chem. B* 116, 14029–14039. doi: 10.1021/jp3098044
- Vinciguerra, B., Cao, L., Cannon, J. R., Zavalij, P. Y., Fenselau, C., and Isaacs, L. (2012). Synthesis and self-assembly processes of monofunctionalized cucurbit[7]uril. *J. Am. Chem. Soc.* 134, 13133–13140. doi: 10.1021/ja3058502

- Walker, S., Kaur, R., McInnes, F. J., and Wheate, N. J. (2010). Synthesis, processing and solid state excipient interactions of cucurbit[6]uril and its formulation into tablets for oral drug delivery. *Mol. Pharm.* 7, 2166–2172. doi: 10.1021/mp100191b
- Walker, S., Oun, R., McInnes, F. J., and Wheate, N. J. (2011). The potential of cucurbit[n]urils in drug delivery. *Israel J. Chem.* 51, 616–624. doi: 10.1002/ijch.201100033
- Wang, H.-Y., Zhou, Y., Lu, J.-H., Liu, Q.-Y., Chen, G.-Y., Tao, Z., et al. (2018). Supramolecular drug inclusion complex of capecitabine with cucurbit[7]uril and inverted cucurbit[7]uril. *Arab. J. Chem.* doi: 10.1016/j.arabjc.2018.04.011
- Wang, R., Bardelang, D., Waite, M., Udachin, K. A., Leek, D. M., Yu, K., et al. (2009). Inclusion complexes of coumarin in cucurbiturils. *Org. Biomol. Chem.* 7, 2435–2439. doi: 10.1039/b903057c
- Wang, R., and Macartney, D. H. (2008). Cucurbit[7]uril host-guest complexes of the histamine h2-receptor antagonist ranitidine. *Org. Biomol. Chem.* 6, 1955–1960. doi: 10.1039/b801591k
- Wang, X., Liu, Y., Lin, Y., Han, Y., Huang, J., Zhou, J., et al. (2019). Trojan antibiotics: new weapons for fighting against drug resistance. *ACS Appl. Bio Mater.* 2, 447–453. doi: 10.1021/acsabm.8b00648
- Wheate, N. J., Buck, D. P., Day, A. I., and Collins, J. G. (2006). Cucurbit[n]uril binding of platinum anticancer complexes. *Dalton Trans.* 451–458. doi: 10.1039/B513197A
- Wheate, N. J., Vora, V., Anthony, N. G., and McInnes, F. J. (2010). Host-guest complexes of the antituberculosis drugs pyrazinamide and isoniazid with cucurbit[7]uril. *J. Incl. Phenom. Macro. Chem.* 68, 359–367. doi: 10.1007/s10847-010-9795-3
- Wu, W.-Y., Yang, J.-Y., Du, L.-M., Wu, H., and Li, C.-F. (2011). Determination of ethambutol by a sensitive fluorescent probe. *Spectrochim. Acta A* 79, 418–422. doi: 10.1016/j.saa.2011.02.045
- Wu, X., Chen, Y., Yu, Q., Li, F.-Q., and Liu, Y. (2019). A cucurbituril/polysaccharide/carbazole ternary supramolecular assembly for targeted cell imaging. *Chem. Commun.* 55, 4343–4346. doi: 10.1039/C9CC01601E
- Wu, X., Zhang, Y.-M., and Liu, Y. (2016). Nanosupramolecular assembly of amphiphilic guest mediated by cucurbituril for doxorubicin delivery. *RSC Adv.* 6, 99729–99734. doi: 10.1039/C6RA21900D
- Wyman, I. W., and Macartney, D. H. (2010). Host-guest complexations of local anaesthetics by cucurbit[7]uril in aqueous solution. *Org. Biomol. Chem.* 8, 247–252. doi: 10.1039/B915694A
- Yang, L., Tan, X., Wang, Z., and Zhang, X. (2015). Supramolecular polymers: historical development, preparation, characterization, and functions. *Chem. Rev.* 115, 7196–7239. doi: 10.1021/cr500633b
- Yang, X., Li, S., Zhang, Q.-W., Zheng, Y., Bardelang, D., Wang, L.-H., et al. (2017). Concealing the taste of the guinness world's most bitter substance by using a synthetic nanocontainer. *Nanoscale* 9, 10606–10609. doi: 10.1039/C7NR03608F
- Yin, H., Chen, L., Yang, B., Bardelang, D., Wang, C., Lee, S. M. Y., et al. (2017). Fluorescence enhancement and  $pK_a$  shift of a rho kinase inhibitor by a synthetic receptor. *Org. Biomol. Chem.* 15, 4336–4343. doi: 10.1039/C7OB00547D
- Yin, H., Huang, Q., Zhao, W., Bardelang, D., Siri, D., Chen, X., et al. (2018). Supramolecular encapsulation and bioactivity modulation of a halonium ion by cucurbit[n]uril ( $n = 7, 8$ ). *J. Org. Chem.* 83, 4882–4887. doi: 10.1021/acs.joc.8b00543
- Yin, H., and Wang, R. (2018). Applications of cucurbit[n]urils ( $n=7$  or  $8$ ) in pharmaceutical sciences and complexation of biomolecules. *Isr. J. Chem.* 58, 188–198. doi: 10.1002/ijch.201700092
- Yin, H., Wang, Z., and Wang, R. (2019). *Modulation of Chemical and Biological Properties of Biomedically Relevant Guest Molecules by Cucurbituril-Type Hosts*. Singapore: Springer.
- Zhang, Q., Li, G., Xiao, X., Zhan, S., and Cao, Y. (2016). Efficient and selective enrichment of ultratrace cytokinins in plant samples by magnetic perhydroxy-cucurbit[8]uril microspheres. *Anal. Chem.* 88, 4055–4062. doi: 10.1021/acs.analchem.6b00408
- Zhang, S., Assaf, K. I., Huang, C., Hennig, A., and Nau, W. M. (2019a). Ratiometric DNA sensing with a host-guest fret pair. *Chem. Commun.* 55, 671–674. doi: 10.1039/C8CC09126A
- Zhang, S., Domínguez, Z., Assaf, K. I., Nilam, M., Thiele, T., Pischel, U., et al. (2018a). Precise supramolecular control of surface coverage densities on polymer micro- and nanoparticles. *Chem. Sci.* 9, 8575–8581. doi: 10.1039/C8SC03150A
- Zhang, X., Xu, X., Li, S., Li, L., Zhang, J., and Wang, R. (2019b). A synthetic receptor as a specific antidote for paraquat poisoning. *Theranostics* 9, 633–645. doi: 10.7150/thno.31485
- Zhang, X., Xu, X., Li, S., Wang, L.-H., Zhang, J., and Wang, R. (2018b). A systematic evaluation of the biocompatibility of cucurbit[7]uril in mice. *Sci. Rep.* 8:8819. doi: 10.1038/s41598-018-27206-6
- Zhao, J., Chen, C., Li, D., Liu, X., Wang, H., Jin, Q., et al. (2014). Biocompatible and biodegradable supramolecular assemblies formed with cucurbit[8]uril as a smart platform for reduction-triggered release of doxorubicin. *Polym. Chem.* 5, 1843–1847. doi: 10.1039/c3py01538f
- Zhao, Y., Buck, D. P., Morris, D. L., Pourgholami, M. H., Day, A. I., and Collins, J. G. (2008). Solubilisation and cytotoxicity of albendazole encapsulated in cucurbit[n]uril. *Org. Biomol. Chem.* 6, 4509–4515. doi: 10.1039/b813759e
- Zhou, Y., Yu, H., Zhang, L., Xu, H., Wu, L., Sun, J., et al. (2009a). A new spectrofluorometric method for the determination of nicotine base on the inclusion interaction of methylene blue and cucurbit[7]uril. *Microchim. Acta* 164, 63–68. doi: 10.1007/s00604-008-0032-3
- Zhou, Y. Y., Sun, J. Y., Yu, H. P., Wu, L., and Wang, L. (2009b). Inclusion complex of riboflavin with cucurbit[7]uril: study in solution and solid state. *Supramol. Chem.* 21, 495–501. doi: 10.1080/10610270802406553

**Conflict of Interest Statement:** The authors declare that the research was conducted in the absence of any commercial or financial relationships that could be construed as a potential conflict of interest.

Copyright © 2019 Das, Assaf and Nau. This is an open-access article distributed under the terms of the Creative Commons Attribution License (CC BY). The use, distribution or reproduction in other forums is permitted, provided the original author(s) and the copyright owner(s) are credited and that the original publication in this journal is cited, in accordance with accepted academic practice. No use, distribution or reproduction is permitted which does not comply with these terms.





# Molecular Lysine Tweezers Counteract Aberrant Protein Aggregation

Inesa Hadrovic<sup>1</sup>, Philipp Rebmann<sup>1</sup>, Frank-Gerrit Klärner<sup>1</sup>, Gal Bitan<sup>2</sup> and Thomas Schrader<sup>1\*</sup>

<sup>1</sup> Faculty of Chemistry, University of Duisburg-Essen, Essen, Germany, <sup>2</sup> Department of Neurology, University of California, Los Angeles, Los Angeles, CA, United States

## OPEN ACCESS

### Edited by:

De-Xian Wang,  
Institute of Chemistry (Chinese  
Academy of Sciences), China

### Reviewed by:

Lihua Yuan,  
Sichuan University, China  
Guoqiang Feng,  
Central China Normal University, China

### \*Correspondence:

Thomas Schrader  
thomas.schrader@  
uni-duisburg-essen.de

### Specialty section:

This article was submitted to  
Supramolecular Chemistry,  
a section of the journal  
Frontiers in Chemistry

Received: 15 July 2019

Accepted: 13 September 2019

Published: 01 October 2019

### Citation:

Hadrovic I, Rebmann P, Klärner F-G,  
Bitan G and Schrader T (2019)  
Molecular Lysine Tweezers Counteract  
Aberrant Protein Aggregation.  
Front. Chem. 7:657.  
doi: 10.3389/fchem.2019.00657

Molecular tweezers (MTs) are supramolecular host molecules equipped with two aromatic pincers linked together by a spacer (Gakh, 2018). They are endowed with fascinating properties originating from their ability to hold guests between their aromatic pincers (Chen and Whitlock, 1978; Zimmerman, 1991; Harmata, 2004). MTs are finding an increasing number of medicinal applications, e.g., as bis-intercalators for DNA such as the anticancer drug Ditercalinium (Gao et al., 1991), drug activity reverters such as the bisglycoluril tweezers Calabadiol 1 (Ma et al., 2012) as well as radioimmuno detectors such as Venus flytrap clusters (Paxton et al., 1991). We recently embarked on a program to create water-soluble tweezers which selectively bind the side chains of lysine and arginine inside their cavity. This unique recognition mode is enabled by a torus-shaped, polycyclic framework, which is equipped with two hydrophilic phosphate groups. Cationic amino acid residues are bound by the synergistic effect of disperse, hydrophobic, and electrostatic interactions in a kinetically fast reversible process. Interactions of the same kind play a key role in numerous protein-protein interactions, as well as in pathologic protein aggregation. Therefore, these particular MTs show a high potential to disrupt such events, and indeed inhibit misfolding and self-assembly of amyloidogenic polypeptides without toxic side effects. The mini-review provides insight into the unique binding mode of MTs both toward peptides and aggregating proteins. It presents the synthesis of the lead compound CLR01 and its control, CLR03. Different biophysical experiments are explained which elucidate and help to better understand their mechanism of action. Specifically, we show how toxic aggregates of oligomeric and fibrillar protein species are dissolved and redirected to form amorphous, benign assemblies. Importantly, these new chemical tools are shown to be essentially non-toxic *in vivo*. Due to their reversible moderately tight binding, these agents are not protein-, but rather process-specific, which suggests a broad range of applications in protein misfolding events. Thus, MTs are highly promising candidates for disease-modifying therapy in early stages of neurodegenerative diseases. This is an outstanding example in the evolution of supramolecular concepts toward biological application.

**Keywords:** molecular tweezers, amino acids, neurodegeneration, amyloids, protein aggregation

## INTRODUCTION

A major challenge in modern medicine is the field of neurodegenerative diseases. Their pathology is dominated by misfolding and subsequent aggregation of characteristic peptides or proteins in the brain, which is correlated with severe impairment of cognitive functions. As the most prominent example, the amyloid  $\beta$ -peptide ( $A\beta$ ) plays a key role in the development and progression of Alzheimer's disease (AD) (Hardy and Higgins, 1992; Hardy and Selkoe, 2002). Senile plaques composed of aggregated  $A\beta$ , forming extracellular  $\beta$ -sheet fibril morphologies, are histopathological hallmarks found in the brains of AD patients. In recent years however, small soluble  $A\beta$  oligomers were identified as the most neurotoxic species (Shankar et al., 2008; Zhao et al., 2012; Sengupta et al., 2016). Despite intense research, the underlying mechanisms of spontaneous misfolding, aggregation, and lesion of nerve cells are still poorly understood. To date only symptom-relieving drugs are clinically approved for AD treatment. Strategically, it seems desirable to develop drug candidates which are able to interfere with the early stages of the disease mechanism. Classical approaches include the reduction of  $A\beta$  production by inhibitors of  $\beta$ - and  $\gamma$ -secretase, the increase of  $A\beta$  removal via anti- $A\beta$  immunotherapy, and direct interference with  $A\beta$  aggregation (Hardy and Selkoe, 2002; Roland and Jacobsen, 2009). The latter can be achieved with a diverse set of peptides and small molecules. Well-known milestones in this field are Congo red (Podlisny et al., 1998), scyllo-Inositol (McLaurin et al., 2000), amino-propane sulfonic acid (Gervais et al., 2007), Clioquinol (Cherny et al., 2001), methylene blue (Necula et al., 2007), and polyphenol (-)-epigallocatechin (EGCG) (Ehrnhoefer et al., 2008).

However, some of these compounds are toxic, others are only active in cell culture or animal experiments, and until today no drug candidate made it through clinical trial. In addition, little structural information is available about the direct interaction between  $A\beta$  and most aggregation inhibitors. Thus, there is clearly a need for new rational approaches. Supramolecular Chemistry has gained a much-improved understanding and quantitative description of those non-covalent interactions which are involved in protein aggregation. In addition, molecular modeling now allows extended MD simulations of complex ensembles with large sampling times and discrete solvent treatment—resulting in predictive power for new supramolecular binders. In our group we developed a highly selective host molecule for lysine and arginine, which is able to draw their side chains into its cavity and shield them from the environment. These molecular tweezers turned out to completely disrupt existing  $\beta$ -sheets formed by amyloidogenic proteins. Our discovery started an intense and very fruitful collaboration between supramolecular chemists and neurologists, which has reached the state of animal experiments and behavioral testing with transgenic mice and holds promise for the development of disease-modifying therapy. This mini-review summarizes the chemical aspects of the endeavor—from deciphering the

binding mode of the tweezers over structural elucidation of their complexes with aggregating proteins to the characterization of their anti-aggregatory effect on various proteins. Finally, toxicity, metabolism, and bioavailability issues will also be briefly discussed.

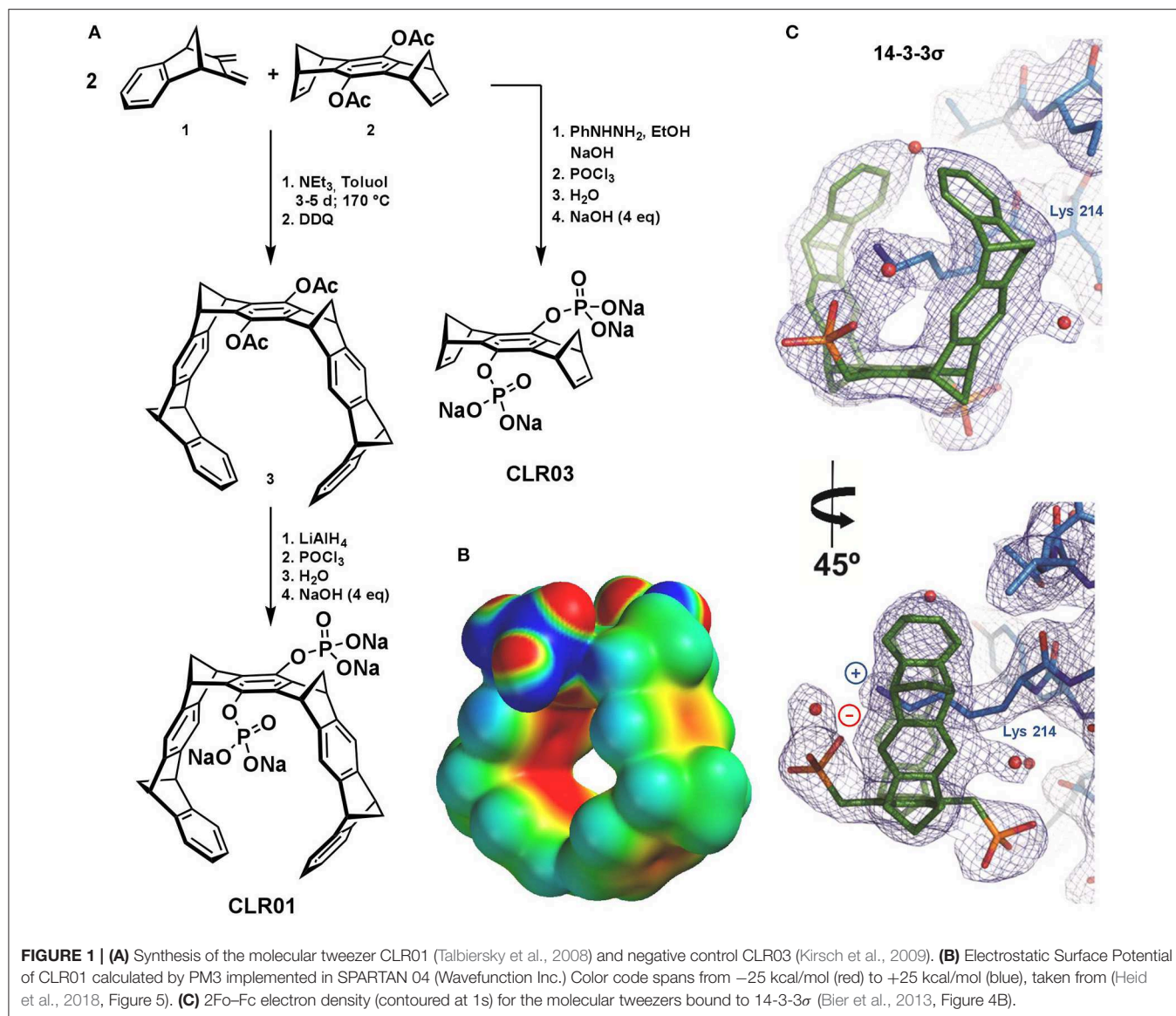
## THE DEVELOPMENT OF MOLECULAR TWEEZERS AS LYSINE AND ARGININE BINDERS

### Structure and Binding Mode of Molecular Tweezers

There are numerous artificial binding motifs for naturally occurring amino acids, but only a few of them are selective and mild enough to find biological application (Crini, 2014; Barrow et al., 2015; Neri et al., 2016). Molecular tweezers were designed rationally, combining supramolecular knowledge, and total synthesis to obtain water-soluble horseshoe-shaped molecules. They are characterized by their well-preorganized torus-shaped, polycyclic non-polar framework, equipped with two hydrophilic phosphate groups. The uniqueness of MTs is reflected in their capability to selectively accommodate exclusively the side chains of basic amino acids, namely lysine and arginine, inside their cavity under physiological conditions. Electrostatic potential surface (EPS) calculations demonstrate that their cavity construction is electron-rich, perfectly symmetric, and open to receive cationic appropriately shaped guests (**Figure 1B**). It appears that even in PBS buffer tweezer dimerization is negligible (Dutt et al., 2013; Heid et al., 2018).

MTs bind cationic amino acid residues via threading their side chains through the cavity in a non-covalent fashion followed by formation of a salt bridge between the tweezer phosphate and the included ammonium or guanidinium cation. This is facilitated by exploiting in a synergistic way van der Waals interactions, substantial electrostatic contributions, and the non-classical hydrophobic effect; this binding mode results in a kinetically fast and reversible recognition process. Quantum chemical and molecular mechanics (QM/MM) calculations and various analytical experiments strongly support this postulated binding mode between MTs and their amino acid guests. Monte Carlo (MC) and molecular dynamics (MD) simulations, isothermal titration calorimetry (ITC) measurements, NMR, and fluorescence titrations, as well as NOESY and variable temperature (VT) experiments clearly point to inclusion of the lysine and arginine side chain inside the tweezer cavity in an enthalpy-driven process. QM/MM calculations confirm the existence of these favorable host-guest complexes in buffered aqueous solution formed via the threading mode (Fokkens et al., 2005; Dutt et al., 2013).

Recently, a crystal structure of the complex between MT and a 14-3-3 protein beautifully demonstrated the threading of the well accessible Lys-214 side chain through the tweezers' cavity accompanied in solution with a substantial inhibition of the complex formation between the 14-3-3 and its natural cargo proteins (Bier et al., 2013).



## Tweezer Synthesis

The characteristic MT framework consists of nine annulated 6-membered rings, which are alternating phenyl and norbornadiene ring systems. The construction of this hydrocarbon torus is achieved in the key step via double Diels-Alder (DA) cycloaddition using two equivalents of diene **1** which forms the walls and one equivalent of dienophile **2** which is the center-piece (**Figure 1A**). The exocyclic diene is obtained in six steps from indene and maleic acid anhydride while the dienophile is made from 1,4-benzophenone in a four-step sequence. The neutral DA reaction requires elevated temperatures; it proceeds stereoselectively *endo* in **1** and *exo* in **2** and thus leads after DDQ (2,3-dichloro-5,6-dicyano-1,4-benzoquinone) oxidation to the desired tweezer (**3**) having the four methylene bridges in all-*syn* configuration (Klärner et al., 1996, 1999; Talbiersky et al., 2008; Schrader et al., 2016).

The two acetoxy-groups can be cleaved in a symmetric or asymmetric fashion, releasing hydroquinone OH groups which can be further functionalized with negatively charged groups for enhanced water-solubility (e.g., phosphates, carboxylates, and sulfates) (Dutt et al., 2013). In the course of several years of intense biophysical and biological testing, the tweezers CLR01 with its two phosphate esters evolved as a lead compound, while its truncated derivative without the side walls, CLR03, served as a negative control. CLR03 represents the central part of the MT molecule; due to the lack of the torus-shaped cavity, it is not able to bind Lys and Arg by inclusion (Schrader et al., 2016).

## INTERACTION WITH BIOACTIVE PEPTIDES

CLR01 was initially tested with small, biologically relevant small peptides (Fokkens et al., 2005). The KLVFF peptide



is located inside the central hydrophobic part of the amyloid- $\beta$  protein, and it was identified as a nucleation site for pathologic protein aggregation, fibril formation, and subsequent plaque occurrence in Alzheimer's disease. NMR and fluorescence titrations with this small peptide revealed inclusion of the *N*-terminal lysine inside CLR01 and a moderate affinity of 10  $\mu$ M ( $K_d$ ) in buffered aqueous solution (PBS) (Dutt et al., 2013).

ITC measurements provide further insight into the postulated binding mode. The binding event between host CLR01 and its KLVFF guest was shown to be a favorable, strongly exothermic process. Here the MT peptide affinity was found to be 15  $\mu$ M, with a 1:1 stoichiometry, and an enthalpic contribution  $\Delta H$  of  $-6.6$  kcal/mol, which is prevailing over the small entropy term  $-T\Delta S$  of  $-0.2$  kcal/mol. Arginine complexation in other peptides was found to be slightly weaker, in the range of 30  $\mu$ M, most likely due to its delocalized guanidinium ion and shorter side chain. The remarkably exothermic character of the binding event correlates well with the assumed threading procedure and the resulting van der Waals interactions between the host cavity and the respective amino acid side chain. The above-reported  $K_d$  values, although moderate in biological terms, place these MT among the most efficient receptor molecules for basic amino acids known today (Fokkens et al., 2005; Dutt et al., 2013).

In general, dissociation constants obtained from ITC measurements agree well with the data determined independently by fluorescence or  $^1\text{H}$  NMR titrations, in spite of the different concentration regimes (NMR  $10^{-3}$  M, ITC  $10^{-4}$  M, Fluoresc.  $10^{-5}$  M). The emission intensity maximum of MTs in fluorescence spectra is found around 330 nm, while the excitation maximum is located at 285 nm ( $\pi, \pi^*$ ). Trapping of guest molecules inside the tweezers cavity results in significant quenching of the fluorescence emission. This proves guest inclusion and allows quantification of the binding event at low concentrations. In most cases affinities for a single lysine inclusion determined by fluorometric titrations are in the range of 5–20  $\mu$ M  $K_d$ . Structurally, the MT's preference for lysine inclusion has been proven in numerous  $^1\text{H}$  NMR titrations in buffer, which reveal drastic upfield shifts of up to 4 ppm ( $\delta\Delta_{\text{max}}$ ) at the  $\delta$ - and  $\varepsilon$ -methylene protons of the basic amino acid side chains. NOESY measurements as well as variable temperature experiments strongly support the guest inclusion (Fokkens et al., 2005).

Molecular tweezers with their unique binding mode for lysine and arginine and their unexpected powerful effect as aggregation inhibitors have attracted the attention of many research groups worldwide in the last decade. Numerous fruitful collaborations demonstrated that these lysine binders represent a widely applicable useful tool against pathologic protein misfolding. In addition, sophisticated analytical methods opened our understanding of the underlying supramolecular mechanism of action. Today we know that advanced MTs are able to specifically disrupt undesired protein-protein interactions; however perhaps even more important is the fact that MTs indeed inhibit misfolding and self-assembly of amyloidogenic polypeptides without toxic side effects (Sinha et al., 2011).

## INTERACTION BETWEEN MOLECULAR TWEEZERS AND AGGREGATING PROTEINS

The pathogenesis of every amyloidosis is caused by aberrant protein aggregation and most likely begins with protein misfolding. AD, Parkinson's disease and type-2 diabetes are the best examined examples of this pathologic process. In the course of AD, the largely unstructured naturally occurring monomeric state of the amyloid- $\beta$  peptides was shown to adopt a conformation rich in  $\beta$ -sheets and which aberrantly forms toxic oligomers and aggregates (Billings et al., 2005).  $A\beta_{40}$ ,  $A\beta_{42}$  and the group of tau proteins mainly participate in this neurologically highly relevant aggregation process which ultimately disposes extracellular plaque formed from  $\beta$ -sheet-rich fibrils. Lysine residues are reported to play an important role in this particular assembly (Usui et al., 2009; Sinha et al., 2012).

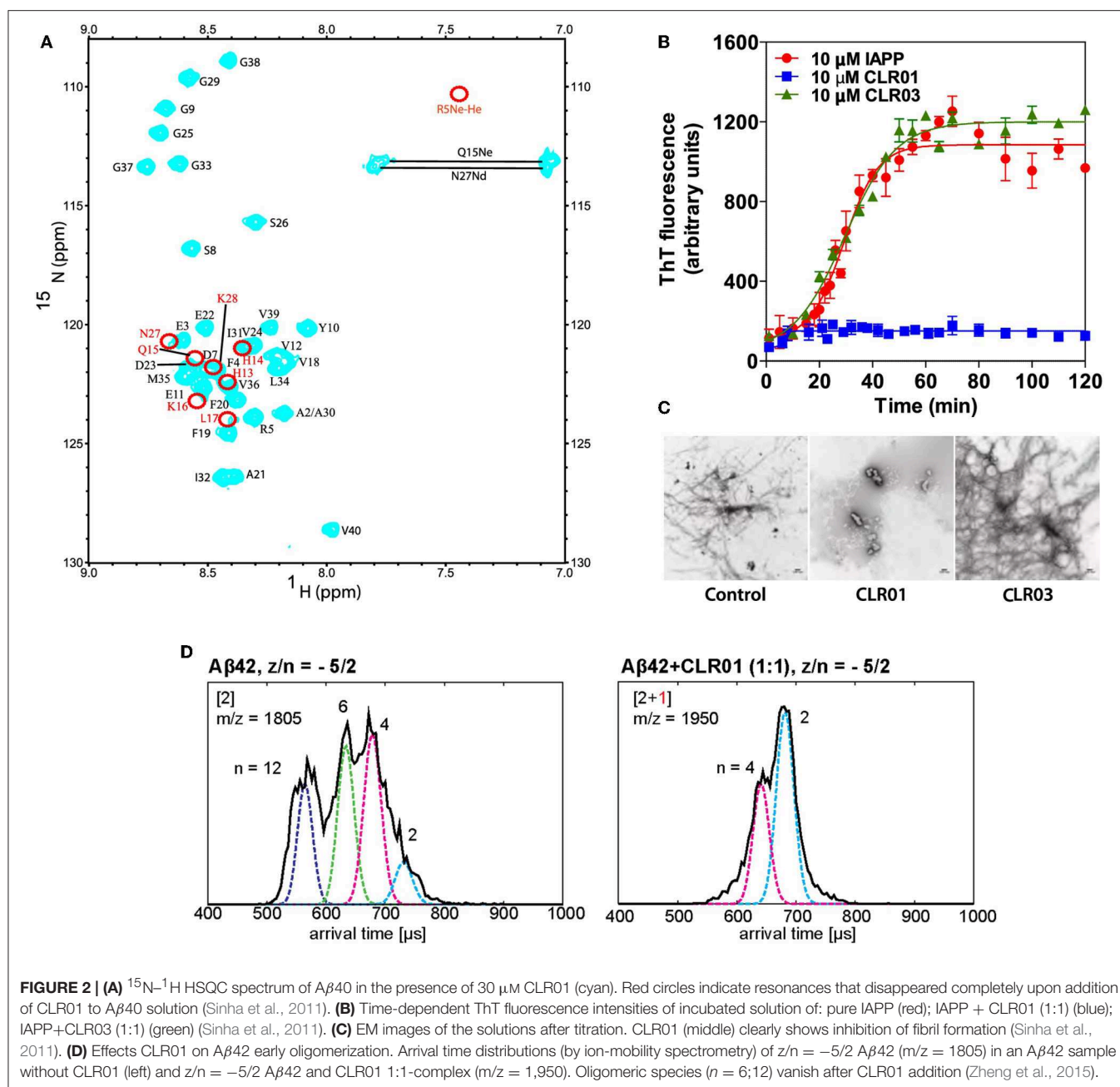
Gratifyingly, MT were found to interfere with the aggregation process of most amyloidogenic proteins. In recent years, many different experiments have been designed and conducted which confirmed CLR01 to be capable of dissolving fibrils, preventing their formation as well as eliminating their toxic precursor oligomers. Structurally, it was important to identify the tweezer binding sites on these proteins. For the most prominent representative, the Alzheimer's peptide, the preferred complexation sites of the tweezers were validated by electron capture dissociation (ECD) mass experiments (EDC-MS/MS) as well as by NMR spectroscopy (Sinha et al., 2011).

### ECD-MS/MS

In the monomeric form of  $A\beta_{40}$  and  $A\beta_{42}$  there are three basic residues, Arg-5, Lys-16, and Lys-28. All of these are simultaneously complexed as confirmed by mass spectrometry. In EDC-MS/MS experiments complexes of MT and a  $A\beta$  protein were collected in a linear ion trap and smoothly fragmented inside. The recorded MS spectra found MT bound to many overlapping protein fragments. The mass spectra show peaks for  $A\beta_{40}$  bound by one, two and three MTs, respectively. In the fragmentation pattern CLR01- $A\beta$ -fragment peaks were only found for fragments bearing a Lys or Arg residue, indicating a retained amino acid selectivity in  $A\beta$  complexation. Most importantly, peptide cleavage did not occur around the two lysine binding sites, because these were protected by the tweezers. The exact binding mode of this complexation event was subsequently investigated by NMR experiments (Sinha et al., 2011).

### NMR Experiments

$^1\text{H}$ - $^{15}\text{N}$  and  $^1\text{H}$ - $^{13}\text{C}$  heteronuclear single quantum coherence (HSQC) NMR experiments confirmed these results. An HSQC spectrum of  $A\beta_{40}$  alone and together with 0.5 equivalents of MT were compared. Upon tweezer binding, the cross peaks of the complexed residue as well as its neighboring amino acids show a significant chemical shift perturbation (CSP) due to the altered magnetic environment. Some signals vanished completely, indicated by red circles in **Figure 2A**. In two-dimensional H(N)CO experiments MT were titrated to a protein solution; already at a 1:10 ratio of CLR01 relative to  $A\beta_{40}$  the CSP



became significant. Amino acid residues surrounding Lys-16 and Lys-28 showed a higher degree of perturbation compared to those in proximity to Arg-5. This implies a stronger affinity of MT for the A $\beta$  Lys residues, consistent with the general Lysine preference of CLR01. At elevated CLR01 concentration all three positions were occupied. The negative control CLR03 showed no effects in the whole NMR-setup (Sinha et al., 2011). Similarly, a three-dimensional HN(CO)CACB NMR experiment was recently used to detect binding sites of MT in the phosphorylated and unphosphorylated tau protein (Despres et al., 2019).

The combination of EDC-MS/MS and NMR spectroscopy underlines the importance of the tweezer cavity for complex

formation with A $\beta$ 40 and A $\beta$ 42, and strongly supports the binding mode elucidated with small peptides (Figure 1C).

If CLR01 binds to every sterically accessible basic residue on a peptide or protein, why is it not toxic then? It was indeed shown that the MT are non-toxic in biological applications at concentrations necessary to inhibit protein aggregation. We believe, that the key lies in kinetically fast reversible binding and moderate affinity. Biophysical experiments indicate fast on and off rates and labile complexation as well as moderate dissociation constants in the low  $\mu\text{M}$  range (Talbiersky et al., 2008; Bier et al., 2013). These key features of our MT safeguard healthy proteins from damage induced by conformational changes, so that they



retain their natural biological function. Indeed, enzymes could be inhibited by MT, albeit only at millimolar concentrations, 100 times higher than those required for the anti-aggregatory effect. The specificity of CLR01 toward the process of aberrant protein aggregation is outstanding because it is a new principle which may be transferred to other drugs as well. It appears that MTs bind their protein guests with the same combination of non-covalent interactions which is also active in the unwanted aggregation process. This unique way of action toward protein aggregation, represents the first example of a “process-specific” aggregation inhibitor; it was examined with various biophysical methods (Schrader et al., 2016).

## PREVENTION OF PATHOLOGIC PROTEIN AGGREGATION

Until 2011 experimental evidence was accumulated for the fact that lysine-specific MT are active against a wide range of aggregating proteins, with detailed experiments performed on the assembly and toxicity of nine prominent amyloid proteins (Sinha et al., 2011).

In this comprehensive investigation a synopsis of various state-of-the-art biophysical experiments gave the full picture: Thioflavin T (ThT) fluorescence, Electron Microscopy (EM), Circular Dichroism spectroscopy (CD), Dynamic Light Scattering (DLS), Mass Spectrometry (MS), and NMR Spectroscopy.

### Thioflavin T (ThT) Fluorescence

ThT is an amyloid dye indicator which turns highly fluorescent upon binding to existing  $\beta$ -sheets (LeVine, 1999). ThT fluorescence was used to monitor the kinetics of  $\beta$ -sheet formation for various amyloid proteins in the presence or absence of CLR01. The tweezers represented the active drug, whereas their truncated derivative, CLR03, was used as negative control. Measurements were performed regularly during a time span of up to 120 h at pH 7.4 in 10 mM phosphate buffer. CLR01 was added in up to 10-fold excess relative to the protein and was able to completely suppress the typical drastic fluorescence enhancement caused by aggregation and protein misfolding. Equimolar concentration of CLR01 was likewise shown to totally disrupt  $\beta$ -sheets of the tau protein. CLR03 displayed no effect in any of the investigated proteins because it lacks the hydrophobic side walls and consequently, the ability to complex Lys residues. Importantly, CLR01 not only inhibited the *de novo* aggregation of amyloidogenic proteins such as A $\beta$ 40/A $\beta$ 42,  $\alpha$ -synuclein and IAPP (Figure 2B) (Prabhudesai et al., 2012), but also disaggregated pre-formed fibrils over several weeks when added at a 10-fold excess, as being confirmed by EM.

### Electron Microscopy (EM)

EM measurements were carried out in parallel to ThT assays, by spotting 10  $\mu$ L aliquots taken from each aggregation reaction, on glow discharged, carbon-coated Formvar grids, using a CX 100 transmission electron microscope. Visualization of the

protein morphology showed that IAPP and other examined amyloidogenic protein samples incubated in the presence of MTs did not form fibrils anymore, strongly supporting conclusions drawn from the ThT measurements (Figure 2C) (Sinha et al., 2011).

### CD Spectroscopy

All  $\beta$ -sheets and therefore also all pathologic protein aggregates produce a dominant characteristic  $\beta$ -sheet band at 215 nm in the CD spectrum. In the presence of a 3-fold excess of CLR01, this band was rapidly reduced and completely disappeared after 1 h, indicating efficient inhibition of  $\beta$ -sheet formation in case of A $\beta$ 40 and A $\beta$ 42. Equimolar CLR01 lead to partial inhibition. Interestingly, CLR01 completely inhibited tau aggregation already at the equimolar level, which correlates with the higher number of exposed Lys residues in the tau sequence in comparison to A $\beta$  (Sinha et al., 2011).

### Dynamic Light Scattering (DLS)

Dynamic light scattering provides a direct and non-invasive way to monitor the formation of larger aggregates. It was employed to monitor the influence of CLR01 on oligomer size and distribution of A $\beta$ . Experiments were performed with CLR01 in 10-fold excess or equimolar relative to A $\beta$ , controls were run with A $\beta$  alone. Intriguingly, the DLS results indicate that CLR01 does not prevent oligomer formation but rather modulates A $\beta$  self-assembly into formation of structures that are neither amyloidogenic nor toxic (Sinha et al., 2011).

### Mass Spectrometry (MS)

In recent years, advanced methods in mass spectrometry have been exploited for the mechanistic elucidation of protein aggregating events. Thus, Bowers et al. used mild ionization conditions and high resolution to monitor the impact of small molecule modulators on A $\beta$  oligomerization (Zheng et al., 2015). The effect of different concentrations of CLR01 and its related derivative, CLR03 on the A $\beta$  assembly was investigated with a custom-built ion mobility spectrometry-mass spectrometer (IMS-MS) which consisted of a nano electrospray ionization (nano-ESI) source, an ion funnel, a temperature-controlled drift cell, and a quadrupole mass filter followed by an electron multiplier for ion detection (Wytenbach et al., 2001). Consistent with earlier studies (Sinha et al., 2011), these experiments confirmed Arg-5, Lys-16, and Lys-28 as preferred binding sites for MT on A $\beta$ . The authors associated four distinct peaks with A $\beta$ 42 alone, while in the presence of a 10-fold CLR01-excess three sets of peaks occurred corresponding to different charge states of the complexes of A $\beta$ 42 with up to four bound tweezers (Bernstein et al., 2009). No dimers or higher oligomers were observed (Figure 2D). This is a good indication that CLR01 not only prevents formation of A $\beta$ 42 dimers, but also of higher order oligomers. Importantly, no free, unbound A $\beta$ 42 was found in the mass spectrum, supporting the assumption that MT bind directly to A $\beta$ 42 with rather high affinity ( $\sim 1 \mu$ M). The authors concluded that CLR01 can remodel the early oligomerization of A $\beta$ 42 not only immediately upon dissolution

but also after the oligomers have already been formed (Zheng et al., 2015).

Native Top-Down Mass Spectrometry and IMS were likewise used to characterize the interaction between MT and the Tau Protein (Nshanian et al., 2018).

Very recently, Loo also reported that no toxic oligomers are left as the result of the efficient interaction between MT and SOD1 (Superoxide Dismutase 1). With ECD, the covalent peptide bonds of the polypeptide could be cleaved, whereas non-covalent forces sufficed to hold the ligand bound to the macromolecule. Tandem MS (MS/MS) or “top-down” MS of the protein–ligand complex allowed to explore the main binding site(s) of MT on the SOD1 surface. Surprisingly, MT preferred to bind to Lys-70 and/or Lys-75 although none of these residues is directly involved in the aggregation process of SOD1. This may explain why at least a 5-fold MT excess is required to affect the aggregation (Malik et al., 2019).

In this investigation, CLR01 inhibited abnormal SOD1 self-assembly *in vitro*, as well as *in vivo*, as being shown on the G93A-SOD1 mouse model of amyotrophic lateral sclerosis (ALS). By applying therapeutic amounts of CLR01 to recombinant wild type and mutant SOD1, their *in vitro* aggregation speed was significantly lowered for all SOD1 forms. *In vivo*, misfolded SOD1 in the spinal cord was significantly reduced, yet not enough to overcome motor deficits, most likely due to the fast disease progression. Further insight came from experiments on SOD1 with ThT and EM at the end of each aggregation. For a potential SOD1 treatment, advanced tweezer derivatives with improved performance must be designed in the future (Malik et al., 2019).

## CONCLUSION AND OUTLOOK

The above-discussed synopsis of structural and biophysical experiments strongly suggests that molecular tweezers dock onto sterically accessible lysine and arginine on aggregating proteins. The resulting Lys/Arg shielding prevents misfolding and/or subsequent protein aggregation into toxic oligomers. It also dissolves existing  $\beta$ -sheets and redirects their path of aggregation to benign amorphous structures.

The same effects are observed with a large number of aggregating proteins, so that these lysine binders seem to act in a process-specific manner and are clearly not protein-specific. In all cases where lysine or arginine residues are involved in the aggregation process, molecular tweezers seem to prevent their ordered aggregation into fibrillar toxic structures. It may be argued that unselective multiple lysine binding should greatly disturb protein function; however, their moderate affinity (10–30  $\mu$ M  $K_d$ ) and fast on- and off-rates apparently preserve natural protein folding and function. Indeed, for enzyme inhibition 100-fold higher concentrations are needed (1 mM), providing a large potential therapeutic window.

After the initial aggregation assays with isolated proteins, cell culture experiments demonstrated powerful protection against

oligomer or fibril lesion from exactly those proteins whose aggregation could also be rescued *in vitro* (Xu et al., 2017; Malik et al., 2018). Finally, triply transgenic mice were treated with low daily doses of CLR01 (40  $\mu$ g/kg) and showed dramatic reduction of plaque load in their cortices (stained histological brain slices). Subsequent behavioral tests (Y-Maze, Pole climbing) revealed significant memory and mobility improvement after treatment with CLR01 (Richter et al., 2017).

Although no systematic metabolism studies have been carried out yet, no degradation product could be found so far, e.g., after treatment with strong acid (pH 0) and base (pH 12) and common phosphatases. We assume that the steric demand of the tweezer skeleton prevents most chemical transformations at the two phosphate groups, and that the doubly phosphorylated stage is recognized as a water-soluble metabolite ready for urinary excretion.

CLR01 was tritium-labeled and could be detected in mouse brains. In addition, HPLC-MS assays of brain extracts revealed 2–3 nM concentrations of CLR01. We are currently optimizing the tweezer structure to generate aggregation inhibitors of lower polarity which will cross the blood-brain barrier (BBB) much more efficiently, hopefully even after oral administration. In some of these projects the results are so promising that we hope to enter clinical trial within the next few years.

Thus, a supramolecular host molecule for basic amino acids was turned into a powerful tool against pathologic protein aggregation and showed highly promising effects in various cell types and animal models. This is an outstanding example in the evolution of supramolecular concepts toward biological application.

## AUTHOR CONTRIBUTIONS

PR wrote the chapters about structure, synthesis, and binding of MTs. IH wrote the chapters about prevention of pathologic protein aggregation by MTs. TS wrote the introduction and conclusions section. F-GK invented the molecular tweezers, GB carried out biological experiments, and both supervised the revision of the mini-review.

## FUNDING

The work summarized in this Mini-Review was performed within the Collaborative Research Centre 1093: Supramolecular Chemistry on Proteins, Subproject A3, which is now in the second grant period and has been funded by the Deutsche Forschungsgemeinschaft DFG. The authors also acknowledge the NIH/NIA R01 AG050721 for the funding and AG050721-02S1 and AG050721-05S1 for administrative supplements.

## ACKNOWLEDGMENTS

Funding by the Deutsche Forschungsgemeinschaft (CRC 1093, Project A3) is gratefully acknowledged.

## REFERENCES

- Barrow, S. J., Kasera, S., Rowland, M. J., del Barrio, J., and Scherman, O. A. (2015). Cucurbituril-based molecular recognition. *Chem. Rev.* 115, 12320–12406. doi: 10.1021/acs.chemrev.5b00341
- Bernstein, S. L., Dupuis, N. F., Lazo, N. D., Wyttenbach, T., Condrón, M. M., Bitan, G., et al. (2009). Amyloid- $\beta$  protein oligomerization and the importance of tetramers and dodecamers in the aetiology of Alzheimer's disease. *Nat. Chem.* 1, 326–331. doi: 10.1038/nchem.247
- Bier, D., Rose, R., Bravo-Rodríguez, K., Bartel, M., Ramirez-Anguaita, J. M., Dutt, S., et al. (2013). Molecular tweezers modulate 14-3-3 protein-protein interactions. *Nat. Chem.* 5, 234–239. doi: 10.1038/nchem.1570
- Billings, L. M., Oddo, S., Green, K. N., McGaugh, J. L., and LaFerla, F. M. (2005). Intraneuronal A $\beta$  causes the onset of early Alzheimer's disease-related cognitive deficits in transgenic mice. *Neuron* 45, 675–688. doi: 10.1016/j.neuron.2005.01.040
- Chen, C. W., and Whitlock, H. W. (1978). Molecular tweezers: a simple model of bifunctional intercalation. *J. Am. Chem. Soc.* 100, 4921–4922. doi: 10.1021/ja00483a063
- Cherny, R. A., Atwood, C. S., Xilinas, M. E., Gray, D. N., Jones, W. D., Mclean, C. A., et al. (2001). Treatment with a copper-zinc chelator markedly and rapidly inhibits  $\beta$ -amyloid accumulation in Alzheimer's disease transgenic mice. *Neuron* 30:665–676. doi: 10.1016/S0896-6273(01)00317-8
- Crini, G. (2014). Review: a history of cyclodextrins. *Chem. Rev.* 114, 10940–10975. doi: 10.1021/cr500081p
- Despres, C., Di, J., Cantrelle, F. X., Li, Z., Huvent, I., Chambraud, B., et al. (2019). Major differences between the self-assembly and seeding behavior of heparin-induced and in vitro phosphorylated tau and their modulation by potential inhibitors. *ACS Chem. Biol.* 14, 1363–1379. doi: 10.1021/acscchembio.9b00325
- Dutt, S., Wilch, C., Gersthagen, T., Talbiersky, P., Bravo-Rodríguez, K., Hanni, M., et al. (2013). Molecular tweezers with varying anions: a comparative study. *J. Org. Chem.* 78, 6721–6734. doi: 10.1021/jo4009673
- Ehrnhöfer, D. E., Bieschke, J., Boeddrich, A., Herbst, M., Masino, L., Lurz, R., et al. (2008). EGCG redirects amyloidogenic polypeptides into unstructured, off-pathway oligomers. *Nat. Struct. Mol. Biol.* 15, 558–566. doi: 10.1038/nsmb.1437
- Fokkens, M., Schrader, T., and Klärner, F. G. (2005). A molecular tweezer for lysine and arginine. *J. Am. Chem. Soc.* 127, 14415–14421. doi: 10.1021/ja052806a
- Gakh, A. A. (2018). "Molecular tweezers," in *Mol Devices - An Introd to Technomimetics Its Biol Appl.* 1st Edn. (Hoboken, NJ: John Wiley & Sons, Inc), 213–310.
- Gao, Q., Williams, L. D., Egli, M., Rabinovich, D., Chen, S. L., Quigley, G. J., et al. (1991). Drug-induced DNA repair: X-ray structure of a DNA-ditercalinium complex. *Proc. Natl. Acad. Sci. U.S.A.* 88, 2422–2426. doi: 10.1073/pnas.88.6.2422
- Gervais, F., Paquette, J., Morissette, C., Krzykowski, P., Yu, M., Azzi, M., et al. (2007). Targeting soluble A $\beta$  peptide with Tramiprosate for the treatment of brain amyloidosis. *Neurobiol. Aging* 28, 537–547. doi: 10.1016/j.neurobiolaging.2006.02.015
- Hardy, J., and Higgins, G. A. (1992). Alzheimer's disease: the amyloid cascade hypothesis. *Science* 256, 184–185. doi: 10.1126/science.1566067
- Hardy, J., and Selkoe, D. J. (2002). The amyloid hypothesis of Alzheimer's disease. *Amyloid Int. J. Exp. Clin. Investig.* 297, 353–357. doi: 10.1126/science.1072994
- Harmata, M. (2004). Chiral molecular tweezers. *Acc. Chem. Res.* 37, 862–873. doi: 10.1021/ar030164v
- Heid, C., Sowislok, A., Schaller, T., Niemeyer, F., Klärner, F.-G., and Schrader, T. (2018). Molecular tweezers with additional recognition sites. *Chem. Eur. J.* 24, 11332–11343. doi: 10.1002/chem.201801508
- Kirsch, M., Talbiersky, P., Polkowska, J., Bastkowski, F., Schaller, T., De Groot, H., et al. (2009). A Mechanism of efficient G6PD inhibition by a molecular clip. *Angew. Chem. Int. Ed.* 48, 2886–2890. doi: 10.1002/anie.200806175
- Klärner, F.-G., Benkhoff, J., Boese, R., Burkert, U., and Kamieth, M. (1996). Molecular tweezers as synthetic receptors in host-guest chemistry: inclusion of cyclohexane and self-assembly of aliphatic side chains. *Angew. Chem. Int. Ed. Engl.* 35, 4–7. doi: 10.1002/anie.199611301
- Klärner, F. G., Burkert, U., Kamieth, M., Boese, R., and Benet-Buchholz, J. (1999). Molecular tweezers as synthetic receptors: molecular recognition of electron-deficient aromatic and aliphatic substrates. *Chem. Eur. J.* 5, 1700–1707. doi: 10.1002/(SICI)1521-3765(19990604)5:6<1700::AID-CHEM1700>3.0.CO;2-9
- LeVine, H. (1999). Quantification of  $\beta$ -sheet amyloid fibril structures with thioflavin T. *Methods Enzymol.* 309, 274–284. doi: 10.1016/S0076-6879(99)09020-5
- Ma, D., Zhang, B., Hoffmann, U., Sundrup, M. G., Eikermann, M., Isaacs, L. (2012). Acyclic cucurbit[n]uril-type molecular containers bind neuromuscular blocking agents in vitro and reverse neuromuscular block in vivo. *Angew. Chem. Int. Ed.* 51, 11358–11362. doi: 10.1002/anie.201206031
- Malik, R., Di, J., Nair, G., Attar, A., Taylor, K., Teng, E., et al. (2018). Using molecular tweezers to remodel abnormal protein self-assembly and inhibit the toxicity of amyloidogenic proteins. *Methods Mol Biol.* 1777, 369–386. doi: 10.1007/978-1-4939-7811-3\_24
- Malik, R., Meng, H., Wongkongkathep, P., Corrales, C. I., Sepanj, N., Atlasi, R. S., et al. (2019). The molecular tweezer CLR01 inhibits aberrant superoxide dismutase 1 (SOD1) self-assembly in vitro and in the G93A-SOD1 mouse model of ALS. *J. Biol. Chem.* 294, 3501–3513. doi: 10.1074/jbc.RA118.005940
- McLaurin, J. A., Golomb, R., Jurewicz, A., Antel, J. P., and Fraser, P. E. (2000). Inositol stereoisomers stabilize an oligomeric aggregate of Alzheimer amyloid  $\beta$  peptide and inhibit A $\beta$ -induced toxicity. *J. Biol. Chem.* 275, 18495–18502. doi: 10.1074/jbc.M906994199
- Necula, M., Breydo, L., Milton, S., Kaye, R., Van Der Veer, W. E., Tone, P., et al. (2007). Methylene blue inhibits amyloid A $\beta$  oligomerization by promoting fibrillization. *Biochemistry* 46, 8850–8860. doi: 10.1021/bi700411k
- Neri, P., Sessler, J. L., and Wang, M.-X. (2016). *Calixarenes and Beyond*. Cham: Springer International Publishing.
- Nshanian, M., Lantz, C., Wongkongkathep, P., Schrader, T., Klärner, F. G., Blümke, A., et al. (2018). Native top-down mass spectrometry and ion mobility spectrometry of the interaction of tau protein with a molecular tweezer assembly modulator. *J. Am. Soc. Mass. Spectrom.* 30, 16–23. doi: 10.1007/s13361-018-2027-6
- Paxton, R. J., Beatty, B. G., Hawthorne, M. F., et al. (1991). A transition metal complex (Venus flytrap cluster) for radioimmunoassay and radioimmunotherapy. *Proc. Natl. Acad. Sci. U.S.A.* 88, 3387–3391. doi: 10.1073/pnas.88.8.3387
- Podlinsky, M. B., Walsh, D. M., Amarante, P., Ostaszewski, B. L., Stimson, E. R., Maggio, J. E., et al. (1998). Oligomerization of endogenous and synthetic amyloid  $\beta$ -protein at nanomolar levels in cell culture and stabilization of monomer by Congo red. *Biochemistry* 37, 3602–3611. doi: 10.1021/bi972029u
- Prabhudesai, S., Sinha, S., Attar, A., Kotagiri, A., Fitzmaurice, A. G., Lakshmanan, R., et al. (2012). A novel "Molecular Tweezer" inhibitor of  $\alpha$ -synuclein neurotoxicity in vitro and in vivo. *Neurotherapeutics* 9, 464–476. doi: 10.1007/s13311-012-0105-1
- Richter, F., Subramaniam, S. R., Magen, I., Lee, P., Hayes, J., Attar, A., et al. (2017). A molecular tweezer ameliorates motor deficits in mice overexpressing  $\alpha$ -synuclein. *Neurotherapeutics* 14, 1107–1119. doi: 10.1007/s13311-017-0544-9
- Roland, J. R., and Jacobsen, H. (2009). Alzheimer's disease: From pathology to therapeutic approaches. *Angew. Chem. Int. Ed.* 48, 3030–3059. doi: 10.1002/anie.200802808
- Schrader, T., Bitan, G., and Klärner, F. G. (2016). Molecular tweezers for lysine and arginine-powerful inhibitors of pathologic protein aggregation. *Chem. Commun.* 52, 11318–11334. doi: 10.1039/C6CC04640A
- Sengupta, U., Nilson, A. N., and Kaye, R. (2016). The role of amyloid- $\beta$  oligomers in toxicity, propagation, and immunotherapy. *EBioMedicine* 6, 42–49. doi: 10.1016/j.ebiom.2016.03.035
- Shankar, G. M., Li, S., Mehta, T. H., Garcia-Munoz, A., Shepardson, N. E., Imelda, S., et al. (2008). Amyloid  $\beta$ -protein dimers isolated directly from Alzheimer brains impair synaptic plasticity and memory. *Nat. Med.* 14, 837–842. doi: 10.1038/nm1782
- Sinha, S., Lopes, D. H. J., and Bitan, G. (2012). A key role for lysine residues in amyloid  $\beta$ -protein folding.pdf. *ACS Chem. Neurosci.* 3, 473–481. doi: 10.1021/cn3000247
- Sinha, S., Lopes, D. H. J., Du, Z., Pang, E. S., Shanmugam, A., Lomakin, A., et al. (2011). Lysine-specific molecular tweezers are broad-spectrum inhibitors of assembly and toxicity of amyloid proteins. *J. Am. Chem. Soc.* 133, 16958–16969. doi: 10.1021/ja206279b
- Talbiersky, P., Bastkowski, F., Kla, F., and Schrader, T. (2008). Molecular clip and tweezer introduce new mechanisms of enzyme inhibition molecular clip and

- tweezer introduce new mechanisms of enzyme inhibition. *J. Am. Chem. Soc.* 130, 9824–9828. doi: 10.1021/ja801441j
- Usui, K., Hulleman, J. D., Paulsson, J. F., Siegel, S. J., Powers, E. T., and Kelly, J. W. (2009). Site-specific modification of Alzheimer's peptides by cholesterol oxidation products enhances aggregation energetics and neurotoxicity. *Proc. Natl. Acad. Sci. U.S.A.* 106, 18563–18568. doi: 10.1073/pnas.0804758106
- Wytenbach, T., Kemper, P. R., and Bowers, M. T. (2001). Design of a new electrospray ion mobility mass spectrometer. *Int. J. Mass Spectrom.* 212, 13–23. doi: 10.1016/S1387-3806(01)00517-6
- Xu, N., Bitan, G., Schrader, T., Klärner, F. G., Osinska, H., and Robbins, J. (2017). Inhibition of mutant  $\alpha$ B crystallin-induced protein aggregation by a molecular tweezer. *J. Am. Heart Assoc.* 6, 1–13. doi: 10.1161/JAHA.117.006182
- Zhao, L. N., Long, H. W., Mu, Y., and Chew, L. Y. (2012). The toxicity of amyloid  $\beta$  oligomers. *Int. J. Mol. Sci.* 13, 7303–7327. doi: 10.3390/ijms13067303
- Zheng, X., Liu, D., Klärner, F. G., Schrader, T., Bitan, G., and Bowers, M. T. (2015). Amyloid  $\beta$ -protein assembly: the effect of molecular tweezers CLR01 and CLR03. *J. Phys. Chem.* 119, 4831–4841. doi: 10.1021/acs.jpcc.5b00692
- Zimmerman, S. (1991). Molecular tweezers: synthetic receptors for  $\pi$ -sandwich complexation of aromatic substrates. *Bioorganic Chem. Front.* 199, 33–71. doi: 10.1007/978-3-642-76241-3\_2

**Conflict of Interest:** The authors declare that the research was conducted in the absence of any commercial or financial relationships that could be construed as a potential conflict of interest.

Copyright © 2019 Hadrovic, Rebmann, Klärner, Bitan and Schrader. This is an open-access article distributed under the terms of the Creative Commons Attribution License (CC BY). The use, distribution or reproduction in other forums is permitted, provided the original author(s) and the copyright owner(s) are credited and that the original publication in this journal is cited, in accordance with accepted academic practice. No use, distribution or reproduction is permitted which does not comply with these terms.





# The Supramolecular Chemistry of Cycloparaphenylenes and Their Analogs

Dapeng Lu<sup>1\*</sup>, Qiang Huang<sup>2</sup>, Shengda Wang<sup>2</sup>, Jinyi Wang<sup>2</sup>, Pingsen Huang<sup>2</sup> and Pingwu Du<sup>2\*</sup>

<sup>1</sup> School of Pharmacy, Anhui Medical University, Hefei, China, <sup>2</sup> Hefei National Laboratory for Physical Sciences at the Microscale, iChEM (Collaborative Innovation Center of Chemistry for Energy Materials), CAS Key Laboratory of Materials for Energy Conversion, Department of Materials Science and Engineering, University of Science and Technology of China, Hefei, China

## OPEN ACCESS

### Edited by:

De-Xian Wang,  
Institute of Chemistry (CAS), China

### Reviewed by:

Han-Yuan Gong,  
Beijing Normal University, China  
Shixin Fa,  
Kyoto University, Japan

### \*Correspondence:

Dapeng Lu  
ludapeng@ahmu.edu.cn  
Pingwu Du  
dupingwu@ustc.edu.cn

### Specialty section:

This article was submitted to  
Supramolecular Chemistry,  
a section of the journal  
Frontiers in Chemistry

**Received:** 11 August 2019

**Accepted:** 19 September 2019

**Published:** 09 October 2019

### Citation:

Lu D, Huang Q, Wang S, Wang J,  
Huang P and Du P (2019) The  
Supramolecular Chemistry of  
Cycloparaphenylenes and Their  
Analogs. *Front. Chem.* 7:668.  
doi: 10.3389/fchem.2019.00668

Cycloparaphenylenes (CPPs) and their analogs have recently attracted much attention due to their aesthetical structures and optoelectronic properties with radial  $\pi$ -conjugation systems. The past 10 years have witnessed a remarkable advancement in CPPs research, from synthetic methodology to optoelectronic investigations. In this present minireview, we highlight the supramolecular chemistry of CPPs and their analogs, mainly focusing on the size-selective encapsulation of fullerenes, endohedral metallofullerenes, and small molecules by these hoop-shaped macrocycles. We will also discuss the assembly of molecular bearings using some belt-persistent tubular cycloarylene molecules and fullerenes, photoinduced electron transfer properties in supramolecular systems containing carbon nanohoop hosts and fullerene guests, as well as the shape recognition properties for structure self-sorting by using dumbbell-shaped dimer of [60]fullerene ligand. Besides, the supramolecular complexes with guest molecules other than fullerenes, such as CPPs themselves, iodine, pyridinium cations, and bowl-shaped corannulene, are also discussed.

**Keywords:** supramolecular chemistry, fullerene guest, non-fullerene guest, carbon nanohoop, cycloparaphenylene

## INTRODUCTION

Supramolecular chemistry is the subject of the association of two or more chemical species held together by intermolecular forces, such as electrostatic interactions, hydrogen bonding, van der Waals forces, etc., which could lead to organized entities of higher complexity (Lehn, 1985, 1988). It is one of today's fastest growing disciplines, crossing a range of subjects from biological chemistry to materials science, and shows great potential in the fields of catalysis, drug delivery, biotherapy, electrochemical sensor, self-healing materials (Zhang and Wang, 2011; Yan et al., 2012; Dong et al., 2015; Yang et al., 2015; Zhang et al., 2017a; Zhou et al., 2017). As one of the most important aspect of supramolecular chemistry, the host-guest molecular recognition requires that the two species must complement each other both in geometry (size and shape) and binding sites (Lehn, 1985, 1988). Macrocyclic structures, in principle, meet the requirements as they usually contain the cavities, clefts, and pockets with appropriate size and shape that provide the framework for substrate species by multiple non-covalent interactions. The representative macrocyclic molecules during the development of supramolecular chemistry, such as crown ether, cyclodextrins, calixarenes, and cucurbiturils, have been the classical structures in this field (Yang et al., 2015; Zhou et al., 2017).



Recently, the introduction of pillar[*n*]arenes (**Figure 1A**) as new types of macrocyclic hosts by Ogoshi et al. (2008), rapidly received significant attention for their prominent host-guest properties.

Meanwhile, another type of carbon-rich macrocyclic molecules with radially oriented  $\pi$  systems pointing inwards to the cavity have emerged as a new class of strained, non-planar aromatic structures, which were named as cycloparaphenylenes (CPPs) or carbon nanohoops because of their structural relationship with carbon nanotubes (CNTs) (Jasti et al., 2008; Jasti and Bertozzi, 2010). Despite their simple structures, however, the synthesis of CPPs was only achieved in 2008 from curved molecular precursors after intensive efforts (Jasti et al., 2008). Following this work, several other novel strategies for CPP synthesis were developed and a number of CPP-related carbon nanorings with various sizes and atomic compositions were prepared (Darzi et al., 2015; Segawa et al., 2016). More importantly, Itami et al. reported the successful synthesis of a carbon nanobelt, [12]carbon nanobelt ([12]CNB) comprising a closed loop of fully fused edge-sharing benzene rings in 2017 (Povie et al., 2017). Furthermore, development of this synthetic strategy to the preparation of [16]CNB and [24]CNB analogs were also reported by the same group (Povie et al., 2018). Using a new ligand system, the yield of the final belt-forming, nickel-mediated reaction for [12]CNB was improved from 1 to 7%, and [16]CNB and [24]CNB were obtained in 6 and 2% yield, respectively. These studies are important steps toward the bottom-up synthesis of other carbon nanobelt structures and CNTs. Another interesting and valuable work which should be mentioned is the thermally induced cycloreversion strategy for the synthesis of carbon nanohoops reported by Huang et al. (2016). They converted the anthracene photodimer synthon into anthracene-incorporated aromatic macrocycle through ring expansion reaction based on the cycloreversion of its dianthracene core. This work sheds light on the utility of the anthracene photodimerization-cycloreversion method for “bottom-up” carbon nanohoop synthesis. The past 10 years have witnessed a remarkable advancement in CPPs research, from synthetic methodology to optoelectronic investigations due to their size-dependent behavior and promising applications in materials (Segawa et al., 2012; Wu et al., 2018; Huang et al., 2019; Toyota and Tsurumaki, 2019; Xu and Delius, 2019).

In a recent work, Delius et al. overviewed the host-guest chemistry of carbon nanohoops, the preparation of mechanically interlocked architectures, and crystal engineering (Xu and Delius, 2019). In this present minireview, we only highlight the supramolecular chemistry of CPPs and their analogs, mainly focusing on the size-selective encapsulation of fullerenes, endohedral metallofullerenes, and small molecules by these hoop-shaped macrocycles. We will also discuss the assembly of molecular bearings using some belt-persistent tubular cycloarylene molecules and fullerenes, photoinduced electron transfer properties in supramolecular systems containing carbon nanohoop hosts and fullerene guests, as well as the shape recognition properties for structure self-sorting by using dumbbell-shaped dimer of [60]fullerene ligand. Besides, the supramolecular complexes with guest molecules other than

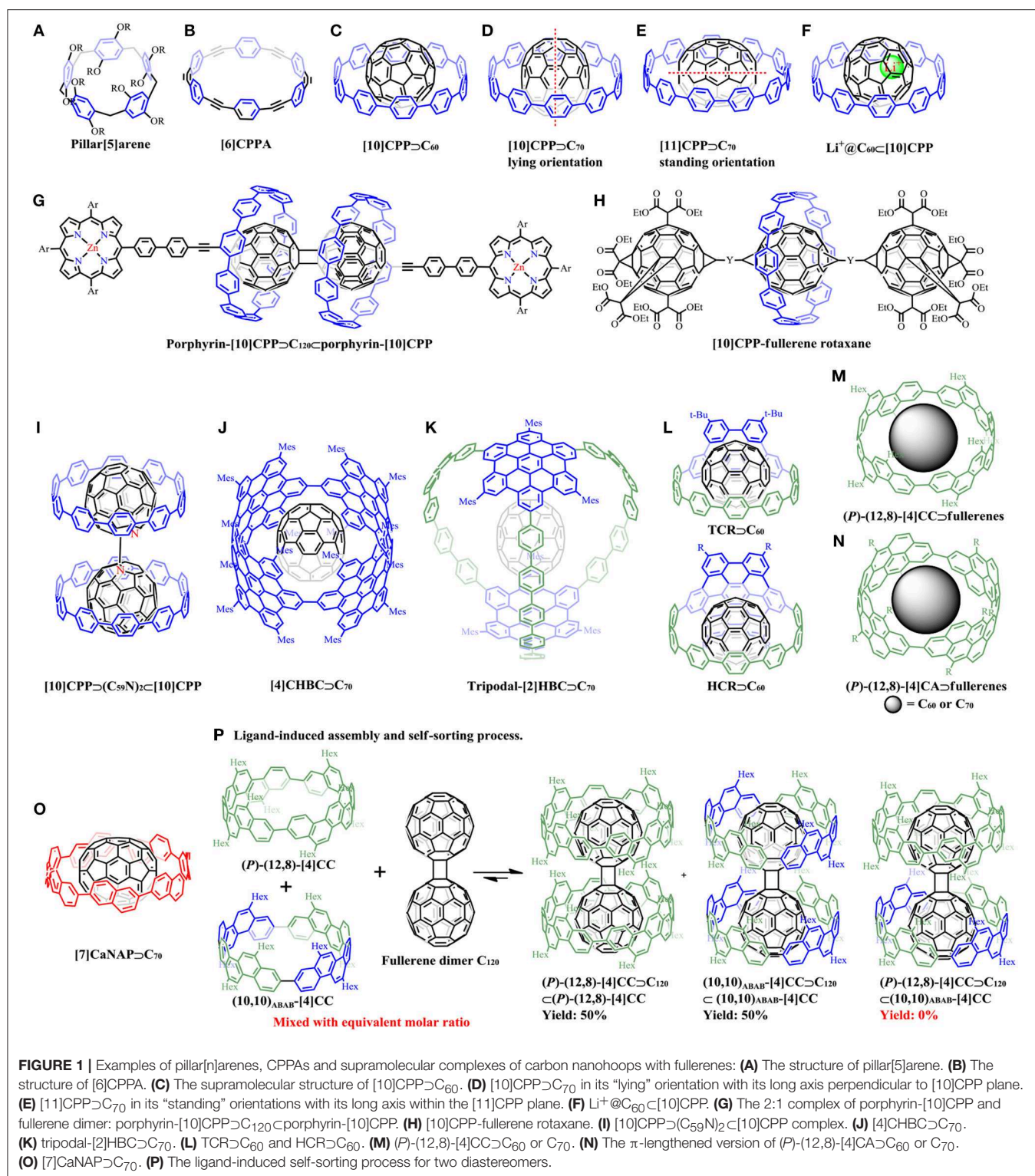
fullerenes, such as CPPs themselves, iodine, pyridinium cations, and bowl-shaped corannulene, are also discussed.

## SUPRAMOLECULAR COMPLEXES CONSISTING OF CPPs AND FULLERENES

The first series of macrocyclic hosts was the molecules with  $sp^2/sp$ -hybridized carbon atoms, cyclic paraphenyleneacetylenes (CPPAs) (**Figure 1B**), reported by Kawase et al. (1996). The complexation between CPPA congeners and fullerenes were extensively studied (Kawase et al., 2003a,b, 2007; Miki et al., 2013). Although CPPA derivatives tend to form tight complexes with  $C_{60}$ , their unstable nature hindered further experimental studies. In contrast, the solely  $sp^2$ -hybridized CPP derivatives without acetylene linkers are sufficiently stable, and could similarly encapsulate fullerene molecules.

The initial example of the host-guest complex of this type was reported by Iwamoto et al. (2011). The CPP receptor with 10 phenylene units ([10]CPP) has an ideal diameter (1.38 nm) to accommodate  $C_{60}$  (0.71 nm) (**Figure 1C**), showing a binding constant  $K_a$  of  $2.79 \times 10^6 \text{ M}^{-1}$  in toluene determined by fluorescence quenching titration, which was two orders of magnitude higher than those obtained for [6]CPPA $\supset C_{60}$  (Kawase et al., 2003a). The variable-temperature NMR (VT-NMR) spectroscopy experiments showed that the rapid exchange between free [10]CPP and [10]CPP $\supset C_{60}$  took place at room temperature, and the energy barrier for the exchange was determined to be  $59 \text{ kJ mol}^{-1}$ . The crystal structure of [10]CPP $\supset C_{60}$  obtained by Jasti' group revealed the presence of convex-concave  $\pi$ - $\pi$  interactions (Xia et al., 2012). It is noteworthy that  $C_{60}$  can be selectively encapsulated by [10]CPP among the mixture of [8]-[12]CPPs, indicating that the cavity sizes of other CPPs were not appropriate for constructing a strong complex with  $C_{60}$ . Interestingly, it was found that  $C_{70}$ , which has an ellipsoidal shape with long axis of 0.796 nm and short axis of 0.712 nm, could also be encapsulated by [10]CPP in its “lying” orientation with its long axis perpendicular to [10]CPP plane (**Figure 1D**), but with reduced association constant  $K_a$  ( $8.4 \times 10^4 \text{ M}^{-1}$  in toluene) compared with [10]CPP $\supset C_{60}$  (Iwamoto et al., 2013). Nevertheless,  $C_{70}$  was adopted the “standing” orientations to be accommodated in the cavity of [11]CPP with its long axis within the [11]CPP plane (**Figure 1E**). Besides, [11]CPP deformed into an ellipsoidal shape to maximize the van der Waals interactions with the long axis of  $C_{70}$ . All these results indicated the size- and orientation selectivity for the CPP $\supset$ fullerene systems. Furthermore, a deep exploration by analyzing geometry structures through theoretical calculations revealed that  $C_{70}$  selectively adopts lying, standing, and half-lying orientations when combined with [10]CPP, [11]CPP, and [12]CPP, respectively (Yuan et al., 2015).

In 2014, Shinohara et al. demonstrated the high binding abilities of [11]CPP toward  $C_{82}$ -based endohedral metallofullerenes, including  $Gd@C_{2v}-C_{82}$ ,  $Tm@C_{2v}-C_{82}$ , and  $Lu_2@C_{2v}-C_{82}$ , which provided a facile non-chromatographic strategy for  $Gd@C_{82}$  extraction and enrichment from crude fullerene mixtures (Nakanishi et al., 2014). Later, another



example of C<sub>82</sub>-based endohedral metallofullerene peapod, [11]CPP $\supset$ La@C<sub>82</sub> was reported (Iwamoto et al., 2014). The solid structure of the complex was determined by X-ray crystallographic analysis, which showed that the La atom was

located near the periphery of [11]CPP rather than the tube axis with the dipole moment of La@C<sub>82</sub> nearly perpendicular to the CPP axis. These evidence demonstrated the different orientations of La@C<sub>82</sub> in CPP and CNT peapods, which suggests that the

orientation of La@C<sub>82</sub> in CNT was mainly determined by interactions among the adjacent ones. More importantly, due to the strong electron accepting properties of La@C<sub>82</sub>, partial charge transfer (CT) from [11]CPP to La@C<sub>82</sub> in the ground state was firstly observed by electrochemical experiments combined with UV/Vis-near-infrared (NIR) titration studies and density functional theory (DFT) calculations, but no fully ionized complex was formed.

The CPP-based fully ionized complex, Li<sup>+</sup>@C<sub>60</sub>⊂[10]CPP, was synthesized and characterized by Ueno et al. (2015) (Figure 1F). The ionic crystal structure was confirmed by X-ray crystallographic analysis. Unlike the empty C<sub>60</sub>, the cationic Li<sup>+</sup>@C<sub>60</sub> core drastically increased the electron accepting ability which could induce strong charge transfer from the electron donors. Cyclic voltammetry experiments revealed that Li<sup>+</sup>@C<sub>60</sub> was harder to be reduced when accommodated by [10]CPP than Li<sup>+</sup>@C<sub>60</sub> itself, which could be ascribed to the higher electron density around the Li<sup>+</sup>@C<sub>60</sub> cage through CPP to Li<sup>+</sup>@C<sub>60</sub> charge transfer interaction. The strong charge transfer interaction also caused the positive charge of the lithium cation delocalized to the outer CPP ring. The broadened absorption bands at around 350 nm and in the NIR region was also related to this interaction. Besides, photoluminescence (PL) lifetime of Li<sup>+</sup>@C<sub>60</sub>⊂[10]CPP (2.5 ns) is shorter than that of [10]CPP (4.3 ns) and C<sub>60</sub>⊂[10]CPP (4.3 ns), suggesting that the charge transfer (CT) interaction may occur.

Recently, Delius et al. reported the synthesis of a porphyrin-[10]CPP conjugate, in which [10]CPP moiety served as a supramolecular junction for charge transfer between a zinc porphyrin electron donor and fullerene electron acceptor (Xu et al., 2018b). Efficient photoinduced electron transfer was observed with a lifetime of charge separation state up to 0.5 μs in the 2:1 complex between [10]CPP and the fullerene dimer (Figure 1G). The intramolecular energy transfer between [10]CPP and porphyrin was also observed. Later, the same group achieved the synthesis of two [2]rotaxanes consisting of one [10]CPP moiety binding to a central fullerene with bis-adduct binding site and another two fullerene hexakis-adduct stoppers using a concave-convex π-π template strategy (Figure 1H) (Xu et al., 2018a). [10]CPP served as an effective supramolecular directing group with the central fullerene as an efficient convex template, steering the reaction exclusively toward two *trans* regioisomers in the final step. The mechanically interlocked structures of [2]rotaxanes were analyzed by variable-temperature NMR (VT-NMR) and mass spectrometry. Transient absorption spectra revealed the interesting consequences of the mechanical bond on charge transfer processes. A later work conducted by Wegner et al. used a dumbbell-shaped dimeric azafullerene [(C<sub>59</sub>N)<sub>2</sub>] as the ligand to combine with two [10]CPP rings, giving [10]CPP⊃(C<sub>59</sub>N)<sub>2</sub>⊂[10]CPP complex (Figure 1I) (Rio et al., 2018). Two stage binding constants were determined to be K<sub>a1</sub> = 8.4 × 10<sup>6</sup> M<sup>-1</sup> and K<sub>a2</sub> = 3.0 × 10<sup>6</sup> M<sup>-1</sup>, respectively, with weak interactions between the two CPP rings. Photoinduced partial charge transfer was observed from [10]CPP to (C<sub>59</sub>N)<sub>2</sub> by differential pulsed voltammetry experiments.

## SUPRAMOLECULAR COMPLEXES CONSISTING OF π-EXTENDED CARBON NANOHOOPS AND FULLERENES

As the π-π interaction operates *via* the surface-to-surface contacts in supramolecular chemistry, it becomes important for large aromatic moieties with increasing π-surface areas. Based on the rapid development of the synthesis strategies, carbon nanohoops with embedded polycyclic aromatic hydrocarbon (PAH) structures, such as hexa-*peri*-hexabenzocoronene (HBC) (Quernheim et al., 2015; Lu et al., 2016; Huang et al., 2019), were subsequently prepared. These π-extended macrocycles usually show larger binding constants with guest molecules due to their larger contact area compared with simple CPP hosts.

The [4]cyclo-2,11-*para*-hexa-*peri*-hexabenzocoronene ([4]CHBC) synthesized in our laboratory was found to selectively incorporate C<sub>70</sub> with a binding constant K<sub>a</sub> of 1.07 × 10<sup>6</sup> M<sup>-1</sup> in toluene (Figure 1J), but no evidence of complexation with C<sub>60</sub> guest was observed, which could be due to the “standing” or “lying” orientations of C<sub>70</sub> in the cavity of the carbon nanoring (Lu et al., 2017). Similarly, another HBC-containing three-dimensional capsule-like carbon nanocage, tripodal-[2]HBC also exhibited the preference of affinity toward C<sub>70</sub> (K<sub>a</sub> = 1.03 × 10<sup>5</sup> M<sup>-1</sup> in toluene) rather than C<sub>60</sub>, which was demonstrated by MS, NMR, and photophysical experiments (Figure 1K) (Cui et al., 2018). More recently, our group achieved the synthesis of two novel π-extended crown-like molecules (TCR and HCR) with embedded curved nanographene units, HBC or TBP (tribenzo[*fj,ij,rst*]pentaphene) (Huang et al., 2019). These two species were found to show high binding affinity toward guest molecule C<sub>60</sub> with the association constants K<sub>a</sub> of 3.34 × 10<sup>6</sup> M<sup>-1</sup> for TCR⊃C<sub>60</sub>, and 2.33 × 10<sup>7</sup> M<sup>-1</sup> for HCR⊃C<sub>60</sub>, respectively (Figure 1L). The gradual increase in binding constants from [10]CPP⊃C<sub>60</sub> (K<sub>a</sub> = 2.79 × 10<sup>6</sup> M<sup>-1</sup>) (Iwamoto et al., 2011) to TCR⊃C<sub>60</sub>, then HCR⊃C<sub>60</sub>, should be ascribed to the increasing π-surfaces that could provide stronger π-π interactions between the hosts and C<sub>60</sub>. Besides, photocurrents were generated when using these molecular crowns or their supramolecular complexes on FTO electrodes under visible light irradiation. Time-resolved spectroscopic measurements suggested fast photoinduced electron transfer in the supramolecular heterojunctions.

The recently reported shape-persistent tubular carbon nanorings demonstrated the binding ability with fullerenes. Five structural isomers of [4]cyclo-2,8-chrysenylene ([4]CC) (Hitosugi et al., 2011), which were named as (P)-(12,8)-, (P)-(11,9)-, (10,10)<sub>AABB</sub>-, (10,10)<sub>ABAB</sub>-, and (+)-(16,0)-[4]CC, can form 1:1 complex with C<sub>60</sub> in solution (Isobe et al., 2013). The highest binding constant among similar complexes was recorded for (P)-(12,8)-[4]CC⊃C<sub>60</sub> (Figure 1M) in *o*-DCB with K<sub>a</sub> = 4.0 × 10<sup>9</sup> M<sup>-1</sup>, while isomers of (P)-(11,9)-, (10,10)<sub>AABB</sub>-, and (10,10)<sub>ABAB</sub>-[4]CC also showed the binding constant above 10<sup>9</sup> M<sup>-1</sup>. The lowest K<sub>a</sub> was recorded for (+)-(16,0)-[4]CC⊃C<sub>60</sub> (2.0 × 10<sup>4</sup> M<sup>-1</sup> in *o*-DCB), but was still higher than that for [10]CPP⊃C<sub>60</sub> (6.0 × 10<sup>3</sup> M<sup>-1</sup> in *o*-DCB) (Iwamoto et al., 2011). These results clearly show that the belt-persistence in tubular



structures also plays a crucial role in binding with fullerenes besides the cavity size. Therefore, a molecular rolling bearing with C<sub>60</sub> in the [4]CC bearing was constructed as the bearing can hold the fullerene molecule tightly to prevent its run-out motion. The C<sub>60</sub> molecule did not exchange and took rapid relative rolling motion on the NMR timescale within the bearing from the <sup>1</sup>H NMR analysis of (*P*)-(12,8)-[4]CC⊃C<sub>60</sub>. The crystal structures of this molecular bearing was further analyzed by X-ray diffraction, demonstrating the presence of smoothly curved surface that allows the dynamic motion of C<sub>60</sub> even in the solid state (Sato et al., 2014). Theoretical studies by density functional theory (DFT) indicates that the calculated association energies were quite method-dependent, and the energy barriers for the rolling motions within the bearing were as low as 2–3 kcal mol<sup>-1</sup> with two distinct rolling motions (precession and spin) (Isobe et al., 2015).

Besides C<sub>60</sub> guest, another twelve fullerenes, including C<sub>70</sub>, nine exohedral functionalized fullerenes, and two endohedral fullerenes, were selected and assessed as rolling journals in the belt-persistent [4]CC bearing (Hitosugi et al., 2013). [4]CC tolerated the modified fullerenes but with reduced binding constant. C<sub>70</sub> was found to be superior guest not only for the high binding constant ( $K_a = 5.0 \times 10^9 \text{ M}^{-1}$  in DCB), but also for its tolerance of introduction of bulky shaft without obvious decrease in binding constant. A lengthened version of (P)-(12,8)-[4]cyclo-2,8-anthanthrenylene ((P)-(12,8)-[4]CA) can also bind with C<sub>60</sub> and C<sub>70</sub> (**Figure 1N**) with enhanced association enthalpy as the increase of the C-C contact area compared with the shorter congener (P)-(12,8)-[4]CC (Matsuno et al., 2013, 2015).

The electronic properties of the molecular bearings were then systematically studied. The bearing systems can generate charge-separated species under light irradiation. (*P*)-(12,8)-[4]CC $\supset$ C<sub>60</sub> system exhibits a rapid back electron transfer to give triplet C<sub>60</sub> journal after the formation of triplet charge-separated species *via* photoinduced electron-transfer (Hitosugi et al., 2014). The lengthened version of [4]CA $\supset$ C<sub>60</sub> could generate a triplet excited state at the outer bearing, whereas the endohedral fullerene Li<sup>+</sup>@C<sub>60</sub> enabled the back electron transfer processes without triplet excited species (Hitosugi et al., 2015).

Although there existed tight association between (P)-(12,8)-[4]CC and C<sub>60</sub>, the solid-state dynamic rotations of C<sub>60</sub> still enabled reorientation by a small energy barrier (+2 kcal mol<sup>-1</sup>). The solid-state rotational motions reached a non-Brownian, inertial regime at 335 K (Matsuno et al., 2018b).

Unlike the relatively rigid conformation of the arylene panels in [4]CC, [7]cyclo-amphi-naphthylene ([7]CaNAP) was rather flexible with its panels rotate rapidly at ambient temperature (Sun et al., 2016). However, this rotation did not significantly affect its binding ability for  $C_{70}$  with the  $K_a$  in the range of  $10^7$ - $10^9$   $M^{-1}$  (depending on the solvents) (**Figure 1O**) (Sun et al., 2019). More importantly, the structure of [7]CaNAP deformed during the rotation to track the orientation changes of the ellipsoidal  $C_{70}$ .

By using dumbbell-shaped C<sub>60</sub> dimer (C<sub>120</sub>) as the ligand with two binding sites, two-wheeled composites can be assembled with the shape-persistent macrocycles as the receptors (Matsuno et al., 2016, 2017). The thermodynamics of the 2:1 complex

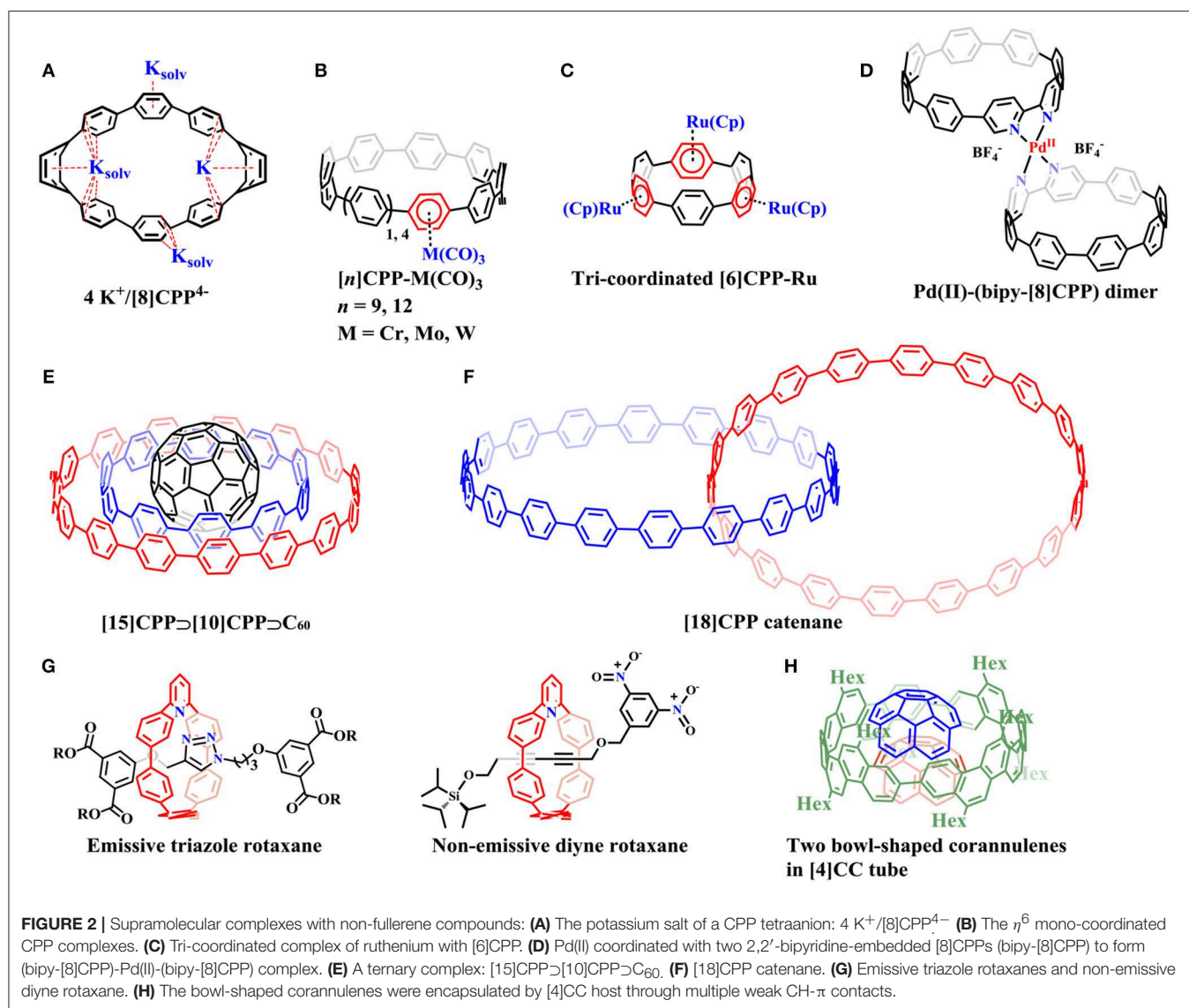
revealed the two-stage association constants, for example  $K_{a1}$  of  $7.3 \times 10^{11} \text{ M}^{-1}$  for the formation of the 1:1 complex  $[(P)-(12,8)-[4]CC \supset C_{120}]$ , and  $K_{a2}$  of  $9.7 \times 10^7 \text{ M}^{-1}$  for the 2:1 complex  $[(P)-(12,8)-[4]CC \supset C_{120} \subset (P)-(12,8)-[4]CC]$ . There was no self-assembly of the two  $[4]CC$  hosts without  $C_{120}$ . The ligand-induced self-sorting phenomena was observed from the  $[4]CC$  family  $\supset C_{120}$ . A moderate level of self-sorting was obtained when mixing a racemic mixture ( $[4]CC$  ( $(P)-(12,8)-[4]CC$  ( $(P)-D_4$ ) and ( $M)-(12,8)-[4]CC$  ( $(M)-D_4$ )) and  $C_{120}$  with equivalent molar ratio: yielding 70% amount of the racemate complexes  $[(P)-D_4 \supset C_{120} \subset (P)-D_4 + (M)-D_4 \supset C_{120} \subset (M)-D_4]$ , and 30% amount of the meso-form  $[(P)-D_4 \supset C_{120} \subset (M)-D_4]$ . A complete self-sorting was obtained when two diastereomers of  $[4]CC$  ( $[(P)-D_4]$  and  $(10,10)_{ABAB}-[4]CC$  [ $D_{2d}$ ]) were applied: yielding 50% amount of  $(P)-D_4 \supset C_{120} \subset (P)-D_4$ , 50% amount of  $D_{2d} \supset C_{120} \subset D_{2d}$ , and no  $(P)-D_4 \supset C_{120} \subset D_{2d}$  was detected (**Figure 1P**). This shape recognition can be explained by the repulsive van der Waals interactions between aliphatic side chains caused by the H–H contacts at the interfaces of the receptors as revealed by the crystal structures.

## SUPRAMOLECULAR COMPLEXES WITH NON-FULLERENE COMPOUNDS

When two aromatic moieties stack in a face-to-face fashion, the  $\pi$ - $\pi$  interaction could hold the two species together, such as the case of CPP analogs with fullerenes. Besides, other non-covalent interactions, such as CH- $\pi$ , metal- $\pi$  interactions also play important roles in various supramolecular systems. The CH- $\pi$  interaction, which is a kind of atom-to-surface hydrogen bond and relatively weak, could also assemble host-guest complex. On the other hand, the metal- $\pi$  coordination usually could strongly stabilize the associated architecture.

In 2013, Petrukhina et al. reported the potassium salt of a CPP tetraanion ( $4\text{ K}^+/[8]\text{CPP}^{4-}$ ) by direct reduction of  $[8]\text{CPP}$  with potassium metal (**Figure 2A**) (Zabula et al., 2013). The X-ray diffraction analysis revealed that  $[8]\text{CPP}^{4-}$  functions as a multisite ligand with its *endo*- and *exo*- surfaces engaged in coordination with the potassium. Similarly,  $[6]\text{CPP}$  were also demonstrated to be reduced by alkali-metal to its mono- and di-anions,  $[6]\text{CPP}^{1-}$  and  $[6]\text{CPP}^{2-}$  (Spisak et al., 2018). Itami et al. synthesized  $\eta^6$  mono-coordinated CPP complexes  $[n]\text{CPP-M}(\text{CO})_3$  where  $n = 9, 12$  and  $\text{M} = \text{Cr}, \text{Mo}, \text{W}$  (**Figure 2B**) (Kubota et al., 2015). The crystal structure of  $[9]\text{CPP-Cr}(\text{CO})_3$  showed that chromium coordinated on the convex surface of  $[9]\text{CPP}$ . Later, Yamago's group succeeded in the preparation of mono-, di-, and tri-coordinated complexes of ruthenium with  $[n]\text{CPP}$  ( $n = 5$  and  $6$ ) (Kayahara et al., 2016). Ru selectively coordinated to alternate phenylene units in multi-coordinated complexes (**Figure 2C**). Single-crystal analysis indicated that Ru also coordinated on the convex surface of CPPs. More recently, Jasti illustrated a general strategy for building up nano hoops that could easily coordinate to transition metals (Van Raden et al., 2017). 2,2'-bipyridine-embedded  $[8]\text{CPP}$  (bipy- $[8]\text{CPP}$ ) synthesized in this work





can readily coordinate to Pd(II) or Ru(II) metal centers, forming (bipy-[8]CPP)-Pd(II)-(bipy-[8]CPP) (**Figure 2D**) or Ru(II)-(bipy-[8]CPP) complexes, respectively.

Besides the role as supramolecular hosts, CPP molecules can also serve as guests to be included in larger nanohoops with the “Russian doll” fashion. The strongest binding was predicted when the host and guest differed by five phenyl rings through theoretical calculations (Fomine et al., 2012; Bachrach and Zayat, 2016). Yamago et al. demonstrated these predictions by experimental studies:  $[n]\text{CPPs}$  ( $n = 5, 6, 7, 8$ , and  $10$ ) did selectively interact with  $[n+5]\text{CPPs}$ , forming  $[n+5]\text{CPP} \supset [n]\text{CPP}$  complexes (Hashimoto et al., 2017). A ternary complex,  $[15]\text{CPP} \supset [10]\text{CPP} \supset \text{C}_{60}$ , could also be assembled (**Figure 2E**).

By analyzing the ions in the gas phase of the complex mixture from CPP synthesis through matrix assisted laser desorption ionization (MALDI) together with ion-mobility

mass spectrometry (IMMS), Müllen’s group provided evidence for the existence of possible catenanes composed of CPPs, such as  $[12]\text{CPP} + [24]\text{CPP}$ ,  $2 \times [18]\text{CPP}$  (**Figure 2F**), or even a trefoil knot (Zhang et al., 2017b). Most recently, Itami et al. reported the synthesis of all-benzene catenanes and trefoil knot through silicon-based template method which adjoined two neighboring CPP fragments in a crossing pattern followed by removal of the silicon tether after macrocyclization (Segawa et al., 2019). Interestingly, the trefoil knot shows only a single proton resonance in  $^1\text{H}$ -NMR spectrum even at  $-95^\circ\text{C}$ , indicating its ultrafast motion on the NMR time scale. The [2]heterocatenane, in which [12]CPP and [9]CPP are mechanically interlocked shows energy transfer from [12]CPP to [9]CPP via the mechanical bond under light irradiation. Cong et al. reported the synthesis of a catenane consisting of two interlocked phenanthroline-containing nanohoops by copper(I)-templated method (Fan et al., 2018). The solid state structure

shows a Möbius topology stabilized by non-covalent interactions. A 2,6-pyridyl embedded nanohoops were recently synthesized for the preparation of nanohoop-based rotaxanes through active metal template reactions (**Figure 2G**; Van Raden et al., 2019). The triazole-embedded [2]rotaxanes showed dramatic changes in fluorescence emission (turn-off) when Pd(II) salt was added, suggesting its possible applications in ion sensing. Inspired by this study, another non-emissive [2]rotaxane was devised and synthesized, which has a fluorescence-quenching 3,5-dinitrobenzyl stopper and a fluoride-cleavable triisopropylsilyl (TIPS) stopper. Upon the addition of tetra-*n*-butylammonium fluoride (TBAF), 123-fold emission was recovered as the nanohoop fluorophore was released, indicating that the nanohoop rotaxanes could effectively serve as turn-on fluorescence sensors.

Itami et al. described the assembly of iodine within [*n*]CPPs (*n* = 9, 10, and 12) (Ozaki et al., 2017). Upon electric stimuli, [10]CPP-I turned out to emit white light, caused by the formation of polyiodide chains inside the [10]CPP cavity through charge transfer between [10]CPP tubes and encapsulated iodine chains.

Gaeta reported the 1,4-dimethoxy modified [8]CPP which exhibits binding ability toward pyridinium cations (Della Sala et al., 2017). Density functional theory (DFT) calculations indicated that the CH... $\pi$  and N<sup>+</sup>... $\pi$ <sup>DMB</sup> (DMB = 1,4-dimethoxybenzene) interactions between the host and pyridinium guest played a crucial role in this supramolecular system. Another multi-(1,4-dimethoxy) modified [9]CPP synthesized by our group showed only weak supramolecular interactions for cationic molecules (Lu et al., 2018).

A novel type of host-guest complex assembled solely by CH- $\pi$  hydrogen bonds rather than  $\pi$ - $\pi$  interactions was devised by the Isobe group (Matsuno et al., 2018a). A bowl-shaped corannulene can be encapsulated by a [4]CC host through multiple weak CH- $\pi$  contacts to form a 1:1 complex in solution, driven by a large association enthalpy. The 1:2 host-guest combination was unveiled in the crystalline solid state (**Figure 2H**). Despite the multiple weak hydrogen bonds, the guest was still allowed dynamic rotational motions in the host. Solid state analysis revealed a single-axis rotation of the bowl in the tube.

## REFERENCES

- Bachrach, S. M., and Zayat, Z. C. (2016). "Planetary orbit" systems composed of cycloparaphenylenes. *J. Org. Chem.* 81, 4559–4565. doi: 10.1021/acs.joc.6b00339
- Cui, S., Zhuang, G., Lu, D., Huang, Q., Jia, H., Wang, Y., et al. (2018). A three-dimensional capsule-like carbon nanocage as a segment model of capped zigzag [12,0] carbon nanotubes: synthesis, characterization, and complexation with C<sub>70</sub>. *Angew. Chem. Int. Ed.* 57, 9330–9335. doi: 10.1002/anie.201804031
- Darzi, E. R., Hirst, E. S., Weber, C. D., Zakharov, L. N., Lonergan, M. C., and Jasti, R. (2015). Synthesis, properties, and design principles of donor-acceptor nanohoops. *ACS Cent. Sci.* 1, 335–342. doi: 10.1021/acscentsci.5b00269

## SUMMARY AND OUTLOOK

In this featured article, we overviewed recent progress on supramolecular properties of CPPs and their analogs. Various types of new carbon nanohoops were prepared by transition metal-catalyzed coupling reactions. These macrocycles usually possess well-defined cavities with rigid conformation and fixed diameters, which makes them good supramolecular hosts for incorporating a wide range of compounds, such as spherical fullerenes through  $\pi$ - $\pi$ , metal- $\pi$ , and/or CH- $\pi$  interactions. These non-covalent interactions enabled efficient molecular recognitions and host-guest energy transfer. Although the synthesis of new carbon nanohoops and related supramolecular complexes has been growing very fast during the past decade, the applications of these carbon-rich architectures in some fields, such as, organic electronic devices, molecular sensing, and molecular machines, is still far from satisfaction. For further advancement, research efforts should be devoted to explore robust synthetic strategies which are essential for the diversification of carbon nanohoop family. Interdisciplinary studies with cooperative material sciences, analytical, biological, physical, and theoretical chemistry, will dramatically expand the understanding and application of the macrocycles and their supramolecular complexes. It is reasonable to expect that these carbon-rich structures will attract further research interests, and lead to the preparation of unique and unprecedented molecular tools and materials in the future.

## AUTHOR CONTRIBUTIONS

PD supervised the project. DL and PD mainly wrote the paper. QH, SW, JW, and PH co-wrote the paper. All authors discussed the results and commented on the manuscript.

## FUNDING

We are grateful for the financial support from the National Natural Science Foundation of China (21801004, 21971229), the National Key Research and Development Program of China (2017YFA0402800), University Natural Science Research Project of Anhui Province (KJ2018A0179), and Grants for Scientific Research of BSKY (XJ201504) from Anhui Medical University.

- Della Sala, P., Talotta, C., Caruso, T., De Rosa, M., Soriente, A., Neri, P., et al. (2017). Tuning cycloparaphenylene host properties by chemical modification. *J. Org. Chem.* 82, 9885–9889. doi: 10.1021/acs.joc.7b01588
- Dong, R., Zhou, Y., Huang, X., Zhu, X., Lu, Y., and Shen, J. (2015). Functional supramolecular polymers for biomedical applications. *Adv. Mater.* 27, 498–526. doi: 10.1002/adma.201402975
- Fan, Y. Y., Chen, D., Huang, Z. A., Zhu, J., Tung, C. H., Wu, L. Z., et al. (2018). An isolable catenane consisting of two Möbius conjugated nanohoops. *Nat. Commun.* 9:3037. doi: 10.1038/s41467-018-05498-6
- Fomine, S., Zolotukhin, M. G., and Guadarrama, P. (2012). "Russian doll" complexes of [*n*]cycloparaphenylenes: a theoretical study. *J. Mol. Model.* 18, 4025–4032. doi: 10.1007/s00894-012-1402-7

- Hashimoto, S., Iwamoto, T., Kurachi, D., Kayahara, E., and Yamago, S. (2017). Shortest double-walled carbon nanotubes composed of cycloparaphenylenes. *Chem Plus Chem* 82, 1015–1020. doi: 10.1002/cplu.201700097
- Hitosugi, S., Iizuka, R., Yamasaki, T., Zhang, R., Murata, Y., and Isobe, H. (2013). Assessment of fullerene derivatives as rolling journals in a finite carbon nanotube bearing. *Org. Lett.* 15, 3199–3201. doi: 10.1021/ol400982r
- Hitosugi, S., Nakanishi, W., Yamasaki, T., and Isobe, H. (2011). Bottom-up synthesis of finite models of helical (n,m)-single-wall carbon nanotubes. *Nat. Commun.* 2, 492. doi: 10.1038/ncomms1505
- Hitosugi, S., Ohkubo, K., Iizuka, R., Kawashima, Y., Nakamura, K., Sato, S., et al. (2014). Photoinduced electron transfer in a dynamic supramolecular system with curved  $\pi$ -structures. *Org. Lett.* 16, 3352–3355. doi: 10.1021/ol501381x
- Hitosugi, S., Ohkubo, K., Kawashima, Y., Matsuno, T., Kamata, S., Nakamura, K., et al. (2015). Modulation of energy conversion processes in carbonaceous molecular bearings. *Chem. Asian J.* 10, 2404–2410. doi: 10.1002/asia.201500673
- Huang, Q., Zhuang, G., Jia, H., Qian, M., Cui, S., Yang, S., et al. (2019). Photoconductive curved-nanographene/fullerene supramolecular heterojunctions. *Angew. Chem. Int. Ed.* 58, 6244–6249. doi: 10.1002/anie.201900084
- Huang, Z. A., Chen, C., Yang, X. D., Fan, X. B., Zhou, W., Tung, C. H., et al. (2016). Synthesis of oligoparaphenylene-derived nanostructures employing an anthracene photodimerization-cycloreversion strategy. *J. Am. Chem. Soc.* 138, 11144–11147. doi: 10.1021/jacs.6b07673
- Isobe, H., Hitosugi, S., Yamasaki, T., and Iizuka, R. (2013). Molecular bearings of finite carbon nanotubes and fullerenes in ensemble rolling motion. *Chem. Sci.* 4, 1293–1297. doi: 10.1039/c3sc22181d
- Isobe, H., Nakamura, K., Hitosugi, S., Sato, S., Tokoyama, H., Yamakado, H., et al. (2015). Theoretical studies on a carbonaceous molecular bearing: association thermodynamics and dual-mode rolling dynamics. *Chem. Sci.* 6, 2746–2753. doi: 10.1039/C5SC00335K
- Iwamoto, T., Slanina, Z., Mizorogi, N., Guo, J., Akasaka, T., Nagase, S., et al. (2014). Partial charge transfer in the shortest possible metallofullerene peapod, La@C<sub>82</sub>@[1]cycloparaphenylene. *Chem. Eur. J.* 20, 14403–14409. doi: 10.1002/chem.201403879
- Iwamoto, T., Watanabe, Y., Sadahiro, T., Haino, T., and Yamago, S. (2011). Size-selective encapsulation of C<sub>60</sub> by [10]cycloparaphenylene: formation of the shortest fullerene-peapod. *Angew. Chem. Int. Ed.* 50, 8342–8344. doi: 10.1002/anie.201102302
- Iwamoto, T., Watanabe, Y., Takaya, H., Haino, T., Yasuda, N., and Yamago, S. (2013). Size- and orientation-selective encapsulation of C<sub>70</sub> by cycloparaphenylenes. *Chem. Eur. J.* 19, 14061–14068. doi: 10.1002/chem.201302694
- Jasti, R., and Bertozzi, C. R. (2010). Progress and challenges for the bottom-up synthesis of carbon nanotubes with discrete chirality. *Chem. Phys. Lett.* 494, 1–7. doi: 10.1016/j.cplett.2010.04.067
- Jasti, R., Bhattacharjee, J., Neaton, J. B., and Bertozzi, C. R. (2008). Synthesis, characterization, and theory of [9]-, [12]-, and [18]cycloparaphenylene: carbon nanohoop structures. *J. Am. Chem. Soc.* 130, 17646–17647. doi: 10.1021/ja807126u
- Kawase, T., Darabi, H. R., and Oda, M. (1996). Cyclic [6]- and [8]Paraphenylacetylenes. *Angew. Chem. Int. Ed.* 35, 2664–2666. doi: 10.1002/anie.199626641
- Kawase, T., Nishiyama, Y., Nakamura, T., Ebi, T., Matsumoto, K., Kurata, H., et al. (2007). Cyclic [5]paraphenyleneacetylene: synthesis, properties, and formation of a ring-in-ring complex showing a considerably large association constant and entropy effect. *Angew. Chem. Int. Ed.* 46, 1086–1088. doi: 10.1002/anie.200603707
- Kawase, T., Tanaka, K., Fujiwara, N., Darabi, H. R., and Oda, M. (2003a). Complexation of a carbon nanoring with fullerenes. *Angew. Chem. Int. Ed.* 42, 1624–1628. doi: 10.1002/anie.200250728
- Kawase, T., Tanaka, K., Seirai, Y., Shiono, N., and Oda, M. (2003b). Complexation of carbon nanorings with fullerenes: supramolecular dynamics and structural tuning for a fullerene sensor. *Angew. Chem. Int. Ed.* 42, 5597–5600. doi: 10.1002/anie.200352033
- Kayahara, E., Patel, V. K., Mercier, A., Kundig, E. P., and Yamago, S. (2016). Regioselective synthesis and characterization of multinuclear convex-bound ruthenium-[n]cycloparaphenylene (n = 5 and 6) complexes. *Angew. Chem. Int. Ed.* 55, 302–306. doi: 10.1002/anie.201508003
- Kubota, N., Segawa, Y., and Itami, K. (2015).  $\eta^6$ -Cycloparaphenylene transition metal complexes: synthesis, structure, photophysical properties, and application to the selective monofunctionalization of cycloparaphenylenes. *J. Am. Chem. Soc.* 137, 1356–1361. doi: 10.1021/ja512271p
- Lehn, J. M. (1985). Supramolecular chemistry: receptors, catalysts, and carriers. *Science* 227, 849–856. doi: 10.1126/science.227.4689.849
- Lehn, J. M. (1988). Supramolecular chemistry—scope and perspectives molecules, supermolecules, and molecular devices. *Angew. Chem. Int. Ed.* 27, 89–112. doi: 10.1002/anie.198800891
- Lu, D., Wu, H., Dai, Y., Shi, H., Shao, X., Yang, S., et al. (2016). A cycloparaphenylene nanoring with graphenic hexabenzocoronene sidewalls. *Chem. Commun.* 52, 7164–7167. doi: 10.1039/C6CC03002E
- Lu, D., Zhuang, G., Wu, H., Wang, S., Yang, S., and Du, P. W. (2017). A large  $\pi$ -extended carbon nanoring based on nanographene units: bottom-up synthesis, photophysical properties, and selective complexation with fullerene C<sub>70</sub>. *Angew. Chem. Int. Ed.* 56, 158–162. doi: 10.1002/ange.201608963
- Lu, D. P., Zhuang, G. L., Jia, H. X., Wang, J. Y., Huang, Q., Cui, S. S., et al. (2018). A novel symmetrically multifunctionalized dodecamethoxy-cycloparaphenylene: synthesis, photophysical, and supramolecular properties. *Org. Chem. Front.* 5, 1446–1451. doi: 10.1039/C8QO00033F
- Matsuno, T., Fujita, M., Fukunaga, K., Sato, S., and Isobe, H. (2018a). Concyclic CH- $\pi$  arrays for single-axis rotations of a bowl in a tube. *Nat. Commun.* 9:3779. doi: 10.1038/s41467-018-06270-6
- Matsuno, T., Kamata, S., Hitosugi, S., and Isobe, H. (2013). Bottom-up synthesis and structures of  $\pi$ -lengthened tubular macrocycles. *Chem. Sci.* 4:3179. doi: 10.1039/c3sc50645b
- Matsuno, T., Kamata, S., Sato, S., Yokoyama, A., Sarkar, P., and Isobe, H. (2017). Assembly, thermodynamics, and structure of a two-wheeled composite of a dumbbell-shaped molecule and cylindrical molecules with different edges. *Angew. Chem. Int. Ed.* 56, 15020–15024. doi: 10.1002/anie.201709442
- Matsuno, T., Nakai, Y., Sato, S., Maniwa, Y., and Isobe, H. (2018b). Ratchet-free solid-state inertial rotation of a guest ball in a tight tubular host. *Nat. Commun.* 9:1907. doi: 10.1038/s41467-018-04325-2
- Matsuno, T., Sato, S., Iizuka, R., and Isobe, H. (2015). Molecular recognition in curved  $\pi$ -systems: effects of  $\pi$ -lengthening of tubular molecules on thermodynamics and structures. *Chem. Sci.* 6, 909–916. doi: 10.1039/C4SC02812K
- Matsuno, T., Sato, S., Yokoyama, A., Kamata, S., and Isobe, H. (2016). Self-sorting of two hydrocarbon receptors with one carbonaceous ligand. *Angew. Chem. Int. Ed.* 55, 15339–15343. doi: 10.1002/anie.201609444
- Miki, K., Matsushita, T., Inoue, Y., Senda, Y., Kowada, T., and Ohe, K. (2013). Electron-rich carbon nanorings as macrocyclic hosts for fullerenes. *Chem. Commun.* 49, 9092–9094. doi: 10.1039/c3cc42561d
- Nakanishi, Y., Omachi, H., Matsuura, S., Miyata, Y., Kitaura, R., Segawa, Y., et al. (2014). Size-selective complexation and extraction of endohedral metallofullerenes with cycloparaphenylene. *Angew. Chem. Int. Ed.* 53, 3102–3106. doi: 10.1002/anie.201311268
- Ogoshi, T., Kanai, S., Fujinami, S., Yamagishi, T. A., and Nakamoto, Y. (2008). *para*-Bridged symmetrical pillar[5]arenes: their Lewis acid catalyzed synthesis and host-guest property. *J. Am. Chem. Soc.* 130, 5022–5023. doi: 10.1021/ja711260m
- Ozaki, N., Sakamoto, H., Nishihara, T., Fujimori, T., Hijikata, Y., Kimura, R., et al. (2017). Electrically activated conductivity and white light emission of a hydrocarbon nanoring-iodine assembly. *Angew. Chem. Int. Ed.* 56, 11196–11202. doi: 10.1002/anie.201703648
- Povie, G., Segawa, Y., Nishihara, T., Miyauchi, Y., and Itami, K. (2017). Synthesis of a carbon nanobelt. *Science* 356, 172–175. doi: 10.1126/science.aam8158
- Povie, G., Segawa, Y., Nishihara, T., Miyauchi, Y., and Itami, K. (2018). Synthesis and size-dependent properties of [12], [16], and [24]Carbon nanobelts. *J. Am. Chem. Soc.* 140, 10054–10059. doi: 10.1021/jacs.8b06842
- Quernheim, M., Golling, F. E., Zhang, W., Wagner, M., Räder, H. J., Nishiuchi, T., et al. (2015). The precise synthesis of phenylene-extended cyclic hexa-peri-hexabenzocoronenes from polyarylated [n]cycloparaphenylenes by the scholl reaction. *Angew. Chem. Int. Ed.* 54, 10341–10346. doi: 10.1002/anie.201500392
- Rio, J., Beeck, S., Rotas, G., Ahles, S., Jacquemin, D., Tagmatarchis, N., et al. (2018). Electronic communication between two [10]cycloparaphenylenes and bis(azafullerene) (C<sub>59</sub>N)<sub>2</sub> induced by cooperative complexation. *Angew. Chem. Int. Ed.* 57, 6930–6934. doi: 10.1002/anie.201713197

- Sato, S., Yamasaki, T., and Isobe, H. (2014). Solid-state structures of peapod bearings composed of finite single-wall carbon nanotube and fullerene molecules. *Proc. Natl. Acad. Sci. U.S.A.* 111, 8374–8379. doi: 10.1073/pnas.1406518111
- Segawa, Y., Fukazawa, A., Matsuura, S., Omachi, H., Yamaguchi, S., Irle, S., et al. (2012). Combined experimental and theoretical studies on the photophysical properties of cycloparaphenylenes. *Org. Biomol. Chem.* 10, 5979–5984. doi: 10.1039/c2ob25199j
- Segawa, Y., Kuwayama, M., Hijikata, Y., Fushimi, M., Nishihara, T., Pirillo, J., et al. (2019). Topological molecular nanocarbons: All-benzene catenane and trefoil knot. *Science* 365, 272–276. doi: 10.1126/science.aav5021
- Segawa, Y., Yagi, A., Matsui, K., and Itami, K. (2016). Design and synthesis of carbon nanotube segments. *Angew. Chem. Int. Ed.* 55, 5136–5158. doi: 10.1002/anie.201508384
- Spisak, S. N., Wei, Z., Darzi, E., Jasti, R., and Petrukhina, M. A. (2018). Highly strained [6]cycloparaphenylene: crystallization of an unsolvated polymorph and the first mono- and dianions. *Chem. Commun.* 54, 7818–7821. doi: 10.1039/C8CC03693D
- Sun, Z., Mio, T., Okada, T., Matsuno, T., Sato, S., Kono, H., et al. (2019). Unbiased rotational motions of an ellipsoidal guest in a tight yet pliable host. *Angew. Chem. Int. Ed.* 58, 2040–2044. doi: 10.1002/anie.201812771
- Sun, Z., Suenaga, T., Sarkar, P., Sato, S., Kotani, M., and Isobe, H. (2016). Stereoisomerism, crystal structures, and dynamics of belt-shaped cyclonaphthylenes. *Proc. Natl. Acad. Sci. U.S.A.* 113, 8109–8114. doi: 10.1073/pnas.1606530113
- Toyota, S., and Tsurumaki, E. (2019). Exploration of nano-saturns: a spectacular sphere-ring supramolecular system. *Chem. Eur. J.* 25, 6878–6890. doi: 10.1002/chem.201900039
- Ueno, H., Nishihara, T., Segawa, Y., and Itami, K. (2015). Cycloparaphenylene-based ionic donor-acceptor supramolecule: isolation and characterization of  $\text{Li}^+@C_{60}C[10]CPP$ . *Angew. Chem. Int. Ed.* 54, 3707–3711. doi: 10.1002/anie.201500544
- Van Raden, J. M., White, B. M., Zakharov, L. N., and Jasti, R. (2017). 2,2'-Bipyridyl-embedded cycloparaphenylenes as a general strategy to investigate nanohoop-based coordination complexes. *J. Am. Chem. Soc.* 139, 2936–2939. doi: 10.1021/jacs.7b00359
- Van Raden, J. M., White, B. M., Zakharov, L. N., and Jasti, R. (2019). Nanohoop rotaxanes from active metal template syntheses and their potential in sensing applications. *Angew. Chem. Int. Ed.* 58, 7341–7345. doi: 10.1002/anie.201901984
- Wu, D., Cheng, W., Ban, X. T., and Xia, J. L. (2018). Cycloparaphenylenes (CPPs): an overview of synthesis, properties, and potential applications. *Asian, J. Org. Chem.* 7, 2161–2181. doi: 10.1002/ajoc.201800397
- Xia, J., Bacon, J. W., and Jasti, R. (2012). Gram-scale synthesis and crystal structures of [8]- and [10]CPP, and the solid-state structure of  $C_{60}@[10]CPP$ . *Chem. Sci.* 3, 3018–3021. doi: 10.1039/c2sc20719b
- Xu, Y., and Delius, M. (2019). The supramolecular chemistry of strained carbon nanohoops. *Angew. Chem. Int. Ed.* doi: 10.1002/anie.201906069. [Epub ahead of print].
- Xu, Y., Kaur, R., Wang, B., Minameyer, M. B., Gsanger, S., Meyer, B., et al. (2018a). Concave-convex  $\pi$ - $\pi$  template approach enables the synthesis of [10]cycloparaphenylene-fullerene [2]rotaxanes. *J. Am. Chem. Soc.* 140, 13413–13420. doi: 10.1021/jacs.8b08244
- Xu, Y., Wang, B., Kaur, R., Minameyer, M. B., Bothe, M., Drewello, T., et al. (2018b). A supramolecular [10]CPP junction enables efficient electron transfer in modular porphyrin-[10]CPP-fullerene complexes. *Angew. Chem. Int. Ed.* 57, 11549–11553. doi: 10.1002/anie.201802443
- Yan, X., Wang, F., Zheng, B., and Huang, F. (2012). Stimuli-responsive supramolecular polymeric materials. *Chem. Soc. Rev.* 41, 6042–6065. doi: 10.1039/c2cs35091b
- Yang, L., Tan, X., Wang, Z., and Zhang, X. (2015). Supramolecular polymers: historical development, preparation, characterization, and functions. *Chem. Rev.* 115, 7196–7239. doi: 10.1021/cr500633b
- Yuan, K., Guo, Y. J., and Zhao, X. (2015). Nature of noncovalent interactions in the [n]cycloparaphenylene $\text{C}_{70}$  ( $n = 10, 11$ , and 12) host-guest complexes: a theoretical insight into the shortest  $C_{70}$ -carbon nanotube peapod. *J. Phys. Chem. C* 119, 5168–5179. doi: 10.1021/jp5129657
- Zabula, A. V., Filatov, A. S., Xia, J., Jasti, R., and Petrukhina, M. A. (2013). Tightening of the nanobelt upon multielectron reduction. *Angew. Chem. Int. Ed.* 52, 5033–5036. doi: 10.1002/anie.201301226
- Zhang, D., Martinez, A., and Dutasta, J. P. (2017a). Emergence of hemicryptophanes: from synthesis to applications for recognition, molecular machines, and supramolecular catalysis. *Chem. Rev.* 117, 4900–4942. doi: 10.1021/acs.chemrev.6b00847
- Zhang, W., Abdulkarim, A., Golling, F. E., Räder, H. J., and Müllen, K. (2017b). Cycloparaphenylenes and their catenanes: complex macrocycles unveiled by ion mobility mass spectrometry. *Angew. Chem. Int. Ed.* 56, 2645–2648. doi: 10.1002/anie.201611943
- Zhang, X., and Wang, C. (2011). Supramolecular amphiphiles. *Chem. Soc. Rev.* 40, 94–101. doi: 10.1039/B919678C
- Zhou, J., Yu, G., and Huang, F. (2017). Supramolecular chemotherapy based on host-guest molecular recognition: a novel strategy in the battle against cancer with a bright future. *Chem. Soc. Rev.* 46, 7021–7053. doi: 10.1039/C6CS00898D

**Conflict of Interest:** The authors declare that the research was conducted in the absence of any commercial or financial relationships that could be construed as a potential conflict of interest.

Copyright © 2019 Lu, Huang, Wang, Wang, Huang and Du. This is an open-access article distributed under the terms of the Creative Commons Attribution License (CC BY). The use, distribution or reproduction in other forums is permitted, provided the original author(s) and the copyright owner(s) are credited and that the original publication in this journal is cited, in accordance with accepted academic practice. No use, distribution or reproduction is permitted which does not comply with these terms.





# Design of a Thiosemicarbazide-Functionalized Calix[4]arene Ligand and Related Transition Metal Complexes: Synthesis, Characterization, and Biological Studies

## OPEN ACCESS

### Edited by:

Carmine Gaeta,  
University of Salerno, Italy

### Reviewed by:

Grazia Maria Letizia Consoli,  
Institute of Biomolecular Chemistry  
(ICB), Italy  
Mauro Mocerino,  
Curtin University, Australia

### \*Correspondence:

Behrouz Shaabani  
shaabani.b@gmail.com

### Specialty section:

This article was submitted to  
Supramolecular Chemistry,  
a section of the journal  
Frontiers in Chemistry

**Received:** 16 July 2019

**Accepted:** 17 September 2019

**Published:** 09 October 2019

### Citation:

Bahojb Noruzi E, Kheirkhahi M,  
Shaabani B, Geremia S, Hickey N,  
Asaro F, Nitti P and Kafil HS (2019)  
Design of a  
Thiosemicarbazide-Functionalized  
Calix[4]arene Ligand and Related  
Transition Metal Complexes:  
Synthesis, Characterization, and  
Biological Studies.  
Front. Chem. 7:663.  
doi: 10.3389/fchem.2019.00663

Ehsan Bahojb Noruzi<sup>1</sup>, Mahsa Kheirkhahi<sup>1</sup>, Behrouz Shaabani<sup>1\*</sup>, Silvano Geremia<sup>2</sup>,  
Neal Hickey<sup>2</sup>, Fioretta Asaro<sup>2</sup>, Patrizia Nitti<sup>2</sup> and Hossein Samadi Kafil<sup>3</sup>

<sup>1</sup> Department of Inorganic Chemistry, Faculty of Chemistry, University of Tabriz, Tabriz, Iran, <sup>2</sup> Department of Chemical and Pharmaceutical Sciences, University of Trieste, Trieste, Italy, <sup>3</sup> Drug Applied Research Center, Tabriz University of Medical Sciences, Tabriz, Iran

In this study, we synthesized a new thiosemicarbazide-functionalized calix[4]arene **L** and its Co<sup>2+</sup>, Ni<sup>2+</sup>, Cu<sup>2+</sup>, and Zn<sup>2+</sup> transition metal complexes. For characterization several techniques were employed: Fourier-transform infrared (FT-IR), <sup>1</sup>H nuclear magnetic resonance (NMR), <sup>13</sup>C-NMR, <sup>15</sup>N-NMR, correlation spectroscopy (COZY), nuclear Overhauser enhancement spectroscopy (NOESY), electrospray ionization (ESI)-mass spectroscopy, scanning electron microscopy (SEM), energy-dispersive X-ray spectroscopy (EDS), and elemental analysis. To explore the capability of the thiosemicarbazide function hosted on a calix[4]arene scaffold for growth inhibition of bacteria, fungi, and cancerous tumor cells, a series of biological evaluations were performed. For **L**, the antimicrobial tests revealed a higher antibacterial activity against gram-positive *Bacillus subtilis* and a lower activity against gram-negative bacteria (*Escherichia coli* and *Pseudomonas aeruginosa*), whereas the gram-positive *Staphylococcus aureus* shows resistance. All examined metal derivatives show an enhancement of the antibacterial activity against gram-negative *E. coli* bacteria, with a more significant improvement for the Ni<sup>2+</sup> and Zn<sup>2+</sup> complexes. MTT assays showed a considerable *in vitro* anticancer activity of Co<sup>2+</sup>, Ni<sup>2+</sup>, and Cu<sup>2+</sup> complexes against Saos-2 bone cancer cell lines. The activity is ascribable to the inorganic ions rather than calixarene ligand. Hemolysis assay results demonstrated that all compounds have high blood compatibility.

**Keywords:** thiosemicarbazide, calix[4]arene, ligand, transition metal complex, antimicrobial, anticancer

## INTRODUCTION

As the third generation of supramolecular hosts, calix[*n*]arenes have attracted considerable attention in a wide range of either demonstrated or potential applications on the basis of their molecular recognition capabilities (Gutsche, 2008; Neri et al., 2016). These applications most notably include direct chemical sensing systems for both ions and neutral molecules (Sliwa and Girek, 2010; Brunetti et al., 2016; Sun et al., 2016; Yeon et al., 2016; Teixeira et al., 2017; Augusto et al., 2018; Cindro et al., 2018; Sarkar et al., 2018), but the host–guest chemistry of calix[*n*]arenes has also been investigated for use in chemical extraction (Du et al., 2018), catalysis (Homden and Redshaw, 2008; Shirakawa and Shimizu, 2018), and various biological/biomedical uses (Perret and Coleman, 2011; Nimse and Kim, 2013; Durso et al., 2016).

The extensive interest in calix[*n*]arenes is correlated with their ease of synthesis and the possibility of successive functionalization of both the upper and lower rims. This offers the possibility to introduce a wide variety of functional groups with different binding properties to fine-tune their supramolecular chemistry. Furthermore, the possibility to functionalize several arms in theory permits them to be multifunctional molecules. Specifically in the case of calix[4]arenes, the high degree of the cavity pre-organization of the cone conformation, combined with this possibility to introduce different functional groups, make them ideal candidates as molecular scaffolds in the design of novel receptors even for metal ions (Sgarlata et al., 2017; Borges et al., 2018; Gaber et al., 2018; Yousef et al., 2018).

Functionalized calixarenes are of particular interest as molecular recognition systems for biomedical applications, and they have been investigated as direct therapeutic agents (William Anthony Coleman, 2010), in drug delivery applications (Rahimi et al., 2018a, 2019), in protein recognition (Doolan et al., 2018), and in imaging applications (Mayer et al., 2018). From this point of view, a potentially interesting strategy that can be applied to calixarenes is functionalization with thiosemicarbazide groups. Thiosemicarbazide groups are functional groups whose derivatives display pharmacological properties that may be further enhanced by incorporation of metal ions (Salah et al., 2018). Thus, both free thiosemicarbazides and their metal complexes have been investigated as anticancer (Güniz Küçüküzül and Coşkun, 2016; Xie and Peng, 2018; Xie et al., 2018), antiviral (Cihan-Üstündag et al., 2016), and antibacterial (Brahma et al., 2018; Molnar et al., 2018) agents.

The application of calix[4]arenes as receptor of hard metal ions, such as alkaline and alkaline-earth ions, is well-known (Sliwa and Girek, 2010). The incorporation of sulfur atoms introduces the possible coordination of softer transition metal ions, such as Co<sup>2+</sup>, Ni<sup>2+</sup>, Cu<sup>2+</sup>, and Zn<sup>2+</sup>, which are of particular biological interest. The metal complexation can occur through S and terminal N atoms in various ways (Campbell, 1975). For example, the metal complexes of the thiosemicarbazide molecule exhibit square planar (Yang et al., 2006), octahedral (Burrows et al., 1996), square pyramidal (Chiesi Villa et al., 1972), or

tetrahedral coordination (Tong et al., 2000) for Co<sup>2+</sup>, Ni<sup>2+</sup>, Cu<sup>2+</sup>, and Zn<sup>2+</sup>, respectively.

The rigid structure of *tert*-butyl-calix[4]arenes means that up to four ligands can be introduced onto the framework through the hydroxy groups in a controlled manner. In general, two thiosemicarbazide groups would be necessary for each calixarene molecule to satisfy the coordination of a single ion. Therefore, the synthetic strategy adopted was to functionalize the 1, 3 positions of the lower rim of the *tert*-butyl-calix[4]arene in cone conformation.

Herein, we report the synthesis and molecular characterization of this novel calix[4]arene-based thiosemicarbazide ligand and its related complexes with some transition metal ions, expressly Co<sup>2+</sup>, Ni<sup>2+</sup>, Cu<sup>2+</sup>, and Zn<sup>2+</sup>. For these compounds, antimicrobial and anticancer activities and biocompatibility were evaluated.

## EXPERIMENTAL

### Materials

All chemical reagents (Merck) and solvents (Merck and Aldrich) were used as purchased without further purification. Human blood was obtained from the Iranian Blood Transfusion Institute. Mueller–Hinton agar (MHA) and Mueller–Hinton broth (MHB) were purchased from Quelab and Merck, respectively. All microorganism strains—*Staphylococcus aureus* (ATCC® 29213™), *Bacillus subtilis* (ATCC® 6633™), *Escherichia coli* (ATCC® 25922™), *Pseudomonas aeruginosa* (ATCC® 27853™), *Candida albicans* (ATCC® 10231™), and *Candida glabrata* (ATCC® 2001™) were provided from Persian Type Culture Collection (PTCC, Karaj, Iran) or Microbiology Department of Drug Applied Research Centre (DARC, Tabriz University, Iran).

### Instrumentation

Fourier-transform infrared (FT-IR) spectra were recorded on a Bruker Tensor 27 spectrometer in the region 4,000–500 cm<sup>−1</sup> using KBr pellets. Nuclear magnetic resonance [<sup>1</sup>H-NMR, <sup>13</sup>C-NMR, <sup>15</sup>N-NMR, correlation spectroscopy (COZY), and nuclear Overhauser enhancement spectroscopy (NOESY)] spectra were taken on a Bruker Spectrospin Avance 400 MHz, Varian 400 and 500 MHz, and Ultra Shield spectrometer with CDCl<sub>3</sub> solvent. For **L**, Zn<sup>2+</sup> titration, aliquots of 4 μL of 1 M Zn(NO<sub>3</sub>)<sub>2</sub>·6H<sub>2</sub>O in perdeuterated methanol were added to 0.016 mmol of **L** in 0.6 mL of CDCl<sub>3</sub> and followed by <sup>1</sup>H-NMR. NMR spectra were recorded at 25°C after 10 min of equilibration time. Mass spectra were recorded on an ion trap Bruker Esquire 4000 and on a Bruker microTOF-Q, both equipped with an electrospray ionization (ESI) system. Microanalyses were carried out using a Heraeus CHN-O-Rapid analyzer. Melting points were measured on an Electrothermal 9100 apparatus. The morphology characteristic, size distribution, and percentage elemental analysis of samples were conducted via scanning electron microscopy (SEM) (field emission SEM–energy-dispersive X-ray (FESEM-EDX); TESCAN 5001). Prior to examination, samples were mounted onto a metal stub using double-sided carbon adhesive tape and covered with a

thin layer of gold, with the aid of a direct current sputter technique (Emitech k450×, England). Furthermore, to evaluate the complexation process, elemental analysis by the energy-dispersive X-ray spectroscopy (EDS) technique was performed.

## Synthesis

*p*-tert-Butylcalix[4]arene **1** was synthesized using the method published by Gutsche et al. (1981). Compound **2** (5,11,17,23-tetra-*p*-tert-butyl-25,27-bis[cianomethoxy]-26,28-dihydroxycalix[4]arene), compound **3** (5,11,17,23-tetra-*p*-tert-butyl-25,27-bis[aminoethoxy]-26,28-dihydroxycalix[4]arene), and compound **4** (5,11,17,23-tetra-*p*-tert-butyl-25,27-bis[2-isothiocyanoethoxy]-26,28-dihydroxycalix[4]arene) were synthesized using procedures reported by Collins et al. (1991), Zhang and Huang (1997), and Quiroga-Campano et al. (2017), respectively.

## Preparation of 5,11,17,23-tetra-tert-butyl-26,28-dihydroxy-25,27-bis(thiosemicarbazidoethoxy)calix[4]arene (L)

Compound **4** (0.15 g, 0.18 mmol) was added at room temperature to a stirred solution of hydrazine hydrate (90  $\mu$ L, 1.8 mmol) in ethanol (5 mL). Stirring was continued for 3 h until a clear yellow solution was obtained. The solvent was evaporated, and the final product was recrystallized from ethanol. Yield 83%. mp: 280°C (dec.). ESI-high-resolution mass spectroscopy (HRMS):  $[\text{C}_{50}\text{H}_{70}\text{N}_6\text{O}_4\text{S}_2+\text{Na}]^+$  calcd: 905.4972 *m/z*; found: 905.4970 *m/z*; FT-IR (KBr,  $\text{cm}^{-1}$ ): 583, 798, 875, 937, 1,043, 1,109, 1,200, 1,297, 1,363, 1,476, 1,542, 1,618, 2,871, 2,957, 3,049, 3,437;  $^1\text{H}$ -NMR: (400 MHz,  $\text{CDCl}_3$ , tetramethylsilane (TMS), 25°C,  $\delta$  ppm), 8.35 (s, 2H; CNHCS), 7.63 (s, 2H; NNHCS), 7.34 (s, 2H; OH), 7.06 (s, 4H; ArH), 6.86 (s, 4H; ArH), 4.21 (d, 4H;  $\text{ArCH}_2\text{Ar}$ ), 4.27–4.17 (m, 8H;  $\text{OCH}_2\text{CH}_2\text{NCS}$ ), 4.12–3.95 (NH<sub>2</sub>; bs, 4H), 3.37 (d, 4H;  $\text{ArCH}_2\text{Ar}$ ), 1.28 (s, 18H; *t*-Bu), 1.00 (s, 18H; *t*-Bu).  $^{13}\text{C}$ -NMR (101 MHz,  $\text{CDCl}_3$ )  $\delta$  ppm: 183.26 (C-S), 150.22, 149.14, 147.81, 142.45, 132.64, 127.82, 125.99, 125.53, 74.60 ( $\text{CH}_2\text{O}$ ), 44.71 ( $\text{CH}_2\text{N}$ ), 34.20 ( $\text{C}(\text{CH}_3)_3$ ), 34.02 ( $\text{C}(\text{CH}_3)_3$ ), 32.05 ( $\text{ArCH}_2\text{Ar}$ ), 31.79 ( $\text{CH}_3$ ), 31.16 ( $\text{CH}_3$ ).  $^{15}\text{N}$ -NMR (50 MHz,  $\text{CDCl}_3$ ,  $\delta$  ppm from  $\text{CH}_3\text{NO}_2$ ): -274.3 ( $\text{CH}_2\text{NH}$ ); other N's are not detected by  $^1\text{H}$ - $^{15}\text{N}$  inverse correlation due to proton exchange. Anal. Calcd. for  $\text{C}_{50}\text{H}_{70}\text{N}_6\text{O}_4\text{S}_2$  (883.27): C, 67.99; H, 7.99; N, 9.51; found: C, 67.54; H, 8.24; N, 10.04.

## Synthesis of Metal Complexes

All of the complexes were synthesized as follows.

An appropriate amount of metal salts (0.11 mmol) was dissolved in methanol (5 mL), and the solution was added to a tetrahydrofuran (THF) solution (10 mL) of ligand L (0.11 mmol). The mixture was stirred and refluxed for 24 h, after which the precipitate was filtered and the solvent was eliminated under reduced pressure. The solid obtained was purified by crystallization using THF.

### Cobalt compound

$\text{Co}(\text{NO}_3)_2 \cdot 6\text{H}_2\text{O}$  salt (0.029 g, 0.11 mmol) was used as the  $\text{Co}^{2+}$  ion source. A dark brown powder was obtained. Yield:

90%. mp: 230°C (dec.). FT-IR (KBr,  $\text{cm}^{-1}$ ), 588, 635, 674, 783, 819, 873, 920, 1,039, 1,120, 1,199, 1,384, 1,482, 1,637, 2,871, 2,958, 3,345. ESI-MS:  $[\text{C}_{50}\text{H}_{69}\text{N}_6\text{O}_4\text{S}_2\text{Co}]^+$  calcd: 940.4 *m/z*; found: 940.4 *m/z*;  $[\text{C}_{50}\text{H}_{68}\text{N}_6\text{O}_4\text{S}_2\text{Co}]^+$  calcd: 939.4 *m/z*; found: 939.4 *m/z*.

### Nickel compound

$\text{Ni}(\text{NO}_3)_2 \cdot 6\text{H}_2\text{O}$  salt (0.029 g, 0.11 mmol) was used as the  $\text{Ni}^{2+}$  ion source. A pale green powder was obtained. Yield: 44%. mp: 276°C (dec.). FT-IR (KBr,  $\text{cm}^{-1}$ ), 587, 685, 747, 814, 873, 922, 1,038, 1,121, 1,197, 1,238, 1,370, 1,481, 1,564, 1,634, 2,095, 2,958, 3,278. ESI-MS:  $[\text{C}_{50}\text{H}_{69}\text{N}_6\text{O}_4\text{S}_2\text{Ni}]^+$  calcd: 939.4 *m/z*; found: 939.4 *m/z*.

### Copper compound

$\text{Cu}(\text{NO}_3)_2 \cdot 3\text{H}_2\text{O}$  salt (0.27 g, 0.11 mmol) was used as the  $\text{Cu}^{2+}$  ion source. A green-brown powder was obtained. Yield: 68%. mp: 270°C (dec.). FT-IR (KBr,  $\text{cm}^{-1}$ ), 583, 632, 689, 806, 873, 1,034, 1,108, 1,196, 1,304, 1,367, 1,479, 1,576, 1,635, 2,957, 3,047, 3,397. ESI-MS:  $[\text{C}_{50}\text{H}_{69}\text{N}_6\text{O}_4\text{S}_2\text{Cu}]^+$  calcd: 944.4 *m/z*; found: 944.4 *m/z*.

### Zinc compound

$\text{Zn}(\text{NO}_3)_2 \cdot 4\text{H}_2\text{O}$  salt (0.026 g, 0.11 mmol) was used as the  $\text{Zn}^{2+}$  ion source. A pale green powder was obtained. Yield: 83%. mp: 208°C (dec.). FT-IR (KBr,  $\text{cm}^{-1}$ ) 581, 674, 783, 1,036, 1,115, 1,198, 1,373, 1,481, 1,635, 2,564, 2,958, 3,270.  $^1\text{H}$ -NMR: (400 MHz,  $\text{CDCl}_3$ , TMS, 25°C,  $\delta$  ppm), 8.49 (s, 2H; -NHCS), 7.00 (bs, 8H; ArH), 4.15 (bs, 4H;  $\text{ArCH}_2\text{Ar}$  and 8H;  $\text{OCH}_2\text{CH}_2\text{NCS}$ ), 3.4 (bs, 4H;  $\text{ArCH}_2\text{Ar}$ ), 1.19 (s, 18H; *t*-Bu), 1.13 (s, 18H; *t*-Bu).  $^{13}\text{C}$ -NMR (101 MHz,  $\text{CDCl}_3$ )  $\delta$  ppm: 149.2 (s), 148.7 (s), 148.0 (s), 143.0 (s), 133.2 (s), 127.5 (d), 127.1 (d), 125.6 (d), 34.4 (s,  $\text{C}(\text{CH}_3)_3$ ), 34.0 (s,  $\text{C}(\text{CH}_3)_3$ ), 32.6 (t,  $\text{ArCH}_2\text{Ar}$ ), 31.6 (q,  $\text{CH}_3$ ), 31.2 (q,  $\text{CH}_3$ ). ESI-MS:  $[\text{C}_{50}\text{H}_{69}\text{N}_6\text{O}_4\text{S}_2\text{Zn}]^+$  calcd: 945.4 *m/z*; found: 945.5 *m/z*.

## Antimicrobial and Antifungal Studies

The minimum inhibitory concentration (MIC) and minimum bactericidal concentration (MBC) of the ligand and related complexes were measured using the microbroth dilution method according to the protocols described by Clinical and Laboratory Standards Institute (CLSI) (Weinstein et al., 2018). Concentration series (15.62–2,000 ppm) of the compounds were prepared in nutrient broth medium. A total of 180  $\mu$ L of prepared diluted solutions was transferred into sterile 96-well microtiter plates, and then 20  $\mu$ L of standardized microorganism suspensions was added and mixed gently to get a homogenous suspension. The concentration of the microorganisms was adjusted to  $5 \times 10^5$  CFU  $\text{mL}^{-1}$  by 0.5 McFarland solution. Then, the plates were incubated at 37°C for 24 h (Bahloul et al., 2018). After incubation, turbidity was evaluated to determine bacterial growth, and the dilution with no turbidity (lack of growth) was considered as MIC. Finally, to determine the MBC, samples (5  $\mu$ L) from tubes in which no growth was observed were cultured in plate (containing MHA medium) and incubated for 24 h at 37°C. In each test, microorganism strain in MHB (without chemicals) and MHB alone (without

bacteria) were used as positive and negative growth controls, respectively (Karimi et al., 2018). This method was applied with *S. aureus* (ATCC<sup>®</sup> 29213<sup>™</sup>) and *B. subtilis* (ATCC<sup>®</sup> 6633<sup>™</sup>) as gram-positive bacteria, *E. coli* (ATCC<sup>®</sup> 25922<sup>™</sup>) and *P. aeruginosa* (ATCC<sup>®</sup> 27853<sup>™</sup>), as gram-negative bacteria, and *C. albicans* (ATCC<sup>®</sup> 10231<sup>™</sup>) and *C. glabrata* (ATCC<sup>®</sup> 2001<sup>™</sup>) as fungal strains.

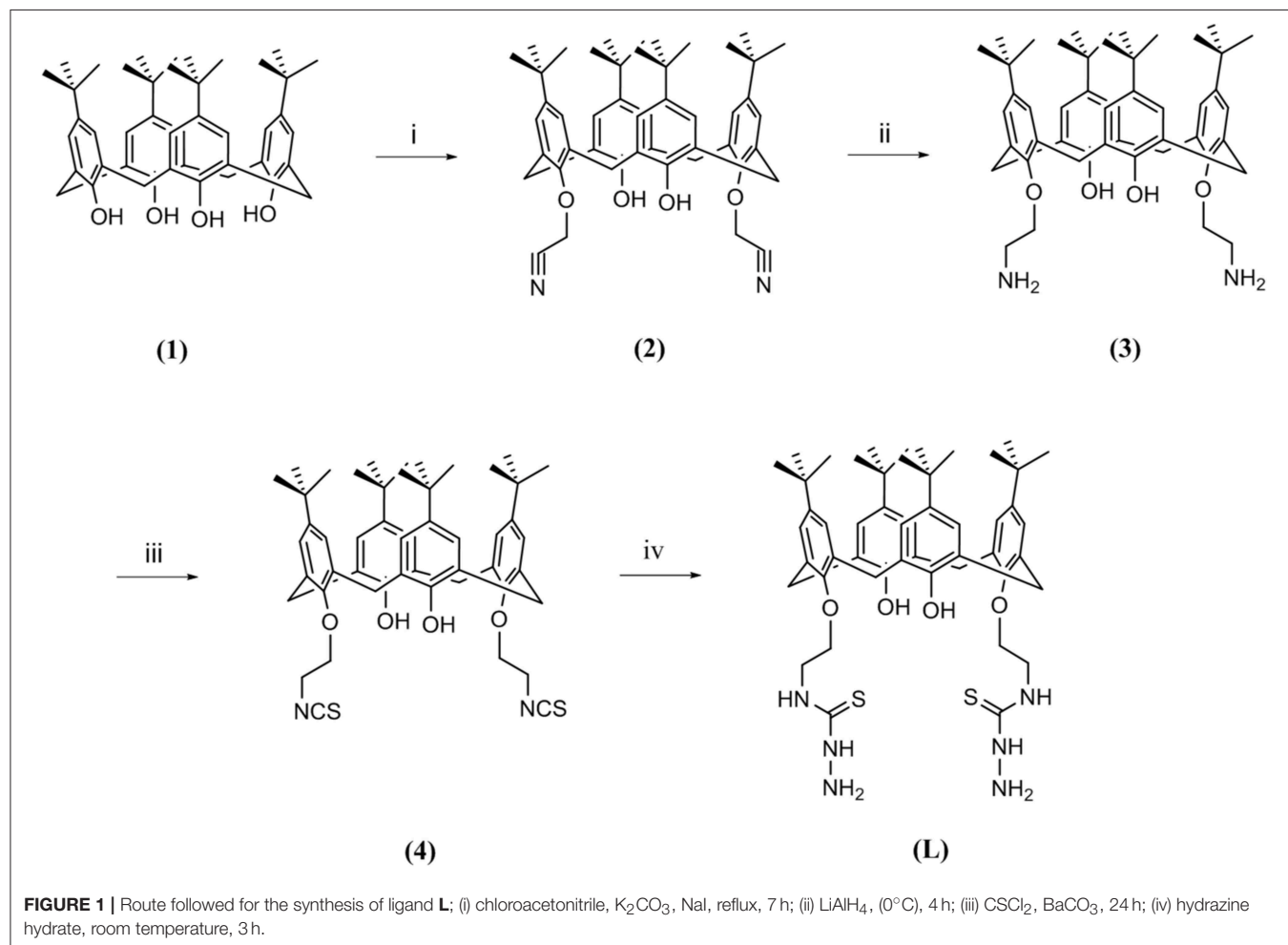
## Cell Culture

MCF-7 cells (human breast cancer cells) and Saos-2 cells (human bone cancer cells) were collected from the Pasteur Institute of Iran, Tehran, Iran, and maintained in RPMI 1640 medium supplemented with 10% fetal bovine serum (FBS) and 1% benzylpenicillin/streptomycin. Further, the MCF-7 and Saos-2 cell lines were maintained at 5% CO<sub>2</sub> in a CO<sub>2</sub> incubator at 37°C for 24 h. Cultures were continuously viewed under a microscope to evaluate the quantity of confluence, and the absence of bacterial and fungal contaminants was confirmed. After 90% confluence was reached, the cells were detached by adding trypsin to the flask. The cell suspensions were collected and centrifuged at 1,500 rpm for 5 min and re-suspended in the growth medium for further steps (Rahimi et al., 2017a).

## MTT Assay

To determine the cytotoxic effect of the synthesized ligand and its related metal compounds, a cell viability study was done with the MTT reduction assay. MCF-7 and Saos-2 cells were seeded at a density of  $1 \times 10^4$  cells/well in 96-well plates. The cells were incubated overnight and treated with **L** or one of the metal complexes at the concentrations of 200, 100, and 50 ppm for 48 h using untreated cells as control. Afterward, the culture media were exchanged with 180 mL of fresh culture media and 20 mL of MTT solution ( $2 \text{ mg mL}^{-1}$ ) and incubated at 37°C for 4 h. The MTT solution was removed and replaced with 200  $\mu\text{L}$  of dimethyl sulfoxide (DMSO) followed by 20-min incubation time. The absorbance of each well (dissolved formazan crystals) was measured at a wavelength of 570 nm using an enzyme-linked immunosorbent assay (ELISA) reader (Shafiei-Irannejad et al., 2018). The results were given as the mean of three independent experiments. The percentage of viability was calculated by absorbance values using the following formula:

$$\text{Cell viability (\%)} = \frac{A_{\text{sample}}}{A_{\text{control}}} \times 100 \quad (1)$$





## Hemolysis Assay

### Blood Collection and Erythrocyte Isolation

Hemolysis assay was performed using fresh human blood. Approximately 5 mL of blood that was stabilized using EDTA was placed into a 15-mL centrifuge tube. Phosphate-buffered saline (PBS) measuring 10 mL was added to wash away blood proteins and serum from the red blood cells (RBCs). The erythrocytes were collected by centrifugation at 4,000 rpm for 10 min at room temperature. The upper layer (plasma) was discarded, and erythrocytes (RBCs) were isolated. The RBCs were washed three times with PBS (pH = 7.4) to obtain a clear supernatant (Rahimi et al., 2018b).

### Hemolytic Activity and RBC Aggregation

The total isolated RBCs were diluted 10 times with PBS. In each microtube, 0.5 mL of ligand **L** or one of the metal complexes was mixed at different concentrations (62.5, 125, 250, 500, and 1,000 ppm) with 0.5 mL of diluted RBCs and incubated at 37°C for 3 h in an incubator shaker. Diluted RBCs treated with 0.5 mL of water and PBS were used as positive and negative controls with 100% and 0% hemolytic effects, respectively. After incubation, all samples were centrifuged at 4,000 rpm for 5 min. The supernatant was taken out and transferred to a 96-well plate (Rahimi et al., 2018b). An ELISA plate reader was used to measure the released hemoglobin (at a wavelength of 540 nm), and the hemolysis rate was calculated via the following formula:

$$\text{Hemolysis (\%)} = \frac{A_{\text{sample}} - A_{\text{negative}}}{A_{\text{positive}} - A_{\text{negative}}} \times 100, \quad (2)$$

where  $A_{\text{sample}}$  is the absorbance of the testing sample, and  $A_{\text{positive}}$  and  $A_{\text{negative}}$  are the absorbance of the positive control and the negative control, respectively.

## RESULTS AND DISCUSSION

### Development of a New calix[4]arene-thiosemicarbazide Ligand and Related Metal Derivatives

The synthetic route for the preparation of 5,11,17,23-tetra-*tert*-butyl-26, 28-dihydroxy-25,27-bis(thiosemicarbazidoethoxy)calix[4]arene (**L**) is shown in Figure 1.

Briefly, starting from *p-tert*-butylcalix[4]arene (**1**), a couple of hydroxyl groups on the lower rim in **1**, 3 alternate positions were transformed to cyanomethoxy by chloroacetonitrile (**2**). The reduction of cyano functional groups with  $\text{LiAlH}_4$  gave the corresponding diamine derivative (**3**). Then, the diisothiocyanate derivative (**4**) was obtained by the reaction of compound **3** with thiophosgene in high yield. Finally, the reaction of compound **4** with an excess amount of hydrazine hydrate in ethanol at room temperature resulted in the new calixarene-thiosemicarbazide derivative (**L**).

Several divalent metal derivatives of **L** ( $\text{Co}^{2+}$ ,  $\text{Ni}^{2+}$ ,  $\text{Cu}^{2+}$ , and  $\text{Zn}^{2+}$ ) were prepared by mixing one equivalent of the metal salt in MeOH with one equivalent of ligand **L** in THF followed by reflux for 24 h.

### Characterization

Several techniques (FT-IR,  $^1\text{H}$ -NMR,  $^{13}\text{C}$ -NMR,  $^{15}\text{N}$ -NMR, COZY, NOESY, MS, CHN analysis, SEM, and EDS analysis) were

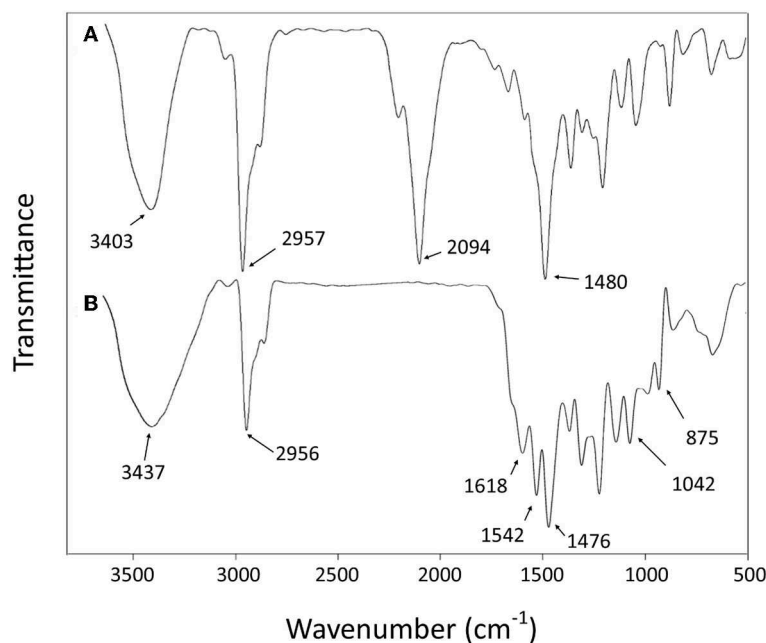


FIGURE 2 | Fourier-transform infrared (FT-IR) spectra of compound **4** (A) and ligand **L** (B).

performed to confirm the preparation route of the ligand and metal derivatives.

## FT-IR

The success of the final step of synthesis is confirmed by the analysis of the FT-IR spectra. The absence of the strong peak at  $2,094\text{ cm}^{-1}$  from the spectrum of **L**, assigned to the stretching mode of CN in the NCS group of **4** (Yamamoto et al., 1992), is the most noteworthy feature that indicates the transformation of isothiocyanate functional group (Figure 2). The disappearance of this peak should be accompanied by the appearance of new bands related to stretching and bending vibrations of the formed thiosemicarbazide group, such as the new bands observed at  $1,620\text{--}1,540\text{ cm}^{-1}$ , which can be attributed to the  $\nu(\text{N}=\text{C}=\text{S})$  vibrations (Rao and Venkataraghavan, 1962). The band at  $875\text{ cm}^{-1}$  can be attributed to the stretching of the C=S group (Mostafa, 2007). Furthermore, the absence of any bands in the  $2,600\text{--}2,550\text{ cm}^{-1}$  range assignable to  $\nu(\text{SH})$  stretching suggests that the CS group remains in thione form (Mostafa, 2007). The expected N–H bond stretching of the thiosemicarbazide group lies within the broad envelope of the peak centered at  $3,437\text{ cm}^{-1}$ , which also contains the O–H stretching (Silverstein et al., 1991; Rastogi et al., 2002). The other bands, corresponding to C–H, C=C, and C–C vibrational modes of aromatic rings (Baldini et al., 2003; Hernández et al., 2016), are conserved in both **4** and **L** spectra.

The comparison of the FT-IR spectra of **L** and the derivative metal complexes evidences a main feature that supports the metal coordination by **L**. The characteristic double peak of the N–C=S vibration observed for **L** in the  $1,620\text{--}1,540\text{ cm}^{-1}$  region shifts to higher wave number in all metal derivatives. These differences are summarized in Table 1, and the corresponding spectra are reported in the Supporting Information.

This observation is in agreement with the hypothesis of a metal coordination by **L** for all bivalent ions, with a possible formation of a five-member cycle involving the terminal N-atom and S-atom responsible for the profile change of the N–C=S vibration bands.

## NMR

The  $^1\text{H}$ -NMR spectra of compound **4** (Figure 3A) show two singlet signals for two sets of 18 *t*-Bu protons ( $\delta$  0.97 and 1.29 ppm), two doublet signals ( $\delta$  3.36 ppm, 4 protons; and  $\delta$  4.25 ppm, 4 protons) assigned to the calixarene  $-\text{CH}_2-$  bridging groups, a multiplet peak ( $\delta$  4.22–4.14 ppm) corresponding to the eight  $\text{OCH}_2\text{CH}_2\text{NCS}$  protons, two types of aromatic protons ( $\delta$  6.86 ppm, 4 protons; and  $\delta$  7.06 ppm, 4 protons) as two singlet signals,

and one singlet peak related to two OH protons ( $\delta$  6.89 ppm) in agreement with literature data (Quiroga-Campano et al., 2017).

The  $^1\text{H}$ -NMR spectra of ligand **L** (Figure 3B) show analogous signals for the protons that correspond to those in **4**, in addition to a broad singlet for the four terminal  $\text{NH}_2$  protons ( $\delta$  4.12–3.95 ppm), a singlet peak attributed to two thiosemicarbazide NH protons ( $\delta$  7.63 ppm), and a singlet signal attributed to two NHCS protons ( $\delta$  8.35 ppm). The singlet peak corresponding to two OH proton ( $\delta$  7.34 ppm) appears at a significantly higher chemical shift than observed for compound **4** ( $\delta$  6.89 ppm). The  $^1\text{H}$ -NMR assignment was supported by the H–H and H–C two-dimensional (2D) NMR spectra (see Supporting Information). Thus, these spectra are in agreement with the synthesis of the new calixarene derivative **L**.

The complexation of the metal ions was investigated by NMR only for the diamagnetic  $\text{Zn}^{2+}$  ion. The addition of a  $\text{Zn}(\text{NO}_3)_2$  solution to the **L** sample provokes a general broadening and shift of  $^1\text{H}$ -NMR signals depending of the type of protons involved. In particular, the signals of protons of the *p*-*tert*-butyl of phenyl groups functionalized by the thiosemicarbazide arms (a) and the corresponding aromatic hydrogens (f) are the most affected (Figure 4).

Owing to the overall broadening of the signals, the two strongest singlets due to sets of 18 *tert*-butyl protons (a, b) are the best indicators to follow the complexation process. The stepwise addition of  $\text{Zn}^{2+}$  ions causes a downfield shift of the (a) protons, whereas the (b) protons are shifted upfield. In particular, the (a) signal shows a slight shift upon the first addition of a  $\text{Zn}^{2+}$ . Then with the second addition of  $\text{Zn}^{2+}$  ion (**L**: $\text{Zn}^{2+}$  ratio = 1:0.5), a split of the (a) signal becomes evident. The two signals (a' and a'') 0.1 ppm apart that have approximately equal intensity can be attributed to species with unbound and bound  $\text{Zn}^{2+}$  ions, respectively. When the titration reaches the 1-to-1 ratio, the (a') signal disappears in favor to the (a'') signal of the  $\text{Zn}^{2+}$  complex. Contemporarily, a significant downfield shift of the aromatic proton (f) is observed. This titration experiment clearly shows the coordination properties of the **L** ligand and the formation of a 1-to-1 stoichiometric complex.

## ESI-MS

The HRMS of ligand **L** showed molecular ion peaks corresponding to the sodium adduct of the **L** ligand (Supporting Information). The most intense peak of  $905.4790\text{ m/z}$  perfectly agrees with a compound with formula  $\text{C}_{50}\text{H}_{70}\text{N}_6\text{O}_4\text{S}_2$  (theoretical  $[\text{M} + \text{Na}]^+$  equal to  $905.4792\text{ m/z}$ ) and confirms the proposed structure for **L**.

Evidence of formation of the complexes was obtained by ESI-MS (Supporting Information). All spectra show peaks

**TABLE 1** | IR spectral data ( $\text{cm}^{-1}$ ) of the ligand and its corresponding complexes in KBr pellets.

Vibrational mode	Frequency ( $\text{cm}^{-1}$ )				
	Ligand <b>L</b>	Complex <b>Co</b>	Complex <b>Ni</b>	Complex <b>Cu</b>	Complex <b>Zn</b>
N–C = S	1,618, 1,542	1,637, sh	1,634, 1,564	1,635, 1,576	1,635, sh

IR, infrared.

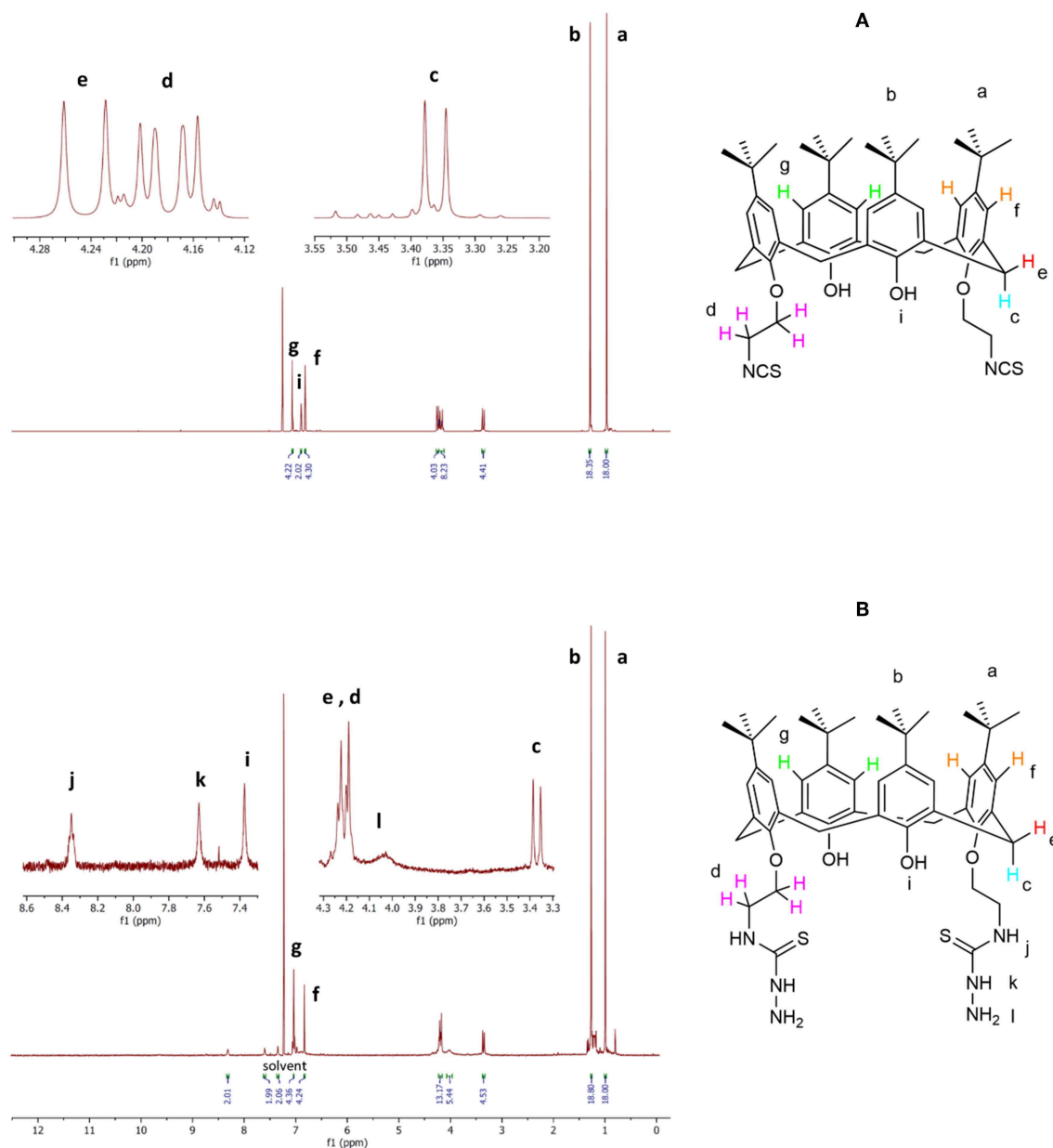


**FIGURE 3 |** Selected portion of the <sup>1</sup>H-NMR spectra of compound 4 (A) and ligand L (B).

related to multiple species along with evidence for formation of the metal ion complexes. The spectrum for the Co adduct shows the presence of Co<sup>2+</sup> bound by a deprotonated L ligand ([C<sub>50</sub>H<sub>69</sub>N<sub>6</sub>O<sub>4</sub>S<sub>2</sub>Co]<sup>+</sup>, *m/z* 940.4) superimposed with an amount of Co<sup>3+</sup> species bound by a doubly deprotonated L ligand ([C<sub>50</sub>H<sub>68</sub>N<sub>6</sub>O<sub>4</sub>S<sub>2</sub>Co]<sup>+</sup>, *m/z* 939.4). It should be noted that the deprotonation of two hydroxy groups of calix[4]arene is consistent with formation of an octahedral coordination environment ideal for complexation of Co<sup>3+</sup> species. The spectrum of Ni derivative, in which an ion is usually involved in octahedral coordination, shows the clearest evidence of metal complexation of those investigated. The

most intense peaks are related to the mono-deprotonated L ligand coordinated to Ni<sup>2+</sup> ion ([C<sub>50</sub>H<sub>69</sub>N<sub>6</sub>O<sub>4</sub>S<sub>2</sub>Ni]<sup>+</sup>, *m/z* 939.4). In the case of Cu<sup>2+</sup> and Zn<sup>2+</sup>, the MS show a series of peaks related to the [C<sub>50</sub>H<sub>69</sub>N<sub>6</sub>O<sub>4</sub>S<sub>2</sub>Cu]<sup>+</sup> (944.4 *m/z*) and [C<sub>50</sub>H<sub>69</sub>N<sub>6</sub>O<sub>4</sub>S<sub>2</sub>Zn]<sup>+</sup> (945.5 *m/z*) complexes, respectively. For both species, the isotopic distribution shows some small discrepancy in the intensity with respect to the calculated distributions.

## SEM

The morphological characteristics of the solid-state aggregation of ligand L and its metal derivatives were evaluated using a SEM

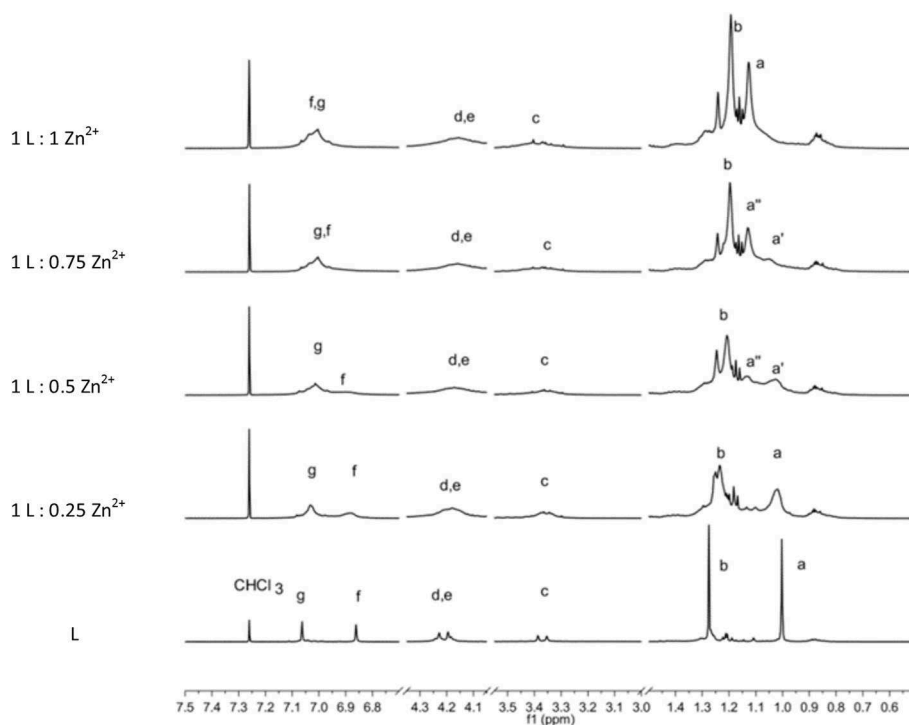


**FIGURE 4** |  $^1\text{H}$ -NMR spectrum sequence of titration of **L** by  $\text{Zn}^{2+}$  ions. The bottom spectra of **L** are scaled by a factor of 0.2.

by applying 15-kV electron acceleration voltage. **Figures 5A–D** shows the SEM images of ligand **L** and of its metal derivatives at  $20\times$  magnification. In comparison with **L**, each metal derivative shows a different morphology of the aggregation state, with a more crystalline tendency in the case of the Zn derivative (**Figure 5E**).

### EDS

EDS or EDX was used to semi-quantitatively measure chemical elements of compounds. As indicated by the EDS chemical maps, the presence of Co, Ni, Cu, and Zn metals is confirmed in the corresponding metal derivative samples (**Figure 6**). The analysis of the data suggests that the percentage of metal ions in the  $\text{Cu}^{2+}$  and  $\text{Zn}^{2+}$  samples is somewhat higher than that observed for the  $\text{Ni}^{2+}$  and  $\text{Co}^{2+}$  derivatives.

### In vitro Antimicrobial Activity and Antifungal Evaluation

The biological properties of thiosemicarbazide derivatives have been studied extensively in recent years by different research groups (Liesen et al., 2010; Plech et al., 2011; Shebl et al., 2013; Rane et al., 2014). Herein, the *in vitro* antimicrobial and antifungal activities of the synthesized compounds (**L** and complexes of **Co**, **Ni**, **Cu**, and **Zn**) were evaluated using the microbroth dilution method against the aforementioned standard strains. None of the investigated compounds show a measurable antifungal activity. However, as shown in **Table 2**, the free ligand **L** has an effective antibacterial activity against gram-positive *B. subtilis*, whereas the gram-positive *S. aureus*

was resistant to it. A lower activity was observed for both investigated gram-negative pathogens (*E. coli* and *P. aeruginosa*). The cobalt complex showed a moderate antibacterial activity against all of the bacteria except *B. subtilis* that showed resistance. The antibacterial properties against the gram-negative strains were significantly enhanced upon coordination of nickel to the thiosemicarbazide ligand, whereas no variations are observed for gram-positive bacteria. Specifically, in the case of *E. coli* strain, the MIC and MBC values show four-fold and two-fold decreases, respectively. The coordination of copper metal to the ligand improved the MIC and MBC values against *S. aureus* and *E. coli* strains. On the other hand, the MIC values against *B. subtilis* and *P. aeruginosa* were not affected by this metal addition, whereas the MBC values against these two strains were enhanced. In comparison with **L**, the zinc complex improved the antibacterial activity toward *S. aureus* and both gram-negative bacteria. In the case of *E. coli* and *P. aeruginosa* strains, the MIC values show eight-fold and two-fold decreases, respectively. On the other hand, the MBC values against all of the microorganisms (except *P. aeruginosa*) were improved significantly, with a 16-fold decrease against *E. coli*. Overall, all compounds have some antibacterial activities against gram-negative strains, and some of them showed an antibacterial activity against gram-positive bacteria. The decreased MIC and MBC values of metal derivatives are consistent with the possibility that they disturb the respiration process of the bacterial cell, blocking the synthesis of proteins, which restricts growth of the microorganism (Dharmaraj et al., 2001).



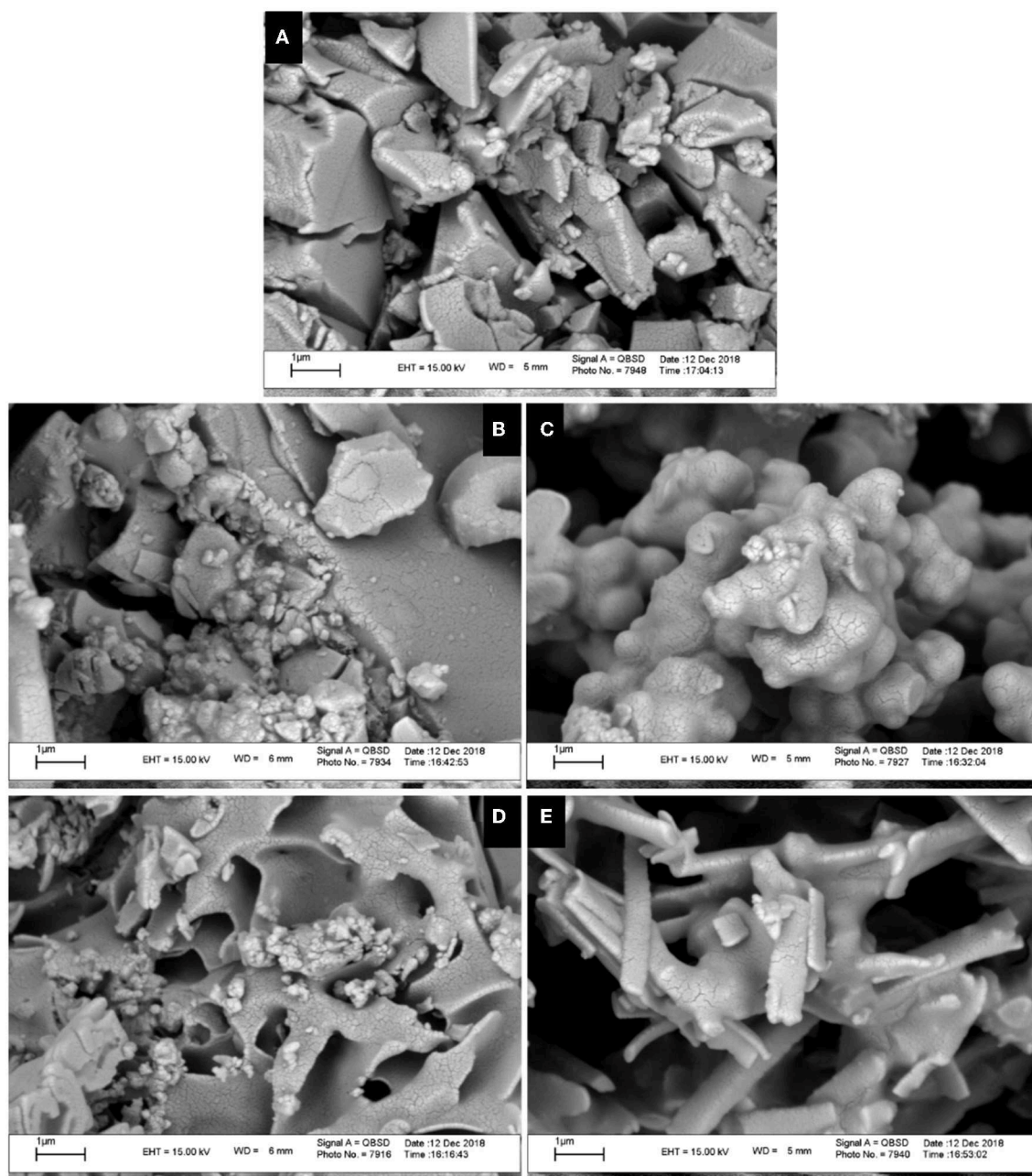


**FIGURE 5 |** Scanning electron microscopy (SEM) images of ligand **L** (A) and complexes **Co** (B), **Ni** (C), **Cu** (D), and **Zn** (E) at the scale of 1  $\mu\text{m}$ .

### MTT Assay

According to previous studies, the anticancer activities of calixarene-based compounds are related to their enzyme inhibition potential (Cherenok et al., 2006, 2012), inhibiting tumor angiogenesis (Dings et al., 2006) and DNA replication of cancer cells (Consoli et al., 2007). The cytotoxicity of the ligand and complexes was studied against the MCF-7 and Saos-2 cell lines by MTT assay. All of the compounds were dispersed in water (and 10% DMSO) and diluted with cell culture medium to reach three required concentrations (50, 100, and

200 ppm). The cytotoxicity impact on cell growth is shown in **Figure 7**. In general, all of the compounds showed a very low antiproliferative activity against MCF-7, whereas for the Saos-2 cells, a more significant dose-dependent antiproliferative activity was observed with exclusion of **L** and the **Zn** derivative. The **Co** derivative showed an excellent anticancer activity against the Saos-2 cell line even at a lower concentration (42.13%), although the most effective toxicity is revealed at a higher concentration (16.34%). At a higher concentration, the activities of **Ni** and **Cu** derivatives are also evident, with inhibition concentrations ( $\text{IC}_{50}$ )

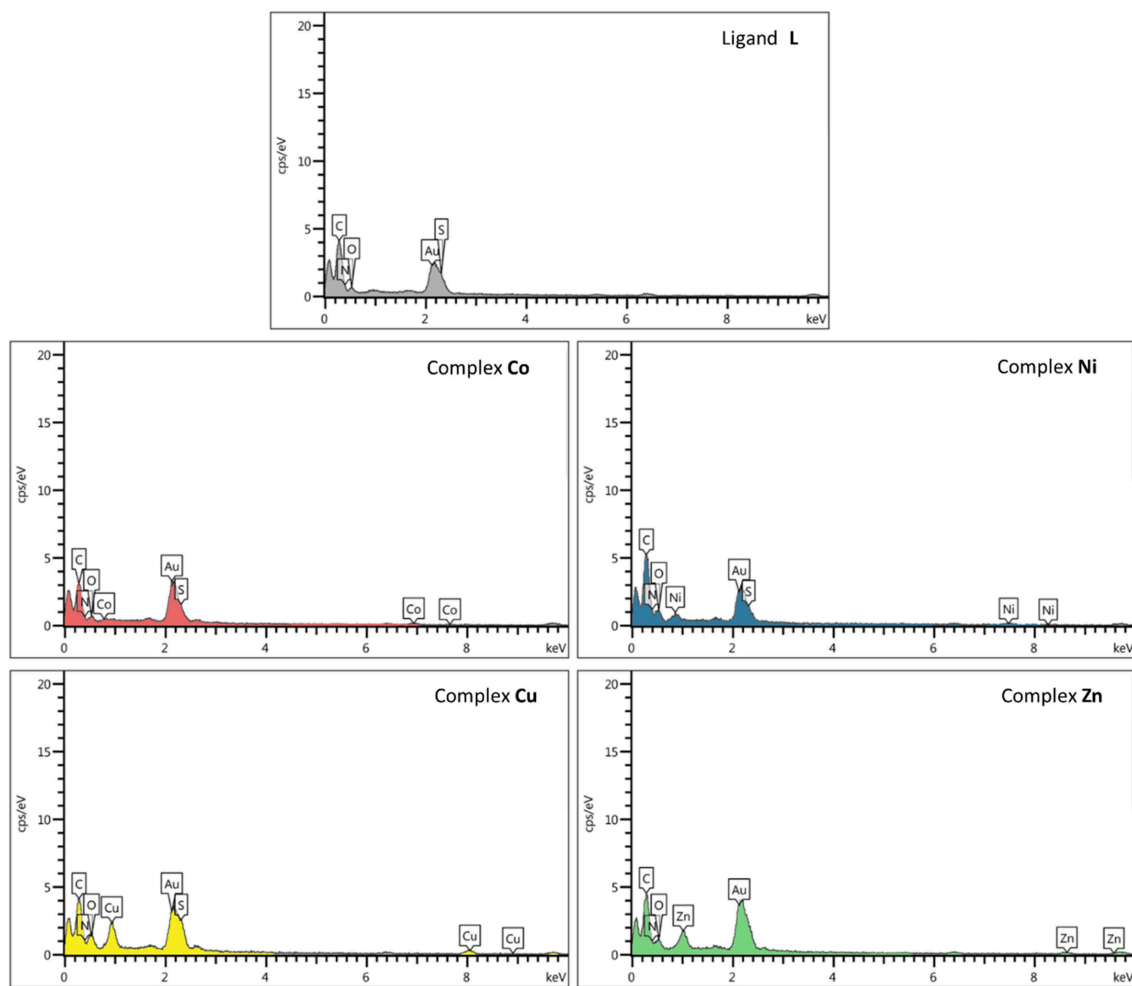


**FIGURE 6 |** Scanning electron microscopy–energy-dispersive X-ray (SEM-EDX) elemental analysis of ligand **L** and complexes **Co**, **Ni**, **Cu**, and **Zn**.

**TABLE 2 |** Antibacterial activity of synthesized compounds against different microorganisms in with the microbroth dilution method.

Microorganisms		Gram positive		Gram negative	
		<i>Staphylococcus aureus</i>	<i>Bacillus subtilis</i>	<i>Escherichia coli</i>	<i>Pseudomonas aeruginosa</i>
<b>MIC</b>	Ligand <b>L</b>	–	31.25	250	62.50
	Complex <b>Co</b>	250	–	125	125
	Complex <b>Ni</b>	–	31.25	62.50	31.25
	Complex <b>Cu</b>	250	31.25	125	62.50
	Complex <b>Zn</b>	500	125	31.25	31.25
	Gentamicin*	0.12	2	0.5	2
<b>MBC</b>	Ligand <b>L</b>	–	–	500	–
	Complex <b>Co</b>	–	–	500	500
	Complex <b>Ni</b>	–	–	250	–
	Complex <b>Cu</b>	250	31.25	250	250
	Complex <b>Zn</b>	500	125	31.25	–
	Gentamicin*	0.25	2	0.5	2

The antibacterial activity is expressed as the MIC and MBC (ppm). MIC, minimum inhibitory concentration; MBC, minimum bactericidal concentration.

\*Gentamicin used as standard control for bacteria.

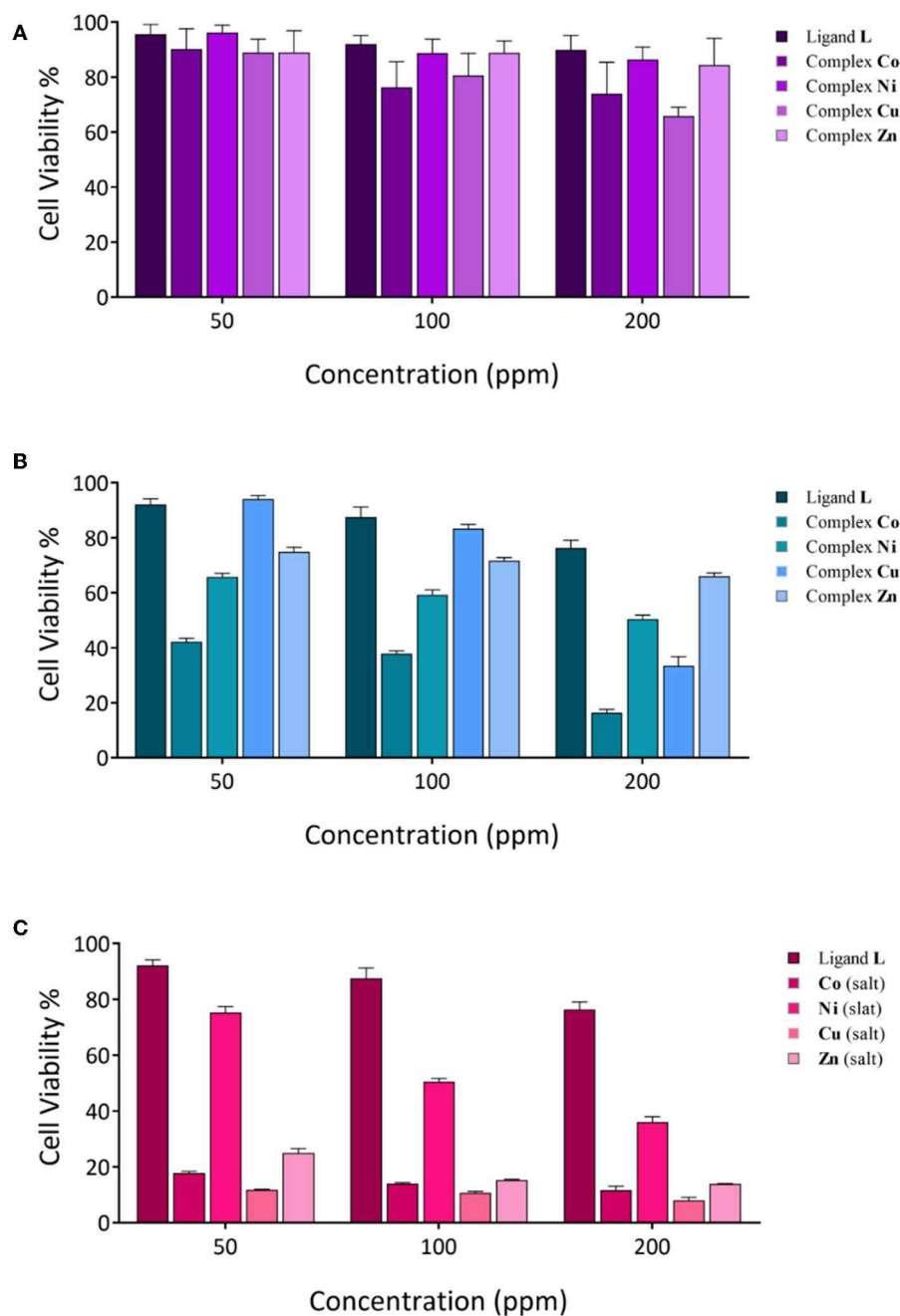


**FIGURE 7** | Cytotoxicity evaluation of synthesized compounds at various concentrations against cancer cell lines; **(A)** MCF-7 cell lines; **(B,C)**, Saos-2 cell lines.

over 48 h of 200 and 170 ppm, respectively. However, control assays performed with the corresponding inorganic salts show that the activity is mainly ascribable to the inorganic component rather than the organic calixarene component. Actually, the L ligand appears to protect the cells against the inherent cytotoxicity of the bivalent ions present in the inorganic salts of these metals.

### Hemolysis Assay

Hemolysis assay was performed to examine the biocompatibility and the cytotoxic effect of ligand and complexes on RBCs at different concentrations. As shown in **Figure 8**, dose-dependent hemolytic effects of the prepared compounds on RBCs were observed, and the results confirm that there are only slight hemolytic effects from the compounds at high dosages. RBCs

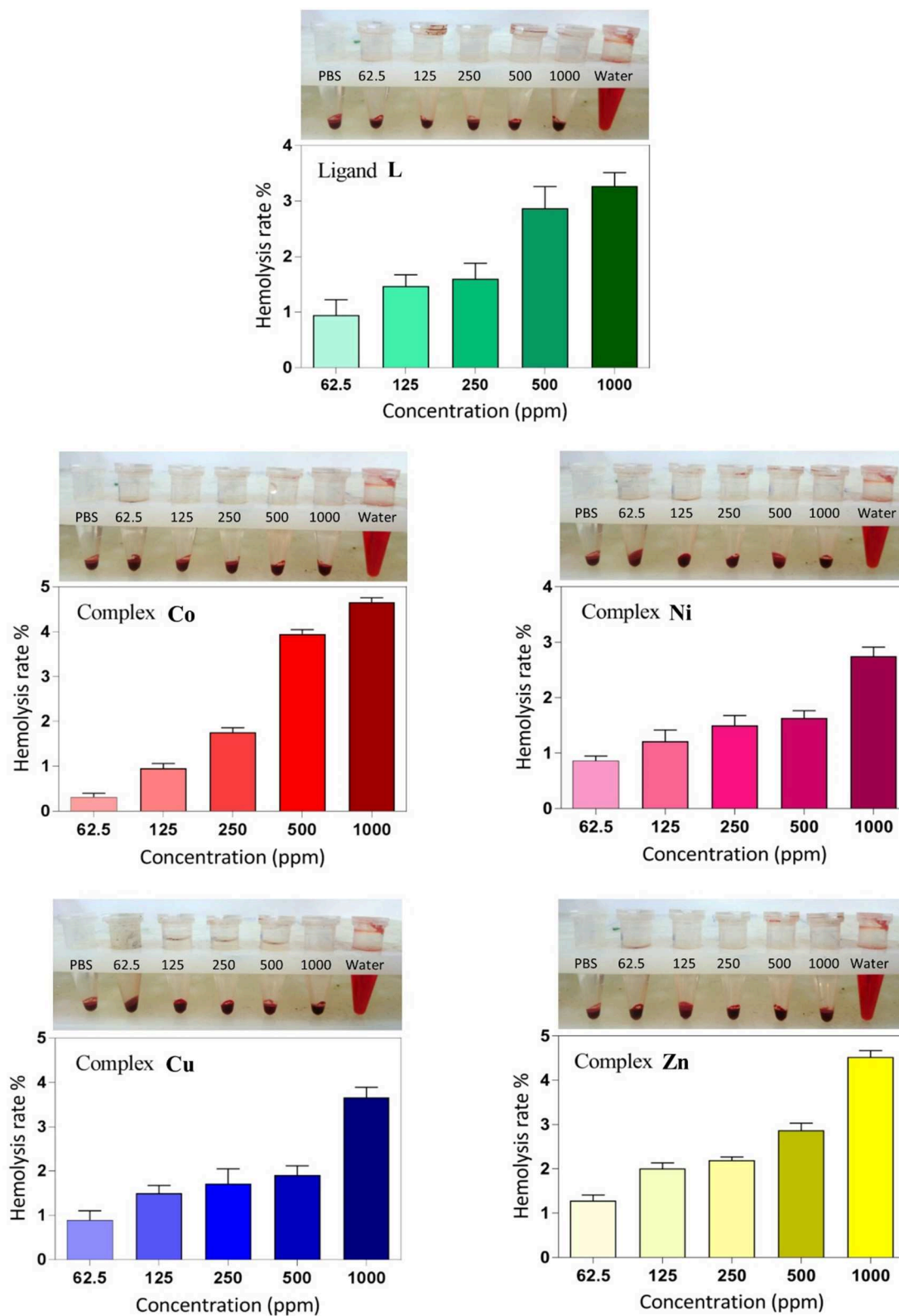


**FIGURE 8 |** Hemolysis rate of human red blood cells (HRBCs) in the presence of the synthesized samples and the visual observation of hemoglobin in the supernatant at different concentrations (ppm).



were also treated with PBS and deionized water as negative and positive controls, respectively. With regard to the results, at the highest concentration investigated (1,000 ppm), the lowest hemolytic activity was observed for the **Ni** derivative (2.6%), whereas at the lowest concentration investigated (62.5 ppm), the lowest hemolytic activity was observed for the **Co** derivative (0.3%). Therefore, on the basis of biocompatibility of the various compound investigated, the **Ni** and **Co** complexes could be the best choices for biological applications in higher and lower concentrations, respectively. Also, the hemolytic activity of the ligand itself is very low (3.18%) and <4.5%, which is an acceptable threshold for hemolytic activity (Rahimi et al., 2017b).

## CONCLUSION

In this study, we designed and synthesized a new calix[4]arene-based thiosemicarbazide molecule, and we used it as a quadridentate ligand to prepare a series of transition metal complexes. The characterization with multiple techniques (FT-IR, <sup>1</sup>H-NMR, <sup>13</sup>C-NMR, <sup>15</sup>N-NMR, COZY, NOESY, ESI-MS, SEM, EDS, and elemental analysis) demonstrated the success of the synthesis of the target ligand, **L**. The ability of **L** to complex metal ions was demonstrated by <sup>1</sup>H-NMR titration experiments with the diamagnetic Zn<sup>2+</sup> ions. On the basis of the known biological properties of thiosemicarbazide derivatives, we performed antimicrobial and anticancer evaluations against human cancer cell lines and biocompatibility studies on **L** and the series of its metal complexes to investigate Co<sup>2+</sup>, Ni<sup>2+</sup>, Cu<sup>2+</sup>, and Zn<sup>2+</sup>. **L** showed a higher antibacterial activity against gram-positive *B. subtilis* and a lower activity against gram-negative bacteria (*E. coli* and *P. aeruginosa*), whereas the gram-positive *S. aureus* shows resistance. All metal derivatives show an enhancement of the antibacterial activity against gram-negative bacteria (except for the Co<sup>2+</sup> and Cu<sup>2+</sup> derivatives for *P. aeruginosa*), with a more significant improvement for the Ni<sup>2+</sup> and Zn<sup>2+</sup> complexes. The anticancer activities of all compounds against the MCF-7 cell line were not relevant, even if the activities of the **Co** and **Cu** complexes slightly improved at a higher concentration. On the other hand, the MTT assay appeared to show a significant anticancer activity of Co<sup>2+</sup>, Ni<sup>2+</sup>, and Cu<sup>2+</sup> complexes against Saos-2 cell line. However, control assays show that this activity is mainly ascribable to the metal ions rather than the organic

calixarene component. Hemolysis assays demonstrated no significant hemolysis rate for all of the compounds even at higher concentrations.

## DATA AVAILABILITY STATEMENT

All datasets generated for this study are included in the manuscript/Supplementary Files.

## ETHICS STATEMENT

All biological studies were carried out under approved protocols with the ethical committee of Tabriz University of Medical Sciences (National Institutes of Health Publication No. 85-23, revised 1996).

## AUTHOR CONTRIBUTIONS

EB and MK: substantial contributions to the conception or design of the work, or the acquisition, analysis or interpretation of data for the work. BS: research have performed under his supervision. SG and NH: substantial contributions to the analysis or interpretation of data for the work. FA: performed the NMR titrations of metal complexes. PN: purified some samples and helped for interpretation of NMR spectra. HK: designed and confirmed antibacterial part of research.

## FUNDING

This study was financially supported by University of Tabriz.

## ACKNOWLEDGMENTS

We thank Drug Applied Research Center (DARC), Tabriz University of Medical Sciences (Tabriz, Iran), and all biological experiments in this report were done in DARC.

## SUPPLEMENTARY MATERIAL

The Supplementary Material for this article can be found online at: <https://www.frontiersin.org/articles/10.3389/fchem.2019.00663/full#supplementary-material>

## REFERENCES

- Augusto, A. S., Miranda, A. S., Ascenso, J. R., Miranda, M. Q., Félix, V., Brancatelli, G., et al. (2018). Anion recognition by partial cone dihomooxalix[4]arene-based receptors bearing urea groups: remarkable affinity for benzoate ion. *Eur. J. Org. Chem.* 2018, 5657–5667. doi: 10.1002/ejoc.201800880
- Bahloul, S., Aghazadeh, Z., Aghazadeh, M., Shojani, S., and Kafil, H. S. (2018). Determining the antibacterial activity of chlorhexidine mouthwashes with and without alcohol against common oral pathogens. *J. Adv. Oral Res.* 9, 15–19. doi: 10.1177/2229411218762045
- Baldini, M., Belicchi-Ferrari, M., Bisceglie, F., Pelosi, G., Pinelli, S., and Tarasconi, P. (2003). Cu(II) complexes with heterocyclic substituted thiosemicarbazones: the case of 5-formyluracil. Synthesis, characterization, x-ray structures, DNA interaction studies, and biological activity. *Inorg. Chem.* 42, 2049–2055. doi: 10.1021/ic026131d
- Borges, A. P., Carneiro, Z. A., Prado, F. S., Souza, J. R., Furlan e Silva, L. H., Oliveira, C. G., et al. (2018). Cu(I) complexes with thiosemicarbazides derived from *p*-toluenesulfonylhydrazide: structural, luminescence and biological studies. *Polyhedron* 155, 170–179. doi: 10.1016/j.poly.2018.08.013
- Brahma, U., Kothari, R., Sharma, P., and Bhandari, V. (2018). Antimicrobial and anti-biofilm activity of hexadentate macrocyclic complex of copper(II) derived from thiosemicarbazide against *Staphylococcus aureus*. *Sci. Rep.* 8:8050. doi: 10.1038/s41598-018-26483-5
- Brunetti, E., Moerkerke, S., Wouters, J., Bartik, K., and Jabin, I. (2016). A selective calix[6]arene-based fluorescent chemosensor for phosphatidylcholine

- type lipids. *Org. Biomol. Chem.* 14, 10201–10207. doi: 10.1039/C6OB01880G
- Burrows, A. D., Mingos, D. M. P., White, A. J. P., and Williams, D. J. (1996). Crystal engineering of metal complexes based on charge-augmented double hydrogen-bond interactions between thiosemicarbazides and carboxylates. *Chem. Commun.* 1996, 97–99. doi: 10.1039/cc9960000097
- Campbell, M. J. M. (1975). Transition metal complexes of thiosemicarbazide and thiosemicarbazones. *Coord. Chem. Rev.* 15, 279–319. doi: 10.1016/S0010-8545(00)80276-3
- Cherenok, S., Vovk, A., Muravyova, I., Shivanyuk, A., Kukhar, V., Lipkowski, J., et al. (2006). Calix[4]arene  $\alpha$ -aminophosphonic acids: asymmetric synthesis and enantioselective inhibition of an alkaline phosphatase. *Org. Lett.* 8, 549–552. doi: 10.1021/ol052469a
- Cherenok, S. O., Yushchenko, O. A., Tanchuk, V. Y., Mischenko, I. M., Samus, N. V., Ruban, O. V., et al. (2012). Calix[4]arene- $\alpha$ -hydroxyphosphonic acids. Synthesis, stereochemistry, and inhibition of glutathione S-transferase. *Arkivoc* 4, 278–298. doi: 10.3998/ark.5550190.0013.421
- Chiesi Villa, A., Manfredotti, A. G., and Guastini, C. (1972). Bis(thiosemicarbazide) copper(II) sulfate. *Cryst. Struct. Commun.* 1:4.
- Cihan-Üstündag, G., Gürsoy, E., Naesens, L., Ulusoy-Güzeldemirci, N., and Çapan, G. (2016). Synthesis and antiviral properties of novel indole-based thiosemicarbazides and 4-thiazolidinones. *Bioorg. Med. Chem.* 24, 240–246. doi: 10.1016/j.bmc.2015.12.008
- Cindro, N., Požar, J., Barišić, D., Bregović, N., Pičuljan, K., Tomaš, R., et al. (2018). Neutral glycoconjugated amide-based calix[4]arenes: complexation of alkali metal cations in water. *Org. Biomol. Chem.* 16, 904–912. doi: 10.1039/C7OB02955A
- Collins, E. M., McKevey, M. A., Madigan, E., Moran, M. B., Owens, M., Ferguson, G., et al. (1991). Chemically modified calix[4]arenes. Regioselective synthesis of 1,3-(distal) derivatives and related compounds. X-ray crystal structure of a diphenol-dinitrile. *J. Chem. Soc. Perkin Trans. 1*, 3137–3142. doi: 10.1039/p19910003137
- Consoli, G. M. L., Granata, G., Galante, E., Di Silvestro, I., Salafia, L., and Geraci, C. (2007). Synthesis of water-soluble nucleotide-calixarene conjugates and preliminary investigation of their *in vitro* DNA replication inhibitory activity. *Tetrahedron* 63, 10758–10763. doi: 10.1016/j.tet.2007.06.123
- Dharmaraj, N., Viswanathamurthi, P., and Natarajan, K. (2001). Ruthenium (II) complexes containing bidentate Schiff bases and their antifungal activity. *Transit. Metal Chem.* 26, 105–109. doi: 10.1023/A:1007132408648
- Dings, R. P., Chen, X., Hellebrekers, D. M., van Eijk, L. I., Zhang, Y., Hoye, T. R., et al. (2006). Design of nonpeptidic topomimetics of antiangiogenic proteins with antitumor activities. *J. Natl. Cancer Inst.* 98, 932–936. doi: 10.1093/jnci/dj247
- Doolan, A. M., Rennie, M. L., and Crowley, P. B. (2018). Protein recognition by functionalized sulfonatocalix[4]arenes. *Chem. Eur. J.* 24, 984–991. doi: 10.1002/chem.201704931
- Du, L. J., Jiao, Y. H., Ye, L. H., Fei, T. H., Wang, Q. Y., Hu, Y. H., et al. (2018). Calixarene-based miniaturized solid-phase extraction of trace triazine herbicides from the honey and milk samples. *Food Anal. Methods* 11, 3283–3292. doi: 10.1007/s12161-018-1270-6
- Durso, A., Brancatelli, G., Hickey, N., Farnetti, E., De Zorzi, R., Bonaccorso, C., et al. (2016). Interactions of a water-soluble calix[4]arene with spermine: solution and solid-state characterisation. *Supramol. Chem.* 28, 499–505. doi: 10.1080/10610278.2015.1125900
- Gaber, M., Fayed, T. A., El-Gamil, M. M., and Abu El-Reash, G. M. (2018). Structural, thermogravimetric, B3LYP and biological studies on some heterocyclic thiosemicarbazide copper(II) complexes and evaluation of their molecular docking. *J. Mol. Struct.* 1151, 56–72. doi: 10.1016/j.molstruc.2017.09.035
- Güniz Küçükgül, S., and Coşkun, G. P. (2016). Macromolecular drug targets in cancer treatment and thiosemicarbazides as anticancer agents. *Anti Cancer Agents Med. Chem.* 16, 1288–1300. doi: 10.2174/1871520616666160219160256
- Gutsche, C. D. (2008). *Calixarenes: An Introduction*. Cambridge: The Royal Society of Chemistry.
- Gutsche, C. D., Dhawan, B., No, K. H., and Muthukrishnan, R. (1981). Calixarenes. 4. The synthesis, characterization, and properties of the calixarenes from *p*-tert-butylphenol. *J. Am. Chem. Soc.* 103, 3782–3792. doi: 10.1021/ja00403a028
- Hernández, W., Vaisberg, A. J., Tobar, M., Álvarez, M., Manzur, J., Echevarría, Y., et al. (2016). *In vitro* antiproliferative activity of palladium(II) thiosemicarbazone complexes and the corresponding functionalized chitosan coated magnetite nanoparticles. *N. J. Chem.* 40, 1853–1860. doi: 10.1039/C5NJ02429C
- Homden, D. M., and Redshaw, C. (2008). The use of calixarenes in metal-based catalysis. *Chem. Rev.* 108, 5086–5130. doi: 10.1021/cr8002196
- Karimi, N., Ghanbarzadeh, B., Hamishehkar, H., Mehramuz, B., and Kafil, H. S. (2018). Antioxidant, antimicrobial and physicochemical properties of turmeric extract-loaded nanostructured lipid carrier (NLC). *Colloid Interface Sci. Commun.* 22, 18–24. doi: 10.1016/j.colcom.2017.11.006
- Liesen, A. P., de Aquino, T. M., Carvalho, C. S., Lima, V. T., de Araujo, J. M., de Lima, J. G., et al. (2010). Synthesis and evaluation of anti-*Toxoplasma gondii* and antimicrobial activities of thiosemicarbazides, 4-thiazolidinones and 1,3,4-thiadiazoles. *Eur. J. Med. Chem.* 45, 3685–3691. doi: 10.1016/j.ejmech.2010.05.017
- Mayer, F., Tiruvadi Krishnan, S., Schuhle, D. T., Eliseeva, S. V., Petoud, S., Toth, E., et al. (2018). Luminescence properties of self-aggregating Tb(III)-DOTA-functionalized calix[4]arenes. *Front. Chem.* 6:1. doi: 10.3389/fchem.2018.00001
- Molnar, M., Tomić, M., and Pavić, V. (2018). Coumarinyl thiosemicarbazides as antimicrobial agents. *Pharm. Chem. J.* 51, 1078–1081. doi: 10.1007/s11094-018-1743-3
- Mostafa, M. M. (2007). Spectroscopic studies of some thiosemicarbazide compounds derived from Girard's T and P. *Spectrochim. Acta* 66, 480–486. doi: 10.1016/j.saa.2006.02.063
- Neri, P., Sessler, J. L., and Wang, M. X. (2016). *Calixarenes and Beyond*. Springer International Publishing, 1–1062.
- Nimse, S. B., and Kim, T. (2013). Biological applications of functionalized calixarenes. *Chem. Soc. Rev.* 42, 366–386. doi: 10.1039/C2CS35233H
- Perret, F., and Coleman, A. W. (2011). Biochemistry of anionic calix[n]arenes. *Chem. Commun.* 47, 7303–7319. doi: 10.1039/c1cc11541c
- Plech, T., Wujec, M., Siwek, A., Kosikowska, U., and Malm, A. (2011). Synthesis and antimicrobial activity of thiosemicarbazides, s-triazoles and their Mannich bases bearing 3-chlorophenyl moiety. *Eur. J. Med. Chem.* 46, 241–248. doi: 10.1016/j.ejmech.2010.11.010
- Quiroga-Campano, C., Gómez-Machuca, H., Moris, S., Jara, P., De la Fuente, J. R., Pessoa-Mahana, H., et al. (2017). Synthesis of bifunctional receptor for fluoride and cadmium based on calix[4]arene with thiourea moieties. *J. Mol. Struct.* 1141, 133–141. doi: 10.1016/j.molstruc.2017.03.089
- Rahimi, M., Karimian, R., Mostafidi, E., Bahojb Noruzi, E., Taghizadeh, S., Shokouhi, B., et al. (2018a). Highly branched amine-functionalized: *p*-sulfonatocalix[4]arene decorated with human plasma proteins as a smart, targeted, and stealthy nano-vehicle for the combination chemotherapy of MCF7 cells. *N. J. Chem.* 42, 13010–13024. doi: 10.1039/C8NJ01790E
- Rahimi, M., Karimian, R., Noruzi, E. B., Ganbarov, K., Zarei, M., Kamounah, F. S., et al. (2019). Needle-shaped amphoteric calix[4]arene as a magnetic nanocarrier for simultaneous delivery of anticancer drugs to the breast cancer cells. *Int. J. Nanomed.* 14, 2619–2636. doi: 10.2147/IJN.S194596
- Rahimi, M., Safa, K. D., and Salehi, R. (2017a). Co-delivery of doxorubicin and methotrexate by dendritic chitosan-g-mPEG as a magnetic nanocarrier for multi-drug delivery in combination chemotherapy. *Polym. Chem.* 8, 7333–7350. doi: 10.1039/C7PY01701D
- Rahimi, M., Shafiei-Irannejad, V., Safa, K. D., and Salehi, R. (2018b). Multi-branched ionic liquid-chitosan as a smart and biocompatible nano-vehicle for combination chemotherapy with stealth and targeted properties. *Carbohydr. Polym.* 196, 299–312. doi: 10.1016/j.carbpol.2018.05.059
- Rahimi, M., Shojaei, S., Safa, K. D., Ghasemi, Z., Salehi, R., Yousefi, B., et al. (2017b). Biocompatible magnetic tris (2-aminoethyl) amine functionalized nanocrystalline cellulose as a novel nanocarrier for anticancer drug delivery of methotrexate. *N. J. Chem.* 41, 2160–2168. doi: 10.1039/C6NJ03332F
- Rane, R. A., Naphade, S. S., Bangalore, P. K., Palkar, M. B., Shaikh, M. S., and Karpoomath, R. (2014). Synthesis of novel 4-nitropyrrole-based semicarbazide and thiosemicarbazide hybrids with antimicrobial and anti-tubercular activity. *Bioorg. Med. Chem. Lett.* 24, 3079–3083. doi: 10.1016/j.bmcl.2014.05.018
- Rao, C. N. R., and Venkataraghavan, R. (1962). The C-S stretching frequency and the “N-C-S bands” in the infrared. *Spectrochim. Acta* 18, 541–547. doi: 10.1016/S0371-1951(62)80164-7

- Rastogi, V. K., Palafox, M. A., Tanwar, R. P., and Mittal, L. (2002). 3, 5-Difluorobenzonitrile: *ab initio* calculations, FTIR and Raman spectra. *Spectrochim. Acta A Mol. Biomol. Spectrosc.* 58, 1987–2004. doi: 10.1016/S1386-1425(01)00650-3
- Salah, B. A., Kandil, A. T., and Abd El-Nasser, M. G. (2018). A therapeutic journey of semicarbazide and thio semicarbazide derivatives and their transition metals complexes: mini review. *Res. Rev. J. Chem.* 7:11.
- Sarkar, T., Ashraf, P. M., Srinives, S., and Mulchandani, A. (2018). Calixarene-functionalized single-walled carbon nanotubes for sensitive detection of volatile amines. *Sens. Actuators B Chem.* 268, 115–122. doi: 10.1016/j.snb.2018.04.078
- Sgarlata, C., Brancatelli, G., Fortuna, C. G., Sciotto, D., Geremia, S., Bonaccorso, C. (2017). Three-dimensional network structures based on pyridyl-calix[4]arene metal complexes. *Chempluschem* 82, 1341–1350. doi: 10.1002/cplu.201700400
- Shafiei-Irannejad, V., Samadi, N., Salehi, B., Yousefi, B., Rahimi, M., Akbarzadeh, A., et al. (2018). Reversion of multidrug resistance by co-encapsulation of doxorubicin and metformin in poly(lactide-co-glycolide)-*d*- $\alpha$ -tocopheryl polyethylene glycol 1000 succinate nanoparticles. *Pharm. Res.* 35:119. doi: 10.1007/s11095-018-2404-7
- Shebl, M., Ibrahim, M. A., Khalil, S. M., Stefan, S. L., and Habib, H. (2013). Binary and ternary copper(II) complexes of a tridentate ONS ligand derived from 2-aminochromone-3 carboxaldehyde and thiosemicarbazide: synthesis, spectral studies and antimicrobial activity. *Spectrochim. Acta A Mol. Biomol. Spectrosc.* 115, 399–408. doi: 10.1016/j.saa.2013.06.075
- Shirakawa, S., and Shimizu, S. (2018). “Inherently chiral calix[4]arenes as supramolecular catalysts,” in *Designed Molecular Space in Material Science and Catalysis*, ed S. Shirakawa (Singapore: Springer), 51–68.
- Silverstein, R. M., Bassler, G. C., and Morrill, T. C. (1991). *Spectrometric Identification of Organic Compounds*, 5th Edn. New York, NY: Wiley.
- Sliwa, W., and Girek, T. (2010). Calixarene complexes with metal ions. *J. Incl. Phenom. Macrocyclic Chem.* 66, 15–41. doi: 10.1007/s10847-009-9678-7
- Sun, Y., Mei, Y., Quan, J., Xiao, X., Zhang, L., Tian, D., et al. (2016). The macroscopic wettable surface: fabricated by calix[4]arene-based host-guest interaction and chiral discrimination of glucose. *Chem. Commun.* 52, 14416–14418. doi: 10.1039/C6CC07956C
- Teixeira, F. A., Marcos, P. M., Ascenso, J. R., Brancatelli, G., Hickey, N., and Geremia, S. (2017). Selective binding of spherical and linear anions by tetraphenyl(thio)urea-based dihomooxalix[4]arene receptors. *J. Org. Chem.* 82, 11383–11390. doi: 10.1021/acs.joc.7b01801
- Tong, Y. X., Su, C. Y., Zhang, Z. F., Kang, B. S., Yu, X. L., and Chen, X. M. (2000). Bis(thiosemicarbazide-S,N)zinc(II) dinitrate. *Acta Crystallogr. Sect. C Cryst. Struct. Commun.* 56, 44–45. doi: 10.1107/S0108270199012974
- Weinstein, M. P., Limbago, B., Patel, J. B., Mathers, A. J., Campeau, S., Mazzulli, T., et al. (2018). *M 100 Performance Standards for Antimicrobial Susceptibility Testing*. Wayne, PA: Clinical and Laboratory Standards Institute.
- William Anthony Coleman, L. G. B. (2010). *Adina Nicoleta Lazar, Mickael Henri Michaud, Sandrine Magnard. Calixarene Derivatives as Anticancer Agent. US Patent 20100056482 A 1.*
- Xie, F., Cai, H., and Peng, F. (2018). Anti-prostate cancer activity of 8-hydroxyquinoline-2-carboxaldehyde-thiosemicarbazide copper complexes *in vivo* by bioluminescence imaging. *J. Biol. Inorg. Chem.* 23, 949–956. doi: 10.1007/s00775-018-1596-y
- Xie, F., and Peng, F. (2018). Anticancer activity of copper complex of (4R)-(-)-2-thioxo-4-thiazolidinecarboxylic acid and 3-rhodaninepropionic acid on prostate and breast cancer cells by fluorescent microscopic imaging. *J. Fluoresc.* 28, 89–96. doi: 10.1007/s10895-017-2177-0
- Yamamoto, T., Sugiyama, S., Akimoto, K., and Hayashi, K. (1992). One-pot synthesis of isothiocyanates from primary amines synthesis using cyanamide? *Org. Preparations Proced. Int.* 24, 346–349. doi: 10.1080/00304949209355899
- Yang, R., Shen, X. Q., Mao, H. Y., Zhang, H. Y., Wu, Q. A., Wang, H., et al. (2006). Synthesis and crystal structure of a novel supra-molecular compound [Co(tsc)2][NPA]2·4H<sub>2</sub>O (tsc = thiosemicarbazide, H<sub>2</sub>NPA = 3-nitro-phthalic acid). *Synth. Reactivity Inorg. Metal Org. Nano Met. Chem.* 36, 617–620. doi: 10.1080/15533170600910538
- Yeon, Y., Leem, S., Wagen, C., Lynch, V. M., Kim, S. K., and Sessler, J. L. (2016). 3-(Dicyanomethylidene)indan-1-one-functionalized calix[4]arene-calix[4]pyrrole hybrid: an ion-pair sensor for cesium salts. *Org. Lett.* 18, 4396–4399. doi: 10.1021/acs.orglett.6b02155
- Yousef, T. A., Abu El-Reash, G. M., El-Gamal, O., and Sharaa, B. M. (2018). Ligational, DFT, optical band gap and biological studies on Mn(II), Co(II) and Ni(II) complexes of ethyl and allyl thiosemicarbazides ending by thiazole group. *J. Mol. Liquids* 251, 423–437. doi: 10.1016/j.molliq.2017.12.022
- Zhang, W.-C., and Huang, Z.-T. (1997). Synthesis of 4-*tert*-butylcalix[4]arenes bearing two Schiff-base units at the lower rim. *Synthesis* 1997, 1073–1076. doi: 10.1055/s-1997-1308

**Conflict of Interest:** The authors declare that the research was conducted in the absence of any commercial or financial relationships that could be construed as a potential conflict of interest.

Copyright © 2019 Bahojb Noruzi, Kheirkhahi, Shaabani, Geremia, Hickey, Asaro, Nitti and Kafil. This is an open-access article distributed under the terms of the Creative Commons Attribution License (CC BY). The use, distribution or reproduction in other forums is permitted, provided the original author(s) and the copyright owner(s) are credited and that the original publication in this journal is cited, in accordance with accepted academic practice. No use, distribution or reproduction is permitted which does not comply with these terms.



# The Hexameric Resorcinarene Capsule as a Brønsted Acid Catalyst for the Synthesis of Bis(heteroaryl)methanes in a Nanoconfined Space

Stefania Gambaro, Pellegrino La Manna, Margherita De Rosa\*, Annunziata Soriente, Carmen Talotta\*, Carmine Gaeta and Placido Neri

Laboratory of Supramolecular Chemistry, Dipartimento di Chimica e Biologia "A. Zambelli", Università degli Studi di Salerno, Salerno, Italy

## OPEN ACCESS

### Edited by:

Ronald K. Castellano,  
University of Florida, United States

### Reviewed by:

Richard J. Hooley,  
University of California, Riverside,  
United States

Adam Urbach,  
Trinity University, United States  
Konrad Tiefenbacher,  
ETH Zürich, Switzerland

### \*Correspondence:

Margherita De Rosa  
maderosa@unisa.it  
Carmen Talotta  
ctalotta@unisa.it

### Specialty section:

This article was submitted to  
Supramolecular Chemistry,  
a section of the journal  
Frontiers in Chemistry

**Received:** 30 August 2019

**Accepted:** 04 October 2019

**Published:** 22 October 2019

### Citation:

Gambaro S, La Manna P, De Rosa M, Soriente A, Talotta C, Gaeta C and Neri P (2019) The Hexameric Resorcinarene Capsule as a Brønsted Acid Catalyst for the Synthesis of Bis(heteroaryl)methanes in a Nanoconfined Space. *Front. Chem.* 7:687. doi: 10.3389/fchem.2019.00687

Herein, we show that the hexameric resorcinarene capsule **C** is able to catalyze the formation of bis(heteroaryl)methanes by reaction between pyrroles or indoles and carbonyl compounds ( $\alpha$ -ketoesters or aldehydes) in excellent yields and selectivity. Our results suggest that the capsule can play a double catalytic role as a H-bond catalyst, for the initial activation of the carbonyl substrate, and as a Brønsted acid catalyst, for the dehydration of the intermediate alcohol.

**Keywords:** supramolecular organocatalysis, resorcinarene hexameric capsule, bis(heteroaryl)methanes, self-assembly, H-bond catalyst, Brønsted acid catalyst

## INTRODUCTION

Supramolecular organocatalysis is an emerging area in supramolecular chemistry whose principal aim is the design of novel systems able to perform catalytic functions mimicking the chemo-, regio-, and stereoselectivity of the natural enzymes (Conn and Rebek, 1997). At this regard, much attention has been focused on designing self-assembled molecular capsules (MCs) able to catalyze organic reaction by confinement of the reactants in their internal cavity (Borsato and Scarso, 2016; Catti et al., 2016; Gaeta et al., 2019). MCs are self-assembled structures sealed by weak non-covalent interactions between the single complementary units. Resembling to an enzyme pocket, the nanoconfined space inside a self-assembled molecular capsule allows the formation of a microenvironment with different physical and chemical features with respect to the external medium. In fact, the nanoconfinement of the reactants inside a MC slows down their molecular mobility determining a different stereo- and regiochemical outcome of the reaction with respect to the bulk conditions. Analogously to the natural systems, when the reactants are hosted inside a MC, the proximity effect between them and the stabilization of the intermediates and transition states induces a reaction acceleration.

Interestingly, Atwood and MacGillivray reported an interesting example of self-assembled capsule **C** ( $\text{I}_6 \cdot (\text{H}_2\text{O})_8$ ) (Figure 1; MacGillivray and Atwood, 1997), which is constituted by six resorcin[4]arene units **1** sealed by eight water molecules, and shows an hydrophobic cavity with an internal volume of  $1,375 \text{ \AA}^3$ . The six resorcinarene units and the eight water molecules are located, respectively, on the sides and on the corners of a cube, and the aggregate is sealed by 60 ( $\text{O} \cdots \text{H} \cdots \text{O}$ ) hydrogen bonding interactions. The 8 bridged-water molecules establish H-bonds with



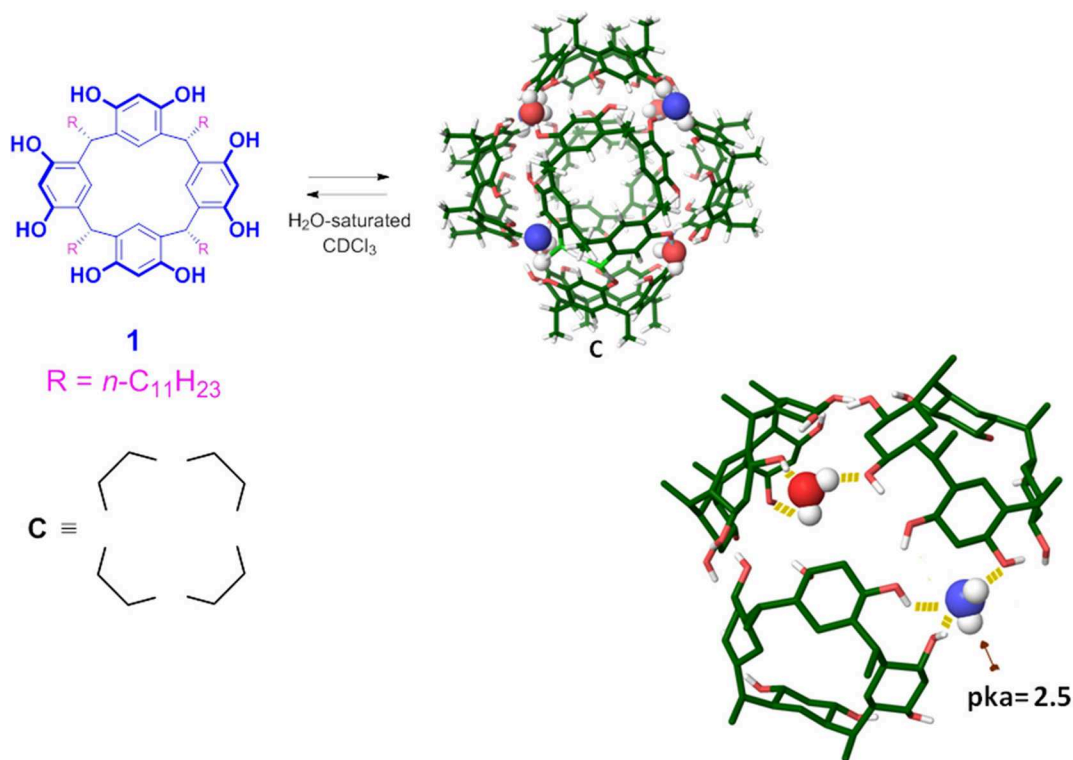


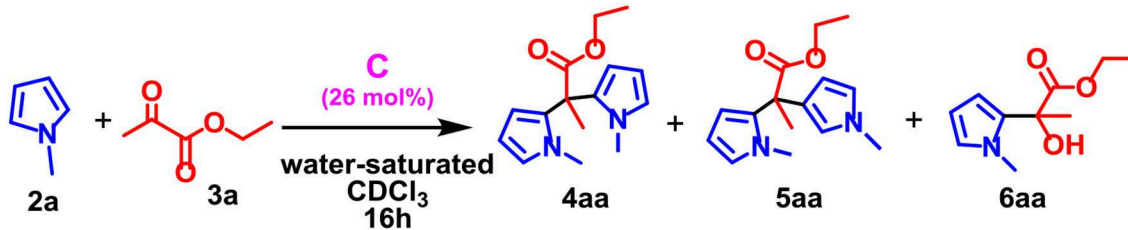
**FIGURE 1** | Chemical drawing of the C-undecyl-resorcin[4]arene **1**. Tube model of the hexameric capsule **C**, the undecyl chains have been omitted for clarity. Chemical drawing of the model representing the hydrogen bond belt between the eight bridged water molecules and the six resorcinarene molecules, in blue the bridging water molecule with one H-bond donating free valence.

the adjacent resorcinol OH groups and, in particular, four of them act as double H-bonds donor (**Figure 1**, H<sub>2</sub>O drawing in red) and single H-bond acceptor, saturating in this way their H-bonding valence. The other four bridged-water molecules act as single H-bond acceptor and single H-bond donor (**Figure 1**, blu), remaining with one H-bond donating free valence. Cohen et al. (Avram and Cohen, 2002b) demonstrated by NMR diffusion experiments, that the capsule **C** is self-assembled also in solution when water-saturated chloroform or benzene is used as a solvent.

The capsule **C** is able to accommodate eight benzene (or chloroform) molecules inside its cavity (Avram and Cohen, 2002a,b, 2004; Shivanyuk and Rebek, 2003). Numerous studies showed that **C** is also able to host in its  $\pi$ -electron rich cavity, complementary guests by H-bonding and/or cation- $\pi$  interactions (Shivanyuk and Rebek, 2001; Avram and Cohen, 2002a; Yamanaka et al., 2004; Evan-Salem et al., 2006). Tiefenbacher et al. demonstrated that **C** behaves as a Brønsted acid (Zhang and Tiefenbacher, 2013; Köster and Tiefenbacher, 2018). In particular, their studies revealed that the hexameric aggregate has an estimated  $pK_a$  value of about 5.5–6.0, a value certainly not comparable with that of the single resorcinarene unit. The acidic behavior of **C** is explained by the stabilization of its conjugate-base due to the delocalization of its negative charge over the phenolic groups and water molecules of the assembly. QM calculations, recently reported by our group (La Manna et al., 2018b) estimated a local  $pK_a$  of  $\approx 2.5$  for the bridged-water

molecules with one H-bond donating free valence (in blue in **Figure 1**), while the mean  $pK_a$  value of all OH groups of **C** is 6.1, in agreement with the experimental datum.

Several reports clearly show that the mild Brønsted acidity of **C** and its ability to stabilize cationic transition states, are crucial factors for the catalytic activity of the capsule (Borsato and Scarso, 2016; Catti et al., 2016; Gaeta et al., 2019). Thus, amazing results have been reported in the last decade regarding the catalysis of chemical reactions into the nanoconfined space of the self-assembled capsule **C**, including the cyclization of terpenes (Zhang and Tiefenbacher, 2015, 2019; Zhang et al., 2017, 2018, 2019; Pahima et al., 2019), the hydration of the alkynes (La Sorella et al., 2016a), the carbonyl-olefin metathesis (Catti and Tiefenbacher, 2018), the sulfoxidation of thioethers (La Sorella et al., 2016b), the synthesis of substituted 1-H-tetrazoles (Giust et al., 2015), the activation of C-F bonds (Köster et al., 2019), and the iminium catalysis (Bräuer et al., 2017; La Manna et al., 2018a). Recently, we showed that the capsule **C** acts as a nanoreactor for a Friedel-Crafts alkylation of arenes and heteroarenes with benzyl chloride (La Manna et al., 2018b) under mild metal-free conditions. We showed that the bridged-water molecules with one H-bond donating free valence exert a crucial role in the activation of the C-Cl bond of benzyl chloride by H-bonding interaction. Analogously, the H-bond donor abilities of the water molecules of **C** have been exploited in the activation of  $\beta$ -nitrostyrenes toward the Michael reaction using pyrroles and indoles as nucleophiles (Gambaro et al., 2019).

**TABLE 1** | Optimization of reaction conditions for the synthesis of BHMs catalyzed by **C**.


Entry <sup>a</sup>	Capsule	T (°C)	2a/3a	Yield (%) <sup>b</sup>	4aa (%) <sup>c</sup>	5aa (%) <sup>c</sup>	6aa (%) <sup>c</sup>
1	No	30	1/1	—	—	—	—
	Yes			35	23	4	8
2	No	50	1/1	—	—	—	—
	Yes			43	30	4	9
3	No	10	1/1	—	—	—	—
	Yes			20	10	5	5
4	No	30	2/1	—	—	—	—
	Yes			60	40	5	15
5	No	30	4/1	—	—	—	—
	Yes			98	60	10	28

<sup>a</sup>Reactions were performed on a 0.16 mmol scale using **2a** (from 1 to 4 equiv.), **3a** (1 equiv.), and capsule **C** (0.26 equiv.) in water saturated  $\text{CDCl}_3$  (1.1 mL) under stirring for 16 h.

<sup>b</sup>Overall yield of all the isolated products. <sup>c</sup>Yields of the isolated products by chromatography on column.

As a part of our research program focused on the extension of the catalytic opportunities offered by the hexameric capsule **C**, we turned our attention to the synthesis of bis(heteroaryl)methanes (BHM) (Palmieri et al., 2010; Shiri et al., 2010; Shiri, 2012). BHM are fundamental building blocks in the synthesis of natural and unnatural porphyrin derivatives (Cho and Lee, 1998; Burrell et al., 2001; Laha et al., 2003). Moreover, they find applications in several fields, ranging from medicine (Sivaprasad et al., 2006; Awuah and You, 2012; Josefsen and Boyle, 2012) to environment and industry (Kursunlu et al., 2012). In particular, bis(indol)methanes (BIM) and bis(pyrrole)methanes, containing two simple or two substituted heteroaryl moieties are molecules with interesting biological properties (Sakemi and Sun, 1991; Gunasekera et al., 1994; Fürstner, 2003; Bao et al., 2005). This class of products is generally obtained by means of strategies relying upon the use of Brønsted (Palmieri et al., 2010; Shiri et al., 2010; Shiri, 2012) and Lewis acids (Ji et al., 2004; Guo et al., 2009; Ling et al., 2019; Qiang et al., 2019; Wu et al., 2019), strong Brønsted acids (Biaggi et al., 2006; Singh et al., 2011; Lucarini et al., 2013; Norouzi et al., 2018; Tran et al., 2018), and electrochemical methods (Du and Huang, 2018).

## RESULTS AND DISCUSSION

Prompted by these considerations and considering our interest in the development of novel organocatalytic strategies, we attempted the synthesis of BHMs derivatives by reaction between

aromatic heterocycles and aldehydes and pyruvates in the presence of capsule **C** as a Brønsted acid catalyst. At this regard, as a model reaction for investigating the catalytic performance of **C**, we chose the reaction between pyrrole **2a** and ethyl pyruvate **3a** in **Table 1**.

We started performing the reaction in **Table 1** in the presence of capsule **C** in water-saturated  $\text{CDCl}_3$  at 30°C and with a 1/1 ratio of **2a/3a**. It was found that the reaction proceeded smoothly to afford preferentially *meso*- $\alpha,\alpha$ -substituted dipyrromethane **4aa** in 23% yield, accompanied by a negligible amount of  $\alpha,\beta$ -linked dipyrromethane **5aa** and monoalkylated adduct **6aa** (entry 1, **Table 1**). No evidence was detected of higher oligomers and other side products. In contrast, when the reaction in **Table 1** was carried out under the same reaction conditions but in the absence of capsule **C**, no products could be evidenced (entry 1, **Table 1**). This result encouraged us to carry out a study for the optimisation of the reaction parameters in order to improve the reaction efficiency.

Initially, the influence of the reaction temperature was investigated (**Table 1**, entries 1–3). When the temperature was decreased to 10°C, both reaction efficiency and selectivity dropped (entry 3, **Table 1**), while an increase in the temperature had a little positive effect on the reaction outcome (entry 4, **Table 1**). Next, we moved to examine the molar ratio of **2a/3a** on the yield of the reaction in **Table 1**. When an excess of **2a** was used, an increase of the reaction efficiency in terms of yield was observed while keeping the selectivity for the adducts substantially unchanged, with the preferential formation of **4aa**

(entries 4–5, **Table 1**). These preliminary results indicated that capsule **C** was capable to promote the reaction in selective and efficient way and suggested that the reaction took place inside the cavity of **C**.

In order to confirm this conclusion, and in accord to a protocol previously reported by us and other groups (Bräuer et al., 2017; La Manna et al., 2018a), we performed a series of control experiments. In details, when the reaction between

**TABLE 2** | Scope of the reaction between different pyrroles **2a–d** and  $\alpha$ -ketoesters **3a–f**.

<p> <b>2a–d</b>      <b>3a–f</b>      <b>C</b> (26 mol%)              water-saturated <math>\text{CDCl}_3</math> 16h  <b>4xx</b>      <b>5xx</b>      <b>7xx</b>      <b>6xx</b> </p>								
<p> <b>a:</b> <math>\text{R}_2 = \text{Me}</math>  <b>b:</b> <math>\text{R}_2 = \text{H}</math>  <b>c:</b> <math>\text{R}_2 = \text{Ph}</math>  <b>d:</b> <math>\text{R}_2 = \text{Bn}</math> </p>								
<p> <b>a:</b> <math>\text{R} = \text{Me}, \text{R}_1 = \text{Et}</math>  <b>b:</b> <math>\text{R} = \text{Me}, \text{R}_1 = \text{Me}</math>  <b>c:</b> <math>\text{R} = i\text{-Pr}, \text{R}_1 = \text{Et}</math>  <b>d:</b> <math>\text{R} = \text{Me}, \text{R}_1 = \text{Bn}</math>  <b>e:</b> <math>\text{R} = \text{Me}, \text{R}_1 = \text{H}</math>  <b>f:</b> <math>\text{R} = \text{CF}_3, \text{R}_1 = \text{Me}</math> </p>								
Entry <sup>a</sup>	Capsule	2	3	Yield (%) <sup>b</sup>	% ( <b>4xx</b> ) <sup>c</sup>	% ( <b>5xx</b> ) <sup>c</sup>	% ( <b>6xx</b> ) <sup>c</sup>	% ( <b>7xx</b> ) <sup>c</sup>
<b>1</b>	No	<b>2a</b>	<b>3a</b>	—	—	—	—	—
	Yes	<b>2a</b>	<b>3a</b>	98	60 ( <b>4aa</b> )	10 ( <b>5aa</b> )	28 ( <b>6aa</b> )	—
<b>2<sup>d</sup></b>	No	<b>2a</b>	<b>3b</b>	—	—	—	—	—
	Yes	<b>2a</b>	<b>3b</b>	99	90 ( <b>4ab</b> )	—	—	—
<b>3</b>	No	<b>2a</b>	<b>3c</b>	—	—	—	—	—
	Yes	<b>2a</b>	<b>3c</b>	55	—	—	55 ( <b>6ac</b> )	—
<b>4</b>	No	<b>2a</b>	<b>3d</b>	—	—	—	—	—
	Yes	<b>2a</b>	<b>3d</b>	76	38 ( <b>4ad</b> )	38 ( <b>5ad</b> )	—	—
<b>5<sup>e</sup></b>	No	<b>2a</b>	<b>3e</b>	—	—	—	—	—
	Yes	<b>2a</b>	<b>3e</b>	64	—	—	—	—
<b>6</b>	No	<b>2a</b>	<b>3f</b>	35	—	—	35 ( <b>6af</b> )	—
	Yes	<b>2a</b>	<b>3f</b>	99	—	—	99 ( <b>6af</b> )	—
<b>7</b>	No	<b>2b</b>	<b>3a</b>	—	—	—	—	—
	Yes	<b>2b</b>	<b>3a</b>	99	99 ( <b>4ba</b> )	—	—	—
<b>8</b>	No	<b>2b</b>	<b>3f</b>	38	—	—	38 ( <b>6bf</b> )	—
	Yes	<b>2b</b>	<b>3f</b>	98	—	—	98 ( <b>6bf</b> )	—
<b>9</b>	No	<b>2c</b>	<b>3a</b>	—	—	—	—	—
	Yes	<b>2c</b>	<b>3a</b>	50	—	—	—	50 ( <b>7ca</b> )
<b>10</b>	No	<b>2d</b>	<b>3a</b>	—	—	—	—	—
	Yes	<b>2d</b>	<b>3a</b>	65	—	—	65 ( <b>6da</b> )	—

<sup>a</sup>Reactions were performed on a 0.16 mmol scale using **2a–d** (4 equiv.), **3a–e** (1 equiv.), and capsule **C** (0.26 equiv.) in water saturated  $\text{CDCl}_3$  (1.1 mL) under stirring for 16 h at 30°C.

<sup>b</sup>Overall yield of all the isolated products. <sup>c</sup>Yields of the isolated products by chromatography on column. <sup>d</sup>9% of adduct of pyrrole with two molecules of pyruvate is present; see **Supporting Information**. <sup>e</sup>Decarboxylated product is present, see **Supporting Information**.

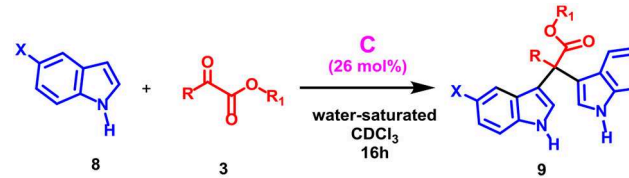
**2a** and **3a** was conducted under the conditions reported in **Table 1** in the presence of **C** and of tetraethylammonium tetrafluoroborate, which is a known competitive guest, no hint of products were detected after 16 h at 50°C. Under these conditions, the ammonium guest occupying the cavity of capsule **C** acts as an inhibitor. In addition, the  $^1\text{H}$  NMR spectrum of the reaction mixture in the presence of tetraethylammonium tetrafluoroborate in **Figure S3** featured shielded signals at negative chemical shifts values attributable to the cation inside the cavity of **C**. Finally, no hint of products was observed when the reaction reported in **Table 1** was performed in the presence of DMSO (**Figure S4**), a hydrogen-bonding competitor solvent able to disaggregate the capsule **C**.

With these results in hand, we next studied the generality of the reaction with regard to both reactants (**Table 2**). Initially, we evaluated the influence of the  $\alpha$ -ketoester structure on the reaction outcome. When  $\alpha$ -ketoester **3c**, bearing an isopropyl group, was reacted with **2a** in the presence of **C** (26 mol%), the formation of the mono-alkylated adduct **6ac** was observed with a yield of 55% (entry 3, **Table 2**), while no hint of other products was detected. Interestingly, under analogous conditions the  $\alpha$ -ketoester **3b** ( $R = \text{Me}$ ) reacted with **2a** giving the *meso*-dipyrromethane product **4ab** (entry 2, **Table 2**) in 90% yield. Probably, by increasing the steric encumbrance of the  $R$  group of **3** from methyl (**3b**) to isopropyl (**3c**) the formation of the di-pyrromethane was hindered. When **3d** (entry 4, **Table 2**), bearing a benzyloxy group, was used as substrate alongside **2a**, then the formation of the double alkylated adducts  $\alpha,\alpha$  and  $\alpha,\beta$  **4ad** and **5ad** was observed in a 1/1 ratio and with a complete loss of selectivity. Differently, using **3b** (entry 2, **Table 2**) only the  $\alpha,\alpha$  adduct **4ab** was obtained. Interestingly, when **3f** bearing an electron-withdrawing trifluoromethyl group was used, the reaction in **Table 2** was almost quantitative displaying a complete selectivity for the mono-alkylated adduct **6af** and no evidence of bis-adduct or other side products (entry 6, **Table 2**). Finally, with  $\alpha$ -ketoacid **3e** no reaction took place and a decarboxylate product was recovered.

At this point, we examined effect of the substitution at the pyrrole nitrogen atom on the reaction outcome. The reaction between pyrrole **2b** and **3a** selectively delivered the *meso* bis-adduct **4ba** in high yield (entry 7, **Table 2**). Even with pyrrole **2b**, the reaction with **3f** afforded to mono-adduct **6bf** as the only reaction product (entry 8, **Table 2**), indicating that the choice of the ketoester influenced the outcome of the reaction.

When a more sterically demanding group was introduced on the nitrogen atom of pyrrole, the yield of the reaction in **Table 2** decreased and the selectivity of the products was influenced. In fact, when pyrrole **2c**, bearing a *N*-benzyl group, was used with **3a** under the conditions reported in **Table 2**, then the mono-adduct **6da** was obtained selectively and in good yield (entry 10, **Table 2**), whereas with *N*-phenyl pyrrole **2d** we observed for the first time the selective formation of a  $\beta, \beta$ -di-adduct (**7ca**) (entry 9, **Table 2**). When the reaction was performed using indole derivatives (**Table 3**), only the formation of di-pyrromethane  $\beta, \beta$ -**9** was observed in high yield

**TABLE 3** | Scope of the reaction with different indoles.



$\text{a: X = H}$   
 $\text{b: X = Me}$   
 $\text{c: X = OMe}$   
 $\text{d: R = Br}$

$\text{b: R = Me, R}_1 = \text{Me}$   
 $\text{d: R = Me, R}_1 = \text{Bn}$

Entry <sup>a</sup>	Capsule	8	3	Yield (%) <sup>b</sup>
1	No	<b>8a</b>	<b>3b</b>	—
	Yes			86
2	No	<b>8b</b>	<b>3b</b>	—
	Yes			90
3	No	<b>8c</b>	<b>3b</b>	—
	Yes			88
4	No	<b>8d</b>	<b>3b</b>	—
	Yes			85
5	No	<b>8a</b>	<b>3d</b>	—
	Yes			80

<sup>a</sup>Reactions were performed on a 0.16 mmol scale using **8** (4 equiv.), **3** (1 equiv.), and capsule **C** (0.26 equiv.) in water saturated  $\text{CDCl}_3$  (1.1 mL) under stirring for 16 h at 30°C.

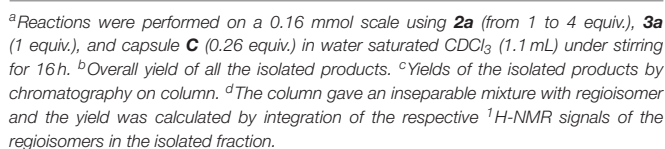
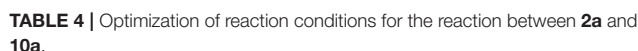
<sup>b</sup>Isolated yield.

independently of the substituents present on the benzene and pyrrole rings.

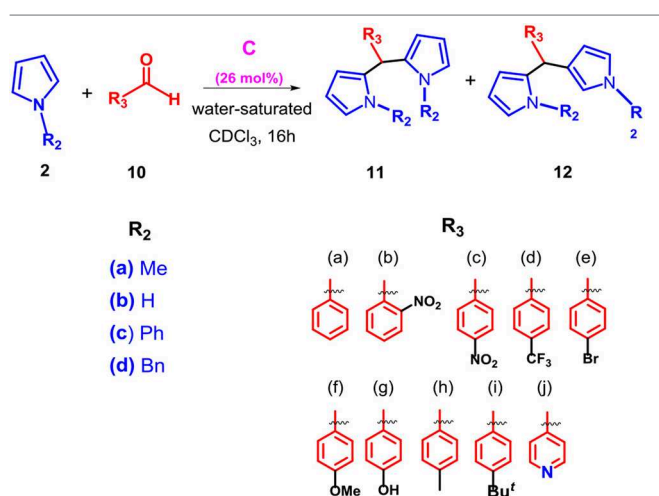
The mechanism proposed for the formation of  $\alpha,\alpha$ -substituted dipyrromethane **4xx** and monoalkylated adduct **6xx** in the nanoconfined space inside the capsule **C**, is outlined in **Scheme 1**. In detail,  $\alpha$ -ketoester **3** is probably stabilized inside the capsule **C** through the formation of a H-bonding interaction with a bridged water molecule (**Scheme 1**).

Previously, we have already shown that pyrrole derivatives are hosted inside the cavity of **C** (La Manna et al., 2018b). At this point, an  $\alpha$ -attack of pyrrole to the activated ketone group of **3** occurs inside the capsule, leading to intermediate **I** (**Scheme 1**) stabilized through H-bonding and cation $\cdots\pi$  interactions, which is re-aromatized to **6xx**. On the basis of the local acidity ( $\text{pK}_a$  of  $\approx 2.5$ ) of the bridged water molecules with H-bond donating free valence, the product **6xx** can be protonated inside the capsule **C** (**II** in **Scheme 1**) and converted to carbocation **III** by losing a water molecule. **III** undergoes an  $\alpha$ -attack of a new pyrrole molecule to give the carbocation **IV** which is stabilized by cation $\cdots\pi$  interactions. This latter is rearomatized to **4xx**, by losing the  $\beta$ -proton and recovering the electroneutrality of the capsule **C**. The mechanism proposed in **Scheme 1** is corroborated by the finding that  $\alpha$ -ketoester





On the basis of these results and in order to extend the scope of the reaction between **2** and carbonyl compounds in the presence of **C**, we studied the procedure with a different carbonyl compound such as benzaldehyde **10a** (**Table 4**). When the substrates **2a** and **10a** were mixed in 1/1 ratio in the presence of **C** in water-saturated CDCl<sub>3</sub> then  $\alpha,\alpha$ -dipyrromethane **11a** was obtained in 34% yield with a regioselectivity ratio of 8.5/1 (entry 1, **Table 4**) with respect to the  $\alpha,\beta$ -isomer **12a**. Interestingly, when the **2a/10a** molar ratio was progressively increased to 2/1 and to 4/1 then the efficiency of the reaction was improved with a 54 and 87% yield of **11a**, respectively (entries 2 and 3, **Table 4**). Interestingly, no hint of product **11a** and **12a** were detected in the reaction mixture in the absence of capsule **C**. The lowering of the reaction temperature from 50 to 25°C (entry 4 in **Table 4**) gives rise to a drop in the yield of **11a**. Once the reaction conditions were optimized (**Table 4**), the substrate scope was then evaluated in order to determine the generality of the reaction.

**TABLE 5 |** Scope of the reaction with different pyrroles **2a–d** and aldehydes **10a–j**.

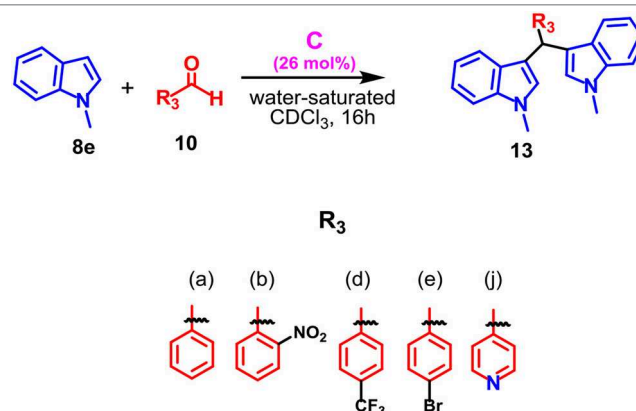
Entry <sup>a</sup>	Capsule	2	10	Yield(%) <sup>b</sup>	% (11) <sup>c</sup>	% (12) <sup>c</sup>
1	No	2b	10a	—	—	—
	Yes			70	70 (11ba) <sup>e</sup>	—
2	No	2c	10a	—	—	—
	Yes			—	—	—
3	No	2d	10a	—	—	—
	Yes			—	—	—
4	No	2a	10b	—	—	—
	Yes			99	90 (11ab)	9 (12ab)
5	No	2a	10c	—	—	—
	Yes			98	96 (11ac)	2 (12ac) <sup>d</sup>
6	No	2a	10d	—	—	—
	Yes			98	88 (11ad)	10 (12ad)
7	No	2a	10e	—	—	—
	Yes			95	93 (11ae)	2 (11ae) <sup>d</sup>
8 <sup>f</sup>	No	2a	10f	—	—	—
	Yes			98	96 (11af)	2 (12af) <sup>d</sup>
9 <sup>f</sup>	No	2a	10g	—	—	—
	Yes			98	96 (11ag)	2 (12ag) <sup>d</sup>
10	No	2a	10h	—	—	—
	Yes			97	95 (11ah)	2 (12ah) <sup>d</sup>

(Continued)

**TABLE 5 |** Continued

Entry <sup>a</sup>	Capsule	2	10	Yield(%) <sup>b</sup>	% (11) <sup>c</sup>	% (12) <sup>c</sup>
11	No	2a	10i	—	—	6 (12ai)
	Yes			97	91 (11ai)	—
12	No	2a	10j	—	—	—
	Yes			85	76 (11aj) <sup>d</sup>	9 (12aj) <sup>d</sup>

<sup>a</sup>Reactions were performed on a 0.16 mmol scale using **2a–d** (4 equiv.), **10a–j** (1 equiv.), and capsule **C** (0.26 equiv.) in water saturated  $\text{CDCl}_3$  (1.1 mL) under stirring for 16 h at 50°C. <sup>b</sup>Overall yield of all the isolated products. <sup>c</sup>Yields of the isolated products by chromatography on column. <sup>d</sup>The column gave an inseparable mixture with the regioisomer and the yield was calculated by integration of the respective <sup>1</sup>H-NMR signals of the regioisomers in the isolated fraction. <sup>e</sup><sup>1</sup>H NMR spectrum on crude reaction mixture showed presence of other species obtained after chromatography purification as a complex and inseparable fraction not characterized. <sup>f</sup>These reactions were performed under stirring for 48 h at 50°C.

**TABLE 6 |** Scope of the reaction between indole **8e** and various aldehydes **10a, b, d, e, j**.

Entry <sup>a</sup>	Capsule	Yield (%) <sup>b</sup>
1	No	—
	Yes	97 (11ea)
2	No	—
	Yes	99 (11eb)
3	No	—
	Yes	98 (11ed)
4	No	—
	Yes	98 (11ee)
5	No	—
	Yes	98 (11ej)

<sup>a</sup>Reactions were performed on a 0.16 mmol scale using **8e** (4 equiv.), **10** (1 equiv.), and capsule **C** (0.26 equiv.) in water saturated  $\text{CDCl}_3$  (1.1 mL) under stirring for 16 h at 50°C. <sup>b</sup>Isolated yield.

As regards the effect of the substitution at the pyrrole nitrogen atom, we found that the introduction of a more hindering group, such as a phenyl or benzyl group, caused a complete loss of reactivity (entries 2–3, **Table 5**). Instead, the reaction with unsubstituted pyrrole **2b** proceeded with a small decrease in yield but preserving the selectivity for adduct **11a** (entry 1, **Table 5**). Interestingly, under the conditions reported in **Table 5** no hint of mono-adduct heteroaryl methane was observed. Successively, we investigated the generality of the reaction between **2a** and several aromatic aldehydes bearing electron-donating or -withdrawing groups (**Table 5**).

The protocol was found to be tolerant to a variety of aromatic aldehydes **10a–j**, independently by the electronic nature and position of the substituents on the aryl group, affording  $\alpha,\alpha$ -adducts **11** in high yields and excellent regioselectivities. In fact, the double attack took place in a completely regioselective way to give **11** as almost the only product with a negligible amount of the corresponding isomer **12**. No evidence of monoalkylated adduct was observed. Additionally, when the protocol was extended to the *N*-methyl indole **8e**, the reaction proceeded smoothly and the adduct **13** was obtained as the only product in high yield (**Table 6**).

## CONCLUSIONS

The resorcinarene hexameric capsule **C** is able to catalyze the reaction between pyrroles or indoles and  $\alpha$ -ketoesters or aldehydes for the formation of bis(heteroaryl)methanes. The reactions take place in the nanoconfined space inside the capsule **C**. The observed results suggested its double catalytic function: **C** can act as H-bond catalyst for the initial activation of the carbonyl functions and as a Brønsted acid catalyst for the dehydration

of the intermediate alcohol. Generally, in the presence of **C** the formation of the  $\alpha,\alpha$ -bis(heteroaryl)methanes occurs with excellent yields and regioselectivity with respect to the  $\alpha,\beta$ - or  $\beta,\beta$ -regioisomers.

## DATA AVAILABILITY STATEMENT

All experimental data are reported in the **Supplementary Material**.

## AUTHOR CONTRIBUTIONS

SG and PL performed the experiments. CT performed NMR studies. CG, AS, and PN participated in manuscript preparation. CT and MD prepared the manuscript.

## ACKNOWLEDGMENTS

The authors thank the Regione Campania (POR CAMPANIAFESR 2007/2013 O.O.2.1, CUP B46D14002660009) for the FT-ICR mass spectrometer facilities, the Farma-BioNet (CUPB25C13000230007), and the Centro di Tecnologie Integrate per la Salute (CITIS) (project PONa3\_00138) for the 600 MHz NMR facilities. Financial support is acknowledged from the Università di Salerno (FARB 2017 Composti Macro ciclici come Organocatalizzatori Supramolecolari in Catalisi Biomimetica).

## SUPPLEMENTARY MATERIAL

The Supplementary Material for this article can be found online at: <https://www.frontiersin.org/articles/10.3389/fchem.2019.00687/full#supplementary-material>

## REFERENCES

- Avram, L., and Cohen, Y. (2002a). The role of water molecules in a resorcinarene capsule as probed by NMR diffusion measurements. *Org. Lett.* 4, 4365–4368. doi: 10.1021/ol0271077
- Avram, L., and Cohen, Y. (2002b). Spontaneous formation of hexameric resorcinarene capsule in chloroform solution as detected by diffusion NMR. *J. Am. Chem. Soc.* 124, 15148–15149. doi: 10.1021/ja0272686
- Avram, L., and Cohen, Y. (2004). Self-recognition, structure, stability, and guest affinity of pyrogallol[4]arene and resorcin[4]arene capsules in solution. *J. Am. Chem. Soc.* 126, 11556–11563. doi: 10.1021/ja047698r
- Awuah, S. G., and You, Y. (2012). Boron dipyrromethene (BODIPY)-based photosensitizers for photodynamic therapy. *RSC Adv.* 2, 11169–11183. doi: 10.1039/c2ra21404k
- Bao, B., Sun, Q., Yao, X., Hong, J., Lee, C. O., Sim, C., et al. (2005). Cytotoxic bisindole alkaloids from a marine sponge *Spongosorites* sp. *J. Nat. Prod.* 68, 711–715. doi: 10.1021/np049577a
- Biaggi, C., Benaglia, M., Raimondi, L., and Cozzi, F. (2006). Organocatalytic synthesis of dipyrromethanes by the addition of *N*-methylpyrrole to aldehydes. *Tetrahedron* 62, 12375–12379. doi: 10.1016/j.tet.2006.09.104
- Borsato, G., and Scarso, A. (2016). “Catalysis within the Self-Assembled Resorcin[4]arene Hexamer,” in *Organic Nanoreactors*, ed S. Sadjadi (London: Academic Press), 203–234. doi: 10.1016/B978-0-12-801713-5.00007-0
- Bräuer, T. M., Zhang, Q., and Tiefenbacher, K. (2017). Iminium catalysis inside a self-assembled supramolecular capsule: scope and mechanistic studies. *J. Am. Chem. Soc.* 139, 17500–17507. doi: 10.1021/jacs.7b08976
- Burrell, K. A., Officer, D. L., Plieger, P. G., and Reid, D. C. W. (2001). Synthetic routes to multiporphyrin arrays. *Chem. Rev.* 101, 2751–2796. doi: 10.1021/cr0000426
- Catti, L., and Tiefenbacher, K. (2018). Brønsted acid-catalyzed carbonyl-olefin metathesis inside a self-assembled supramolecular host. *Angew. Chem. Int. Ed.* 57, 14589–14592. doi: 10.1002/anie.201712141
- Catti, L., Zhang, Q., and Tiefenbacher, K. (2016). Advantages of catalysis in self-assembled molecular capsules. *Chem. Eur. J.* 22, 9060–9066. doi: 10.1002/chem.201600726
- Cho, W.-S., and Lee, C.-H. (1998). Convenient synthesis of difurylmethanes and dithienylmethanes and their application to the syntheses of core-modified porphyrins. *Bull. Korean Chem. Soc.* 19, 314–319. doi: 10.1002/chin.199838113
- Conn, M. M., and Rebek, J. Jr. (1997). Self-assembling capsules. *Chem. Rev.* 97, 1647–1668. doi: 10.1021/cr9603800
- Du, K.-S., and Huang, J.-M. (2018). Electrochemical synthesis of bisindolylmethanes from indoles and ethers. *Org. Lett.* 20, 2911–2915. doi: 10.1021/acs.orglett.8b00968
- Evan-Salem, T., Baruch, I., Avram, L., Cohen, Y., Palmer, L. C., and Rebek, J. Jr. (2006). Resorcinarenes are hexameric capsules in solution. *Proc. Natl. Acad. Sci. U.S.A.* 103, 12296–12300. doi: 10.1073/pnas.0604757103
- Fürstner, A. (2003). Chemistry and biology of roseophilin and the prodigiosin alkaloids: a survey of the last 2500 years. *Angew. Chem. Int. Ed.* 42, 3582–3603. doi: 10.1002/anie.200300582
- Gaeta, C., Talotta, C., De Rosa, M., La Manna, P., Soriente, A., and Neri, P. (2019). The hexameric resorcinarene capsule at work: supramolecular catalysis in confined spaces. *Chem. Eur. J.* 25, 4899–4913. doi: 10.1002/chem.201805206
- Gambaro, S., De Rosa, M., Soriente, A., Talotta, C., Floresta, G., Rescifina, A., et al. (2019). A hexameric resorcinarene capsule as a hydrogen bonding catalyst in the conjugate addition of pyrroles and indoles to nitroalkenes. *Org. Chem. Front.* 6, 2339–2347. doi: 10.1039/C9QO00224C

- Giusti, S., La Sorella, G., Sporni, L., Fabris, F., Strukul, G., and Scarso, A. (2015). Supramolecular catalysis in the synthesis of substituted 1 H-tetrazoles from isonitriles by a self-assembled hexameric capsule. *Asian J. Org. Chem.* 4, 217–220. doi: 10.1002/ajoc.201402229
- Gunasekera, S. P., McCarthy, P. J., and Kelly-Borges, M. (1994). Hamacanthins A and B, new antifungal bis indole alkaloids from the deepwater marine sponge. *J. Nat. Prod.* 57, 1437–1441. doi: 10.1021/np50112a014
- Guo, X., Pan, S., Liu, J., and Li, Z. (2009). One-pot synthesis of symmetric and unsymmetric 1,1-bis-indolylmethanes via tandem iron-catalyzed C–H bond oxidation and C–O bond cleavage. *J. Org. Chem.* 74, 8848–8851. doi: 10.1021/jo902093p
- Ji, S.-J., Zhou, M.-F., Gu, D.-G., Jiang, Z.-Q., and Loh, T.-P. (2004). Efficient Fe<sup>III</sup>-catalyzed synthesis of bis(indolyl)methanes in ionic liquids. *Eur. J. Org. Chem.* 2004, 1584–1587. doi: 10.1002/ejoc.200300719
- Josefsen, L. B., and Boyle, R. W. (2012). Unique diagnostic and therapeutic roles of porphyrins and phthalocyanines in photodynamic therapy, imaging and theranostics. *Theranostics* 2, 916–966. doi: 10.7150/thno.4571
- Köster, J. M., Häussinger, D., and Tiefenbacher, K. (2019). Activation of primary and secondary benzylic and tertiary alkyl(sp<sup>3</sup>)C–F bonds inside a self-assembled molecular container. *Front. Chem.* 6:639. doi: 10.3389/fchem.2018.00639
- Köster, J. M., and Tiefenbacher, K. (2018). Elucidating the importance of hydrochloric acid as a cocatalyst for resorcinarene-capsule-catalyzed reactions. *Chem. Cat. Chem.* 10, 2941–2944. doi: 10.1002/cctc.201800326
- Kursunlu, A. N., Guler, E., Ucan, H. I., and Boyle, R. W. (2012). A novel bodipy-dipyrin fluorescent probe: synthesis and recognition behaviour towards Fe (II) and Zn (II). *Dyes Pigm.* 94, 496–502. doi: 10.1016/j.dyepig.2012.02.006
- La Manna, P., De Rosa, M., Talotta, C., Gaeta, C., Soriente, A., Floresta, G., et al. (2018a). The hexameric resorcinarene capsule as an artificial enzyme: ruling the regio and stereochemistry of a 1,3-dipolar cycloaddition between nitrones and unsaturated aldehydes. *Org. Chem. Front.* 5, 827–837. doi: 10.1039/C7QO00942A
- La Manna, P., Talotta, C., Floresta, G., De Rosa, M., Soriente, A., Rescifina, A., et al. (2018b). Mild friedel–crafts reactions inside a hexameric resorcinarene capsule: C–Cl bond activation through hydrogen bonding to bridging water molecules. *Angew. Chem. Int. Ed.* 57, 5423–5428. doi: 10.1002/anie.201801642
- La Sorella, G., Sporni, L., Ballester, P., Strukul, G., and Scarso, A. (2016a). Hydration of aromatic alkynes catalyzed by a self-assembled hexameric organic capsule. *Catal. Sci. Technol.* 6, 6031–6036. doi: 10.1039/C6CY00307A
- La Sorella, G., Sporni, L., Strukul, G., and Scarso, A. (2016b). Supramolecular activation of hydrogen peroxide in the selective sulfoxidation of thioethers by a self-assembled hexameric capsule. *Adv. Synth. Catal.* 358, 3443–3449. doi: 10.1002/adsc.201600430
- Laha, J. K., Dhanalekshmi, S., Taniguchi, M., Ambroise, A., and Lindsey, J. S. (2003). A scalable synthesis of meso-substituted dipyrromethanes. *Org. Process. Rev. Dev.* 7, 799–812. doi: 10.1021/op034083q
- Ling, Y., An, D., Zhou, Y., and Rao, W. (2019). Ga(OTf)<sub>3</sub>-catalyzed temperature-controlled regioselective Friedel–Crafts alkylation of trifluoromethylated 3-indolylmethanols with 2-substituted indoles: divergent synthesis of trifluoromethylated unsymmetrical 3,3'- and 3,6'-bis(indolyl)methanes. *Org. Lett.* 21, 3396–3401. doi: 10.1021/acs.orglett.9b01135
- Lucarini, S., Mari, M., Piersanti, G., and Spadoni, G. (2013). Organocatalyzed coupling of indoles with dehydroalanine esters: synthesis of bis(indolyl)propanoates and indolacrylates. *RSC Adv.* 3, 19135–19143. doi: 10.1039/c3ra42922a
- MacGillivray, L. R., and Atwood, J. L. (1997). A chiral spherical molecular assembly held together by 60 hydrogen bonds. *Nature* 389, 469–472. doi: 10.1038/38985
- Norouzi, M., Elhamifar, D., and Mirbagheri, R. (2018). Self-assembled alkyl imidazolium based organosilica as efficient support for sulfonic acid catalyst in the synthesis of bis(indolyl)methanes. *Polyhedron* 154, 229–235. doi: 10.1016/j.poly.2018.07.047
- Pahima, E., Zhang, Q., Tiefenbacher, K., and Major, D. T. (2019). Discovering monoterpene catalysis inside nanocapsules with multiscale modelling and experiments. *J. Am. Chem. Soc.* 141, 6234–6246. doi: 10.1021/jacs.8b13411
- Palmieri, A., Petrini, M., and Shaikh, R. R. (2010). Synthesis of 3-substituted indoles via reactive alkylideneindolenine intermediates. *Org. Biomol. Chem.* 8, 1259–1277. doi: 10.1039/B919891A
- Qiang, W., Liu, X., and Loh, T.-P. (2019). Supported iridium catalyst for the green synthesis of 3,3'-bis(indolyl)methanes using methanol as the bridging methylene source. *ACS Sustain. Chem. Eng.* 7, 8429–8439. doi: 10.1021/acssuschemeng.9b00094
- Sakemi, S., and Sun, H. H. (1991). Nortopsentins A, B, and C. Cytotoxic and antifungal imidazole-diylbis[indoles] from the sponge *Spongosorites ruetzleri*. *J. Org. Chem.* 56, 4304–4307. doi: 10.1021/jo00013a044
- Shiri, M. (2012). Indoles in multicomponent processes (MCPs). *Chem. Rev.* 112, 3508–3549. doi: 10.1021/cr2003954
- Shiri, M., Zolfigol, M. A., Kruger, H. G., and Tanbakouchian, Z. (2010). Bis- and trisindolylmethanes (BIMs and TIMs). *Chem. Rev.* 110, 2250–2293. doi: 10.1021/cr900195a
- Shivanyuk, A., and Rebek, J. Jr. (2001). Reversible encapsulation by self-assembling resorcinarene subunits. *Proc. Natl. Acad. Sci. U.S.A.* 98, 9662–9665. doi: 10.1073/pnas.141226898
- Shivanyuk, A., and Rebek, J. Jr. (2003). Assembly of resorcinarene capsules in wet solvents. *J. Am. Chem. Soc.* 125, 3432–3433. doi: 10.1021/ja027982n
- Singh, K., Sharma, S., and Sharma, A. (2011). Unique versatility of Amberlyst 15. An acid and solvent-free paradigm towards synthesis of bis(heterocyclyl)methane derivatives. *J. Mol. Catal. A Chem.* 347, 34–37. doi: 10.1016/j.molcata.2011.07.007
- Sivaprasad, G., Perumal, P. T., Prabavathy, V. R., and Mathivanan, N. (2006). Synthesis and anti-microbial activity of pyrazolylbisindoles—promising anti-fungal compounds. *Bioorg. Med. Chem. Lett.* 16, 6302–6305. doi: 10.1016/j.bmcl.2006.09.019
- Tran, P. H., Nguyen, X.-T. T., and Chau, D.-K. N. (2018). A brønsted-acidic ionic liquid gel as an efficient and recyclable heterogeneous catalyst for the synthesis of bis(indolyl)methanes under solvent-free sonication. *Asian J. Org. Chem.* 7, 232–239. doi: 10.1002/ajoc.201700596
- Wu, Z., Wang, G., Yuan, S., Wu, D., Liu, W., Ma, B., et al. (2019). Synthesis of bis(indolyl)methanes under dry grinding conditions, promoted by a Lewis acid surfactant–SiO<sub>2</sub>-combined nanocatalyst. *Green Chem.* 21:3542. doi: 10.1039/C9GC01073D
- Yamanaka, M., Shivanyuk, A., and Rebek, J. (2004). Kinetics and thermodynamics of hexameric capsule formation. *J. Am. Chem. Soc.* 126, 2939–2943. doi: 10.1021/ja037035u
- Zhang, Q., Catti, L., Pleiss, J., and Tiefenbacher, K. (2017). Terpene cyclizations inside a supramolecular catalyst: leaving-group-controlled product selectivity and mechanistic studies. *J. Am. Chem. Soc.* 139, 11482–11492. doi: 10.1021/jacs.7b04480
- Zhang, Q., Catti, L., Syntrivani, L.-D., and Tiefenbacher, K. (2019). En route to terpene natural products utilizing supramolecular cyclase mimetics. *Nat. Prod. Rep.* doi: 10.1039/C9NP00003H. [Epub ahead of print].
- Zhang, Q., Rinkel, J., Goldfuss, B. M., Dickschat, J. S., and Tiefenbacher, K. (2018). Sesquiterpene cyclizations catalysed inside the resorcinarene capsule and application in the short synthesis of isolongifolene and isolongifolenone. *Nat. Catal.* 1, 609–615. doi: 10.3390/catal8120609
- Zhang, Q., and Tiefenbacher, K. (2013). The hexameric resorcinarene capsule is a brønsted acid: investigation and application to synthesis and catalysis. *J. Am. Chem. Soc.* 135, 16213–16219. doi: 10.1021/ja4080375
- Zhang, Q., and Tiefenbacher, K. (2015). Terpene cyclization catalysed inside a self-assembled cavity. *Nat. Chem.* 7, 197–202. doi: 10.1038/nchem.2181
- Zhang, Q., and Tiefenbacher, K. (2019). Sesquiterpene cyclizations inside the hexameric resorcinarene capsule: total synthesis of  $\delta$ -selinene and mechanistic studies. *Angew. Chem. Int. Ed. Early View* 58, 12688–12695. doi: 10.1002/anie.201906753

**Conflict of Interest:** The authors declare that the research was conducted in the absence of any commercial or financial relationships that could be construed as a potential conflict of interest.

Copyright © 2019 Gambaro, La Manna, De Rosa, Soriente, Talotta, Gaeta and Neri. This is an open-access article distributed under the terms of the Creative Commons Attribution License (CC BY). The use, distribution or reproduction in other forums is permitted, provided the original author(s) and the copyright owner(s) are credited and that the original publication in this journal is cited, in accordance with accepted academic practice. No use, distribution or reproduction is permitted which does not comply with these terms.





# Ditopic Receptors Based on Dihomooxacalix[4]arenes Bearing Phenylurea Moieties With Electron-Withdrawing Groups for Anions and Organic Ion Pairs

Alexandre S. Miranda<sup>1,2</sup>, Defne Serbetci<sup>1</sup>, Paula M. Marcos<sup>1,3\*</sup>, José R. Ascenso<sup>4</sup>, Mário N. Berberan-Santos<sup>2</sup>, Neal Hickey<sup>5</sup> and Silvano Geremia<sup>5</sup>

<sup>1</sup> Centro de Química Estrutural, Faculdade de Ciências da Universidade de Lisboa, Lisbon, Portugal, <sup>2</sup> Centro de Química-Física Molecular, Institute of Nanoscience and Nanotechnology (IN) and IBB-Institute for Bioengineering and Biosciences, Instituto Superior Técnico, Universidade de Lisboa, Lisbon, Portugal, <sup>3</sup> Faculdade de Farmácia da Universidade de Lisboa, Lisbon, Portugal, <sup>4</sup> Centro de Química Estrutural, Instituto Superior Técnico, Lisbon, Portugal, <sup>5</sup> Department of Chemical and Pharmaceutical Sciences, Centre of Excellence in Biocrystallography, University of Trieste, Trieste, Italy

## OPEN ACCESS

### Edited by:

Carmine Gaeta,  
University of Salerno, Italy

### Reviewed by:

Corrada Geraci,  
Institute of Biomolecular Chemistry  
(ICB), Italy  
Ivan Stoikov,  
Kazan Federal University, Russia  
Behrouz Shaabani,  
University of Tabriz, Iran

### \*Correspondence:

Paula M. Marcos  
pmmarcos@fc.ul.pt

### Specialty section:

This article was submitted to  
Supramolecular Chemistry,  
a section of the journal  
Frontiers in Chemistry

Received: 01 August 2019

Accepted: 22 October 2019

Published: 08 November 2019

### Citation:

Miranda AS, Serbetci D, Marcos PM, Ascenso JR, Berberan-Santos MN, Hickey N and Geremia S (2019) Ditopic Receptors Based on Dihomooxacalix[4]arenes Bearing Phenylurea Moieties With Electron-Withdrawing Groups for Anions and Organic Ion Pairs. *Front. Chem.* 7:758. doi: 10.3389/fchem.2019.00758

Two bidentate dihomooxacalix[4]arene receptors bearing phenylurea moieties substituted with electron-withdrawing groups at the lower rim via a butyl spacer (CF<sub>3</sub>-Phurea **5b** and NO<sub>2</sub>-Phurea **5c**) were obtained in the cone conformation in solution, as shown by NMR. The X-ray crystal structure of **5b** is reported. The binding affinity of these receptors toward several relevant anions was investigated by <sup>1</sup>H NMR, UV-Vis absorption in different solvents, and fluorescence titrations. Compounds **5b** and **5c** were also tested as ditopic receptors for organic ion pairs, namely monoamine neurotransmitters and trace amine hydrochlorides by <sup>1</sup>H NMR studies. The data showed that both receptors follow the same trend and, in comparison with the unsubstituted phenylurea **5a**, they exhibit a significant enhancement on their host-guest properties, owing to the increased acidity of their urea NH protons. NO<sub>2</sub>-Phurea **5c** is the best anion receptor, displaying the strongest complexation for F<sup>−</sup>, closely followed by the oxoanions BzO<sup>−</sup>, AcO<sup>−</sup>, and HSO<sub>4</sub><sup>−</sup>. Concerning ion pair recognition, both ditopic receptors presented an outstanding efficiency for the amine hydrochlorides, mainly **5c**, with association constants higher than 10<sup>9</sup> M<sup>−2</sup> in the case of phenylethylamine and tyramine.

**Keywords:** dihomooxacalix[4]arenes, phenylurea anion receptors, biogenic amine hydrochlorides, ditopic receptors, proton NMR titrations, UV-Vis absorption studies, fluorescence studies, X-ray diffraction

## INTRODUCTION

Anion recognition by synthetic receptors continues to attract much attention, as documented by the reviews published recently (Evans and Beer, 2014; Busschaert et al., 2015; Gale et al., 2016). Anions play essential roles in numerous biological systems, as well as in many environmental and industrial processes.

Macrocyclic compounds have been developed as anion receptors, in which the interactions are mainly established by hydrogen bond donor groups, such as ureas and thioureas, incorporated in

the macrocycle scaffolds. These receptors are able to recognize anions with different geometries through effective and directional H-bonds. However, to bind a charged species these monotopic receptors need to overcome the tendency of the target ion to form an ion pair with its counter ion, especially in non-polar solvents. Thus, heteroditopic receptors, molecules capable of simultaneously bind both ions of a given ion pair, have been obtained and are an emerging area in supramolecular chemistry (Kim and Sessler, 2010; McConnell and Beer, 2012). These systems have important applications, as membrane transport agents, and in salt extraction and solubilisation. The binding ability of these ditopic receptors toward organic ion pairs, namely ammonium and amino acid salts, has been more investigated in the last years. Alkylammonium moieties are a constant presence in compounds of biological interest, such as biogenic amines, trace amines and amino acids (Mutihac et al., 2011).

Calixarenes are a particularly attractive class of macrocyclic compounds owing to the relatively ease functionalization of both the upper and the lower rims, and to the presence of a pre-organized cavity available in different sizes and conformations (Gutsche, 2008). These compounds have been largely used as anion receptors. In particular, calix[4]arenes (Quinlan et al., 2007; Babu et al., 2009; Curinova et al., 2009; De Solis et al., 2015; Klejch et al., 2016; Rezankova et al., 2017) and calix[6]arenes (Hamon et al., 2008; Nehra et al., 2016) bearing phenylurea moieties incorporating electron-withdrawing groups, such as NO<sub>2</sub> and CF<sub>3</sub>, have been investigated. These groups are expected to increase the acidity of the urea NH protons, thus enhancing the anion binding ability of the receptors. Calixarenes have also been used as building blocks for the construction of ditopic receptors able of simultaneous binding of anions and cations. Examples of such receptors based on calix[4] (Pescatori et al., 2009), calix[5] (Capici et al., 2010), and mainly calix[6]arenes (Hamon et al., 2008; Lascaux et al., 2010; Cornut et al., 2015; Moerkerke et al., 2017) are reported in the literature.

In the course of our studies on anion binding by disubstituted dihomooxalix[4]arenes (calix[4]arene analogs in which one CH<sub>2</sub> bridge is replaced by one CH<sub>2</sub>OCH<sub>2</sub> group) (Marcos, 2016) with phenylurea units (Marcos et al., 2014a,b), we were interested in determine the enhancement on the anion binding affinity of the receptors by the introduction of electron-withdrawing groups. Along with this research, the phenylurea derivatives were also evaluated as ditopic receptors (Gattuso et al., 2015). They combine in the same molecule two different binding sites, i.e., an ureido anionic site and a hydrophobic cavity suitable for organic cations.

In this paper we describe the synthesis of two new disubstituted dihomooxalix[4]arenes bearing, via a butyl spacer, *para* CF<sub>3</sub>- (**5b**) or NO<sub>2</sub>-phenylurea (**5c**) moieties, at the 1,3-positions of the lower rim. The host-guest properties of these receptors, obtained in the cone conformation, toward several relevant anions were established by proton NMR and UV-Vis absorption titrations in chloroform (or dichloromethane) and acetonitrile. Some photophysical properties of these receptors (due to their intrinsic fluorescence) were evaluated and, in a few cases, fluorescence studies were also performed to investigate the calixarene binding affinity. These dihomooxa

derivatives were also tested as heteroditopic receptors for *n*-alkylammonium chlorides, and monoamine neurotransmitters and trace amine hydrochlorides by proton NMR studies. The results are compared to those obtained with the analog unsubstituted phenylurea (**5a**). The solid state structure of **5b** is also presented.

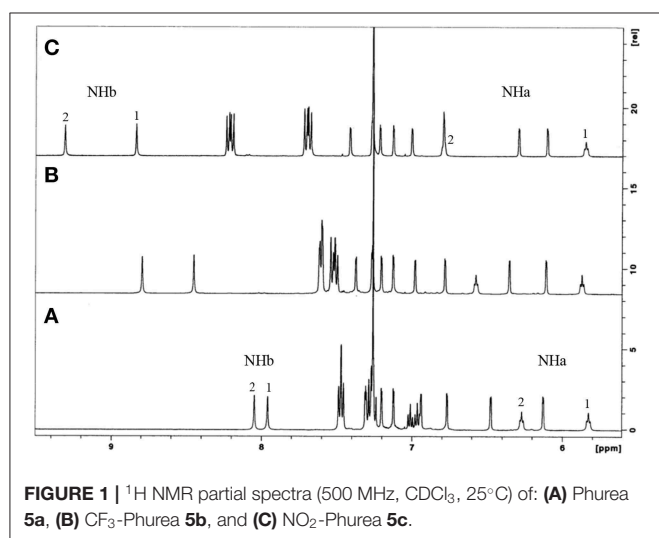
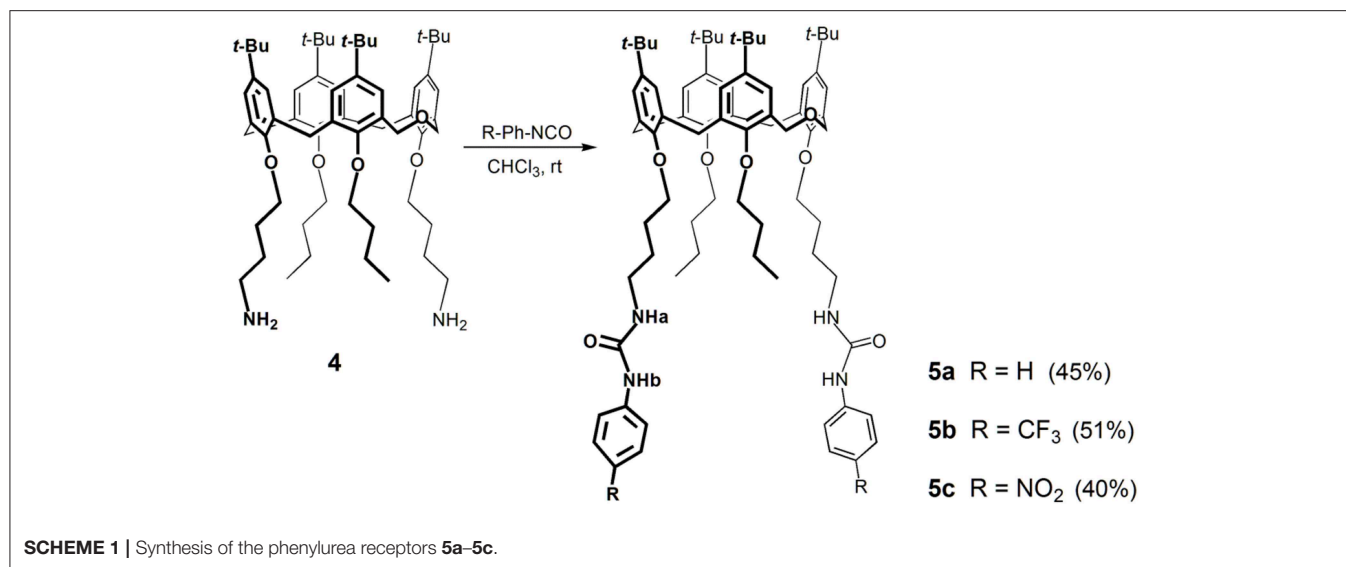
## RESULTS AND DISCUSSION

### Synthesis and Structural Analysis

Previously, we have reported the synthesis of a lower rim 1,3-disubstituted dihomooxalix[4]arene receptor containing two phenylurea moieties and two *n*-butyl groups (Marcos et al., 2014a). Following this line of research, we synthesized two new ureido-dihomooxalix[4]arenes bearing CF<sub>3</sub> or NO<sub>2</sub> groups at the *p*-position of the phenylurea moiety, via a butyl spacer. The binding ability of these receptors is expected to be increased by the introduction of the electron-withdrawing groups. Thus, the alkylation reaction of the parent *p*-*tert*-butyldihomooxalix[4]arene (**1**) with 4-bromobutyronitrile and K<sub>2</sub>CO<sub>3</sub> gave the dicyano-dihydroxy compound **2**, which was further alkylated with *n*-butyl iodide and NaH, yielding the dicyano-dibutoxy derivative **3**. Reduction of the cyano groups with NaBH<sub>4</sub>/CoCl<sub>2</sub> afforded diamine **4**. These reactions and products were already described (Marcos et al., 2014a). Diamine **4** reacted with *p*-(trifluoromethyl)- or *p*-nitro-phenylisocyanate to yield the corresponding *p*-CF<sub>3</sub>-phenylurea **5b** and *p*-NO<sub>2</sub>-phenylurea **5c**, in the cone conformation (**Scheme 1**).

These receptors are inherently chiral, as indicated by their NMR spectra in CDCl<sub>3</sub>. The proton spectra show four singlets for the *tert*-butyl groups, five AB quartets for the CH<sub>2</sub> bridge protons, four pairs of doublets for the aromatic protons, and two triplets and two singlets for the NHa and NHb protons, respectively. The aromatic and NH region of the three phenyl ureas is shown in **Figure 1**. Increasing downfield shifts for the NH protons, mainly the NHb, can be observed from Phurea **5a** to NO<sub>2</sub>-Phurea **5c**, indicating the increased acidity of these protons. Moreover, the proton spectra display two triplets and several multiplets for the methyl and methylene protons of the butyl spacers and *n*-butyl groups. The <sup>13</sup>C spectra exhibit three ArCH<sub>2</sub>Ar resonances in the range 28.8–31.5 ppm, indicative of a cone conformation (Jaime et al., 1991). The proton assignments were confirmed by COSY spectra.

Small colorless single crystal needles were obtained by slow evaporation of a chloroform solution containing compound **5b**. The X-ray structure was determined using synchrotron radiation with crystals frozen at 100 K. The asymmetric unit of the monoclinic crystal (space group P2<sub>1</sub>/c) is composed of one molecule of **5b** and a disordered co-crystallized chloroform solvent molecule with a total occupancy factor of 0.7. The dihomooxalixarene macrocycle adopts the expected cone conformation, producing an inherently chiral molecule due to the 1,3-substitution pattern on the lower rim (**Figure 2**, rings A and C). The centrosymmetric space group implies the presence of a racemic mixture of the two enantiomers in the crystals. The mean planes of the two ureido substituted phenyl rings (A and C) make large outward (dihedral) angles of 125° and



$131^\circ$ , respectively, with respect to the dihomooxacalixarene mean plane, defined by the methylene bridging groups (**Figure 2B**). With regard to the butoxy substituted phenyl rings, the one connected with the homooxo bridge (B) shows a mean plane of the phenyl ring inclined inwards with a dihedral angle of  $66^\circ$ . As a result, its *p*-*tert*-butyl group partially occupies the calixarene cavity. The facing butoxy substituted phenyl ring (D) is inclined slightly outwards, with a dihedral angle of  $101^\circ$ . Consistently with previous reports, the ureido groups form an intramolecular  $\text{N–H}\cdots\text{O}$  bifurcated hydrogen bond (Marcos et al., 2014b; Augusto et al., 2018). In this case the H-bond is rather asymmetric, with the  $\text{N}\cdots\text{O}$  distance of the NH directly bonded to the phenyl ring, *para* to the electron-withdrawing  $\text{CF}_3$  group, shorter with respect to the other  $\text{N}\cdots\text{O}$  distance (2.89 vs.  $3.06\text{ \AA}$ ). The relative orientations of the skeletons of the NCONH ureido moieties show a mean plane dihedral angle of  $28^\circ$ , while the terminal phenyl groups form dihedral angles of about  $20^\circ$  (Ring A) and  $40^\circ$  (Ring C) with respect to their corresponding

planar ureido groups. The overall result is that these phenyl groups show a dihedral angle of about  $74^\circ$  between their mean planes (**Figure 2**).

The crystal packing shows that the ureido groups are involved in an intermolecular  $\text{N–H}\cdots\text{O}$  hydrogen bonds network. More specifically, one-dimensional chains of bifurcated H-bonds, formed by iso-orientated calixarenes (generated by crystallographic glide planes), are propagated antiparallel along the *c*-axis (**Figure 3**). The resulting intermolecular  $\text{N}\cdots\text{O}$  distances show that these bifurcated intermolecular H-bonds are even more asymmetric than the intramolecular H-bonds. In this case the NH group directly bound to the phenyl ring forms a weaker H-bond with the carbonyl oxygen of a symmetry related molecule in comparison to the second NH group ( $\text{N}\cdots\text{O}$  distances are  $3.14$  and  $2.85\text{ \AA}$ , respectively). The antiparallel chains are related by crystallographic screw axes and stacked along the *b*-axis with the calix cups facing the  $\text{CF}_3$ -phenyl rings (**Figure 3**). The chloroform molecules at partial occupancy fill the voids created by the crystal packing of the calixarene molecules.

The comparison with the solid state structure of **5a** containing two crystallographic independent molecules, previously reported (Gattuso et al., 2015), shows an analogous crystal packing arrangement, despite the significant differences in the unit cells and the different space groups. However, in **5a** the orientations of the  $\text{NHCONH}$  ureido moieties are quite different in the two crystallographic independent molecules, being almost parallel in one (similar to the conformation found in **5b**) and orthogonally oriented in the other (Gattuso et al., 2015). For each independent molecules of **5a**, the cone macrocycle adopts a similar conformation to **5b**, in which the *p*-*tert*-butyl groups of the B rings lean into the cavity. More specifically, for the molecule with the almost parallel orientation of the ureido groups, the four dihedral angles formed by the mean planes of the phenyl rings and the dihomooxacalixarene bridging mean plane are within two degrees of the molecule found in **5b**. On the other hand, the **5a** molecule having an orthogonal orientation of the  $\text{NHCONH}$  ureido moiety shows a more

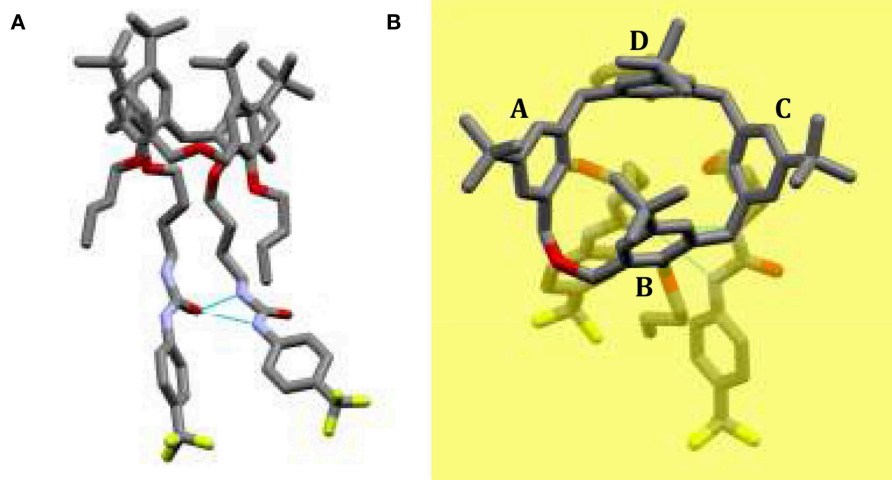


**FIGURE 2** | Solid state structure of  $\text{CF}_3$ -Phurea **5b**. **(A)** The molecule shows a cone conformation, with the phenylureido moieties involved in an intramolecular  $\text{N-H}\cdots\text{O}$  bifurcated hydrogen bond. **(B)** Orthogonal view of **5b** with respect to the dihomooxalixarene mean plane (yellow) defined by the methylene bridging groups.

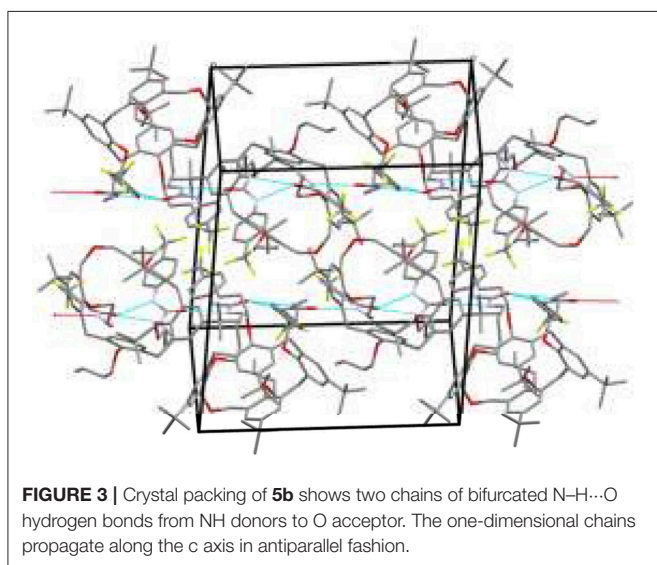


**FIGURE 3** | Crystal packing of **5b** shows two chains of bifurcated  $\text{N-H}\cdots\text{O}$  hydrogen bonds from NH donors to O acceptor. The one-dimensional chains propagate along the c axis in antiparallel fashion.

open cone conformation ( $121^\circ$ ,  $74^\circ$ ,  $137^\circ$ ,  $97^\circ$  for A, B, C, and D angles, respectively). This comparison suggests that the openness of the cone is to some degree related to the conformation and reciprocal orientation of the  $\text{NHCONH}$  ureido moieties.

## Photophysical Properties

Owing to the intrinsic fluorescence of receptors **5**, and to evaluate the changes caused by the introduction of the substituent groups at the *p*-position of the phenylurea ring, some photophysical properties of **5a** and **5b** were determined, following previous studies (Miranda et al., 2017).

The absorption and steady-state fluorescence spectra of Phurea **5a** and  $\text{CF}_3$ -Phurea **5b** in dichloromethane are shown

in **Figure 4**. The compounds present a well-defined absorption in the UV region, exhibiting a blue shift of 28 nm for **5b** (**Figure 4A**). The same trend is observed in the emission spectrum, the normalized spectra being again similar for both compounds (**Figure 4B**).

Relevant photophysical properties of the two Phureas are collected in **Table 1**. Stokes shifts were calculated as the difference between the excitation and the emission peak wavelengths. The results show that  $\text{CF}_3$ -Phurea **5b** presents a higher value compared to **5a**. The fluorescence lifetimes ( $\tau_f$ ) and quantum yields ( $\phi_F$ ) were also determined. Overall, fluorescence lifetimes and yields do not change much upon *para* substitution, the fluorescence quantum yields are significant (0.2–0.6) and lifetimes moderate (1–2 ns). The quantum yield decreases and the lifetime increases upon *para* substitution, both effects resulting mainly from a decrease of the radiative rate constant ( $k_r$ ) (**Table 1**).

## Anion Recognition Proton NMR Studies

The binding properties of bidentate  $\text{CF}_3$ -Phurea **5b** and  $\text{NO}_2$ -Phurea **5c** toward several relevant anions of different geometries (spherical, linear, trigonal planar, and tetrahedral) were studied in  $\text{CDCl}_3$  through  $^1\text{H}$  NMR titrations using tetrabutylammonium (TBA) salts. The association constants (as  $\log K_{\text{ass}}$ ) reported in **Table 2** were determined using the WinEQNMR2 program (Hynes, 1993) and following the urea NH chemical shifts. In a few cases where those protons became broad or disappeared, the association constants were calculated through the complexation induced shifts of the aromatic protons of the calixarene skeleton.

Hydrogen bonding interactions between the anions and the urea groups of the receptors were clearly evidenced by the downfield shifts of their NH protons, as shown in **Figure 5**. In all the studied cases, the complexation process occurs under fast exchange conditions on the



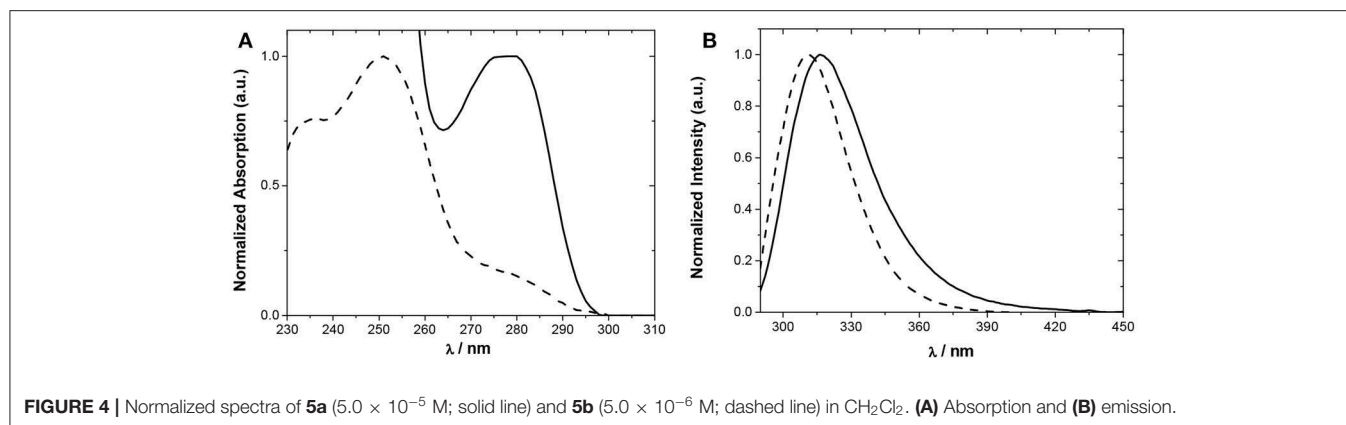


**FIGURE 4** | Normalized spectra of **5a** ( $5.0 \times 10^{-5}$  M; solid line) and **5b** ( $5.0 \times 10^{-6}$  M; dashed line) in  $\text{CH}_2\text{Cl}_2$ . **(A)** Absorption and **(B)** emission.

**TABLE 1** | Photophysical properties of Phureas **5a** and **5b** in  $\text{CH}_2\text{Cl}_2$  at  $25^\circ\text{C}$ .

	$\lambda_{\text{max,abs}}$ (nm)	$\lambda_{\text{max,em}}$ (nm)	$\epsilon$ ( $\text{M}^{-1} \text{cm}^{-1}$ )	Stokes shift <sup>a</sup> (nm)	$\tau_f$ (ns)	$\phi_F$	$k_r$ ( $\text{ns}^{-1}$ )	$k_{nr}$ ( $\text{ns}^{-1}$ )
<b>5a</b>	278	316	$5.0 \times 10^3$	38	1.15	0.59 <sup>b</sup>	0.51	0.36
<b>5b</b>	250	310	$7.1 \times 10^4$	60	1.57	0.21 <sup>c</sup>	0.13	0.50

<sup>a</sup>Compute as  $\lambda_{\text{max,em}} - \lambda_{\text{max,abs}}$ .

<sup>b</sup>Against quinine sulfate  $\phi_F = 0.60$  in  $\text{HCl}$  0.1 M.

<sup>c</sup>Against tryptophan  $\phi_F = 0.12$  in water.

**TABLE 2** | Association constants ( $\log K_{\text{ass}}$ )<sup>a</sup> of dihomooxa ureas **5a–5c** determined by  $^1\text{H}$  NMR in  $\text{CDCl}_3$  at  $25^\circ\text{C}$ .

	Spherical				Linear		Trigonal planar			Tetrahedral		
	$\text{F}^-$	$\text{Cl}^-$	$\text{Br}^-$	$\text{I}^-$	$\text{CN}^-$	$\text{SCN}^-$	$\text{NO}_3^-$	$\text{AcO}^-$	$\text{BzO}^-$	$\text{HSO}_4^-$	$\text{H}_2\text{PO}_4^-$	$\text{ClO}_4^-$
I. Radius/ $\text{\AA}^b$	1.33	1.81	1.96	2.20	1.91	2.13	1.79	2.32	—	1.90	2.00	2.40
Phurea <b>5a</b> <sup>c</sup>	3.10	2.73	2.23	1.59	2.71	1.90	2.42	2.88	2.93	2.58	2.69	1.65
$\text{CF}_3$ -Phurea <b>5b</b>	3.48	3.12	2.68	2.18	3.13	2.18	2.68	3.34	3.46	3.07	3.15	2.04
$\text{NO}_2$ -Phurea <b>5c</b>	3.88	3.65	3.07	2.65	3.66	2.67	3.15	3.67	3.83	3.61	3.49	2.37

<sup>a</sup>Estimated error <10%.

<sup>b</sup>Data quoted in Marcus (1997).

<sup>c</sup>Data taken from Marcos et al. (2014a).

NMR time scale at room temperature. The titration curves obtained (Figure S1) indicate the formation of 1:1 host-guest complexes. This stoichiometry was also confirmed by Job plots (Figure S2).

The anion binding results obtained by proton NMR titrations (Table 2) show that both phenylureas bearing the electron-withdrawing groups  $\text{CF}_3$  and  $\text{NO}_2$  are better receptors than Phurea **5a** (with no substituents), due to the increased acidity of their NH protons. All the receptors follow the same trend: the association constants decrease in general with decreasing anion basicity. The data show that  $\text{NO}_2$ -Phurea **5c** is the best anion receptor, exhibiting high association constants. Among the spherical halides, **5c** displays the strongest complexation for  $\text{F}^-$  ( $\log K_{\text{ass}} = 3.88$ ). The results with  $\text{F}^-$  showed no evidence for the formation of the  $\text{HF}_2^-$  species (Amendola et al., 2006, 2010; Babu et al., 2009) Although the acidity of Phureas **5b** and **5c** is higher compared to that of **5a**, the solvent used, chloroform, is a weakly competitive one,

contributing to stabilize the H-bond complexes. Moreover, small downfield and upfield shifts for the *ortho* and *meta* protons, respectively, of the phenylurea groups of **5c** were also observed (Figure S3), corroborating the expected effects for the formation of hydrogen-bonding complexes (Amendola et al., 2010). In the case of the pseudo-halides, the more basic  $\text{CN}^-$  anion was complexed with higher selectivity with respect to  $\text{SCN}^-$  ( $K_{\text{ass}} \text{CN}^-/K_{\text{ass}} \text{SCN}^- = 8.9$  and  $9.8$  for **5b** and **5c**, respectively). With regard to the planar oxoanions, receptors **5b** and especially **5c** show a very efficient binding toward the carboxylates  $\text{BzO}^-$  and  $\text{AcO}^-$  ( $\log K_{\text{ass}} = 3.83$  and  $3.67$ , respectively, for **5c**). As observed before with **5a** and with other dihomooxa ureas (Marcos et al., 2014b; Teixeira et al., 2017), there is a slight inversion of the basicity order.  $\pi$  stacking interactions may contribute to this slight increase of the  $\text{BzO}^-$  complexation over that of  $\text{AcO}^-$ . The inorganic oxoanions,  $\text{HSO}_4^-$  and  $\text{H}_2\text{PO}_4^-$ , are also tightly bound by these receptors.

### UV-Vis Absorption and Fluorescence Studies

The binding properties of CF<sub>3</sub>- and NO<sub>2</sub>-Phureas (**5b** and **5c**) were complemented through UV-Vis absorption titrations. Thus, the interactions between these receptors and some selected anions of different geometries (F<sup>−</sup>, Cl<sup>−</sup>, Br<sup>−</sup>, NO<sub>3</sub><sup>−</sup>, AcO<sup>−</sup>, BzO<sup>−</sup>, HSO<sub>4</sub><sup>−</sup>, and H<sub>2</sub>PO<sub>4</sub><sup>−</sup>) as TBA salts were studied in chloroform (or dichloromethane) and acetonitrile solvents.

In chloroform, NO<sub>2</sub>-Phurea **5c** displays an absorption band centered at approximately 335 nm. Upon addition of increasing amounts of F<sup>−</sup> ion, this band decreases in intensity while a new one is progressively formed, reaching a maximum at 356 nm (red shift of 21 nm) and exhibiting an isosbestic point at 341 nm, which reveals the existence of only two species (**Figure 6A**). Similar absorption spectral changes were observed for the carboxylates AcO<sup>−</sup> and BzO<sup>−</sup>, both leading to red shifts of 15 nm and presenting isosbestic points, as well as for the inorganic oxoanions HSO<sub>4</sub><sup>−</sup> and H<sub>2</sub>PO<sub>4</sub><sup>−</sup>, although to a smaller extent. In the case of addition of the spherical Cl<sup>−</sup> and Br<sup>−</sup> anions, and the planar NO<sub>3</sub><sup>−</sup>, successive increases of the absorption were recorded, but with almost no shifts in their maxima. Similar absorption spectra were obtained for NO<sub>2</sub>-Phureido-calix[4]arene analogs (Babu et al., 2009; Curinova et al., 2009). CF<sub>3</sub>-Phurea **5b** exhibits a similar behavior in dichloromethane. In this case it was not possible to use chloroform solvent due to absorption overlapping with urea **5b**. The addition of increasing amounts of F<sup>−</sup>, AcO<sup>−</sup>, BzO<sup>−</sup>, and H<sub>2</sub>PO<sub>4</sub><sup>−</sup> anions to a solution of **5b** leads to a decrease of the intensity of its absorption peak at 250 nm, while a new band appears and progressively moves to longer wavelength. Isosbestic points can also be observed, as illustrated in **Figure 7A** for the BzO<sup>−</sup> anion. The other anions studied showed no new band formation at higher wavelengths; only a gradual increase of the absorption band centered at 250 nm was observed as the anion concentration increased. In acetonitrile, both receptors showed identical behaviors toward all the anions: a successive increase of the absorption in the presence of the anions, with no significant modification of their band shapes (**Figures 6B, 7B**).

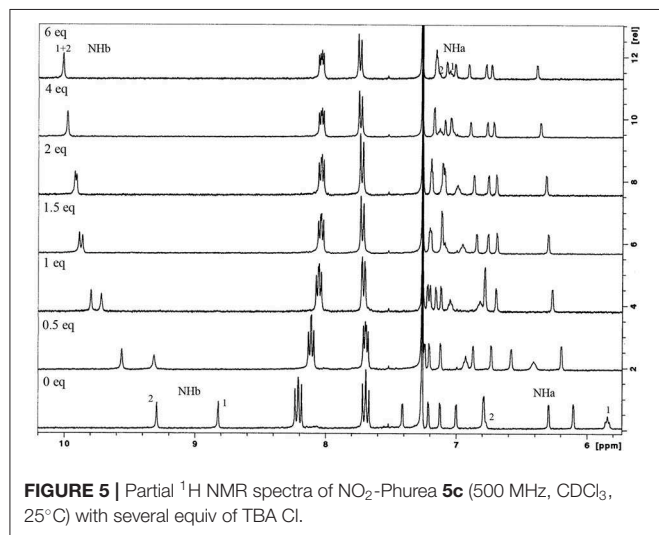


**FIGURE 5** | Partial <sup>1</sup>H NMR spectra of NO<sub>2</sub>-Phurea **5c** (500 MHz, CDCl<sub>3</sub>, 25°C) with several equiv of TBA Cl.

In all cases, the spectral variations were sufficiently important to allow the determination of the corresponding binding constants. The data presented in **Table 3** show a stronger complexation in chloroform (or dichloromethane in the case of **5b**) than in acetonitrile for both ureas, in agreement with the competitiveness of the solvents. The association constants in both solvents are higher than those obtained by NMR, but follow the same trend: F<sup>−</sup>, AcO<sup>−</sup>, and BzO<sup>−</sup> are the best bound anions. The UV concentrations are more than 200 times less than those used in the NMR titrations, and this fact influences the association constants. The more diluted solutions used in the UV experiments favor the dissociation of the salts, thereby providing a higher concentration of the anions available for binding and resulting in higher association constants.

The NO<sub>3</sub><sup>−</sup> and HSO<sub>4</sub><sup>−</sup> anion binding constants with CF<sub>3</sub>-Phurea **5b** were also determined by fluorescence in CH<sub>2</sub>Cl<sub>2</sub>. The data obtained (log *K*<sub>ass</sub>: NO<sub>3</sub><sup>−</sup> = 3.87 and HSO<sub>4</sub><sup>−</sup> = 4.00) are

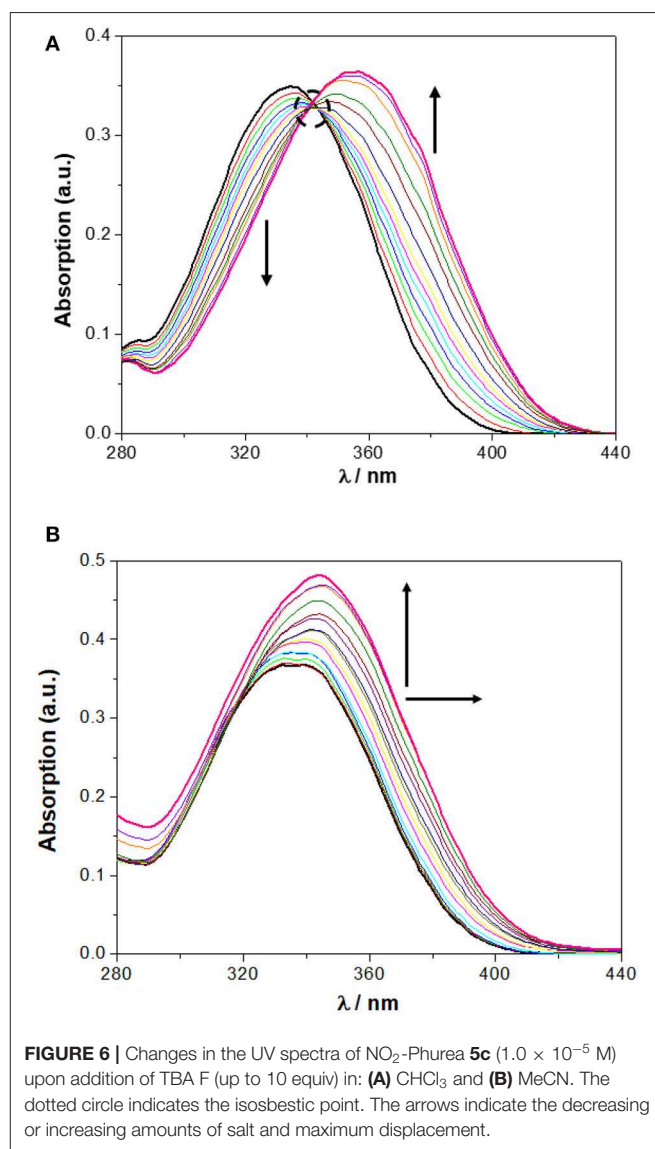
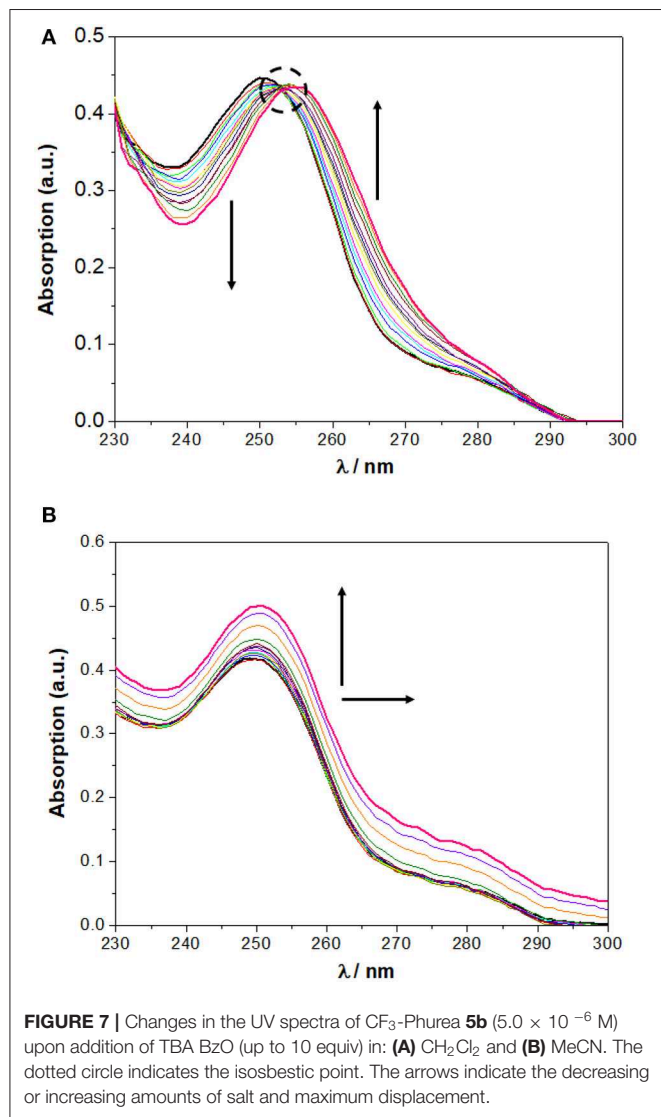


**FIGURE 6** | Changes in the UV spectra of NO<sub>2</sub>-Phurea **5c** ( $1.0 \times 10^{-5}$  M) upon addition of TBA F (up to 10 equiv) in: **(A)** CHCl<sub>3</sub> and **(B)** MeCN. The dotted circle indicates the isosbestic point. The arrows indicate the decreasing or increasing amounts of salt and maximum displacement.

higher, as expected, than those obtained for **5a** ( $\log K_{\text{ass}} = 3.5$  and 3.7) (Miranda et al., 2017), but follow the same trend. The results are also similar to those obtained by UV-Vis absorption (Table 3), indicating that fluorescence can also be a good method for the determination of the receptor-anion association constants.



## Organic Ion Pair Recognition

Based on our earlier good results obtained with Phurea **5a** (Gattuso et al., 2015), dihomooxa receptors **5b** and **5c** have also been tested as heteroditopic receptors for *n*-propyl and *n*-butylammonium chlorides in a preliminary study to evaluate their complexation behavior. Besides the presence of a hydrophobic cavity and an anionic binding site in close proximity, CF<sub>3</sub>- and NO<sub>2</sub>-Phureas displayed an enhancement of their binding efficiency for Cl<sup>−</sup> anion compared to that of **5a** (almost one log unity in the case of **5c**), being expected a higher positive effect on the salt complexation.

Proton NMR titrations were performed in CDCl<sub>3</sub> by adding increasing amounts (up to two equiv) of the salts to solutions of the receptors **5b** and **5c**. Three sets of resonances corresponding to the free and complexed receptors, and to the guest bound to the host were observed on addition of the first aliquot of the salts. The alkylammonium cation inclusion inside the dihomooxa cavity is demonstrated by the appearance of the alkyl group resonances in the negative region of the spectrum. On the other side, simultaneous chloride binding to the urea moiety is shown by the downfield shifts observed for all the NH protons, indicating complexation of the anion through hydrogen-bond interactions (Figure 8). This Figure also shows the pairs of enantiotopic hydrogen atoms of the α- and β-CH<sub>2</sub> groups of the included

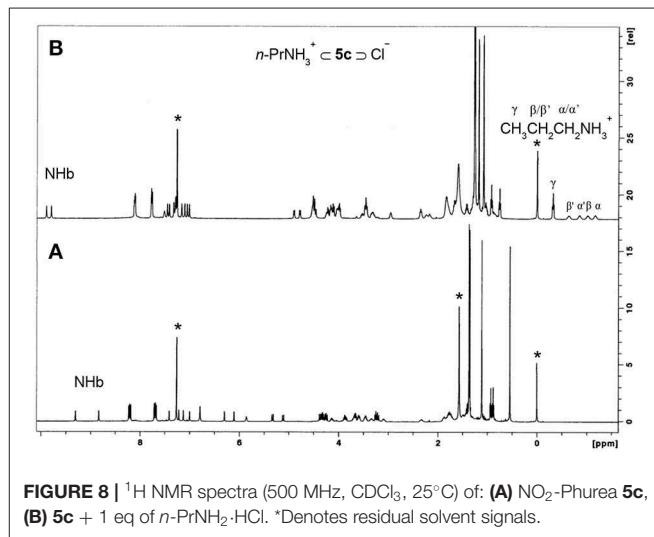


**TABLE 3** | Association constants ( $\log K_{\text{ass}}$ )<sup>a</sup> of dihomooxa ureas **5b** and **5c** determined by UV-Vis absorption at 25°C.

	Solvent	Spherical			Trigonal planar			Tetrahedral	
		F <sup>−</sup>	Cl <sup>−</sup>	Br <sup>−</sup>	NO <sub>3</sub> <sup>−</sup>	AcO <sup>−</sup>	BzO <sup>−</sup>	HSO <sub>4</sub> <sup>−</sup>	H <sub>2</sub> PO <sub>4</sub> <sup>−</sup>
CF <sub>3</sub> -Phurea <b>5b</b>	CH <sub>2</sub> Cl <sub>2</sub>	4.57	4.02	3.66	3.72	4.54	4.65	3.93	3.93
	MeCN	4.10	3.81	3.54	3.50	4.03	4.20	3.81	3.60
NO <sub>2</sub> -Phurea <b>5c</b>	CHCl <sub>3</sub>	4.74	4.30	3.90	3.97	4.65	4.72	4.19	4.24
	MeCN	4.52	4.04	3.61	3.63	4.13	4.30	3.77	3.83

Estimated error <10%.

guest displaying non-equivalent signals owing to the chiral environment of the host. The free host signals disappeared with subsequent additions of the salts. This binding process occurs under slow exchange condition on the NMR time scale. All these host-guest pairs studied displayed percentages of complexation higher than 95%, corresponding to association constants higher than  $10^9 \text{ M}^{-2}$ .

These ureas were then tested in the recognition of the monoamine neurotransmitter and trace amine hydrochlorides

shown in **Figure 9**. The studies were done in a  $\text{CDCl}_3/\text{CD}_3\text{OD}$  solvent mixture (5:1, v/v) for a better solubility of the guests. The addition of one equiv. of the guests to a solution of the hosts at room temperature (**Figure 10A**) induced a large broadening of all signals, indicating a strong host-guest interaction (**Figure 10B**). To obtain a clear interpretation of the spectra, it was however necessary to lower the temperature to 233 K. As illustrated in **Figure 10C** for **5b** with dopamine-HCl, four high field signals for the  $\alpha$ - and  $\beta$ - $\text{CH}_2$  protons of the guest were observed,

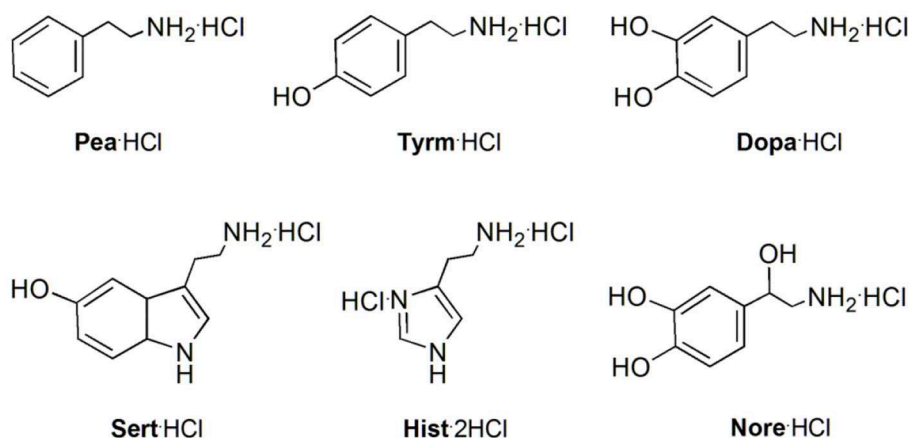


**FIGURE 9** | Structures of the monoamine neurotransmitters and trace amine hydrochlorides studied: 2-phenylethylamine (Pea-HCl), tyramine (Tyrm-HCl), dopamine (Dopa-HCl), serotonin (Sert-HCl), histamine (Hist-2HCl), and norepinephrine (Nore-HCl).

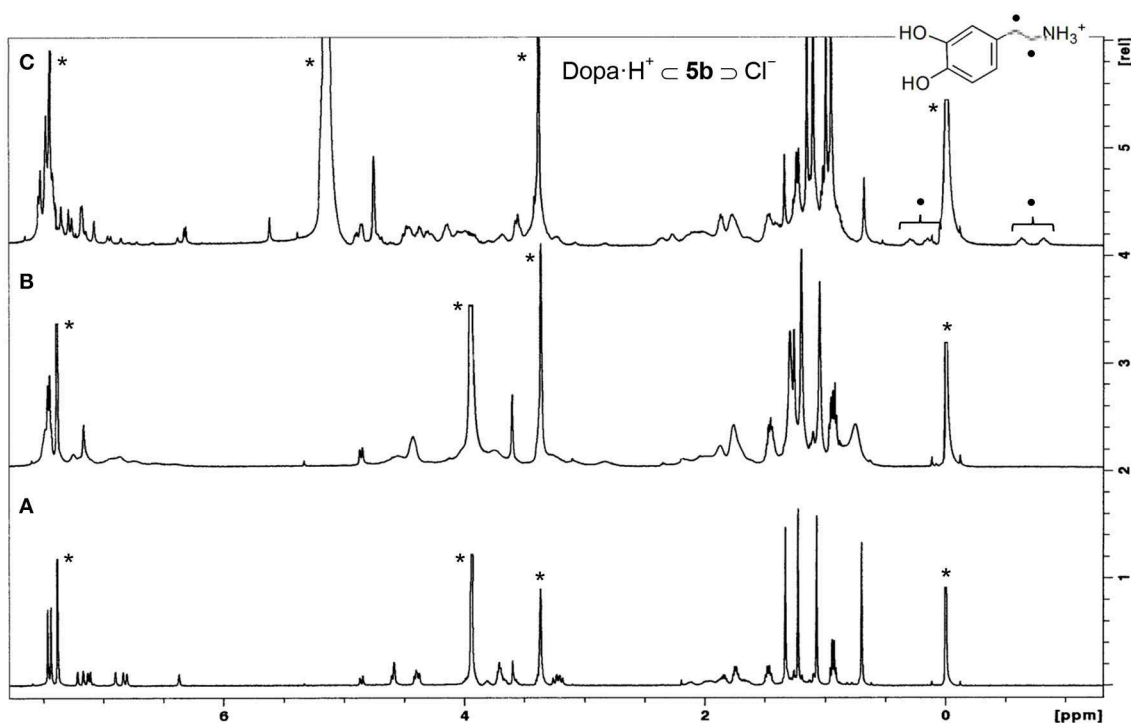


**FIGURE 10** |  $^1\text{H}$  NMR spectra (500 MHz,  $\text{CDCl}_3/\text{CD}_3\text{OD}$ , 5:1, v/v) of: **(A)**  $[\text{CF}_3\text{-Phurea } \mathbf{5b}] = 1.0 \text{ mM}$  at 298 K, **(B)**  $[\mathbf{5b}] = [\text{Dopa-HCl}] = 1.0 \text{ mM}$  at 298 K, and **(C)**  $[\mathbf{5b}] = [\text{Dopa-HCl}] = 1.0 \text{ mM}$  at 233 K. \*Residual solvent signals.



showing their inclusion inside the asymmetric cavity of the host. The slow exchange rate between the free and the complexed receptors allowed the determination of the percentages of complexation and of the corresponding association constants, by direct integration of the peaks. The data (Table 4) show that both ureas display an outstanding efficiency toward the biogenic amines, being as expected better than Phurea 5a. Both ureas present very high percentages of complexation and association constants, even preventing us from calculating  $K_{\text{ass}}$  for phenylethylamine and also tyramine in the case of NO<sub>2</sub>-Phurea 5c. This urea is more efficient than CF<sub>3</sub>-Phurea 5b, but the latter is slightly more selective. Ureas 5b and 5c display a similar affinity trend, comparable with 5a, showing some selectivity for Pea and Tyrm and no interaction with histamine and norepinephrine. As mentioned before (Gattuso et al., 2015), it seems that the less bulky Pea and Tyrm guests fit better inside the dihomooxa cavity.

## CONCLUSIONS

Two new 1,3-disubstituted dihomooxalix[4]arene receptors containing *para* CF<sub>3</sub>- (5b) or NO<sub>2</sub>-phenylurea (5c) moieties on the lower rim linked by a butyl spacer were obtained in the cone conformation in solution. The X-ray structure of 5b was obtained and confirms the cone conformation with one *tert*-butyl-phenyl group oriented toward the center of the cup. The 1,3-substitution pattern on the lower rim results in inherently chiral molecules, present as racemic mixture in the centrosymmetric crystals. In the crystal structure, the ureido groups are involved in asymmetric intra- and inter-molecular bifurcated H-bonds.

The anion binding affinity of 5b and 5c was established by <sup>1</sup>H NMR, UV-Vis and fluorescence studies. These receptors form 1:1 complexes with anions of different geometries through hydrogen bonding. Comparing to the unsubstituted phenylurea 5a, CF<sub>3</sub>-Phurea and especially NO<sub>2</sub>-Phurea showed, as expected, a relevant enhancement on their binding efficiency, due to the increased acidity of their urea NH protons. Compound 5c displayed the strongest complexation for F<sup>−</sup> (log  $K_{\text{ass}}$  = 3.88), closely followed by the oxoanions BzO<sup>−</sup>, AcO<sup>−</sup>, and HSO<sub>4</sub><sup>−</sup>. The association constants obtained by UV-Vis absorption titrations followed the same trend of those obtained by NMR, and were higher in CHCl<sub>3</sub> (or CH<sub>2</sub>Cl<sub>2</sub>) than in MeCN, according to the competitiveness of the solvents.

As heteroditopic receptors, both compounds exhibited remarkable ion pair recognition, displaying very high association

constants for the monoamine neurotransmitters tyramine, dopamine and serotonin, and the trace amine phenylethylamine hydrochlorides. The more efficient ditopic receptor 5c presented  $K_{\text{ass}}$  higher than 10<sup>9</sup> M<sup>−2</sup> in the case of Pea and Tyrm, which turns it into a potential candidate for biogenic amine chemosensors in biological fluids.

## EXPERIMENT

### Synthesis

All chemicals were reagent grade and were used without further purification. Chromatographic separations were performed on Merck silica gel 60 (particle size 40–63 μm, 230–400 mesh). Melting points were measured on a Stuart Scientific apparatus and are uncorrected. FTIR spectra were recorded on a Shimadzu Model IRAffinity-1 spectrophotometer. <sup>1</sup>H and <sup>13</sup>C NMR spectra were recorded on a Bruker Avance III 500 MHz spectrometer, with TMS as internal reference. The conventional COSY experiment was collected as 256 × 2 K complex points. Elemental analysis was determined on a Fisons EA 1108 microanalyser.

### Procedure for the Synthesis of Ureas 5b and 5c

To a solution of 4 (0.71 g, 0.762 mmol) in CHCl<sub>3</sub> (35 mL) was added 1.53 mmol of the appropriate isocyanate. The mixture was stirred at room temperature under N<sub>2</sub> for 4 h. Evaporation of the solvent yielded the crude products which were purified as described below.

### 7,13,19,25-Tetra-Tert-Butyl-27,29-Bis[[N'-(p-Trifluoromethylphenylureido)butyl]oxy]-28,30-dibutoxy-2,3-dihomo-3-oxacalix[4]arene (5b)

Flash chromatography (SiO<sub>2</sub>, eluent CH<sub>2</sub>Cl<sub>2</sub>/MeOH, 99.7:0.3): it was obtained in 51% yield (0.51 g); mp 151–152°C; IR (KBr) 3,350 cm<sup>−1</sup> (NH), 1,647 cm<sup>−1</sup> (CO); <sup>1</sup>H NMR (CDCl<sub>3</sub>, 500 MHz) δ 0.55, 1.10, 1.34, 1.37 [4s, 36H, C(CH<sub>3</sub>)], 0.89, 0.93 (2t, 6H, *J* = 7.4 Hz, CH<sub>3</sub>), 1.33–1.54 (m, 8H, OCH<sub>2</sub>CH<sub>2</sub>CH<sub>2</sub>CH<sub>3</sub> and OCH<sub>2</sub>CH<sub>2</sub>CH<sub>2</sub>CH<sub>2</sub>NH<sub>a</sub>), 1.77, 1.89, 2.31 (3m, 8H, OCH<sub>2</sub>CH<sub>2</sub>CH<sub>2</sub>CH<sub>3</sub> and OCH<sub>2</sub>CH<sub>2</sub>CH<sub>2</sub>CH<sub>2</sub>NH<sub>a</sub>), 3.16, 3.37, 3.59 (3m, 4H, OCH<sub>2</sub>CH<sub>2</sub>CH<sub>2</sub>CH<sub>2</sub>NH<sub>a</sub>), 3.20, 4.28 (ABq, 2H, *J* = 12.6 Hz, ArCH<sub>2</sub>Ar), 3.22, 4.26 (ABq, 2H, *J* = 14.1 Hz, ArCH<sub>2</sub>Ar), 3.24, 4.38 (ABq, 2H, *J* = 12.5 Hz, ArCH<sub>2</sub>Ar), 3.45, 3.71, 3.90, 4.07 (4m, 4H, OCH<sub>2</sub>CH<sub>2</sub>CH<sub>2</sub>CH<sub>2</sub>NH<sub>a</sub>), 3.59, 3.66, 3.82 (3m, 4H, OCH<sub>2</sub>CH<sub>2</sub>CH<sub>2</sub>CH<sub>3</sub>), 4.32, 5.26 (ABq, 2H, *J* = 12.4 Hz, CH<sub>2</sub>OCH<sub>2</sub>), 4.33, 5.04 (ABq, 2H, *J* = 12.7 Hz, CH<sub>2</sub>OCH<sub>2</sub>), 5.87, 6.57 (2t, 2H, NH<sub>a</sub>), 6.11, 6.35, 6.78, 6.98, 7.12, 7.20, 7.27, 7.37

**TABLE 4** | Percentages of complex formation and corresponding association constants,  $K_{\text{ass}}$  (M<sup>−2</sup>)<sup>a</sup>.

	Pea-HCl	Tyrm-HCl	Dopa-HCl	Sert-HCl	Hist-2HCl	Nore-HCl
Phurea 5a <sup>b</sup>	86% 41,000	85% 36,000	67% 6,300	61% 4,100	c	c
CF <sub>3</sub> -Phurea 5b	>95% >10 <sup>9</sup>	91% 1,23,000	79% 18,000	81% 22,000	c	c
NO <sub>2</sub> -Phurea 5c	>95% >10 <sup>9</sup>	>95% >10 <sup>9</sup>	87% 51,000	86% 42,000	c	c

<sup>a</sup>CDCl<sub>3</sub>/CD<sub>3</sub>OD (5:1, v/v), 233 K; Estimated error ≤15%.

<sup>b</sup>Data taken from Gattuso et al. (2015).

<sup>c</sup>No complexation observed.

(8d, 8H, ArH), 7.50, 7.53 (2d, 4H, Ph-H<sub>o</sub>), 7.60, 7.61 (2d, 4H, Ph-H<sub>m</sub>), 8.45, 8.79 (2s, 2H, NH<sub>b</sub>); <sup>13</sup>C NMR (CDCl<sub>3</sub>, 125.8 MHz) δ 13.9, 14.1 [O(CH<sub>2</sub>)<sub>3</sub>CH<sub>3</sub>], 19.3, 19.4 (OCH<sub>2</sub>CH<sub>2</sub>CH<sub>2</sub>CH<sub>3</sub>), 25.0, 25.5, 25.8, 28.8 (OCH<sub>2</sub>CH<sub>2</sub>CH<sub>2</sub>CH<sub>2</sub>NH<sub>a</sub>), 28.9, 31.0, 31.3 (ArCH<sub>2</sub>Ar), 31.2, 31.4, 31.6, 31.7 [C(CH<sub>3</sub>)], 32.2, 32.6 (OCH<sub>2</sub>CH<sub>2</sub>CH<sub>2</sub>CH<sub>3</sub>), 33.6, 33.9, 34.21, 34.22 [C(CH<sub>3</sub>)], 39.3, 39.4 (OCH<sub>2</sub>CH<sub>2</sub>CH<sub>2</sub>CH<sub>2</sub>NH<sub>a</sub>), 71.7, 71.9 (CH<sub>2</sub>OCH<sub>2</sub>), 73.2, 74.8, 75.0, 75.6 (OCH<sub>2</sub>CH<sub>2</sub>CH<sub>2</sub>CH<sub>2</sub>NH<sub>a</sub> and OCH<sub>2</sub>CH<sub>2</sub>CH<sub>2</sub>CH<sub>3</sub>), 117.7, 117.8, 123.7, 125.4, 125.6, 126.0, 126.1, 126.3, 126.49, 126.52, 126.9, 129.5 (ArH), 123.3, 124.1 (q, *J* = 32 Hz, CF<sub>3</sub>), 128.6, 130.2, 131.8, 132.7, 133.1, 134.3, 134.6, 136.2, 143.1, 143.4, 144.4, 145.0, 145.1, 145.7, 152.7, 153.1, 153.9, 155.3 (Ar), 155.6, 156.7 (CO). Anal. Calcd for C<sub>77</sub>H<sub>100</sub>N<sub>4</sub>O<sub>7</sub>F<sub>6</sub>: C, 70.73; H, 7.71; N, 4.28. Found: C, 70.78; H, 8.01; N, 4.02.

### 7,13,19,25-Tetra-Tert-Butyl-27,29-Bis[[N'-(p-Nitrophenylureido)Butyl]oxy]-28,30-dibutoxy-2,3-dihomo-3-oxacalix[4]arene (5c)

Flash chromatography (SiO<sub>2</sub>, eluent CH<sub>2</sub>Cl<sub>2</sub>/MeOH, 99.7:0.3) followed by recrystallization from CH<sub>2</sub>Cl<sub>2</sub>/*n*-hexane: it was obtained in 40% yield (0.38 g); mp 157–159°C; IR (KBr) 3,367 cm<sup>-1</sup> (NH), 1,647 cm<sup>-1</sup> (CO); <sup>1</sup>H NMR (CDCl<sub>3</sub>, 500 MHz) δ 0.54, 1.11, 1.35, 1.37 [4s, 36H, C(CH<sub>3</sub>)], 0.88, 0.93 (2t, 6H, *J* = 7.4 Hz, CH<sub>3</sub>), 1.38–1.50 (m, 4H, OCH<sub>2</sub>CH<sub>2</sub>CH<sub>2</sub>CH<sub>3</sub>), 1.48, 1.76, 1.87, 2.34 (4m, 12H, OCH<sub>2</sub>CH<sub>2</sub>CH<sub>2</sub>CH<sub>2</sub>NH<sub>a</sub> and OCH<sub>2</sub>CH<sub>2</sub>CH<sub>2</sub>CH<sub>3</sub>), 3.09, 3.34, 3.45, 3.59 (4m, 4H, OCH<sub>2</sub>CH<sub>2</sub>CH<sub>2</sub>CH<sub>2</sub>NH<sub>a</sub>), 3.20, 4.26 (ABq, 2H, *J* = 12.7 Hz, ArCH<sub>2</sub>Ar), 3.23, 4.24 (ABq, 2H, *J* = 14.0 Hz, ArCH<sub>2</sub>Ar), 3.26, 4.37 (ABq, 2H, *J* = 12.6 Hz, ArCH<sub>2</sub>Ar), 3.45, 3.59, 3.66, 4.14 (4m, 4H, OCH<sub>2</sub>CH<sub>2</sub>CH<sub>2</sub>CH<sub>2</sub>NH<sub>a</sub>), 3.66, 3.87 (2m, 4H, OCH<sub>2</sub>CH<sub>2</sub>CH<sub>2</sub>CH<sub>3</sub>), 4.31, 5.33 (ABq, 2H, *J* = 12.3 Hz, CH<sub>2</sub>OCH<sub>2</sub>), 4.33, 5.12 (ABq, 2H, *J* = 12.3 Hz, CH<sub>2</sub>OCH<sub>2</sub>), 5.85, 6.79 (2t, 2H, NH<sub>a</sub>), 6.10, 6.29, 6.79, 7.00, 7.12, 7.21, 7.26, 7.41 (8d, 8H, ArH), 7.68, 7.71 (2d, 4H, Ph-H<sub>o</sub>), 8.20, 8.23 (2d, 4H, Ph-H<sub>m</sub>), 8.83, 9.31 (2s, 2H, NH<sub>b</sub>); <sup>13</sup>C NMR (CDCl<sub>3</sub>, 125.8 MHz) δ 13.9, 14.1 [O(CH<sub>2</sub>)<sub>3</sub>CH<sub>3</sub>], 19.3, 19.4 (OCH<sub>2</sub>CH<sub>2</sub>CH<sub>2</sub>CH<sub>3</sub>), 24.8, 25.2, 25.7, 28.81 (OCH<sub>2</sub>CH<sub>2</sub>CH<sub>2</sub>CH<sub>2</sub>NH<sub>a</sub>), 28.84, 31.1, 31.4 (ArCH<sub>2</sub>Ar), 31.2, 31.4, 31.5, 31.7 [C(CH<sub>3</sub>)], 32.2, 32.6 (OCH<sub>2</sub>CH<sub>2</sub>CH<sub>2</sub>CH<sub>3</sub>), 33.6, 34.0, 34.24, 34.23 [C(CH<sub>3</sub>)], 39.3 (2C) (OCH<sub>2</sub>CH<sub>2</sub>CH<sub>2</sub>CH<sub>2</sub>NH<sub>a</sub>), 71.7, 72.1 (CH<sub>2</sub>OCH<sub>2</sub>), 73.9, 74.9, 75.1, 75.6 (OCH<sub>2</sub>CH<sub>2</sub>CH<sub>2</sub>CH<sub>2</sub>NH<sub>a</sub> and OCH<sub>2</sub>CH<sub>2</sub>CH<sub>2</sub>CH<sub>3</sub>), 117.0, 117.1, 123.6, 125.3, 125.56, 125.60, 125.63, 126.0, 126.1, 126.6, 126.9, 130.0 (ArH), 128.3, 129.7, 131.6, 132.7, 133.1, 134.3, 134.6, 136.2, 141.6, 142.1, 144.4, 145.1, 145.2, 145.8, 146.1, 146.7, 152.7, 153.2, 153.8, 154.9 (Ar), 155.7, 156.3 (CO). Anal. Calcd for C<sub>75</sub>H<sub>100</sub>N<sub>6</sub>O<sub>11</sub>: C, 71.40; H, 7.99; N, 6.66. Found: C, 70.99; H, 7.99; N, 6.48.

### Determination of the Crystallographic Structure of Compound 5b

Small colorless single crystal needles were obtained by slow evaporation of a chloroform solution containing compound 5b. The single crystals investigated were very small (0.01, 0.01, 0.05 mm) and synchrotron radiation was necessary to obtain a dataset suitable to solve the structure. The data was also collected with frozen crystal at 100 K. Despite these provisions, the best small crystal showed poor diffraction data with a

maximum resolution of 0.98 Å. Data collection was carried out at the Macromolecular crystallography XRD1 beamline of the Elettra synchrotron (Trieste, Italy), employing the rotating-crystal method with a Dectris Pilatus 2M area detector. Single crystals were dipped in PEG200 cryoprotectant, mounted on a loop and flash-frozen under a liquid nitrogen stream at a 100 K. Diffraction data were indexed and integrated using the XDS package (Kabsch, 2010a), while scaling was carried out with XSCALE (Kabsch, 2010b). The structure was solved using the SHELXT program (Sheldrick, 2015) and structure refinement was performed with SHELXL-14 (Sheldrick, 2008), operating through the WinGX GUI (Farrugia, 2012) by full-matrix least-squares (FMLS) methods on F<sup>2</sup>.

The structure was solved using the SHELXT program (Sheldrick, 2015). The asymmetric unit of the monoclinic crystal (space group P2<sub>1</sub>/c) is composed of one molecule of 5b and disordered co-crystallized chloroform solvent molecule with a total occupancy factor of 0.7. The chloroform molecule shows disorder over two positions, which were isotropically refined at 0.4/0.3 partial occupancies. All other non-hydrogen atoms were anisotropically refined at full occupancy. Hydrogen atoms were added at the calculated positions and refined using the riding model. Crystallographic data and refinement details are reported in Table S1.

### <sup>1</sup>H NMR Titrations

The anion association constants (as log *K*<sub>ass</sub>) were determined in CDCl<sub>3</sub> by <sup>1</sup>H NMR titration experiments. Several aliquots (up to 10 equiv) of the anion solutions (as tetrabutylammonium salts) were added to 0.5 mL solution of the receptors (2.5 × 10<sup>-3</sup> – 5 × 10<sup>-3</sup> M) directly in the NMR tube. The spectra were recorded after each addition of the salts, and the temperature of the NMR probe was kept constant at 25°C. For each anion-receptor system titrations were repeated at least two times. The association constants were evaluated using the WinEQNMR2 program (Hynes, 1993) by following the urea NH chemical shifts. When possible, *K*<sub>ass</sub> was calculated as a mean value of the four NH chemical shifts. The Job plots were performed keeping the total concentration in the same range as before. Concerning ion-pair recognition experiments, the percentage of complex formation, necessary for the calculation of the corresponding *K*<sub>ass</sub>, was determined by direct <sup>1</sup>H NMR integration of the free and complexed resonances of the hosts and/or the guests, present at equilibrium. The samples were prepared by mixing aliquots of stock solutions of the host (600 μl) and guests (60 μl) to obtain a final equimolar host-guest solution of 1.0 × 10<sup>-3</sup> M. Details related to these experiments have already been described (Gattuso et al., 2015).

### UV-Vis Absorption and Fluorescence Studies

Absorption and fluorescence studies were done using an UV-3101PC UV-Vis-NIR spectrophotometer and a Fluorolog F112A fluorimeter in right-angle configuration, respectively. The association constants were determined in CHCl<sub>3</sub> (or CH<sub>2</sub>Cl<sub>2</sub>) and MeCN by UV-Vis absorption spectrophotometry at 25°C. A few anion complexation studies were also done by steady-state

fluorescence in  $\text{CH}_2\text{Cl}_2$ . The spectra were recorded between 230 and 300 nm or 280–440 nm, in the case of  $\text{NO}_2$ -Phurea **5c**, and using quartz cells with an optical path length of 1 cm. Several aliquots (up to 10 equiv) of the anion solutions (as TBA salts) were added to a 2 mL solution of the receptors ( $5.0 \times 10^{-6}$  –  $5.0 \times 10^{-5}$  M) directly in the cell. The spectral changes were interpreted using the HypSpec 2014 program (Gans et al., 1996). Details concerning the photophysical properties determination are given in the **Supporting Information**.

## DATA AVAILABILITY STATEMENT

The datasets generated for this study are available on request to the corresponding author.

## AUTHOR CONTRIBUTIONS

AM synthesized and characterized the compounds, carried out the UV-Vis absorption, and fluorescence studies. DS contributed to the synthesis, characterization, and UV-Vis titrations of one of the compounds. PM designed the study, performed the NMR experiments, their analysis and interpretation, and wrote the manuscript. JA carried out some NMR experiments, their analysis and interpretation, contributed also

to the writing, and critical review of the manuscript. MB-S performed the analysis, interpretation, and writing of the photophysics results. NH did the crystallization and structure determination by X-ray diffraction, the analysis, interpretation, and manuscript preparation for structural data. SG performed the analysis, interpretation, and manuscript preparation for structural data.

## FUNDING

This work was funded by Fundação para a Ciência e a Tecnologia.

## ACKNOWLEDGMENTS

Authors thank *Fundação para a Ciência e a Tecnologia*, Project ref. UID/UI/00100/2013; AM thanks a Ph.D. Grant ref. SFRH/BD/129323/2017. DS thanks to UPMC (Paris) for an internship grant.

## SUPPLEMENTARY MATERIAL

The Supplementary Material for this article can be found online at: <https://www.frontiersin.org/articles/10.3389/fchem.2019.00758/full#supplementary-material>

## REFERENCES

- Amendola, V., Esteban-Gómez, D., Fabbri, L., and Licchelli, M. (2006). What anions do to N-H containing receptors. *Acc. Chem. Res.* 39, 343–353. doi: 10.1021/ar050195l
- Amendola, V., Fabbri, L., and Mosca, L. (2010). Anion recognition by hydrogen bonding: urea-based receptors. *Chem. Soc. Rev.* 39, 3889–3915. doi: 10.1039/b822552b
- Augusto, A. S., Miranda, A. S., Ascenso, J. R., Miranda, M. Q., Félix, V., Brancatelli, G., et al. (2018). Anion recognition by partial cone dihomooxacalix[4]arene based receptors bearing urea groups: remarkable affinity for benzoate ion. *Eur. J. Org. Chem.* 5657–5667. doi: 10.1002/ejoc.201800880
- Babu, J. N., Bhalla, V., Kumar, M., Puri, R. K., and Mahajan, R. K. (2009). Chloride ion recognition using thiourea/urea based receptors incorporated into 1,3-disubstituted calix[4]arenes. *New J. Chem.* 33, 675–681. doi: 10.1039/b816275a
- Busschaert, N., Caltagirone, C., Van Rossom, W., and Gale, P. A. (2015). Applications of supramolecular anion recognition. *Chem. Rev.* 115, 8038–8155. doi: 10.1021/acs.chemrev.5b00099
- Capici, C., De Zorzi, R., Gargiulli, C., Gattuso, G., Geremia, S., Notti, A., et al. (2010). Calix[5]crown-3-based heteroditopic receptors for n-butylammonium halides. *Tetrahedron* 66, 4987–4993. doi: 10.1016/j.tet.2010.05.021
- Cornut, D., Moerkerke, S., Wouters, J., Bruylants, G., and Jabin, I. (2015). A biomimetic heteroditopic receptor for zwitterions in protic media. *Chem. Asian J.* 10, 440–446. doi: 10.1002/asia.201403082
- Curinova, P., Stibor, I., Budka, J., Sykora, J., Kamil, L., and Lhotak, P. (2009). Anion recognition by diureido-calix[4]arenes in the 1,3-alternate conformation. *New J. Chem.* 33, 612–619. doi: 10.1039/b816790g
- De Solis, S., Elisei, F., and Gunnlaugsson, T. (2015). Lower rim amide (1,3) functionalized calix[4]arene amido-thiourea derivatives as dimetallic Zn(II) coordination complexes for anion recognition/sensing. *Supramol. Chem.* 27, 697–705. doi: 10.1080/10610278.2015.1079633
- Evans, N. H., and Beer, P. D. (2014). Advances in anion supramolecular chemistry: from recognition to chemical applications. *Angew. Chem. Int. Ed.* 53, 11716–11754. doi: 10.1002/anie.201309937
- Farrugia, L. J. (2012). WinGX and ORTEP for windows: an update. *J. Appl. Cryst.* 45, 849–854. doi: 10.1107/S0021889812029111
- Gale, P. A., Howe, E. N. W., and Wu, X. (2016). Anion receptor chemistry. *Chem* 1, 351–422.
- Gans, P., Sabatini, A., and Vacca, A. (1996). Investigation of equilibria in solution. Determination of equilibrium constants with the HYPERQUAD suite of programs. *Talanta* 43, 1739–1753. doi: 10.1016/0039-9140(96)01958-3
- Gattuso, G., Notti, A., Parisi, M. F., Pisagatti, I., Marcos, P. M., Ascenso, J. R., et al. (2015). Selective recognition of biogenic amine hydrochlorides by heteroditopic dihomooxacalix[4]arenes. *New J. Chem.* 39, 817–821. doi: 10.1039/c4nj01423e
- Gutsche, C. D. (2008). *Calixarenes (Monographs in Supramolecular Chemistry)*. Cambridge: The Royal Society of Chemistry.
- Hamon, M., Ménand, M., Le Gac, S., Luhmer, M., Dalla, V., and Jabin, I. (2008). Calix[6]tris(thio)ureas: heteroditopic receptors for the cooperative binding of organic ion pairs. *J. Org. Chem.* 73, 7067–7071. doi: 10.1021/jo800712q
- Hynes, M. J. (1993). EQNMR: a computer program for the calculation of stability constants from nuclear magnetic resonance chemical shift data. *J. Chem. Soc. Dalton Trans.* 311–312. doi: 10.1039/DT9930000311
- Jaime, C., de Mendoza, J., Prados, P., Nieto, P., and Sanchez, C. (1991). Carbon-13 NMR chemical shifts. A single rule to determine the conformation of calix[4]arenes. *J. Org. Chem.* 56, 3372–3376. doi: 10.1021/jo00010a036
- Kabsch, W. (2010a). XDS. *Acta Cryst. D* 66, 125–132. doi: 10.1107/S0907444909047337
- Kabsch, W. (2010b). Integration, scaling, space-group assignment and post-refinement. *Acta Cryst. D* 66, 133–144. doi: 10.1107/S0907444909047374
- Kim, S. K., and Sessler, J. L. (2010). Ion pair receptors. *Chem. Soc. Rev.* 39, 3784–3809. doi: 10.1039/c002694h
- Klejš, T., Slavicek, J., Hudecek, O., Eigner, V., Gutierrez, N. A., Curinova, P., et al. (2016). Calix[4]arenes containing a ureido functionality on the lower rim as highly efficient receptors for anion recognition. *New J. Chem.* 40, 7935–7942. doi: 10.1039/c6nj01271j
- Lascaux, A., le Gac, S., Wouters, J., Luhmer, M., and Jabin, I. (2010). An allosteric heteroditopic receptor for neutral guests and contact ion pairs with

- a remarkable selectivity for ammonium fluoride salts. *Org. Biomol. Chem.* 8, 4607–4616. doi: 10.1039/c0ob00211a
- Marcos, P. M. (2016). "Functionalization and properties of homooxalixarenes," in *Calixarenes and Beyond*, eds P. Neri, J. L. Sessler, M. X. Wang (Switzerland: Springer International Publishing), 445–466. doi: 10.1007/978-3-319-31867-7\_17
- Marcos, P. M., Teixeira, F. A., Segurado, M. A. P., Ascenso, J. R., Bernardino, R. J., Brancatelli, G., et al. (2014b). Synthesis and anion binding properties of new dihomooxalix[4]arene diurea and dithiourea receptors. *Tetrahedron* 70, 6497–6505. doi: 10.1016/j.tet.2014.07.020
- Marcos, P. M., Teixeira, F. A., Segurado, M. A. P., Ascenso, J. R., Bernardino, R. J., Michel, S., et al. (2014a). Bidentate urea derivatives of *p*-tert-butylidihomooxalix[4]arene: neutral receptors for anion complexation. *J. Org. Chem.* 79, 742–751. doi: 10.1021/jo4026012
- Marcus, Y. (1997). *Ion Properties*. New York, NY: Marcel Dekker, 50–51.
- McConnell, A. J., and Beer, P. D. (2012). Heteroditopic receptors for ion-pair recognition. *Angew. Chem. Int. Ed.* 51, 5052–5061. doi: 10.1002/anie.201107244
- Miranda, A. S., Martelo, L. M., Fedorov, A. A., Berberan-Santos, M. N., and Marcos, P. M. (2017). Fluorescence properties of *p*-tert-butylidihomooxalix[4]arene derivatives and the effect of anion complexation. *New J. Chem.* 41, 5967–5973. doi: 10.1039/c7nj00652g
- Moerkerke, S., Malytskyi, V., Marcéls, L., Wouters, J., and Jabin, I. (2017). Selective recognition of quaternary ammonium ions and zwitterions by using a biomimetic bis-calix[6]arene-based receptor. *Org. Biomol. Chem.* 15, 8967–8974. doi: 10.1039/c7ob02031g
- Mutihac, L., Lee, J. H., Kim, J. S., and Vicens, J. (2011). Recognition of amino acids by functionalized calixarenes. *Chem. Soc. Rev.* 40, 2777–2796. doi: 10.1039/c0cs00005a
- Nehra, A., Bandaru, S., Yarramala, D. S., and Rao, C. P. (2016). Differential recognition of anions with selectivity towards F<sup>−</sup> by a calix[6]arene-thiourea conjugate investigated by spectroscopy, microscopy, and computational modeling by DFT. *Chem. Eur. J.* 22, 8903–8914. doi: 10.1002/chem.201600844
- Pescatori, L., Arduini, A., Pochini, A., Secchi, A., Massera, C., and Ugozzoli, F. (2009). Monotopic and heteroditopic calix[4]arene receptors as hosts for pyridinium and viologen ion pairs: a solution and solid-state study. *Org. Biomol. Chem.* 7, 3698–3708. doi: 10.1039/b906409e
- Quinlan, E., Matthews, S. E., and Gunnlaugsson, T. (2007). Colorimetric recognition of anions using preorganized tetra-amidourea derived calix[4]arene sensors. *J. Org. Chem.* 72, 7497–7503. doi: 10.1021/jo070439a
- Rezankova, M., Budka, J., Miksatko, J., Eigner, V., Cisarova, I., Curinova, P., et al. (2017). Anion receptors based on intramolecularly bridged calix[4]arenes bearing ureido functions. *Tetrahedron* 73, 742–749. doi: 10.1016/j.tet.2016.12.054
- Sheldrick, G. M. (2008). A short history of SHELX. *Acta Cryst. A* 64, 112–122. doi: 10.1107/S0108767307043930
- Sheldrick, G. M. (2015). SHELXT - Integrated space-group and crystal-structure determination. *Acta Cryst. A* 71, 3–8. doi: 10.1107/S2053273314026370
- Teixeira, F. A., Marcos, P. M., Ascenso, J. R., Brancatelli, G., Hickey, N., and Geremia, S. (2017). Selective binding of spherical and linear anions by tetraphenyl(thio)urea-based dihomooxalix[4]arene receptors. *J. Org. Chem.* 82, 11383–11390. doi: 10.1021/acs.joc.7b01801

**Conflict of Interest:** The authors declare that the research was conducted in the absence of any commercial or financial relationships that could be construed as a potential conflict of interest.

Copyright © 2019 Miranda, Serbetci, Marcos, Ascenso, Berberan-Santos, Hickey and Geremia. This is an open-access article distributed under the terms of the Creative Commons Attribution License (CC BY). The use, distribution or reproduction in other forums is permitted, provided the original author(s) and the copyright owner(s) are credited and that the original publication in this journal is cited, in accordance with accepted academic practice. No use, distribution or reproduction is permitted which does not comply with these terms.





# $\beta$ -D-Galactose-Functionalized Pillar[5]arene With Interesting Planar-Chirality for Constructing Chiral Nanoparticles

Guangping Sun<sup>1</sup>, Liangtao Pu<sup>4</sup>, Srikala Pangannaya<sup>1</sup>, Tangxin Xiao<sup>3</sup>, Xiao-Yu Hu<sup>1,2\*</sup>, Juli Jiang<sup>1\*</sup> and Leyong Wang<sup>1,3</sup>

<sup>1</sup> Key Laboratory of Mesoscopic Chemistry of Ministry of Education, Jiangsu Key Laboratory of Advanced Organic Materials, School of Chemistry and Chemical Engineering, Nanjing University, Nanjing, China, <sup>2</sup> College of Material Science and Technology, Nanjing University of Aeronautics and Astronautics, Nanjing, China, <sup>3</sup> School of Petrochemical Engineering, Changzhou University, Changzhou, China, <sup>4</sup> State Key Laboratory of Pollution Control and Resource Reuse, School of Environment, Nanjing University, Nanjing, China

## OPEN ACCESS

### Edited by:

De-Xian Wang,  
Institute of Chemistry (CAS), China

### Reviewed by:

Min Xue,  
Zhejiang Sci-Tech University, China  
Yuxin Pei,  
Northwest A&F University, China

### \*Correspondence:

Xiao-Yu Hu  
huxy@nuaa.edu.cn  
Juli Jiang  
jjl@nju.edu.cn

### Specialty section:

This article was submitted to  
Supramolecular Chemistry,  
a section of the journal  
Frontiers in Chemistry

**Received:** 30 August 2019

**Accepted:** 17 October 2019

**Published:** 14 November 2019

### Citation:

Sun G, Pu L, Pangannaya S, Xiao T, Hu X-Y, Jiang J and Wang L (2019)  $\beta$ -D-Galactose-Functionalized Pillar[5]arene With Interesting Planar-Chirality for Constructing Chiral Nanoparticles. *Front. Chem.* 7:743. doi: 10.3389/fchem.2019.00743

Planar-chiral pillar[5]arenes bearing  $\beta$ -D-galactose substituents on both rims have been successfully synthesized and effectively separated by silica gel chromatography with a high yield. The obtained (*S<sub>p</sub>*)- and (*R<sub>p</sub>*)- $\beta$ -D-galactose functionalized pillar[5]arenes [(*S<sub>p</sub>*-D)-GP5 and (*R<sub>p</sub>*-D)-GP5] exhibit the *S<sub>p</sub>* and *R<sub>p</sub>* planar chirality. Furthermore, (*S<sub>p</sub>*-D)-GP5 and (*R<sub>p</sub>*-D)-GP5 can not racemize according to dynamic <sup>1</sup>H NMR and CD spectra. Notably, GP5 is able to capture a guest molecule (DNS-CPT) to form a host-guest supramolecular amphiphile, which can further self-assemble into chiral nanoparticles with the *S<sub>p</sub>* and *R<sub>p</sub>* planar chirality of (*S<sub>p</sub>*-D)-GP5 and (*R<sub>p</sub>*-D)-GP5 still being retained, suggesting GP5 could be as reliable chiral sources to transfer the *S<sub>p</sub>* and *R<sub>p</sub>* planar chirality.

**Keywords:** supramolecular macrocycles,  $\beta$ -D-galactose-functionalized pillar[5]arenes, planar chirality, self-assembly, nanoparticles

## INTRODUCTION

Supramolecular macrocycles, such as cyclodextrins, cucurbiturils, and calixarenes, have played a very important role in supramolecular chemistry (Moghaddam et al., 2011; Zhang and Wang, 2011; Jie et al., 2015; Choi et al., 2017). Compared with these traditional macrocycles, pillar[n]arenes have attracted more attention due to their unique planar chirality (Ogoshi et al., 2011b). The planar chirality of pillar[n]arenes is very useful for chiral molecular recognition, chirality switches, and catalysis because of the outstanding host-guest properties of pillar[n]arenes to capture different guest molecules (Yao et al., 2017; Lee et al., 2018; Park et al., 2019).

As many literatures have presented (Ogoshi et al., 2011a, 2012, 2013a,b, 2016; Kitajima et al., 2014), the planar chirality of pillar[n]arenes is mainly caused by the substitution position of the alkoxy moieties. Ogoshi et al. (2012) and Kitajima et al. (2014) found that all of the synthesized pillar[5]arenes are racemic mixtures and racemization takes place by rotation of units. These racemic mixtures could be divided into eight conformers including diastereomeric conformers: (*S<sub>p</sub>*, *S<sub>p</sub>*, *S<sub>p</sub>*, *S<sub>p</sub>*, *S<sub>p</sub>*), (*R<sub>p</sub>*, *S<sub>p</sub>*, *S<sub>p</sub>*, *S<sub>p</sub>*, *S<sub>p</sub>*), (*R<sub>p</sub>*, *R<sub>p</sub>*, *S<sub>p</sub>*, *S<sub>p</sub>*, *S<sub>p</sub>*), (*R<sub>p</sub>*, *S<sub>p</sub>*, *R<sub>p</sub>*, *S<sub>p</sub>*, *S<sub>p</sub>*) and their antipodal enantiomers: (*R<sub>p</sub>*, *R<sub>p</sub>*, *R<sub>p</sub>*, *R<sub>p</sub>*, *R<sub>p</sub>*), (*S<sub>p</sub>*, *R<sub>p</sub>*, *R<sub>p</sub>*, *R<sub>p</sub>*, *R<sub>p</sub>*), (*S<sub>p</sub>*, *S<sub>p</sub>*, *R<sub>p</sub>*, *R<sub>p</sub>*, *R<sub>p</sub>*), (*S<sub>p</sub>*, *R<sub>p</sub>*, *S<sub>p</sub>*, *R<sub>p</sub>*, *R<sub>p</sub>*). In order to isolate the different pillar[5]arene enantiomers, they have functionalized pillar[5]arene with 10 bulky cyclohexylmethyl groups at both rims to inhibit the rotation of the units (Ogoshi et al., 2011a). Then, two special enantiomers [(*S<sub>p</sub>*, *S<sub>p</sub>*, *S<sub>p</sub>*, *S<sub>p</sub>*, *S<sub>p</sub>*) and

(*R<sub>p</sub>*, *R<sub>p</sub>*, *R<sub>p</sub>*, *R<sub>p</sub>*, *R<sub>p</sub>*) were successfully separated by chiral high performance liquid chromatography (HPLC). The circular dichroism (CD) spectra of the two enantiomers were clearly defined with a complete mirror image, which was defined as (*S<sub>p</sub>*)- and (*R<sub>p</sub>*)-pillar[5]arenes, respectively. Simultaneously, Strutt et al. (2012, 2014) reported the separation of pillararene-based enantiomers by introducing one  $\pi$ -conjugated unit, which expressed good and selective encapsulation of neutral and positively charged electron poor aromatic guests. Moreover, some other researches (Yao et al., 2017; Lee et al., 2018; Park et al., 2019) about planar chirality of pillar[5]arenes have been performed to achieve chiral inversion, chiral transfer and so on. Besides the above mentioned pillar[n]arene derivatives,  $\beta$ -D-galactose-functionalized pillar[5]arene (GP5), as a new-type of sugar modified supramolecular amphiphile, has been widely used in biologically relevant fields for the construction of antibacterial and targeted drug delivery systems (Nierengarten et al., 2013; Yu et al., 2013; Liu et al., 2017; Wu et al., 2017). However, all the results above never revealed the planar chirality of GP5, and there was no report about the investigation of (*S<sub>p</sub>*)- and (*R<sub>p</sub>*)- $\beta$ -D-galactose-functionalized pillar[5]arene [(*S<sub>p</sub>*)-GP5 and (*R<sub>p</sub>*)-GP5]. In our previous work (Liu et al., 2017), we have obtained a similar  $\beta$ -D-galactose-based water-soluble pillar[5]arene (GalP5), which showed no planar chirality, because GalP5 possessed one methylene group at the position of  $\beta$ -D-galactose, resulting in the disappearance of planar chirality induced in the progress of functionalized pillar[5]arenes. Herein, we have successfully designed a new  $\beta$ -D-galactose functionalized pillar[5]arene without the presence of methylene group connected with  $\beta$ -D-galactose, and first achieved the separation of diastereoisomers possessing planar chirality by silica gel chromatography to obtain (*S<sub>p</sub>*)-GP5 and (*R<sub>p</sub>*)-GP5 with a high yield. Their rotational and planar chiral properties were investigated by NMR, UV-Vis and CD measurements, respectively.

## RESULTS AND DISCUSSION

### Planar Chirality of GP5

The synthesis of GP5 relies on the copper-catalyzed alkyne-azide cycloaddition (CuAAC) reaction, which was used to introduce the bulky  $\beta$ -D-acetylgalactose moieties on both rims of the pillar[5]arene building block. In this way, it can effectively inhibit the rotation of the units and thus achieve the separation of the (*S<sub>p</sub>*)- and (*R<sub>p</sub>*)- $\beta$ -D-acetyl-galactose pillar[5]arene [(*S<sub>p</sub>*)-AP5 and (*R<sub>p</sub>*)-AP5] (Figures 1, 9). From the  $^1\text{H}$  NMR spectrum of AP5, we can clearly find that the resonances of the aromatic protons ( $\text{H}_1$ ) show two single peaks, identifying the existence of (*S<sub>p</sub>*)-AP5 and (*R<sub>p</sub>*)-AP5 (Figure S19). In order to further investigate the planar chirality of AP5, (*S<sub>p</sub>*)-AP5 and (*R<sub>p</sub>*)-AP5 were successfully obtained by silica gel chromatography with DCM/MeOH = 40:1 as fluent solvent. As shown in Figure S19, every signal of (*S<sub>p</sub>*)-AP5 and (*R<sub>p</sub>*)-AP5 is different from each other, but corresponding well to the protons of AP5.

The circular dichroism (CD) and UV-Vis spectra of (*S<sub>p</sub>*)-AP5, (*R<sub>p</sub>*)-AP5, and AP5 were further investigated to explain the planar chirality of AP5. As expected, two different kinds

of CD signals could be observed between (*S<sub>p</sub>*)-AP5 and (*R<sub>p</sub>*)-AP5, and AP5 showed no obvious signal, which suggested (*S<sub>p</sub>*)-AP5 and (*R<sub>p</sub>*)-AP5 were mirror images in the planar chirality and they were separated effectively by silica gel chromatography (Figure 2).

With compounds (*S<sub>p</sub>*)-AP5 and (*R<sub>p</sub>*)-AP5 in hand, (*S<sub>p</sub>*)-GP5 and (*R<sub>p</sub>*)-GP5 were successfully obtained by reacting with sodium methoxide solution, respectively. Similar to (*S<sub>p</sub>*)-AP5 and (*R<sub>p</sub>*)-AP5,  $^1\text{H}$  NMR and  $^{13}\text{C}$  NMR spectra of (*S<sub>p</sub>*)-GP5 and (*R<sub>p</sub>*)-GP5 are different. However, there is no obvious difference between (*S<sub>p</sub>*)-GP5 and (*R<sub>p</sub>*)-GP5 in  $^1\text{H}$ - $^1\text{H}$  COSY, NOESY, and HSQC spectra. To further investigate the planar chirality of (*S<sub>p</sub>*)-GP5 and (*R<sub>p</sub>*)-GP5, CD and UV-Vis spectra were performed and two kinds of chiral signals were observed. As shown in Figure 3, the CD signals of (*S<sub>p</sub>*)-GP5 and (*R<sub>p</sub>*)-GP5 were fully symmetrical, which indicated (*S<sub>p</sub>*)-GP5 and (*R<sub>p</sub>*)-GP5 were mirror images in the planar chirality. However, no obvious CD signal could be found from GP5, which further confirmed (*S<sub>p</sub>*)-GP5 and (*R<sub>p</sub>*)-GP5 owned opposite planar chirality. For comparison, a control molecule (compound 4) was synthesized (Scheme S2 and Figure 10) and no CD signal could be observed, which showed the planar chirality of pillar[5]arene was mainly attributed to the cyclization of moiety to form the pillararene backbone.

As we all know, CD spectroscopy is a well-established tool for detecting and tracking the dynamic behavior of molecule and supramolecular chirality. Pillar[5]arene derivatives could show strong CD extrema ( $\text{CD}_{\text{ex}}$ ) at ca. 310 nm in the absence of any other attached chromophoric groups. According to previous reports (Ogoshi et al., 2012; Yao et al., 2017), the results showed (*S<sub>p</sub>*)-pillar[5]arene derivatives exhibited negative  $\text{CD}_{\text{ex}}$  and (*R<sub>p</sub>*)-pillar[5]arene derivatives exhibited positive  $\text{CD}_{\text{ex}}$ . Therefore, combining the CD spectra calculated by DFT method (Figure 4 and Figure S21), we deduced the compound with higher retention factor ( $R_f$ ) value obtained from silica gel chromatography should be the *S<sub>p</sub>* conformer and show negative  $\text{CD}_{\text{ex}}$  signal. The compound with lower  $R_f$  value was the *R<sub>p</sub>* conformer and positive  $\text{CD}_{\text{ex}}$  signal.

### Racemization Investigation of (*S<sub>p</sub>*)-GP5 and (*R<sub>p</sub>*)-GP5

According to previous literatures (Ogoshi et al., 2010a,b, 2011a; Nierengarten et al., 2013), the planar chirality of pillar[5]arene is unstable and will be racemized. In order to explore whether (*S<sub>p</sub>*)-GP5 and (*R<sub>p</sub>*)-GP5 could exchange with each other, dynamic  $^1\text{H}$  NMR and CD measurements were further carried out. According to the planar chirality of (*S<sub>p</sub>*)-GP5 and (*R<sub>p</sub>*)-GP5, the two protons from the methylene moieties adjacent to the O atoms ( $\text{H}_4$ ) were different in chemical environment and could split into two groups of double peak in 1:1 integration ratio at 298 K (Figure S20). Thus, the split proton resonances are a useful marker to determine whether the rotation of pillar[5]arenes takes place on the NMR time scale (Ogoshi et al., 2010a,b, 2011b). Moreover, as shown in Figure 5, although the chemical shift of  $\text{D}_2\text{O}$  exhibited upfield shift changes due to the weakening of intermolecular hydrogen bonding of  $\text{D}_2\text{O}$  with increasing temperature, almost no peak changes for (*S<sub>p</sub>*)-GP5 and (*R<sub>p</sub>*)-GP5 could

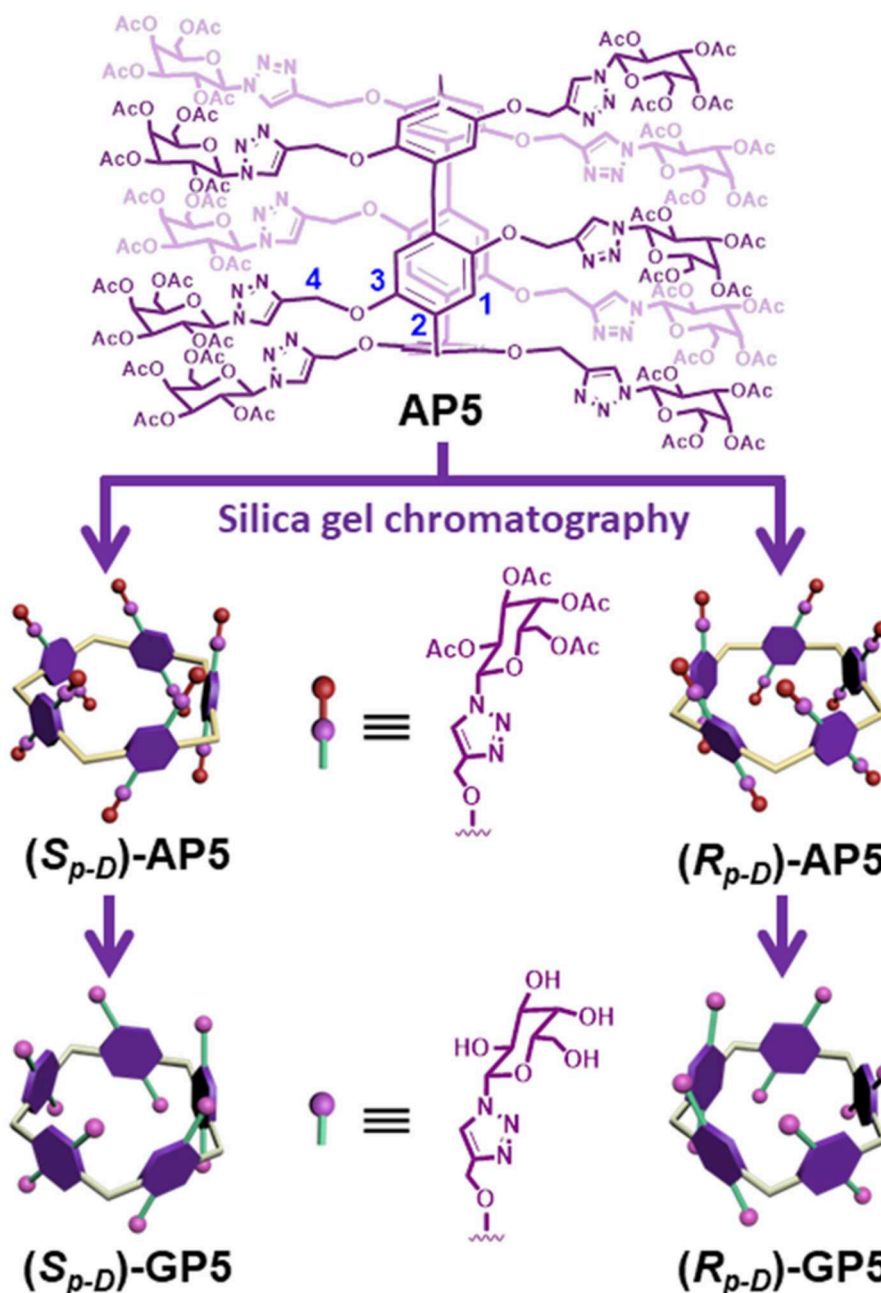


**FIGURE 1** | Schematic structure illustration of **AP5** and **GP5**.

be observed (TMS as the reference). More important, the split of  $H_{4'}$  and  $H_4$  still retained during the progress of heating, indicating  $(S_{p-D})$ -GP5 and  $(R_{p-D})$ -GP5 were stable and hardly racemized on the NMR time scale in the measured temperature range.

Subsequently, dynamic CD experiments were investigated, and the results indicated the intensity of  $(S_{p-D})$ -GP5 and  $(R_{p-D})$ -GP5 were stable and symmetric, confirming the planar chirality of  $(S_{p-D})$ -GP5 and  $(R_{p-D})$ -GP5 was absolutely independent

and the racemization of  $(S_{p-D})$ -GP5 and  $(R_{p-D})$ -GP5 didn't happen even under higher temperature. Whereas, when more attention was paid to the wavelength from 290 to 310 nm, which was ascribed to  $\pi$ - $\pi^*$  transitions of the aromatic moieties in the pillar[5]arene backbone, both  $(S_{p-D})$ -GP5 and  $(R_{p-D})$ -GP5 trended to racemize with increasing temperature (Figure 6 and Figure S22). However, due to the large molecular size of bulky substituent on the rim of GP5, neither  $(S_{p-D})$ -GP5 nor  $(R_{p-D})$ -GP5 could racemize actually, which is consistent with

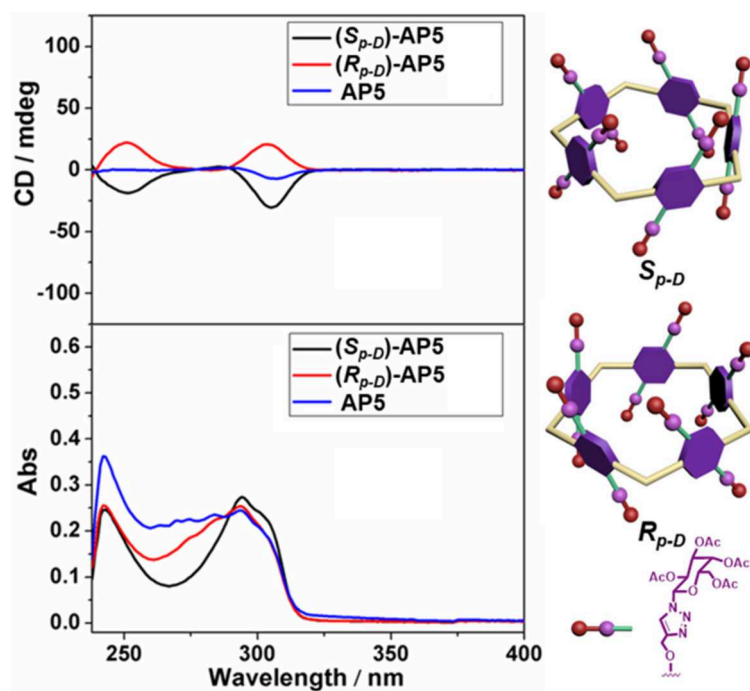


**FIGURE 2** | CD and UV-Vis spectra of  $(S_{p-D})$ -AP5 ( $8 \mu\text{M}$  in  $\text{CHCl}_3$ ),  $(R_{p-D})$ -AP5 ( $8 \mu\text{M}$  in  $\text{CHCl}_3$ ), and AP5 ( $8 \mu\text{M}$  in  $\text{CHCl}_3$ ).

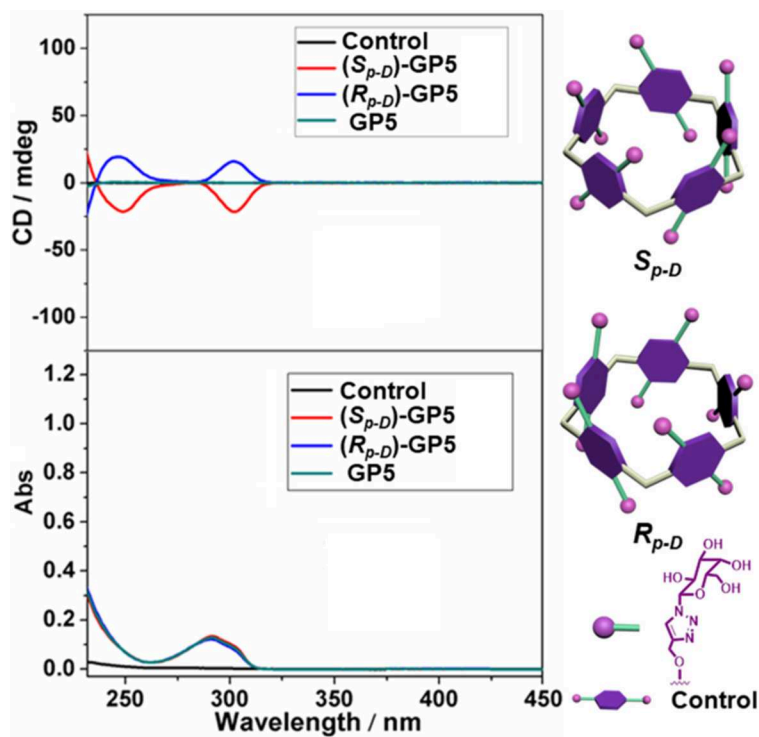


**FIGURE 3** | CD and UV-Vis spectra of  $(S_{p-D})$ -GP5 ( $8 \mu\text{M}$  in  $\text{H}_2\text{O}$ ),  $(R_{p-D})$ -GP5 ( $8 \mu\text{M}$  in  $\text{H}_2\text{O}$ ), and GP5 ( $8 \mu\text{M}$  in  $\text{H}_2\text{O}$ ), and control molecule ( $40 \mu\text{M}$  in  $\text{H}_2\text{O}$ ).



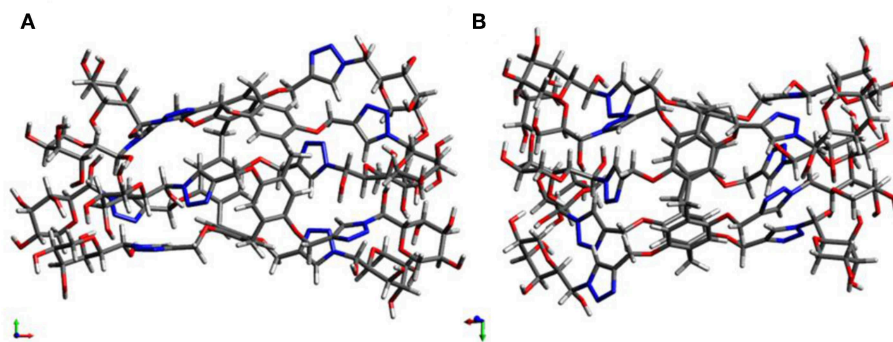


**FIGURE 4** | Optimized structure: **(A)** (*S<sub>p-D</sub>*)-GP5 and **(B)** (*R<sub>p-D</sub>*)-GP5.

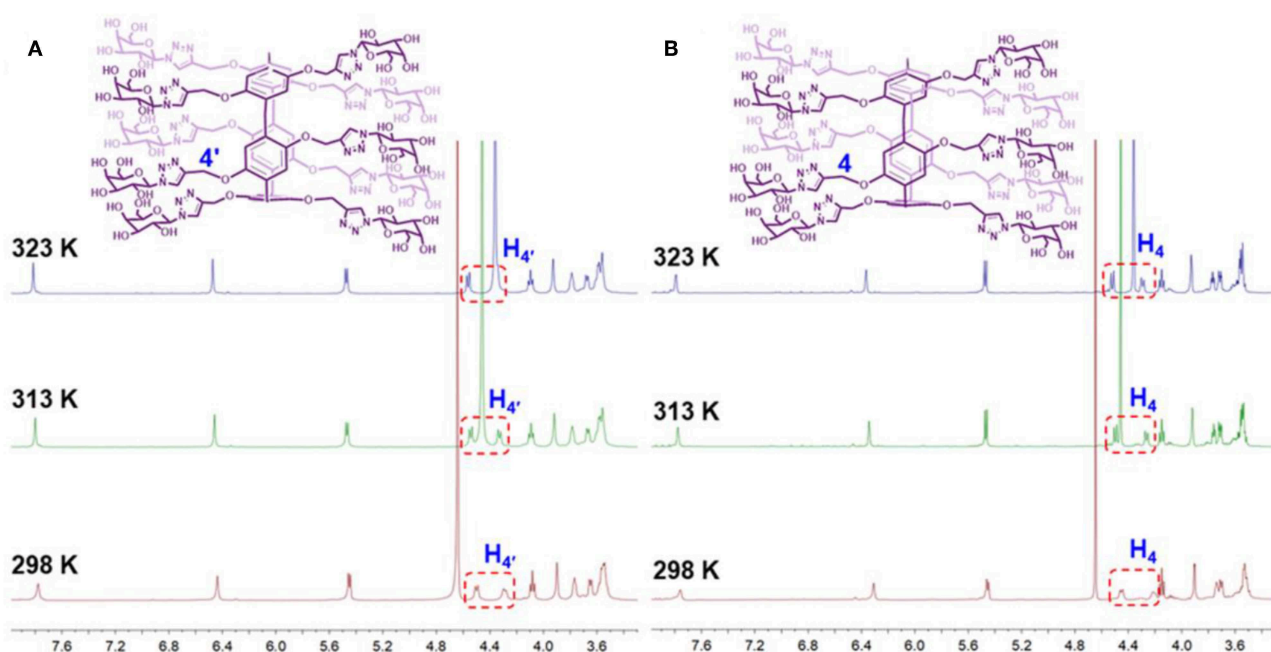


**FIGURE 5** | Dynamic  $^1\text{H}$  NMR spectra of **(A)** (*S<sub>p-D</sub>*)-GP5 (4 mM in  $\text{D}_2\text{O}$ ) and **(B)** (*R<sub>p-D</sub>*)-GP5 (4 mM in  $\text{D}_2\text{O}$ ).

the dynamic  $^1\text{H}$  NMR results (Ogoshi et al., 2011a, 2016). In summary, different from many traditional pillar[5]arene derivatives, the planar chirality of (*S<sub>p-D</sub>*)-GP5 and (*R<sub>p-D</sub>*)-GP5 are very stable and unchangeable, which can be used as a reliable chiral source to induce and transfer the *S<sub>p</sub>* and *R<sub>p</sub>* planar chirality.

Simultaneously, after dialysis with distilled water, the CD spectra of the (*S<sub>p-D</sub>*)-nanoparticles and (*R<sub>p-D</sub>*)-nanoparticles were obtained, respectively. The results confirmed the planar chirality of these chiral nanoparticles still existed and displayed symmetrical signal, indicating that (*S<sub>p-D</sub>*)-GP5 and (*R<sub>p-D</sub>*)-GP5 could be used as reliable chiral sources to transfer the *S<sub>p</sub>* and *R<sub>p</sub>* planar chirality (Figure 8).

## The Construction of Chiral Nanoparticles

Based on the outstanding host-guest properties of pillar[5]arene, one of our previously reported guest molecule (DNS-CPT) (Sun

et al., 2019) was used to investigate the construction of nanoparticles with planar chirality (Figure 11). As shown in Figure 7, when (*S<sub>p-D</sub>*)-GP5 or (*R<sub>p-D</sub>*)-GP5 was added into the DNS-CPT solution, an obvious Tyndall effect could be observed, indicating the formation of large sized aggregates. The diameter of these nanoparticles was confirmed to be 39 and 38 nm by dynamic light scattering (DLS), respectively. The morphology of the nanoparticles was further investigated by transmission electron microscopy (TEM), and the results showed both (*S<sub>p-D</sub>*)- and (*R<sub>p-D</sub>*)-GP5 could form nanoparticles with the presence of the guest molecule DNS-CPT (Figure 7 and Figure S23). Moreover, Zeta potential measurements showed that the obtained nanoparticles possess relatively high positive  $\zeta$ -potentials (32.85 and 35.93 mV, respectively), suggesting their good stability in solution (Figure S24).

## EXPERIMENTAL

### Synthesis of GP5

As shown in **Figure 9**, GP5 was synthesized based on the click reaction between compound **1** and **2** to generate compound AP5 successfully. Then, AP5 was reacted with sodium methoxide in methanol for 24 h under an inert atmosphere at ambient temperature. The resulting reaction mixture was filtered and washed with methanol, which gave the target macrocycle GP5 in 99% yield. A combination of  $^1\text{H}$ ,  $^{13}\text{C}$ ,  $^1\text{H}$ - $^1\text{H}$  COSY, NOESY,

and HSQC nuclear magnetic resonance spectroscopy (NMR) confirmed (**Figures S7–S16**) the formation of GP5.

### Synthesis of Compound 4

Compound **4** was synthesized based on the click reaction between 1,4-bis(prop-2-yn-1-yloxy)benzene and compound **2** to generate compound **3** successfully. Then, compound **3** was reacted with sodium methoxide in methanol for 24 h under an inert atmosphere at ambient temperature. The resulting reaction mixture was filtered and washed with methanol,

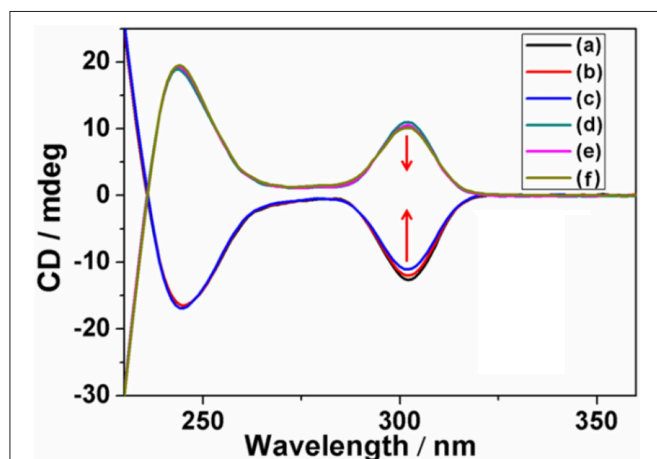


**FIGURE 6** | Dynamic CD spectra of (*S*<sub>p-D</sub>)-GP5 [(A–C)] 8  $\mu\text{M}$  in H<sub>2</sub>O and (*R*<sub>p-D</sub>)-GP5 [(D–F)] 8  $\mu\text{M}$  in H<sub>2</sub>O at 298, 313, and 323 K, respectively.

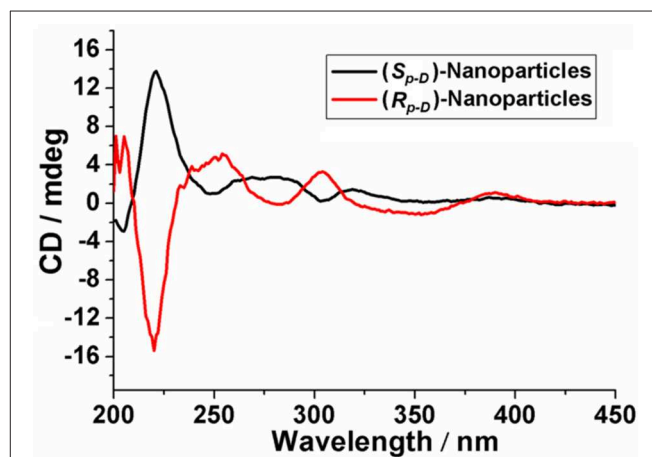


**FIGURE 8** | CD spectrum of chiral nanoparticles.

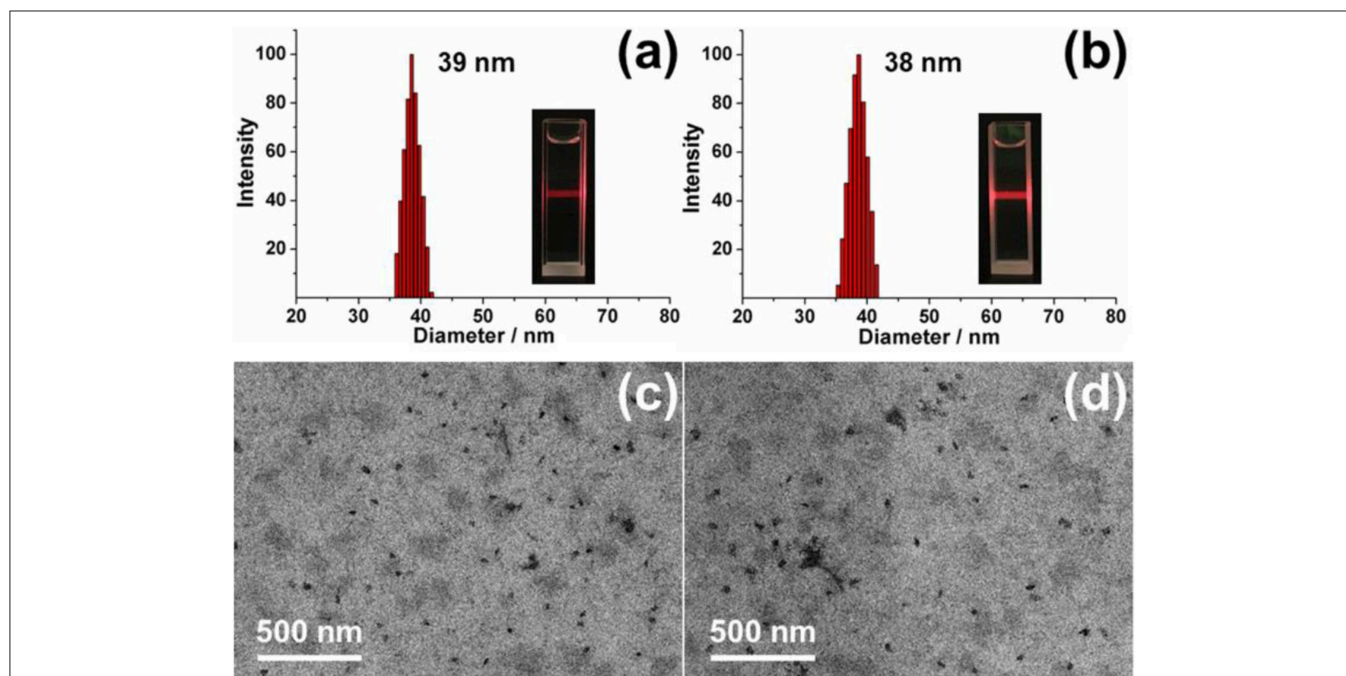


**FIGURE 7** | DLS data of chiral nanoparticles: (a) (*S*<sub>p-D</sub>)-nanoparticles. Inset photo: Tyndall effect. (b) (*R*<sub>p-D</sub>)-nanoparticles. Inset photo: Tyndall effect. TEM images of chiral nanoparticles: (c) (*S*<sub>p-D</sub>)-nanoparticles. (d) (*R*<sub>p-D</sub>)-nanoparticles.

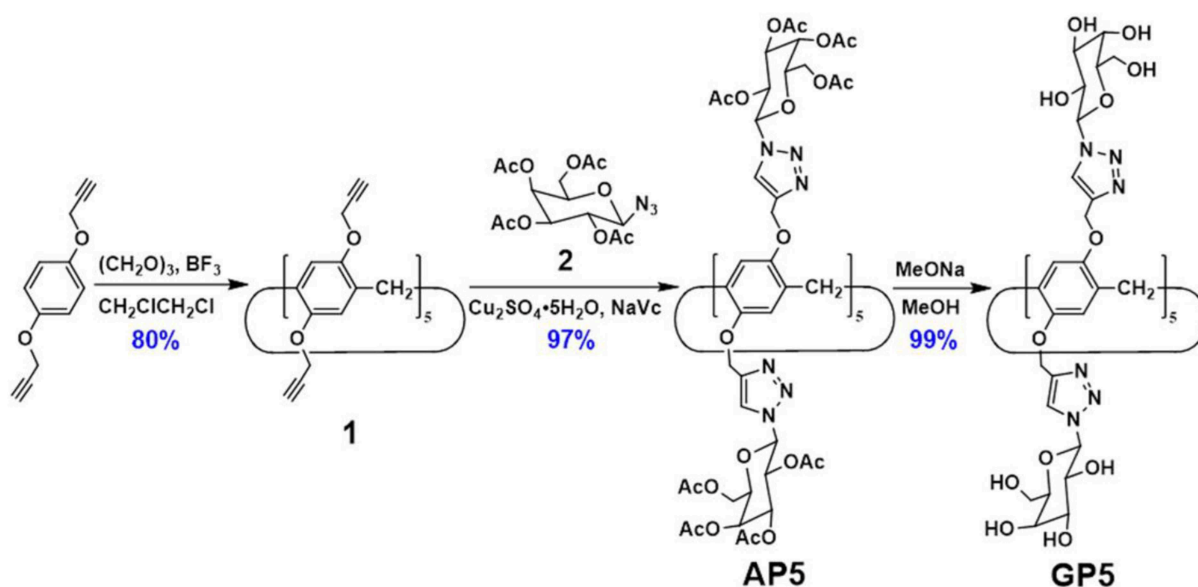


FIGURE 9 | Synthesis route of GP5.

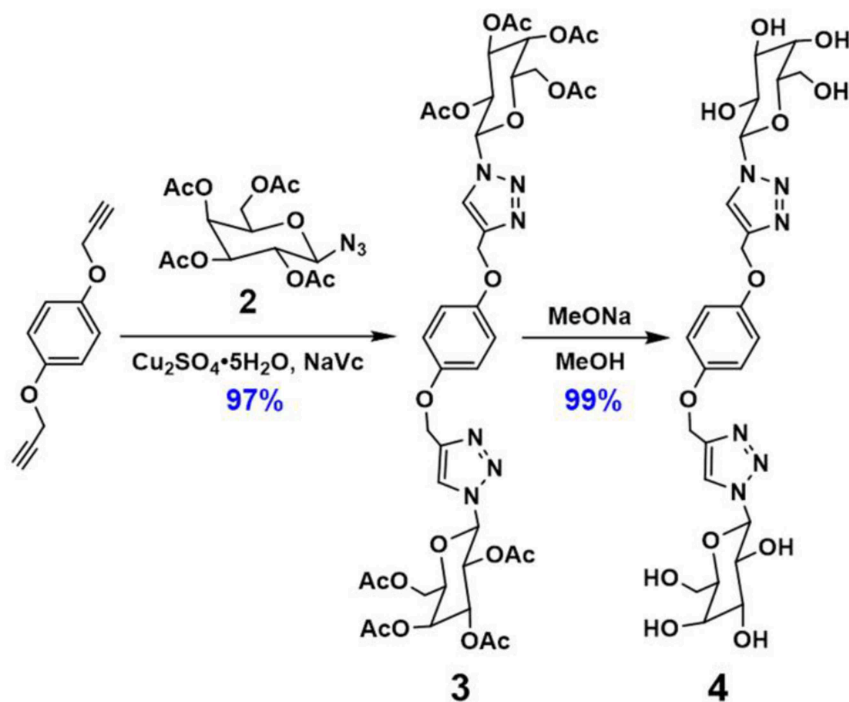


FIGURE 10 | Synthesis route of compound 4.

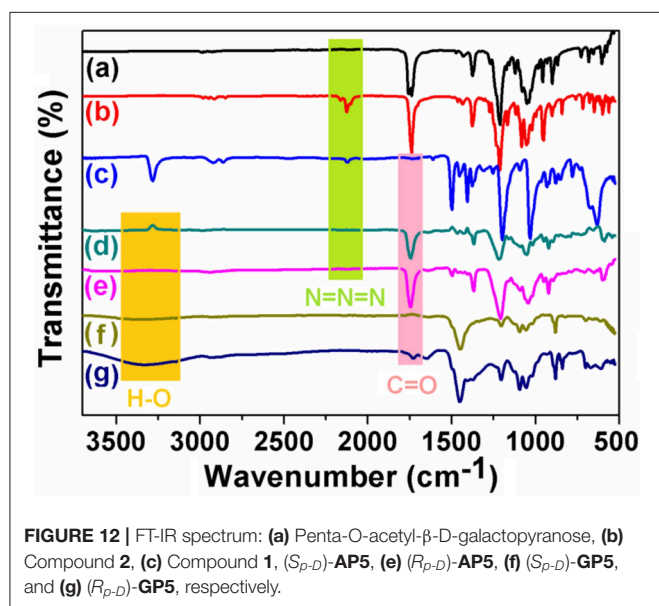
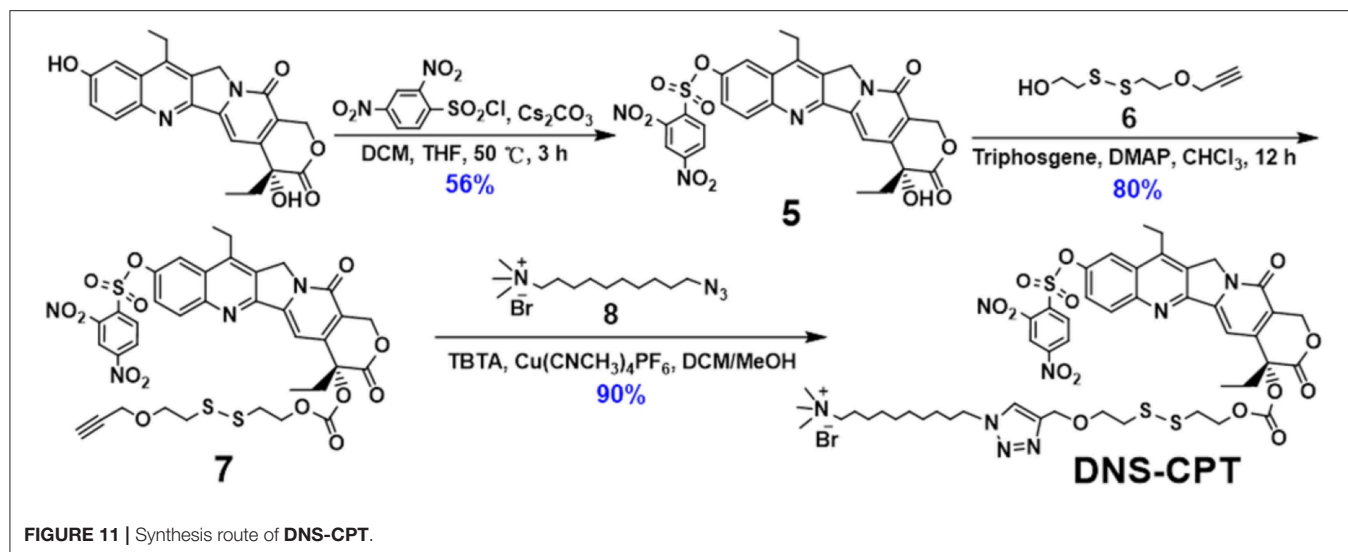
which gave the control molecule compound 4 in 99% yield.  $^1\text{H}$  NMR (Figures S17, S18) confirmed the formation of compounds 3 and 4.

### Synthesis of DNS-CPT

DNS-CPT was synthesized and characterized according to our previous work (Sun et al., 2019).

### Fourier Transform Infrared Spectrometer (FT-IR) Spectrum

FT-IR experiments of 1,2,3,4,6-penta-*o*-acetyl- $\beta$ -D-galactopyranose, compound 1, compound 2, (*S<sub>p</sub>-D*)-AP5, (*R<sub>p</sub>-D*)-AP5, (*S<sub>p</sub>-D*)-GP5, and (*R<sub>p</sub>-D*)-GP5 were carried out to track the functionalization process of pillar[5]arene. As shown in Figure 12, after reaction with trimethylsilyl azide



(TMS- $N_3$ ), a typical  $N=N=N$  peak at  $2,100\text{ cm}^{-1}$  could be observed. However, the  $N=N=N$  peak disappeared after the click reaction with compound 1, which indicated the 1,2,3,4,6-penta-o-acetyl-β-D-galactopyranose group had been modified to pillar[5]arene to obtain AP5 successfully. Meanwhile, the stretching vibration peak of  $C=O$  was detected at  $1750\text{ cm}^{-1}$ . Moreover, when the acetyl group of AP5 was removed, the characteristic absorption peak of  $C=O$  disappeared and a wide peak of  $O-H$  at  $3300\text{ cm}^{-1}$  was observed at the same time, which showed the successful formation of GP5.

## CONCLUSION

In conclusion, we successfully obtained  $(S_p\text{-D})$ -AP5,  $(R_p\text{-D})$ -AP5,  $(S_p\text{-D})$ -GP5, and  $(R_p\text{-D})$ -GP5 through silica gel chromatography with a high yield at room temperature. Dynamic CD and

$^1\text{H}$  NMR experiments revealed the  $S_p$  and  $R_p$  planar chirality of these pillar[5]arene derivatives (GP5) were very stable and unracemized, which could be used as reliable chiral sources to construct chiral nanoparticles, showing the  $S_p$  and  $R_p$  planar chirality of GP5 could be transferred by the host-guest interaction based on GP5 and DNS-CPT.

## DATA AVAILABILITY STATEMENT

All datasets generated for this study are included in the article/Supplementary Material.

## AUTHOR CONTRIBUTIONS

LW, X-YH, and JJ conceived the project, supervised the study, and revised the manuscript. GS conducted the experiments, wrote the draft manuscript, and prepared the supporting information. LP conducted the TEM experiments. SP conducted the calculation experiments. All authors analyzed and interpreted the data.

## FUNDING

This work was supported by the National Natural Science Foundation of China (Nos. 21572101 and 21871136) and the Natural Science Foundation of Jiangsu Province (No. BK20180055).

## ACKNOWLEDGMENTS

We thank Yuan Chen and Yukun Shi from our group for the helpful discussion.

## SUPPLEMENTARY MATERIAL

The Supplementary Material for this article can be found online at: <https://www.frontiersin.org/articles/10.3389/fchem.2019.00743/full#supplementary-material>



## REFERENCES

- Choi, H., Cho, K. J., Seo, H., Ahn, J., Liu, J., Lee, S. S., et al. (2017). Transfer and dynamic inversion of coassembled supramolecular chirality through 2D-sheet to rolled-up tubular structure. *J. Am. Chem. Soc.* 139, 17711–17714. doi: 10.1021/jacs.7b09760
- Jie, K., Zhou, Y., Yao, Y., and Huang, F. (2015). Macrocyclic amphiphiles. *Chem. Soc. Rev.* 44, 3568–3587. doi: 10.1039/C4CS00390J
- Kitajima, K., Ogoshi, T., and Yamagishi, T. T. (2014). Diastereoselective synthesis of a [2]catenane from a pillar[5]arene and a pyridinium derivative. *Chem. Commun.* 50, 2925–2927. doi: 10.1039/c3cc49794a
- Lee, E., Ju, H., Park, I. H., Jung, J. H., Ikeda, M., Kuwahara, S., et al. (2018). Pseudo[1]catenane-type pillar[5]thiacrown whose planar chiral inversion is triggered by metal cation and controlled by anion. *J. Am. Chem. Soc.* 140, 9669–9677. doi: 10.1021/jacs.8b05751
- Liu, X., Shao, W., Zheng, Y., Yao, C., Peng, L., Zhang, D., et al. (2017). GSH-Responsive supramolecular nanoparticles constructed by  $\beta$ -D-galactose-modified pillar[5]arene and camptothecin prodrug for targeted anticancer drug delivery. *Chem. Commun.* 53, 8596–8599. doi: 10.1039/C7CC04932C
- Moghaddam, S., Yang, C., Rekharsky, M., Ko, Y. H., Kim, K., Inoue, Y., et al. (2011). New ultrahigh affinity host-guest complexes of cucurbit[7]uril with bicyclo[2.2.2]octane and adamantane guests: thermodynamic analysis and evaluation of M2 affinity calculations. *J. Am. Chem. Soc.* 133, 3570–3581. doi: 10.1021/ja109904u
- Nierengarten, I., Buffet, K., Holler, M., Vincent, S. P., and Nierengarten, J. F. (2013). A mannosylated pillar[5]arene derivative: chiral information transfer and antiadhesive properties against uropathogenic bacteria. *Tetrahedron Lett.* 54, 2398–2402. doi: 10.1016/j.tetlet.2013.02.100
- Ogoshi, T., Akutsu, T., Yamafuji, D., Aoki, T., and Yamagishi, T. A. (2013a). Solvent- and achiral-guest-triggered chiral inversion in a planar chiral pseudo[1]catenane. *Angew. Chem. Int. Ed.* 52, 8111–8115. doi: 10.1002/anie.201302675
- Ogoshi, T., Kitajima, K., Aoki, T., Yamagishi, T. A., and Nakamoto, Y. (2010a). Synthesis and conformational characteristics of alkyl-substituted pillar[5]arenes. *J. Org. Chem.* 75, 3268–3273. doi: 10.1021/jo100273n
- Ogoshi, T., Kitajima, K., Aoki, T., Yamagishi, T. A., and Nakamoto, Y. (2010b). Effect of an intramolecular hydrogen bond belt and complexation with the guest on the rotation behavior of phenolic units in pillar[5]arenes. *J. Phys. Chem. Lett.* 1, 817–821. doi: 10.1021/jz900437r
- Ogoshi, T., Masakai, K., Shiga, R., Kitajima, K., and Yamagishi, T. A. (2011a). Planar-chiral macrocyclic host pillar[5]arene: no rotation of units and isolation of enantiomers by introducing bulky substituents. *Org. Lett.* 13, 1264–1266. doi: 10.1021/ol200062j
- Ogoshi, T., Shiga, R., Yamagishi, T. A., and Nakamoto, Y. (2011b). Planar-chiral pillar[5]arene: chiral switches induced by multiexternal stimulus of temperature, solvents, and addition of achiral guest molecule. *J. Org. Chem.* 76, 618–622. doi: 10.1021/jo1021508
- Ogoshi, T., Yamafuji, D., Akutsu, T., Naito, M., and Yamagishi, T. A. (2013b). Achiral guest-induced chiroptical changes of a planar-chiral pillar[5]arene containing one  $\pi$ -conjugated unit. *Chem. Commun.* 49, 8782–8784. doi: 10.1039/c3cc44672g
- Ogoshi, T., Yamafuji, D., Aoki, T., Kitajima, K., Yamagishi, T. A., Hayashi, Y., et al. (2012). High-yield diastereoselective synthesis of planar chiral [2]- and [3]rotaxanes constructed from per-ethylated pillar[5]arene and pyridinium derivatives. *Chem. Eur. J.* 18, 7493–7500. doi: 10.1002/chem.201200122
- Ogoshi, T., Yamagishi, T. A., and Nakamoto, Y. (2016). Pillar-shaped macrocyclic hosts pillar[n]arenes: new key players for supramolecular chemistry. *Chem. Rev.* 116, 7937–8002. doi: 10.1021/acs.chemrev.5b00765
- Park, J., Choi, Y., Lee, S. S., and Jung, J. (2019). Critical role of achiral guest molecules in planar chirality inversion of alanine-appended pillar[5]arenes. *J. Org. Lett.* 21, 1232–1236. doi: 10.1021/acs.orglett.9b00277
- Strutt, N. L., Fairen-Jimenez, D., Iehl, J., Lalonde, M. B., Snurr, R. Q., Farha, O. K., et al. (2012). Incorporation of an A1/A2-difunctionalized pillar[5]arene into a metal-organic framework. *J. Am. Chem. Soc.* 134, 17436–17439. doi: 10.1021/ja3082523
- Strutt, N. L., Zhang, H., and Stoddart, J. F. (2014). Enantiopure pillar[5]arene active domains within a homochiral metal-organic framework. *Chem. Commun.* 50, 7455–7458. doi: 10.1039/c4cc02559h
- Sun, G., He, Z., Hao, M., Xu, Z., Hu, X.-Y., Zhu, J.-J., et al. (2019). Bifunctional supramolecular prodrug vesicles constructed from camptothecin derivative with water-soluble pillar[5]arene for cancer diagnosis and therapy. *Chem. Commun.* 55, 10892–10895. doi: 10.1039/c9cc05859a
- Wu, X., Zhang, Y., Lu, Y., Pang, S., Yang, K., Tian, Z., et al. (2017). Synergistic and targeted drug delivery based on nano-CeO<sub>2</sub> capped with galactose functionalized pillar[5]arene via host-guest interactions. *J. Mater. Chem. B.* 5, 3483–3487. doi: 10.1039/C7TB00752C
- Yao, J., Wu, W., Liang, W., Feng, Y., Zhou, D., Chruma, J. J., et al. (2017). Temperature-driven planar chirality switching of a pillar[5]arene-based molecular universal joint. *Angew. Chem. Int. Ed.* 56, 6869–6873. doi: 10.1002/anie.201702542
- Yu, G., Ma, Y., Han, C., Yao, Y., Tang, G., Mao, Z., et al. (2013). A sugar-functionalized amphiphilic pillar[5]arene: synthesis, self-assembly in water, and application in bacterial cell agglutination. *J. Am. Chem. Soc.* 135, 10310–10313. doi: 10.1021/ja405237q
- Zhang, X., and Wang, C. (2011). Supramolecular amphiphiles. *Chem. Soc. Rev.* 40, 94–101. doi: 10.1039/b919678c

**Conflict of Interest:** The authors declare that the research was conducted in the absence of any commercial or financial relationships that could be construed as a potential conflict of interest.

Copyright © 2019 Sun, Pu, Pangannaya, Xiao, Hu, Jiang and Wang. This is an open-access article distributed under the terms of the Creative Commons Attribution License (CC BY). The use, distribution or reproduction in other forums is permitted, provided the original author(s) and the copyright owner(s) are credited and that the original publication in this journal is cited, in accordance with accepted academic practice. No use, distribution or reproduction is permitted which does not comply with these terms.



# Enantiomeric Recognition of $\alpha$ -Aminoacids by a Uranyl Salen-Bis-Porphyrin Complex

Chiara M. A. Gangemi<sup>1</sup>, Ugne Rimkaite<sup>2</sup>, Federica Cipria<sup>1</sup>, Giuseppe Trusso Sfrazzetto<sup>1,3</sup> and Andrea Pappalardo<sup>1,3\*</sup>

<sup>1</sup> Department of Chemical Sciences, University of Catania, Catania, Italy, <sup>2</sup> Faculty of Chemistry and Geosciences, University of Vilnius, Vilnius, Lithuania, <sup>3</sup> I.N.S.T.M. - Consorzio Interuniversitario Nazionale per la Scienza e Tecnologia dei Materiali, University of Catania, Catania, Italy

A novel uranyl salen-bis-porphyrin complex, in which two porphyrin subunits and salen moiety were directly linked, was synthesized for the recognition of tetrabutylammonium (TBA) amino acids. This uranyl salen complex, due to the presence of porphyrins with their fluorescence properties, represents the first example of a luminescence of uranyl salen complexes. UV/Vis measurements indicate the formation of 1:1 host-guest complexes, whereas UV-vis and fluorescence studies revealed that this complex acts as a receptor for the enantiomeric recognition of  $\alpha$ -aminoacids derivatives, with high association constants and an excellent enantiomeric discrimination between the two enantiomers of phenylalanine-TBA.

## OPEN ACCESS

### Edited by:

Carmine Gaeta,  
University of Salerno, Italy

### Reviewed by:

Paula M. Marcos,  
University of Lisbon, Portugal  
Silvano Geremia,  
University of Trieste, Italy

### \*Correspondence:

Andrea Pappalardo  
andrea.pappalardo@unict.it

### Specialty section:

This article was submitted to  
Supramolecular Chemistry,  
a section of the journal  
Frontiers in Chemistry

**Received:** 27 September 2019

**Accepted:** 18 November 2019

**Published:** 03 December 2019

### Citation:

Gangemi CMA, Rimkaite U, Cipria F,  
Trusso Sfrazzetto G and Pappalardo A  
(2019) Enantiomeric Recognition of  
 $\alpha$ -Aminoacids by a Uranyl  
Salen-Bis-Porphyrin Complex.  
Front. Chem. 7:836.  
doi: 10.3389/fchem.2019.00836

**Keywords:** porphyrins, salen ligands, uranyl complexes, luminescence, enantiomeric recognition

## INTRODUCTION

Salen ligands are a class of molecules that have been widely explored in the field of supramolecular chemistry. The most fascinating and promising use of salen derivatives is due to their chiral complexes with numerous metals. The salen structure, due to two contiguous stereogenic carbon atoms in the diimine bridge, creates a chiral pocket which can coordinate a metal cation (*via* imine nitrogen and phenolic oxygen atoms). Salen ligands rose to prominence thanks to the pioneering work of Jacobsen and Katsuki that paved the way to one of the most well-designed protocol for the enantioselective epoxidation of unfunctionalized alkenes catalyzed by chiral manganese salen complexes (Jacobsen, 1993; Katsuki, 2000; Yoon and Jacobsen, 2003; La Paglia Fragola et al., 2012; Trusso Sfrazzetto et al., 2015; Ballistreri et al., 2016, 2018; Zammataro et al., 2019). Furthermore, salen ligands are structures of great value in homogeneous catalysis (Katsuki, 1995; Jacobsen, 2000; Cozzi, 2004; McGarrigle and Gilheany, 2005; Baleizao and Garcia, 2006; Wezenberg and Kleij, 2008; Whiteoak et al., 2012).

In recent years, our research group exploited these chiral salen-metal complexes as enantiomeric receptors for chiral guests. In fact, depending on the metal ion and different substituents in the aromatic ring of salen framework, these salen-metal complexes can be used as efficient enantioselective catalysts and highly sensitive chemosensors (D'Urso et al., 2014; Puglisi et al., 2017, 2018, 2019). In particular, chiral uranyl salen complexes have proved to be excellent receptors for amino acid salts (Amato et al., 2007, 2010, 2011; Ballistreri et al., 2010; Pappalardo et al., 2012a), since the uranyl metal center, acting as a Lewis acid, possesses an equatorial fifth position able to coordinate one molecule of carboxylate anion (Ballistreri et al., 2012; Brancatelli et al., 2013). These synthetic enantioselective receptors could help to better understand the mechanisms of drugs action; processes that are involved in immunological responses and processes of the storage of

genetic information. Besides, slightly modification of their structures could lead to chemosensors, which due to their simple use, relatively low cost and high sensitivity are particularly significant in the chemical analysis.

Taking into account the salen ligand applications in the field of catalysis and enantiomeric recognition, previous studies have inspired us to extend current research on the synthesis of salen receptors comprising porphyrin macrocycles which, with their high stability and fluorescence properties, could greatly extend the use of salen ligands as chemosensors. Porphyrins, due to their rigid molecular structure, tunable substituents, large skeleton dimensions, and additional metallation sites in the core, are very attractive macrocycles for their applications in many technological fields (Beletskaya et al., 2009; Drain et al., 2009). In our strategy, the rational combination of porphyrin derivatives with chiral uranyl-salen ligands in one structure, would lead to chemosensors that possess unprecedented luminescence properties, that till now were precluded in uranyl-salen complexes due to the presence of uranyl metal center. Here we report on the synthesis of a novel uranyl salen-bis-porphyrin complex, in which two porphyrin subunits and the salen ligand are directly connected, and the enantiomeric recognition properties of this receptor toward selected  $\alpha$ -aminoacids derivatives assessed by UV-vis and fluorescence measurements (Figure 1).

## MATERIALS AND METHODS

### General Experimental Methods

The NMR experiments were carried out at 27°C on a Varian UNITY Inova 500 MHz spectrometer ( $^1\text{H}$  at 499.88 MHz,  $^{13}\text{C}$  NMR at 125.7 MHz) equipped with pulse field gradient module (Z axis) and a tuneable 5 mm Varian inverse detection probe (ID-PFG). ESI mass spectra were acquired on a API 2000–ABSciex using  $\text{CH}_3\text{OH}$  (positive ion mode). A JASCO V-560 UV-Vis spectrophotometer equipped with a 1 cm path-length cell was used for the UV-Vis measurements. Luminescence measurements were carried out using a Cary Eclipse Fluorescence spectrophotometer with resolution of 0.5 nm, at room temperature. The emission was recorded at 90° with respect to the exciting line beam using 10:10 slit-widths for all measurements. All chemicals were reagent grade and were used without further purification.

### General Procedure for the Synthesis of TBA Amino Acid Derivates (Ballistreri et al., 2010)

An aqueous solution of tetrabutylammonium hydroxide (40% w/w, 13 mmol) was added to an aqueous suspension of the desired amino acid (13 mmol). The resultant reaction mixture was heated at 60°C for 2 h. Water was removed in vacuo at 80°C. The residue was dissolved in  $\text{CH}_2\text{Cl}_2$  (10 mL), filtered and the solvent was evaporated in vacuo to afford in high yield the desired product.

## Procedure for UV-vis and Fluorescence Titrations

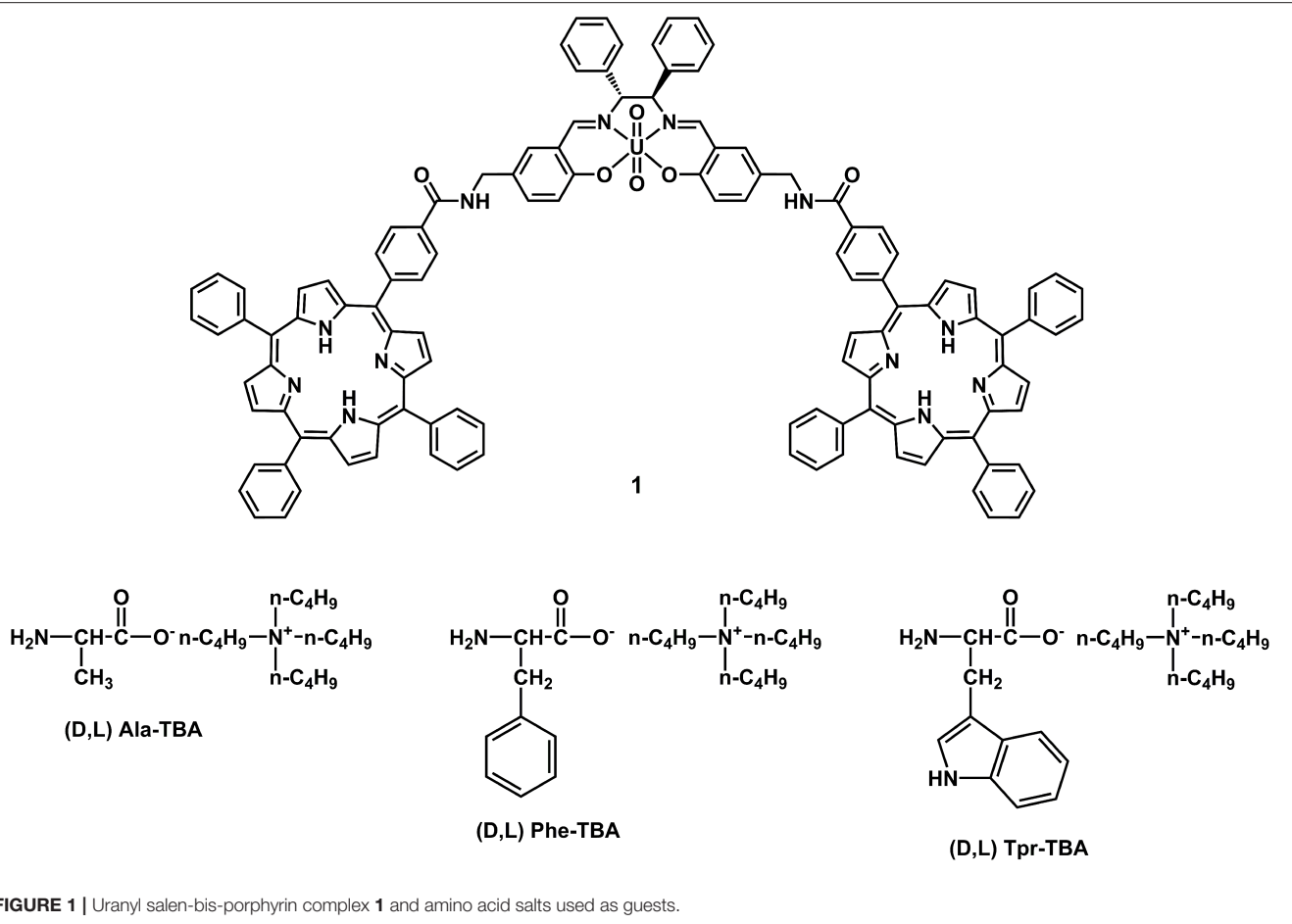
Two stock solutions of host and guest ( $1.0 \times 10^{-3}$  M) in dry chloroform were prepared. From these, different solutions with different ratio receptor/guest (host concentration =  $1.0 \times 10^{-6}$  M) were prepared, and UV-vis and emission spectra were recorded at 25°C. Fluorescence titrations were carried out using  $\lambda_{\text{ex}} = 350$  nm in dry chloroform, recording at  $\lambda_{\text{em}} = 650$  and 715 nm. With this data treatment, the apparent binding affinities of receptor with amino acid guests were estimated using HypSpec (version 1.1.33) (Pappalardo et al., 2012b), a software designed to extract equilibrium constants from potentiometric and/or spectrophotometric titration data. HypSpec starts with an assumed complex formation scheme and uses a least-squares approach to derive the spectra of the complexes and the stability constants.  $\chi^2$ -test (chi-square) was applied, where the residuals follow a normal distribution (for a distribution approximately normal, the  $\chi^2$ -test value is around 12 or less). In all of the cases,  $\chi^2 \leq 10$  were found, as obtained by 3 independent measurement sets.

### Synthesis of Compound 4 (Johansson et al., 2003)

5.0 g (0.0300 mol) of compound 2 (Dalla Cort et al., 2006) and 5.97 g of potassium phthalimide 3 (0.0322 mol) were placed in a 250 mL round-bottom flask. The reagents were dissolved in 100 mL of DMF. The reaction mixture was allowed to stir at room temperature for 48 h and then was heated at 55°C for 4 h. The reaction mixture was cooled down to room temperature and diluted with 250 mL of EtOAc and washed with water ( $3 \times 200$  mL). The organic layer was dried over anhydrous  $\text{Na}_2\text{SO}_4$ , filtered and evaporated. The product was purified by silica gel column chromatography ( $\text{CHCl}_3$ ) to afford 3.37 g (40 % yield) of compound 4.  $^1\text{H}$  NMR (500 MHz,  $\text{CDCl}_3$ ):  $\delta = 10.99$  (s, 1H); 9.88 (s, 1H); 7.86–7.84 (m, 2H); 7.73–7.71 (m, 2H); 7.67 (s, 1H); 7.65–7.63 (dd,  $J = 8.5$  Hz,  $J = 2.0$  Hz, 1H); 6.95 (d,  $J = 8.5$  Hz, 1H); 4.82 (s, 2H).

### Synthesis of Compound 5

0.662 g (2.36 mmol) of compound 4 and 0.0171 g (0.036 mmol) of tetrabutylammonium tribromide were placed in a 20 mL round-bottom flask. In this flask 3.60 mL of 1,3-propanediol and 3.90 mL of triethyl orthoformate were added. The reaction mixture was allowed to stir at room temperature for 48 h, then diluted with 45 mL of EtOAc. The organic solution was washed with water ( $3 \times 20$  mL), dried over anhydrous  $\text{Na}_2\text{SO}_4$ , filtered and evaporated. The product was purified by silica gel column chromatography (cyclohexane/EtOAc 3:1) affording 0.732 g of white compound 5 (92% yield).  $^1\text{H}$  NMR (500 MHz,  $\text{CDCl}_3$ ):  $\delta = 7.85$  (s, 1H); 7.83–7.81 (m, 2H); 7.70–7.68 (m, 2H); 7.36–7.34 (dd,  $J = 8.5$  Hz,  $J = 2.5$  Hz, 1H); 7.28 (s, 1H); 6.84 (d,  $J = 8.5$  Hz, 1H); 5.61 (s, 1H); 4.74 (s, 2H); 4.30–4.27 (m, 2H); 4.02–3.96 (m, 2H); 2.30–2.20 (m, 1H); 1.52–1.48 (m, 1H).  $^{13}\text{C}$  (125 MHz,  $\text{CDCl}_3$ ):  $\delta = 25.6, 31.4, 40.9, 67.2, 102.9, 117.4, 122.1, 123.2, 127.6, 128.6, 131.3, 132.1, 133.9, 154.9, 168.0$ .



## Synthesis of Compound 6

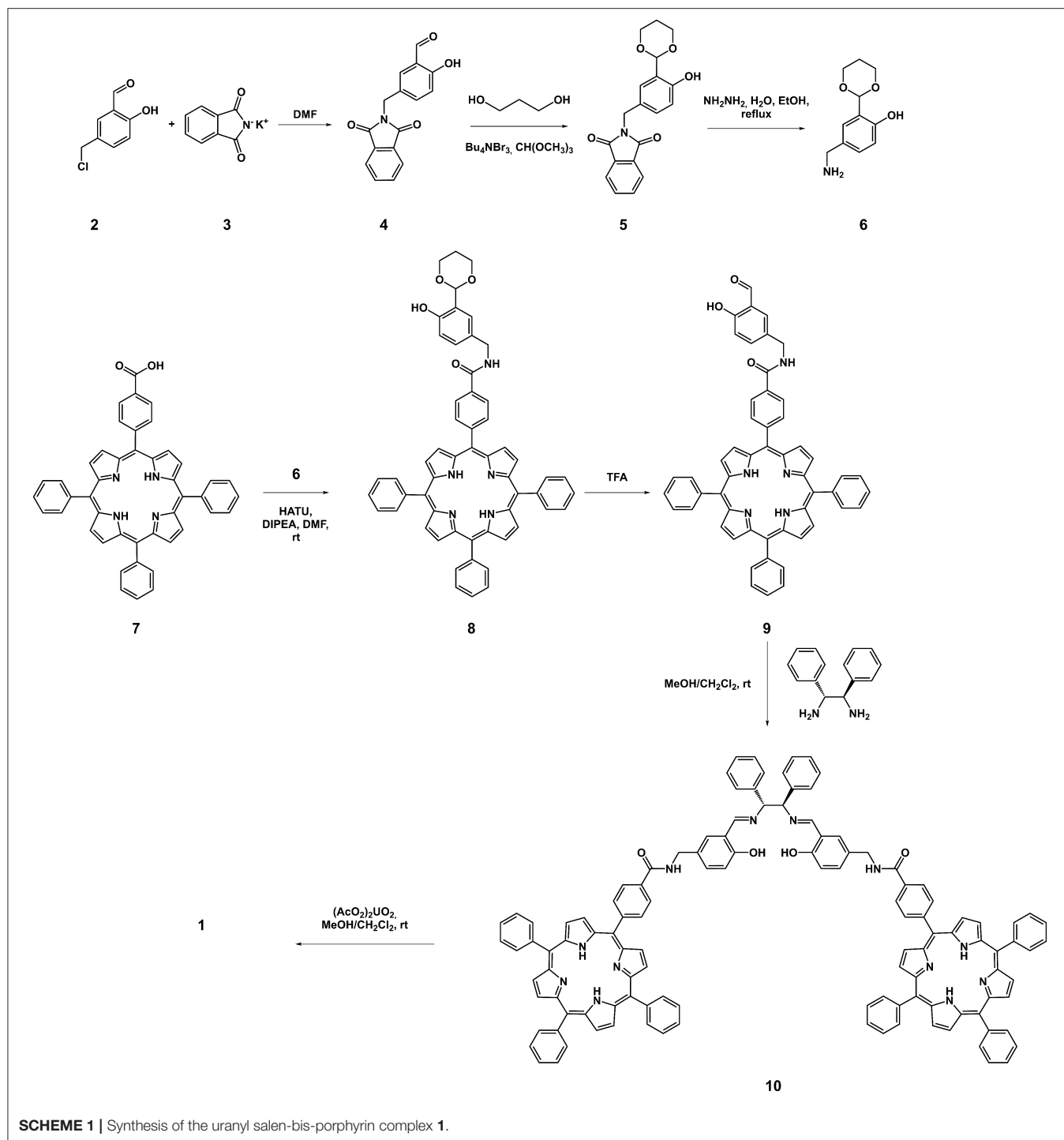
0.440 g (1.298 mmol) of compound **5** and 0.704 mL (0.713 mmol) of hydrazine monohydrate in 30 mL of EtOH were added in a round-bottomed flask of 50 mL. The reaction was heated at 90°C and monitored by TLC. After 20 min, the heating was interrupted. The reaction mixture was cooled down to room temperature and solvent was evaporated. The obtained white precipitate was diluted in 30 mL of water. The aqueous solution was extracted with CHCl<sub>3</sub> (2 × 20 mL) which was previously passed through Al<sub>2</sub>O<sub>3</sub> layer. The CHCl<sub>3</sub> solution was dried over anhydrous Na<sub>2</sub>SO<sub>4</sub>, filtered and evaporated. Compound **6** (0.154 g, 57%) was obtained as a yellow oil. <sup>1</sup>H NMR (500 MHz, CDCl<sub>3</sub>): δ = 7.18–7.16 (dd, *J* = 8.5 Hz, *J* = 2.0 Hz, 1H); 7.14 (s, 1H); 6.87–6.85 (d, *J* = 8.5 Hz, 1H); 5.65 (s, 1H); 4.33–4.30 (m, 2H); 4.04–3.99 (m, 2H); 3.77 (s, 2H); 2.32–2.30 (m, 1H); 1.54–1.50 (m, 1H). <sup>13</sup>C NMR (125 MHz, CDCl<sub>3</sub>): 26.6; 45.7; 67.4; 102.4; 117.1; 122.2; 126.3; 129.2; 134.3; 154.0.

## Synthesis of Compound 8

0.394 g (0.598 mmol) of compound **7** (Gaware et al., 2017) were dissolved in 20 mL of anhydrous DMF, in a round-bottomed flask. To this stirred solution 0.273 g (0.718 mmol) of HATU was added, and the resulting mixture was left to stir under N<sub>2</sub>

atmosphere at room temperature for 20 min. Then, solution of 0.130 g (0.623 mmol) of compound **6** in 5 mL of anhydrous DMF was poured into the reaction mixture, which was stirred under N<sub>2</sub> atmosphere and room temperature, for other 40 min. Finally, 0.105 mL (0.623 mmol) of *N,N*-diisopropylethylamine was added to the reaction mixture. The reaction was carried out in N<sub>2</sub> atmosphere for 70 h. After this period, the reaction mixture was evaporated. The resulting precipitate was dissolved in 30 mL of CH<sub>2</sub>Cl<sub>2</sub>. The organic solution was washed with water (3 × 40 mL), dried over anhydrous Na<sub>2</sub>SO<sub>4</sub> filtered and evaporated. Compound **8** was purified by silica gel column chromatography (CH<sub>2</sub>Cl<sub>2</sub>/MeOH 100:2) affording 80 mg (16% yield) of a purple solid. <sup>1</sup>H NMR (500 MHz, CDCl<sub>3</sub>): δ = 8.85–8.61 (m, 8H); 8.29–8.26 (d, *J* = 8.0 Hz, 2H); 8.24–8.18 (m, 6H); 8.11–8.05 (d, *J* = 8.0 Hz, 2H); 7.90 (s, 1H); 7.78–7.72 (m, 9H); 7.37–7.33 (dd, *J* = 8.5 Hz, *J* = 2.0 Hz, 1H); 7.31 (d, *J* = 2.0 Hz, 1H); 6.96–6.93 (d, *J* = 8.5 Hz, 1H); 6.57 (s, 1H); 5.70 (s, 1H); 4.64 (d, 2H); 4.38–4.32 (m, 2H); 4.20–4.02 (m, 2H); 2.35–2.25 (m, 1H); 1.52–1.48 (m, 1H); –2.81 (s, 2H). <sup>13</sup>C (125 MHz, CDCl<sub>3</sub>): δ = 25.7, 29.7, 43.9, 67.5, 102.9, 117.8, 118.5, 120.3, 125.3, 126.5 (x3), 126.7 (x3), 127.5 (x3), 127.7 (x3), 127.9, 129.2, 130.6, 131.7, 132.1, 134.4 (x2), 134.5, 134.6, 142.0, 142.7, 145.6, 150.3, 155.0.





## Synthesis of Compound 9

0.080 g (0.094 mmol) of compound **8** were dissolved in 1.74 mL of TFA, in a round-bottomed flask, and the resulting mixture was allowed to stir at room temperature for 3 h. Then, 10 mL of diethyl ether were added to the organic solution affording a green precipitate, that was filtered and crystallized using MeOH, to give 50 mg (67% yield) of a red solid.  $^1\text{H}$ NMR (500 MHz,  $\text{CDCl}_3$ ):  $\delta$

= 11.04 (s, 1H); 9.96 (s, 1H); 8.96–8.86 (m, 8H); 8.33–8.29 (d,  $J$  = 8.0 Hz, 2H); 8.24–8.19 (m, 6H); 8.26–8.22 (d,  $J$  = 8.0 Hz, 2H); 7.80–7.72 (m, 9H); 7.70 (d,  $J$  = 2.0 Hz, 1H); 7.68–7.64 (dd,  $J$  = 8.5 Hz,  $J$  = 2.0 Hz, 1H); 7.05 (d,  $J$  = 8.5 Hz, 1H); 6.77 (t, 1H); 4.76 (d, 2H); –2.77 (s, 2H).  $^{13}\text{C}$  (125 MHz,  $\text{CDCl}_3$ ):  $\delta$  = 43.0, 118.0, 118.1, 120.4, 121.2, 125.0, 125.2, 126.5, 126.7, 127.5, 127.8, 128.5, 129.0, 131.4, 132.1, 132.2, 132.6, 132.8, 132.9, 134.4, 134.5, 134.6,

136.6, 136.7, 142.0, 142.8, 149.5, 150.1, 150.3, 150.4, 167.2, 196.3. MS (ESI):  $m/z = 790.2$   $[M + H]^+$ .

### Synthesis of Salen-Bis-Porphyrin Ligand **10**

In a round bottom flask, to a solution of 27.6 mg of salicylic-porphyrin **9** (0.0349 mmol) in absolute EtOH (10 mL) was added (1*R*,2*R*)-(+)-1,2-diphenylethylenediamine (3.7 mg, 0.0175 mmol). The reaction was stirred for 48 h at room temperature and monitored by TLC ( $\text{CH}_2\text{Cl}_2/\text{CH}_3\text{OH}$ , 100:2). The reaction was quenched by evaporation of the solvent under reduced pressure, and salen-bis-porphyrin ligand **10** was purified by PLC ( $\text{CH}_2\text{Cl}_2/\text{CH}_3\text{OH}$ , 100:2) to afford 24 mg of a red/purple solid compound (78% yield).  $^1\text{H}$ NMR (500 MHz,  $\text{CDCl}_3$ ):  $\delta = 14.41$  (bs, 2H); 8.86–8.74 (m, 16H); 8.30 (s, 2H); 8.25–8.07 (m, 20H); 7.77–7.66 (m, 20H); 7.29–7.15 (m, 12H); 6.97 (d,  $J = 8.5$  Hz, 2H); 6.83 (t, 2H); 4.73 (s, 2H); 4.56 (d, 4H);  $-2.78$  (s, 4H).  $^{13}\text{C}$  (125 MHz,  $\text{CDCl}_3$ ):  $\delta = 43.3$ , 80.1, 117.2 (x2), 118.47, 118.53, 120.3 (x2), 120.5, 125.4 (x2), 126.3, 126.7 (x2), 127.7 (x3), 127.8 (x2), 128.4, 128.6, 131.0, 132.3, 133.5, 134.4 (x3), 134.5 (x2), 134.6, 139.0, 141.9, 142.0, 145.6, 160.4, 166.2, 167.4. MS (ESI):  $m/z = 1760.4$   $[M + H]^+$ ,  $m/z = 891.0$   $[M + \text{Na}]^{2+}$ .

### Synthesis of Uranyl Salen-Bis-Porphyrin Complex **1**

To a solution of **10** (22 mg, 0.0125 mmol) dissolved in absolute ethanol (10 mL) was added uranyl acetate (5.3 mg, 0.0125 mmol). The reaction was stirred overnight at room temperature, and the resulting solid was filtered and dried to yield 27 mg of uranyl salen-bis-porphyrin complex **1** as a red powder (98% yield).  $^1\text{H}$ NMR (500 MHz,  $\text{DMSO}-d_6$ ):  $\delta = 9.49$  (s, 2H); 9.33 (s, 2H); 8.82–8.76 (m, 16H); 8.32–8.20 (m, 20H); 7.83–7.80 (m, 20H); 7.74–7.59 (m, 8H); 7.21 (t, 2H); 7.15 (m, 2H); 7.05 (d, 2H); 6.35 (s, 2H); 4.67–4.57 (m, 4H);  $-2.93$  (s, 4H).  $^{13}\text{C}$  (125 MHz,  $\text{DMSO}-d_6$ ):  $\delta = 42.2$ , 79.5, 119.0 (x2), 120.1, 120.2 (x2), 120.3, 122.7, 125.9 (x3), 126.6 (x2), 127.0 (x3), 127.2 (x2), 127.4 (x3), 127.5, 128.1, 128.2, 133.7, 133.9, 134.2 (x3), 135.2, 141.1, 141.6, 144.0, 166.0, 168.6, 171.2. MS (ESI):  $m/z = 1058$   $[M+2\text{EtOH}+2\text{H}]^{2+}$ ;  $m/z = 1077$   $[M+2\text{EtOH}+\text{Na}+\text{H}]^{2+}$ .

## RESULTS AND DISCUSSION

Target uranyl salen-bis-porphyrin complex **1** was synthesized in seven steps starting from 5-Cl-methyl-salicylaldehyde **2** (Dalla Cort et al., 2006; Saffar-Telur, 2015) as shown in **Scheme 1**. In the first step potassium phthalimide was treated with compound **2** to yield compound **4** (40%), which was then reacted with 1,3-propanediol to afford the acetal intermediate **5** (92%). Conversion of the phthalimido moiety into an amino group by treatment with hydrazine, under standard Gabriel conditions, yielded the compound **6** (57%). The condensation reaction between compound **6** and 5-(4-Carboxyphenyl)-10,15,20-triphenylporphyrin **7** (Gaware et al., 2017) which was activated using HATU (Gangemi et al., 2015), afforded the porphyrin derivative **8** (16%), which was then treated with TFA to remove the acetal moiety and yield the salicylic-porphyrin **9** (67%). Condensation of **9** with the (1*R*,2*R*)-(+)-1,2-diphenylethylenediamine yielded salen ligand **10** (78%), which

was finally converted into the corresponding salen complex **1** (98 %) by uranyl acetate. The proposed structures for this new chiral uranyl-salen complex and all the intermediates compounds are consistent with the  $^1\text{H}$  and  $^{13}\text{C}$  NMR spectroscopy data as well as the ESI mass spectrometry data (see **Supplementary Material**).

The UV-vis spectrum of uranyl salen-bis-porphyrin complex **1** dissolved in  $\text{CHCl}_3$  solution shows an intense Soret band centered at 419 nm ( $\epsilon = 6,26 \cdot 10^5 \text{ M}^{-1} \text{ cm}^{-1}$ ) and four Q-bands (515 nm; 550 nm; 590 nm; 646 nm) (**Figure 2**). The UV-vis spectrum is similar to the 5-(4-Methoxycarbonylphenyl)-10,15,20-triphenylporphyrin (TPPCOOMe, the precursor of 5-(4-Carboxyphenyl)-10,15,20-triphenylporphyrin **7**) in the same solvent (Rong et al., 2012), suggesting that the insertion of the salen- $\text{UO}_2$  does not change the spectroscopic behavior of the porphyrin. Furthermore, there is no evidence of aggregation even at higher concentration (2.5  $\mu\text{M}$ ), as confirmed by UV-Vis and fluorescence data. In addition, the luminescence measurements are in accordance with literature data for similar porphyrins, with two main emission bands centered at 650 and 715 nm ( $\lambda_{\text{ex}}$  350 nm), respectively (**Figure 2**).

After proving the luminescent properties of uranyl salen-bis-porphyrin complex **1**, enantioselective recognition properties were evaluated by UV-vis and fluorescence measurements in chloroform, in particular for fluorescence titrations, following the emission changes at these two emission wavelengths of porphyrin moiety (650 nm and 715 nm, by using  $\lambda_{\text{ex}}$  350 nm). Unfortunately, the fluorescence titrations showed a small intensity variation with all the selected amino acid guests except for the *L*-tryptophan derivative, which led to a poor data fitting. For that reasons, binding constant values between uranyl salen-bis-porphyrin complex **1** and amino acid derivatives were determined by UV-vis titrations, following a decrease of the absorption at 419 nm upon addition of increasing aliquots of guests. A representative example of UV-vis titration and the fluorescence titration of uranyl salen-bis-porphyrin complex **1** with *L*-Trp-TBA are shown in **Figure 3**.

**Table 1** reports the pertinent binding constant values with selected amino acid derivatives, the detection limit observed (DL) and the corresponding enantiomeric excess. In all cases, binding constant values have been calculated using 1:1 stoichiometry, suggested by Job's plots (see **Supplementary Material**).

Notably, due to the presence of the porphyrin moieties, receptor **1** is able to detect the amino acid guests at low concentration. In fact, 1  $\mu\text{M}$  solution of uranyl salen-bis-porphyrin complex **1** is able to detect amino acid derivatives at very low concentrations (ppb).

Enantiomeric recognition is very efficient with the *L*-Phe-TBA, which is recognized more than 8 times respect to the *D*-enantiomer ( $K_L/K_D = 8.51$ ). A good enantioselectivity is also observed for the *D*- and *L*-Trp-TBA pair ( $K_D/K_L = 4.04$ ). Moreover, for the *L*-Trp-TBA we were able to determine the binding constant value by fluorescence titration ( $K$  ( $\text{M}^{-1}$ ) =  $2.63 \pm 0.03 \times 10^6$ ), in good agreement with the value calculated by UV-vis titration. In particular, a decrease of the emission intensity has been observed, probably due to a photoinduced electron transfer mechanism (PET) (Trusso Sfrassetto et al.,

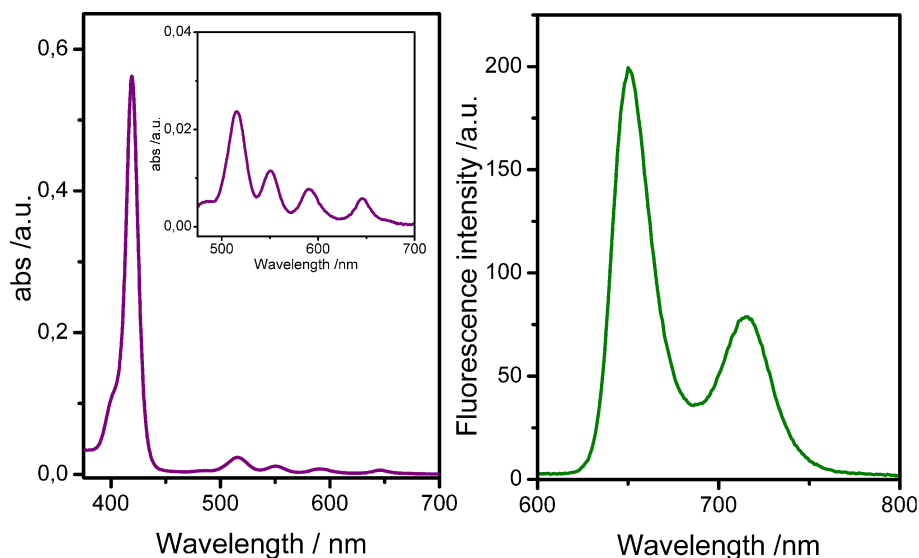


**FIGURE 2** | UV-Vis spectra (**Left**) and fluorescence spectra (**Right**) of uranyl salen-bis-porphyrin complex **1** in  $\text{CHCl}_3$  (1  $\mu\text{M}$ ).

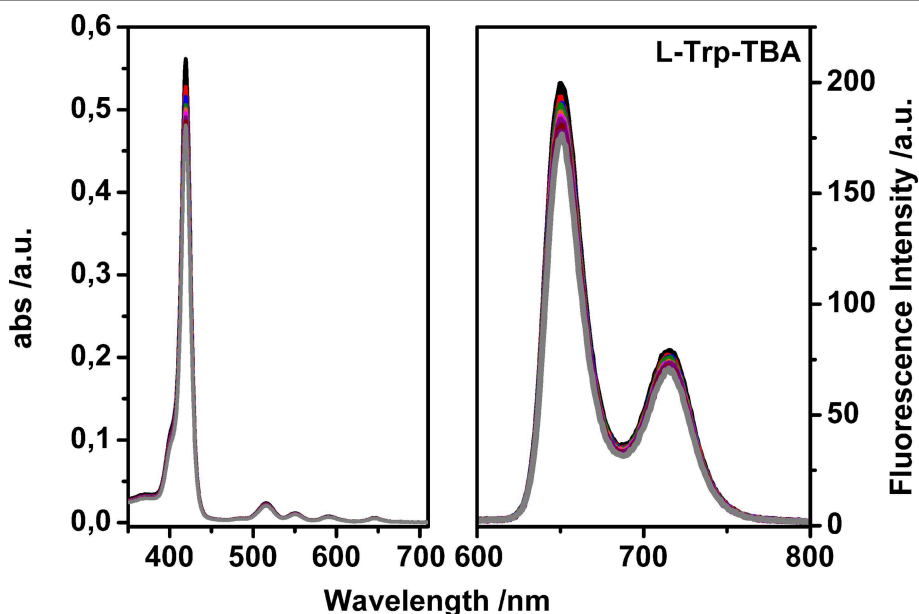


**FIGURE 3** | Representative UV-vis titration (**Left**) and fluorescence titration (**Right**) of uranyl salen-bis-porphyrin complex **1** with **L-Trp-TBA** ( $\lambda_{\text{ex}} = 350 \text{ nm}$  in dry chloroform).

2016). Only the *D*- and *L*-Ala-TBA ( $K_D/K_L = 1.70$ ) pair shows a slight selective recognition. With the smaller amino acid guest, coordination to the uranyl metal center appears less susceptible to the different configurations of the carbon atom stereocenter and then the molecular recognition is less selective. With aromatic amino acid derivatives, the possibility for the carboxylate anion to bind the fifth equatorial coordination site of the uranyl metal and, at the same time, to exploit CH- $\pi$  interactions with the salen moiety and the porphyrin

macrocycles of receptor **1** might be responsible for the strong observed enantioselectivity. Moreover, the strong recognition for the *L*-Phe-TBA enantiomer is in contrast with respect to those observed with our previous receptors having the same configuration of the chiral diamine bridge (*R,R*) (Ballistreri et al., 2010; Amato et al., 2011; Pappalardo et al., 2012a; Forte et al., 2015). Probably, the presence of the two porphyrin arms not only increase the limit of detection by the presence of a fluorescence signal, but also plays a fundamental role in the recognition event.

**TABLE 1** | Binding constant values  $K$  ( $M^{-1}$ ) with selected amino acid derivatives, detection limit observed (DL), and enantiomeric excess calculated by UV-vis titrations in dry chloroform at 25°C.

Guest	DL <sup>b</sup>	$K$ ( $M^{-1}$ ) <sup>a</sup>	e.e.
D-Phe-TBA	2.5 ppb	$(8.13 \pm 0.08) \times 10^4$	$K_L/K_D = 8.51$
L-Phe-TBA	1.6 ppb	$(6.92 \pm 0.07) \times 10^5$	
D-Ala-TBA	1.7 ppb	$(9.77 \pm 0.59) \times 10^6$	$K_D/K_L = 1.70$
L-Ala-TBA	1.3 ppb	$(5.75 \pm 0.05) \times 10^6$	
D-Trp-TBA	1.6 ppb	$(4.33 \pm 0.09) \times 10^6$	$K_D/K_L = 4.04$
L-Trp-TBA	1.1 ppb	$(1.07 \pm 0.01) \times 10^6$	

<sup>a</sup>Calculated by HypSpec v1.1.33.<sup>b</sup>Calculated by method of the calibration curve using the formula  $DL = 3\sigma/K$ , where  $\sigma$  is the standard deviation of the blank, and  $K$  is the slope of the calibration curve.

## CONCLUSION

We have synthesized a new chiral uranyl salen complex bearing two porphyrin macrocycles and evaluated the enantiomeric recognition properties of this complex toward  $\alpha$ -amino acid derivatives by UV-vis titrations. The presence of porphyrin arms lead to a receptor that possesses luminescence properties that are not quenched by the coordination with the uranyl cation, which decreases the fluorescence intensity in uranyl salen complexes. UV/Vis measurements and Job plots indicate the formation of 1:1 host-guest complexes. This receptor displays a very high selectivity toward amino acid derivatives, in particular for the two enantiomers of Phe-TBA. The two porphyrin macrocycles play a key role in the enantioselectivity interacting through

CH- $\pi$  with the aromatic moiety of aminoacids, leading to high binding affinities. Work is in progress in our laboratory to better understand the rules governing the interactions of this salen receptor with amino acid guests in order to design new host-guest systems that possess luminescence properties.

## DATA AVAILABILITY STATEMENT

All datasets generated for this study are included in the article/**Supplementary Material**.

## AUTHOR CONTRIBUTIONS

CG, UR, FC, and AP performed the synthesis of uranyl porphyrin-salen complex. GT acquired UV-vis and luminescence data. AP writing-original draft preparation. CG, UR, FC, GT, and AP writing-review and editing.

## FUNDING

This work was supported by the University of Catania, Department of Chemical Sciences (Piano per la Ricerca 2016-2018-Linea Intervento 2).

## SUPPLEMENTARY MATERIAL

The Supplementary Material for this article can be found online at: <https://www.frontiersin.org/articles/10.3389/fchem.2019.00836/full#supplementary-material>

## REFERENCES

- Amato, M. E., Ballistreri, F. P., D'Agata, S., Pappalardo, A., Tomaselli, G. A., Toscano, R. M., et al. (2011). Enantioselective molecular recognition of chiral organic ammonium ions and amino acids using cavitand-salen-based receptors. *Eur. J. Org. Chem.* 21, 5674–5680. doi: 10.1002/ejoc.201100955
- Amato, M. E., Ballistreri, F. P., Gentile, S., Pappalardo, A., Tomaselli, G. A., and Toscano, R. M. (2010). Recognition of achiral and chiral ammonium salts by neutral ditopic receptors based on chiral salen-UO<sub>2</sub> macrocycles. *J. Org. Chem.* 75, 1437–1443. doi: 10.1021/jo902328y
- Amato, M. E., Ballistreri, F. P., Pappalardo, A., Sciotto, D., Tomaselli, G. A., and Toscano, R. M. (2007). Synthesis and conformational aspects of 20- and 40-membered macrocyclic mono and dinuclear uranyl complexes incorporating salen and (R)-BINOL units. *Tetrahedron* 63, 9751–9757. doi: 10.1016/j.tet.2007.07.014
- Baleizao, C., and Garcia, H. (2006). Chiral salen complexes: an overview to recoverable and reusable homogeneous and heterogeneous catalysts. *Chem. Rev.* 106, 3987–4043. doi: 10.1021/cr050973n
- Ballistreri, F. P., Gangemi, C. M., Pappalardo, A., Tomaselli, G. A., Toscano, R. M., and Trusso Sfrazzetto, G. (2016). (Salen)Mn(III) catalyzed asymmetric epoxidation reactions by hydrogen peroxide in water: a green protocol. *Int. J. Mol. Sci.* 17:1112. doi: 10.3390/ijms17071112
- Ballistreri, F. P., Lombardo, G., Pappalardo, A., Punzo, F., Thompson, A., Tomaselli, G. A., et al. (2012). An integrated X-ray and molecular dynamics study of uranyl-salen structures and properties. *Dalton Trans.* 41, 1951–1960. doi: 10.1039/C1DT11758K
- Ballistreri, F. P., Pappalardo, A., Toscano, R. M., Tomaselli, G. A., and Trusso Sfrazzetto, G. (2010). Heteroditopic chiral uranyl-salen receptor for molecular recognition of amino acid ammonium salts. *Eur. J. Org. Chem.* 20, 3806–3810. doi: 10.1002/ejoc.201000566
- Ballistreri, F. P., Toscano, R. M., Amato, M. E., Pappalardo, A., Gangemi, C. M. A., Spidalieri, S., et al. (2018). A new Mn-salen micellar nanoreactor for enantioselective epoxidation of alkenes in water. *Catalysts* 8:129. doi: 10.3390/catal8040129
- Beletskaya, I., Tyurin, V. S., Tsivadze, A. Y., Guillard, R., and Stern, C. (2009). Supramolecular chemistry of metalloporphyrins. *Chem. Rev.* 109, 1659–1713. doi: 10.1021/cr800247a
- Brancatelli, G., Geremia, S., Notti, A., Pappalardo, A., and Trusso Sfrazzetto, G. (2013). Mono- and dinuclear uranyl(VI) complexes with chiral Schiff base ligand. *Inorg. Chim. Acta* 396, 25–29. doi: 10.1016/j.ica.2012.12.034
- Cozzi, P. G. (2004). Metal-Salen Schiff base complexes in catalysis: practical aspects. *Chem. Soc. Rev.* 33, 410–421. doi: 10.1039/B307853C
- Dalla Cort, A., Mandolini, L., Pasquini, C., and Schiaffino, L. (2006). A novel ditopic zinc-salophen macrocycle: a potential two-stationed wheel for [2]-pseudorotaxane. *Org. Biomol. Chem.* 4, 4543–4546. doi: 10.1039/b613705a
- Drain, C. M., Varotto, A., and Radiovojevic, I. (2009). Self-organized porphyrinic materials. *Chem. Rev.* 109, 1630–1658. doi: 10.1021/cr8002483
- D'Urso, A., Tudisco, C., Ballistreri, F. P., Condorelli, G. G., Randazzo, R., Tomaselli, G. A., et al. (2014). Enantioselective extraction mediated by a chiral cavitand-salen covalently assembled on a porous silicon surface. *Chem. Commun.* 50, 4993–4496. doi: 10.1039/C4CC00034J
- Forte, G., D'Urso, A., Ballistreri, F. P., Toscano, R. M., Tomaselli, G. A., Trusso Sfrazzetto, G., et al. (2015). Enantiomeric recognition of  $\alpha$ -amino acid derivatives by chiral uranyl-salen receptors. *Tetrahedron Lett.* 56, 2922–2926. doi: 10.1016/j.tetlet.2015.04.092
- Gangemi, C. M. A., Randazzo, R., Fragalà, M. E., Tomaselli, G. A., Ballistreri, F. P., Pappalardo, A., et al. (2015). Hierarchically controlled



- protonation/aggregation of a porphyrin-spermine derivative. *New J. Chem.* 39, 6722–6725. doi: 10.1039/C5NJ01264C
- Gaware, V. S., Hakerud, M., Juzeniene, A., Høgset, A., Berg, K., and Måsson, M. (2017). Endosome targeting meso-tetraphenylchlorin–chitosan nanoconjugates for photochemical internalization. *Biomacromolecules* 18, 1108–1126. doi: 10.1021/acs.biomac.6b01670
- Jacobsen, E. N. (1993). “Asymmetric catalytic epoxidation of unfunctionalized olefins,” in *Catalytic Asymmetric Synthesis*, ed I. Ojima (New York, NY: VCH), 159–202.
- Jacobsen, E. N. (2000). Asymmetric catalysis of epoxide ring-opening reactions. *Acc. Chem. Res.* 33, 421–431. doi: 10.1021/ar960061v
- Johansson, A., Abrahamsson, M., Magnuson, A., Huang, P., Mårtensson, J., Styring, S., et al. (2003). Synthesis and photophysics of one mononuclear Mn(III) and one dinuclear Mn(III,III) complex covalently linked to a ruthenium(II) tris(bipyridyl) complex. *Inorg. Chem.* 42, 7502–7511. doi: 10.1021/ic0344822
- Katsuki, T. (1995). Catalytic asymmetric oxidations using optically active (salen)manganese(III) complexes as catalysts. *Coord. Chem. Rev.* 140, 189–214. doi: 10.1016/0010-8545(94)01124-T
- Katsuki, T. (2000). “Asymmetric oxidations and related reactions: asymmetric epoxidation of unfunctionalized olefins and related reactions,” in *Catalytic Asymmetric Synthesis, 2nd Edn*, ed I. Ojima (New York, NY: Wiley-VCH), 287–325.
- La Paglia, Fragola, V., Lupo, F., Pappalardo, A., Trusso Sfrazzetto, G., Toscano, R. M., Ballistreri, F. P., et al. (2012). A surface-confined O=MnV(salen) oxene catalyst and high turnover values in asymmetric epoxidation of unfunctionalized olefins. *J. Mater. Chem.* 22, 20561–20561. doi: 10.1039/c2jm34847k
- McGarrigle, E. M., and Gilheany, D. G. (2005). Chromium- and manganese-salen promoted epoxidation of alkenes. *Chem. Rev.* 105, 1563–1602. doi: 10.1021/cr0306945
- Pappalardo, A., Amato, M. E., Ballistreri, F. P., Tomaselli, G. A., Toscano, R. M., and Trusso Sfrazzetto, G. (2012a). Pair of diastereomeric uranyl salen cavitands displaying opposite enantiodiscrimination of  $\alpha$ -amino acid ammonium salts. *J. Org. Chem.* 77, 7684–7687. doi: 10.1021/jo301098d
- Pappalardo, A., Ballistreri, F. P., Li Destri, G., Mineo, P. G., Tomaselli, G. A., Toscano, R. M., et al. (2012b). Supramolecular polymer networks based on calix[5]arene tethered poly(*p*-phenyleneethynylene). *Macromolecules* 45, 7549–7556. doi: 10.1021/ma3015239
- Puglisi, R., Ballistreri, F. P., Gangemi, C. M. A., Toscano, R. M., Tomaselli, G. A., Pappalardo, A., et al. (2017). Chiral Zn–salen complexes: a new class of fluorescent receptors for enantiodiscrimination of chiral amines. *New J. Chem.* 41, 911–915. doi: 10.1039/C6NJ03592B
- Puglisi, R., Mineo, P. G., Pappalardo, A., Gulino, A., and Trusso Sfrazzetto, G. (2019). Supramolecular detection of a nerve agent simulant by fluorescent Zn–salen oligomer receptors. *Molecules* 24:2160. doi: 10.3390/molecules24112160
- Puglisi, R., Pappalardo, A., Gulino, A., and Trusso Sfrazzetto, G. (2018). Supramolecular recognition of CWAs simulant by metal–salen complexes: the first multi-topic approach. *Chem. Commun.* 54, 11156–11159. doi: 10.1039/C8CC06425C
- Rong, Y., Chen, P., Wang, D., and Liu, M. (2012). Porphyrin assemblies through the air/water interface: effect of hydrogen bond, thermal annealing, and amplification of supramolecular chirality. *Langmuir* 28, 6356–6363. doi: 10.1021/la3005294
- Saffar-Telur, A. (2015). Direct covalent attachment of Mn(III) salen complex to the hydroxyapatite-encapsulated  $\gamma$ -Fe<sub>2</sub>O<sub>3</sub> nanocrystallites: an efficient magnetic and reusable catalyst for oxidation of alcohols. *RSC Adv.* 5, 70577–70585. doi: 10.1039/C5RA08594B
- Trusso Sfrazzetto, G., Millesi, S., Pappalardo, A., Toscano, R. M., Ballistreri, F. P., Tomaselli, G. A., et al. (2015). Olefin epoxidation by a (salen)Mn(III) catalyst covalently grafted on glass beads. *Cat. Sci. Technol.* 5, 673–679. doi: 10.1039/C4CY00831F
- Trusso Sfrazzetto, G., Satriano, C., Tomaselli, G. A., and Rizzarelli, E. (2016). Synthetic fluorescent probes to map metallosis and intracellular fate of zinc and copper. *Coord. Chem. Rev.* 311, 125–167. doi: 10.1016/j.ccr.2015.11.012
- Wezenberg, S. J., and Kleij, A. W. (2008). Material applications for salen frameworks. *Angew. Chem., Int. Ed.* 47, 2354–2364. doi: 10.1002/anie.200702468
- Whiteoak, C. J., Salassa, G., and Kleij, A. W. (2012). Recent advances with  $\pi$ -conjugated salen systems. *Chem. Soc. Rev.* 41, 622–631. doi: 10.1039/C1CS15170C
- Yoon, T. P., and Jacobsen, E. N. (2003). Privileged chiral catalysts. *Science* 299, 1691–1693. doi: 10.1126/science.1083622
- Zammataro, A., Gangemi, C. M. A., Pappalardo, A., Toscano, R. M., Puglisi, R., Nicotra, G., et al. (2019). Covalently functionalized carbon nanoparticles with a chiral Mn–Salen: a new nanocatalyst for enantioselective epoxidation of alkenes. *Chem. Commun.* 55, 5255–5258. doi: 10.1039/C9CC01825E

**Conflict of Interest:** The authors declare that the research was conducted in the absence of any commercial or financial relationships that could be construed as a potential conflict of interest.

The reviewer SG declared a past co-authorship with one of the authors AP to the handling editor.

Copyright © 2019 Gangemi, Rimkaite, Cipria, Trusso Sfrazzetto and Pappalardo. This is an open-access article distributed under the terms of the Creative Commons Attribution License (CC BY). The use, distribution or reproduction in other forums is permitted, provided the original author(s) and the copyright owner(s) are credited and that the original publication in this journal is cited, in accordance with accepted academic practice. No use, distribution or reproduction is permitted which does not comply with these terms.



# Synthesis and Host–Guest Properties of Acyclic Pillar[*n*]naphthalenes

Yuanyin Jia<sup>1†</sup>, Ming Dong<sup>2†</sup>, Bin Wang<sup>2\*</sup> and Chunju Li<sup>1,2,3\*</sup>

<sup>1</sup> School of Chemical and Environmental Engineering, Shanghai Institute of Technology, Shanghai, China, <sup>2</sup> Key Laboratory of Inorganic–Organic Hybrid Functional Material Chemistry, Ministry of Education, Tianjin Key Laboratory of Structure and Performance for Functional Molecules, College of Chemistry, Tianjin Normal University, Tianjin, China, <sup>3</sup> Department of Chemistry, Center for Supramolecular Chemistry and Catalysis, Shanghai University, Shanghai, China

## OPEN ACCESS

### Edited by:

De-Xian Wang,  
Institute of Chemistry (CAS), China

### Reviewed by:

Lyle Isaacs,  
University of Maryland, College Park,  
United States  
Liu-Pan Yang,  
Southern University of Science and  
Technology, China

### \*Correspondence:

Bin Wang  
hxywangb@mail.tjnu.edu.cn  
Chunju Li  
cjl@shu.edu.cn

<sup>†</sup>These authors have contributed  
equally to this work

### Specialty section:

This article was submitted to  
Supramolecular Chemistry,  
a section of the journal  
Frontiers in Chemistry

**Received:** 15 August 2019

**Accepted:** 14 November 2019

**Published:** 03 December 2019

### Citation:

Jia Y, Dong M, Wang B and Li C  
(2019) Synthesis and Host–Guest  
Properties of Acyclic  
Pillar[*n*]naphthalenes.  
Front. Chem. 7:828.  
doi: 10.3389/fchem.2019.00828

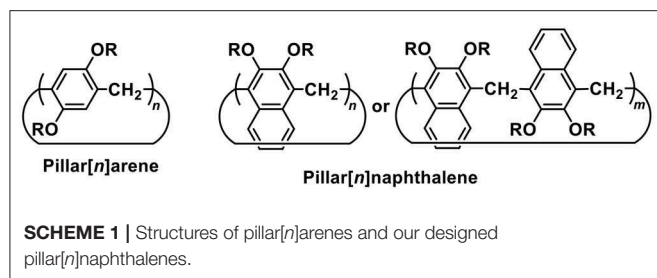
Here we report a new class of synthetic receptors, acyclic pillar[*n*]naphthalene (*n* = 2–4, **Dimer**, **Trimer**, and **Tetramer**) oligomers, which are made up of 2,3-diethoxynaphthalene units linked by methylene bridges at the 1- and 4-positions. They can be synthesized through a one-step condensation of 2,3-diethoxynaphthalene monomer and paraformaldehyde in the presence of BF<sub>3</sub>•(Et)<sub>2</sub>O catalyst. The crystal structure of **Tetramer** has an interesting pseudo-cycle shaped structure in the solid state. Their complexation behaviors toward several organic ammonium cations (**1**<sup>+</sup>–**15**<sup>+</sup>) and electron-deficient neutral guests (**16**–**17**), were examined by means of <sup>1</sup>H NMR spectroscopy. **Tetramer** shows good host-guest properties toward the ammonium guests, giving association constants (*K*<sub>a</sub>) in the magnitude of 10<sup>2</sup>–10<sup>4</sup> M<sup>–1</sup>, which are comparable with those for some macrocyclic hosts.

**Keywords:** pillararenes, calixarenes, acyclic hosts, molecular recognition, host-guest chemistry

## INTRODUCTION

Since the discover of crown ethers, the development of hosts for recognizing various guest species has mainly focused on macrocyclic structures (Cram, 1988; Lehn, 1988; Pedersen, 1988; Gong et al., 2010; Chun et al., 2013; Jurícek et al., 2014; Liu et al., 2019). Methylene-bridged macrocyclic arenes, for example calixarenes (Baldini et al., 2007; Guo and Liu, 2012), pillararenes (Ogoshi et al., 2008; Xue et al., 2012; Wang et al., 2016; Yang et al., 2016), coronarenes (Wang, 2018), helic[6]arene (Zhang et al., 2016), biphenarenes (Chen et al., 2015; Dai et al., 2017; Li et al., 2019; Wang et al., 2019b), and etc. (Guo et al., 2018; Luo et al., 2018; Ma et al., 2018) have been widely used in host-guest chemistry, self-assembly materials, and biomedical field (Song and Yang, 2015; Alsbaiee et al., 2016; Li et al., 2017; Jie et al., 2018; Chen et al., 2019; Yang et al., 2019). Naphthalene-based macrocyclic arenes, termed as calixnaphthalenes, have also been produced (Poh et al., 1989; Andreetti et al., 1993; Shorthill et al., 2004; AlHujran et al., 2012; Avetta et al., 2012). However, calixnaphthalenes have not become highly popular receptors because they do not have unique molecular recognition properties. Considering that pillararenes with pillar-shape topologic structures have shown nice host-guest properties, we wondered whether we can create acyclic pillarnaphthalenes (**Scheme 1**), which would have deep, pillar-shape, and π-rich cavities, and maybe better binding abilities than calixnaphthalenes. As detailed below, we did not get such macrocycles, but succeed in making acyclic pillarnaphthalene oligomers.

Acyclic hosts that contain partially enclosed cavities capable of binding guests provided alternatives with unique synthetic and functional advantages (Goodman et al., 2007; Seebach and Gardiner, 2008; Pan et al., 2017; Wang et al., 2019a). For example, foldamers may provide cavities that are adaptive in recognizing different guest molecules (Zhang et al., 2012; Yashima et al., 2016).



Molecular tweezers have made the way from a supramolecular host to a drug candidate, due to their ability to inhibit peptide and protein aggregation through the complexation toward amino acids (Sinha et al., 2011; Schrader et al., 2016).

Isaacs and his co-workers created acyclic cucurbit[n]uril-type receptors, which can function as solubilizing agents for insoluble drugs. Interestingly, the solubility of paclitaxel was increased 2,750 times through the formation of soluble container–drug complex (Ma et al., 2012). These highly soluble acyclic cucurbiturils could also solubilize individual single-walled carbon nanotubes (SWNTs) in water even at a concentration 100–1,000 times lower than typically required for surfactants (Shen et al., 2012). The groups of Schrader and Yoshizawa synthesized beautiful water-soluble clip and tweezer-shaped hosts based on norbornene and anthracene building blocks (Bier et al., 2013; Jono et al., 2017).

Herein, we wish to report the synthesis of a new type of receptors, acyclic pillar[n]naphthalene ( $n = 2-4$ , **Dimer**, **Trimer**, and **Tetramer**) oligomers, which are made up of 2,3-diethoxynaphthalene units linked by methylene bridges at the 1- and 4-positions. **Tetramer**, bearing a pseudo-cavity, has good host-guest properties toward a series of model organic cationic guests.

## MATERIALS AND METHODS

All the reagents involved in this research were commercially available and used without further purification unless otherwise noted.  $^1\text{H}$  NMR,  $^{13}\text{C}$  NMR, 2D NOESY, and COSY spectra (see **Supplementary Material**) were recorded with a Bruker AVANCE III 500 MHz instrument. Chemical shifts were referred to TMS. High-resolution mass spectra (HRMS) were determined on a Bruker Daltonics, Inc. APEXIII 7.0 TESLA FTMS instrument. The single crystal X-ray data were measured by direct methods using SHELXS-971 and refined by fullmatrix least-squares procedures on F2 with SHELXL-97.2. All non-hydrogen atoms were obtained from the difference Fourier map and subjected to anisotropic refinement by full-matrix least squares on F2. Hydrogen atoms were obtained geometrically and treated as riding on the parent atoms or were constrained in the locations during refinements. Test parameters and detailed experimental data are shown in the **Supplementary Material**.

## Synthesis and Characterization

To the solution of 2,3-diethoxy naphthalene (2.6 g, 12 mmol) in  $\text{CHCl}_3$  (150 mL) was added paraformaldehyde (0.36 g, 12

mmol). Boron trifluoride diethyl etherate (2.5 mL, 20 mmol) was then added to the reaction mixture. The mixture was stirred at  $25^\circ\text{C}$  for 1 h. Then the reaction was quenched by addition of 50 mL water. The organic phase was separated and washed with saturated aqueous  $\text{NaHCO}_3$ , and water. The organic layer was dried over anhydrous  $\text{Na}_2\text{SO}_4$  and concentrated. The residue was purified by column chromatography on silica gel (eluent: 1/1, v/v, dichloromethane: petrol ether) to afford **Dimer** (21%), **Trimer** (9%), and **Tetramer** (15%), as white solids.

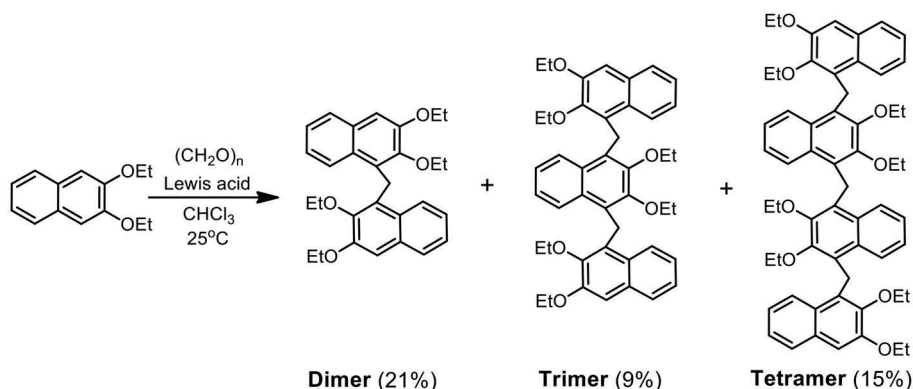
**Dimer.** m.p.  $155-156^\circ\text{C}$ .  $^1\text{H}$  NMR (500 MHz,  $\text{CDCl}_3$ , 298 K):  $\delta$  (ppm): 8.10 (d,  $J = 8.4$  Hz, 2H), 7.61 (d,  $J = 7.7$  Hz, 2H), 7.28–7.24 (m, 2H), 7.23–7.20 (m, 2H), 7.07 (s, 2H), 5.00 (s, 2H), 4.22 (q,  $J = 7.0$  Hz, 4H), 4.02 (q,  $J = 7.0$  Hz, 4H), 1.57 (t,  $J = 7.0$  Hz, 6H), 1.33 (t,  $J = 7.0$  Hz, 6H).  $^{13}\text{C}$  NMR (125 MHz,  $\text{CDCl}_3$ , 298 K):  $\delta$  (ppm): 151.36, 146.37, 131.43, 129.97, 128.57, 126.80, 124.88, 124.65, 123.71, 106.85 (C of acyclic dimer), 69.11, 63.80 (C of methylene in ethoxy group), 23.55 (C of methylene bridge of acyclic dimer), 15.58, 14.86 (C of methyl in ethoxy group). HRMS (ESI):  $\text{C}_{29}\text{H}_{32}\text{O}_4\text{NH}_4^+$ , calcd  $m/z$  462.2644; found  $m/z$  462.2641.

**Trimer.** m.p.  $171-172^\circ\text{C}$ .  $^1\text{H}$  NMR (500 MHz,  $\text{CDCl}_3$ , 298 K):  $\delta$  (ppm): 8.17 (d,  $J = 8.6$  Hz, 2H), 8.04 (dd,  $J = 6.5$ , 3.3 Hz, 2H), 7.57 (d,  $J = 7.8$  Hz, 2H), 7.23 (dd,  $J = 11.0$ , 4.0 Hz, 2H), 7.14–7.09 (m, 4H), 7.01 (s, 2H), 4.93 (s, 4H), 4.20–4.11 (m, 8H), 3.87 (q,  $J = 7.0$  Hz, 4H), 1.51 (t,  $J = 7.0$  Hz, 6H), 1.35 (t,  $J = 7.0$  Hz, 6H), 1.13 (t,  $J = 7.0$  Hz, 6H).  $^{13}\text{C}$  NMR (125 MHz,  $\text{CDCl}_3$ , 298 K):  $\delta$  (ppm): 151.37, 148.98, 146.30, 131.42, 130.70, 130.15, 128.93, 128.49, 126.81, 125.16, 124.90, 124.53, 124.39, 123.24, 106.78 (C of acyclic trimer), 69.21, 69.10, 63.79 (C of methylene in ethoxy group), 23.37 (C of methylene bridge of acyclic trimer), 15.77, 15.43, 14.84, 14.22 (C of methyl in ethoxy group). HRMS (ESI):  $\text{C}_{44}\text{H}_{48}\text{O}_6\text{NH}_4^+$ , calcd  $m/z$  690.3795; found  $m/z$  690.3786.

**Tetramer.** m.p.  $212-213^\circ\text{C}$ .  $^1\text{H}$  NMR (500 MHz,  $\text{CDCl}_3$ , 298 K):  $\delta$  (ppm): 8.19 (d,  $J = 8.2$  Hz, 2H), 8.13 (d,  $J = 8.5$  Hz, 2H), 8.02 (d,  $J = 8.2$  Hz, 2H), 7.58 (d,  $J = 8.0$  Hz, 2H), 7.23 (t,  $J = 7.6$  Hz, 2H), 7.16–7.04 (m, 6H), 7.02 (s, 2H), 4.92 (s, 4H), 4.89 (s, 2H), 4.17 (q,  $J = 7.0$  Hz, 4H), 4.13 (q,  $J = 7.0$  Hz, 4H), 3.95 (q,  $J = 7.0$  Hz, 4H), 3.88 (q,  $J = 7.0$  Hz, 4H), 1.52 (t,  $J = 6.9$  Hz, 6H), 1.33 (t,  $J = 7.0$  Hz, 3H), 1.16 (t,  $J = 7.0$  Hz, 6H), 1.05 (t,  $J = 7.0$  Hz, 6H).  $^{13}\text{C}$  NMR (125 MHz,  $\text{CDCl}_3$ , 298 K):  $\delta$  (ppm): 151.36, 149.00, 148.89, 146.25, 131.42, 130.71, 130.66, 130.17, 129.29, 128.78, 128.46, 126.80, 125.21, 125.19, 124.91, 124.56, 124.29, 123.92, 123.18, 106.72 (C of acyclic tetramer), 69.25, 69.13, 69.08, 63.77 (C of methylene in ethoxy group), 23.34 (C of methylene bridge of acyclic tetramer), 15.78, 15.48, 15.46, 14.85 (C of methyl in ethoxy group). HRMS (ESI):  $\text{C}_{59}\text{H}_{64}\text{O}_8\text{NH}_4^+$ , calcd  $m/z$  918.4945; found  $m/z$  918.4922.

## RESULTS AND DISCUSSION

2,3-Diethoxy naphthalene was selected as the building block to condense with paraformaldehyde. Due to the electron-donating ethoxy groups, great regioselectivity can be rationalized, and the reactive sites should be 1- and 4-positions in Friedel–Crafts reaction. It was expected to produce pillar-shape macrocycles, pillar[n]naphthalenes. However, no cyclic oligomers have been obtained after many attempts; a possible reason is that big



**SCHEME 2** | Synthesis of acyclic pillar[n]naphthalenes **Dimer**, **Trimer**, and **Tetramer**.

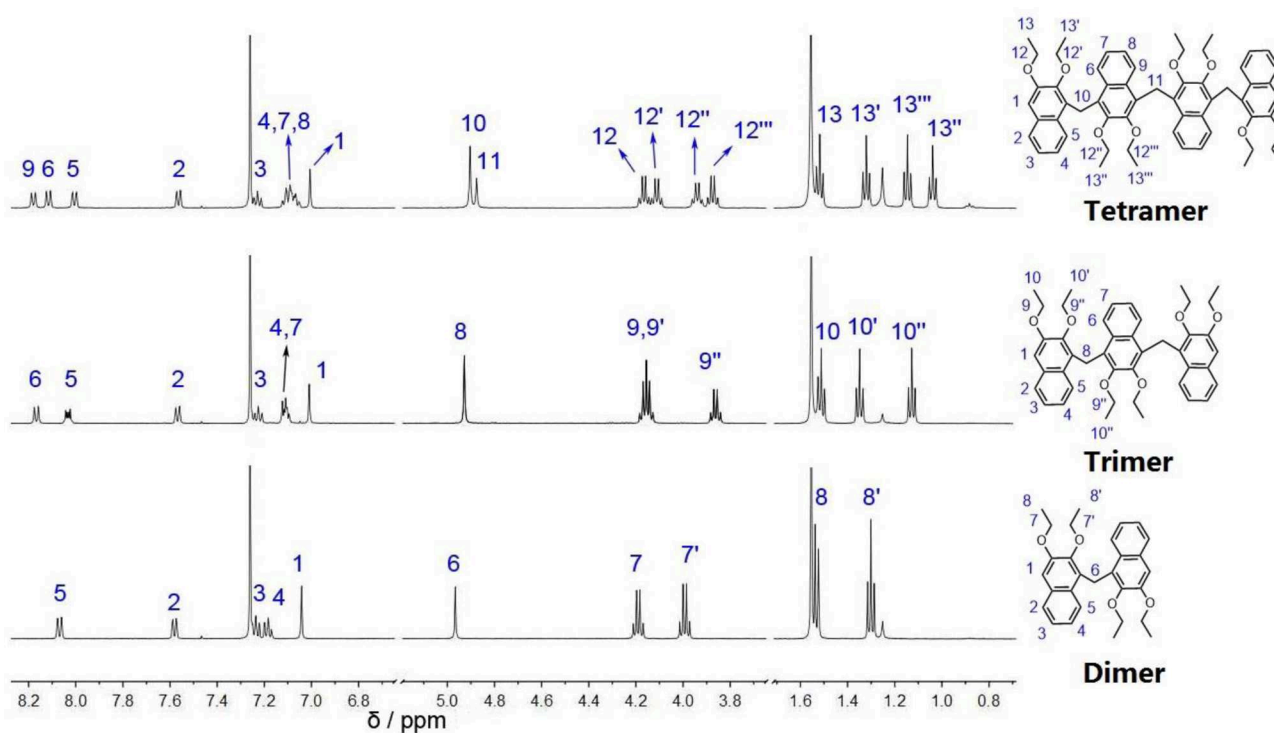


**FIGURE 1** |  $^1\text{H}$  NMR spectra (500 MHz, 2.0 mM,  $\text{CDCl}_3$ ) of **Dimer**, **Trimer**, and **Tetramer**.

naphthalene units make the final cyclization quite difficult due to the steric hindrance. Fortunately, we got acyclic pillar[n]naphthalenes ( $n = 2-4$ ).

Using  $\text{BF}_3 \cdot (\text{Et})_2\text{O}$  as the catalyst, the condensation reaction of 2,3-diethoxy naphthalene and paraformaldehyde in  $\text{CHCl}_3$  at room temperature (Scheme 2) produced oligomers **Dimer**, **Trimer**, and **Tetramer** with yields of 21, 9, and 15%, respectively. Other Lewis acid catalysts, for example  $\text{TfOH}$ ,  $\text{FeCl}_3$ , and  $\text{AlCl}_3$ , could also work, but the reaction yields were lower than that for  $\text{BF}_3 \cdot (\text{Et})_2\text{O}$ . The synthesis was considerably easy since it just involved a one-step reaction of commercial starting materials

and the isolation was also convenient by column chromatography on silica gel.

**Dimer**, **Trimer**, and **Tetramer** were well characterized by  $^1\text{H}$  NMR,  $^{13}\text{C}$  NMR, NOESY, and COSY spectra (Figure 1 and Supplementary Figures 1–11), and high-resolution mass spectrometry (HRMS). They have rather complex patterns of aromatic and ethoxy peaks in  $^1\text{H}$  NMR spectra (Figure 1) because they are not highly symmetrical macrocycles, but acyclic oligomers with low symmetry.

Single crystals of **Dimer**, **Trimer**, and **Tetramer** suitable for X-ray analysis were obtained by diffusion of hexane into a solution



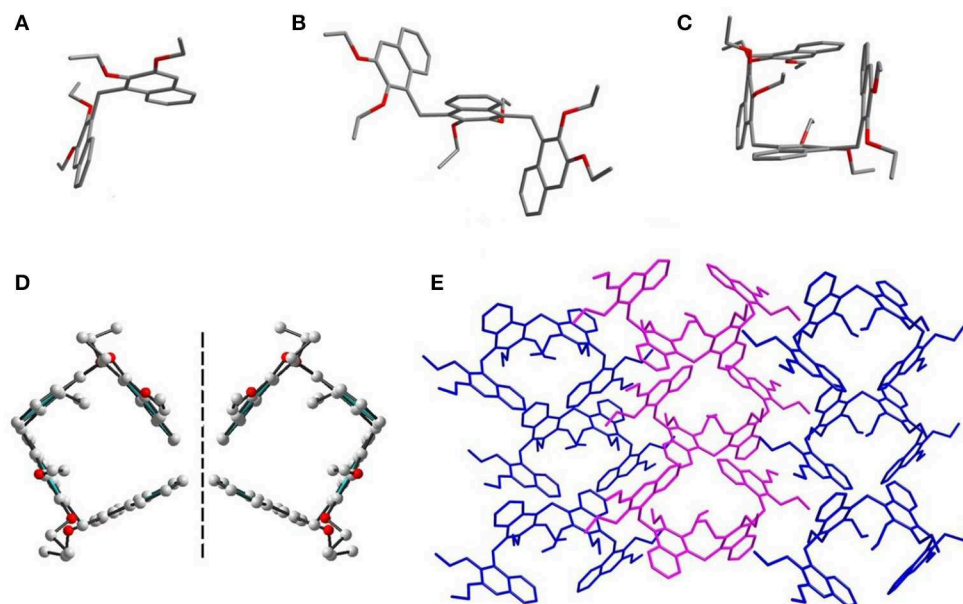


**FIGURE 2 |** Crystal structures of **Dimer (A)**, **Trimer (B)**, and **Tetramer (C)**. **(D)** A pair of enantiomers of **Tetramer**. **(E)** Packing mode of **Tetramer**.

of the compounds in dichloromethane at room temperature (**Figure 2**). As expected, these three acyclic oligomers had the same connecting style, i.e., 2,3-diethoxy naphthalene units were connected by methylene at 1,4-positions. As shown in **Figures 2A,B**, the acyclic **Dimer** and **Trimer**, possessing two and three naphthalene moieties, have ill-defined cavities. Particularly, the **Tetramer** exhibits a pseudocycle-shaped structure, with all the methylene bridges being orientated outwardly. There exist intramolecular sextuple C–H $\cdots$  $\pi$  interactions, with H $\cdots$ ring center distances of 2.75–3.23 Å (**Supplementary Figure 12**), between the middle two ethoxy groups and naphthalenes, resulting in the formation of a pseudo cycle rather than a zigzag structure. More interestingly, the single crystal structures of **Tetramer** molecules exist in a pair of enantiomers in the solid state (**Figure 2D**).

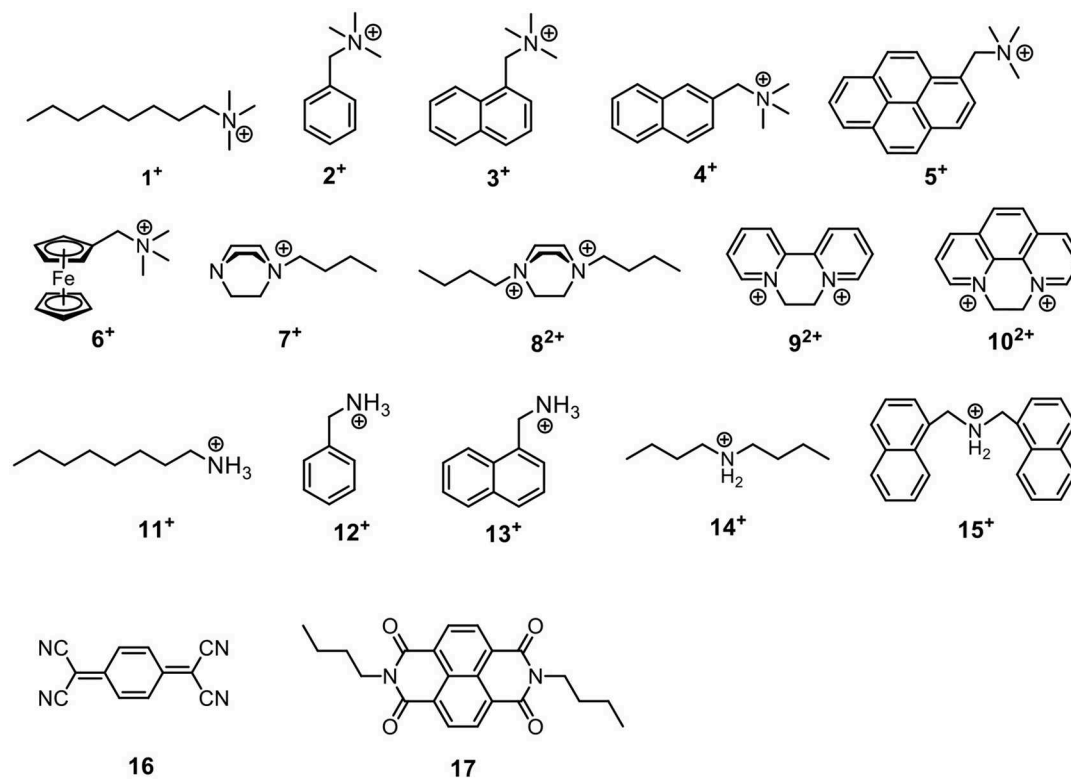
The host-guest properties of the acyclic receptors were then tested. Since they possess  $\pi$ -rich cavities, several cationic guests (**1**<sup>+</sup>–**15**<sup>+</sup>) and electron-deficient neutral guests (**16**–**17**) (**Scheme 3**) were chosen as model guest molecules to investigate their host-guest chemistry. In most cases, CDCl<sub>3</sub> was used as solvent during the <sup>1</sup>H NMR experiments of host-guest mixture and following NMR titrations; for guests **7**<sup>2+</sup>, **9**<sup>2+</sup>, and **10**<sup>2+</sup>, CD<sub>2</sub>Cl<sub>2</sub> was used because of their poor solubility in CDCl<sub>3</sub>.

**Figure 3** shows the <sup>1</sup>H NMR spectra recorded for quarternary ammonium guest **1**<sup>+</sup> in the absence and presence of **Tetramer**. As can be readily seen, upon addition of **Tetramer**, protons H<sub>a</sub>, H<sub>b</sub>, and H<sub>c</sub> of **1**<sup>+</sup> display substantial upfield shifts ( $\Delta\delta = -0.39$ ,  $-0.29$ , and  $-0.21$  ppm) due to complexation-induced shielding effects, indicating that **1**<sup>+</sup> was located inside the acyclic host's pseudo-cavity to form a host-guest inclusion complex, and the main binding site is the N<sup>+</sup>(Me)<sub>3</sub> moiety. In contrast, protons H<sub>n-i</sub> undergo indistinct NMR changes, suggesting

they are located outside the cavity of **Tetramer**. [24] In the NOESY spectrum of **1**<sup>+</sup> and **Tetramer**, NOE correlations were observed between methyl protons H<sub>a</sub> of the guest and the aromatic protons H<sub>5</sub>, H<sub>7</sub> and H<sub>8</sub> of **Tetramer**, also suggesting the host-guest encapsulation (**Supplementary Figure 13**). The formation of **1**<sup>+</sup>•**Tetramer** complex was further supported by ESI mass spectrometry analysis of an equimolar mixture of **1**•BArF and **Tetramer**, where an intense peak for the 1:1 complex ( $m/z$  1072.66, calcd. for **1**<sup>+</sup>•**Tetramer** = 1072.67) was observed (**Supplementary Figure 14**). The encapsulation could also be rationalized by energy-minimized molecular modeling (**Figure 3D**): the oligomers wrapped around the guest to enhance the host-guest contacts driven by cation $\cdots$  $\pi$ /C–H $\cdots$  $\pi$  interactions.

The addition of **Dimer** and **Trimer** could also induce the upfield shifts of guest **1**<sup>+</sup>, but the  $\Delta\delta$  values are smaller than those for **Tetramer** (**Supplementary Figure 15**). These results indicated relatively weak binding interactions occurred for **Dimer** and **Trimer** in comparison with **Tetramer**. These observations were consistent with the association constants ( $K_a$ ) obtained from <sup>1</sup>H NMR titration experiments. As shown in **Table 1**, the  $K_a$  value of **1**<sup>+</sup> with **Tetramer** [ $(4.4 \pm 0.6) \times 10^2 \text{ M}^{-1}$ ] is 18 times larger than that for **Trimer**, and the affinity for **Dimer** was too small to be accurately calculated ( $< 5 \text{ M}^{-1}$ ).

Since **Tetramer** showed interesting structure and good recognition behavior, we then examined its binding capacity toward other cationic guests (**Table 1** and **Supplementary Figures 16–29**), revealing that **Tetramer** can form host-guest complexes with them but the binding affinities are totally different. For the trimethyl ammonium guests **1**<sup>+</sup>–**6**<sup>+</sup>, **3**<sup>+</sup> [ $K_a = (1.2 \pm 0.2) \times 10^3 \text{ M}^{-1}$ ] and **4**<sup>+</sup> [ $K_a =$



**SCHEME 3** | Structures of guest molecules. The counter anions of **1<sup>+</sup>**-**15<sup>+</sup>** are tetrakis[3,5-bis(trifluoromethyl)phenyl] borate ( $\text{BArF}^-$ ).

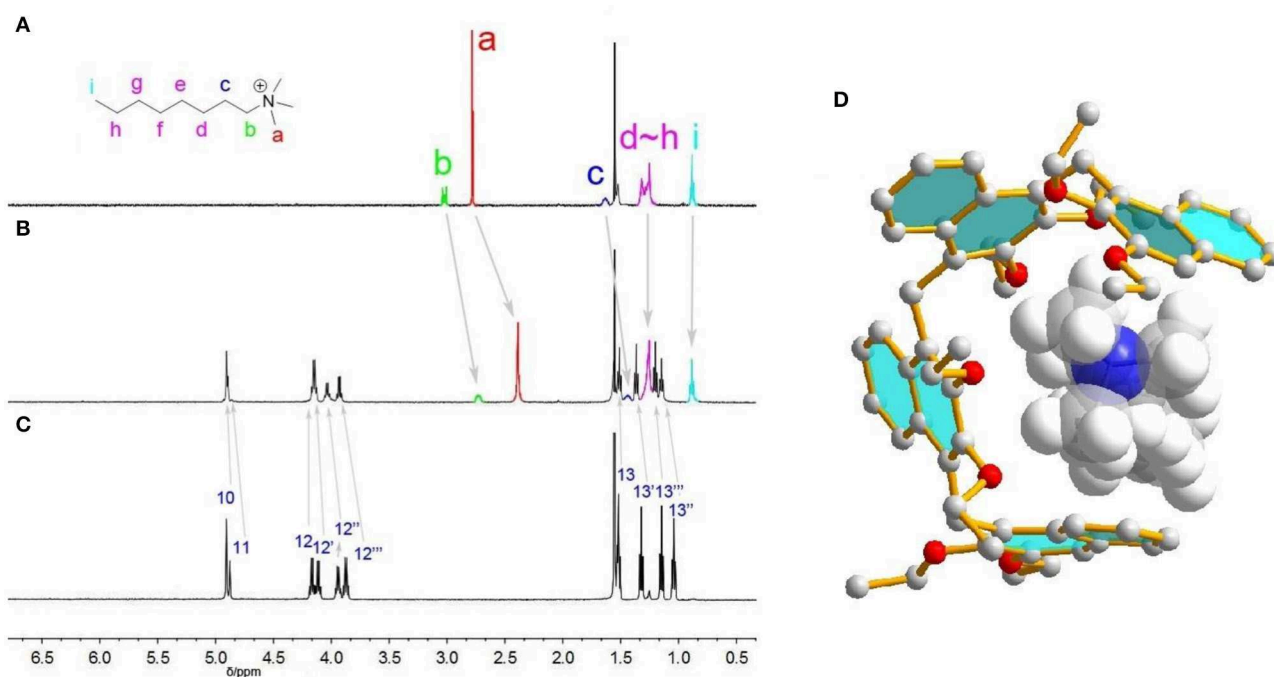


**FIGURE 3** |  $^1\text{H}$  NMR spectra ( $\text{CDCl}_3$ , 298 K, 1.0 mmol) of **(A)** guest **1<sup>+</sup>**, **(B)** **1<sup>+</sup>** and **Tetramer** (1:1 mixture), **(C)** **Tetramer**. **(D)** Energy-minimized structures of **1<sup>+</sup>•Tetramer** at the semiempirical PM6 level of theory.

**TABLE 1** | Association constants ( $M^{-1}$ ) of **Dimer**, **Trimer**, and **Tetramer** with different guests (500 MHz, 298 K).

Guest	Host	Solvent	$K_a$ ( $M^{-1}$ ) <sup>a</sup>
1 <sup>+</sup>	<b>Dimer</b>	CDCl <sub>3</sub>	— <sup>b</sup>
1 <sup>+</sup>	<b>Trimer</b>	CDCl <sub>3</sub>	25±7
1 <sup>+</sup>	<b>Tetramer</b>	CDCl <sub>3</sub>	$(4.4 \pm 0.6) \times 10^2$
2 <sup>+</sup>	<b>Tetramer</b>	CDCl <sub>3</sub>	$(2.9 \pm 0.4) \times 10^2$
3 <sup>+</sup>	<b>Tetramer</b>	CDCl <sub>3</sub>	$(1.2 \pm 0.2) \times 10^3$
4 <sup>+</sup>	<b>Tetramer</b>	CDCl <sub>3</sub>	$(2.1 \pm 0.4) \times 10^3$
5 <sup>+</sup>	<b>Tetramer</b>	CDCl <sub>3</sub>	$(1.6 \pm 0.2) \times 10^2$
6 <sup>+</sup>	<b>Tetramer</b>	CDCl <sub>3</sub>	$(1.8 \pm 0.2) \times 10^2$
7 <sup>2+</sup>	<b>Tetramer</b>	CDCl <sub>3</sub>	$(2.0 \pm 0.1) \times 10^2$
8 <sup>+</sup>	<b>Tetramer</b>	CD <sub>2</sub> Cl <sub>2</sub>	$(1.4 \pm 0.1) \times 10^2$
9 <sup>2+</sup>	<b>Tetramer</b>	CD <sub>2</sub> Cl <sub>2</sub>	$(1.2 \pm 0.2) \times 10^2$
10 <sup>2+</sup>	<b>Tetramer</b>	CD <sub>2</sub> Cl <sub>2</sub>	$(1.7 \pm 0.3) \times 10^2$
11 <sup>+</sup>	<b>Tetramer</b>	CDCl <sub>3</sub>	$(2.5 \pm 0.4) \times 10^4$
12 <sup>+</sup>	<b>Tetramer</b>	CDCl <sub>3</sub>	$(4.3 \pm 0.3) \times 10^3$
13 <sup>+</sup>	<b>Tetramer</b>	CDCl <sub>3</sub>	$(1.4 \pm 0.1) \times 10^4$
14 <sup>+</sup>	<b>Tetramer</b>	CDCl <sub>3</sub>	$(1.4 \pm 0.2) \times 10^3$
15 <sup>+</sup>	<b>Tetramer</b>	CDCl <sub>3</sub>	$(3.0 \pm 0.3) \times 10^2$
16–17	<b>Tetramer</b>	CDCl <sub>3</sub>	— <sup>c</sup>

<sup>a</sup>The  $K_a$  values were determined by NMR titrations (Supplementary Figure 30).

<sup>b</sup>The  $K_a$  value was too small ( $<5 M^{-1}$ ) to be accurately calculated.

<sup>c</sup>No interactions were found (Supplementary Figures 28, 29).

$(2.1 \pm 0.4) \times 10^3 M^{-1}$ ] bearing naphthyl moieties give stronger affinities, which should be due to host-guest fitted  $\pi \cdots \pi$  interactions and large contacts. The substitution of naphthyl for smaller phenyl or bigger pyrenyl in **3<sup>+</sup>** and **4<sup>+</sup>**, affording **1<sup>+</sup>** or **5<sup>+</sup>**, considerably decreases the association constants by one order of magnitude.

Binding affinities of **Tetramer** toward primary ammonium guests **11<sup>+</sup>**–**13<sup>+</sup>** were stronger than those of the corresponding quaternary ammonium guests **1<sup>+</sup>**–**3<sup>+</sup>**. For example, the  $K_a$  value of **Tetramer** and octylammonium **11<sup>+</sup>** [ $(2.5 \pm 0.4) \times 10^4 M^{-1}$ ] is about 56-fold higher than that for trimethyloctylammonium **1<sup>+</sup>** [ $(4.4 \pm 0.6) \times 10^2 M^{-1}$ ]. Similarly, the selectivity factors of **12<sup>+</sup>**/**2<sup>+</sup>** and **13<sup>+</sup>**/**2<sup>+</sup>** are 15 and 12, respectively. The reason for such high selectivity would be that big and spherical  $N^+(Me)_3$  group is too larger compared with **Tetramer**'s size, and small  $NH_3^+$  is a suitable one. It should be noted that the binding affinities of **Tetramer** and organic ammonium salts, with  $K_a$  values in the magnitude of  $10^2$ – $10^4 M^{-1}$ , are

## REFERENCES

- AlHujran, T. A., Dawe, L. N., and Georgiou, P. E. (2012). Synthesis of functionalized acenaphthenes and a new class of homooxacalixarenes. *Org. Lett.* 14, 3530–3533. doi: 10.1021/ol301538s
- Alsaiee, A., Smith, B. J., Xiao, L., Ling, Y., Helbling, D. E., and Dichtel, W. R. (2016). Rapid removal of organic micropollutants from water by a porous  $\beta$ -cyclodextrin polymer. *Nature* 529, 190–194. doi: 10.1038/nature16185
- Andreotti, G. D., Boehmer, V., Jordon, J. G., Tabatabai, M., Ugozzoli, F., Vogt, W., et al. (1993). Dissymmetric calix [4] arenes with C4- and C2-symmetry.

comparable to those for macrocyclic arenes such as pillararenes and biphenarenes.

Due to its  $\pi$ -electron rich cavity, the complexation of **Tetramer** and two  $\pi$ -deficient neutral guests, **16** and **17**, were also investigated. From Supplementary Figures 28, 29, no obvious NMR changes were detected, indicating no stable complexes can be formed.

## CONCLUSIONS

In summary, acyclic pillarnaphthalenes with 2,3-diethoxynaphthalene units bridged by methylenes at 1,4-positions were synthesized through a one-pot reaction of 2,3-diethoxy naphthalene monomer and paraformaldehyde by using Lewis acid as the catalyst. Acyclic pillar[4]naphthalene **Tetramer** is able to interact organic ammonium guests cations by wrapping around them, giving association constants in the magnitude of  $10^2$ – $10^4 M^{-1}$ . We expect that **Tetramer** bearing pseudo-cycle cavity, could have significant potential for the applications in host-guest chemistry and self-assembly.

## DATA AVAILABILITY STATEMENT

All datasets generated for this study are included in the article/Supplementary Material.

## AUTHOR CONTRIBUTIONS

CL, BW, and YJ conceived this project and designed the experiments. YJ and MD contributed to most of the experimental work. CL, MD, and BW co-wrote the paper. All authors discussed and commented on the paper and analyzed the data.

## FUNDING

This work was supported by the National Natural Science Foundation of China (21772118 and 21472122), the Shanghai Pujiang Program (16PJD024), and the Shuguang Program.

## SUPPLEMENTARY MATERIAL

The Supplementary Material for this article can be found online at: <https://www.frontiersin.org/articles/10.3389/fchem.2019.00828/full#supplementary-material>

- Synthesis, X-ray structures, conformational fixation, and proton NMR spectroscopic studies. *J. Org. Chem.* 58, 4023–4032. doi: 10.1021/jo00067a040
- Avetta, C. T., Shorthill, B. J., Ren, C., and Glass, T. E. (2012). Molecular tubes for lipid sensing: tube conformations control analyte selectivity and fluorescent response. *J. Org. Chem.* 77, 851–857. doi: 10.1021/jo201791a
- Baldini, L., Casnati, A., Sansone, F., and Ungaro, R. (2007). Calixarene-based multivalent ligands. *Chem. Soc. Rev.* 36, 254–266. doi: 10.1039/B603082N
- Bier, D., Rose, R., Bravo-Rodriguez, K., Bartel, M., Ramirez-Anguila, J. M., Dutt, S., et al. (2013). Molecular tweezers modulate 14-3-3 protein–protein interactions. *Nat. Chem.* 5, 234–239. doi: 10.1038/nchem.1570

- Chen, H., Fan, J., Hu, X., Ma, J., Wang, S., Li, J., et al. (2015). Biphen[n]arenes. *Chem. Sci.* 6, 197–202. doi: 10.1039/C4SC02422B
- Chen, J., Ni, H., Meng, Z., Wang, J., Huang, X., Dong, Y., et al. (2019). Supramolecular trap for catching polyamines in cells as an anti-tumor strategy. *Nat. Commun.* 10:3546. doi: 10.1038/s41467-019-11553-7
- Chun, Y., Singh, N. J., Hwang, I. C., Lee, J. W., Yu, S. U., and Kim, K. S. (2013). Calix [n] imidazolium as a new class of positively charged homo-calix compounds. *Nat. Commun.* 4:1797. doi: 10.1038/ncomms2758
- Cram, D. J. (1988). The design of molecular hosts, guests, and their complexes. *Science* 240, 760–767. doi: 10.1126/science.3283937
- Dai, L., Ding, Z. J., Cui, L., Li, J., Jia, X., and Li, C. (2017). 2, 2'-Biphen[n]arenes (n = 4–8): one-step, high-yield synthesis, and host-guest properties. *Chem. Commun.* 53, 12096–12099. doi: 10.1039/C7CC06767D
- Gong, H. Y., Rambo, B. M., Karnas, E., Lynch, V. M., and Sessler, J. L. (2010). A "Texas-sized" molecular box that forms an anion-induced supramolecular necklace. *Nat. Chem.* 2, 406–409. doi: 10.1038/nchem.597
- Goodman, C. M., Choi, S., Shandler, S., and DeGrado, W. F. (2007). Foldamers as versatile frameworks for the design and evolution of function. *Nat. Chem. Biol.* 3, 252–262. doi: 10.1038/nchembio876
- Guo, D. S., and Liu, Y. (2012). Calixarene-based supramolecular polymerization in solution. *Chem. Soc. Rev.* 41, 5907–5921. doi: 10.1039/C2CS35075K
- Guo, S., Song, Y., He, Y., Hu, X. Y., and Wang, L. (2018). Highly efficient artificial light-harvesting systems constructed in aqueous solution based on supramolecular self-assembly. *Angew. Chem. Int. Ed.* 57, 3163–3167. doi: 10.1002/anie.201800175
- Jie, K., Zhou, Y., Li, E., and Huang, F. (2018). Nonporous adaptive crystals of pillararenes. *Acc. Chem. Res.* 51, 2064–2072. doi: 10.1021/acs.accounts.8b00255
- Jono, K., Suzuki, A., Akita, M., Albrecht, K., Yamamoto, K., and Yoshizawa, M. (2017). A polyaromatic molecular clip that enables the binding of planar, tubular, and dendritic compounds. *Angew. Chem. Int. Ed.* 129, 3570–3574. doi: 10.1002/anie.201612489
- Juríček, M., Strutt, N. L., Barnes, J. C., Butterfield, A. M., Dale, E. J., Baldrige, K. K., et al. (2014). Induced-fit catalysis of corannulene bowl-to-bowl inversion. *Nat. Chem.* 6, 222–228. doi: 10.1038/nchem.1842
- Lehn, J. M. (1988). Supramolecular chemistry—scope and perspectives molecules, supermolecules, and molecular devices (Nobel Lecture). *Angew. Chem. Int. Ed.* 27, 89–112. doi: 10.1002/anie.198800891
- Li, B., Meng, Z., Li, Q., Huang, X., Kang, Z., Dong, H., et al. (2017). A pH responsive complexation-based drug delivery system for oxaliplatin. *Chem. Sci.* 8, 4458–4464. doi: 10.1039/c7sc01438d
- Li, B., Wang, B., Huang, X., Dai, L., Cui, L., Li, J., et al. (2019). Terphen[n]arenes and quaterphen[n]arenes (n = 3–6): one-pot synthesis, self-assembly into supramolecular gels, and iodine capture. *Angew. Chem. Int. Ed.* 58, 3885–3889. doi: 10.1002/anie.201813972
- Liu, Y., Zhao, W., Chen, C. H., and Flood, A. H. (2019). Chloride capture using a C–H hydrogen bonding cage. *Science* 365, 159–161. doi: 10.1126/science.aaw5145
- Luo, J., Ao, Y. F., Wang, Q. Q., and Wang, D. X. (2018). Diversity-oriented construction and interconversion of multicavity supermacrocycles for cooperative anion- $\pi$  binding. *Angew. Chem. Int. Ed.* 57, 15827–15831. doi: 10.1002/anie.201810836
- Ma, D., Hettiarachchi, G., Nguyen, D., Zhang, B., Wittenberg, J. B., Zavalij, P. Y., et al. (2012). Acyclic cucurbit [n] uril molecular containers enhance the solubility and bioactivity of poorly soluble pharmaceuticals. *Nat. Chem.* 4, 503–510. doi: 10.1038/nchem.1326
- Ma, Y. L., Ke, H., Valkonen, A., Rissanen, K., and Jiang, W. (2018). Achieving strong positive cooperativity through activating weak non-covalent interactions. *Angew. Chem. Int. Ed.* 57, 709–713. doi: 10.1002/anie.201711077
- Ogoshi, T., Kanai, S., Fujinami, S., Yamagishi, T. A., and Nakamoto, Y. (2008). para-Bridged symmetrical pillar [5] arenes: their Lewis acid catalyzed synthesis and host-guest property. *J. Am. Chem. Soc.* 130, 5022–5023. doi: 10.1021/ja711260m
- Pan, S. J., Ye, G., Jia, F., He, Z., Ke, H., Yao, H., et al. (2017). Regioselective synthesis of methylene-bridged naphthalene oligomers and their host-guest chemistry. *J. Org. Chem.* 82, 9570–9575. doi: 10.1021/acs.joc.7b01579
- Pedersen, C. J. (1988). The discovery of crown ethers. *Science* 241, 536–540. doi: 10.1126/science.241.4865.536
- Poh, B. L., Lim, C. S., and Khoo, K. S. (1989). A water-soluble cyclic tetramer from reacting chromotropic acid with formaldehyde. *Tetrahedron Lett.* 30, 1005–1008. doi: 10.1016/S0040-4039(00)95302-4
- Schrader, T., Bitan, G., and Klärner, F. G. (2016). Molecular tweezers for lysine and arginine-powerful inhibitors of pathologic protein aggregation. *Chem. Commun.* 52, 11318–11334. doi: 10.1039/C6CC04640A
- Seebach, D., and Gardiner, J. (2008).  $\beta$ -peptidic peptidomimetics. *Acc. Chem. Res.* 41, 1366–1375. doi: 10.1021/ar700263g
- Shen, C., Ma, D., Meany, B., Isaacs, L., and Wang, Y. (2012). Acyclic cucurbit [n] uril molecular containers selectively solubilize single-walled carbon nanotubes in water. *J. Am. Chem. Soc.* 134, 7254–7257. doi: 10.1021/ja301462e
- Shorthill, B. J., Avetta, C. T., and Glass, T. E. (2004). Shape-selective sensing of lipids in aqueous solution by a designed fluorescent molecular tube. *J. Am. Chem. Soc.* 126, 12732–12733. doi: 10.1021/ja047639d
- Sinha, S., Lopes, D. H., Du, Z., Pang, E. S., Shanmugam, A., Lomakin, A., et al. (2011). Lysine-specific molecular tweezers are broad-spectrum inhibitors of assembly and toxicity of amyloid proteins. *J. Am. Chem. Soc.* 133, 16958–16969. doi: 10.1021/ja206279b
- Song, N., and Yang, Y. W. (2015). Molecular and supramolecular switches on mesoporous silica nanoparticles. *Chem. Soc. Rev.* 44, 3474–3504. doi: 10.1039/C5CS00243E
- Wang, M. X. (2018). Coronarenes: recent advances and perspectives on macrocyclic and supramolecular chemistry. *Sci. China Chem.* 61, 993–1003. doi: 10.1007/s11426-018-9328-8
- Wang, Y., Liu, T., Jiang, J., Chen, Y., Cen, M., Lu, D., et al. (2019a). Syntheses of water-soluble acyclic naphthalene oligomers and their applications in water. *Dalton Trans.* 48, 6333–6336. doi: 10.1039/C9DT00709A
- Wang, Y., Ping, G., and Li, C. (2016). Efficient complexation between pillar [5] arenes and neutral guests: from host-guest chemistry to functional materials. *Chem. Commun.* 52, 9858–9872. doi: 10.1039/C6CC03999E
- Wang, Y., Xu, K., Li, B., Cui, L., Li, J., Jia, X., et al. (2019b). Efficient separation of cis- and trans-1, 2-dichloroethene isomers by adaptive biphen[3]arene crystals. *Angew. Chem. Int. Ed.* 58, 10281–10284. doi: 10.1002/anie.201905563
- Xue, M. I. N., Yang, Y., Chi, X., Zhang, Z., and Huang, F. (2012). Pillararenes, a new class of macrocycles for supramolecular chemistry. *Acc. Chem. Res.* 45, 1294–1308. doi: 10.1021/ar2003418
- Yang, B., Zhang, X. D., Li, J., Tian, J., Wu, Y. P., Yu, F. X., et al. (2019). *In situ* loading and delivery of short single- and double-stranded dna by supramolecular organic frameworks. *CCS Chem.* 1, 156–165. doi: 10.31635/ccschem.019.20180011
- Yang, K., Pei, Y., Wen, J., and Pei, Z. (2016). Recent advances in pillar [n] arenes: synthesis and applications based on host-guest interactions. *Chem. Commun.* 52, 9316–9326. doi: 10.1039/C6CC03641D
- Yashima, E., Ousaka, N., Taura, D., Shimomura, K., Ikai, T., and Maeda, K. (2016). Supramolecular helical systems: helical assemblies of small molecules, foldamers, and polymers with chiral amplification and their functions. *Chem. Rev.* 116, 13752–13990. doi: 10.1021/acs.chemrev.6b00354
- Zhang, D. W., Zhao, X., Hou, J. L., and Li, Z. T. (2012). Aromatic amide foldamers: structures, properties, and functions. *Chem. Rev.* 112, 5271–5316. doi: 10.1021/cr300116k
- Zhang, G. W., Li, P. F., Meng, Z., Wang, H. X., Han, Y., and Chen, C. F. (2016). Triptycene-based chiral macrocyclic hosts for highly enantioselective recognition of chiral guests containing a trimethylamino group. *Angew. Chem. Int. Ed.* 55, 5304–5308. doi: 10.1002/anie.201600911

**Conflict of Interest:** The authors declare that the research was conducted in the absence of any commercial or financial relationships that could be construed as a potential conflict of interest.

Copyright © 2019 Jia, Dong, Wang and Li. This is an open-access article distributed under the terms of the Creative Commons Attribution License (CC BY). The use, distribution or reproduction in other forums is permitted, provided the original author(s) and the copyright owner(s) are credited and that the original publication in this journal is cited, in accordance with accepted academic practice. No use, distribution or reproduction is permitted which does not comply with these terms.



# Advantages of publishing in Frontiers



## OPEN ACCESS

Articles are free to read  
for greatest visibility  
and readership



## FAST PUBLICATION

Around 90 days  
from submission  
to decision



## HIGH QUALITY PEER-REVIEW

Rigorous, collaborative,  
and constructive  
peer-review



## TRANSPARENT PEER-REVIEW

Editors and reviewers  
acknowledged by name  
on published articles

## Frontiers

Avenue du Tribunal-Fédéral 34  
1005 Lausanne | Switzerland

**Visit us:** [www.frontiersin.org](http://www.frontiersin.org)

**Contact us:** [info@frontiersin.org](mailto:info@frontiersin.org) | +41 21 510 17 00



## REPRODUCIBILITY OF RESEARCH

Support open data  
and methods to enhance  
research reproducibility



## DIGITAL PUBLISHING

Articles designed  
for optimal readership  
across devices



## FOLLOW US

[@frontiersin](https://twitter.com/frontiersin)



## IMPACT METRICS

Advanced article metrics  
track visibility across  
digital media



## EXTENSIVE PROMOTION

Marketing  
and promotion  
of impactful research



## LOOP RESEARCH NETWORK

Our network  
increases your  
article's readership